Astrophysics and Space Science Library 375

Gennady P. Chernov

Fine Structure of Solar Radio Bursts

ASSL

Springer

Fine Structure of Solar Radio Bursts

For further volumes:
http://www.springer.com/series/5664

Astrophysics and Space Science Library

EDITORIAL BOARD

Gennady Pavlovich Chernov

Fine Structure of Solar Radio Bursts

Springer

G.P. Chernov
IZMIRAN
Russian Academy of Sciences
Troitsk The Moscow Area
Russia
gchernov@izmiran.rssi.ru

ISSN 0067-0057
ISBN 978-3-642-20014-4 e-ISBN 978-3-642-20015-1
DOI 10.1007/978-3-642-20015-1
Springer Heidelberg Dordrecht London New York

Library of Congress Control Number: 2011932229

Cover image: Motive from the image "Assortment of solar burst types" taken with the Frequency Agile Solar Radiotelescope Subsystem Testbed (FST) at Owens Valley Solar Array (http://www.ovsa.njit.edu/). Courtesy of Dale E. Gary.

Cover design: eStudio Calamar S.L.

Printed on acid-free paper

Springer is part of Springer Science+Business Media (www.springer.com)

Seek, and you will find…

The Gospel, St. Matthew VII, 7

Preface

The first steps of research of Solar Radio Bursts are described in the famous monographs by Zheleznyakov (1964) and Kundu (1965). The rapid progress of the Solar Radio Astronomy was regarded in the excellent book by Kruger (1979). This survey covers successive development of radioheliographic observations, the detection of spectral fine structure and various kinds of extraterrestrial observations. A theoretical description of radio emission mechanisms was published by Zheleznyakov (1998): "*Radiation in Astrophysical Plasmas*". The solar radio physics has grown to be an extended field, making it rather impossible for a single person to review many topics.

The recent review by Pick and Vilmer (2008), A&A Rev. 16, 1–153: "*Sixty-five years of solar radioastronomy*:" is a general historical description of the solar radio emission in a wide aspect of its relation with X-ray emission, CME, interplanetary shock waves, etc. This is a very useful review and may be unique, after the monograph by Kruger (1979).

All these editions do not almost contain however any information about the fine structure of radio bursts. The study of the fine structure of the solar radio emission is a key to understanding the plasma processes in the solar corona. It remains a reliable means for both diagnosing the solar corona and verifying the results of laboratory plasma experiments on the wave–wave and wave–particle interactions. The high time and frequency resolution data have improved our studies of similar fine structures in stellar flares.

Already the first spectral observations of large type IV (and II+IV) bursts revealed the rich variety of the fine structure of the radio emission in the form of wide-band pulsations in emission and absorption with different periods, rapid bursts (spikes) and narrow-band patches. Modulation of the continuum emission in the form of narrow stripes in emission and absorption (zebra pattern (ZP) and fiber bursts (FB)) appeared to be the most intriguing elements of the fine structure. Pulsations and spikes usually accompany ZP and FB in the dynamical radio spectra.After the short review of some elements of fine structures by Fomichev and Chertok (1976) and the short theoretical description of the emission mechanisms by Kuijpers (1980), only the atlas by Slottje (1981) (with a small number of copies) gives exhaustive experimental results about ZP and FB. If pulsations and

spikes obtained sufficiently adequate interpretation, then for ZP and FB during several decades more than ten different mechanisms were developed.

During last almost two decades with the space missions, such as soft X-ray observations with Yohkoh, extreme-ultraviolet (EUV) observations with SOHO and TRACE and now RHESSI and Hinode, we have rich information about the flare evolution in different spectral ranges. And now, it should be studied how they could help us to understand the processes of formation of different fine structures. The exhaustive description of Physics of the solar corona in Aschwanden (2004) represents a comprehensive source for this purpose.

The plan for this book resulted from a desire to have a concise up-to-date survey of the fine structure of solar radio bursts. This volume has grown out of more than 40-year-old experience of the author in the study of spectral fine structure.

In this book we shall show the entire diversity of experimental data with the development of the observational techniques, with the goal to confirm or disprove theoretical models. The author does not pretend however to give an exhaustive survey of all published works in the field of fine structure. This cannot be presented in one volume. The author tried rather to present materials not illuminated earlier in any reviews. Moreover, the exposition of the materials is most likely an author's view, without pretending to have achieved a universal description "of all and entire". The reader will notice that many of the figures are taken from the author's own work based on observations of fine structure in the meter range conducted over more than 40 years (Markeev and Chernov 1970). To our knowledge no other observatory in the world possesses similar high-resolution data. Therefore, the author apologizes in advance before the colleagues who might have the impression that their work did not receive proper citation.

Chapter 2 is devoted to radio pulsations. After several excellent reviews (Slottje 1981; Roberts et al. 1984; Aschwanden 1987, 2004), here, the preference is given to the description of millisecond pulsations, which have not yet been described properly.

Perhaps, the largest number of works was devoted to the fastest bursts, the spikes. In Chap. 3, a view of the author on number of problems is given. And again, the preference is there given to the description of the models of millisecond spikes, which is continued in Chap. 4, since they were discovered as the superfine structure of the zebra pattern (ZP).

Chapter 4, the largest chapter, gives a sufficiently complete description of the historical development of both the experimental data and theoretical models of ZP and FB.

Chapter 5 is devoted to recent observations with the highest resolution (~1 ms, and partially much less), when several new details of the fine structure were discovered. The description of new mechanisms of the ZP was continued, a special attention was given to works on the improvement of model at double plasma resonance (DPR), since in the past 3–4 years more than 10 articles were published on this theme.

Since this book deals with the observation and theoretical models of the fine structure of solar radio bursts, it covers a wide field of Solar Radio Physics and will be useful to graduate students and researchers.

Troitsk (IZMIRAN) G.P. Chernov
November 2010

Acknowledgments

The author is grateful for support to the Chinese Academy of Sciences and NSF of China that enabled him to work with colleagues at NAOC (Fu, Q.J., Yan Y., Huang G.L.). The author thanks also K.L. Klein for the preparation and discussion of the Nançay radioheliograph data and M. Poquerusse for the ARTEMIS spectrograph data (Meudon). The author is most indebted to P. Zlobec for the data from the Trieste Astronomical Observatory polarimeter, discussion and comments.

The author is grateful to the colleagues and friends who provided the spectra and graphics: Marian Karlicky, Jan-Louis Bougeret, Michael Kaiser, Gregory Fleishman, Dale Gary, Yihua Yan, Chengmin Tan, Baolin Tan, Guangli Huang, Robert Sych, Natalia Meshalkina, Aleksandr Altyntsev, Aleksei Kuznetsov, B.P. Dabrowsky. . .

The SOHO, TRACE and RHESSI data were obtained from the SOHO, TRACE, RHESSI, and Hinode databases and the X-ray data – from the Yohkoh/SXT database (ISAS, Japan). The author is grateful to SOHO, TRACE, RHESSI, Hinode, Nobeyama RH and SSRT teams for operating the instruments and performing the basic data reduction, and especially, for the open data policy.

This book was supported by the Russian Foundation of Basic Research, grants No. 08-02-00270, 11-02-91151.

The author wants to acknowledge his colleagues for an efficient help with spectral observations at IZMIRAN: A.K. Markeev, V.V. Fomichev, D. Sobolev, R. Gorgutsa.

I express special appreciation to my entire family, my daughter Karina and my son Pavel, who enabled me to work freely on the manuscript amid our difficult times, and to my wife Valentina to whom this book is dedicated with eternal love and wishes of the fastest victory over a grave ailment.

Contents

Chapter 1

Introduction

Solar radio astronomy has grown into an extensive scientific branch since its birth in the forties of the 20-th century, initiated by the subsequent discovery of the main basic components of solar radio emission: the quiet Sun, the slowly varying component and various types of radio bursts including noise storms (Krüger, 1979). It was quickly revealed that radio bursts are observed during chromospheric flares.

The radio bursts were classified in five distinctive types at the dynamical spectrum (Wild, Smerd and Weiss, 1963) and the noise storms in the meter wave range proved to be the most widespread manifestation of solar activity, when against the background of the prolonged increased continuous emission numerous narrow-band short-term bursts of type I appear at different frequencies.

Type III bursts are obviously the most frequent bursts observed from the solar corona. They are characterized by their short duration and rapid drift from high to low frequencies in the decimeter and meter wave ranges. It is assumed that radio emission is generated by the beams of fast electrons at the levels of the local plasma frequency or its second harmonic (*'plasma hypothesis'*).

Slow-drift type II bursts are outstanding events associated with large flares. They occur much more rarely. The frequency drift to low frequencies is found to correspond to the velocity of the order of 10^3 km s^{-1} and the moving agency is identified with a collisionless MHD shock wave set up as a result of explosion at the time of the flare flash phase (Wild and Smerd, 1972).

Type IV bursts are a continuum radiation following type II bursts, or they are superimposed on the time, and then such events are called type II+IV. Their radio sources can be stationary or moving, and the continuum can be extended from meter into decimeter and microwave ranges almost simultaneously (Zheleznyakov, 1964; Kundu, 1965; Wild and Smerd, 1972).

The type V burst is a broad-band continuum radiation following a type III burst as a diffuse prolongation (usually below 150 MHz). It is assumed to be the emission of the part of electrons, producing the type III burst trapped in a magnetic loop.

The recent review by Pick & Vilmer (2008) gives the input of radio observations to our understanding of solar and solar–terrestrial physics.

Already the first spectral observations of the large type IV (and II+IV) bursts revealed a rich variety of the fine structures of radio emission in the form of wide-band pulsations in emission and absorption with different periods, rapid bursts (spikes), narrow-band patches. Modulation of the continuum emission in the form

of narrow stripes in the emission and absorption (zebra patterns and fiber bursts) appeared to be the most intriguing elements of the fine structure (Krüger, 1979).

Studies of the fine structure of solar radio bursts are of great importance for both the refinement of the burst generation mechanisms and the diagnostics of the corona plasma. The most intriguing fine structure is, undoubtedly, the zebra pattern (ZP) in continuous type-IV radio bursts.

The study of the fine structure of the solar radio emission is a key to understanding the plasma processes in the solar corona. It remains a reliable means for both diagnosing the solar corona and verifying the results of laboratory plasma experiments on the wave-wave and wave-particle interactions. High time and frequency resolution data have improved our studies of similar fine structures in star flares. So, the continuum radio emission of type IV was associated for a long time with the synchrotron emission of electrons trapped into a magnetic cloud (after the work of Boischot (1957), but the analysis of the fine structure testified that the plasma mechanism is predominant in the meter and decimeter wave band.

We will try to describe the development of the investigation of fine structures from the period going from their first discovery in the solar radio emission to the present days.

So, we intend to describe fast pulsations of solar radio emission in Chapter 2, radio spikes, the most short-living solar bursts ($\lesssim 0.1$ s) (Chapter 3), zebra patterns and fiber bursts (Chapter 4), and the recent results of theirs study (Chapter 5).

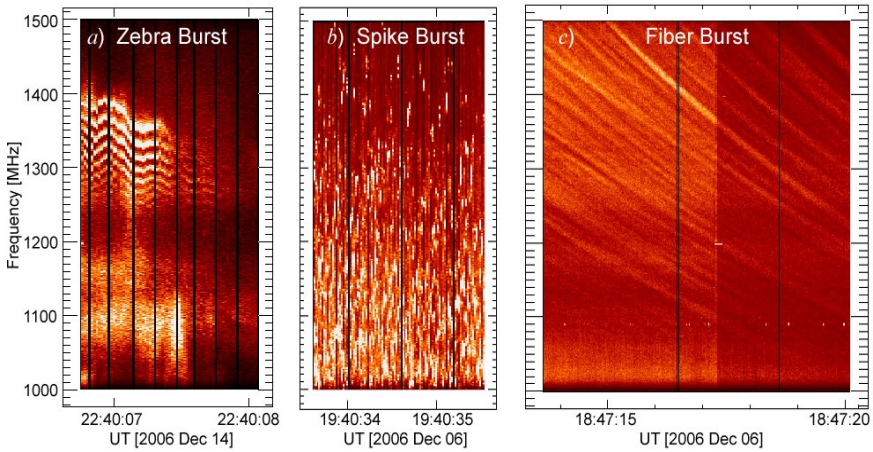

Fig. 1.1 Examples of a zebra pattern (*a*), spike bursts (*b*), and fiber bursts (*c*) observed by a new system of Frequency Agile Solar Radiotelescope (Owens Valley Radio Observatory in California, http://www.ovsa.njit.edu/) (courtesy of D.Gary).

Figure 1.1 shows an excellent illustration of such fine structures in the decimeter range with a high time resolution, observed by a new system of Frequency Agile Solar Radiotelescope (FASR, http://www.ovsa.njit.edu/). Figure 1.2 illustrates millisecond spikes, fast pulsations, and several stripes of the zebra pattern observed simultaneously in a unique solar event of 13 December 2006 with the Chinese spectrometer in the range 2.6 – 3.8 GHz.

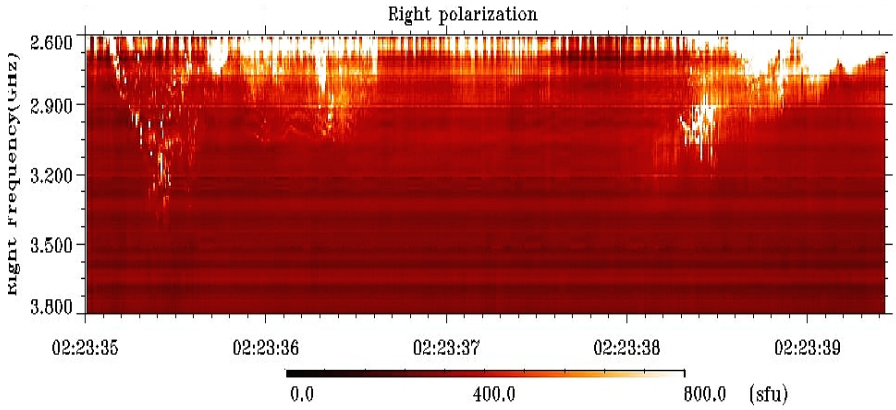

Fig. 1.2 Millisecond spikes, fast pulsations and several stripes of the zebra pattern observed simultaneously in a unique solar event of 13 December 2006 in the range 2.6 – 3.8 GHz with the spectrometer of National Astronomical Observatory of China (NAOC) (private communication of prof. Y.Yan).

For over more than four decades radio astronomers have been observing pulsating structures in solar radio emission. 'Pulsations' include a wide range of phenomena of quasi-periodic patterns or fine structures observed in the metric/ decimetric/ microwave frequency ranges. They were usually described as series of fast drift bursts. Pulsations are rarely observed in pure form. Usually, they are superimposed on other elements of the fine structure: spikes, fiber bursts, zebra patterns.

Slottje (1981) was the first to summarize the observed properties of the pulsations. Aschwanden (1987, 2004) presented an extensive review of all kinds of models for the pulsating events. Therefore it would be superfluous to repeat here in detail the entire content of these excellent reviews (and of a number of others). We will note only their basic conclusions, and let us try to call the reader's attention to experimental data and theoretical models that were not yet previously described, using both the old sources and the recent publications.

Thus, primary attention will be given to millisecond pulsations because, in the recent years, the new solar broadband radio spectrometers of NAOC (China, Huairou station) have allowed us to obtain unique information on the fine structures at frequencies 1 – 7.6 GHz with high resolution (10 MHz and 5 – 8 ms, and partially

1.25 ms) (Fu et al., 2004). And it was discovered that in the microwave range the same variety of fine structures was observed as in the meter range.

The "spike" type radio bursts were isolated as a special kind of the most short-time and narrow-band bursts in the meter and decimeter wave bands with the beginning of observation with high resolution. There are bursts with the duration of $d_f \leq 0.1$ s at one frequency. The spikes riveted at once the attention of researchers, since the brightness temperatures of the spikes T_b can reach (and even exceed) 10^{15} K. Such a high brightness temperature, along with the extremely short duration of the bursts and the strong circular polarization of radio emission, can only be provided by some coherent mechanism. From the first years of the study, the spikes are generally agreed to be an emission closely connected with the particle acceleration and primary energy release in flares.

The most complete experimental study of spikes was executed by Tarnstrom & Philip (1971). Then, the basic observed properties of spikes in the meter range are summarized in the short review by Slottje (1981). Benz (1985; 1986) described spikes in the decimeter range at the base of observations with the digital spectrometer IKARUS (Zurich). At last, we obtained exhaustive review of all basic mechanisms of the excitation of spikes and their relevance to the observed parameters thanks to Fleishman & Melnikov (1998). Although now, the nature of spikes remains not explained completely, and we will try to show this in Chapter 3.

The nature of the zebra pattern (ZP) has been a subject of wide discussion for more than 40 years. The ZP in the solar radio emission is the simultaneous excitation of waves at many (up to a few tens) of closely spaced, nearly equidistant frequencies. The basic parameters of ZP in the meter wave band are represented in the atlas by Slottje (1981). Now it is authentically known that in a regular ZP the frequency separation between the stripes grows with frequency: from 4 – 5 MHz at 200 MHz to ~ 80 MHz at 3000 MHz and to ~150 – 200 MHz at 5700 MHz. It is important to note that the relative frequency bandwidth of a separate stripe in emission remains almost stably constant with frequency, $\Delta f_e/f \approx 0.005$.

More than ten different models have been proposed for ZPs; most of them include some emission of electrostatic plasma waves at the upper hybrid frequency (ω_{UH}) (Kuijpers, 1975a; Zheleznykov and Zlotnik, 1975a; Mollwo, 1983; 1988; Winglee and Dulk, 1986). In order to explain the ZP dynamics in the framework of this mechanism, it is necessary that the magnetic field in the radio source varied sufficiently rapidly, which, however, contradicts the fairly low field values determined from the frequency separation between the stripes. Over the past five years, there appeared dozens of papers concerning the refinement of this mechanism, because, in its initial formulation, it failed to describe many features of the ZP. Kuznetsov and Tsap (2007) assumed that the velocity distribution function of hot electrons within the loss cone can be described by a power law with an exponent of 8–10. In this case, a fairly deep modulation can be achieved, but the excitation of waves at multiple double plasma resonance (DPR) levels is still impossible.

Fiber bursts differ from ZP stripes only by a constant negative frequency drift, and one of the first models explained the radio emission (t) of fiber bursts by the coalescence of plasma waves (l) with whistlers (w), $l + w \rightarrow t$ (Kuijpers, 1975a).

In spite of the fact that then some more models were proposed (Alfvénic solitons, whistler solitons, MHD oscillations), this first model remains now most accepted. After the brief review by Kuijpers (1980) the situation in this sphere of activity was cleared up only in the review of Chernov (2006).

In Chernov (1976a; 1990), the mechanism $l + w \rightarrow t$ was proposed as an unified model in which the formation of ZPs in the emission and absorption spectra was attributed to the oblique propagation of whistlers, while the formation of stripes with a stable negative frequency drift (the fiber bursts) was explained by the ducted propagation of waves along a magnetic trap. This model explains occasionally observed transformation of the ZP stripes into fibers and vice versa.

The discovery of the superfine structure of the ZP, in the form of millisecond spikes was the most significant new effect in the microwave range (Chernov et al., 2003). The reliability of such a study strongly grew over the past few years in connection with numerous observations of fast radio bursts (millisecond spikes) during the stellar flares (Abada-Simon et al., 1995). It is amazing that the period of star spikes in the radio burst of the classical red dwarf AD Leo coincides with the period of spikes in the superfine structure of solar zebra stripes (~30 ms) (Osten and Bastian, 2006).

To overcome difficulties arising in different models, a new ZP theory based on the emission of auroral choruses (magnetospheric bursts) via the escape of the Z mode captured by regular plasma density inhomogeneities was recently proposed (LaBelle et al. 2003). This theory, however, fails to explain the high intensity of radiation emitted by separate incoherent sources. In addition, the theory imposes some stringent conditions, such as the presence of a large–amplitude ion–acoustic wave.

The existence of a ZP in the solar radio emission can be attributed to the existence of discrete eigenmodes in the nonuniform solar atmosphere. Several aspects of this mechanism were considered in Laptukhov and Chernov (2006); Barta and Karlicky (2006); Ledenev, Yan, and Fu (2006). In Laptukhov and Chernov (2006), dispersion relations were derived for a discrete spectrum of eigenmodes of a spatially periodic medium in the form of nonlinear structures formed due to the onset of thermal instability. The spectrum of eigenfrequencies of a system of spatially periodic cavities is calculated, and it is shown that such a system is capable of generating a few tens of ZP stripes, the number of which is independent of the ratio of the plasma frequency to the gyrofrequency in the source.

In practically all models the discussion deals with regular ZP. Problems appear with the interpretation of the frequently observed uncommon stripes of a ZP. For example, for explaining the so-called “tadpoles” (submerged in a developed ZP) special mechanisms were elaborated (Zheleznykov and Zlotnik, 1975a; Chernov, 2006). Rare attempts were made to explain other uncommon forms of ZPs (in the form of zigzags, complex splittings of stripes into the superfine structure). They cause big problems for the known models.

It is important to note that the model with the whistlers successfully explains the zigzags of stripes and their splitting, and also the variations in the frequency drift of stripes synchronously with the spatial drift of the sources of radio emission (Chernov, 2006). Since each new phenomenon provides its uncommon parameters

of fine structure, and the entire variety of the parameters does not succeed in the statistical systematizing, below primary attention is given to the analysis of separate phenomena. Just such a situation stimulates many authors to elaborate on new mechanisms.

In the present book, an attempt is made to evaluate what model most adequately describes the new observational data and to find out where the ZP stripes form (during the excitation of waves in the source or in the course of their further propagation). Calculations show that the DPR-based mechanism fails to describe the generation of a large number of ZP stripes in any coronal plasma model. Some other unsolved problems or difficulties in the DPR model are also examined in detail.

Here, it is shown that the new varieties of ZP succeed in explaining these phenomena within the framework of known mechanisms by taking into account the special features of plasma parameters and fast particles in the source. On the other hand, the formation of ZP stripes due to radio wave propagation through the coronal heterogeneities can be recognized as the most natural mechanism of ZP. The mechanism related to the excitation of discrete eigenmodes of the periodically nonuniform plasma (Laptukhov and Chernov, 2006, 2009) can yield the observed number of harmonics. However, in this case, only the possibility of generating harmonics in a one-dimensional stationary problem is considered, i.e., the frequency dynamics of stripes is not analyzed.

During the last several years some new varieties of ZP have been recorded. Now, it is necessary to estimate the possibility of their interpretation by taking into account all known models of ZPs.

Chapter 2

Pulsations

2.1 Overview of oscillation phenomena

For over more than four decades radio astronomers have been observing pulsating structures in the solar radio emission. 'Pulsations' include a wide range of phenomena of quasi-periodic patterns or fine structures observed in the metric/decimetric/ microwave frequency ranges. At the early stage they attracted the attention of solar radio astronomers by oscillating shapes of the time profiles of radio bursts. With the development of spectral observations it became clear that the pulsations occur almost simultaneously over a wide frequency range. They were described as series of fast drift bursts.

Slottje (1981) was the first who summarized the observational properties of the pulsations (see also Krüger (1979). High resolution observations revealed that some pulsations consists of series of broad-band short-lived absorption pulses. Here, "absorption" does not mean the physical process. On the contrary, sometimes such pulsations were more likely the result of interruption of the emission process. Kuijpers (1975a) as well as Zaitsev & Stepanov (1975) and Benz & Kuijpers (1976) preferred, in view of their interpretation, the name "sudden reductions" of intensity.

All the available results and reports of observations show that pulsations appear at a wide range of the periods (from several minutes to sub-seconds) and emission frequencies, from meter (Rosenberg, 1970; McLean & Sheridan, 1973; Trottet et al., 1981), decimeter (Gotwols, 1972; Bernold, 1980), and to centimeter waves (Fu et al. 1990; Qin & Huang, 1994), among others.

Aschwanden (1987; 2004b) presented an extensive review of all kinds of models for the pulsating events, and classified them into three groups: (1) MHD flux tube oscillations, which modulate the radio emissivity with a standing or propagating MHD wave (slow-mode magneto-acoustic oscillation, fast kink mode, fast sausage mode); (2) periodic selforganizing systems of plasma instabilities (wave-particle, wave-wave interactions); and (3) modulation of acceleration (repetitive injection of particles into a loss-cone configuration). The third type may explain the shortest periods (< 1s), and it can include nonstationary magnetic reconnection.

Pulsations are rarely observed in pure form. Usually, they are superimposed on other elements of the fine structure: spikes, fiber bursts, zebra patterns.

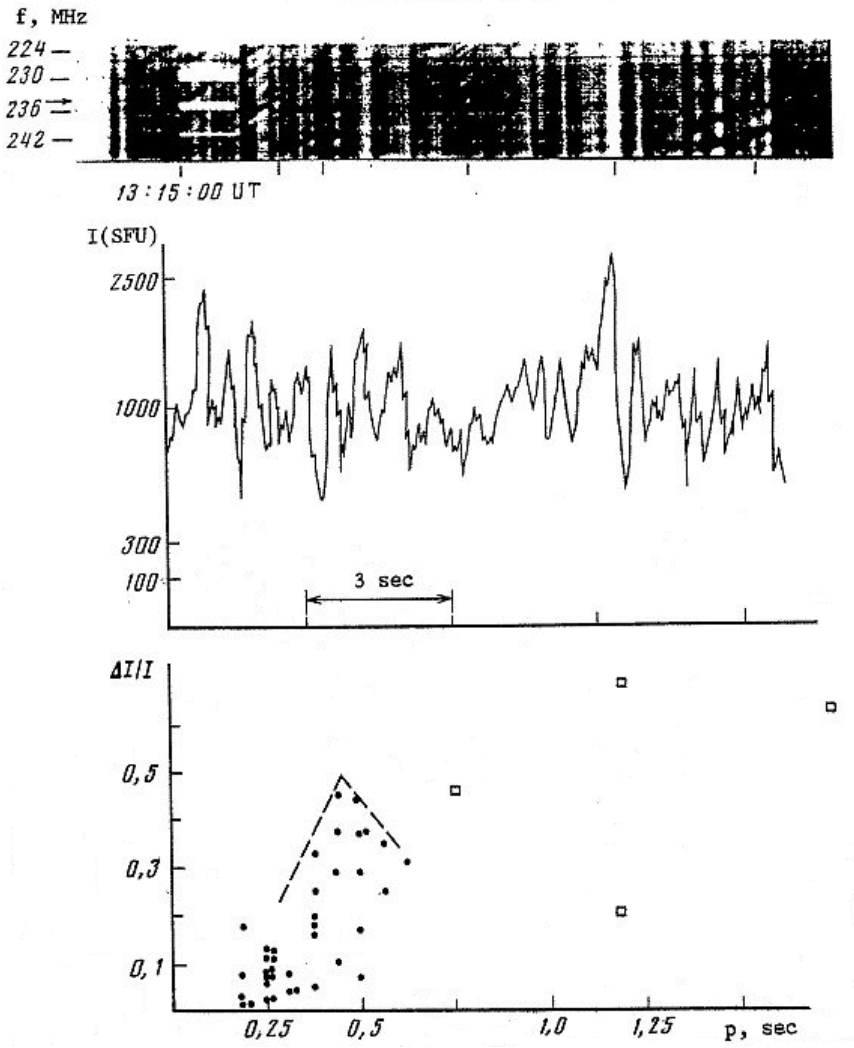

Fig. 2.1**.** Fast pulsations in emission and absorption superimposed onto fiber bursts in a prolonged type IV burst 5 February 1986. At the top is dynamic spectrum in the 224-245 MHz range (IZMIRAN); in the middle is the time profile of the radio emission flux (1 sfu = 10^{-22} W m^{-2} Hz^{-1}) at 234 MHz (Potsdam) and in the bottom is the distribution of the modulation depth of the radio emission, $\Delta I/I = (I_{max} - I_{min})/(I_{max} + I_{min})$, as a function of the pulsation period p (s). Dots denote single pulsations, the empty small squares are complex long-period oscillations (Chernov & Kurths, 1990).

As such a complex example in Figure 2.1 the subsecond pulsations in a prolonged type IV burst of 5 February 1986 are shown. The pulsations in emission alternate with sudden reductions with a nonrigourous period of 0.2 – 0.8 s and both are superimposed onto fiber bursts. The time profile in Figure 2.1 shows a large modulation depth of the intensity I in the fast pulsations, $\Delta I/I \simeq 0.6$, and the dependence of $\Delta I/I$ on the period p reveals a maximum with the value of $p \simeq 0.5$ s. The statistical analysis of the modulation depth executed in Chernov & Kurths (1990) with five other events with fast pulsations in the meter range showed a similar behaviour of these parameters. Therefore, in order to understand the nature of such fast pulsations, let us briefly examine the possibilities of different models.

2.2 Brief characteristics of pulsation models

The plasma model of radio pulsations in the context of beam instability is based on nonlinear wave scattering into the nonresonant range of the wave spectrum, in which they are damped by collisions and are converted into electromagnetic radiation (Zaitsev et al. 1985; Aschwanden, 1987). It should yield a strict period $p \simeq 2\pi / \nu_{ei}$ (ν_{ei} is the frequency of electron-ion collisions), but it can operate efficiently only for protons (Zaitsev et al. 1984).

Oscillations of loss-cone instability are determined by quasilinear effects of damping of plasma waves on fast particles that are precipitating into the loss-cone. The main properties of the plasma model of pulsations near the excitation threshold ($\gamma \geq \gamma_{ei}$) for loss-cone instability are an increase in the modulation depth and a decrease in the intensity of the pulsations with an increase of their period. The strongest pulsations should have should have the shortest period (Zaitsev et al. 1985), which may be of millisecond value ($p \sim 1/\gamma$). But since the growth rate γ is proportional to the density of fast particles and the plasma frequency

$$\gamma \sim \frac{n_h}{n_c} \omega_{Pe},$$

a pronounced modulation may be expected only in the interior of the corona, such as in flare loops, in which $\omega_{Pe} \sim 10^{10}$ s^{-1} and $n_h / n_c \geq 10^{-5}$. Their most likely application has therefore been in terms of microwave millisecond (spike) oscillations (Zaitsev et al. 1985).

Relaxation oscillations of beam instability on electrons must be maintained by a periodic source of fast electrons and must have a low quality factor (Q, a small number of pulsations per series).

MHD models of pulsations are based on modulation of the plasma density in a magnetic trap, mainly by fast magnetosonic (FMS) waves excited by protons in Cherenkov or bounce resonance. Their period is determined only by the size of the trap and therefore it cannot be very short. Under conditions of bounce resonance, for example, $p = R/V_A = l/V$, where R and l are the radius and length of the trap, V is the velocity of the fast particles, and V_A is the Alfvén velocity, $V_A \cong (c/43)(f_{He}/f_{Pe})$ (f_{He} and f_{Pe} are the cyclotron and plasma frequencies of electrons), for a preiod $p = 0.05$ s we must assume the magnetic arch high in the corona with the improbably small dimensions, $R \approx 10^6$ cm and $l \approx 5 \cdot 10^8$ cm ($V_A \approx 3.5 \cdot 10^7$ cm for $f_{He}/f_{Pe} \approx 1/20$ and $V = 10^{10}$ cm s^{-1}).

MHD oscillation modes propagating in dense traps may yield the typical variation of the one-second periods and the modulation depth, including three phases: i) a periodic phase associated with the arrival from the flare region of a low-frequency disturbance with a maximum group velocity; ii) a quasiperiodic phase with increasing modulation due to the interaction of the first disturbance and subsequent higher-frequency disturbance which arrives at the same level in the corona with the minimum group velocity; iii) and a decay phase (Roberts et al. 1984; Aschwanden, 1987; 2004).

MHD pulsations are determined by weak oscillations of the magnetic field in a FMS wave, $\Delta B << B_0$ (B_0 is undisturbed field), so they must shallow modulation $\Delta I / I \approx \Delta B / B_0$ (Rosenrauh and Stepanov, 1986).

Zaitsev et al. (1984) shown that the duration of pulse train (with the period of several seconds) in type IV radio bursts decreases with increasing hardness of the spectrum of high-energy protons and increases with decreasing proton flux from the Sun (in the Earth's orbit). Such a correlation (shown in Figure 2.2.) corresponds to a MHD model of pulsations and inexplicable within the framework of a nonlinear periodical regime of plasma instabilities.

In this case the oscillation period is determined only by the parameters of the trap and is independent of the density and spectrum of trapped particles. The duration of a pulsating structure is determined by the trapping time of the energetic protons sustaining MHD oscillations of the source (FMS waves). As the result of diffusion by small-scale Alfvén waves, the characteristic time required for the protons to escape the trap decreases with increasing density and hardness of the protons, which is essentially in agreement with observational data (Zaitsev et al. 1984).

The physical coupling of the pulsations and the energetic protons is as follow. The electrons and protons produced during the flare are partially trapped in a coronal magnetic trap (loop) with an enhanced plasma density, the loop being a source of type IV radio emission as well as a resonator for the fast mode MHD wave. The energetic electrons are rather rapidly (over approximately a few seconds) released from the trap, after which their density within the trap is maintained at a comparatively low level, providing only the intensity required for type IV radio emission. The residence time of >10 MeV protons in the trap is substantially

longer, and they excite and sustain MHD oscillations at the source, thus determining the duration of pulsating structures.

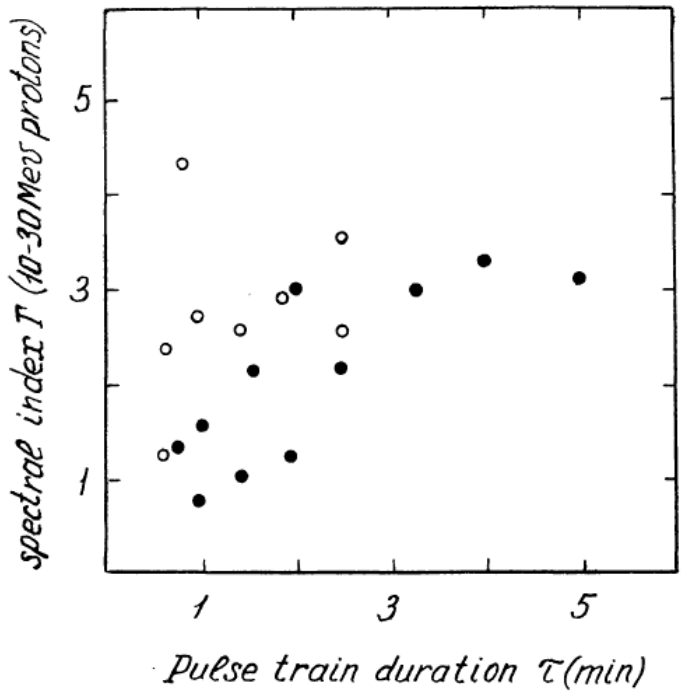

Fig. 2.2 The variation of integral spectral index (Γ) in the 10 – 30 MeV range versus pulse train duration (τ , min). The filled circles indicate 11 western flares, the open circles 8 eastern flares (Zaitsev et al. 1984).

The protons trapped in the magnetic loop can, moreover, make a substantial contribution to the cosmic ray flux near the Earth as well. At times less the diffusion time, such protons drift with the speed $\upsilon_D \approx \upsilon^2 / \omega_i R \approx 10^6$ cm s^{-1} (ω_i is the proton gyrofrequency, *R* is the radius of loop) toward the open magnetic field lines and escape into interplanetary space. Therefore, the pulsations of type IV radio emission are predictors of the appearance of protons in the vicinity of the Earth.

Sudden reductions (SRs) represent a special class of pulsations which are often superimposed onto sub-second pulsations in emission and complicate the picture. They are caused by a quench of loss-cone instability of plasma waves upon the injection of new particles into the loss-cone (Zaitsev & Stepanov, 1975; Benz & Kuijpers, 1976). They have the nature of deep troughs of radio intensity, so in an

analysis of the modulation depth they must be separated from pulsations in emission, although this is difficult to do on a dynamic spectrum, since SRs, like MHD pulsations , have a one-second scale.

Oscillations of loss-cone instability of plasma waves at the boundary between weak and strong diffusion of fast electrons on whistlers, including the quench of instability during the injection of new particles into the loss-cone (Trottet et al. 1981) or the model of torsional oscillations of a magnetic flux tube (Tapping, 1983) may apply only to pulsations with a long period (>> 1 s).

Thus, the known models of pulsations do not enable us to explain millisecond pulsations with deep modulation of radio emission. In this connection Chernov (1989) proposed the mechanism of coalescence of plasma waves with whistler waves in which the whistler spectrum is determined by the pulsating regime of their interaction with ion-sound waves.

Model with whistler waves. In the pulsed regime of energy transfer between whistlers (w) and ion-sound waves (s) the combining mechanism of radio emission (t) due to the coalescence of whistlers with plasma waves (l) $l + w \rightarrow t$ yields pulses of radio emission in a wide frequency range at times of maximum of whistler energy (W^w). As a result of decay processes, a flat spectrum of whistlers W^w = Const (with respect to frequency and angle) is established, so the absorption bands typical for fiber bursts and zebra pattern will be washed out, and we should observe brief wideband pulses with a period of ~ 0.01 – 1 s that depends on W^w.

The main process resulting fast pulsations is associated with the pulsating regime of coalescence and decay of s- waves with whistlers: $s + s' \leftrightarrow w$. From experiments it is well known that this process proceeds at both the sum and difference frequencies. The maximum increment of s- waves falls at frequencies close to the ion plasma frequency ω_{Pi} . In the solar corona at the altitudes of meter and decimeter ranges, the approximate equality $\omega_{Pi} \approx \omega_{Be}/4$ is satisfied, which favors the realization of conservation laws for processes $s + s' \leftrightarrow w$ at the difference frequency and the maximum increment (Chernov, 1989). Such a condition is not satisfied in the Earth's magnetosphere.

A second necessary condition for satisfying the conservation laws for this pulsating process is isotropization of the wave vectors k^s and k^w , since the process proceeds for two oppositely directed vectors k^s and $k^{s'}$ and the vector k^w directed at an angle $\vartheta^w > 70^o$ (Tsytovich, 1977). In this case, the slowest process (determining the pulsation period) is scattering of whistlers on thermal electrons. For the usual whistler energy density (relative to thermal energy of the background plasma) $W^w/nT \approx 10^{-7}$, this scattering time is ~ 0.3 – 0.2 s.

The merging process of plasma wave with whistlers $l + w \rightarrow t$ is very fast (about 10^{-3} s), so the duration of one pulsation actually will not exceed the collisional damping time $\nu_{ei}^{-1} \approx 10^{-2}$ s.

The source of such pulsations may be located in a region of reconnection (of high coronal loops) with a vertical size ~ (2 –5) 10^9 cm , for instance, between magnetic islands after a flare. Such a region must contain a neutral magnetic point of the X type with diverging shock fronts, between which the nonisothermicity develops ($T_e >> T_i$) and ion-sound waves are excited. Even in an initially isothermal plasma in the reconnection region, the ion-sound waves are excited by Cherenkov mechanism with a large increment due to the electron drift relative to ions V_d in the current sheet. The ion-sound instability changes smoothly into Buneman instability for $V_d > V_{Te}$ (the thermal velocity of electrons), maintaining the nonisothermicity in the reconnection region (Kaplan & Tsytovich, 1973). The heating occurs simultaneously over a wide altitude range between shock wave fronts. The conservation laws for the processes $s + s' \leftrightarrow w$ and $l + w \rightarrow t$ can be satisfied simultaneously over entire reconnection region only after the spectra of s- and w-waves become isotropic due to scattering.

All these nonlinear processes are accelerated with increase in W^s and W^w and if $p > \nu_{ei}^{-1}$, then the period will decrease with increasing of W^w (i.e. with increasing pulse intensity and modulation depth), regardless of the level W^l of the plasma waves (i.e. the continuum level). For high levels of W^w, when $p < \nu_{ei}^{-1}$, the pulse modulation depth $\Delta I / I$ will decrease sharply with decreasing period due to the coalescence of individual pulses, when the intermittence disappears. Therefore, the dependence of $\Delta I / I$ on period p should typically have a maximum at $p = \nu_{ei}^{-1}$.

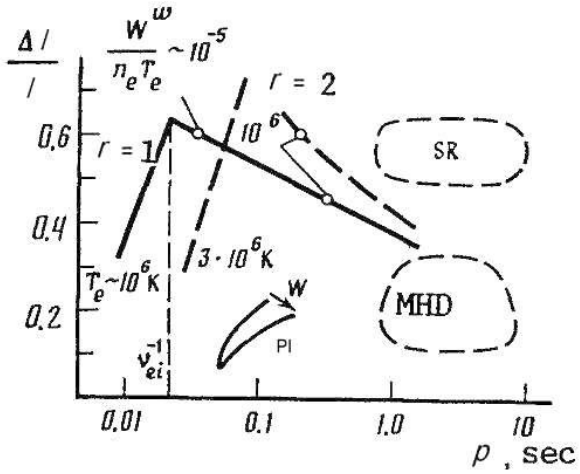

Fig. 2.3. Calculation of the modulation depth $\Delta I / I$ of radio emission as a function of the pulse period p in the model based on whistlers whose level is maintained by ion-sound turbulence. (Chernov, 1989).

Figure 2.3 shows the modulation depth as a function of period calculated for several values of W^w, temperature $T_e = 10^6$ and $3 \cdot 10^6$, $f_{Pe}/f_{Be} = 30$ and two values of the parameter r – the ration of rates of rise of the radio emission in two processes, $l + w \rightarrow t$ and $l + i \rightarrow t$. The approximate domains of the pulse parameters in the models of MHD oscillations, plasma oscillations of loss-cone instability (Pl) and sudden reductions (SR) are also shown qualitatively. The presence of a maximum in the dependence of $\Delta I / I$ on p at the value $p = \nu_{ei}^{-1}$ is the main indicator for the model with whistlers. The number of electron-ion collisions decreases with increasing T_e approximately as $\sim T_e^{-3/2}$, so a shift in the maximum with time provides information about the variation of T_e in the source. The amplitude of the pulses increases sharply with increasing r. Then strong pulses should be observed even against a weak continuum emission. The sharp maximum may be smoothed out if W^w does not exceed $10^{-6}\ n_e T_e$. If a fiber burst is superposed on the pulses, then the modulation depth should increase due to the contribution of low-frequency absorption.

The nonlinear oscillatory regime of loss-cone instability discussed in Zaitsev et al.(1985) for microwave pulses, can also yield pulses in the meter-wave range. The period of such plasma oscillations, $p \approx 2\pi / \nu_{ei}$, increases with increasing modulation depth and intensity.

Pulses in the model of MHD oscillations of coronal traps with FMS waves in bounce resonance have relatively long period ($\gtrsim$ 1 s), determined only by the size of magnetic trap, and a small modulation depth, proportional to the magnetic field oscillation in the FMS wave, $\Delta I / I \approx \Delta B / B$, ($\Delta B << B$).

Thus, in this mechanism of pulsations with whistlers, the modulation depth may be considerably higher than in other models, and its dependence on the period is characterized by a nearly linear increase with increasing period (with different slopes, determined by the energy level of whistlers and ion-sound waves and by the degree to which T_e exceeds T_i) up to some maximum value at a period $p \propto \nu_{ei}^{-1}$.

In Figure 2.1 fiber bursts and SRs are superimposed onto pulsations, and since they have absorption features, the modulation depth would be increased, which we do observe and a "tail" distribution is associated with these additional structure. Here, we see clear characteristic shape in the distribution with a maximum at $p \approx$ 0.45 s, which indicates the value of $T_e \approx$ (7-8) $\cdot 10^6$ K.

The statistical analysis carried out by Chernov & Kurths (1990) revealed a similar dependence $\Delta I / I$ (p) in numerous series of the fast pulsations observed in five other radio bursts. One of the most interesting events was a small type IV bursts on 13 July 1982 shown in Figure 2.4. Following a strong group of type III bursts clearly defined pulsations in emission simultaneously with SR and fibers bursts in absorption were observed for about 10 min. The $\Delta I / I$ (p) distribution for six selected fragments display a similar form with maxima at p $\approx$ 0.4 – 0.5 s.

The slope of this distribution becomes stepper with time and a small decrease is noted in the modulation depth, which indicate (in accordance with the model of pulsations with whistlers) a gradual equalization of temperatures and a decrease in the whistler energy in the source. This event can be related with a magnetic reconnection high in the corona, since the start of the corresponding microwave burst was delayed by about 1 min relative to the meter bursts. The type III bursts (that immediately preceded the pulsations) were probably produced by fast electrons accelerated in a pulsed mode in the current sheet.

The mechanism of millisecond pulsations with whistlers is attractive in that it does not require a pulsing source of fast particles or a pulsing disturbance that propagates from the flare region.

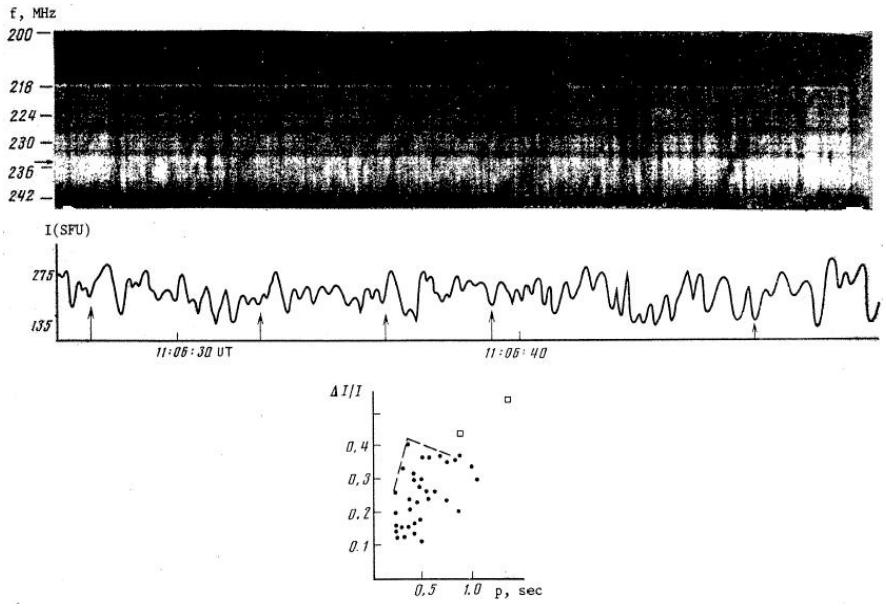

Fig. 2.4**.** Pulsation in emission and absorption and fiber bursts in absorption in brief type IV bursts on 13 July 1982. All the notations are analogous to that in Fig. 2.1 (Chernov & Kurths, 1990).

.

2.3 Microwave pulsations

2.3.1 New observations

The microwave emission region is very close to the flaring region, therefore their periodic pulsations must carry important information about the physical conditions in flaring energy-releasing regions (Fu et al. 1990; Qin & Huang, 1994). There is a series of new good observational data in the frequency range of 2.60 – 3.80 GHz taken with a Solar Broadband Radio Spectrometers (SBRS, Huairou, NAOC) (Fu et al. 2004; Tan et al. 2007). The frequency resolution of SBRS is 10 MHz, and the cadence is 8 ms in the frequency range 2.6 – 3.8 GHz. This provides us with a good opportunity to study the temporal behavior of the microwave quasi-periodic pulsations.

Figure 2.5 shows three typical examples of the pulsating phenomena (in right polarization) in big event on 13 December 2006 observed equally with other kinds of fine structures: fiber bursts, zebra patterns, spikes (in emission and absorption).

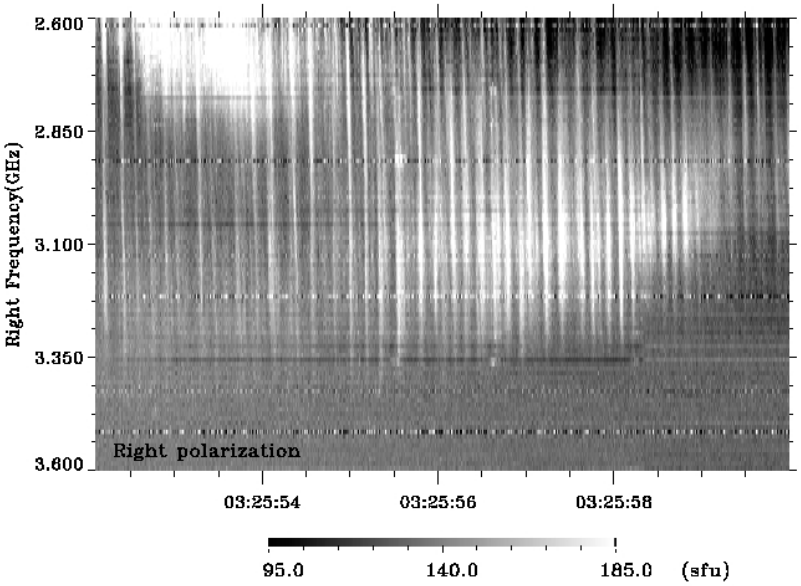
2.600
2.850
3.100
3.350
3.600
Right Frequency(GHz)
Right polarization
03:25:54
03:25:56
03:25:58
95.0
140.0
185.0
(sfu)

a

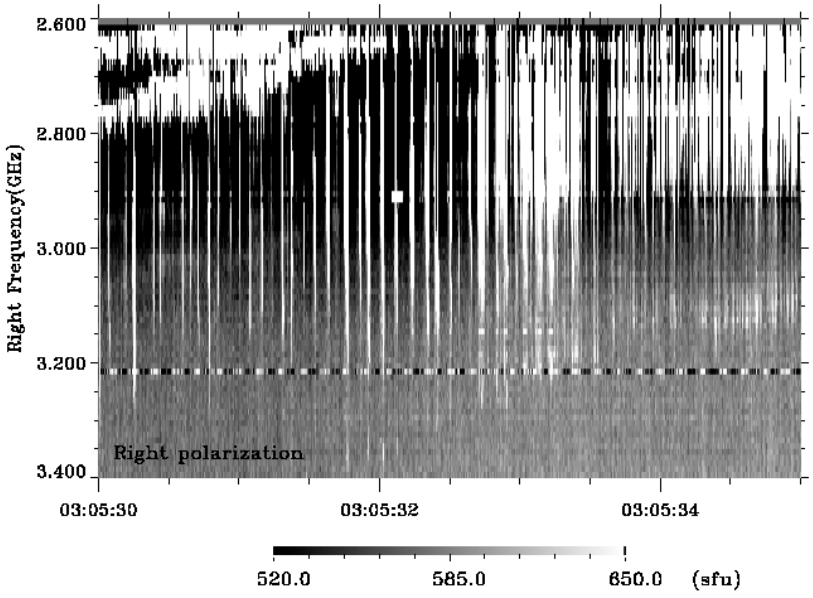
2.600
2.800
3.000
3.200
3.400
Right Frequency(GHz)
Right polarization
03:05:30
03:05:32
03:05:34
520.0
585.0
650.0
(sfu)

b

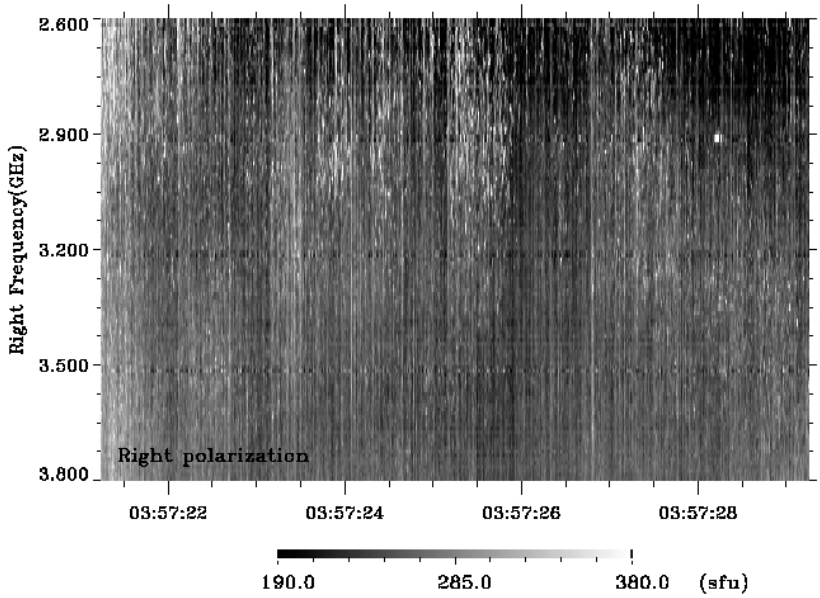

c

Fig. 2.5. The pulsations structures in the long-lasting event on 13 December 2006. The panel a) shows an fragment that occurred during 03:25:52.0 - 03:25:59.0 UT, after the peak of the flare. The panel b) shows an fragment that occurred during 03:05:30.0 – 03:05:32.7 UT, just after the peak of the flare. The panel c) shows snowflake-like spikes distributed along the vertical lines of the microwave pulsations during 03:57:21 – 03:57:29 UT, quite a bit after the peak of the flare (SBRS/Huairou) (adapted from Tan et al. 2007).

Tan et al. (2007) carried out the statistical analysis of pulsations in this event. There are more than 40 cases of pulsations with periods of <1.0 s. They were observed at rising phase of the flare as well as at peak and post maximum phases. The mean pulsation duration was about 10 – 13.0 s. About 75% of pulsations events (31 in 41) had the period of p <100 ms.

2.3.2 Theoretical models

It is still an open question as to which pulsating mechanisms are relevant for the interpretation of the observing features, and how the proposed model works in detail, especially for the very short period pulsations.

Models known earlier usually dealt with the considerably larger periods of microwave pulsations. There is much evidence showing the existence of the electric

current system in the flaring region. The disturbances of the current system produced by some beams of fast electrons propagating in the magnetic tube will lead to dynamic processes, which in turn will stimulate radiation of the system in X-rays and microwaves, which appeared in additional to the beam-generated radio bursts. By this process, a pulsating regime can be triggered with the global sausage mode (Nakariakov 2007); its period is in the range from several seconds to several tens of seconds.

As the pulsations may indicate the existence of the longitudinal electric current in the solar plasma loops, Zaitsev et al. (1998) provided another model of an LRC circuit analog of current-carrying magnetic loop to diagnose the electric current in the solar plasma loops.

Kliem et al. (2000) proposed another model in which the radio pulsations are caused by quasi-periodic particle acceleration episodes that result from a highly dynamic regime of magnetic reconnection in an extended large scale current sheet above the soft X-ray flare loop. They think that radio pulsation is a signature of dynamic magnetic reconnection, and that the reconnection is dominated by repeated formation and subsequent coalescence of magnetic islands, known as secondary tearing modes. With this model, Kliem et al. may explain the pulsations with periods of 0.5 – 5 s.

However, up to now we have not had a good model for accurately interpreting fast pulsating events with a very short period (VSP) of several tens of milliseconds at a frequency of microwaves.

Tan et al. (2007) proposed a new model of the tearing-mode oscillation in current-carrying flare loops to explain the very short pulsation period. The flaring region must consist of many current-carrying compact loops. 2. In each current-carrying flare loop, the resistive tearing mode instability will trigger the formation of a series of multiscale magnetic islands (with different poloidal number m). The positions of X-points is between two magnetic islands. Electron accelerations occur in the regions near each X-points, and the energetic electrons are distributed mainly along the X-lines of the magnetic configuration in the current-carrying flare loops. Such an electron acceleration process is a bit similar to the stochastic particle acceleration model. The resistive tearing-mode oscillation will modulate the plasma emission, turning the emission spectrogram into pulsating structures. The evolution of the tearing-mode instability dominates the duration of the pulsating events, and the period of the tearing-mode oscillation governs the period of the pulsating events.

The period of the oscillations mainly depends on several factors:

1. For the total electric current (I), $p \propto 1/I$.
2. For the geometrical parameters of the loop, a and R_0, the loop section radius a is especially sensitive to the period of the pulsations, $p \propto a^2$.
3. For the plasma density ρ , $p \propto \sqrt{\rho}$; here, $\rho \approx Nm_i$.

The calculated values of period are shown in Figure 2.6.

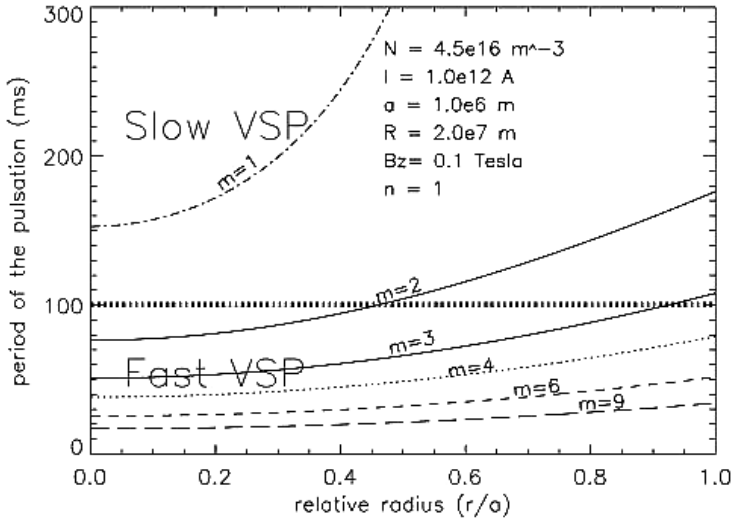

Fig. 2. 6. Pulsation period due to the tearing-mode oscillation with different poloidal mode numbers in the flare loops. The fast VSP is located below the broad dashed line at 100 ms, where the poloidal number is $m > 2$, and the slow VSP is located above the broad dashed line, where $\mathbf{m} < 2$ (courtesy of Tan et al. 2007).

From Figure 2.6 we find that the shorter the period of the oscillation, the greater the poloidal number *m*.

So, the main conclusion is that the pulsations of the microwave emission are the result of the modulation of the resistive tearing mode oscillation in the current-carrying flare loops.

Tan (2008) defined a set of observable parameters of short pulsations and then discussed the possible relations among these observed parameters and their physical implications for the dynamical processes of solar eruptive events, and applied them to interpret the nature of the pulsations.

2.4 Summary

Pulsations in the solar radio emission have been observed during more than four solar cycles. Many theoretical models were developed several decades earlier and described in numerous reviews and several books. However, new spectral observations have shown that all known models do not explain the large modulation depth, and the most developed MHD model cannot explain fast (millisecond) pulsations both in the meter and in microwave ranges. Here, we described, possibly, the unique model of pulsations with the whistlers, which explains the large modulation depth in the fast pulsations (§ 2.2). It is presented

lation depth in the fast pulsations (§ 2.2). It is presented for the meter and decimeter ranges, although, possibly, with the larger probability it can explain millisecond pulsations in the microwave range. However, more contemporary recent developments connect millisecond pulsations in the microwave range with the resistive tearing-mode oscillations in the current-carrying flare loops (§ 2.3.2). In any case, the plasma model does not correspond to radio-pulsations, first of all in the modulation depth of pulsations, possibly, because of a large extent of the source of pulsations in height in the corona, when nonlinear oscillations from different parts of the source become dephased, and pulsations wash off. So, if we obtain microwave spectrograms with high cadence and a high frequency resolution, in addition to radioheliographs with high resolution in space instantaneously, then we can distinguish the detailed electromagnetic structure of the flaring region, and this will help us to understand the physical mechanism of the eruptive processes.

Chapter 3

Spike bursts

Radio bursts of the type "spike" were isolated in a special kind of the most short-time and narrow-band bursts in the meter and decimeter wave bands with the beginning of observation with high resolution by Elgarøy (1961) and independently by Droge & Riemann (1961) and De Groot (1962). There are bursts with a duration of $d_f \lesssim 0.1$ s at one frequency, total duration of $d_0 \approx 0.1 - 0.5$ s, and the total frequency band at the dynamical spectrum of $b_0 \approx 1 - 20$ MHz. Then, the most complete experimental study was executed by Tarnstrom & Philip (1971). The most part of their observations concerns the spikes in the noise storms in three frequency intervals between 135 – 255 MHz. An important result of the statistical study of time profiles of Zimmermann (1971) was the determination of the rise time of the emission to the maximum equal to about 0.05 s.

Spikes are generally agreed to be a non-thermal, coherent emission closely connected with the particle acceleration and energy release in flares, and during the subsequent years the interest to research of spikes increased. In particular, fast bursts were discovered in the decametric range of wavelengths (at some fixed frequencies in the interval of 18 – 26 MHz) (Barrow & Sounders, 1972). Spikes were observed in the microwave range (Droge, 1977; Stahli & Magun, 1986). The basic observed properties of spikes in the meter range are summarized in the short review by Slottje (1981). Benz (1985; 1986) described spikes in the decimeter range at the base of observations with the digital spectrometer IKARUS (Zurich). In five events, clear time and frequency profiles were presented; a good correlation was found with type III bursts and hard X-ray bursts. From the flare configuration a typical upper limit of the dimension of spike sources of 200 km is found. It was proposed that the observed fragmentation in the radio emission should already occur in the exciter due to the fragmentation of the primary energy release (Bastian et al. 1998).

However, the nature of the spikes remained unexplained completely for a long time. Finally, we obtained exhaustive review of all basic mechanisms of the excitation of spikes and their relevance to observed parameters thanks to Fleishman & Melnikov (1998). After a short examination of some variations of the plasma mechanism (Zheleznykov & Zaitsev, 1975; Zaitsev et al. 1985; Melrose, 1991) the authors conclude that none of the modifications of the plasma mechanism can explain the totality of observational data. Being based on the observations of spikes at the harmonic frequencies and the partial registrations of the radio emission of spikes in the extraordinary mode they conclude that the spikes can be excited only by the cyclotron maser mechanism (the loss-cone instability of the 1-st and 2-nd electromagnetic cyclotron harmonics, see also Kuznetsov and Vlasov (2003)).

The electron cyclotron maser mechanism is examined in Fleishman & Melnikov (1998) in detail. Here it does not have sense to present the content of the large review. Let us simply note that the basic objection against this mechanism was based by many authors on the estimations of the absorption of radio emission at the third gyro-resonance level in the corona. Furthermore, this mechanism is effective only in the sources, where the ratio of plasma and cyclotron frequencies is less than unity ($\omega_{Pe}/\omega_{Be} < 1$), while practically all observational data provide evidence of the inverse relationship ($\omega_{Pe}/\omega_{Be} >> 1$), not only in the meter but even in the microwave range. Still, it is important to note that the harmonic relationship of the frequencies (distant from the values 2:1) of the clusters of spikes was observed only in several events in the decimeter range (Benz & Güdel, 1987; Güdel, 1990; Krucker & Benz, 1994). In the majority of events the harmonic relationships was not discovered both in the meter and microwave ranges. Below, we will show the important properties of spikes not taken into account by Fleishman & Melnikov (1998) and will describe an alternative generation mechanism.

3.1 Morphological analysis of spikes in the meter range

The predominant majority of spikes are observed during noise storms, and therefore in describing their properties it is convenient to adhere to the spectral classification used for type I bursts (Elgaroy, 1961; Chernov et al. 1972). The bursts not displaying frequency drift will be classified as the *s* type bursts (stable). Those drifting to lower frequencies, as the *d* type (direct) and those drifting to higher frequencies as the *r* type bursts (reverse). The letter *f* (fast) can be added to the latter two designations if the drift rate exceeds ± 40 MHz s^{-1}. Bursts of type *s* in the form of bright dots (or "sprays" (Kundu, 1965, p.260)) should also be distinguished from the brief wide-band bursts, although both of them are characterized by an instantaneous bandwidth equal to the total bandwidth ($b_t = b_0$). Therefore, spikes in the form of bright dots should be designated by the symbol *ss* (stable sprays), in contrast to the latter.

Spectral observations with high resolution (0.5 MHz, 0.02 s) in the 180 – 230 MHz range performed at IZMIRAN (near Moscow) with simultaneous recording of the circular polarization at 204 MHz gave numerous examples of all types of spikes (Markeev & Chernov, 1970; Chernov, 1977; 1978). Examples of three typical groups of spikes of different spectral types that were observed in a noise storm on 3 September 1973 are shown in Figure 3.1. Recordings of the left- and right-polarized emission components at 204 MHz are presented below the spectra. Regardless of the magnitude and direction of the frequency drift, the emission of all spikes is fully polarized and is observed only in the right polarimeter channel I_R, although the polarization of the continuum emission and of type I bursts sometimes revealed changes. The recording at the fixed frequency 204 MHz gives us

information on the form of the time profiles of the spikes, on the duration d_f and on the emission intensity above the continuum level.

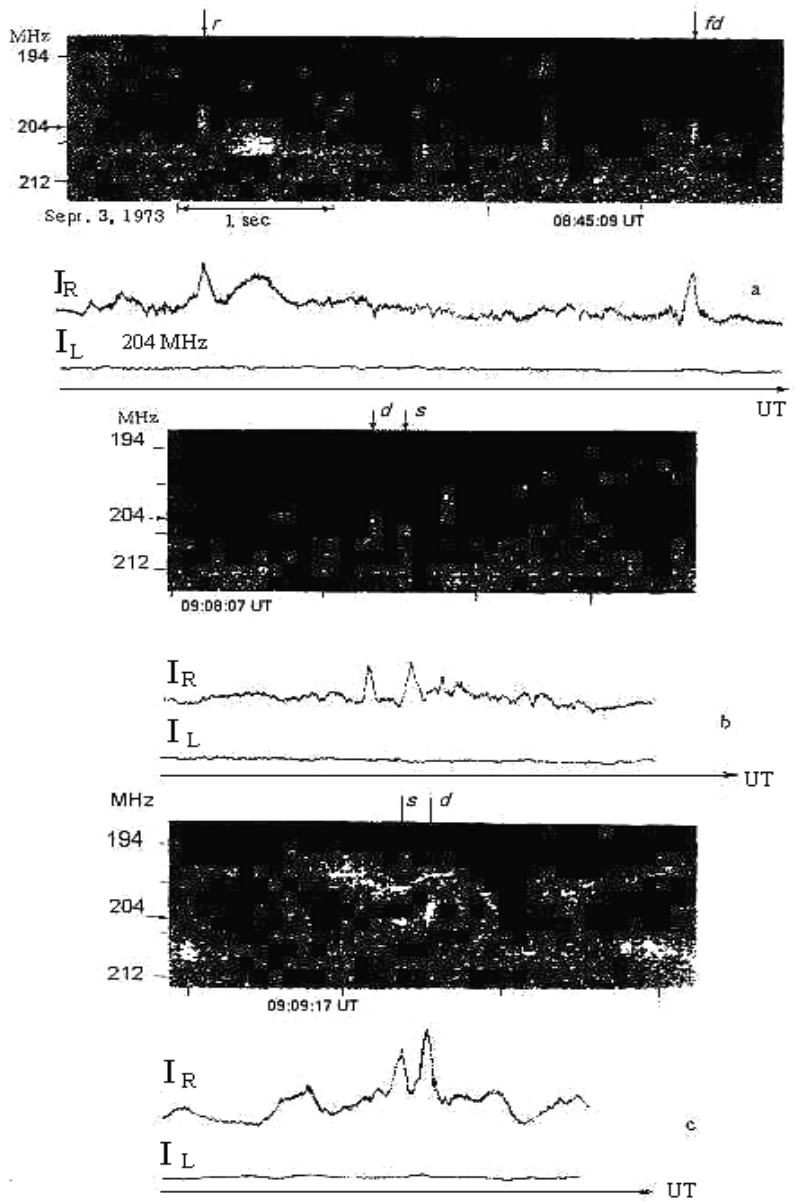

Fig. 3.1 Spectra and polarization profiles of three groups of spikes. I_R and I_L – right and left polarization channels. The continuum level was ~ 50 10^{-22} $Wm^{-2}Hz^{-1}$ and was strongly polarized (~80%R) (Chernov, 1977).

We see that the spikes have different frequency drift even in the same group, and this fact could be easily explained in the plasma model, when small particle beams are accelerated in different directions. Therefore, it is very strange that many authors of different models try explain only short peaks of emission in a narrow frequency band with the relative bandwidth $\Delta f / f \sim 1 - 2\ \%$.

The clusters of spikes are similar to the spark interferences in the dynamic spectrum, although they were always observed during the flares simultaneously with other types of bursts. Therefore since the beginning of the first observations the specific doubts remained in the solar origin of spikes. Simultaneous observations in far distant observatories were necessary for the checking. This checking was realized via the comparison of dynamic spectra of IZMIRAN with the multichannel profiles near the frequency of 169 MHz of the interferometer of Nançay observatory. Such a comparative presentation is shown in the Figure 3.2. We see that spikes of type *ss* in the noise storm on 30 October 1971 coincide exactly in frequency (at 169 MHz) and in time, which indicates the solar origin of the bursts.

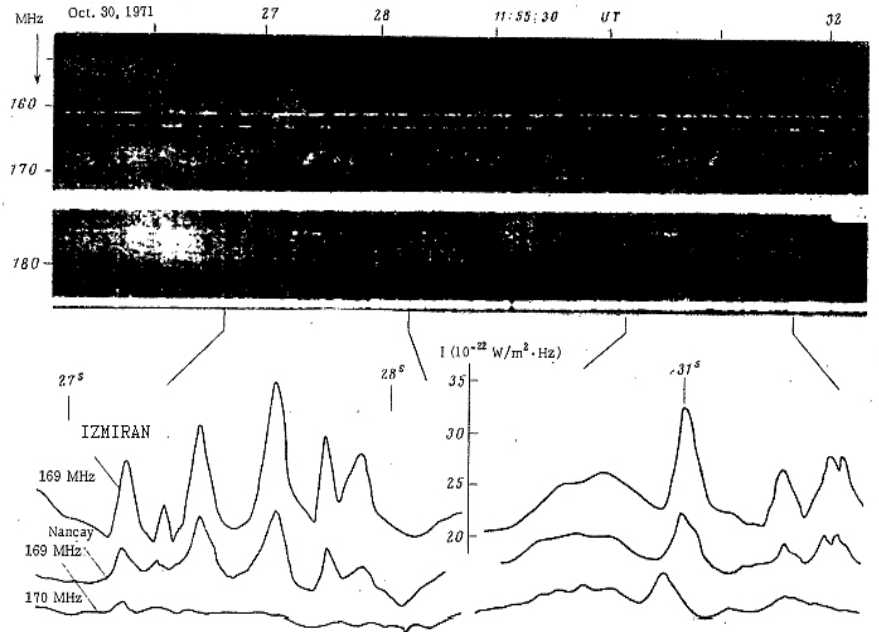

Fig. 3.2 Spectrum of a group of spikes (*ss* type) and their time profiles at 169 MHz at IZMIRAN and Nançay observatory (France) in the noise storm on 30 October 1971 (Chernov, 1977).

In contrast to type I bursts, spikes display a grater variety of spectra which do not always enter into the classification adopted above. Spectra of unusual spikes are presented in Figures 3.3 and 3.4.

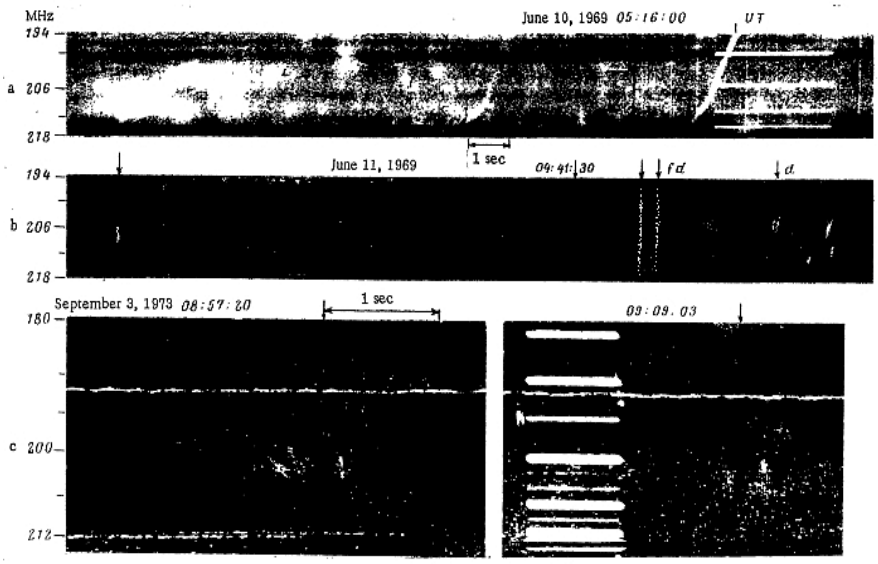

Fig. 3.3 Spikes with unusual spectra: a) wide-range spikes with variable frequency drift; b) spikes forming pairs (a splitting in time); c) spikes displaying a frequency splitting (Chernov, 1977) .

In Figure 3.3a, about 5.5 s before a strong type *d* spike drifted through the entire range (218 – 194 MHz) there appeared two spikes repeating on the time with the second one revealing a halt in frequency drift (a step), after which the drift resumed but now the emission gradually faded. Such an appearance of complex spike – forerunners was repeated three times in a few minutes in a noise storm on 10 June 1969. All spikes were fully polarized with the same sign as strongly polarized continuum emission (Markeev & Chernov, 1970). Several pairs of spikes split in the time and frequency are shown in Figure 3.3b. The microstructural splitting in frequency is shown in Figure 3.3c. The instantaneous bandwidth of each of the split spikes in the first two pairs (on the left) is ~ 0.3 MHz.

A most unusual group of spikes in the form of J bursts is presented in Figure 3.4. In the highest-frequency burst one observes a bend in the initial section toward an increase in the frequency drift. Two reversal points (or two stages of descending branches are observed. The burst developed further at lower frequencies with individual fadings, also lining up in the form of a J burst. The behavior of polarization in this group of spikes was also unusual. The first burst has the higher degree of right circular polarization (~40% at the maximum) while the complex second burst is polarized to an even lower degree (~15%). This group of spikes was observed against a background of low unpolarized continuum. The type I bursts observed in this period were also weakly polarized, with degree of polarization varying from burst to burst. Thus, the unusual polarization of the spikes in

this case reflects the complex nature of the behavior of the polarization in the noise storm.

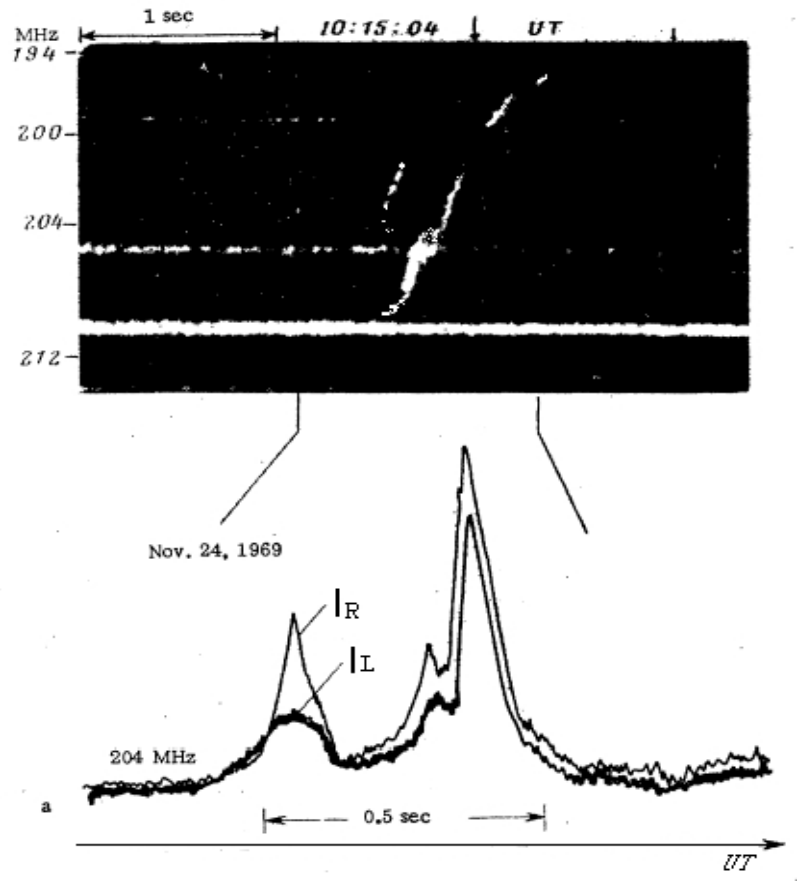

Fig. 3.4 Spectrum and polarization profiles (I_R, I_L) at 204 MHz of a complex group of spikes in the form of J bursts. The emission is weakly polarized (Chernov, 1977).

The characteristic parameters of these spikes were: duration at fixed frequency $d_f \approx 0.1$ s, instantaneous bandwidth $b_t \approx$ 1- 1.5 MHz, bandwidth of occupied frequencies $b_0 \approx 6 - 30$ MHz, and rate of frequency drift $df/dt \approx -20$ MHz s^{-1} (considerably less than for type III bursts).

So, all presented examples of drifting spikes testify in favor of the plasma mechanism when spikes are excited by small particle beams with velocities less than velocities of beams for type III bursts.

The instantaneous bandwidth and the duration of the spikes are considerably smaller than for type I bursts, with intermediate bursts being observed even more

rarely than spikes. The instantaneous bandwidth of a burst depends strongly on the rate of frequency drift, while the total bandwidth of spikes varies within wide limits. Thus, in one storm one may observe spikes of type *ss* having a bandwidth $b_0 \approx 1$ MHz and spikes of type *r* or *d* drifting within a wide band sometimes exceeding 15 – 20 MHz. Therefore, one can actually compare spikes with type I bursts in their duration at a fixed frequency d_f. Distributions of the numbers of spikes with respect to their duration d_f plotted for bursts observed in one storm and in several storms usually differ little and have a maximum near $d_f \approx 0.1$ s. An example of such a distribution for spikes observed on 3 and 4 September 1973 is shown in Figure 3.5. The spike duration was determined from the time profile at 204 MHz as a total time during which the emission was above the continuum level. The distribution was plotted for 97 spikes of different spectral classes. It reflects the general character of the appearance of spikes of different duration: ~ 70% of the bursts have duration $d_f \approx 0.10 – 0.15$ s, for 20% of the bursts $d_f \approx 0.15 – 0.25$ s and rare cases one observes very brief spikes with $d_f \approx 0.05 – 0.07$ s, with the latter including both drifting (*r* and *d*) and stable (*s*) spikes. A similar distribution of spikes was also observed in neighboring frequency ranges (Tarnstrom & Philip, 1971) and in the decimeter range (Elgarøy and Sveen 1973).

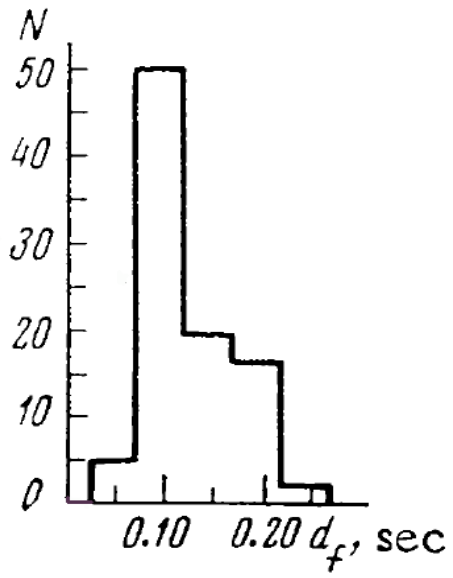

Fig. 3.5 Distribution of numbers of spikes with respect their duration d_f at the fixed frequency 204 MHz for the noise storm on 3 – 4 September 1973 (Chernov, 1977)

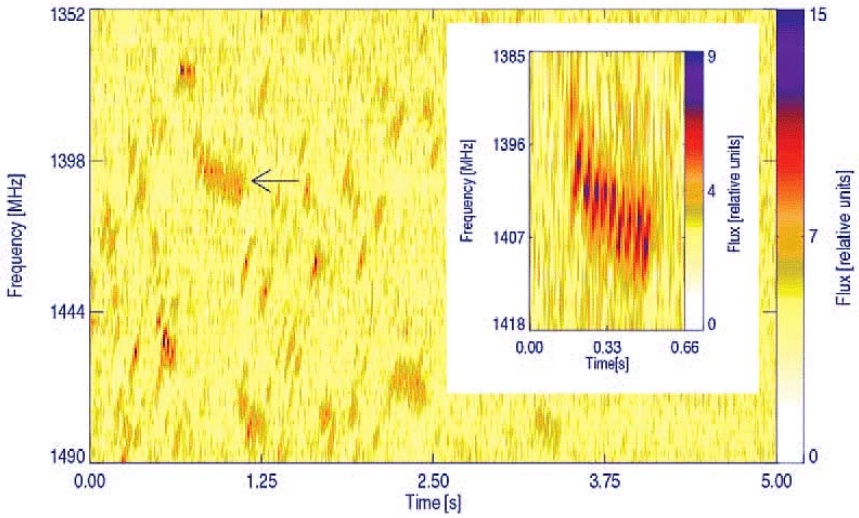

Fig. 3.6 Dynamic spectrum of the radio spikes recorded at the Torun Centre for Astronomy (Poland) on 26 March 2000, beginning at 10:38:00 UT, with time resolution of 80 μs. Some drifting spikes form chains with drift in frequency (Dąbrovsky et al. 2005).

Spikes in the decimeter range have usually very high drifting rate (almost vertical at the dynamic spectrum) (Benz, 1985; 1986). However, Dąbrovsky et al. (2005) discussed several events with drifting spikes (Figure 3.6) with a similarity with the spikes in the meter range. Moreover, some drifting spikes form chains with drift in frequency. Dąbrovsky et al. (2005) single out essentially two different kinds of spike event: one class is composed of spike clusters originating in a post-flare phase and located far away from the main flare location (Benz et al. 2002), and the other is composed of the clusters appeared in the main flare phase and well correlated with other nonthermal flare emission: HXR (Aschwanden & Güdel 1992).

The many years of observations of spikes indicate that they are observed most often in the decimeter range (at frequencies > 300 MHz (Benz, 1986). According to observations with several spectrographs in IZMIRAN, they are observed more rarely at frequencies 180 – 260 MHz, and considerably more rarely at frequencies 90 – 180 MHz. Observations with IZMIRAN's spectrograph in the range 90 – 180 MHz made it possible to verify the appearance of spikes at frequencies forming harmonic ratios, which was predicted by Zheleznyakov & Zaitsev (1975). Later, the appearance of spikes at the harmonic frequencies in the decimeter range was discussed by Benz & Güdel (1987) and by Güdel (1990).

A case of the appearance of spikes at harmonic frequencies in the meter range is shown in Figure 3.7. We can see two groups of spikes at 08:57:19.7 UT (noted by arrows) exactly at the harmonic frequencies 200 and 100 MHz, but the spikes do not repeat the spectral forms and they belong to different spectral types.

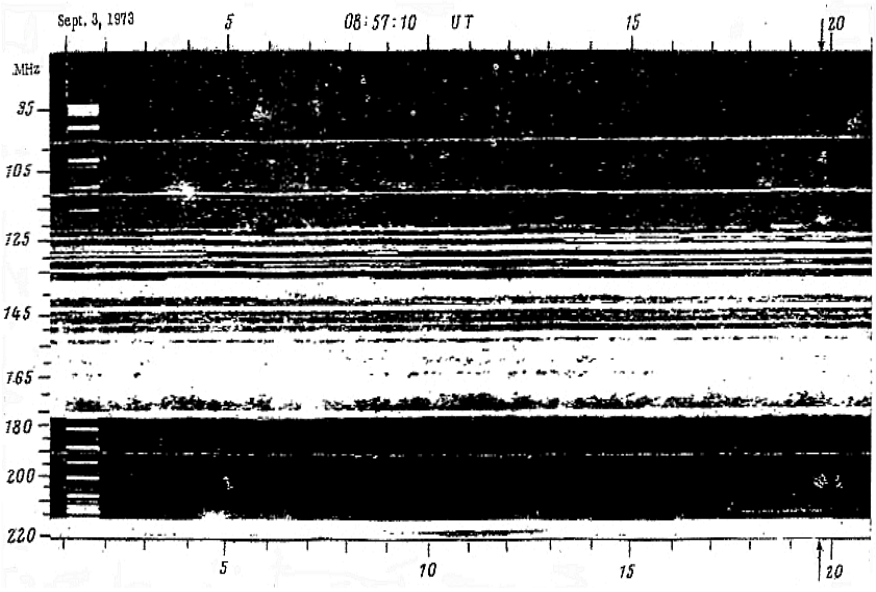

Fig. 3.7 Spikes at harmonic frequencies in the meter range in the noise storm on 3 September 1973 (Chernov, 1977).

At 101 – 102 MHz we see a pair of *ss* type spikes while three type *r* spikes (displaying a microstructure) correspond to them at 202 – 204 MHz. For other spikes (see the interval 05 – 08 s) we do not find corresponding bursts. Such a checking was made for three noise storms, and clear harmonic pairs of spikes at harmonic frequencies were not found.

Spikes are most frequently observed in the noise storms in the composition of complex groups of type I bursts. As a general property of the active regions it can be noted that in all the cases of the appearance of spikes in noise storms the noise centers were not farther than 40° from the central meridian, on the basis of which one can conclude that the emission of spikes is probably more directional than that of type I bursts.

Sometimes a closer relationship between spikes and type I bursts is displayed. In the noise storm on 10 October 1974 several events were observed in which spikes with fast reverse drift (*rf*) were the forerunners of type I bursts (Figure 3.8*a*. The opposite relationship appears in the spectrum *b*: a spike appeared as an after-effect of type I burst, in the form of bright dot at the high-frequency edge of a reverse-drifting type I burst. A fine structure in the form of a drifting type d spike observed against the background of a weaker nondrifting type I burst is shown in Figure 3.8*c*. It should be noted that the fine structure of type I emission was observed rather rarely. An exception was the noise storm on 3 September 1973, when bursts with fine structure followed for several hours, although the storm was

weak. According to the Nançay radio heliograph maps at 169 MHz the noise center was located near the central meridian.

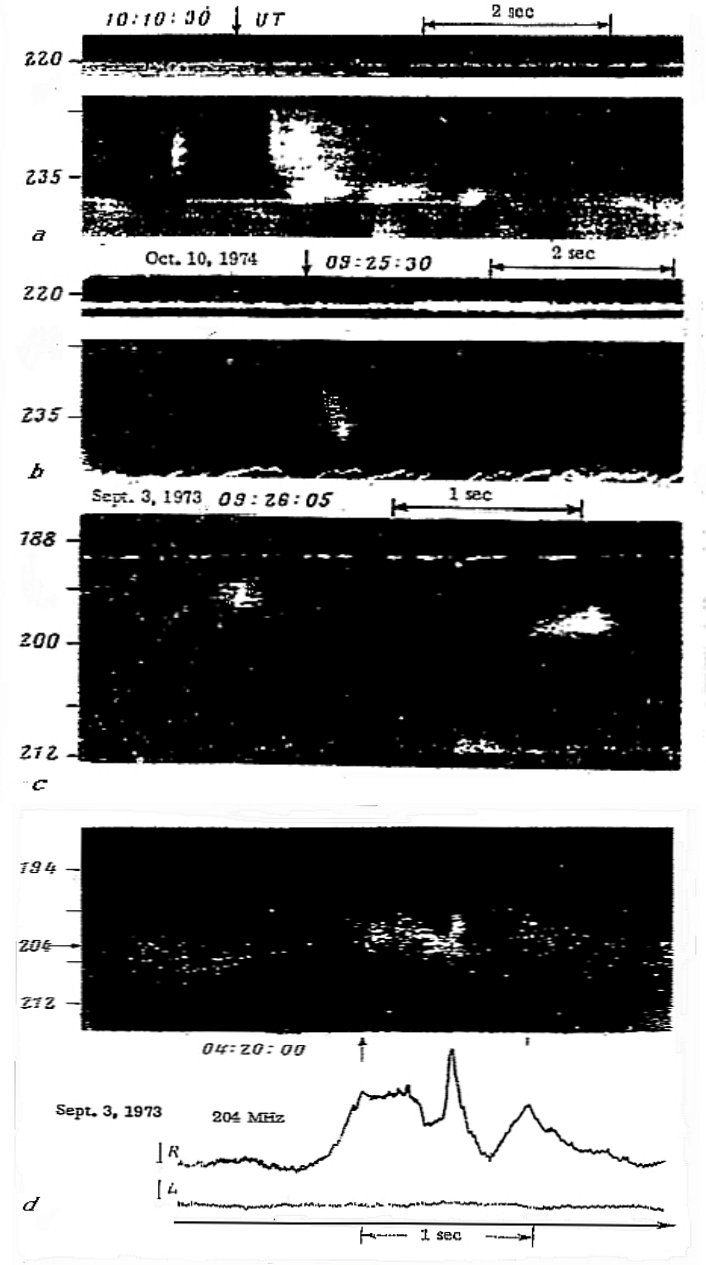

Fig. 3.8 Relationship between spikes and type I bursts (Chernov, 1977).

An example of the best expressed fine structure of the type I burst is shown in Figure 3.8d. The burst really consists of a set of spikes with different frequency drifts. The reality of this microstructure of the type I emission is confirmed by the corresponding fluctuations in the time profiles of the polarization channels at 204 MHz obtained with another receiver. The polarization of these elements has no features: the emission was fully polarized during the entire storm. Not having measurements of the positions of the radio sources with a sufficiently high angular resolution (< 1'), one cannot say with certainty whether the emission of individual elements of the fine structure escapes from one source.

3.1.1 Dimensions of spike radio sources

The absence of the observations of the sizes of the sources of spikes always impoverished studies. Many authors usually use a rough estimate of the source dimension l of a spike by the bandwidth of the spike $\Delta\omega/\omega$ according to the simple formula:

$$l \approx L \ \Delta\omega/\omega \ \lesssim 200 \text{ km} \qquad (3.1)$$

with the magnetic (or plasma) scale length L is about 10000km and $\Delta\omega/\omega$ = 0.02. This is an order of magnitude smaller than the 'speed of light dimension' derived from the duration of spikes at 600 MHz (but compatible if the Alfvén speed is used (Slottje, 1978)). The magnitude, derived from (3.1) is high limit of the dimension, and it agrees with the possible observation of a spike by *VLBI* technique yielding a diameter of approximately 50 km (Tapping 1983). *VLBI* baseline gives a maximum angular resolution on the Sun of 0.07'' corresponding to a spatial scale of 45 km. This spike was observed at the fixed frequency 1663 MHz and it was not accompanied by a dynamic spectrum. In literature, the cases are available, when the authors discuss pulsations (without the dynamic spectrum), whereas a zebra pattern on the spectrum is observed, or spikes are discussed, although the wide-band pulsations are really observed. However, the equating of diameter with the linear dimension l (along the height in the corona) assumes the spherical form of radio source. Actually, taking into account the mechanism of generation, the diameter can considerably exceed l.

In the meter range the angular resolution is much worse. On 19 July 1971 two spikes were observed in IZMIRAN with spectrograph covering the frequency band 151 – 187 MHz and a radiometer at 169 MHz, and in Nançay Station with a multichannel 159 – 179 MHz spectrograph and a 169 MHz radio heliograph. Absolute positions were measured to 1' accuracy, the angular resolution was $\approx$3.4' and the time resolution was 0.05 s. All the data are assembled in Figure 3.9 in a common time scale. Two spikes, each lasting ~ 0.1 s, occurred $\approx$ 0.32 s apart at

12:18:31.7 UT. They covered the 165 – 176 MHz frequency band and showed no frequency drift.

The 151 – 187 MHz spectrograph had a sensitivity of ≈ 5 sfu (1 sfu = 10^{-22} W m^{-2} Hz^{-1}). The spikes were recorded during a noise storm with a weak continuum of ≈ 16 sfu. The storm was associated with the active region situated near the central meridian. Both spikes were weak, reaching an intensity of only ≈ 14 sfu.

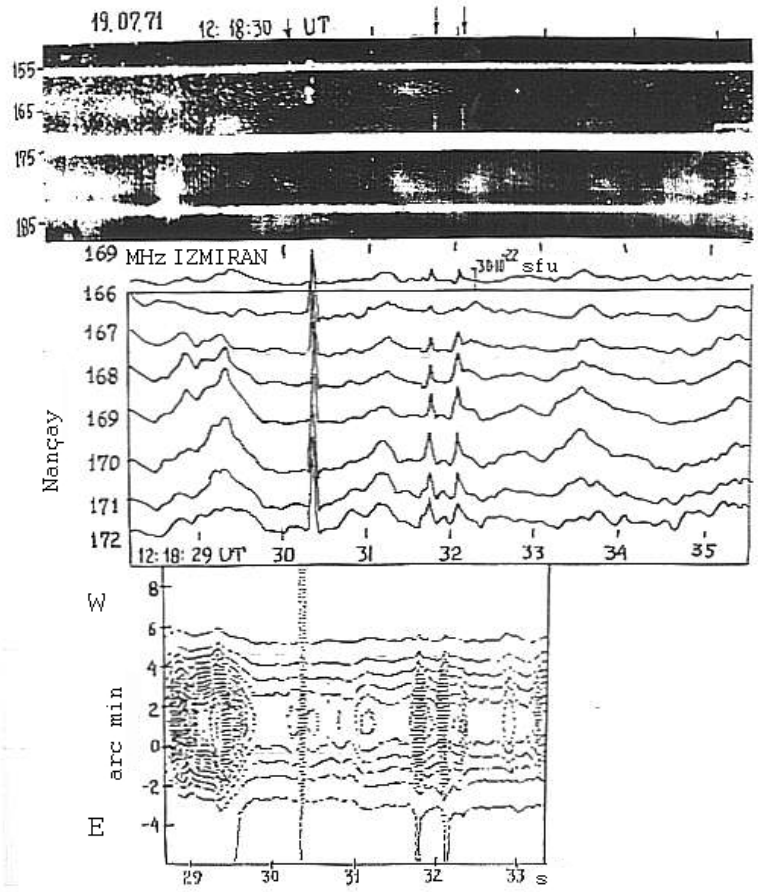

Fig. 3.9 Dynamic spectrum and radiometer profile at 169 MHz recorded on 19 July 1971 at IZMIRAN, compared on the same time scale with multichannel spectrograph and radio heliograph tracing obtained in Nançay. The isophote contour interval is 2 sfu. The pair of arrows at the top marks the spikes (Chernov, 1982).

Since the bursts had coincident time profiles despite the widely separated stations, they were evidently of solar origin. The vertical scale in the bottom panel is

the distance in arc minutes in East – West (E – W) direction from the central meridian (0').

Despite the presence of an interference (vertical features in the isophotes) it is clear that at the instance when spikes occurred, all the isophotes associated with the noise center between 3.5'E and 5.5'W broadened. If we estimate the size of the spike sources from the half-broadening of the noise storm source ($\approx$4') and the instrument resolving power (3.4'), we obtain the value $[(4')^2 - (3.4')^2]^{1/2}$ = 2.1'. If the spike sources were fairly large, comparable in size with the background burst sources ($\approx$ 5' – 10'), then their excitation might have attributable to mechanisms that could briefly involve an entire extended background source. These observations suggest, however, that the spike sources actually are several times smaller in diameter than noise storm sources and even type I burst sources.

The first two-dimensional observations with VLA enabled the visible spike source size (70") at 333 MHz (Krucker et al. 1995). This value will be coordinated with the sizes of spikes at the frequency of 169 MHz given above. The time resolution of VLA is low ($\approx$1.667 s), nevertheless, it was firmly established that the center of mass of sources slightly changed (by 10" – 25") between the main intensity peaks (separated by 2 ± 4 s) on the time profile.

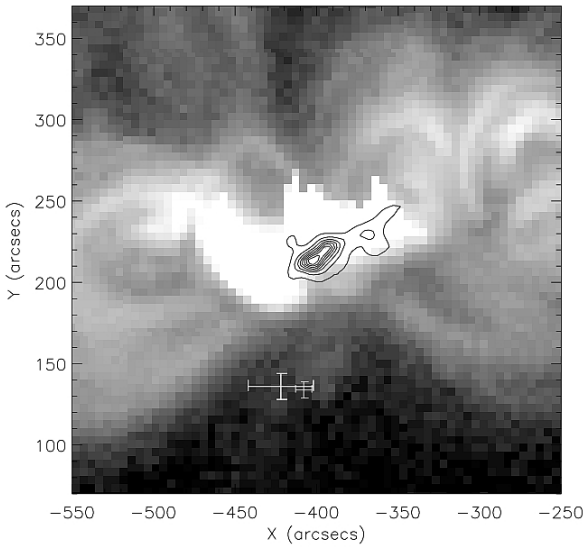

Fig. 3.10 Spike positions in the course of the X1.9 event on 2000/07/12 superposed on an SXT/Yohkoh image (AlMg filter, 5" resolution) taken at 10:21:18 UT. The centroid positions of the spike sources at 432 MHz as observed by the NRH are drawn with error bars representing their scatter in time. Group 2 (large error bars): 10:53:20--10:53:40 UT; group 3 (small error bars): 11:01:00--11:01:10 UT. The hard X-ray intensity at 10:30:40 UT as observed by HXT/Yohkoh (M1 channel) is displayed by isophotes (Benz et al. 2002).

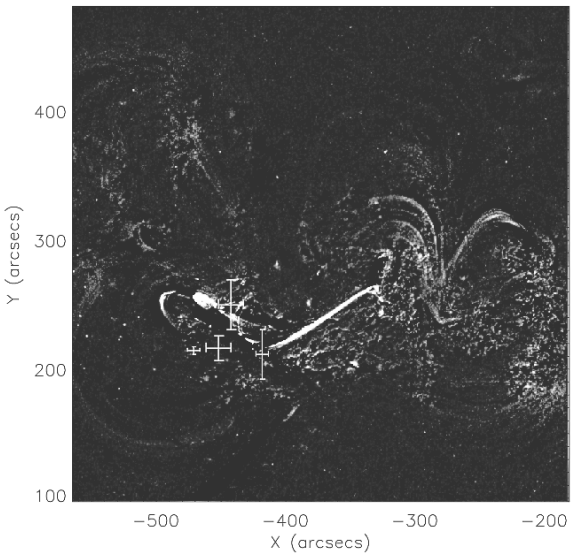

Fig. 3.11 Centroid positions of spikes observed on 2000/07/12 13:38--13:40 UT at 432, 410, 327, and 236 MHz by the NRH (from left to right). They are superimposed on a TRACE image at 195 Å with 1" resolution showing the difference between the image at the end of the spike event and the image just before (Benz et al. 2002).

In the more recent paper of Benz et al. (2002), the spike positions (with the Nan›cay Radioheliograph) have been compared with the location of hard X-ray emission and the thermal flare plasma in soft X-rays and EUV lines. Two examples are presented in Figures 3.10 and 3.11. The decimetric spikes are found to be single sources located some 20" to 400" away from the flare site in hard or soft X-rays. In most cases there is no bright foot-point nearby. In at least two cases the spikes are near loop tops. These observations do not confirm the widely held view that the spike emission is produced by some loss-cone instability near the foot-points of flare loops. On the other hand, the large distance to the flare sites and the fact that these spikes are all observed in the flare decay phase make the analyzed spike sources questionable sites for the main flare electron acceleration. They possibly indicate coronal post-flare acceleration sites.

3.1.2 Relationship of spikes with other bursts

A great variety of spikes was observed simultaneously with type III bursts. A special attention was paid to the appearance of spikes in the high-frequency edge of type III bursts (Tarnstrom & Philip, 1971, Bastian et al. 1998). Long-standing observations in IZMIRAN showed that spikes appeared not only at the moments of the type III emission but also in the intervals between bursts, and in the entire

spectrograph band. One can distinguish two types of spikes connected with type III emission. The first is a series of similar drifting spikes, miniature type III bursts (see e.g. Figure 2 in Chernov (1974a)). Spikes with duration of ~0.1 – 0.15 s were superposed on longer and more intense type III emission and had about the same frequency drift –60 – -80 MHz s^{-1}. But the emission of the spikes was sharply distinguished on the polarization recordings. All the type III bursts had a weak degree of polarization or were unpolarized while the spikes were fully polarized.

The spikes of the second type in the type III emission were not similar to the latter, they occupied a small frequency band, and belonged to different type. But here, they were also strongly polarized. An excellent example of such spikes is shown in Figure 3.12. The spikes interleaved with type I bursts and both drifted from 220 MHz to 190 MHz in one minute. Therefore, it is possible that they are emitted from the different sources.

Spikes were observed in several type II burst. They accompany the main type II emission harmonics in low- or high-frequency edge. Their spectral characteristics are about the same as for spikes in noise storm: the most spikes drift in frequency. But they are, however, unpolarized like the whole type II burst, in contrast with strongly polarized spikes in the noise storms (Chernov et al. 1975).

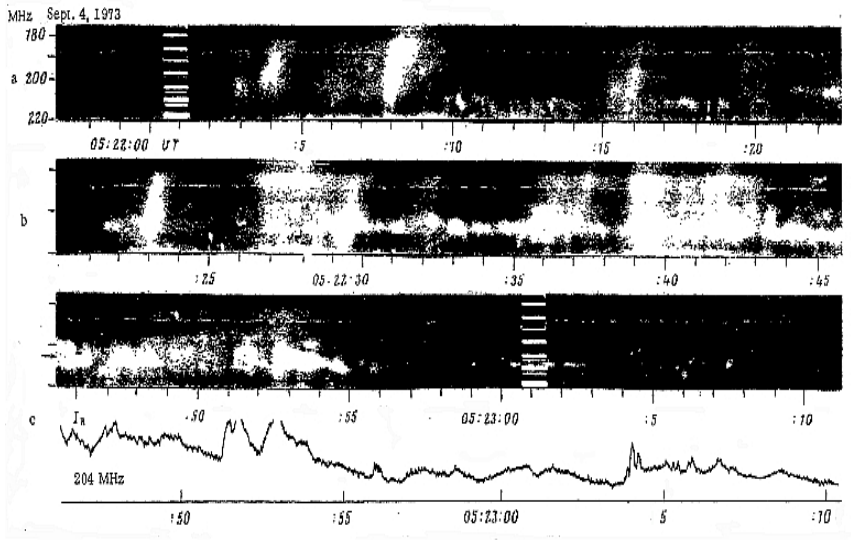

Fig. 3.12 Numerous spikes of type *ss* and a chain of type I bursts observed in a complex of type III bursts on September 4, 1973 (Chernov, 1977).

These spikes differ from the well-known 'herringbone' structure observed in type II bursts in their considerably smaller duration, emission bandwidth and inconstant frequency drift.

A complexity of registration of weak spikes at the high level of type IV continuum bursts explains the reason of their rare detection. In the meter range it is possible to select two types of spikes observing in the type IV bursts.

1) Very short-time ($\approx$ 0.02 – 0.05 s) spikes in the narrow bandwidth, from point like bursts up to 5 –10 MHz, usually without frequency drift. Such spikes are most frequently being observed in the decimeter range where they appear by klusters (or spray) of hundreds (and even thousands) of spikes in a broad frequency bandwidth.
2) Broadband short-lived spikes; they look like the instantaneous strengthening of continuum, therefore, they are called even as spike brightenings (Bakunin & Chernov, 1985). They differ from fast pulsation by absence of a strong periodicity, they look like isolated bursts arbitrarily scattered in the spectrum.

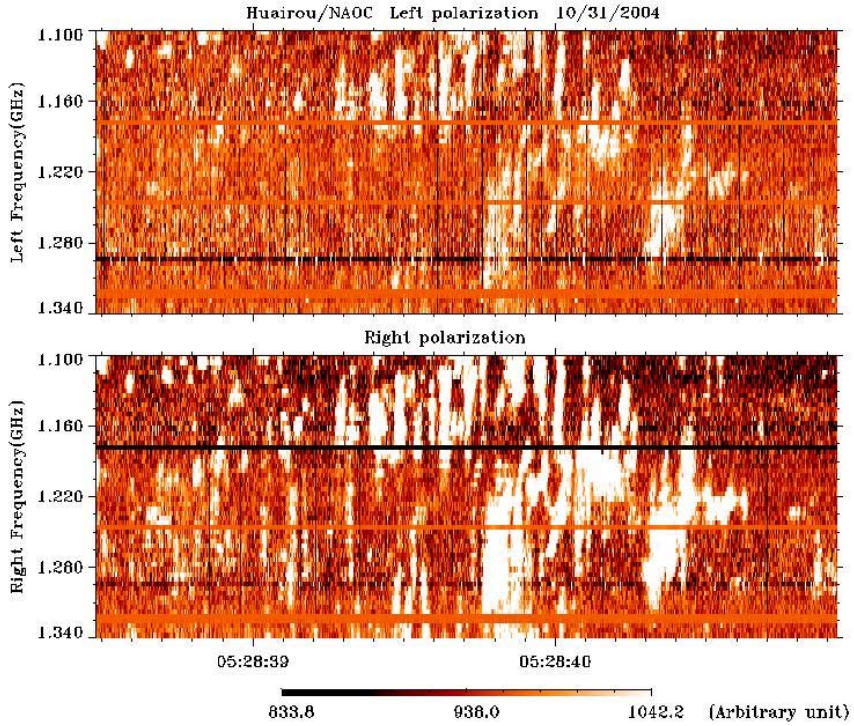

Fig. 3.13 Klusters of spikes in the range 1.1 – 1.34 GHz with extremely high time resolution, of 1.25 ms in the spectrum of the *NAOC* spectrometer (private communication of prof. Yan Y.).

An excellent example of such a kluster of both kinds of spikes in the range 1.1 – 1.34 GHz (with extremely high time resolution, of 1.25 ms) in the spectrum of the *NAOC* spectrometer is shown in Figure 3.13. These spikes have complex po-

larization, we can see as moderate polarized spikes as well as very strongly polarized.

In spite of noticeable differences in their properties, many authors explain both these two kind of spikes by the maser instability (Fleishman & Melnikov, 1998, and references therein).

3.2 Millisecond spikes in the microwave range

In the microwave range the spikes are observed in the most diverse forms: from the instantaneous in the broad band to the points-like at the limit of instrument resolution. The drifting spikes can possess the most diverse drift and even zigzag shape. Besides, as it was found out in recent years, the instantaneous spikes are superfine structure of other elements of the fine structure, in particular, different fibers and zebra-stripes.

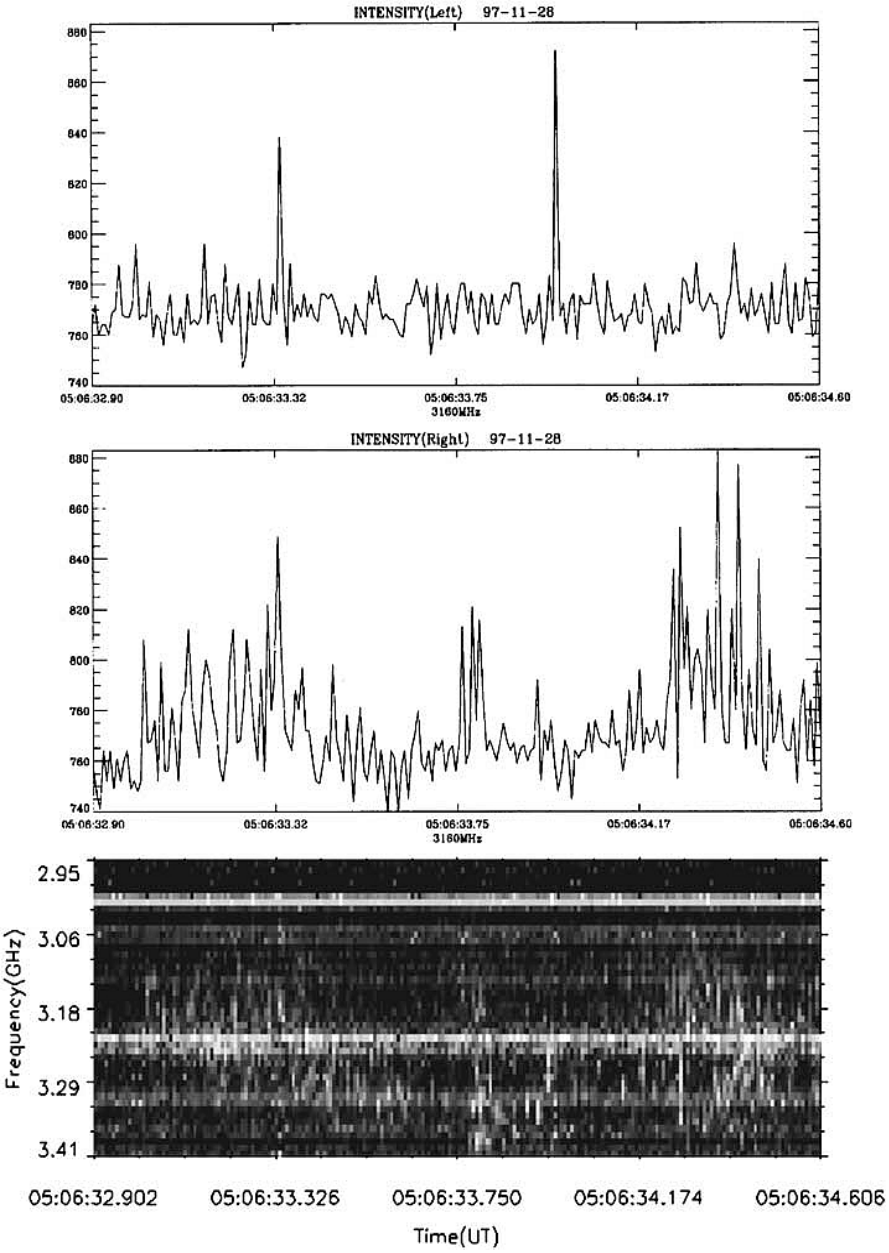

Fig. 3.14 The event on 28 November 1997 with instantaneous millisecond spikes: the top two panels show left and right polarization profiles at 3160 MHz, bottom panel – dynamic spectrum in the range 2.95 – 3.41 GHz. All spikes are fully right hand polarized (Chernov et al. 2001a).

Chernov et al. (2001a) the first presented the detailed analysis of two events with millisecond spikes observed with SBRS (NAOC, Huairou station) in the range 2.6 – 3.8 GHz (120 channels). Figure 3.14 shows the dynamic spectra and left and right polarization profiles of a cluster of spikes. The spectrometer had the frequency resolution of 10 MHz and the time resolution of 8 ms.

The duration of each spike is at the 8 ms limit of the instrument resolution. Spikes are visible in only one right polarization channel, i.e. the spike emission is fully polarized. In the dynamic spectrum each spike is visible only in several frequency pixels, i.e. their frequency bandwidth is less or equal to 10 – 30 MHz ($\Delta f / f \leq 0.007$).

Several examples of millisecond spikes with a strong polarization in the same frequency band were analysed in Wang et al. (2008), in a unique long lasting (> 2 hours) event with spikes in emission and absorption on 13 December 2006.

In some experiments spikes were observed with short-base interferometers. From these observations, upper limits on the visible source sizes can be derived. The first such observations were done with a two-element interferometer at a frequency of 2.8 GHz (Gary et al.(1991)). From an analysis of a burst with a time profile consisting of a continuum and spikes superimposed on it, an upper size to the spike source was derived to be 28".

Huang and Nakajima (2004) defined the location of microwave spikes (in the range 2.6 – 3.8 GHz) using simultaneous source positions at 17 GHz with Nobeyama Radio Heliograph. The source at 17 GHz was located in one foot-point of a small bright coronal loop with strong photospheric magnetic field, and the authors assumed that the electron cyclotron maser instability and gyro-resonance absorption dominate, respectively, the rising and decay phase of the spike event.

Measurements of spatial characteristics of drifting spike sources are made available, through a combined analysis of the data from the Siberian Solar Radio Telescope (SSRT) (Smolkov *et al.*, 1986) and from the NAOC spectropolarimeter (Fu *et al.*, 1995). Such a combination was made for the first time by Meshalkina et al. (2004). Figure 3.15 shows the time profiles of intensity (R+L) and polarization V (R-L) and 1D position of the sources of SSRT and the dynamic spectrum of SBRS (5.2 - 7.6 GHz) for drifting spikes with positive frequency drift. The subsecond pulse (SSP) belongs rather to spike with the duration d_f ~ 0.15 s. The polarization degree was moderate ~ 30%.

The fine temporal structure of flare bursts was recorded by the EW and NS arrays separately to provide 1D images (scans) of the solar disk. The time taken to record the information for a full two-dimensional image is too large (every 2–3 min) to be feasible for observing sub-second events, whereas one-dimensional scans can be made in a much shorter time (every 14 ms). The top right panel shows that according the one-dimensional (1D) map the source position of the spike burst was about 30 arcsec apart from the center of the background burst source. The intersection point of 1D scan projections passing through the source emission maximum gives us its location on the two-dimensional map. This is shown in Figure 3.16. Bottom panels show the superposition of SSRT radio maps and MDI magnetograms.

Meshalkina et al. (2004) presented results of data analysis for 18 similar spike events. A high degree of polarization was recorded in the all SSP events of different spectral type. Despite the high polarization the photospheric magnetic field under the SSP source does not exceed 250 G. Typically the sources of subsecond pulses are far from AR sunspots with large magnetic fields. Most of the SSP sources are very close to the neutral line. Such an arrangement indicates that SSP sources are located at the tops of magnetic loops. As a consequence, the predominant mode of the electromagnetic wave can be confidently determined only for events with a large distance from the SSP source to the neutral line.

In half the background bursts, the sign of the degree of polarization suggests the extraordinary wave mode. This mode can be generated in an optically thin layer of emitting flare plasma by the gyrosynchrotron mechanism. In 6 events the spike sources were located well apart from the neutral line (no less than about 10 arc sec), and they were polarized, as a rule, in the sense of an ordinary wave. Note that the source positions of the spikes, recorded in the same flare, are close to one another, and no reversal of the polarization was observed in this case. Interpretation in terms of a maser mechanism is in conflict with these observations.

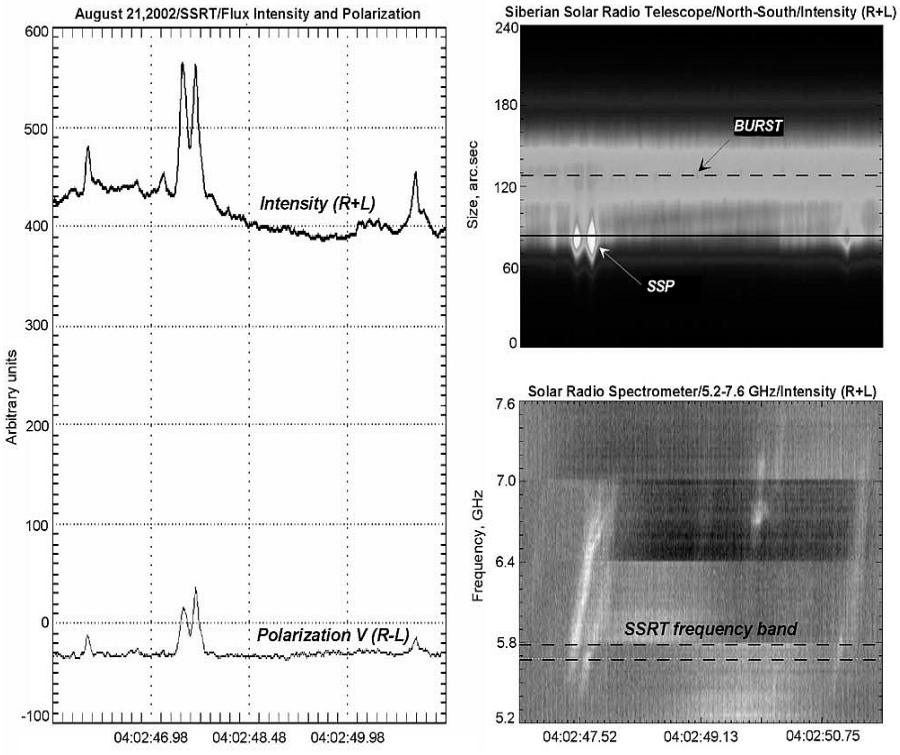

Fig. 3.15 21 August 2002. *Left:* 1D time profiles in intensity and polarization from SSRT at 5.7 GHz. Top right: time development of 1D scans SSRT. Bottom right: dynamic spectrum from NAOC (Meshalkina et al. 2004).

As a rule, the SSP sources are well apart from the strong magnetic field, and the SSP emission corresponds to not less than the 5–10 cyclotron frequency harmonics, if we take the value of magnetic field at the photospheric level. At such high harmonics maser mechanisms are not effective (Fleishman and Melnikov, 1998).

The size of spike sources is unexpectedly high value, of several tens of arcseconds (top 1D scans in Figure 3.16). From the total set of SSRT data for 30 events, the size of spike sources varies from 3.5 to 46 arcseconds. (Altyntsev et al. 1996; 2003). Although, Alekseev et al. (1997) found by VLBI method much less size (< 1 arcsecond) in the decimeter range.

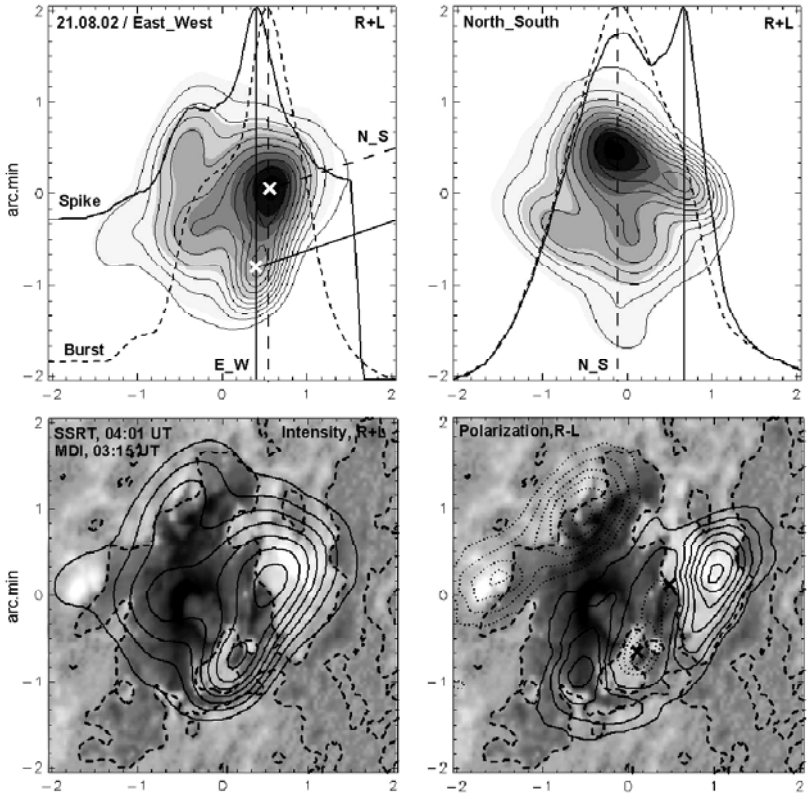

Fig. 3.16 Top: the SSP source position relative to the background burst from 1D scans for NS and EW, respectively (solid line – 1D scan of SSP source (time 04:02:32 UT), dashed line – 1D scan of background burst (time 04:02:51 UT) (these scans were normalized), contour – 2D intensity (the nearest to SSP, time 04:03:25 UT), shading – intensity (2D map of background burst – time 04:01:09 UT). Bottom: superposition of 2D SSRT maps (contour left – intensity of the nearest 2D map to the SSP – time 04:03:25 UT), contour right – polarization) on the MDI magnetograms (white color – N, black – S, dashed line – neutral line) Black cross shows radio SSP source. Scale in arc min, north on the top (Meshalkina et al. 2004).

The most intriguing phenomenon with spikes on 29 May 2003 is analyzed by Chernov et al. (2011). Figure 3.17 shows the dynamic spectrum of NAOC in the range 5.2 – 7.6 GHz (two bottom panels) in Left and Right polarization channels and simultaneous profiles in intensity (R+L) and polarization (R-L) of NAOC coincided with corresponding profile of SSRT at 5.7GHz (two top panels). The spectrum shows that the emission consists in whole of spikes. The spikes with duration of 5 – 10 ms and frequency bandwidth of 70 – 100 MHz do not present any frequency drift, and they formed fast drifting bursts, slow-drifting fibers, zebra pattern stripes etc. Latin numbers I - V mark five fragments of zebra stripes with different drift and frequency separation.

Eight spike peaks marked by numbers 1 – 8 above the profiles well coincide in both stations. The source positions of these spikes are shown in Figure 3.18 presenting also the source position of the background bursts at 5.7 GHz (SSRT) and at 17 GHz (the Nobeyama Radio Heliograph (NoRH)).

The spike source positions were defined by the crossing of two N-S and E-W 1D scans. These 1D scans yield intensity profiles with maximum time resolution (14 ms) and intensity distribution of isolated spikes in comparison with intensity distribution of the background burst. Such data for the spike number 8 are shown in Figure 3.19. The diagram of SSRT did not reveal a broadening of the spike sources; therefore their sizes can be estimated as <15 arcseconds. The spike emission was weakly polarized (20 – 30%). The determination of the wave mode encounters the difficulties of the precision determination of the polarity of magnetic field near the neutral line.

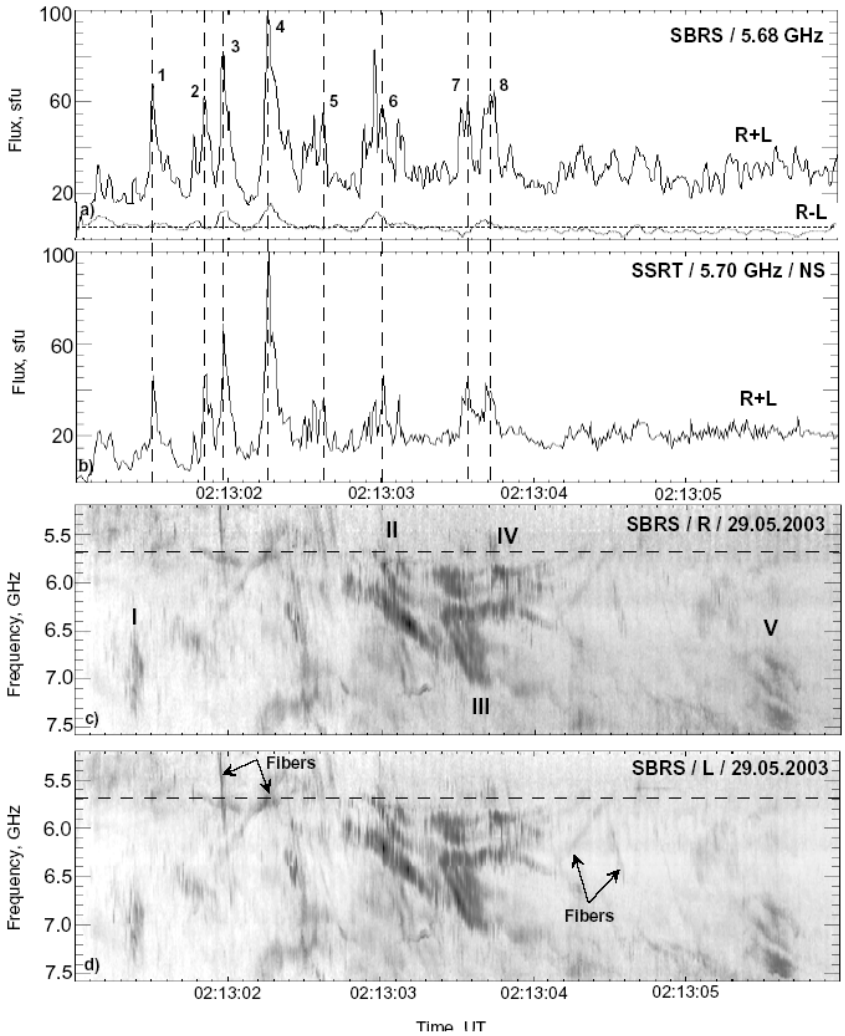

Fig. 3.17 Comparison of 1D time profile (NS) of SSRT (b) with time profiles in intensity (R+L) and polarization (R-L) (a) and dynamic spectrum in L and R polarization channels (d and c) of NAOC (Huairou). All the emission consists in whole of spikes (Chernov et al. 2011).

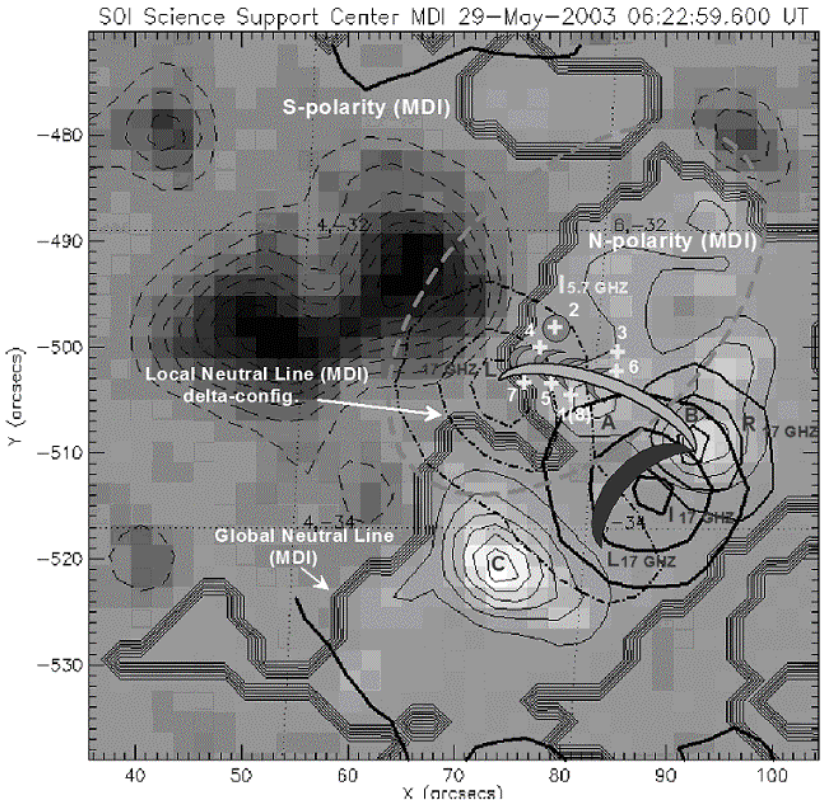

Fig. 3.18 Positions of the radio sources at 5.7 GHz (SSRT) and 17 GHz (NoRH) overlaid on the MDI magnetogram (the broad line is neutral magnetic line). The position of Left polarized local source at 5.7 GHz at the moment 02:17:54.8 UT is marked by gray dashed line. The position of Left polarized source at 17 GHz (elongated along the S-W direction) is shown by bold dashed-dot line. Crosses are positions of centers of spike sources with numbers 1 – 8 (Chernov et al. 2010).

Thus, with this example of the event 29 May 2003 we can conclude that the spikes are emitted by a mechanism of the background burst emission. In this case, it is completely improbable so that the spikes would be excited by miniature beams of fast particles or so that they would be the consequence of the primary flare energy release. All other elements of the fine structure (such as different fibers and zebra patterns with the spiky superfine structure) could be related with a modulation of the background burst emission, e.g. due to the nonlinear interaction of high-frequency plasma waves with low-frequency waves, such as ion-acoustic and whistler waves.

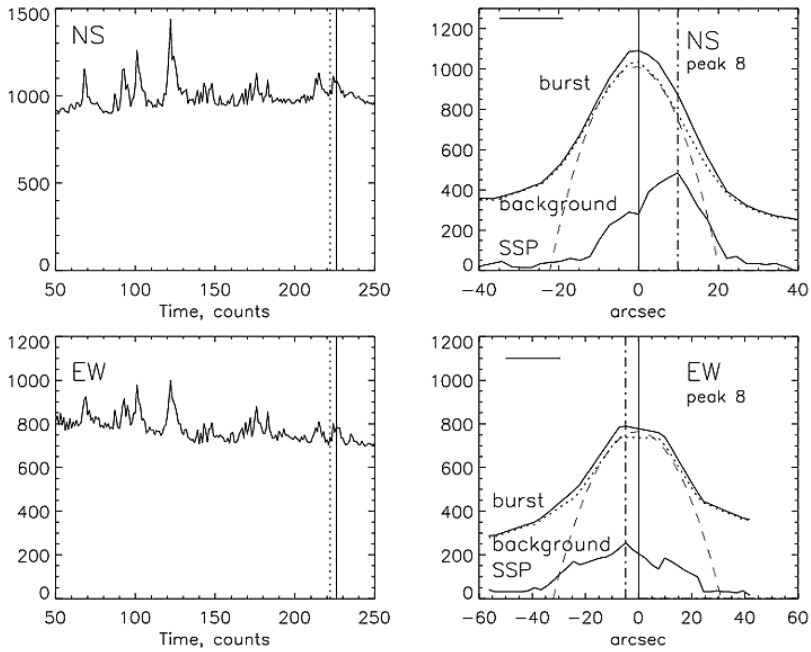

Fig. 3.19 Left two panels: time intensity profiles received by time display of the 1D scans. Right two panels: 1D NS and EW scans of the intensity distribution at the maximum of spike number 8 relative to intensity distribution of the background burst. The horizontal line in the upper left angles shows the dimension of the point source at the half intensity level (spatial resolution) (Chernov et al. 2010).

In Chapter 4 one more event on April 10, 2001 is described (in connection with zebra pattern) in which all the emission also consisted of spikes. The clusters of the spikes in the range of 4.5-7.5 GHz were tightly saturated, and the spikes are superimposed on each other, which hampered to measure their parameters even with the resolution of 5 ms. In this connection Rozhansky et al. (2008) suggested a tool with which to decompose the cluster onto individual Gaussian spikes. Nita et al.(2008) develop the algorithm of this an automated technique for fitting the spectral components of solar microwave spike burst. The method helps to study the variation of the spike distribution parameters, such as amplitude, bandwidth, and related derived physical parameters, as a function of time. The authors conclude that the spikes are a secondary phenomenon, rather than a manifestation of the primary energy release and particle acceleration.

3.3 Interpretation of the spike emission

3.3.1 The generation of the spike bursts by electron beams

The dynamic spectra of drifting spikes in the noise storms can seem like the spectra of miniature type III bursts. Sometimes these two types of bursts are hard to distinguish, from which one can assume that the mechanism of generation of spikes and type III bursts are similar. The closer connection between spikes and type I bursts is not a contradiction, since the plasma hypothesis is also the most popular for type I bursts while the great variety of spikes in noise storms can be connected with different conditions in the source.

Duration and instantaneous band of spikes

Long time there were only some hypotheses on the generation of spikes in the first stage of quasi linear relaxation (Tarnstrom & Philip, 1971). Only detailed examination relates to the spikes in the HF edge of type III bursts (Zheleznykov & Zaitsev, 1975). The broadband drifting and instantaneous spikes require special examination. First of all, it is important to examine the kinematic effects of the motion in the corona of the small beams, which radiate in the narrow frequency band. In contrast to type III bursts the parameters of the electron beams producing spikes provide the rapid switching on of the emission (for which the instantaneous injection of the beam is required) and cessation of the generation of plasma waves after characteristic time of a plateau formation in the electron velocity distribution function due to the effect of quasi linear relaxation (Kaplan & Tsytovich, 1972, Sec. 8):

$$\tau_{pl} \approx 40\, n_e / n_b \omega_{Pe} \,, \tag{3.2}$$

where n_e and n_b are the concentrations of background plasma and of beam, ω_{Pe} is the electron plasma frequency. Conversely, type III bursts are characterized by a slow rise in the beam concentration in the injection region and the subsequent efficient flying-off of the electrons with a distribution function which is in a quasi steady state (Zheleznykov & Zaitsev, 1970). For a concentration ratio $n_e / n_b \approx 10^7$ and $\omega_{Pe} = 2\pi \cdot 200$ MHz the time is $\tau_{pl} \approx 0.3$ s. It determines the total duration of a spike. The establishment of a plateau and the absence of efficient flying-off of the electrons generating the spikes indicate a small velocity dispersion in the

beam. The assumption that the velocity dispersion is small, ($\Delta V / V < 0.1$) is also needed to explain the narrow instantaneous spectral band of the spikes.

Because of the electron velocity dispersion the emission at a fixed frequency escape from an extended region in the corona. Let us estimate the value of the velocity dispersion and the extend ΔX of the beam required to explain the narrow instantaneous emission band $b_t \approx 1 - 2$ MHz.

It is known that the driving of the plasma waves takes place on the inner slope of the particle velocity distribution function where its derivative is positive $\partial f_V / \partial V > 0$. In accordance with the dispersion equation for the plasma waves, an electron beam with a velocity dispersion from V to $V + \Delta V$ moving into outer layers of the corona emits in a band from the highest frequency, emitted by the slowest particles in the tail section of the beam (where $f_{Pe} = f_{Pet}$), $f_{hf} \approx f_{Pet} (1 + 3 V_{Te}^2 /2V^2)$, to the lowest frequency, emitted at the front of the beam (where $f_{Pe} = f_{Pefr}$), $f_{lf} \approx f_{Pefr} [1 + 3 V_{Te}^2 /2(V + \Delta V)^2]$.

Here, it is assumed that the particle velocity V is approximately equal to the phase velocity V_{ph} of the wave, which is >> V_{Te} (the electron thermal velocity). From this we obtain:

$$b_t = f_{hf} - f_{lf} \approx \Delta f_{Pe} + 3 f_{Pet} (V_{Te}^2 /(V + \Delta V)^2 (\Delta V / V). \qquad (3.3)$$

For a more precise estimate of the band b_t we must also allow for a small contribution of the emission from the region already abandoned by the beam. If the plasma waves decay in a finite time, due to electron-ion collisions ν_e, for example, then the residual emission widens the band b_t on the HF edge by an amount ~ $V \nu_e^{-1} \, grad \, f_{Pe}$. In order to obtain the value of $b_t \approx 1$ MHz one must assume in (3.3) that the extent of the beam is $\Delta X = \Delta f_{Pe} / grad \, f_{Pe} \approx 0.5 \cdot 10^8$ cm, while the velocity dispersion must be << 1, $\Delta V / V \approx 0.05$, which was taken into account in the last approximation in (3.3). The estimates were made for f_{Pe} = 200 MHz, $V_{Te} = 5 \cdot 10^8$ cm ($T_e = 10^6$K), $V = 5 \cdot 10^9$ cm s^{-1}, and $grad \, f_{Pe} \approx 1$ MHz/10^8 cm (in Newkirk's model).

In estimating the duration of the emission at a fixed frequency f_l we consider that the plasma waves at one frequency are generated in the height interval Δh corresponding to the interval $\Delta f_{Pe} = f_{Pe2} - f_{Pe1}$ of plasma levels from which the radiation of this frequency, generated by electrons with velocities V and $V + \Delta V$, escapes. We find size of this interval by analogy with Eq.(3.3):

$$\Delta f_{Pe} \approx 3 f_l (V_{Te}^2 /(V + \Delta V)^2 (\Delta V / V). \qquad (3.4)$$

What we said above is explained in Figure 3.18 by a graph of the dependence of the plasma frequency on the velocity of the particles emitting at the fixed fre-

quency f_l. Figure 3.20 shows two particle beams moving along *grad* f_{Pe} and having the following parameters:

a) $\Delta X = 10^8$ cm and $V = (5.1 - 5.3) \cdot 10^9$ cm s^{-1} (this velocity corresponds to a frequency drift of~ – 50 MHz s^{-1} in Newkirk's model of n_e for a coronal streamer);

b) $\Delta X = 0.5 \cdot 10^8$ cm, and $V = (3.1 - 3.3) \cdot 10^9$ cm s^{-1} (the frequency drift ~ – 30 MHz s^{-1}.

The slope of the leading and trailing fronts are connected with the flying-off of the particles (the slow ones lag behind) and depend on the time of injection. The brief duration of the spikes allows one to assume that instantaneous injection occurs directly in the source. The initial position of beam b is shown by a dashed line.

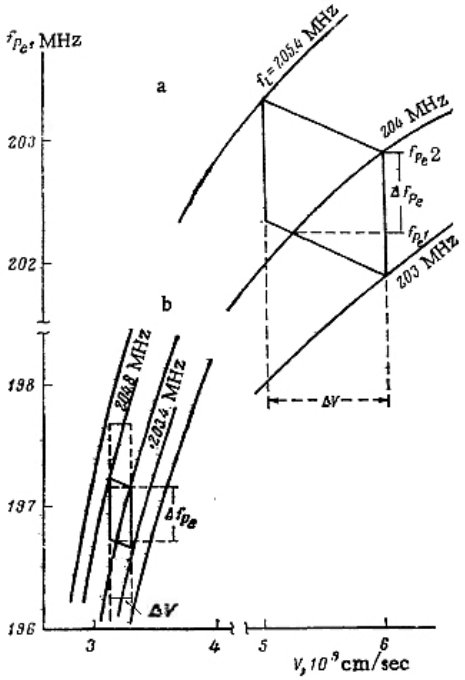

Fig. 3.20 Dependence of plasma frequency f_{Pe} on velocity V of fast particles emitting at one frequency $f_l \approx f_{Pe} (1 + (3/2)(V_{Te}^2 / V^2)$: a) $\Delta X = 10^8$ cm, $V = (5.1 - 5.3) \cdot 10^9$ cm s^{-1}, and $\Delta V / V = 0.2$; b) $\Delta X = 0.5 \cdot 10^8$ cm, $V = (3.1 - 3.3) \cdot 10^9$ cm s^{-1}, and $\Delta V / V = 0.07$ (Chernov, 1978).

These two diagrams give a comparative idea of the particle beams generating a type I bursts (beam a) emitting in the frequency band $b_t \approx 3.5$ MHz and a spike burst (beam b, $b_t \approx 1.4$ MHz). It is shown that the fixed frequency $f_l = 204$ MHz is emitted from the height interval Δf_{Pe} determined by Eq. (3.4).

After a short excitation time of the plasma waves, connected with the time scale of the beam, the plasma waves must decay owing to collisions in the corona. At frequencies of ~ 200 MHz the damping constant, defined as the collision time ν_e^{-1}, is ~ 0.03 – 0.5 s, comparable with the time in which the beam passes through the region $\Delta h = \Delta f_{Pe} / grad\, f_{Pe}$ emitting at the fixed frequency. Therefore, the duration of the emission at one frequency will be composed of the sum of these times:

$$d_f \approx (\Delta h + \Delta X)/V + \nu_e^{-1}. \qquad (3.5)$$

Taking the parameters of beam b in Figure 3.20 as $\Delta h = 0.5 \cdot 10^8$ cm, $\Delta X = 0.6 \cdot 10^8$ cm, and $\nu_e^{-1} \approx 0.05$ s, we obtain $d_f \approx 0.09$ s.

In this model the frequency drift of spikes must be a consequence of the movement of the beam in the inhomogeneous solar corona. The very fast reverse drift observed in groups of spikes ("rain" like events) may be explained by the group delay of radio emission in the height interval ΔX.

Rise and decay times of emission

It is known that for type III bursts the flying-off of the beam reveals in an increase in the duration of the burst with a decrease in frequency (Aubier & Boischot, 1972). The velocity dispersion in the electron beams producing spikes is very small, so that their dispersion is weakly expressed (see Figures 3.3 and 3.4). This effect can be detected, however. Spectra of four spikes, obtained by the spectrograph of the IZMIRAN and profiles at several fixed frequencies, obtained simultaneously by the multichannel receiver in Nançay are shown in Figure 3.21 (Chernov, 1978).

The values of the frequency drift of each burst ($\dot{f}$), the duration d_f of the emission at the corresponding frequency at the 1/e level, the ratio of the rise time t_r of the emission from the 1/e level to the maximum value, and the decay time t_d from the maximum to 1/e level are entered alongside the profiles. The profiles of drifting bursts a) and c) reveal a clear increase in duration with a decrease in frequency. The ratio t_r / t_d grows at the same time. Thus, the time profiles of the spikes reveal properties characteristic of type III bursts. The only difference from type III bursts is that the durations of the drifting spikes increases mainly through an increase in the rise time t_r, while type III bursts display an increase in the decay time of the emission with an increase in the total duration at different frequencies (Aubier & Boischot, 1972). A study of the time profiles of spikes at several frequencies indicates that the decay time of the emission is about the same in all the bursts. No definite dependence between the rise and decay times for each burst is revealed in this case. A similar result was obtained by Elgarøy & Rosekild (1973)

as a result of an analysis of a large number of spike profiles observed at several frequencies. We note one more property characteristic of spikes, which can be traced in Figure 3.21: the ratio t_r / t_d grows with a decrease in the drift rate. Thus, spikes display properties characteristic of the emission caused by a beam of fast particles traveling the corona. In contrast to type III bursts, however, the emission ceases in a section of the profile close to the maximum. Further, the profile is characterized only by damping of the emission, as a consequence of which one observes an increase in t_r / t_d with a decrease in frequency for drifting spikes of type *d* and *fd* and about the same damping time for all the bursts. Instantaneous spikes of type *s* in Figure 3.21 do not display such a clear dependence, so that in this case the electron beam is probably not able to travel any appreciable amount in the corona during the lifetime of the burst, i.e. type *s* spikes are characterized by instantaneous emission in a wide frequency band (~ 5 MHz for burst b)), after which the emission only decays.

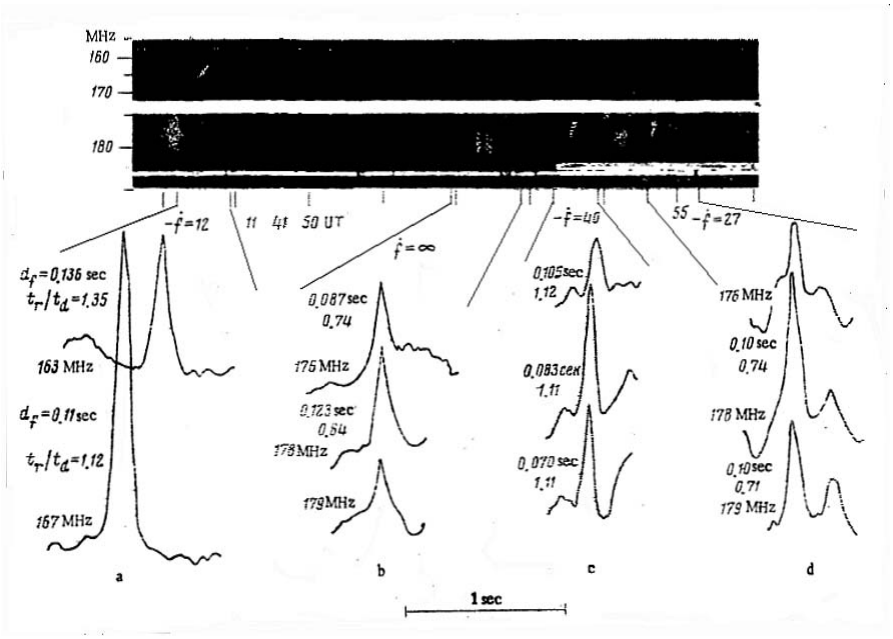

Fig. 3.21 Spectrum (IZMIRAN) and time profiles, obtained with the multichannel spectrograph (Nançay), for four spikes (a, b, c, d) observed in noise storm on 24 October 1971. The duration of the drifting spikes (d_f, s) at the 1/e level grows with a decrease in frequency together with the ratio t_r / t_d of the rise time to the decay time of the emission (Chernov, 1978).

An analysis of the sections of decay of the emission in the profiles of 19 spikes at frequencies of from 163 to 179 MHz and of 31 bursts at 204 MHz indicates an

exponential damping of the emission (Chernov, 1978). An example of time profiles plotted on a logarithmic scale of intensity (I) at two successive frequencies for a drifting spike is presented in Figure 3.22.

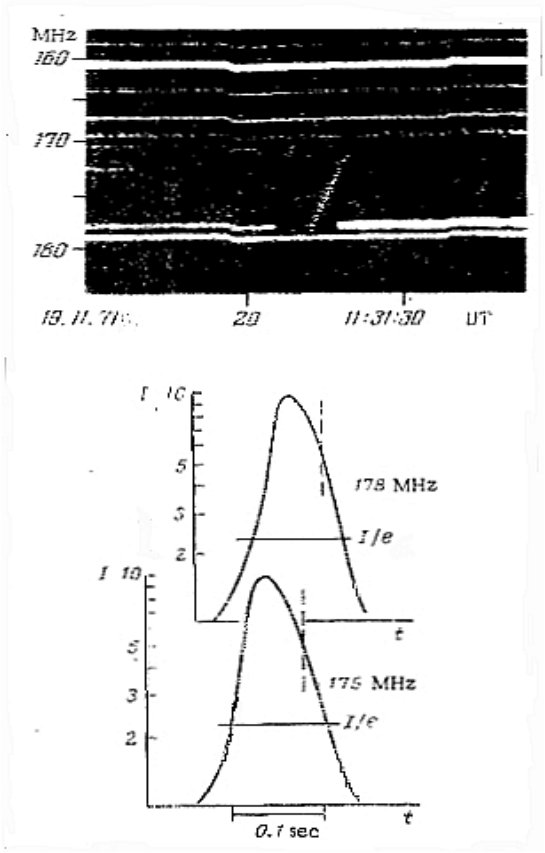

Fig. 3.22 Dynamic spectrum of a spike (IZMIRAN) and its time profiles (Nançay) (Chernov, 1978) .

The sections of the profiles below the dashed line are nearly straight, which indicate an exponential decay of the emission. Assuming that the process of damping of the plasma waves on electron-ion collisions is the most likely cause of the decay of the emission, we obtain a method for determining the plasma temperature in the emission source by measuring the damping constant τ_d (as the time of an e-fold decay of the emission on the exponential sections of the spike profiles by the well-known equation (Zheleznyakov, 1964; Aubier & Boischot, 1972)):

$$T_e = 0.65 \cdot 10^{-4} \; f^{4/3} \tau_d^{2/3}. \qquad (3.6)$$

Numerous reports are known on determination of the kinetic temperature in the solar corona from the rate of damping of type III bursts emission (Zimmerman, 1971; Aubier & Boischot, 1972 and others). The unsatisfactory nature of the results consisted in the fact that overstated values of the temperature (up to (5-6) $\cdot 10^6$K) were obtained for the most part. The errors in the determination of coronal temperature were pointed out in Fomichev & Chertok, (1970) and Riddle (1974). The results of Zheleznyakov & Zaitsev (1970), Zaitsev et al.(1972) and Zaitsev et al.(1974) indicate that the purely exponential damping due to collisions cannot take part at all in the decay of type III emission. The profiles of spikes are therefore very interesting as one of source for determining the coronal temperature.

The cessation of the action of the emitting agent at time close to the emission maximum is due to the rapid passage of the miniature beam through the region of generation at a fixed frequency. For example, the beam b) in Figure 3.20 crosses the region Δf_{Pe} in a time not exceeding 0.03 s. To determine the damping constant we selected single spikes whose profiles were not distorted by neighboring bursts or fluctuations in the background emission. The damping constant τ_d and values T_e averaged over N bursts observed on different days at different frequencies are presented in Table 3.1

Table 3.1: Coronal temperature T_e determined from the damping constant τ_d in the spike profiles (adapted from Chernov,1978).

Date	F(MHz)	N	τ_d (s)	T_e (10^6 K)
10.06.69	204	6	0.021	0.59
17.06.70	204	3	0.023	0.63
3.09.73	204	22	0.019	0.55
24.10.71	179	3	0.016	0.42
19.11.71	179	3	0.022	0.51
24.10.71	176	4	0.019	0.44
19.07.71	169	4	0.026	0.53
30.10.71	169	3	0.030	0.58
24.10.71	163	2	0.029	0.54

All the values of T_e determined from separate bursts lay in the range of (0.41 – 0.72) $\cdot 10^6$ K the size of which is probably connected with the error in determining the damping constant, since T_e does not display a definite frequency dependence.

These values of T_e are found to be lower than the values usually adopted for active regions un the corona (~ (1 –2) $\cdot 10^6$ K) obtained from other sources. These estimates thereby confirm the hypothesis advanced by Elgarøy (1963) that the kinetic temperature of the plasma in noise centers (which are identified with filaments lying far from coronal condensations) can be somewhat lower than in neighboring regions as a result of their screening by the magnetic field.

Another alternative explanation is possible, however, for the faster damping of plasma waves than fallows from the collision time $\nu_e^{-1} = \tau_d \approx 0.05$ s for $T_e \sim 10^6$ K. First of all, we consider that the excited plasma waves are driven to lower wave numbers (into a region of higher phase velocities) as a result of differential scattering on thermal ions. A more efficient mechanism of damping of the plasma waves is probably turned on in successive stages of scattering. Such a mechanism may be Landau damping on fast beam particles corresponding to the outer slope of the hump in the particle velocity distribution function f_V, where $\partial f_V / \partial V < 0$. These particles do not radiate, but they hardly absorb either, since the energy density of the plasma waves in this region of phase velocities is low. Efficient damping on fast particles will occur only in the case when the phase velocity grows by a small amount in one act of differential scattering, as a consequence of which the wave does not go out of resonance with the beam. Let us estimate the size of the jump in phase velocity of a wave in one act of scattering.

It is known that scattering on ions will be efficient if the relative change $\Delta k/k$ in the wave vectors during scattering satisfies the inequality:

$$\frac{\Delta k}{k} < \frac{V_{Ti}}{3V_{Te}^2} V_{ph}, \tag{3.7}$$

which follows from the conservation laws and the dispersion equation for plasma waves (Tsytovich, 1970, Eq. 8.21).

Let us assume that V_{ph} is approximately equal to V, the particle velocities, which for spikes must in the range of (3 – 6) $\cdot 10^9$ cm s^{-1} (less than for type III bursts and greater than $6V_{Te}$, so that Landau damping on the surrounding plasma would be unimportant). Then for $V_{Te} = 5 \cdot 10^8$ cm s^{-1} and $V = 3.1 \cdot 10^9$ cm s^{-1} the quantity on the right side in (3.7) will be ≈ 0.048, which indicates the differential character of the scattering. The phase velocity varies in approximate the same ratio, $\Delta k/k \approx \Delta V_{ph}/V_{ph}$, so that with a velocity dispersion $\Delta V/V \approx 0.1$ in the beam the plasma waves will not go out of resonance with the beam during the first two acts.

If we assume that the spectrum of the plasma waves remains one-dimensional during the lifetime of a burst, then the time for single scattering on ions in an isothermal plasma will be determined by the relation (Tsytovich, 1970):

$$\tau_i \approx \frac{4}{43} \frac{n_e m_e}{\omega_{Pe} W^l} V_{Te} V \ . \qquad (3.8)$$

Since spikes are usually more than an order of magnitude weaker than type III bursts we can assume that here the energy of excited plasma waves does not exceed $W^l \approx 10^{-2} n_b m_e V^2$. Then, adopting the values of $n_e/n_b \approx 10^7$, $\omega_{Pe} = 4\pi \cdot 10^8$ Hz, $V_{Te} = 5 \cdot 10^8$ cm s^{-1}, and $V = 3.1 \cdot 10^9$ cm s^{-1}, we obtain $\tau_i \approx 10^{-2}$ s. The time for Landau damping on fast beam particles also comprises about the same value (for example, see Eq. (6.1.2.2) in Akhiezer et al. (1974)). Thus Landau damping can accelerate the absorption of the plasma waves, which probably explains the somewhat understated temperatures determined from the time profiles of spikes with allowance only for collisional damping.

Landau damping on fast beam particles becomes especially efficient in velocity-nonmonotonic beams in which all the faster particles arrive at the leading front of the beam from behind during the lifetime of the burst. Then the plasma waves excited ahead of the beam will remain in resonance with the beam during multiple scatterings on ions. The majority of spikes are probably generated by such velocity –nonmonotonic beams in which the generation of plasma waves can cease before the establishment of a plateau, as soon as the fast rear particles reach the leading front, i.e. after a time $d_0 \sim \Delta X / \Delta V$, where ΔV is the total velocity dispersion in the beam.

Calculation of time profile

The fast electrons are not able to expand in the short lifetime of the beam producing a spike. But an analysis of the time dependence of the emission power of spikes is complicated by the fact that the emission damping constant τ_d comprises a value comparable with the entire duration of the burst, and τ_d can be determined only by Landau damping on fast beam particles. Because of this, one observes spike profiles with different relations of the rise and decay times of the emission. In this case wave absorption is one of the important factors forming the time profile. Therefore, in contrast to type III bursts, for spikes one needs a more systematic allowance for plasma wave absorption in the system of quasi-linear equations describing the time dependence of the plateau level and the particle momentum (Eq. (9) and (10) in Zaitsev et al. (1972)). This fact and the need to choose a concrete nonuniform particle distribution function make the above mentioned system of equations unsolvable and prevent the transition to self-similar solutions.

But during the short rise time of the spike emission ($t_r = 0.03$ s) the profile must be determined mainly by the shape of the distribution function along the beam, which allows one to neglect quasi-linear effects in the first moment after injection and to pass on to some model representation.

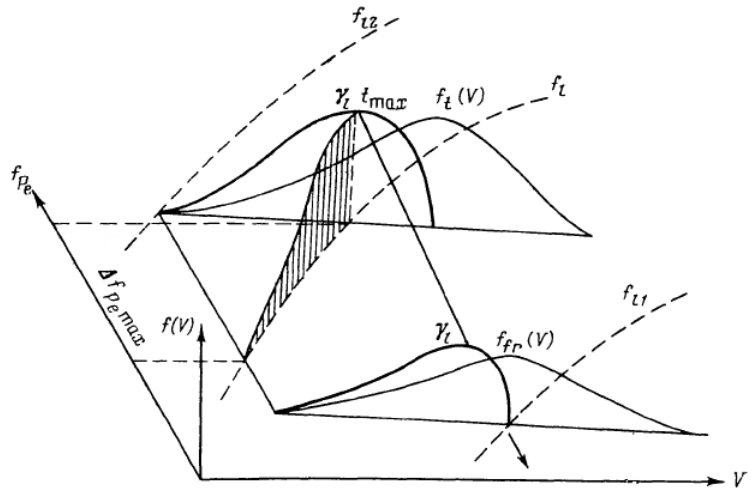

Fig. 3.23 Shape of particle distribution function in a nonuniform beam, at the front of the beam f_{fr} (V) and at the its trailing front f_t (V). A symbolic volume with a positive increment γ_l of beam instability is distinguished by a heavy line. Particles emitting at one frequency f_l in the interval of plasma levels Δf_{Pe} at the moment of the emission maximum at this frequency are distributed along the hatched surface (Chernov, 1978).

But the allowance for the integration of emission in an extended region (radiating at one frequency) is a difficult problem. This is clarified by the diagram in Figure 3.23, where the particle velocity distribution functions at the leading front of the beam (f_{fr} (V)) and its tail sections (f_t (V)) are shown. Particles with different velocities, distributed along the hatched surface whose projection onto (f_{Pe}; V) plane is the curve $f_{Pe} \approx f_l\,(1 - (3/2)(V_{Te}^2 / V^2))$, emit at one frequency f_l at a fixed time. Plasma oscillations are driven on the inner slope of the distribution function. The symbolic volume with a positive increment $\gamma_l \propto n_b (\Delta V / V)^{-2}$ of the beam instability in this region is distinguished by a heavy line. As the beam moves in the direction – *grad* f_{Pe} the emission at the frequency f_l begins to rise as soon as its leading front crosses the curve f_l = const. The efficient generation of the plasma waves is maintained through the increased concentration of fast particles at the trailing front. Then, the maximum in the generation at the frequency f_l comes at the moment when the emission is integrated within the maximum height interval ($\Delta f_{Pe}\,max$) and the intersecting surface covers a region with the maximum increment at the trailing front of the beam (it is shown hatching at just this moment t_{max} in Figure 3.23).

Thus, at each moment in the interval Δf_{Pe} the increment takes values located along the envelope of such an intersecting surface. Since its area is a complicated

function of the plasma frequency f_{Pe}, the velocity dispersion $\Delta V/V$, and the concentration n_b (which varies with time), the time dependence of the energy of the plasma waves, which must have the form

$$W(t) \sim \int_{\Delta f_{Pe}} \int_0^T e^{2\gamma(f_{Pe};\Delta V/V;n_b)t}\, e^{-(T-t)\tau_d}\, dt\, df_{Pe}\,, \qquad (3.9)$$

cannot be reduced to an analytical form suitable for calculation. In this case the group delay of the radio emission at the frequency f_l from the interval Δf_{Pe} is not taken into account in (3.9), since its maximum value $\Delta t_{gr} = \Delta h/V_{gr}$ is a small quantity: $\Delta t_{gr} = 0.5\cdot10^8/7.5\cdot10^9 \approx 0.007$ s.

We note, however, that the time profile of the emission at the frequency f_l from the height interval Δf_{Pe} can be represented as the result of the passage through this interval of an instantaneous emission band whose low-frequency slope is determined by the variation of the distribution function along the beam while its high-frequency slope is determined by the particle velocity distribution at the trailing front of the beam (since the slowest particles from the deepest plasma levels contribute to the emission at the highest frequencies). Such an instantaneous band can be called the idealized band, since it reflects the nonuniformity of the beam at the initial time without allowance for plasma wave absorption.

To simplify the calculations we assume that the beam instantly emits plasma waves in the frequency band from f_{l1} to f_{l2} (see Figure 3.24) with a linear frequency profile of intensity. These considerations allow us to pass to the solution of a simpler problem which qualitatively accurately reflects the physical process of formation of the time profile and permits numerical calculations to be made. In Figure 3.24 the height interval from the level f_0 to $f_0 + \Delta f$ in which emission at one frequency can be generated is marked on the axis of plasma frequency f_{Pe} (or of height in the corona). We assume that the emission power in this interval declines with height from the maximum W = 1 at the level $f_0 + \Delta f$ (corresponding to the level of escape of the ordinary wave) to zero at the level f_0 by the linear low $W_{\Delta f} = (1/\Delta f)(f - f_0)$. The start of the emission is due to the arrival of this interval of the instantaneous band whose low-frequency slope occupies the frequencies from f_{fr} to f_{fr} +b/2, and for simplicity it is also given by a straight line $W_b \approx (2/b)(f - f_{fr})$. The instantaneous band crosses the interval Δf at the rate of the frequency drift $df/dt = -a$ (direct drift), which determines the time dependence of the frequency in the form $f_{fr} = f_0 + \Delta f - at$. Thus, the power of the plasma waves generated at the given time will be proportional to the area under the curve determined by the product of the straight line $W_{\Delta f}$ and W_b (it is hatched in Figure 3.24a).

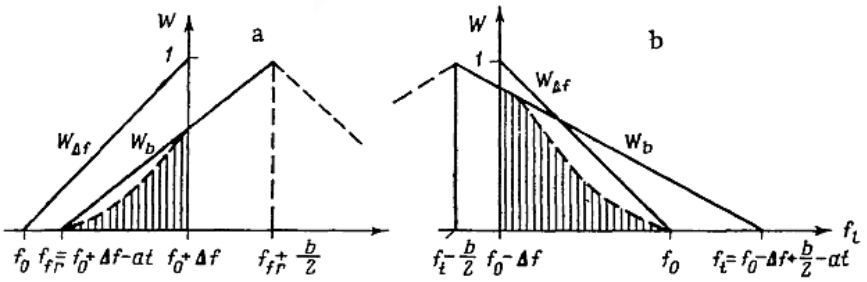

Fig. 3.24 Diagram explaining the simplified model for calculating the time profile of a burst: a) the rise of the emission is connected with the passage of the instantaneous band b of the burst through the interval Δf in which the emission at one frequency declines from 1 to 0; b) analogous diagram explaining the decay of the emission (Chernov, 1978).

But the time dependence of the emission power with allowance for the exponential factor determining the damping of the plasma waves can be approximated by the expression:

$$W_1 \sim \int_0^T e^{-(T-t)/\tau_d}\,dt \int_{f_{fr}}^{f_0+\Delta f} W_{\Delta f}\, W_b\, df$$

$$= \frac{2}{b\,\Delta f}\, e^{-T/\tau_d} \int_0^T e^{t/\tau_d}\,dt \int_{f_{fr}}^{f_0+\Delta f} (f - f_0)(f - f_{fr})\,df \qquad (3.10)$$

After the time $T_1 = b/2a$ the emitting activity of the beam begins to decay, which is connected with the passage through the interval Δf of the decaying HF slope of the band b. Since the HF slope of b is determined by the shape of the beam at its trailing front, the inclination of the straight line $W_{\Delta f}$ must be reversed in accordance with Figure 24b. The generation ceases at the time $T_3 = b/a$ when $f_t = f_0 - \Delta f$, after which the time profile is characterized only by damping of the plasma waves with a damping constant τ_d. Taking the integrals and simplifying the expressions it is easy to obtain four stage-by-stage equations for calculating the time profile of a burst. Here, it is assumed that the flux of electromagnetic waves is proportional to the power of the plasma waves, i.e. the source remains optically thin to radio emission in the process of wave conversion.

36 time profiles were calculated for different combinations of burst parameters within the limits of the following values: $a = 10 - 50$ MHz s^{-1}, $b = 1 - 2$ MHz, $\Delta f = 0.5 - 1.1$ MHz, and $\tau_d = 0.050 - 0.0125$ s. Since the observed profiles have a diverse character, individual profiles of single spikes, not distorted by neighboring bursts, rather than averaged profiles were compared with the calculated profiles.

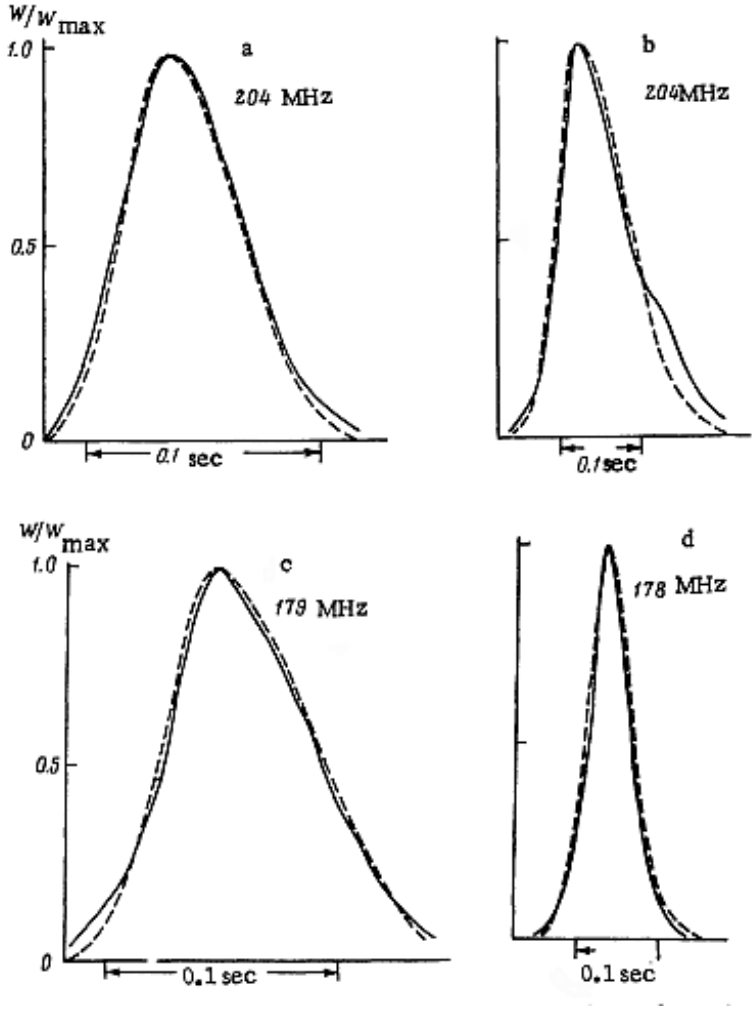

Fig. 3.25 Calculated (dashed line) and experimental (solid line) normalized profiles of spikes with direct frequency drift (Chernov, 1978).

Figure 3.25 shows that one is able to find a calculated profile (dashed line), characterized by only one set of parameters a, b, Δf, and τ_d which is in satisfactory agreement with each observed profile (solid line). The damping constant is uniquely determined from the matching of the final sections of decay of the emission, since the generation of plasma waves ceases at a time pertaining to the decay on the section nearer the maximum. By assigning a model of the electron concentration, we can estimate the size ΔX of the electron beam and the velocity disper-

sion $\Delta V/V$, using Eq. (3.3) and (3.4), for each burst from the parameters Δf and b obtained from the matching of the profiles.

Later, an analysis focusing on the temporal properties of spikes was carried out by Güdel & Benz (1990) who organized dedicated observations of decimeter wave spikes at several frequencies between f = 361 MHz and f = 1110 MHz with high time resolution (from 0.5 to 10 ms). A steep rise and a short saturation phase were normally followed by an exponential decay. They did not find a distinct correlation between the spike duration and the decay rate, nor between the peak flux and the decay rate. This and a rather fixed value of the decay rate ($\tau_d \approx 29 - 32$ ms) suggests a decay mechanism inherent to the plasma at a given density level (collisional damping).

Güdel & Benz (1990) found that the rise phase does not display an exponential growth; a better description, although lacking any straightforward physical meaning, is given by the Gaussian profile.

In the above calculations of spike profiles in the meter range, the not exponential rise phase is described by a spline exciter function (3.10). Güdel and Benz deconvolve the exciter function (*f(t)*) from an observed profile, using a similar expression:

$$W(t) \sim \frac{1}{\tau} \int_{-\infty}^{t} e^{-(t-t')\tau} f(t')\,dt' , \qquad (3.10a)$$

the convolution of *f(t)* and damping function $e^{-t/\tau}$.

Güdel & Benz (1990) obtained also an important dependence of the spike duration d_f on frequency in a broad frequency range of 200 – 1000 MHz. The durations follow an inverse power law dependence, $d_f \sim f^{-1.34 \pm 0.13}$. In the subsequent years this dependence was refined at other frequencies (Zlobec & Karlicky, 1998) and with the more high resolution, of 1 ms (Meszarosova et al. 2002; 2003). It was expanded to 3GHz, and this refined law $d_f \sim f^{-1.29 \pm 0.08}$ differs significantly in a statistical sense from the intuitively expected behavior $d_f \sim f^{-1}$, which requires a physical interpretation based on ECME mechanism (Sirenko and Fleishman, 2009).

The experimental data in Figure 3.26 correspond to frequencies from 0.2 to 3 GHz. Though radio spikes have been observed at frequencies at least up to 5.5 GHz, their durations at such frequencies do not exceed 2.5 ms, and so have not been measured reliably. Therefore, a new modeling in frames of ECME was performed for the frequency range 0.3–3 GHz in Sirenko and Fleishman (2009). Only the results of the model for the second harmonic of the extraordinary wave are consistent with the observed behavior. Thus, this wave is a probable candidate for the dominant mode in spike bursts. Let's remind that this mechanism is effective

only in the sources, where the ratio of plasma and cyclotron frequencies is near unity ($\omega_{Pe}/\omega_{Be} \approx 1$).

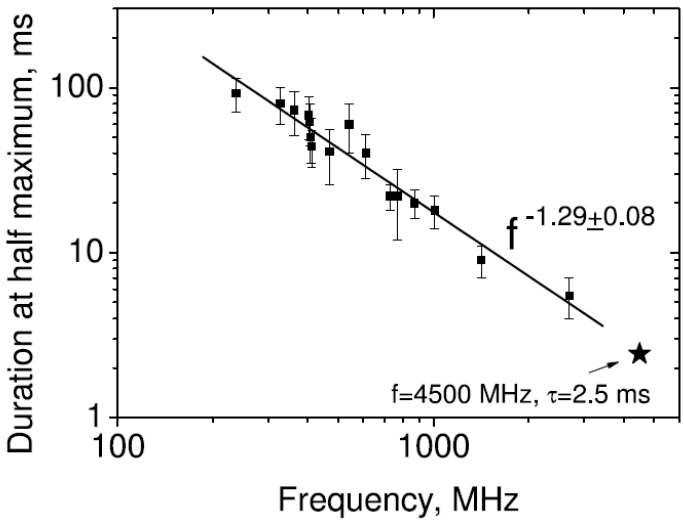

Fig. 3.26 Observational data on the frequency dependence of the durations of solar millisecond narrow-band radio spikes at 0.2–3 GHz. The best fit to these observations is a power law with exponent 1.29 ± 0.08 (Rozhansky et al. 2008).

In this connection, let us note that estimations of the magnetic field strength according to the parameters of ZP and fiber bursts give only value of B =125 G at the plasma level of 5 GHz, which will be coordinated with the extrapolated values (see Fig. 10 in Chernov et al. (2006)).

Furthermore, the spikes are generated most likely by different mechanisms in meter-decimeter and microwave ranges.

Polarization

The data presently available indicate a strong circular polarization of spikes observed simultaneously with bursts of types I, III, and IV. In this case the signs of polarization of the spikes and types I and III bursts coincide, i.e. they correspond to the ordinary wave. The unpolarized spikes observed in the form of the microstructure of a type II burst on 3 May 1973, are an exception.

The polarization may be connected both with the mechanism of generation and with the conditions of the escape and propagation of the radio emission. But if one mechanism of generation is adopted for the spikes observed in different events then the presence of unpolarized emission indicate that the mechanism yields unpolarized emission, and the degree of polarization is determined by the conditions

of escape and propagation of the emission in the corona. In this connection, it is known that a difference in the optical depths for the ordinary (*o*) and extraordinary (*e*) waves cannot provide a high degree of circular polarization (Zheleznyakov, 1964). Let us therefore consider the influence of the conditions of escape of the radio emission from the corona.

It is known that only the *o*-wave may emerge from the source if its frequency satisfies the inequality (Zheleznyakov, 1964):

$$\frac{f_{Pe}^2}{f^2} > 1 - \frac{f_{Be}}{f} \tag{3.11}$$

Since in the process of transformation of plasma waves into electromagnetic emission as a result of induced scattering on ions the emission frequency remains close to the frequency of the Langmuir waves, $f^2 \approx f_{Pe}^2 (1+3V_{Te}^2/V^2)$, by substituting this expression into the inequality (3.11) and dropping the small terms we obtain the following condition for fully polarized emission:

$$\frac{f_{Be}}{f_{Pe}} < 3\frac{V_{Te}^2}{V^2}. \tag{3.12}$$

From this we can find the lower limit for the magnetic field strength in the source. For a frequency f = 204 MHz, $V_{Te} = 5 \cdot 10^8$ cm s^{-1}, and velocities $V \approx (3.3 - 5) \cdot 10^9$ cm s^{-1} (see Figure 3.18 for the corresponding plasma frequencies) the magnetic field strength must exceed the values B ≈ 4.8 – 2.2 G respectively, which are probably easily realized in noise storm centers where the majority of electron beams producing spikes are created.

But the condition (3.11) may not be satisfied for the spikes observed in type II bursts, since the frequency of the fundamental tone for type II bursts corresponds to the plasma concentration behind the shock front, where it exceeds the undosturbed plasma concentration by two to three times. As a result, unpolarized spikes should be observed in type II bursts, since all the unpolarized type II emission emerges from a region lying above the level of escape of the *e*- wave.

It should be noted that the emission of spikes can be fully polarized in somewhat smaller fields also if one allows for the driving of the plasma waves into a region of higher phase velocities, as suggested in Zheleznyakov & Zaitsev, 1975). In this report they also predict the existence of spikes at the second harmonic of the local plasma frequency, for which the absence of appreciable polarization should be a characteristic difference from spikes at the fundamental frequency. But spikes at the second harmonic were not detected in the observations discussed in Chernov (1977). If the second harmonic is not formed, this may be connected with an inefficiency of the process of Raman scattering of plasma waves on each other owing to the weak intensity of the waves in the nonresonance region of the

spectrum. In contrast to the situation for type III bursts, in the sources of weak spikes the plasma waves are not able to grow to the required level during a few acts of differential scattering.

Influence of group delay of radio emission on the frequency drift of solar radio bursts

The effect in which radio waves are subject to group delay in the corona should result in distortion in the dynamic spectra of solar radio bursts at meter wavelengths, since emission usually occurs at frequencies just above the local plasma frequency. It is especially important to isolate the group delay effect in pure form, i.e. the group delay of radio frequencies emitted instantaneously in a broad frequency band, to understand whether this effect could have distorted published values of the frequency drift in various bursts. Let us attempt to consider the actual conditions in the source, primarily the extent of the source in the corona and the velocity dispersion of the emitted electrons. As we know, the emission at each frequency propagates at its own group velocity, which is also different for different modes (Ginzburg, 1967):

$$V_{\mathrm{gr}} = c/[N_{\mathrm{o,e}} + f(dN_{\mathrm{o,e}}/df)], \tag{3.13}$$

where $N_{\mathrm{o,e}}$ is the refractive index for for *o*- and *e*- waves, c is velocity of light. The group velocity varies only at the frequencies for which the refractive index $N_{\mathrm{o.e}}$ <<1. Therefore the group delay in the solar corona can be taken into account on a distance of the order of three solar radii. The group propagation time can be calculated from the expression:

$$t_{\mathrm{gr}} = \int_{\rho_s}^{4R_\odot} \frac{d\rho}{V_{gr}} \ , \tag{3.14}$$

where ρ_s is the distance from the emitting source to the center of the Sun in solar radii $R_\odot$. Simple estimates (Zheleznyakov & Zatsev, 1975) and certain calculations (Elgarøy, 1969; Chertok, 1973) indicate that the propagation time difference for signals of different frequencies (and different modes) is usually small ($\approx$0.1-0.2 s). The mechanism of emission and the extent of the generating region at one frequency were usually left out of account, although these both factors would probably play an important role in forming the dynamic spectra of short-lived bursts.

The group propagation time was calculated on the basis of (3.14) using quasi-longitudinal approximation for $N_{\mathrm{o,e}}$:

$$N_{o,e}^2 = 1 - \frac{f_{Pe}^2 / f^2}{1 \pm (f_{Be} / f) |\cos\alpha|}, \qquad (3.15)$$

where α is the angle between the propagation direction and the magnetic field. A plasma mechanism was assumed for generation of the emission, whose frequency was set equal to the Langmuir frequency $f = f_{Pe}(1+3V_{Te}^2/V^2)^{1/2}$, where the approximation $k_t \approx \omega/V$ was used for the wave number of the Langmuir waves. Substituting (3.15) into (3.13) and (3.13) into (3.14), we obtain:

$$t_{gr} = \frac{R_\otimes}{c} \int_{\rho_s}^{4} \left\{ \left(1 - \frac{f_{Pe}^2 / f^2}{1 \pm (f_{Be}/f)|\cos\alpha|} \right)^{1/2} + \frac{f_{Pe}^2 / f^2}{2\left(1 - \frac{f_{Pe}^2 / f^2}{1 \pm (f_{Be}/f)|\cos\alpha|} \right)^{1/2}} \right\} d\rho$$
$$\times \left[(1 \pm (f_{Be}/f)|\cos\alpha|)^{-1} + (1 \pm (f_{Be}/f)|\cos\alpha|)^{-2} \right] \qquad (3.16)$$

The value of $\cos\alpha$ was assumed to be near unity. Since the calculation is made only for the meter range, it is possible to use the corresponding models for the electron density $n_e = 16.52 \cdot 10^4 \cdot 10^{4.32/\rho}$ cm^{-3}, which is double the density in Newkirk's model (Newkirk, 1961), and the magnetic field strength $B = 0.05\rho^{-1} \cdot 10^{2.16/\rho}$ G. This last model was obtain from radio observations (Fomichev & Chertok, 1968) and it ensures a magnetic field of about 2 G at the level of f_{Pe} = 200 MHz.

Then the relations for f_{Pe}/f and f_{Be}/f are simplified to $f_{Pe}/f = 1/(1+3V_{Te}^2/V^2)^{1/2} = 1/b$, $f_{Be}/f_{Pe} = a/\rho$, where a is a constant equal, for example, to 0.385 for B = 2.3 G. After substitutions, expression (3.16) is reduced to tabular integrals, and we can obtain an analytic expression that greatly reduces the volume of the calculations (see in details Chernov, 1990c).

It is important to note that simple replacement of the transverse-wave frequency by the Langmuir frequency for the integration of (3.16) (this is implied in the calculations of many authors (in particular, of Elgaroy (1969) and Chertok (1973)) may give incorrect results, since in so doing we replace the dependence of V_{gr} on the wave number of the transverse wave, $V_{gr} = \partial\omega/\partial k_t$, by the dependence of multiplier b on the velocity V, i.e. use the wave number of the Langmuir waves, $k_t = \omega/V$. Since $k_t << k_t$ the calculation should replace the dependence of b on V with the dependence of b on k_t, which is a function of k_l as a result of differential scattering of plasma waves on thermal ions. Such an expression for k_t was used in Chernov (1990c), based on formula (12.6.1.5) in Akhiezer (1974).

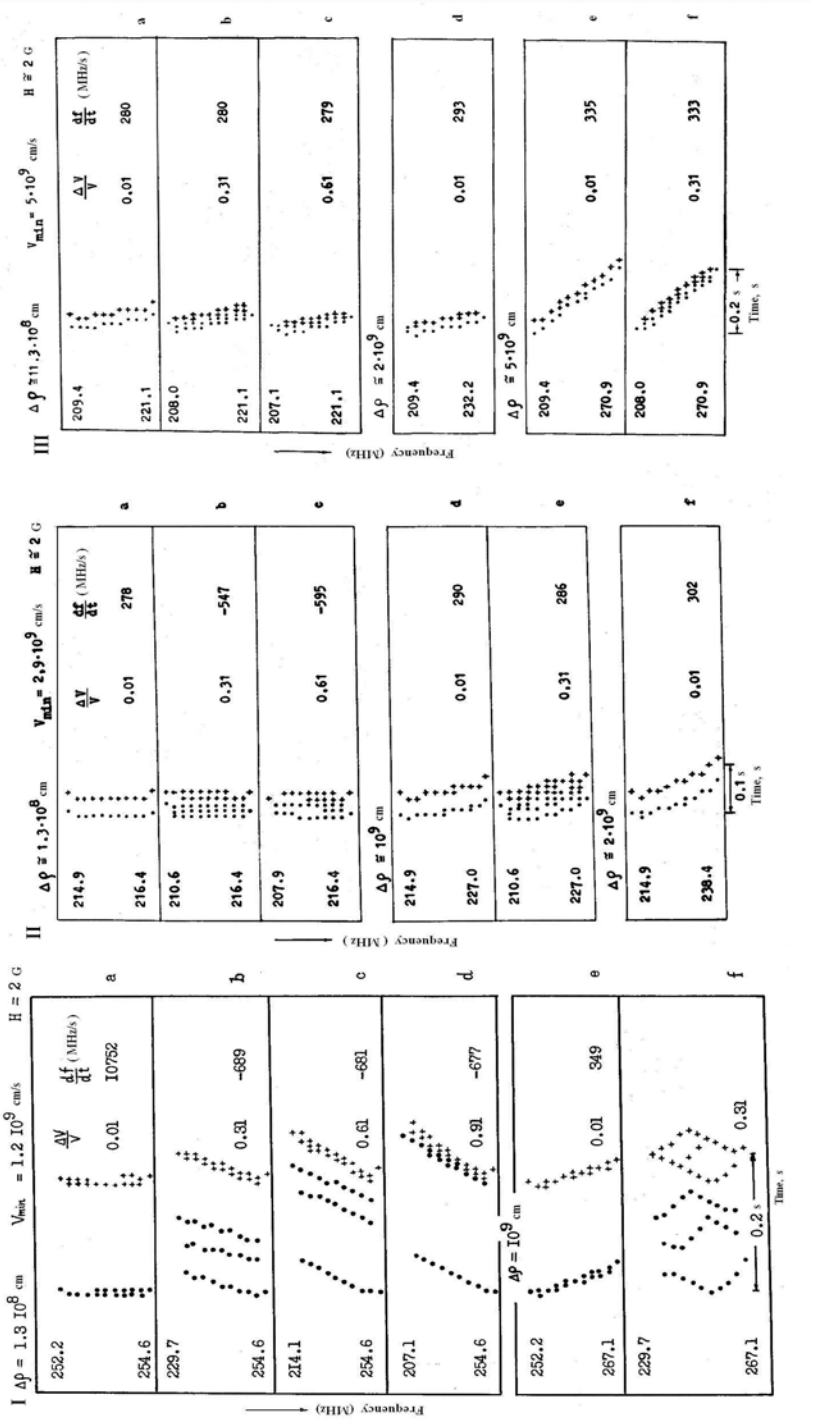
I
II
III
Frequency (kHz)
Time, s
0.2 s
0.1 s

Fig. 3.27 Examples of dynamic spectra (in three columns, I, II, III) calculated for instantaneous burst distorted by group delay of radio emission at minimum electron velocity $V_{min} = 1.2 \cdot 10^9$ cm s^{-1} in a magnetic field $B = 2$ G for two source sizes ($\Delta\rho$). The dots represent the position of the ordinary wave and the crosses those of the extraordinary wave; the frequency ranges studied are indicated at the left, the time scales at the bottom, and the values used for the velocity dispersion $\Delta V/V$ and the calculated frequency drift rates df/dt at the right of the spectra (Chernov, 1990c).

The calculations covered various combinations of source dimensions $\Delta\rho$, electron velocities, and velocity dispersion $\Delta V/V$. The source leading edge was located at the plasma level $f_{Pe,fr} = 206.866$ MHz, where, according to the model, $\rho_{fr} = 1.231853$, and ten source sizes were taken at intervals of about 10^8 cm for small dimensions and 10^9 cm for more extended sources.

It was assumed that radio emission is excited instantaneously in this fixed source. The calculation was performed for the *o*- and *e*- waves with several magnetic field values (from 1 to 10 G) with a preliminary check of the condition for escape of the latter from the source. The entire burst frequency band was divided into 11 equally spaced fixed frequencies. The program constructed the dynamic spectrum of the instantaneous frequency band with distortion by the group delay. The results are presented in Figure 3.27 in three columns (I, II, III).

The calculations indicated that in most cases the group delay in the burst band is so small that it is difficult to detect it in the dynamic spectrum. Thus, the group delay $\Delta t_{gr} \approx 0.07 - 0.09$ s is obtained for a velocity $5 \cdot 10^9$ cm s^{-1} and source sizes from 10000 to 20000 km (Figure 3.27, columns IIIa and IIId). The most interesting effects are observed with low electron velocities (column I) as a natural result of the approach of the source to the level at which the waves can escape from the corona, i.e. with the decrease of V_{gr}. In this case, the group delay from a compact source (of ~10^8 cm) creates a negative frequency drift (about –680 MHz s^{-1} (Figure 27, Ib, c, d). As the source became larger (of ~10^9 cm), the delay in propagation through the source becomes noticeable at high frequencies and results in a positive frequency drift (Ie). At large velocity dispersion we then observe a sign change of the frequency drift in the burst band (If). This is a very subtle effect, however, because the burst front curves on a time segment of 0.036 s. It is interesting that the trailing edge of the burst is also cured, but antisymmetrically with respect to the leading edge. This unsteadiness of the frequency drift results from the fact that when the velocity dispersion is large, radiation at a given frequency escape from the corona in a rather extended range of heights. Here, the roles of the two competing group-delay effects (high-frequency delay in propagation through the source and low-frequency delay due to the decrease in V_{gr} near escape level) are opposed to one another at the upper and lower points of this interval.

At small velocity dispersion ($\Delta V/V < 0.1$), the difference between the delays of the o- and e- waves causes splitting of the burst into two parts with different polarization. This splitting was predicted in Elgarøy (1969) for double bursts with reverse drift, for which delays of approximately 1 – 2 s were obtained. These calculations indicate that when the emission mechanism and the extent of the generating region at a given frequency are taken into account, the split components may have either positive or negative drift, depending on the

have either positive or negative drift, depending on the dimensions of the source (negative drift is associated with compact sources). However, the maximum splitting is only about 0.16 s (Ia, d, e), and the second component has mixed polarization in the case of wide dispersion in a compact source (Ic, d). This splitting is attained only as a result of the delay of the *e*- wave near its escape level with low particle velocities of $V \approx 2.5\ V_{Te}$. In this case the Landau damping by the thermal plasma becomes significant, with the result that the split bursts can only be extremely weak. It is weak type I bursts that have shown variation (and even sign changes) of polarization in noise storms (Chernov et al. 1972).

As we go to higher velocities, the splitting between *o*- and *e*- waves decreases: at $V = 2.9 \cdot 10^9$ cm s^{-1} it is approximately of 0.05 s (Figure 3.27, IIa, d, f), and at $V = 5 \cdot 10^9$ cm s^{-1} it is difficult to detect (see column III), consistent with the observations of Chernov et al (1972).

Another important inference follows from these calculations. We see from Id, IIf, IIId, f that if the source parameters support an instantaneous broad emission band ($\geq 30 - 50$ MHz), the group delay produces no noticeable frequency drift (high slope in dynamic spectrum). The radiation from the compact source acquires a negative drift of – 600 MHz s^{-1} (Figure 3.27.I). In this case, screening of the e-wave may even mean that there are no paired bursts with different polarization. Calculations indicate that this wave would not escape from the source if the magnetic field exceeds of 5 G.

A positive frequency drift of about 300 MHz s^{-1} occurs with high particle velocities in an extended source. It is these weak broadband spike bursts that are sometimes observed during noise storms and type IV bursts (Bakunun & Chernov, 1985).

Thus, the group delay is too small, it can cause only very large frequency drift. This means that the frequency drift due to motion of the radiating agent in the corona (which, for example, amounts to about – 100 MHz s^{-1} for type III bursts at the discussed frequencies) cannot be affected noticeably by group delay. Such increases are too small that they cannot be used to explain the total compensation of frequency drift as proposed in Elgarøy (1980). If such compensation did indeed occur, type III bursts with moderate drift rates would never be observed because the group delay cannot be switched in for some bursts and switched out for others. It is always created in the corona, but this effect is weak. It is also impossible to use group delay to explain the frequency drift of '*s*'- burst as proposed in Zaitsev & Zlotnik (1986).

3.3.2 Ion-sound model of microwave spikes

As we noted above, the ECME mechanism is encountered serious problems at interpretation of microwave spikes, though the authors forget often to remind about that in their conclusions (Fleishman & Melnikov, 1998). The main obstacles are

the high values of the magnetic field strength in a source, at times exceeding those at photosphere level.

To avoid some difficulties Wang & Li (1991) proposed a model of nonlinear parametric instability for millisecond spikes. But except definitive difficulties with the carrying-out of the matching conditions for the coupling process of two electromagnetic waves with whistler wave, the pump electromagnetic wave must be strong for the nonlinear parametric instability. It should be to propose also enough seldom conditions high in the solar corona for a whistler instability with very small whistler wave numbers $k_w << \omega_{Pe}/c$. Moreover such model can explain only strictly periodic spikes.

The solution of the nonlinear Shrödinger equation for the pump wave in Wang & Li (1991) with the consideration of the Miller force (ponderomotive force in the equation of the electron motion) contradicts to the conclusion of Wentzel & Aschwanden (1991): the maximum energy density inferred in the spike emission by ECME is at least two order of magnitude less than the energy density at which electron entrainment sets in.

Thus we have not so far a well accepted emission mechanism to explain main spike parameters at microwaves. Although there is general agreement, that the emission mechanism has to be coherent, it is unclear whether it is by gyroemission or plasma emission as one proposed in Altyntsev et al. (1998).

Chernov et al. (2001a) proposed that the propagation of fast shock fronts through the microwave source could generate fast bursts of spikes. They discuss the model of spike emission due to the coalescence of Langmuir waves with ion-sound waves.

According the observations discussed in Chernov et al. (2001a), spatial and time coincidence of HXR and microwave sources testifies about the same fast particles responsible for those emissions and a common acceleration source which is usually proposed connected with magnetic reconnection at middle heights in the corona ($\geq$ 10000 km). Fast particles accelerated in such a region can propagate upward direction and cause meter radio bursts and downward direction and cause successively decimetric, microwave and HXR emissions. Similar scheme was proposed for spikes by Fu et al. (1990) at the wavelength =21 cm.

According to well accepted ideas shock fronts are the place of Langmuir, ion-sound and whistler instabilities. All these waves are usually observed in situ observations in interplanetary shocks and in the front of earth bow shock (Gurnett et al., 1979).

According to conclusions from the observations of microwave spikes (Figure 3.14) a mechanism of spike emission must operate in direct association with shock fronts, where Langmuir and ion-sound waves instabilities are developed. Therefore the most probable mechanism of spike emission may be the interaction of plasma Langmuir waves with ion-sound waves $l+s \rightarrow t$. This process is well studied by Tsytovich (1970), and for type I bursts by Melrose (1980) and Benz & Wentzel (1981), and in a direct connection with decimetric spikes was firstly proposed by Kaastra (1985).

As Benz and Wentzel (1981) proposed, ion-sound waves are generated by current driven instability in a current sheet in a small magnetic reconnection region.

The waves generate an anomalous resistance and create the conditions for their existence with $T_e >> T_i$. Although Melrose (1989) believes, that the mechanism by which these wave are generated is not understood and there is no basis for expecting them to be present in the corona other than by analogy with the interplanetary medium (Gurnett et al.1979). In such a case ion-sound waves could be really present only in the narrow shock fronts. In the same time all energetic estimations of Benz & Wentzel (1981) for the coalescence $l+s \rightarrow t$ remain available for our consideration here. However the three wave matching conditions was not strictly verified.

To be certain in a reality of the resonance coupling l and s waves in the solar corona we must verify the matching conditions of frequency and wave vector at the sum frequency $l+s \rightarrow t$ and at the difference frequency $l \rightarrow t+s$ (the decay process):

$$\omega_l \pm \omega_s = \omega_t , \qquad k_l \pm k_s = k_t \tag{3.17}$$

to determine the ranges of possible angles between the wave vectors of all resonance modes and magnetic field direction **B** (θ_l, θ_s, θ_t).

Therefore we use simple dispersion relations for all modes but with allowance for the magnetic field:

$$\omega_l^2 = \omega_{Pe}^2 + 3k_l^2 V_{Te}^2 + \omega_{Be}^2 \sin^2 \theta_l , \tag{3.18}$$

$$\omega_t^2 = k_t^2 c^2 + \omega_{Pe}^2 \left(1 + \frac{\omega_{Be}}{\omega_t} \cos \theta_t \right)^{-1} , \tag{3.19}$$

$$\omega_s^2 = k_s^2 \upsilon_s^2 . \tag{3.20}$$

It is evident from the dispersion curves that only ordinary wave can participate in such an interaction, at least for usual wave numbers k_l and $k_s \geq \omega_{Pe}/c$ which are the most probable when the emission source is located between the escape levels of ordinary and extraordinary waves, although according to Tsytovich (1970) in the whole range of k_s, i.e. $\omega_{Pi}/\upsilon_s < k_s < \omega_{Pe}/V_{Te}$ ion-sound waves can interact with Langmuir waves. We simplify the first two equations using expansions subject to the condition that their second and third terms are small and $\omega_{Pe}/\omega_{Be} >> 1$:

$$\omega_l \approx \omega_{Pe} \left(1 + \frac{3k_l^2 V_{Te}^2}{2\omega_{Pe}^2} + \frac{\omega_{Be}^2 \sin^2 \theta_l}{2\omega_{Pe}^2} \right) , \tag{3.21}$$

$$\omega_t \approx \omega_{Pe} \left(1 + \frac{k_t^2 c^2}{2\omega_{Pe}^2} - \frac{\omega_{Be}}{2\omega_{Pe}} \cos \theta_t \right) . \tag{3.22}$$

We substitute these expansions in the first resonance condition (3.17) $\omega_l \pm \omega_s = \omega_t$, then determine k_t^2 from the result, and substitute it in the relation for wave numbers:

$$k_t^2 = k_l^2 + k_s^2 \pm 2k_l k_s \cos\theta \ , \tag{3.23}$$

where θ is the angle between the vectors $\mathbf{k}_l$ and $\mathbf{k}_s$. We obtain:

$$k_t^2 = \frac{1}{c^2}\left(\omega_{Pe}\omega_{Be}\cos\theta_t + \omega_{Be}^2 \sin^2\theta_l + 3k_l^2 V_{Te}^2 + 2k_s \upsilon_s\right) . \tag{3.24}$$

Using the procedure to eliminate k_t we estimate $\cos\theta_t$:

$$\cos\theta_t = \frac{k_s^2 c^2}{\omega_{Pe}\,\omega_{Be}}\left[\frac{k_l^2}{k_s^2}\left(1 - 3\frac{V_{Te}^2}{c^2}\right) \mp 2\frac{k_l}{k_s}\cos\theta + 1\right] - \frac{\omega_{Be}}{\omega_{Pe}}\sin^2\theta_l \pm 2\frac{k_s \upsilon_s}{\omega_{Be}} \ . \tag{3.25}$$

Here the ratio k_l/k_s is used as a convenient parameter. It is easy to verify that for small values of θ_l and θ, justified by the evident fact that the coalescence $l+s \rightarrow t$ and the decay $l \rightarrow t + s$ take place respectively with almost antiparallel or parallel wave vectors $\mathbf{k}_l$ and $\mathbf{k}_s$ (an analogy exists with the similar processes of Langmuir waves and whistlers (Fomichev and Fainstein, 1988; Chernov and Fomichev, 1989)) and for a small magnitude of the ratio $\omega_{Be}/\omega_{Pe} \sim 0.1$, the quantity $\cos\theta_t$ is determined mainly by the last term in (3.25). Taking into account that the lower sign corresponds to the process at the sum frequency $l + s \rightarrow t$ with $k_l \approx -k_s$ and the upper sign to the process at the difference frequency $l \rightarrow t + s$ with $k_l \approx k_s$ and that $k_s \upsilon_s = \omega_s$, we can write:

$$\theta_t \approx \mp \arccos 2\frac{\omega_s}{\omega_{Be}} \ . \tag{3.26}$$

The angle θ_t is somewhat larger or smaller than this value, depending on the sign of the bracketed term in (3.25); the sign, in turn, is governed mainly by the ratio k_l/k_s , which is very close to unity, i.e., k_t is directed in the side of the biggest from k_l, k_s . The bracketed term in (3.25) changes sign when

$$\left(\frac{k_l}{k_s}\right)^2\left(1 - 3\frac{V_{Te}^2}{c^2}\right) - 2\left(\frac{k_l}{k_s}\right)\cos\theta + 1 = 0 \ . \tag{3.27}$$

In such a case

$$\frac{k_l}{k_s} = \frac{\pm\cos\theta \pm \sqrt{\cos^2\theta - (1 - 3V_{Te}^2/c^2)}}{1 - 3V_{Te}^2/c^2} \ . \qquad (3.28)$$

In order for k_l/k_s to be real-valued, it is necessary that $\cos^2\theta - (1 - 3V^2_{Te}/c^2) > 0$, i.e., $\cos\theta > \pm\sqrt{1 - 3V_{Te}^2/c^2}$, so the upper bound of the angle $\theta < 1.28^\circ$ is obtained at the coronal temperature $T_e = 10^6$ K, or for $V_{Te} \approx 3.89 \times 10^8$ cm s^{-1}, and $\theta < 8.14^\circ$ for $T_e = 2 \times 10^7$ K. We then obtain from (3.28) the two values k_l/k_s = 1.00235 and 0.99816, i.e., the bracketed term in (3.28) changes sign when the ratio k_l/k_s passes through unity. The evident condition $|\cos\theta| < 1$ leads to the limitation of k_s from above: $k_s < 0.5\omega_{Be}/v_s$. This value is about two times bigger than the Debye length $k_D = \omega_{Pe}/V_{Te}$, therefore the interaction is possible in the whole range of k_s and $k_l \approx k_s$. The range of θ_t for a simple rough estimation from (3.26) will determined by the frequency range of *s*-waves: $\omega_{Bi} < \theta_s < \omega_{Pi}$. Substituting these limiting frequencies in (3.26), we obtain that the decay at the difference frequency yields the emission of *t*-waves in the range of angles $62^\circ < \theta_t < 89^\circ$ and, respectively, for the coalescence at the sum frequency $91^\circ < \theta_t < 118^\circ$.

According to Benz and Wentzel (1981) *ls*-interaction becomes the most efficient with a high intensity of *s* waves, when unit optical thickness is reached over merely a few meters. It is easy to show that in an optically thick source the interactions at the frequencies $\omega_t = \omega_l \pm \omega_s$ can be equally efficient and the maximum brightness temperature can be derived (similar to the procedure in Benz and Wentzel (1981) and in Chernov and Fomichev (1989)):

$$T_b = \frac{h\omega_{Pe}}{K_B} \frac{N_s N_l}{N_s \pm N_l} \ , \qquad (3.29)$$

where h is Planck's constant, K_B is Boltzmann's constant, and N_l, N_s are the dimensionless wave intensities ($N_l << N_s$) (or wave quantum densities). That is the theoretical estimation. From the observation we obtain:

$$T_b = \frac{2\pi^2}{K_B} \frac{W_t}{k_t^2 \Delta k_t} = \frac{0.143 \cdot 10^7 S}{f^2 l_{10}^2} exp^{\tau} \ , \qquad (3.30)$$

where τ is the optical depth of the solar corona for the electromagnetic emission. Here, the designations are similar to Fomichev and Fainstein (1988): S(s.f.u.) is the burst flux in solar flux units, f is the frequency in GHz, and l_{10} is the linear source size perpendicular to the line of sight in units of 10^{10} cm. So that with a flux emission 100 s.f.u. and a burst source of 10^8 cm we obtain the observed $T_b \approx 7 \times 10^{13}$ K, i.e., close to the value predicted in Benz and Wentzel (1981), for instance, with a small value of density energy of plasma wave $W_l \approx 10^{-7}$ erg cm^{-3}

for isotropic *l*-waves, and $W_l = (h/(2\pi)^3)\omega_{Pe}N_l k_l^2\, \Delta k_l \Omega_l$. So with a solid angle $\Omega_l \leq 1$, $k_l \approx \Delta k_l \approx 5 \times 10^{-2}$ cm^{-1} we find from (3.29) for $N_l << N_s$, $T_b \approx 5.7 \times 10^{13}$ K.

Here, the duration of a separate spike is not connected with the parameters of a beam of fast particles (as in the beam instability). It can be determined by the local very short time of recovery of the nonisothermicity of plasma (after a burst from the miniature region) and subsequent temperature balance. Specifically, this chaotic process of spike release from the turbulent plasma can explain the chaotic appearance of spikes in the clusters, which count hundreds and thousands of bursts.

The model under discussion helps us to propose a new explanation of the observations of decimetric spikes at harmonics '*s*' = 2–6 (Güdel, 1990). The relativistic ECME seems implausible in the decimeter range, where the plasma emission mechanism usually plays a main role. As a detail, conformity of spikes at different harmonics was not observed. We may relate the emission of consecutive frequency bands of spikes with consecutive magnetic islands with X- point configurations along a vertical magnetic current sheet. Frequency bandwidths at each harmonic show the vertical size of a zone between two fast shock fronts propagating from one X- point, and the frequency separation between the centers of each spike band (or harmonic frequency) is defined by the size of magnetic islands between X-points. Multiple magnetic islands are usually supposed during the restoration of the magnetic structure after the escape of CMEs and were obtained in multiple numerical modelling of magnetic reconnection.

3.4 Summary

We have presented all the currently available observational data on radio spikes, the most short-living solar bursts ($\lesssim 0.1$ s). We have tried to analyze through meter, decimeter and microwave ranges, since such a full analysis is absent in any review or book. In the meter range the spikes are more often observed in noise storms, and sometimes they are a superfine structure of type I bursts. Although, spikes reveale their own superfine structure, in the form of frequency and time splitting. Spikes are also observed in the type III group bursts, but they appeared independently of the latter. The spikes are usually strongly polarized with the same sign as type I and III bursts. Therefore, the spike emission was rather related with ordinary wave. Only spikes observed in type II bursts were unpolarized, as the whole type II emission. Several available positional observations gave unexpectedly large dimensions of the spike sources, of 70'' – 400'' in the meter range and $\lesssim$ 15'' at microwaves. It is possible to select two types of spikes observed in the type IV bursts: very short-time ($\approx$ 0.02 – 0.05 s) dot-like spikes (most frequently being observed in the decimeter range where they appear as klusters of hundreds of bursts), and broadband short-lived spikes (spike brightenings). All parameters of spikes in the meter range indicate the plasma generation mechanism (the beam instability). The high degree of polarization and the absence of spikes at

the harmonic (2:1) frequencies testify that spikes emit at frequencies near the local plasma frequencies. The modeling of spike profiles and calculations of the group delay from the spike source confirm the plasma emission mechanism for spikes. The ECME mechanism runs into serious problems when interpretating the microwave millisecond spikes: the main obstacles are too high values of the magnetic field strength in the source ($\omega_{Pe} \leq \omega_{Be}$). The probable mechanism is the interaction of plasma Langmuir waves with ion-sound waves ($l+s \rightarrow t$) in a source related with shock fronts in the reconnection region. In such a case, the duration of a separate spike is not connected with the parameters of fast particles (as in the ECME mechanism). It can be determined by the local very short time of recovery of the nonisothermicity of plasma (after a burst from the miniature region) and subsequent temperature balance. Specifically, this chaotic process of spike release from the turbulent plasma can explain the chaotic appearance of spikes in the clusters. Below, section 5.3.1 will be dedicated to the analysis of millisecond spikes in the absorption, because of their connection with the zebra pattern.

Chapter 4

Zebra pattern and fiber bursts

Already the first spectral observations of the large type IV (and II+IV) bursts revealed a rich variety of the fine structures of the radio emission, in particular, a modulation of the continuum emission in the form of narrow stripes in the emission and absorption. Stripes in emission and absorption against the continuum background of solar type IV radio bursts in the meter and decimeter wave ranges are traditionally subdivided into two kinds: zebra pattern (ZP) and fiber bursts (FB) (or intermediate drift bursts (IDB)). (Kuijpers 1975a; Slottje 1981). Since the end of the seventies, microwave observations of solar emission with high temporal and spectral resolution have also shown fine structures: millisecond spikes (with a duration of single spikes of a few tens of milliseconds), and fast pulsations, usually superimposed on a smooth continuum emission (Benz, 1993). We could also find some indications of a probable zebra pattern in the microwave range in Isliker and Benz (1994).

The new solar broadband radio spectrometers of NAOC (China, Huairou station) with higher resolution (10 MHz and 5 – 8 ms) can observe detailed zebra patterns and fiber bursts at high frequencies, 2.6 – 7.6 GHz (Chernov et al. 2001b). In the microwave range, the same variety of fine structures is observed. Thus the relative frequency parameters of zebra structures in microwave and meter wave bands appear identical. This testifies to the identical nature of the formation of fine structure in different frequency ranges. Some recent observations with a time resolution of 0.1 s, using Ondˇrejov radiospectrographs in the range 0.8-4 GHz, have allowed us to find new properties of zebra structures and to verify theoretical models (Ledenev et al. 2001; Karlicky et al. 2001; Sawant et al. 2002b).

We have to examine the historical interval of studies of ZP and FB for four solar cycles, since the previous surveys were either very brief (Fomichev and Chertok 1977)), or limited only to the description of the observed properties of fine structure in the meter range (Slottje 1981) or to short theoretical description of the generation mechanisms (Kuijpers 1980). It is important to emphasize the most significant moments of all past studies without repeating all details, contained in the well-known reviews. In the recent years, observations of fine structures have been considerably expanded and new properties of ZP and FB have been revealed. At present, the analysis of new events usually implies a more thorough study of flare processes in the X-ray emission (Yohkoh, RHESSI) and the ultraviolet lines (SOHO, TRACE). It is therefore important at this stage to identify new properties of the fine structure observed at various frequencies and to analyze them in the context of various theoretical models; this is the goal of the current section.

4.1 Observations

ZP and FB were recorded at the end of the fifties by observations with the first spectrographs. The first narrow stripes in emission and absorption were observed in the event on 4 November, 1957 (Boischot et al. 1960). The short description of this event entered in the monographs on 1964 (Zheleznyakov 1970; Kundu, 1964), where a special attention was turned to the very characteristic property of stripes - close mutual arrangement of the stripes in emission and absorption. The name 'zebra pattern' was introduced by Slottje (1972) as most adequate to observations, after the detailed measurements of the frequency separation between stripes by Elgarøy (1971), testifying about, that they are not always parallel between themselves. But the first front-pager about the observations of zebra structure was made by Elgarøy (1959, 1961) in the event August,18, 1959 (Figure 4. 1).

The basic properties of ZP were already visible based on this example: preferred drift to the high frequencies, at times the non-parallelism of stripes, the frequency separation between stripes increases with frequency, abrupt changes in frequency drift (hooks and jumps) and even a transition into the braided zebra pattern with drifting spikes as elements of such patterns. Then the set of the descriptions of separate events appeared, and between others *parallel drifting bursts* (PDB) in Tarnstrom and Plilips (1971), PDB- events, similar to ZP. Slottje(1972) opened new stage in study of non-stationary ZP in the event March 2, 1970.The first short survey about ZP and FB was included in the review of Fomichev and Chertok (1977), devoted to the fine structure. But the most complete description of properties of the ZP and FB in the meter wave band was represented in atlas of Slottje (1981). Young et al.(1961) the first reported observations of 'intermediate drift bursts' in the range 500 – 950 MHz in five events of 1959 (Figure 4.2).The authors noticed almost all basic properties of IDB: the presence of absorption ('shadow'), moreover as from the high-frequency edge, so from the low-frequency one; the wide spread of frequency drift to low frequencies and even the reverse drift; the bursts occur usually in regular groups with almost constant frequency spacing, but on some occasions as isolated bursts.

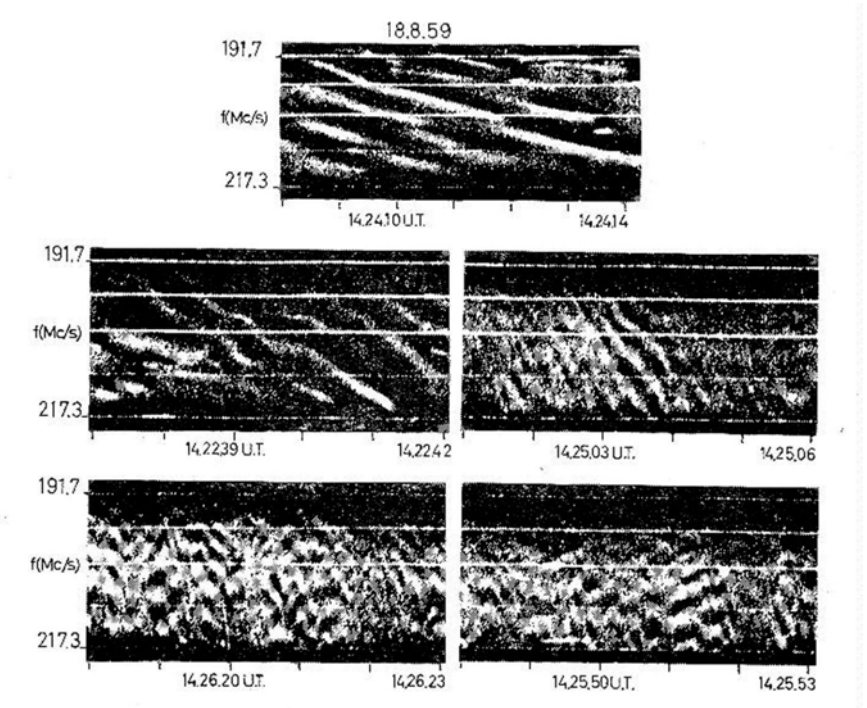

Fig. 4.1 An example of zebra structure in the event August 18, 1959 (from Elgarøy1961).

With the development of observations it became obvious, that this name 'intermediate drift bursts' (intermediate between the drift of types II and III bursts) did not always prove to be accurate, since the fibers were frequently observed with different frequency drift, also even of opposite sign. And gradually all authors began to call them simply 'fiber bursts', (finally after Slottje (1972)). The basic properties of FB are successfully represented by Kuijpers (1975a) (Figure 4.3), from the event March 6, 1972.

Kuijpers (1980) summarized basic observed properties of ZP and FB in the following Table 4.1.

If we do not turn attention to the different frequency drift of stripes, then all other parameters of ZP and FB have close values. Let us note, that in the section of Table 4.1 for the ZP there are no two lines (Duration and Single frequency

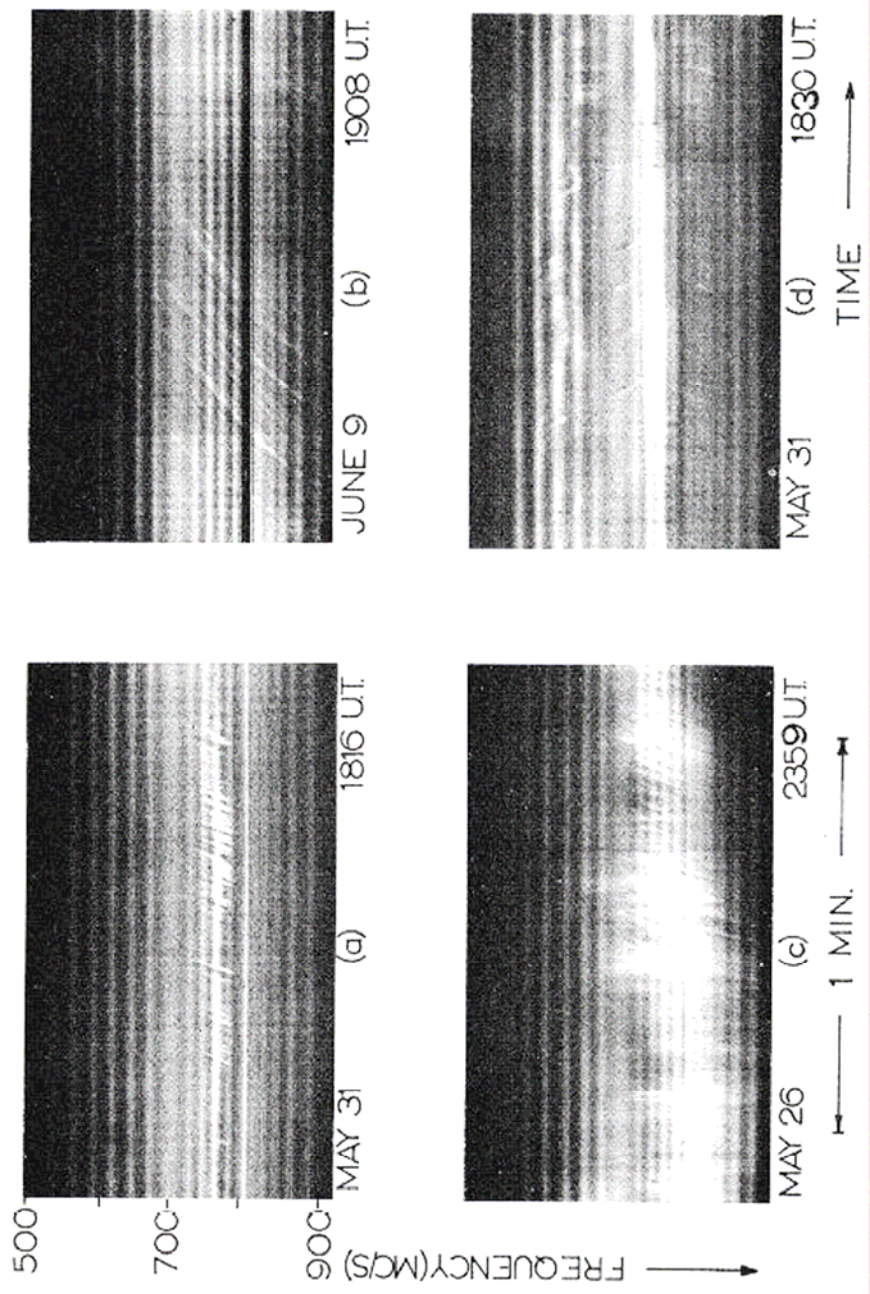

Fig. 4.2 Intermediate drift bursts in three events of 1959 (from Young et al., 1961).

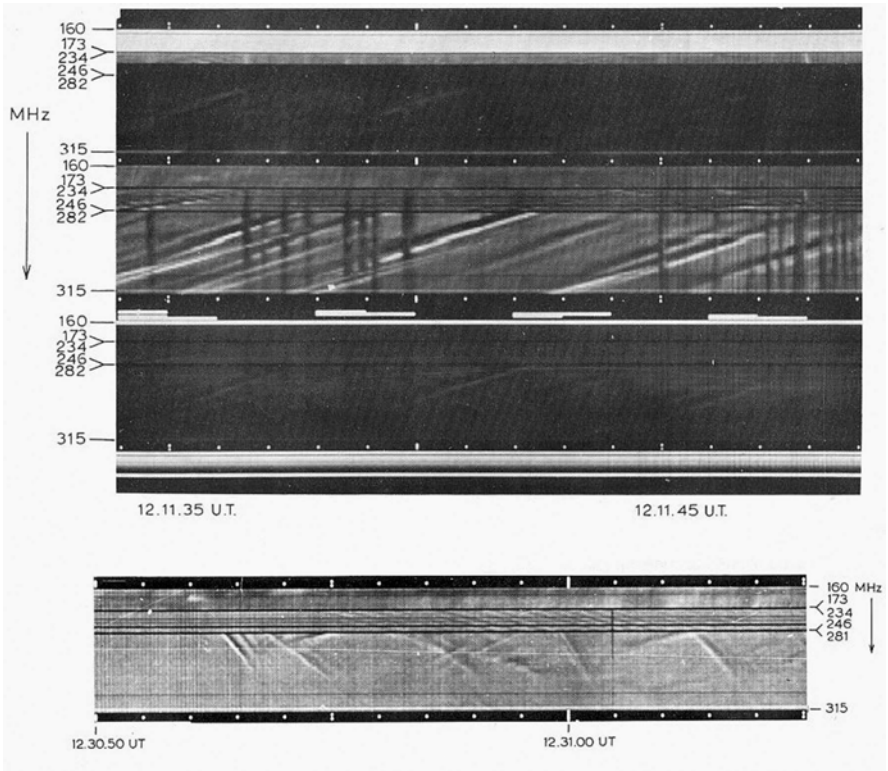

Fig. 4.3 Two examples of intermediate drift bursts observed with 60-channel Utrecht spectrograph on March 6, 1972. Each channel has a width of 0.9 MHz. In the top panel fibers are clearly visible on the sensitive channels in the middle. Lower part - normal channel, upper part - circular polarization (from Kuijpers, 1975).

duration), although for ZP approximately the same values are characteristic. Furthermore, generally there is no parameter of the frequency separation between emission and absorption (characteristic to both types of the structures). The large contribution to the statistics of observations of FB in the broad frequency range 150 – 1000 MHz was made by Elgarøy (1982) (Table II). He has found a linear dependence between frequency drift velocity and observed bandwidth, the duration at one frequency t_f is determined by the length of exciter rather, but not by electron collision time. He proposed to define the magnetic field strength B in different ways: the values obtained with frequency separation between emission and absorption $\Delta f_{ea} \approx b_t = f_w \approx 0.25 f_{Be}$, (where f_w - whistler frequency, f_{Be} - electron cyclotron frequency) are compared with values defined using df/dt in the

Table 4.1: Observed characteristics of ZP and FB (from Kuijpers, 1980)

Zebra patterns	
Frequency extent	$\geq$ 40 MHz
Number of consecutive stripes	5 – 20 (up to 70)
Stripe spacing at 160 – 200 MHz	2 – 3 MHz
at 800 – 900 MHz	20 MHz
Fiber bursts	
Frequency extent	30 MHz (up to 120 MHz)
Duration	5 – 10 s
Single frequency duration	0.2 – 0.4 s
Instantaneous bandwidth	$\leq$ 1 MHz
Drift rate, $-df/dt$	$10^{-2}f + 6\cdot10^{-5}f^2$ (Elgarøy, 1982)
number in one group	10 -30 (up to 300)
Flux at 160 – 320 MHz	200 sfu
at 50 – 600 MHz	500 sfu

form:

$$B=6.4(\ln f - 1.3)^{-2}\,|df/dt|, \tag{4.1}$$

if to identify the exciter velocity, defined by df/dt in the double Newkirk model with the group velocity of whistlers. He got a magnetic field of 1.4-1.8 G at 150 MHz, and about 13.5 G at 1000 MHz. These values give the plasma $\beta = nk_BT=(B^2/8\pi)$ nearest to 1 ($n = n_e + n_i$; $T = 1.5\cdot10^6 K$; k_B - Boltzman's constant, *e, i* - designate electrons and ions).

Sometimes the regularity of the ZP is not particularly strong and individual stripes show a FB profile. In this connection let us note, that for their more detailed comparison it is convenient to use the following parameters: the instantaneous frequency separation between the stripes (or spacing) Δf_s; the frequency separation between adjacent intensity peaks in emission and absorption Δf_{ea}; the instantaneous frequency bandwidth of a single emission stripe Δf_e; the full frequency bandwidth of all stripes in the spectrum Δf; the total number of stripes and their frequency drift df/dt.

Slottje (1981) and Elgarøy (1982) discuss the absorption mainly in FB. Elgarøy (1982) obtained the frequency profiles, using the microphotometer, and he found a nice symmetry between absorption and emission. The absorption was observed usually at the low frequency side in about

Table 4.2: Summary of observed parameters for FB (From Elgarøy, 1982)

	Frequency			
Parameters	150	300	500	1000
$\|df/dt\|$ (MHz/s)	3.1	7.5	23	66.5
t_f (s)	0.37	0.29	0.18	0.08
b_t (MHz)	1.1	2.1	3.6	>5
t_i (s)	0.2	0.2	0.1	(0.05)
b_i (MHz)	0.5	1.0	2.0	>2

$|df/dt|$- frequency drift velocity; t_f - duration at one frequency;
b_t - instantaneous bandwidth; t_i - intrinsic (or exciter) duration;
b_i - intrinsic bandwidth: $b_t = b_i + t_i|df/dt|$; $t_f = t_i + b_i|df/dt|$.

30% of all cases. Slottje (1981) noted that the absorption-emission character is also true for ZP. He measured the frequency separation between emission and absorption for FB and the frequency spacing between emission stripes for ZP. Two such distributions are shown in Figure 4.4.

The regularity of the instantaneous frequency spacing (Δf_s) is the most striking aspect of ZP. A closer look reveals that generally Δf_s increases with frequency (Chernov, 1976a). But sometimes, in one event the spacing changes with time up to a factor of two (Slottje, 1981).

The distribution shown in Figure 4a was constructed by Slottje (1981) using 79 events with ZP near 300 MHz. The histograms are cut of below 2 MHz due to the resolution limit of the spectrograph (the frequency spacing between channels).

The distribution of Δf_{ea} for FB (Figure 4b) continues up to zero values, but the values less than 2 MHz were obtained in frames of an assumption that $\Delta f_{ea} \approx \Delta f_e$, then the value of Δf_e, can be calculated more precisely using the drifting time between the channels. Slottje (1981) found, that about 56% of FB have the separation $\Delta f_{ea} < 1$ MHz.

Slottje (1981) denotes, that ZP often demonstrates some particularities. For example, discontinuous stripes within patterns (an intriguing phenomenon, crucial for the interpretation of ZP), appearance and disappearance of stripes amidst a continuous pattern. Hooks and jumps of stripes or wave-like frequency drift put also some additional questions for the interpretation.

Without repeating all properties of ZP, described in Slottje (1981), let us note the basic parameters of ZP and FB, which with the development of observations proved to be very important.

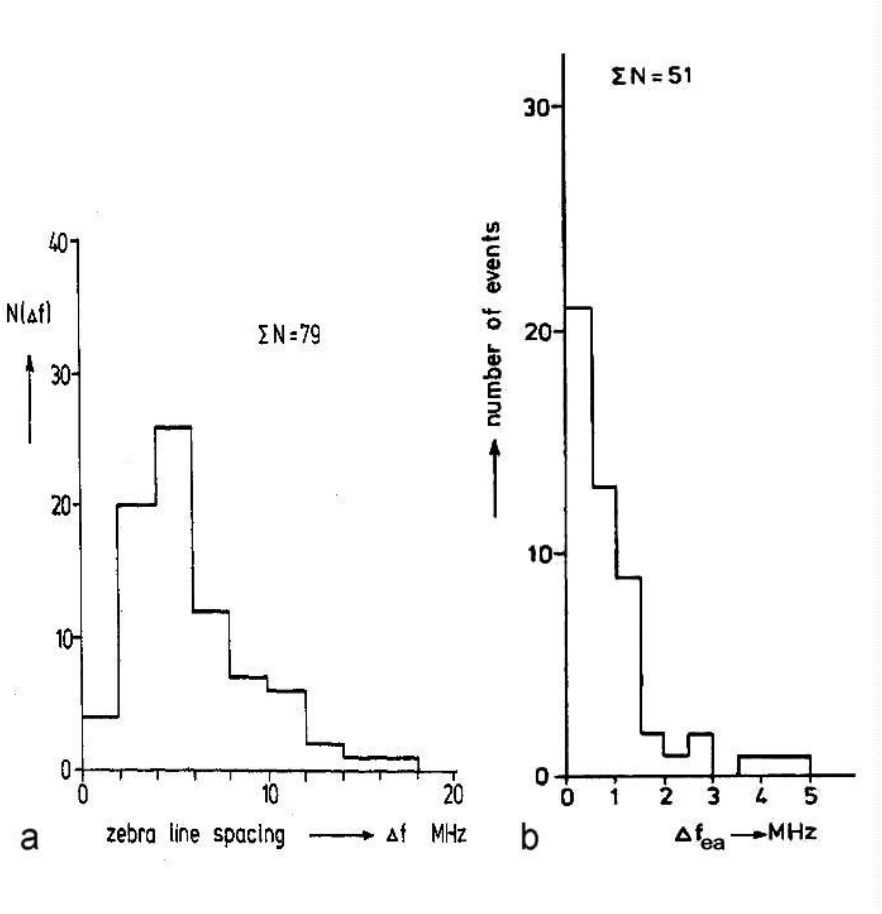

Fig. 4.4 The distribution of frequency spacing in zebra patterns in 79 events where a value was found *(a)*; and the distribution of the apparent frequency separation of emission and absorption of fiber bursts in 51 events where a value was found *(b)* (from Slottje, 1981).

The full frequency bandwidth of ZP and the total number of stripes are difficult to determine, because of the narrow frequency bandwidth of spectrographs. ZP and FB are usually observed as a modulation of the strong circularly polarized continuum emission, and zebra stripes as FB are also strong polarized in the same sign as continuum emission (Chernov et al., 1975, Chernov, 1976). Let us note the first important property: ZP and FB are usually observed against the background of type IV continuum emission with wide-band pulsations of radio emission. Among the latter Slottje (1981) has alluded, first of all, to pulsation in the absorption BSA (broad-band short-lived absorption pulses or 'sudden reductions' of background continuum intensity) and BEP (broad-band emission pulses), though

far less abundantly than BSA. This property must be considered as very important condition during the construction of a model of the formation of the stripes in emission and absorption.

The survey of the first observations showed already, that the frequency separation Δf_s smoothly increases with the frequency from 1 – 1.5 MHz at 150 MHz up to 10 MHz at 700 MHz (see figure 9 in Chernov (1976a)). Slottje encountered the difficulty of determining this dependence since the multichannel spectrograph (NERA station and Dwingeloo station after 1972, respectively with 60 channels between 160 – 320 MHz with the bandwidth of one channel of $\approx$0.9 MHz) did not make possible to accurately determine this parameter.

Slottje showed, that the instantaneous frequency bandwidth of a single emission stripe Δf_e is equal about to one half of the frequency spacing $\Delta f_s \approx 2 - 4$ MHz at a frequency range 160 – 320 MHz.

For fiber bursts Slottje (1981) draws conclusion, that $\Delta f_e \approx \Delta f_{ea} \approx 1 - 2$ MHz. This is rather true also for ZP, taking into account the conclusion of Slottje (1981), that the emission-absorption character of zebra stripes and FB is about the same. This was shown in figures 5, 6 and 7 in Chernov et al. (1975).

ZP and FB differ in the frequency drift: the zebra stripes drift usually synchronously (sometimes detecting very rapid oscillations), and FB have usually the constant (more often negative) drift velocity. However, in the atlas of Slottje (1981) it is shown already, that it is sometimes difficult to distinguish zebra stripes and FB, when they are almost continuously transforming into each other (e.g. see spectrum August 18 1970, 16:43 UT). Therefore Chernov et al. (1975) and Slottje (1981) draw conclusion, that the origin of both types of strips can be determined by the same mechanism.

The large spread of the values of all parameters indicates not a wide spectrum of the observed frequencies, but more likely the big variety of values in the different events. Therefore it is more important to compare the relative values of those parameters (relative to the observing frequency). Such a comparison of the ZP parameters in five events, observed in the recent time is given in Table 4.3.

In the Table 4.3 for 4 events (besides 1994 10 25) ZP and FB were observed practically simultaneously and their parameters were coincided on the value. The parameters $\Delta f_s/f$ and $\Delta f_{ea}/f$ grow with frequency, clearly in connection with the faster growth of the magnetic field than the density with decrease of the height. The parameter $\Delta f/f$ decreases with frequency, which corresponds to a decrease in the size of the radio sources in the lower corona. Only the quantity $\Delta f_e/f$ remains more stable. In four events, the radio fine structure corresponded to the ordinary mode. Since the statistical evidence is inconclusive, in the following presentation the primary attention we will give to several individual events.

Table 4.3: Parameters of the zebra pattern in five events (from Chernov, 2004).

Date Time UT	f(MHz) Frequency range	Flare Imp. Coordinates	$\Delta f_s/f$	$\Delta f_{ca}/f$	$\Delta f/f$	$\Delta f_c/f$	Magnenic polarity	Sign of polariza-tion Wave mode
1998 05 02 14:41	35 20 – 70	3B X1.1 S15W15	0.0036	0.0024	0.88	0.0035	S(N)	L R ?
1994 10 25 10:08	175 100 – 500	1N C4.7 S09W12	0.015	0.006	0.4	0.0049	S	R O
1999 07 28 08:15	360 45 – 520	1B M2.3 S15E03	0.014	0.006	0.22	0.0054	N	L O
1998 09 23 08:00	360 100 – 700	3B M7.1 N18E09	0.064	0.032	0.3	0.014	N	L O
2000 10 29 02:20	3000 1000 – 3800	2B M4.4 S25E35	0.033	0.015	0.16	0.0059	S	R O

4.2 Polarization

A question about the polarization of ZP and FB is one of the most crucial items for the construction of theoretical models. Let us pause at it in more detail, since in the old reviews the polarization was barely discussed (in the absence of authentic observations). Generally the ZP appears merely as positive and negative modulation of the strong polarized continuum emission. Quite often polarization outputs of the Utrecht spectrograph were saturated, and some quantitative values for the polarization degree were obtained by Chernov et al. (1975) for the event May 3, 1973, shown in the Figure 4.5.

Above north magnetic polarity of the leading spot in AR McMath 12336 (S14E51) the fully left polarized emission in this event corresponds to the ordinary mode.

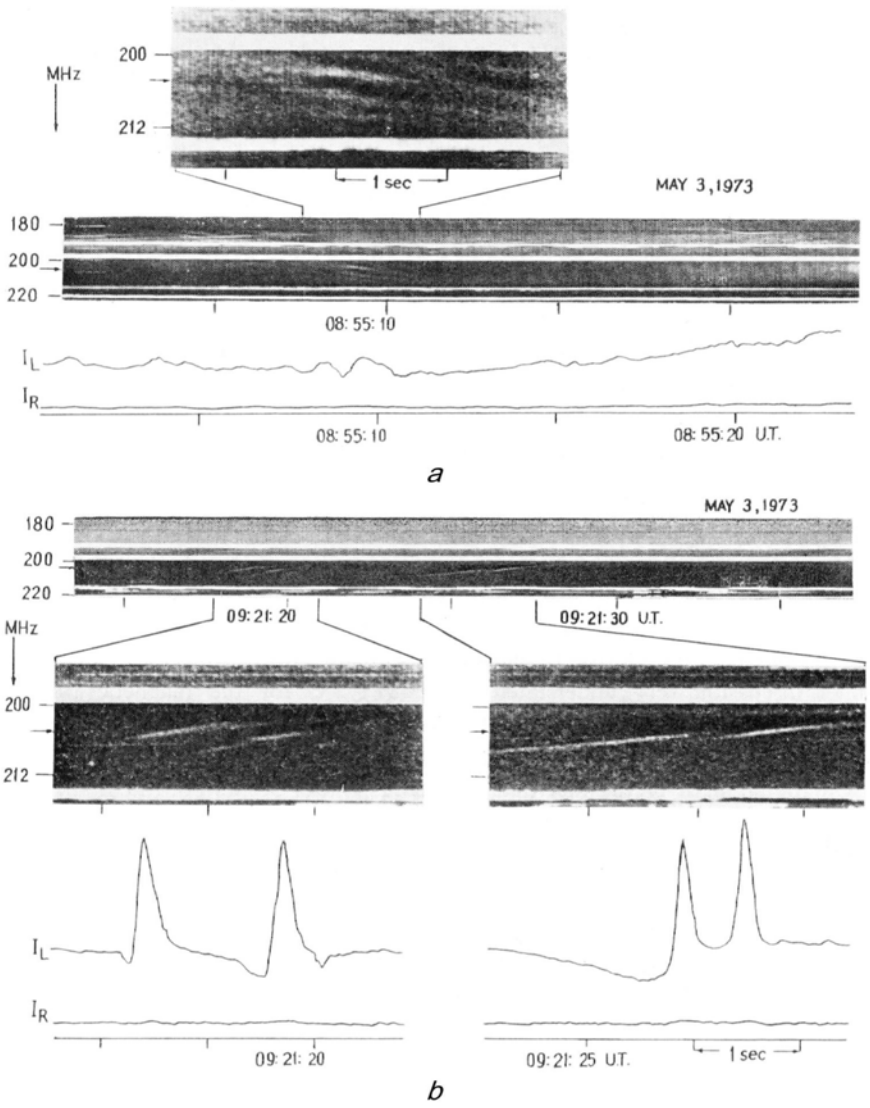

Fig. 4.5 Spectra and polarization profiles of ZP *(a)* and FB *(b)* with time resolution 0.02 s (IZMIRAN data) in the event May 3, 1970. The emission is fully left circularly polarized as for continuum as for fine structure. The frequency bandwidth of low-frequency absorptions is varying during different time moments (Chernov et al. 1975).

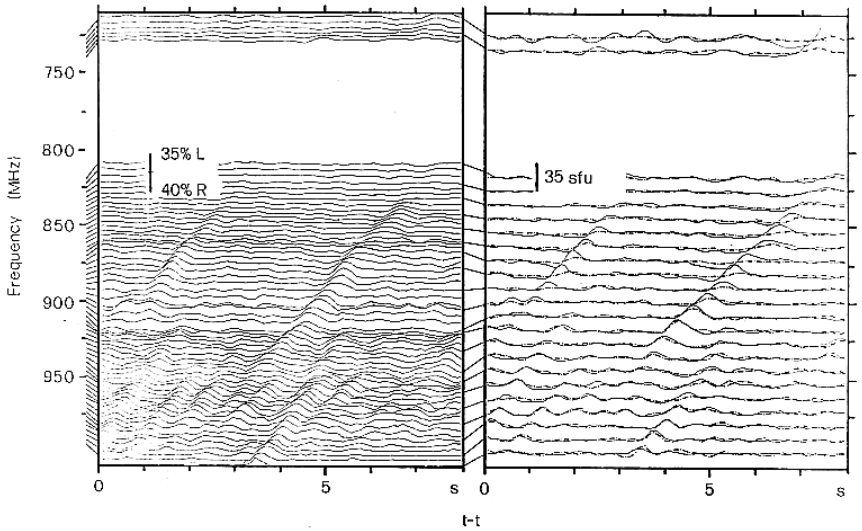

Fig. 4.6 Time profiles of the intensity (*left profiles*) and right (*dotted lines*) and left (*full lines*) circular polarization (*right profiles*) after subtraction of the continuum in the event November 22, 1981 (from Bernold, 1983).

The detailed polarization profiles in the decimeter range have been subsequently presented by Bernold, 1983. In Figure 4.6 an example of very interesting profiles in right and left circular polarization is shown. These data have not been included in Bernold and Treumann (1983), and Bernold (1983) does not discuss behavior of polarization in time, though evolution of polarization from almost zero in the beginning up to strong in the middle and again weak in the end of a fiber represents a difficulty at the interpretation in any theoretical model. The main conclusion there: in two events the polarization indicates the ordinary mode for the radiation (on the criterion of the leading spot magnetic polarity).

The more detailed analysis of polarization of ZP and FB is realized by Chernov and Zlobec (1995), owing to comparison of the dynamic spectra (IZMIRAN) and polarization recordings at the fixed frequency (Trieste AO). In Figure 4.7 an unusual fiber is shown. The position of the absorption changed from high frequency edge in the beginning to low frequency edge in the end of the fiber in emission. Note an undulation in the polarization plot during the absorption and a time delay of the L- component relative to R- component on approximately 0.02 s. This particularity means that the noted undulation is not due to a real change in polarization but to a small delay of the signal of the weaker polarimetric channel, the L-handed one, in respect to the stronger one, R- handed, because the radiation was R- handed polarized on about 80%.

Even the more complex behavior of the polarization in ZP was observed in the event of April of 24, 1985, shown in Figure 4.8. In the left time interval the more pronounced delay of R- polarization channel was recorded (≈ 0.03 s). But in the

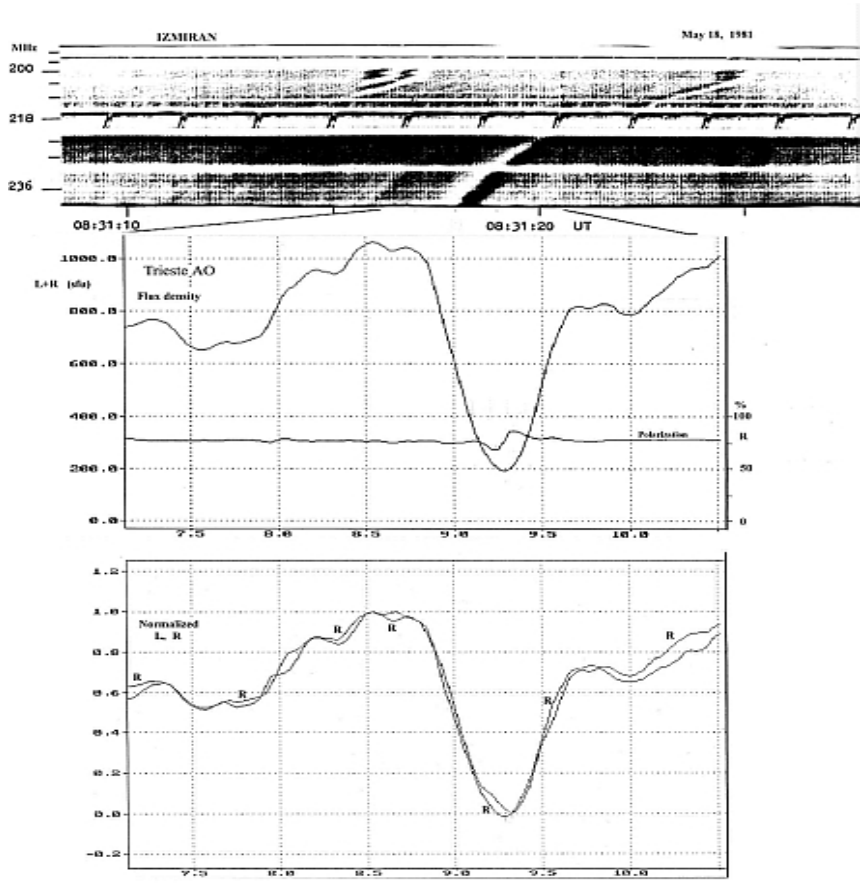

Fig. 4.7 The dynamical spectrum in the range 190 – 240 MHz (IZMIRAN) and flux density, polarization profiles and normalized (separately L and R components at 237 MHz , Trieste AO) for an unusual isolated fiber during the short impulsive type IV burst May 18, 1981 (from Chernov and Zlobec, 1995).

right interval we can see in the same series of ZP very complicated behavior of polarization due to the different (noisy) delays between L- and R- channels. The

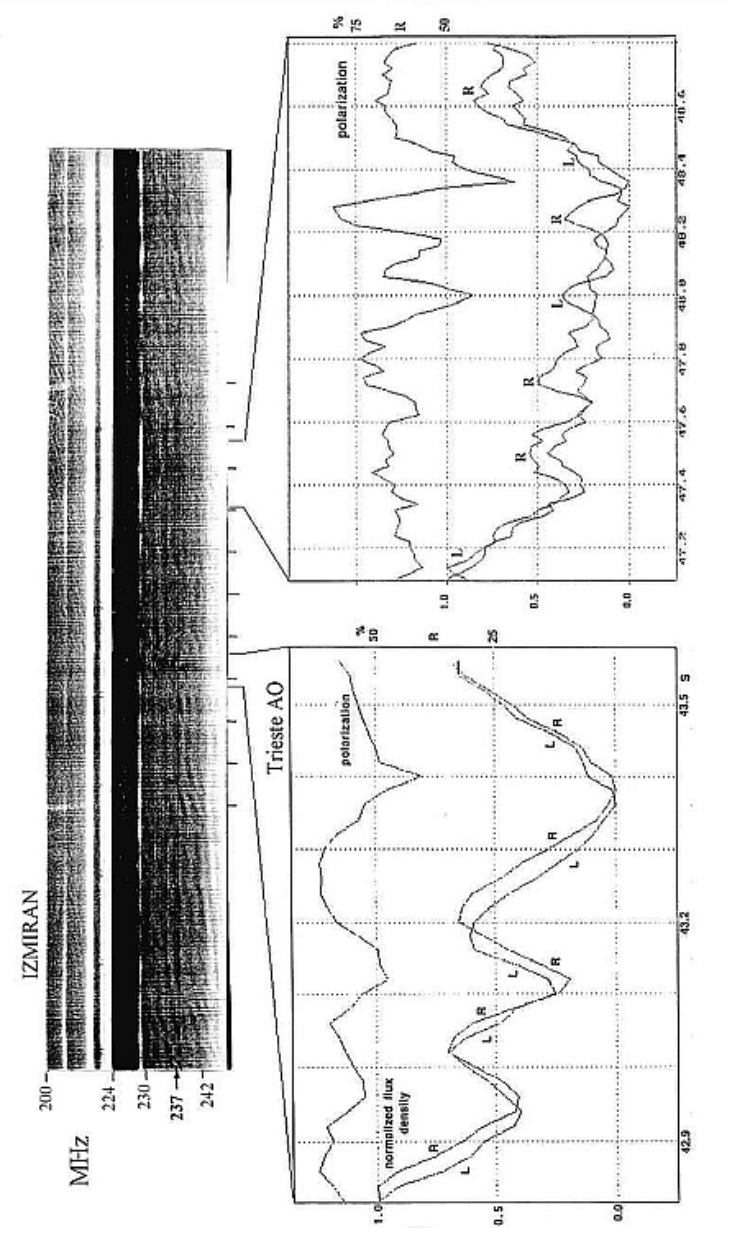

Fig. 4.8 Under the dynamic spectrum of the zebra normalized L and R components are presented. In the same box the polarization trend is also given (after the accurate subtraction of the continuum radiation) (from Chernov and Zlobec, 1995).

polarization was R- handed and very variable between 20 – 80%, but the noted delay of R- channel is the most important detail here, that is the delay of the more intense channel. The similar delay of the strongest component (of $\approx$ 0.8 s) was also registered in the short complex event April 26, 1984 during a transformation of second pulsations into zebra pattern (shown below in Figure 4.20).

In both events (May 18 and April 24) the radiation was rather in the ordinary mode (on the criterion of the leading spot magnetic polarity), and if in the May 18 event it is possible to recognize the delay as expected one, the weak polarization component was delayed, i.e. the extraordinary (*e*) wave, in the event of April 24 the strong component was delayed, *o*- mode. The emission in the ordinary mode looks to be the most probable one not only on the criterion of the polarity of leading spot, as this was done for the event of May 3, 1973 and for many other events with fine structure (Zlobec *et al.* (1987)), but also with the information of the position observations with the Nançay radioheliograph (NRH) (Chernov et al.,1994; 2001c).

The study of the moderate polarization is of significant interest, in order to be disentangled, whether actually in the source only one mode is emitted, and polarization depends on propagation conditions. However, the moderate polarization of fine structure was observed very rarely, 4 events are only analyzed in Chernov and Zlobec (1995). More than in 90% of cases the completely polarized radiation is usually recorded.

Chernov and Zlobec (1995) conclude that the moderate polarization is result in the course of propagation in the corona. When waves cross a quasi-transverse (or zero magnetic field) this should affect the propagation time of the *o*- and *e*- waves in a different way, in particular the weakest X- mode should be more delayed. The change of the polarization degree is very critical on the dependence of the angle to the magnetic field very near 90^o: the polarization sign can change in the angle interval $89.4_i 89.8^o$ (see Table III in Chernov and Zlobec (1995)). Meanwhile for the delay of *o*- mode (in the events April 26, 1984 and April 24, 1985 (Figure 4.8)) the probable explanation is related to the reflection of waves from density inhomogeneities. The reflections and delays of *o*-mode were described by Hayes (1985).

In Chernov et al. (1994) an attempt is undertaken to analyze polarization time profiles together with the positions of the radio sources of the separate zebra stripes by means of Nançay Radio Heliograph (NRH) at 164 and 236.6 MHz. In the IZMIRAN's dynamic spectrum of Figure 4.9, zebra stripes with opposite frequency drift are seen in the event of June 5, 1990 (09:35 – 11:50 UT). This long lasting type IV event is related possibly with a filament activation and eventual eruption, but is not initiated by a conspicuous flare. In such a case it was very simply to show that the radio source positions were connected to a region of southern magnetic polarity near the active region (AR) 6086. The radio emission was fully R-handed polarized and is thus likely to be in the ordinary mode.

In this case ZP was more pronounced in absorption (see in Figure 4.9, below spectra, the flux density time profiles in left-hand and righthand polarization of Trieste AO at 237 MHz), and the stripes with the negative frequency drift are

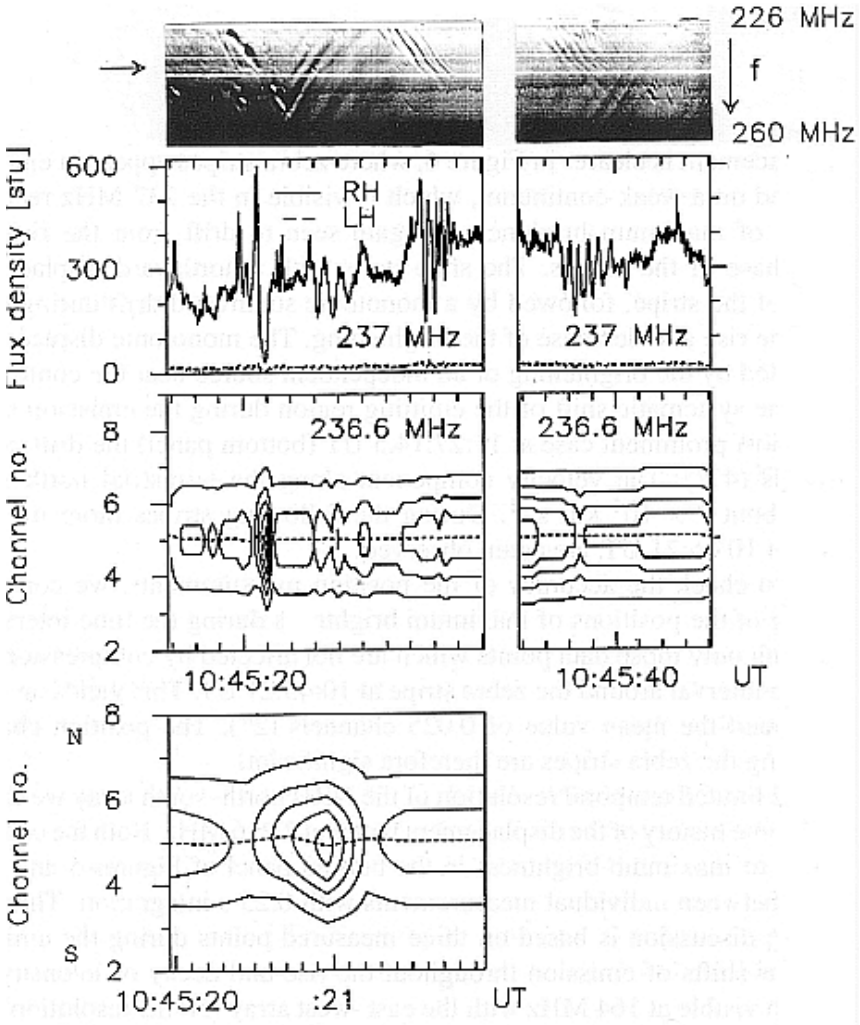

Fig. 4.9 Oppositely drifting zebra stripes in the event June 5, 1990. The *two top panels* give the dynamic spectrum (IZMIRAN, the arrow points to 237 MHz) and the 237 MHZ records of the flux density in RH and LH polarization (Trieste AO). The abscissa is graded in steps of 1 s. The *third panels* from the top give the evolution of radio brightness and source position at 236.6 MHz (Nançay Radio Heliograph (NRH)), north-south array) with contours from 9 to 89% of the biggest intensity, in steps of 20%. The *dashed line* through the centre of highest contour gives the position of peak brightness. The vertical axis is graded in 1.4', channel numbers of NRH from terrestrial south to north. The projected position of the centre of the solar disk is in channel 0. The *fourth panel* shows a zoom of the zebra source around 10:45:21 UT (from Chernov et al., 1994).

similar to fiber bursts with low-frequency absorption. When an emission stripe from one set intersects an absorption stripe from another set, the emission stripe is strongly reduced. The process by which the continuum is extinguished therefore also reduces the emission stripe. This can only occur if the emission and absorption stripes are generated in the same volume.

The absorption may be very pronounced: at 10:45:21 UT the modulation depth *md* at 237 MHz is about 90%. It is defined as $m_d = (I_{max} - I_{min})/(I_{max} + I_{min})$, where *I*, denoting the whole Sun flux density. It varies with time, e.g. after 6 s m_d decreases gradually from 66 to 27%. However near the end of the event a series of zebra stripes only in emission is observed.

Position data in Figure 8 will be discussed in the following section.

Some conclusions from polarization data

- The zebra patterns are usually strong polarized, in about of 90% cases.
- The radio emission corresponds to ordinary wave mode.
- In several events a moderate polarization was observed, and complex behavior of polarization is defined by propagation effect and depends of a delay of the extraordinary wave relative to the ordinary one.
- The polarizations parameters of zebra stripes and fiber bursts are usually identical.

4.3 Spatial Size and Positions Shifts of Zebra Pattern (ZP) Radio Sources

4.3.1. The June 5, 1990 event

In Chernov et al. (1994) the first detailed position measurements are executed, therefore it is worthwhile to extract the meaningful results of this work. The spatial properties of the ZP radio sources are approximately identical, in spite of different kinds of the zebra stripes in the investigated event of June 5, 1990: stripes with their degeneration in the course of drift into the almost dot elements in emission and absorption shown in Figure 4.9, or more regular ones, but accompanying by several wiggles, almost simultaneous in entire occupied frequency range (Figure 4.10).

The sources of zebra stripes are not point-like. Sizes up to 1.9' are observed. During the absorption stripes, slightly larger sources are seen ($\approx$ 2.1'). These sizes are close to those of the unperturbed continuum.

Apparent displacements of radio sources are observed during many zebra stripes. Due to the limited time resolution of the NRH northsouth array (the integration time of 0.25 s) we cannot describe the time history of displacements of all

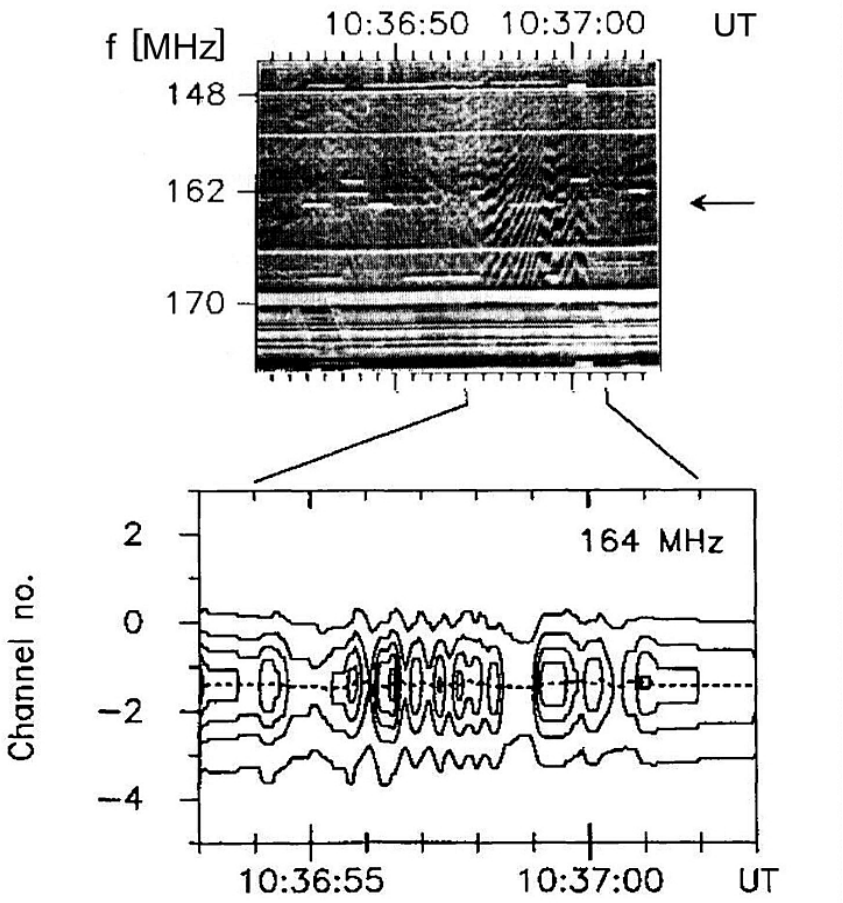

Fig. 4.10 Temporal evolution of the dynamic spectrum (IZMIRAN) and source position (NRH) during an interval of zebra pattern in the event June 5 1990 near 164 MHz (the horizontal arrow on the right indicates 164 MHz). *Below* - the one-dimensional map at 164 MHz with east-west array; the position of maximum brightness is noted by the *dotted line*; 1 channel $\approx$ 1.0', time resolution 0.05 s (from Chernov et al., 1994).

rapid variations seen e.g. in Figure 4.9 in the spectra and Trieste polarization profiles with the integration time of 0.02 s. The centroid of the continuum source, plotted by the dashed line through the center of the strongest contour (3rd row in Figure 4.9) was stable during the 13-s interval. However, during the zebra stripe the centroid undergoes an oscillating drift (the bottom panel): northward at the onset of the stripe, then southward near the brightest emission. The monotonic

southward displacements were also observed in other series of zebra

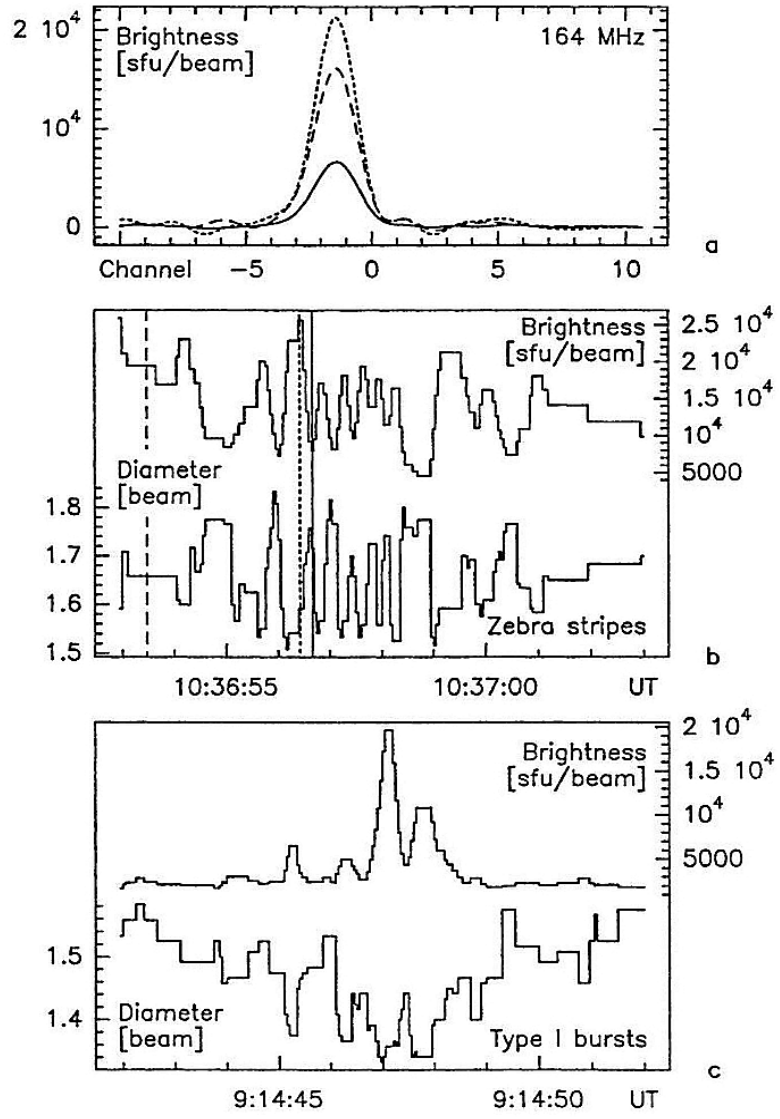

Fig. 4.11 Temporal evolution of zebra pattern shown in Figure 4.10 at 164 MHz. *(a)* One-dimensional brightness distributions with 50 ms integration time during unperturbed continuum (10:36:53.5 UT, *long* dashes), an emission stripe (10:36:56.45 UT, *short dashes*) and the subsequent extinction stripe (10:36:56.70 UT, *solid line*). *(b)* Time history of the brightness (*top*) and half-power diameter (*bottom*) during the zebra-pattern. *(c)* Time history of brightness and diameter of type I bursts during the noise storm preceding the type IV event. The brightness and diameter in *(b)* and *(c)* are those of a Gaussian fit to the observed source profiles (from Chernov *et al.*, 1994).

stripes in emission with the positive frequency drift (see Figure 6 in Chernov et al.(1994)). The maximum shift covered 0.56 channels (about 47'') that corresponds to the velocity component along the terrestrial north-south baseline of about $7 \cdot 10^4$ km s^{-1}. The measured r.m.s. variation around the mean value was of 0.025 channels (2''), therefore the position changes detected during zebra stripes are significant.

Similar shifts of emission throughout isolated zebra stripes are also visible at 164 MHz with the east-west array (50 ms resolution). For example, during the interval of zebra stripes shown in Figure 10 the centroid of the source starts at a position east of the preceding continuum and drifts westward throughout the maximum brightness of the three emission stripes between 10:36:55 – 57 UT with the negative frequency drift. The total distance covered by the space drift is of the order of $2 \cdot 10^4$ km and the projected velocity $\approx 10^5$ km s^{-1}.

The zebra stripes undergo several wiggles with a spasmodic (sawtooth) sign change of the frequency drift. We can note two such moments, 10:36:58 and 10:37:01 UT, and in both cases the space drift changes direction, to eastward. Furthermore, during one second into 10:36:59 – 10:37:00 UT the frequency drift was almost zero, and the spatial drift in this source was also retarded. Thus, we observe specific relation between the directions of the frequency drift on the spectrum and the spatial drift of sources.

Figure 4.11 represents source structure and dimensions during zebra pattern (shown in Figure 4.10). One-dimensional scans are displayed in Figure 4.11(a) for three features: the unperturbed continuum before zebra stripes (10:36:53.5 UT, long dashes), an emission stripe (10:36:56.45 UT, short dashes, and the subsequent absorption stripe (10:36:56.7 UT, solid line). The sources are structureless, and no qualitative difference is apparent between them. The main remarkable feature is the brightness, which is reduced in the whole source of unperturbed continuum emission during the absorption stripe and enhanced during the emission stripe. Figure 4.11(b) shows the time history of the peak brightness (top) and of the size (bottom) of the emitting source. Near the brightest phase of the zebra stripes, the source width is 1.5 – 1.6 times the beam of the NRH. The measured half width is 1.9', and gives a brightness temperature of roughly 10^{10} K (for a circular source) during the brightest peak at 10:36:56.45 UT. During the phase of absorption and of the unperturbed continuum emission the source appears slightly broader, typically 2.1' and 2.0', respectively.

Thus, in absorption stripes we see the whole continuum source. For this reason we always notice the shift of the center of source upon transfer from the emission stripe into the absorption stripe, (see Figures 4.9 and 4.10) since the position of the maximum brightness of continuum, as a rule, is considerably displaced from the maximum in the emission stripe. The similar behavior of radio sources we observe upon the comparison of type I bursts in the noise storm which preceded the type IV event (Figure 4.11(c)). The diameter of type I sources is also less than the diameter of the continuum. The source of type I bursts is also not point-like (~ 1.3 times the beam). The source sizes of the zebra emission stripe and the type I bursts are therefore comparable.

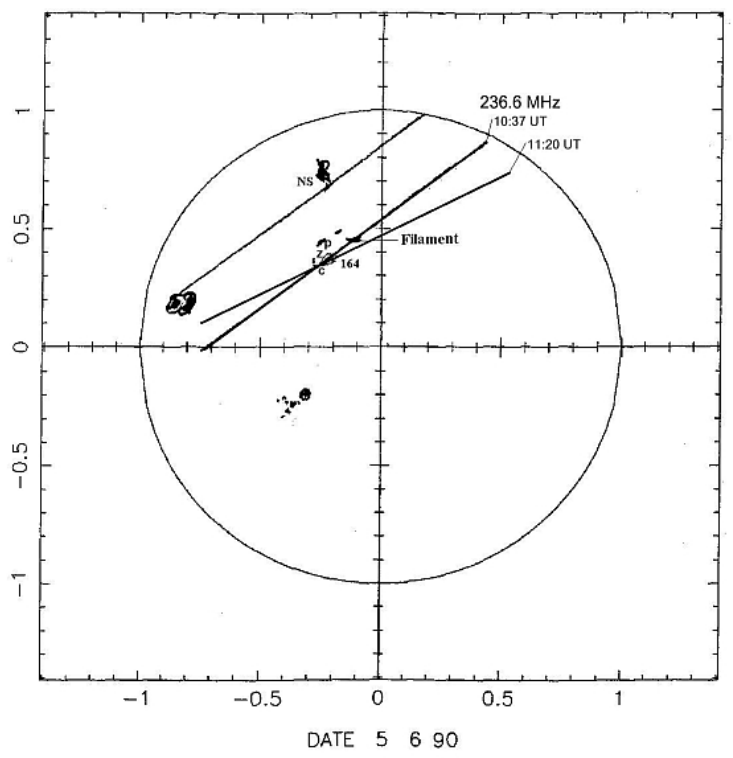

Fig. 4.12 Two-dimensional positions of radio sources at different moments of the event June 5, 1990 with NRH, of zebra patterns (marked by z) and fast pulsations (p). All radio sources were tightly related with an active filament. Positions of the burst continuum at 164 MHz is marked by c, and at 236.6 MHz by an intersection of two one-dimensional scans at 10:37 and 11:20 UT. Sources of ZP at 164 MHz were located under the filament (marked by a cloud) (from Chernov *et al.*, 2001c).

In these measurements the great significance has the mutual arrangement of the sources of continuum and fine structure. They rarely coincide. It is shown in Figure 4.12 two-dimensional positions of radio sources in the event June 5, 1990: sources of the continuum (marked by c), zebra stripes in emission (z) and fast pulsations (p) are spread in the projection on the disk along the active filament.

4.3.2. The March 12, 1989 event

In the event March 12, 1989 zebra patterns were observed during almost three hours (09:00 – 11:40 UT) and were also related with an active filament. Without the determination of the positions of radio sources we could not understand at all polarization data in this event, since the zebra pattern was observed against the background of weak continuum in the RH polarimeter channel, and a strong continuum with pulsations only in LH channel. Spectral features and position data of radio sources of the zebra pattern during one minute, 11:18 – 11:19 UT are shown in Figure 4.13.

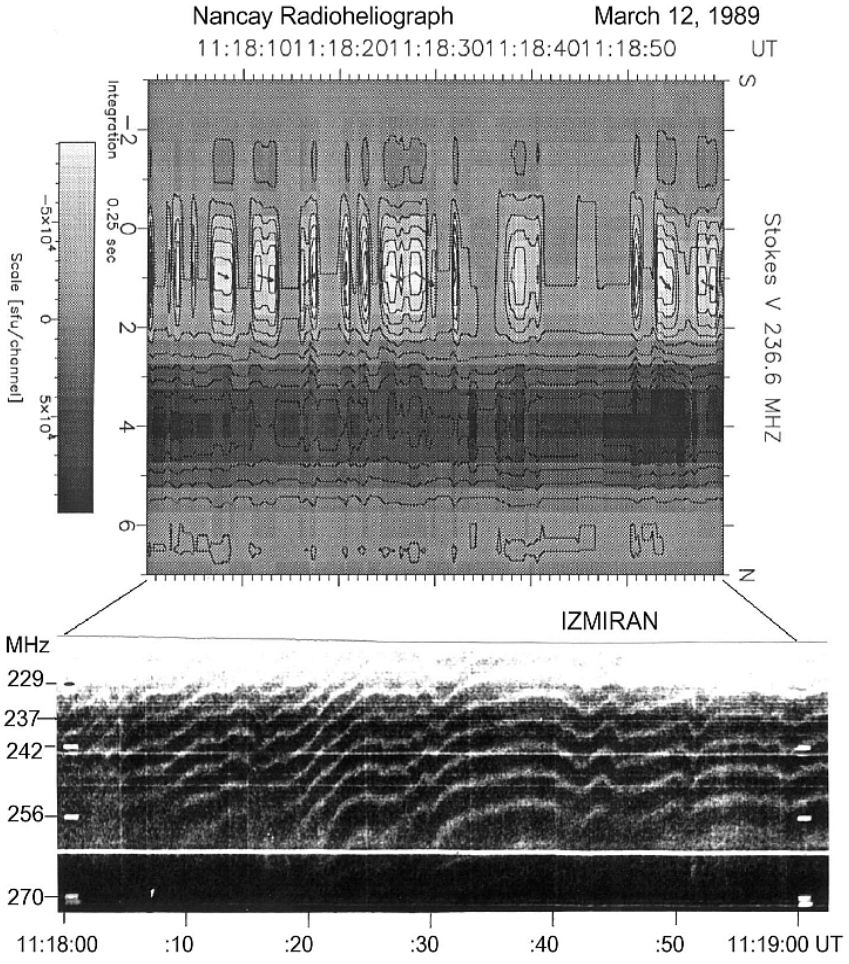

Fig. 4.13 Radio source positions and dynamic spectrum of zebra pattern in the event March 12, 1989 during one minute 11:18 – 11:19 UT. The *upper panel* represents gray-scale plots of one-dimensional (North-South) brightness distribution in polarization (Stokes V, white - RH- and black - LH polarization) measured by NRH at frequency 236.6 MHz. The vertical axis gives the coordinate along the terrestrial N-S direction in units of channel numbers of NRH with one channel ≈ 2.2' (0 indicates the center of the solar disk). *Short arrows* in some white source centers show direction of spatial drift of maximum brightness during some wiggles of zebra stripes at the dynamic spectrum (*lower panel*) obtained with the IZMIRAN spectrograph in the range 220 – 270 MHz (from Chernov et al., 1999).

The upper panel represents grayscale plots of one-dimensional (North-South) brightness distribution in polarization (Stokes V) measured by NRH at 236.6 MHz. The emission sources of the zebra stripes are visible in white (RH-polarized) at about the position of the NRH channel number +1, the strong continuum source was located in the channel number +4. It appears in black (LHpolarized) with numerous pulsating sources, chaotically shifted from the center of the continuum source, predominantly directed towards the position of the zebra sources. Chernov et al. (1999) note the explicit shifts of the centers of sources of absorption stripes (weak remnant continuum emission, clear-gray) in respect to the white sources of the emission stripes, predominantly directed towards North, the position of the strong continuum. According to a more precise profile evaluation of source positions the displacement at Figure 4.13 was about 0.4 channel ($38 \cdot 10^8$ cm). This property remained distinctive during the whole event, i.e. for about 3 hours, and sometimes of a more value, $(50 – 70) \cdot 10^8$ cm.

We can also note the specific correlation between the frequency drift of zebra stripes in emission on the spectrum and the spatial drift of their sources, that it was already noted above, in the event on 5 June 1990. The frequency of 236.6 MHz in essence came to the stripes with the negative drift with its gradual flattening to the zero value. At these moments the sources detected displacement towards the North. Such displacements are marked at the position plot in Figure 4.13 by short arrows. Only in 11:18:16 – 17 UT along the frequency of 236.6 MHz the zebra stripe experienced the jump of drift to the reverse side (with the positive drift), and then the source was displaced towards the South. Such displacements were even more pronounced in other zebra pattern series during the event.

One should note, that the source of the zebra against the background of weak continuum (30 – 60 s.f.u., 1 solar flux unit = 10^{-22} W m^{-2} Hz^{-1})) in the course of the event, was also slowly displaced towards the north. So, in one hour 10:20 – 11:20 UT it was displaced from channel -1 to +1, i.e. up to distance of $190 \cdot 10^8$ cm, with an average speed of about 50 km s^{-1}. The source of strong continuum (200 – 600 s.f.u.) was also displaced towards the North, but up to the noticeably smaller distances. We constructed a two-dimensional position of the zebra source in Figure 4.14, using the crossing of one dimensional scans of NRH at 236.6 MHz during the event. The strong continuum source was located near the AR 5395 (Spots), meanwhile the zebra sources was located (in projection) near a dark (in the line *Hα*) filament. According to Stanford magnetogram in SGD 537, part 1 (1989) the

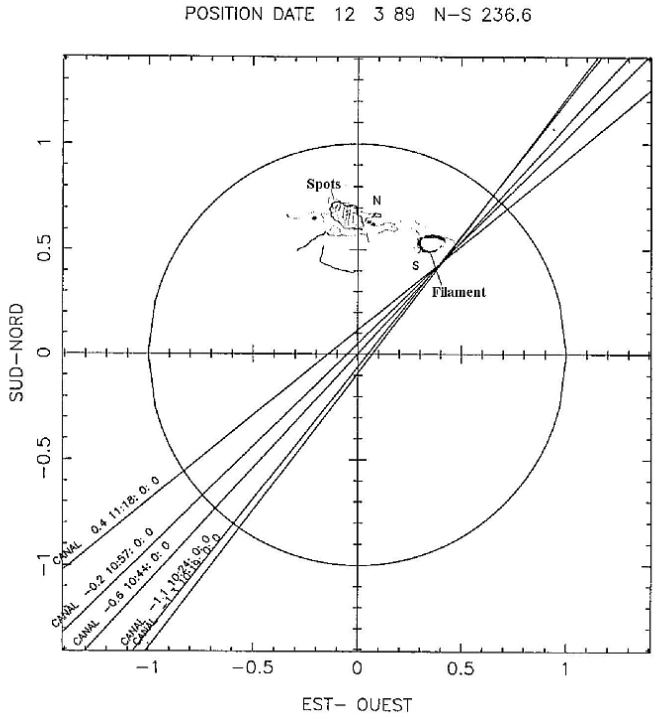

Fig. 4.14 Two-dimensional positions of radio sources of zebra patterns (LH polarized) in the event March 12, 1989 at 236.6 MHz obtained by intersections of one-dimensional S – N scans of NRH in different moments. The radio sources positions were tightly related with an active filament in the south magnetic polarity (S). The strong burst continuum source (RH polarized) was located near AR NOAA 5395 with the predominant north magnetic polarity (marked by N) (from Chernov et al., 1999).

predominant magnetic polarity near Spots was North (N), and near the filament it was South (S). Hence we assume that the radio emission of both sources corresponded to the ordinary wave. The radio event started after the end of the 2B *Hα* flare (N28E05) in AR 5395 and after a small maximum (08:28 UT), of importance M6.7 of SXR (GOES-7). The zebra patterns had been observed during the three hours lasting interval between two CMEs. Taking into account that the maximum energy release taken place in the meter radio range and a source merging of zebra absorption stripes and pulsations (in the strong continuum) we assume that the radio event was caused by a global magnetic reconnection high in the corona, and the radio sources of the zebra patterns were related with magnetic islands during a long-lasting restoration of the magnetic structure after the CME.

4.3.3. The February 17, 1992 event

In the event February 17, 1992 the zebra patterns were observed in a complex type IV event during about four hours in the time interval 08 – 12 UT, and the radio source was also connected with an active dark filament without a big $H\alpha$ flare and microwave activity (Chernov et al., 1998). For the first time we can see an entire frequency range occupied by ZP in a oscillating regime in the interval 180 – 350 MHz (Figure 15). The polarization changed the sign during the event from LH into RH beginning from 236.6 MHz (10:00 UT) then at 327 MHz (10:52 UT) and 407 MHz (10:58 UT), i.e. beginning from the upper corona layers to the lower ones.

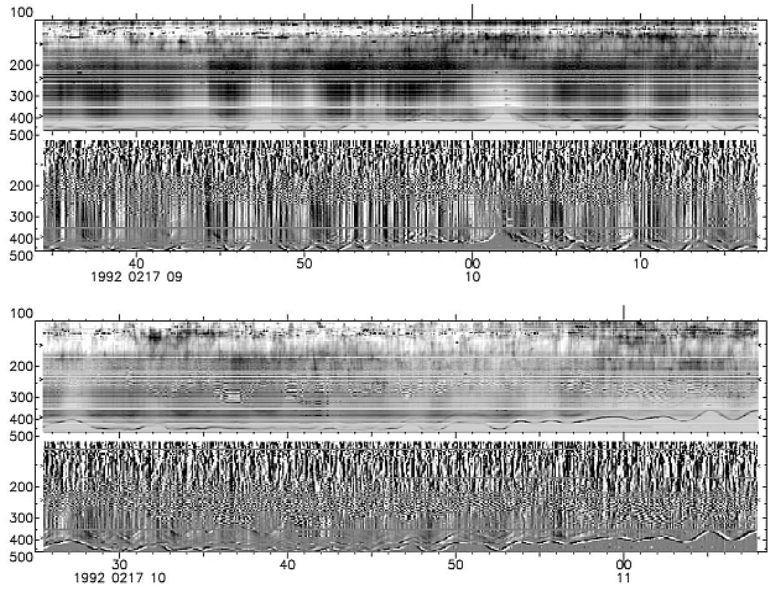

Fig. 4.15 ARTEMIS dynamic spectrum over a 1 h 45 min period (flux density / time derivative). Besides the 3 min pulsations (in phase with the EEL around 400 MHz), additional pulsations with periods of ≈ 20 s can be seen, as well as zebra patterns between 190 and 350 MHz, and noise storm at frequencies < 190 MHz (from Chernov et al., 1998).

The change of the polarization sign was accompanied by a smooth decrease in the emission, as continuum so zebra patterns (in the time interval 10:00 – 10:02

UT the zebra pattern almost disappeared). Figure 4.16 gives representation about

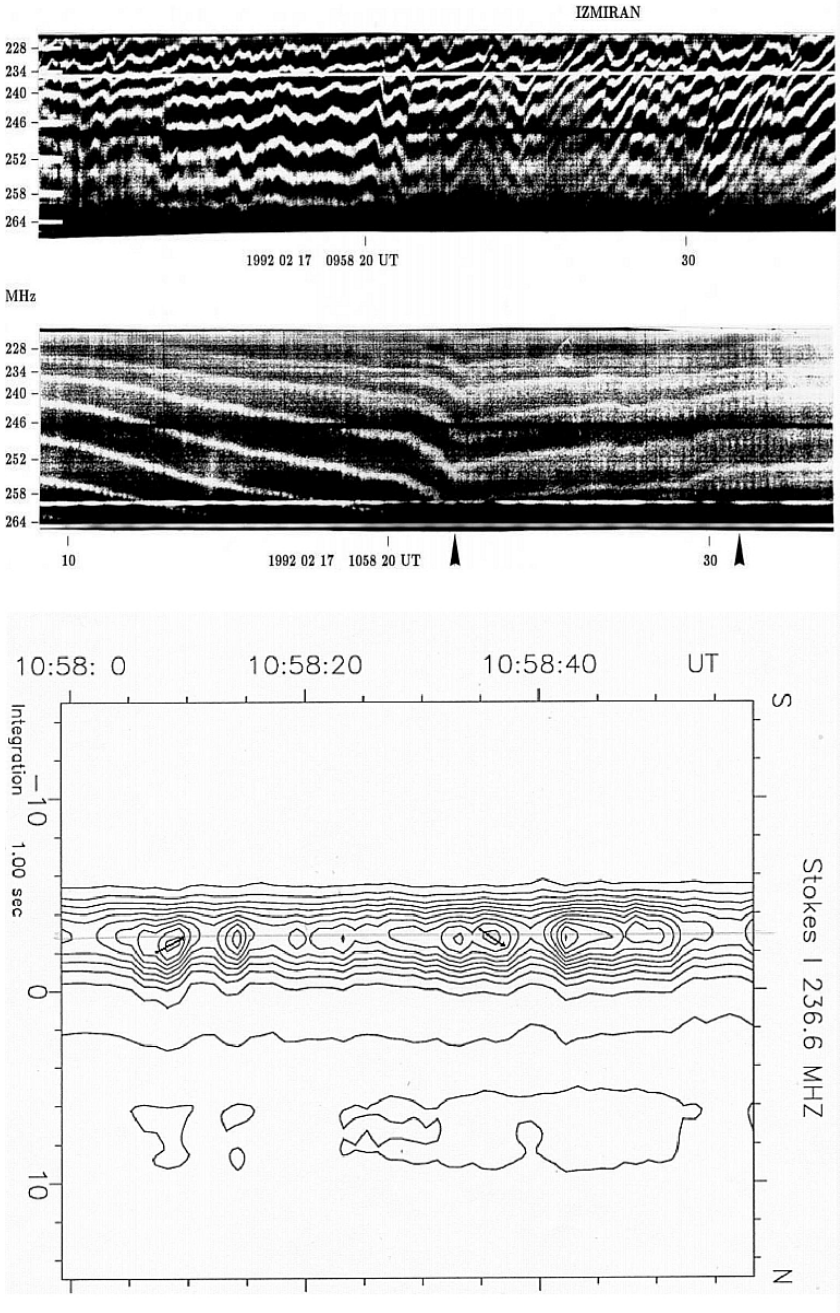

Fig. 4.16 *Top*: Two fragments of zebra patterns recorded with the IZMIRAN spectrograph, (before and after the change of polarization sign) illustrating two kinds of sub-structures discovered. The top spectrum shows numerous sudden frequency shifts of zebra stripes. The bottom spectrum shows a case of stripe splitting (first arrow is the beginning) and dot-like structure of the upper frequency component (second arrow). *Bottom*: Contour plots of the one-dimensional SN brightness distribution measured by NRH at 236.6 MHz in intensity. The 0 channel gives the center of the solar disk. The arrows in the centers of sources at 10:58:07-10 UT and 10:58:34 – 37 UT show the direction of the spatial drift of sources (from Chernov et al., 1998).

the change the nature of zebra pattern before the change of the polarization sign (with the sharp jumps of drift) and after the change of sign (with a slow drift, when the stripes are almost parallel to time axis). The frequency range of the zebra patterns began gradually to become narrow. It is possible to explain this by a capture of the zebra radio source into a magnetic cloud.

It is remarkable, that the radio emission of the oscillating fiber limiting all the emission from the high frequency edge, discussed in Chernov et al. (1998) as *Evolving Emission Line* (EEL), retained the sign of polarization even during several minutes to 11:06.5 UT, although the continuum at 407 MHz changed the sign of polarization rapidly at 10:58.5 UT. Probably, its source was located in the corona in the old configuration of the magnetic field lower than the new magnetic cloud. Thus, in the February 17, 1992 event it was difficult to define the wave mode, because the polarization changes were probably caused due to the magnetic reconnection high in the corona.

However we could compare the frequency drift with the spatial source shifts during one of unusual frequency splitting of zebra stripes. For the larger persuasiveness we added to Figure 16 the one-dimensional SN distribution of zebra-stripe sources. We had time resolution of NRH only 1 s, but the zebra stripes changed the sign of frequency drift at 10:58:22 UT from positive into negative with enough low frequency drift (remaining almost parallel to the time axis). Therefore this time resolution make it possible to recognize the spatial drift of sources as significant. So, we see the spatial drift at 236.6 MHz in the beginning of this interval (about 10:58:08 UT) towards South and in the end (about 10:58:35 UT) towards North. In Figure 16 the direction of the spatial drift are marked by arrows in the centers of sources at the corresponding moments of SN distribution. Looking at Figure 3 in Chernov et al. (1998) and being based on several Yohkoh/SXT images, it is tempting to locate the radio source of zebra patterns in this event within a large trans-equatorial closed loop connecting AR 7056 and 7058. The source displacements in the direction S – N are quite anticipated therefore.

Some main conclusions from positional observations.

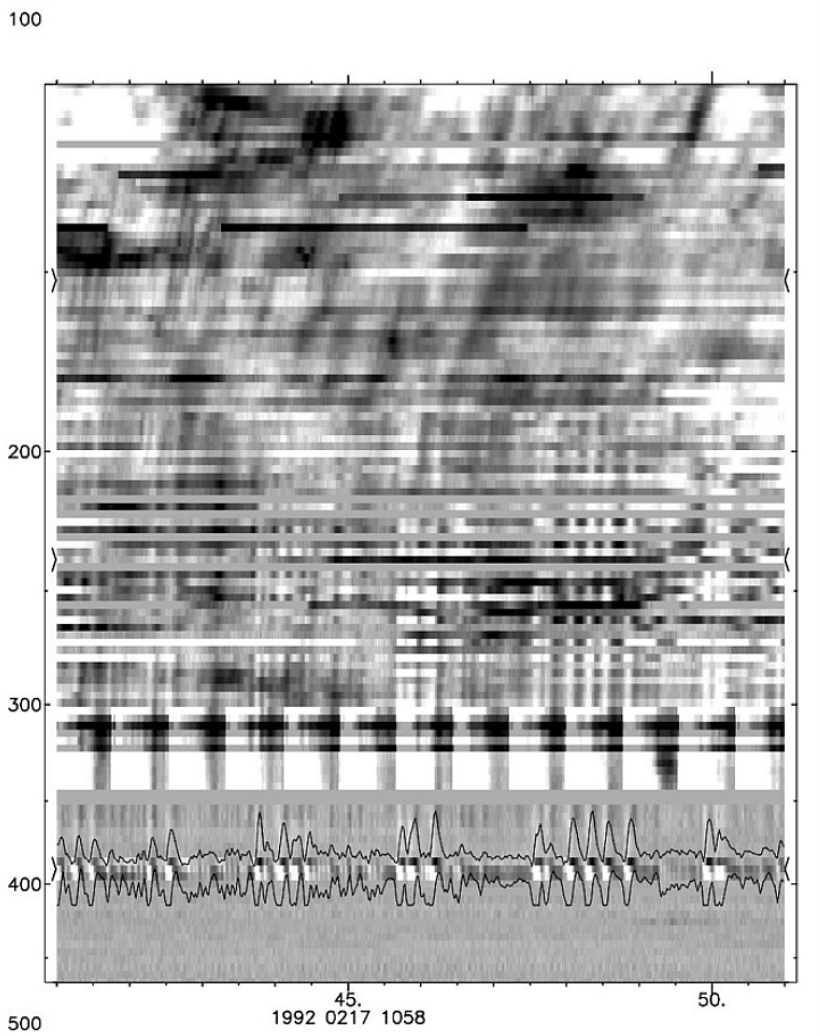

Fig. 4.17 ARTEMIS spectrum at high time resolution, over a time interval when zebra patterns exhibited marked sub-structures. Zebra stripes are the horizontal black bands around 250 MHz; each one is visible in a given frequency channel for a few seconds only, because of its frequency drift. The EEL is visible on 2 channels around 400 MHz; we superimposed the 2 corresponding time profiles showing the 0.25 s period clearly. This set-up emphasizes the spectral structure of the EEL, made up of emission (black) and absorption (white) dots, synchronized with zebra stripe dots and 0.25 s sudden reductions. At frequencies < 200 MHz, we notice fast structures drifting at type III rates (from Chernov et al., 1998).

- The zebra pattern radio sources are not point-like, they occupy the noticeable part of the background continuum source or even of entire active region (AR). The measured half width is 1.9', and gives a brightness temperature of roughly 10^{10}K.

- Different positions (or displacements) of the sources of stripes in emission and absorption are almost always observed, they prove to be maximum in cases when the sources of zebra patterns and continuum are strongly spread. In the absorption stripes we see actually not real motions, but rapid switchings towards the center of the continuum source.

- A correlation is noticed between the directions of frequency drift of stripes on the spectrum and the spatial drift of sources at the fixed frequency. The speeds of motion in the projection on the solar disk prove to be very large, $\geq 10^{10}$ cm s^{-1}.

Below, in the section 4.4.1 a more detailed description of source displacements of zebra stripes in the event October 25, 1994 is presented.

4.4. Sub-structure of zebra stripes

Two new kinds of sub-structures are visible in the zebra patterns recorded by IZMIRAN spectrograph on February 17, 1992. The first new feature is a rapid frequency shift of the whole zebra pattern, like at 09:58:21 UT (Figure 16, upper panel). All zebra stripes jump by an amount comparable to the zebra stripe separation. They do not do it simultaneously, but with a frequency drift rate $df/dt \approx 50$ MHz s^{-1}, comparable to type III burst drift rates. The zebra pattern seems to be broken along a slanted "fault". These frequency shifts occur frequently and randomly during the whole event, without any characteristic time period, sometimes within a second, sometimes episodically during one minute.

The second new feature consists in sub-splitting of a zebra stripe into two separate stripes, like at 10:58:21 – 22 UT (Figure 4.16, middle panel, after the hook). The split stripes have different characteristics: the lowfrequency stripe is continuous, while the high-frequency stripe consists of regular dots with a characteristic period ≈ 0.25 s. These frequency splittings last for minutes. Occasionally two continuous stripes exhibit chaotic frequency drifts, or cross each other.

The oscillating fiber in the event February 17, 1992 had the frequency bandwidth in emission 10 – 15 MHz (Figure 4.15). It oscillates almost sinusoidally and in phase with flux density of broadband pulsations. One or two weaker additional stripes (15 – 20 MHz wide) appear episodically on the low frequency side of the EEL, at 20 to 100 MHz from it. The EEL is distinctly different from zebra stripes at lower frequencies. It mostly consists of one single emission stripe instead of many, with a larger relative bandwidth $\Delta f/f \approx 12/450 \approx 0.03$, instead of $\approx 1.3/250 \approx 0.005$ for zebra stripes. It is also continuous over two hours instead of being intermittent.

Very dilated plots using ARTEMIS high time resolution (Figure 4.17), reveal that the EEL is structured into a succession of dots every 0.25 s or so. Each dot consists of an emission (black) on its low-frequency side and an absorption (white) on its high-frequency side. The duration of each dot is about half their pe-

riod, that is ≈ 0.12 s. The dots are synchronized with zebra stripe dots (after the splitting, Figure 4.16) and 0.25 s sudden reductions. The source position of the EEL is also different: it is north of the continuum/zebra pattern common position.

4.4.1. Braided zebra patterns

In some events the overlap of different fine structures may be just a chance. Slottje (1981) shown statistics of the simultaneous appearance of fast pulsations, spike bursts and fiber burst with the zebra patterns: the percentage of such event is low and their occurrence may be independent, e.g. because they arise in spatially different sources. A number of events were observed where zebra stripes are not continuous emissions, but the trajectories of a substructure of narrow-band short-lived elements (spike bursts), which themselves show different drift rates. Such a degeneracy of regular zebra stripes into different substructure elements can be seen already based on the first example, given by Elgarøy (1959) (see Figure 4.1, two bottom panels). Slottje (1981) consider drifting spikes, organized in zebra-like patterns as distinctive structure which was called 'braided zebra pattern'. After the conclusion of Slottje (1981) that the braided zebra patterns are events themselves, all consequent observations shown that in many events the regular zebra pattern sometimes degenerates into the braided one. Karlicky *et al.* (2001) named similar structures as *lace bursts*.

4.4.2. Tadpoles

In one event (March 2, 1970) Slottje (1972) observed a degeneracy of zebra stripes into so-called tadpoles. These burst got their name because of their aspect on the spectrum: an absorption "body" with a low frequency emission "tail" and a high frequency emission spike, the "eye" (Figure 4.18). Tadpoles were very developed, and Slottje isolated this element as a special structure. They were described in detail also in Slottje (1981). The 3-dimensional scheme of one tadpole is also described in monographs Krüger (1979) and Zheleznyakov (1995).

Although it is possible to find examples also in other events when the unsteady (irregular) zebra stripes produce on the spectrum whimsical forms, including the tadpoles. Such an example is shown in Figure 4.19. In the middle panel a small tadpole is marked by an arrow. In this event (July 3, 1974) the regular zebra stripes appeared only during very short time interval, as this is shown (by the arrows) in two other panels. The frequency profiles shown at the right of each spectrum present modulation depth typical for ZP.

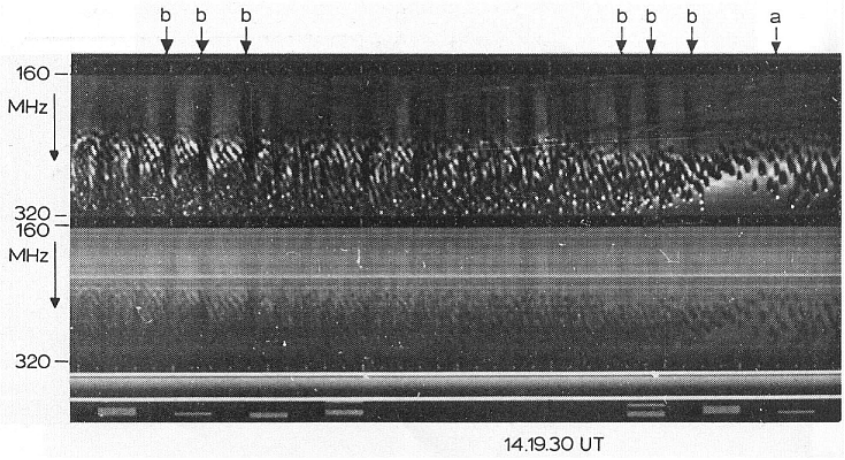

Fig. 4.18 ZP ending in separate tadpoles in the event March 2, 1970 (from Slottje, 1972).

These examples already show, what a wide variety the irregular ZP presents in each event. However, this in no way indicates, that each new element is excited by new mechanism. Most likely, entire diversity of stripes on the spectrum is determined by the parameters of plasma in the radio source and by the form of the distribution function of fast particles, which, naturally, cannot be strictly identical in the different events.

4.4.3. Unusual behavior of ZP

The April 26, 1984 event

An intriguing conversion of the second pulsations into ZP was observed on April 26, 1984, shown in Figure 4.20. The continuum burst began after a group of type III+V burst (and after the small 1B flare). In the high frequency part of the spectrum (200 – 242 MHz) the burst has the form of instantaneous pulsations in emission and absorption (sudden reductions) with the time scale of seconds.

At lower frequencies the frequency drift of pulsations becomes measurable, and it decreases gradually from $\approx$ - 180 MHz s^{-1} to $\approx$ - 0.5 MHz s^{-1} and pulsations turn into arch stripes similar to the ZP (or fiber bursts, shown by dashed lines in Figure 4.20). The stripes are not continued below 130 MHz, but in the frequencies 84 – 72 MHz some drifting fibers (or striae) are also present in the continuum of type V burst .

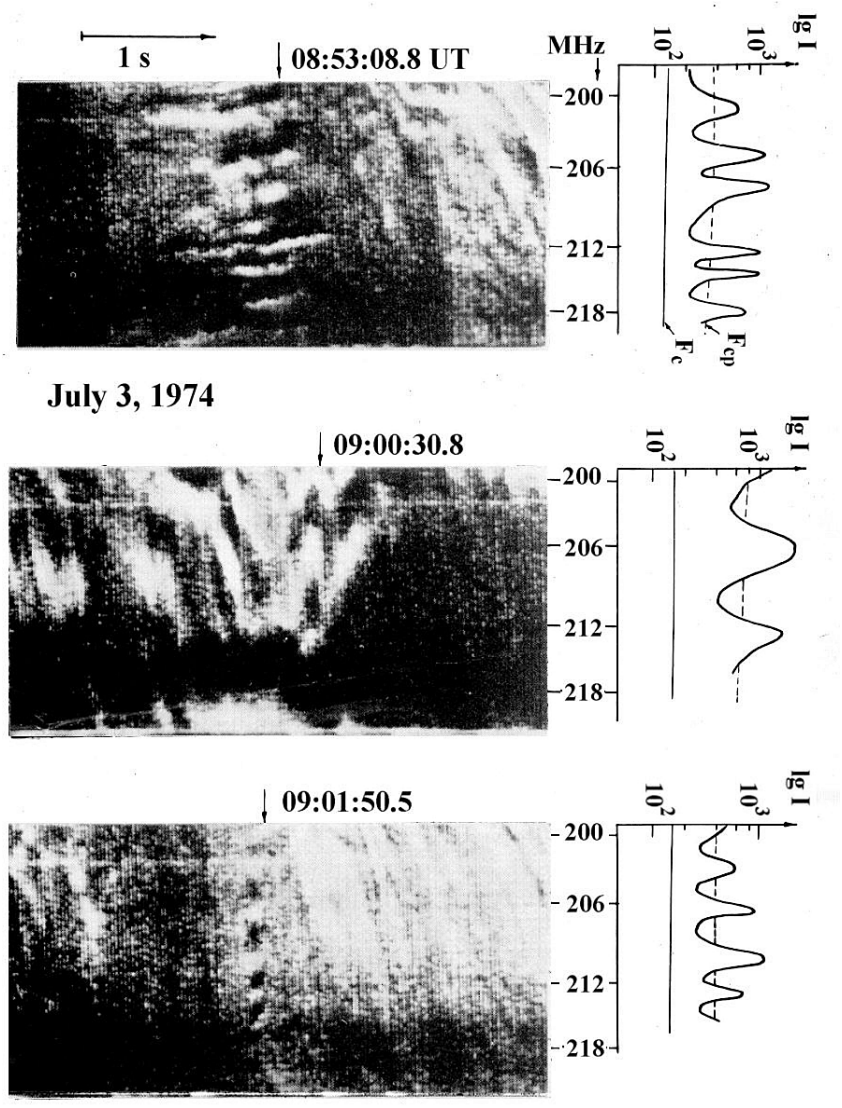

Fig.4.19 Three fragments of spectra with non stationary ZP on July 3, 1974, registered by IZMIRAN spectrograph (time resolution is 0.02 s, frequency resolution ≈ 0.15 MHz). Frequency profiles obtained by microphotometry of the spectra in relative logarithmic units at the time marked by arrows above the spectra are presented in the same frequency scale as the spectra (from Chernov, 1976a).

At the end of the event it is clearly visible that the stripes are superimposed to spike-like pulsations with a strict period of 0.8 – 1.0 s. All the emission consists of the second pulsations and drift stripes. Sudden reductions in the range 242 – 220

MHz correspond to the spaces between the pulsations in the emission at the lower frequencies (shown by arrows in Figure 4.20).

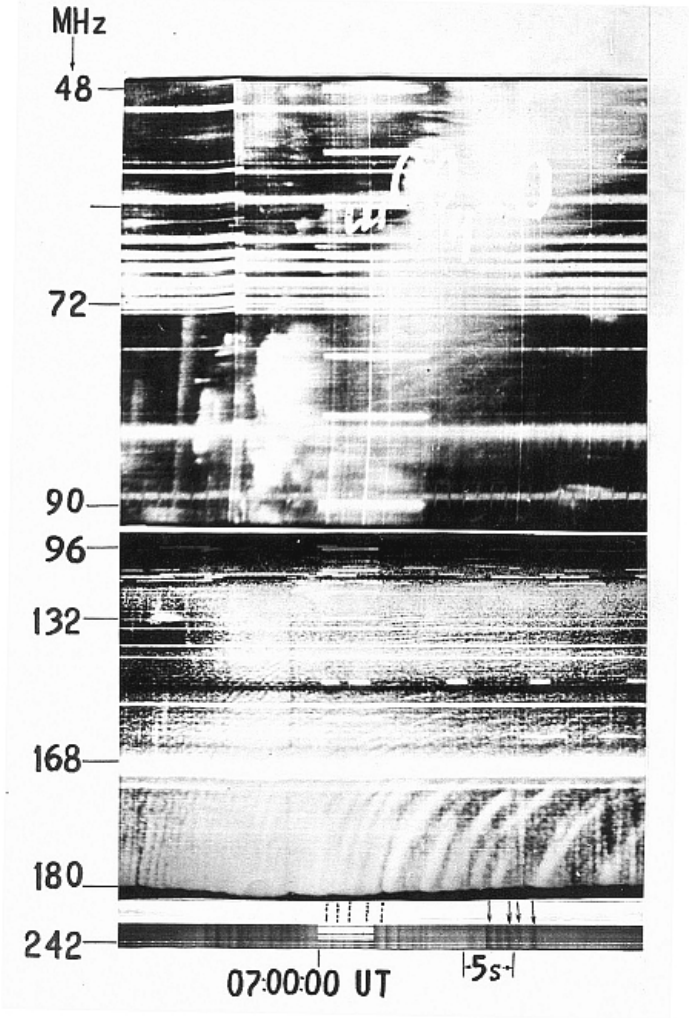

Fig. 4.20 Dynamic spectrum of type V on April 26, 1984 showing a transformation of pulsations in HF part (220 – 240 MHz) into ZP between 120 – 180 MHz (spectrograph of IZMIRAN) (from Chernov et al., 1984).

Thus, in this event a continuous conversion of second pulsations at HF part of the spectrum into zebra stripes with gradually decreasing frequency drift at lower frequencies was observed. This testifies on a close connection of the nature of sudden reductions and stripes of ZP.

The July 28, 1999 event

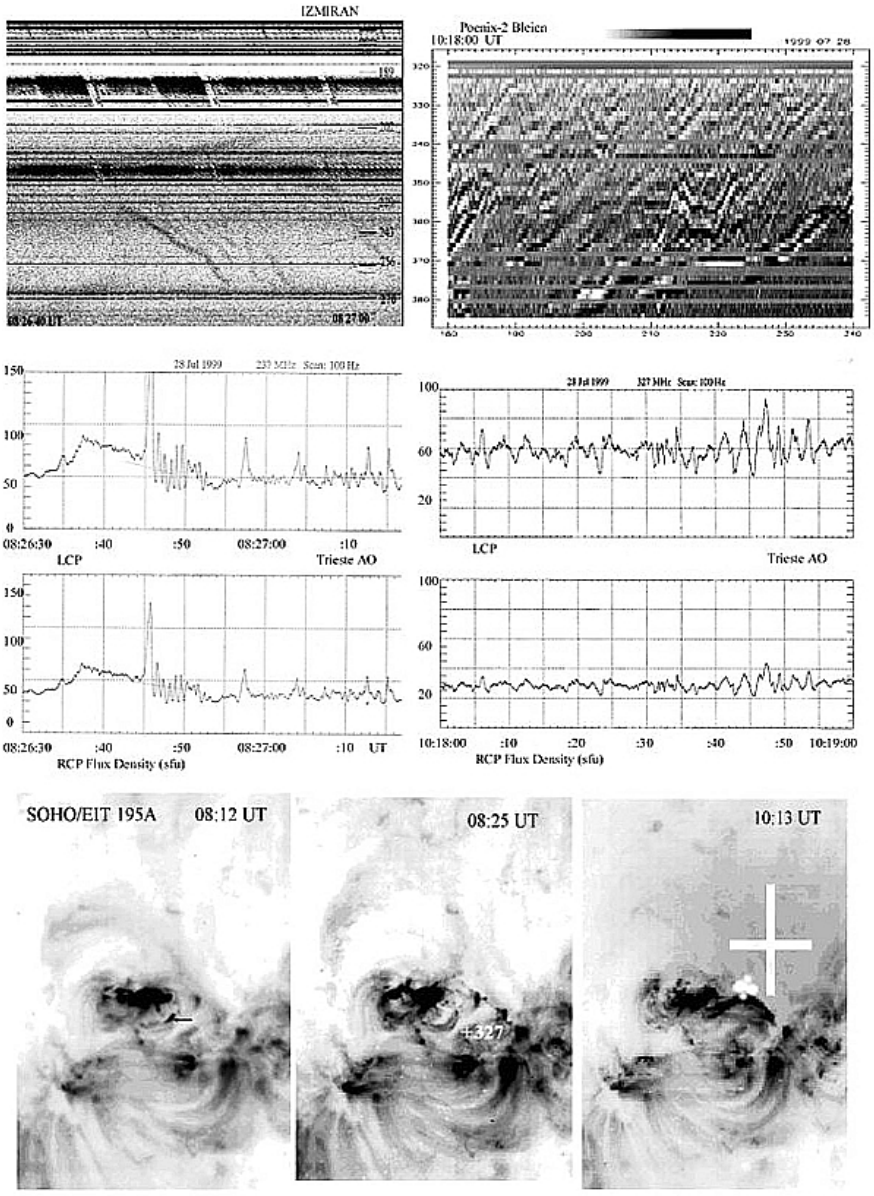

Fig. 4.21 *Top panel*: Two spectra showing zebra-patterns at about 08:26 between 189 and 270 MHz recorded by IZMIRAN (left) and at about 10:18 between 320 and 385 MHz by Phoenix-2 (right). *Middle panel*: time profiles of the Trieste AO polarimeter at 237 (left) and 327 MHz (right). *Bottom panel*: Flare evolution in EUV line 195 Å (SOHO/EIT). The arrow in the left panel indicates a new rising bright loop. The positions of the NRH radio source centers are shown by *crosses* (*small cross* -327, *big cross* -164 MHz) (from Chernov, 2004).

The analysis of the zebra-patterns is based on the dynamic spectra of IZMIRAN and Phoenix-2 (Messmer et al., 1999), single frequency polarization data of the Trieste AO and spatial positions of the Nancay Radioheliograph (NRH). This event included long-lasting zebrapatterns between 08:15 and 10:30 UT related to a small flare (1B M2.3) in AR 8649 localized at S15 E03 with maximum at 08:14. The event was accompanied by a CME of HALO type at 09:06. The peak radio flux in the decimetric range was 42000 s.f.u. at 606 MHz at about 08:48.

Concerning fine structures, three main phases can be selected: the impulsive (08:15 – 08:30), followed by the peak (08:50 – 09:25) and the decay (10:15–10:30). During the first two phases narrow banded zebrapatterns with 50 – 150 MHz bandwidth appeared in the frequency range from 200 up to 1500 MHz (Ondrejov spectra). The interval between different bursts was lasting about one minute. During the decay phase zebra-patterns appeared mainly at frequencies between 300 and 400 MHz.

The two top panels of Figure 4.21 show examples of the zebra-patterns during the impulsive phase (left, IZMIRAN) and the decay phase (right, Phoenix-2). In the left panel zebra stripes drift towards higher frequencies. In the later decay phase the zebra lines show different frequency drifts with tendency towards lower frequencies. With this frequency drift behavior zebra stripes resemble fiber bursts. A common property of both zebra and fiber burst was the absorption of the continuum emission at the low frequency edge of each stripe. The middle panels in Figure 21 show evident absorption in the L- and R-plots of the Trieste AO at 237 MHz (left) and 327 MHz (right). The circular polarization was weak at the beginning of the event (weakly R-handed at 327 and 408 MHz during the impulsive phase at 08:15) and moderately L-polarized (about 30-40%) after 08:25. At the maximum the L-polarization increased to about 60-80% and then towards the end became once more moderate.

After the event maximum (08:55) some unusual fiber bursts appeared with absorption at both low and high frequency edges of the emission stripe (Figure 4.22). Additionally, some stripes were observed in absorption only. After 10:19 almost all zebra stripes and fiber bursts showed absorption at the high frequency edge (Figure 4.22, bottom). During that interval zebra-stripes formed some cascades with U-burst like change of the frequency drift (from negative to positive). In such cases fiber bursts were continuously converted into zebra-stripes.

SOHO/EIT data show two new bright loops that appeared earlier than the two intervals of zebra-pattern structures (bottom panels at the Figure 4.21). According to NRH data the radio sources were located above these loops. During the impulsive phase, the zebra-patterns between 450 – 550 MHz can be connected with the appearance of new bright kernels (arrow in Figure 4.21, left SOHO/EIT panel). According to SOHO/MDI magnetograms these evolving kernels appeared above the neutral magnetic line, that explains the change of polarization sign at that moment. Afterwards, flare kernels form the raising bright loop and the radio source at 327 MHz were localised just above this loop.

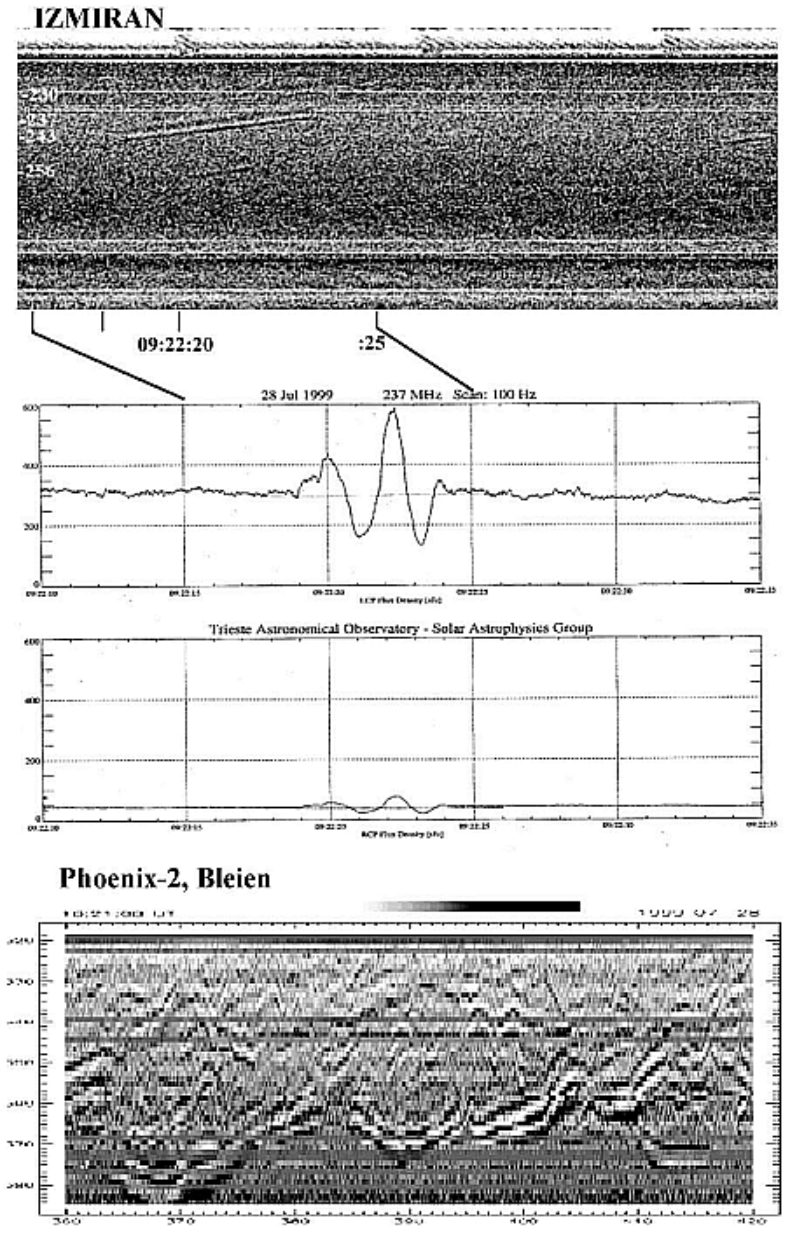

Fig.4. 22 *Top panel*: IZMIRAN spectrogram showing the absorption at both low and high frequency edge of the emission in a fiber burst, confirmed by the Trieste AO polarization measurements (*middle panel*). *Bottom panel*: Phoenix-2 spectrum between 320 and 385 MHz displays an unusual zebra-pattern with absorptions at high frequency edge of the emission stripes (from Messmer et al., 2002).

A common interpretation of the above observations is that the zebrapatterns occurred in the new formed coronal flare loops. The narrow bandwidth of the zebrapatterns is determined by the vertical dimensions of these emergent loops. The change in frequency drift can be interpreted as the change of the density gradient at the radio source and of the whistler group velocity direction due to the quasilinear scattering of whistlers on fast particles. The partial L-polarization suggests ordinary emission mode.

The striking feature is the inverted position of the absorption stripe in the zebrapattern during the decay phase, i.e. at the high-frequency side of the emission stripe. This has to be accounted for by any theory of the zebra-burst emission mechanisms. A similar behavior of fiber bursts was considered in Chernov (1990b) where it was shown that in such a case the observed emission is obtained by wave decay $l \rightarrow t + w$, with emission at the frequency difference between *l*- and *w*- waves. The continuous conversion of fiber bursts into zebra-lines with positive frequency drift, considering that the other parameters of both structures are identical, testifies an unique origin of both structures in frames of whistler model.

The September 23, 1998 event

According to Solar Geophysical Data (SGD), a 3B M7.1 flare began at 06:40 UT in the active region NOAA 8340 (N18E09), reaching its maximum at 07:13 UT. The radio event was observed from 06:52 to 11:00 UT, and included a type II outburst (06:52 – 07:02 UT) and a prolonged type IV outburst with several maxima. Zebra structure was observed in the interval 08:00 – 08:10 UT. In the spectrum in the upper panel of Figure 4.23, obtained with the new ARTEMIS IV spectrograph (Greece) at 250 – 450 MHz (Caroubalos et al., 2001), we can see a fiber burst (08:03 – 08:04 UT), rib-like zebra structure (08:05 – 08:06 UT), and rapid pulsations in emission and absorption (08:08 – 08:09 UT). Below the spectrum, a rare property of the fine structure is visible in the 327-MHz polarization profiles obtained at the Trieste Astronomical Observatory: the radiation displayed very weak left-circular polarization. These profiles also show that the dips in intensity in the absorption stripes comprise about 20 – 30 % of the mean continuum level. The zebra structure observed at 08:06 – 08:07 UT was most pronounced in absorption, and the rapid pulsations observed at 08:08 – 08:09 UT were also purely in absorption (i.e., they were of type sudden reductions).

The evolution of the flare is illustrated in four different panels in the lower part of Figure 4.23. A two-ribbon *Hα* flare was observed over three hours along the eastern and western parts of a neutral line of the magnetic field. The two TRACE 195 Å frames show numerous bright loops that appear (and disappear) between these two parts of the neutral line. A new bright loop appeared in the southern part of the flare region at 08:00 UT, and the center of the 327 MHz radio source observed at 08:08 UT (NRH) coincides with this new loop in the 195 Å TRACE frame.

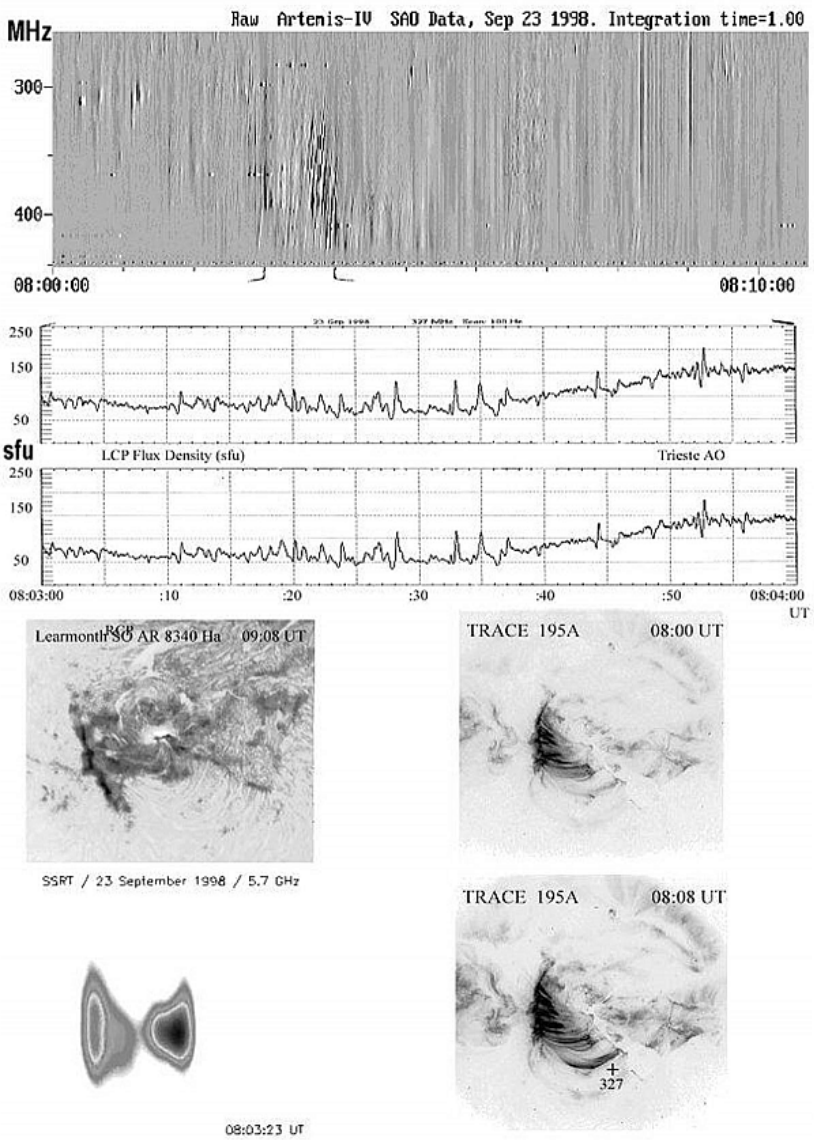

Fig. 4.23 The event of September 23 1998. *The upper panel* shows the fine structure displayed between 08:00 and 08:10 UT at 250 – 450 MHz (the ARTEMIS-IV spectrograph, Greece). *The next panel* presents time profiles of the L and R channels of the Trieste Astronomical Observatory polarimeter at 327 MHz, which shows weak left-circular polarization. *The lower set of panels* presents the development of the *Hα* flare (upper left; Learmonth Solar Observatory), two EUV 195 Å frames, which show numerous hot loops between two parts of the neutral line (*right*, TRACE), and the radio brightness distribution at 5.7 GHz (*lower left*, SSRT). The position of the center of the radio source at 327 MHz (NRH) is indicated by *the cross* above the new loop at 08:08 UT (from Hillaris et al., 2002).

Thus, the analysis of all the available observational data for these event show that fine structure was observed simultaneously with the appearance of new, hot magnetic loops, and that the frequency bandwidth occupied by the fine structure in the spectrum (280 – 450 MHz) could realistically be determined by the extent of these new loops in the corona. Again, the data demonstrate that the zebra structure consists not only of stripes of emission, but also of stripes with appreciable absorption, which are sometimes even dominant.

4.4.4. Unusual fibers

Slow drifting fibers in the type II bursts

The term 'unusual fibers' we use only in connection with unusual frequency drift, characteristic for fiber bursts (IDB), (on classification of Slottje and Kuijpers), since in many events fibers as separate bursts have different speed of frequency drift (almost as zebra), which is already obvious based on the example of the first spectra of slow drifting fibers of Thopmson and Maxwell (1962) (Figure 4.24). They showed such unusual fibers in type IV burst at frequencies 100 – 180 MHz and at frequencies 25 – 50 MHz in the end of type V burst in its low frequency part.

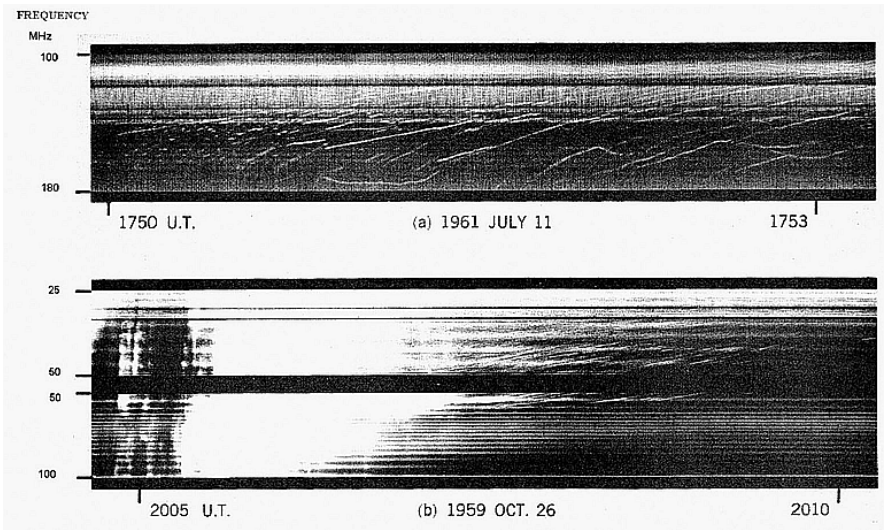

Fig. 4.24 The first example of unusual fibers in the range 25 – 180 MHz (from Thompson and Maxwell, 1962).

The subsequent observations showed, that the unusual fibers appear more frequently in the the type II bursts. Sometimes the II type emission degenerates simply into the narrow-band fibers. An example of such fibers is given by Chernov (1990a) in Figure 3. But more frequently slow drifting fibers appear in the flare continuum immediately after the type II burst. Specifically, such fibers at frequencies 72 – 140 MHz are analysed in detail by Bakunin et al. (1991) in the event February 3, 1983. The similar bursts are analyzed by Chernov (1997) at more high frequencies 186-236 MHz in a strong flare continuum in the event of October 12, 1981 (Figure 4.25). The unusual fibers were observed on the impulsive phase of flare, and the zebra patterns appeared just the same time and continued more than half hour. The microwave burst of the type gradual rise and fall (GRF) had the maximum (delayed relatively metric burst) and just the maximum phase of zebra pattern. The slow drifting fibers differ from the fiber bursts by many parameters: larger instantaneous frequency bandwidth (≈3 MHz at 115 MHz); slower frequency drift (about equal to drift of type II bursts); long duration (about one minute instead of some seconds). Nevertheless, sometimes they reveal low frequency absorption (Bakunin et al. 1991), typical for FB.

The first, natural suggestion that the emission from elongated density irregularities are observed (when a shock wave propagates through them), do not support by the registration some second after of the subsequent type II burst without similar fibers at the same frequencies in the same event. Since the formation and disruption of dense extended irregularities cannot occur in only a few second, we would suggest that in each case the fibers are created by an emission mechanism, rather than by the structure of the corona.

A number of data on interplanetary shocks indicate the presence of plasma wave and whistler in the upstream of fronts. It is, therefore, logical to consider the fiber structure of type II bursts to be the result of the propagation of whistlers through clumps of plasma waves ahead of a shock front. The absence of bounce motions of the fast particles ahead of the shock front explains the lack of strict periodicity of the fibers. Without diffusion of fast particles on whistlers the absorption at low-frequency edge cannot created, as confirmed by the observations. Whistler wave packets can be almost standing before the front (when the whistler group velocity is about equal to the velocity of the shock) which explains the prolonged whistler propagation (without the cyclotron damping), i.e. longtime fibers.

The slowly drifting fibers in the flare continuum (after the type II burst) shown in Figure 4.25 (see also Figure 12 in Bakunin et al. (1991)) can be related with whistlers generated between two shock fronts or between shock front and CME propagating with almost equal velocities (see in more detail Chernov (1997).

Rope-like fibers

For the first time, Aurass et al. (1987) reported on a new fine structure observed by IZMIRAN spectrograph during the type IV radio burst on April 24, 1985 (Figure 4.26). It was named as slowly drifting chains of narrowband fiber bursts, then as envelope of fibers (Mann et al. 1989) and as rope-like fibers (Chernov, 1997). This last name in the best way reflects their view of dynamic spectrum, and it will be used in the following presentation. The rope-like structures are characterized by

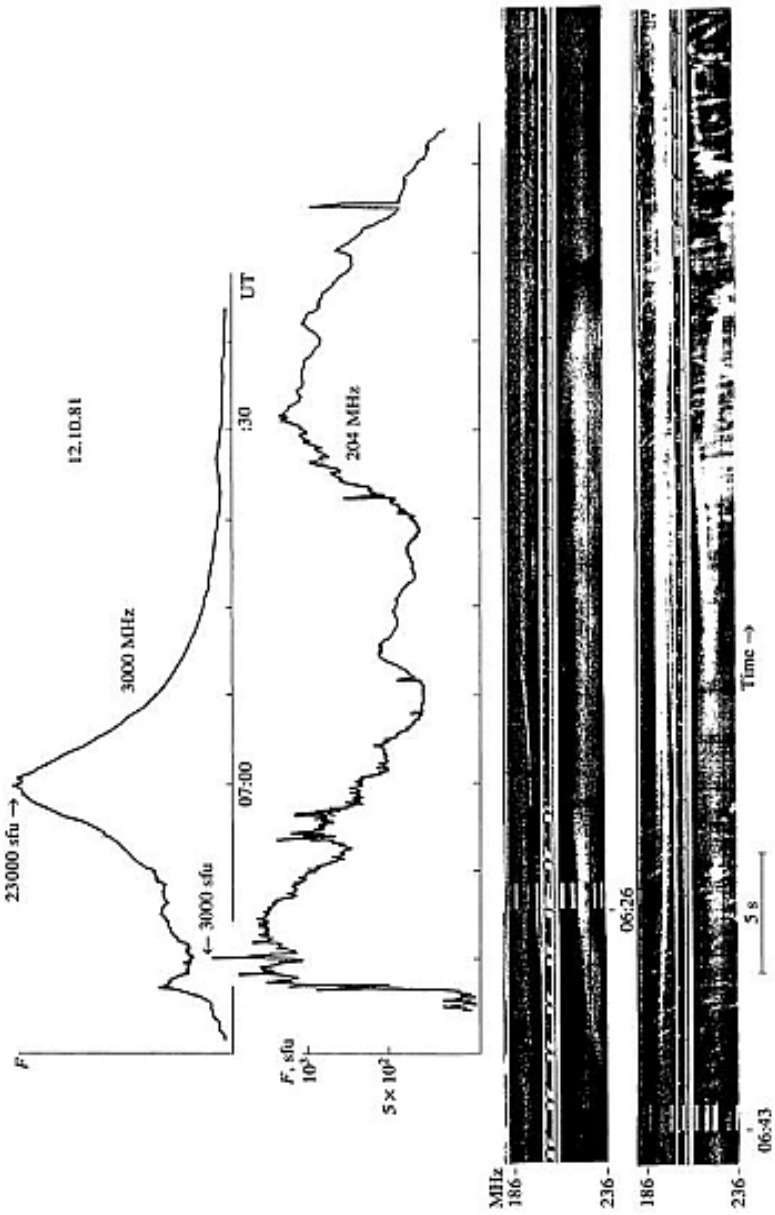

Fig.4.25 *Two bottom panels*: slow-drifting fibers recorded by IZMIRAN spectrograph in the strong flare continuum after the type II burst on 12 October 1981 (at 06:26 UT) and at the background of a braided zebra pattern (at 06:43 UT). *Two top panels*: time profiles at frequencies 3000 and 204 MHz; the maximum of microwave bursts (of type gradual rise and fall) delays noticeably relatively the burst maximum at 204 MHz (from Chernov, 1997).

a slowly positively or negatively drifting rope of narrowband, always negatively drifting fiber bursts. The fibers possess very pronounced absorptions at the low frequency side confirmed by a strong modulation depth presented by the radio flux profile at 234 MHz at the bottom of Figure 4.26.

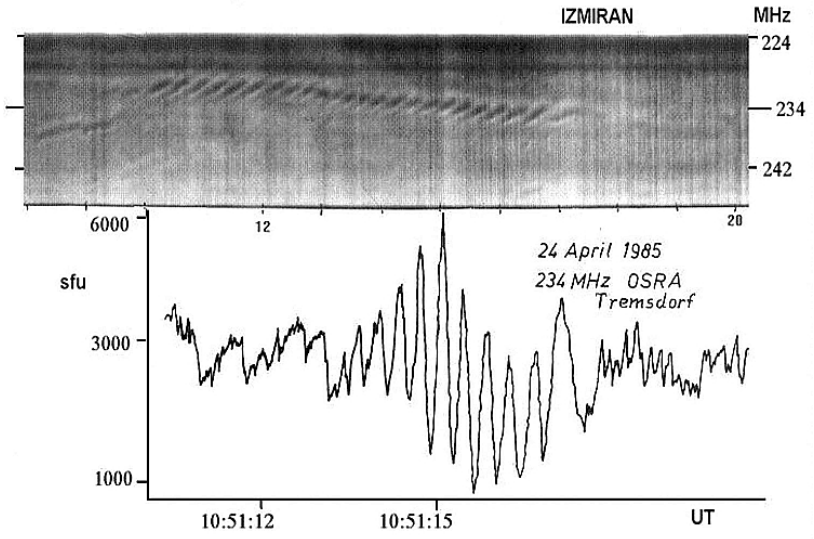

Fig. 4.26 IZMIRAN spectrogram in the 224 – 247 MHz range of rope-like chains of fibers and corresponding radio flux registration at 234 MHz of the Tremsdorf Observatory (from Aurass et al., 1987).

In the same time the majority of ropes is accompanied by its own low frequency absorption, which sometimes proves to be more expressed, than emission, as this is shown in Figure 4.27: rope began from a black stripe only in the absorption. The instantaneous bandwidth of the ropes is roughly 2 MHz and of narrowband fibers is 0.5 MHz. The fibers have typical drift rates of -5 MHz s^{-1} and the ropes have slow oscillating drift, not exceeding $\pm 1 \div 1.5$ MHz s^{-1}. Thus, the fibers in a rope represent typical features of FB in the frequency range around 200 MHz, with exception of their small frequency extent of 2 MHz. The individual fibers in the rope have approximately the same characteristics. The time distance between the fibers in the rope is strictly constant, and on the average equal to 0.4 s, with the average duration at one frequency $\lesssim$ 0.1 s. Both these parameters are much less than for usual FB, according to Elgarøy (1982) and Kuijpers (1975a). So, we must stretch to explain the more rapid repetition of the fibers in the ropes.

In the section Polarization it was shown a weak polarization degree of $20 \div 30\%$ in this event, which can be connected with depolarization effects during propagation. The rope-like fibers were observed in the event April 24, 1985 during more than one hour. It is important to still note, that the ropes were observed against the background of broadband fast pulsations with the period $\lesssim$ of 0.1 s.

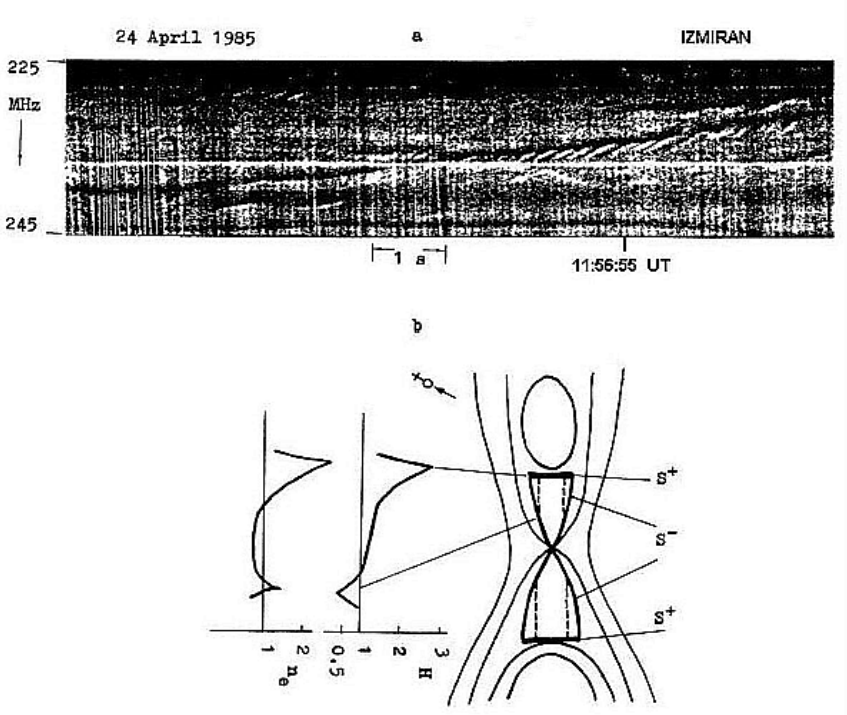

Fig. 4.27 *(a)*: the rope which has begun from pure absorption. *(b)*: qualitative scheme of a possible radio source of the ropes in the form of a quasi-stationary magnetic reconnection with a type X neutral point (Forbes and Priest (1983) and the approximate variation of density and magnetic field strength in the reconnection region (Sidneva and Semenov, 1985); S^- - slow shock fronts, S^+ - fast shock fronts, *dashed lines* denote whistler wave packet trajectories (from Chernov, 1990).

Rope-like fibers in other events

It is not possible to say that a structure of such type is very rare. With small variations in the parameters they appear at different phases of the flare. A number of ropes similar to those of April 24, 1985 were observed in the event October 12, 1981 shown in Figure 4.25. They lasted more than an hour at the post maximum phase. Sometimes ropes appear simply in the composition of ZP. Specifically, such an example is shown in Figure 4.28. A set of ropes embedded in the developed ZP was observed during two minutes in a short event July 18, 2000. The fine structure appeared after strong group of type III+V bursts during a small, 1F C9.3 flare in AR 9087 (S13E16). However, attempts are made to rename similar structures as a new type of bursts. A rope (named as sawtooth bursts) in the event November 3, 1997 are discussed in two versions of the work: Klassen et al. (2001)

and Karlicky et al. (2002). For the comparison we show this event recorded simultaneously by spectrographs in Tremsdorf and

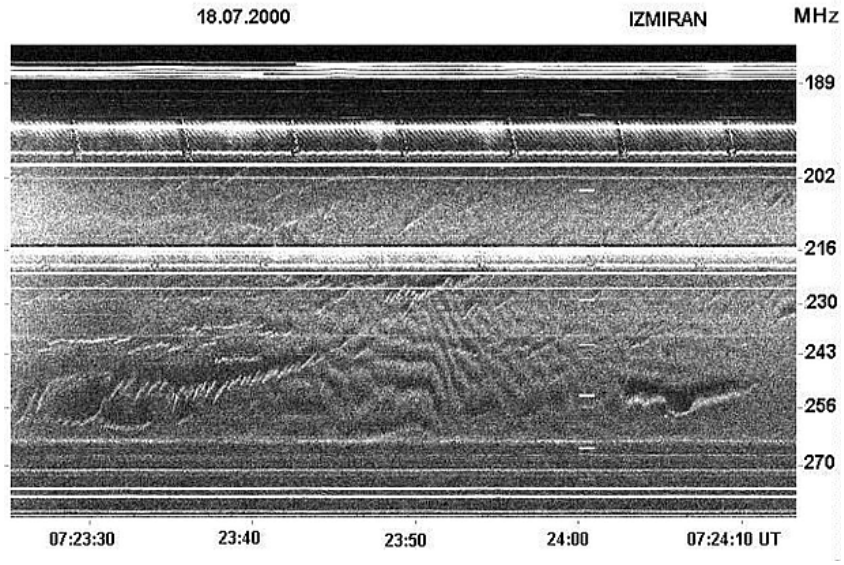

Fig. 4.28 A set of ropes embedded in the developed ZP in the event July 18, 2000 (from Chernov, 2008).

IZMIRAN in Figure 4.29. Both papers are devoted to the analysis of fibers after 09:09 UT around 150 MHz, but one minute before two other chains of fibers are visible: one at about the same frequency range, and another at frequencies 210 – 215 MHz. And in both these chains the fibers overlap on the time. According to IZMIRAN spectrum the chain at 09:09 UT do not also completely satisfy condition, that the subsequent fiber begins only after the termination of the emission of previous one, although precisely this condition should justify the new name. It is undertaken by analogy with X- ray traces (obtained in TOKAMAK plasmas) generated by disruptive instability. Although, entire process more suits for explanation of simultaneous impulsive X-ray bursts and of type III bursts. The new name stimulated the authors for the creation of new mechanism, moreover even without any references on their previous interpretations of similar bursts (Mann et al, 1989). There is also no basis to use the interpretation of these fibers to Lace-bursts (or braided zebra), since as the regular fibers in the narrow frequency band are not similar to disorderly Lace- bursts on all parameters. Besides, the mentioned authors do not discuss remarkable splitting of fibers before the termination, regular frequency drift of fibers and the entire rope. Since these periodic fibers in the dynamic spectrum are actually similar in general appearance to a rope, here we will use this term. In contrast to the terms mentioned above, it does not simultaneously imply a model of their formation. Comparing the ropes of fibers in Figures

4.26 – 4.29, we can conclude, that these are identical phenomena. A certain variety of ropes in the different events does not exceed variety of ZP, depending on the concrete plasma parameters in the source.

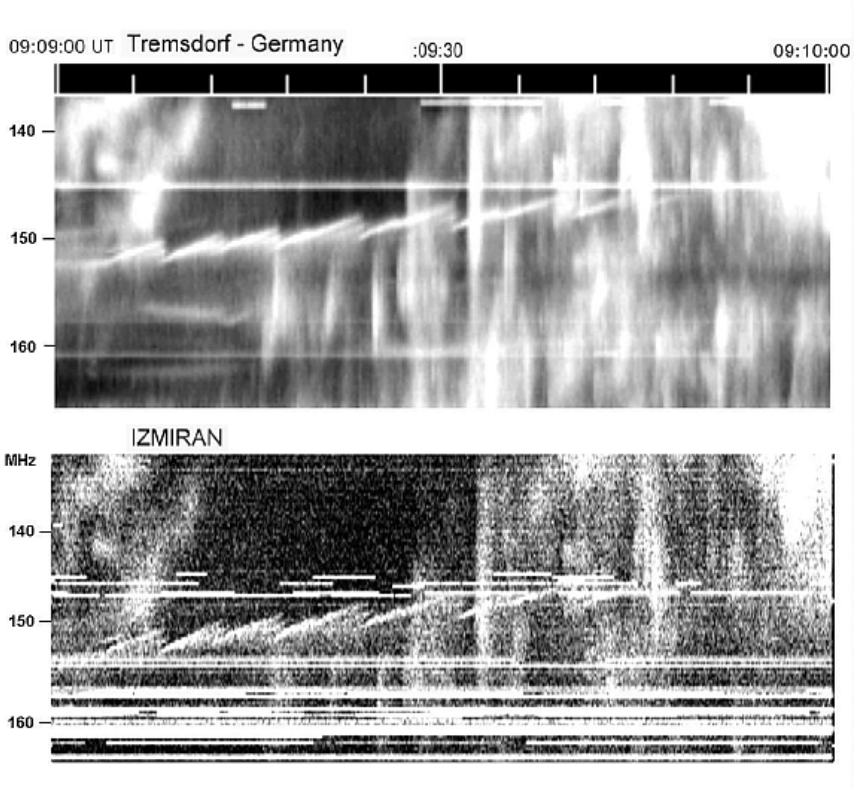

Fig. 4.29 Magnified fragments of the Tremsdorf and IZMIRAN spectra (on the same time scale) showing a close coincidence between the rope of fibers and all of the accompanying bursts in the November 3, 1997 event at impulsive phase of flare during the strong type II burst (from Chernov, 2008).

The analysis of several events carried out by Chernov (2008), showed that the ropes of fibers are usually observed in the time interval when the hock front catches up with the leading edge of a coronal mass ejection. Thus, the radio emission source should be located in a height interval between the CME and the shock front catching up with it.

Rope-like fibers at decametric range; the May 2, 1998 event

For the event May 2, 1998 ZP structures were first observed at frequencies between 22 – 46 MHz with Nançay DCM spectrometer-polarimeter (Figure 4.30). The radio event was simultaneous with a large 3B X1.1 flare at 13:30–13:42–15:13 UT in the active region NOAA 8210, with coordinates S15W15. The SOHO LASCO telescope detected a major halo-type coronal mass ejection (CME) extending to 26 $R\odot$. The radio event included a large group of type III bursts, two type II bursts, and type IV continuum radiation. A global dynamical spectrum is presented by Leblanc *et al.* (2000). The maximum energy release in the corona occurred at the heights where the decimeter radiation was generated (22 000 s.f.u. at 606 MHz), but the event extended to lower frequencies and into interplanetary space, as type II and III radio bursts. Zebra pattern structures were first observed over approximately three minutes between 22 – 46 MHz (Nan¸cay DCM spectrometer-polarimeter) against the flare continuum after the strong type II and type III bursts. The dynamical spectrum in the upper panel of Figure 4.30 shows that the zebra structure consists of numerous fragments of stripes with various frequency drift. The most evident long fragment resembles a narrowband rope of fibers with a constant frequency drift. This main rope of fibers with the duration of about two minutes forms the low-frequency boundary of all the zebra-pattern fragments some of them also forming ropes of fibers at higher frequencies. The frequency drift of the main rope is approximately -0.13 MHz s^{-1} near 35 MHz. The frequency drift of separate fibers is much less, ~ -0.04 MHz s^{-1}. We should note two more important properties of the main rope: its frequency width increased from 0.25 MHz at 43 MHz to 0.8 MHz at 22 MHz, accompanied by an appreciable decrease in the left-circular polarization.

The width of the frequency bands for individual stripes of emission was approximately the same for all the zebra-structure fragments, $\Delta f_e \approx 0.08$ MHz, with the relative width of these bands being $\Delta f_e/f \approx 0.0024$. However, the frequency separations between the stripes of emission were appreciably different in different fragments ($\Delta f_s \approx 0.08 \div 0.17$ MHz), and the short-time-scale fibers within the main rope are not strictly periodic in frequency. In some fragments, a low frequency absorption is observed, and frequency separation between an emission stripe and the neighboring absorption, Δf_{ea} is approximately equal to Δf_e.

The radio emission of all components of the type II and type III bursts was essentially unpolarized, while the main rope displayed strong left-circular polarization (black at the spectrum in Figure 4.30). Other fragments of the zebra structure displayed moderate right-circular polarization (white in Figure 4.30). Two-dimensional NRH radio source images of at 164 MHz show four radio sources above active region NOAA 8210. The complex behavior of the polarization of the fine structure may indicate that different radio sources are located in regions with different magnetic polarities.

The lower part of Figure 4.30 displays the evolution of the flare in the 195 Å EUV line (five frames from SOHO/EIT sequence), while the sixth lower panel shows the onset of the $H\alpha$ flare.We can see in this last panel that a helmet-like ejection has already formed above the sigmoid flare ribbon by 13:24 UT. The continuation of this ejection is clearly visible in the first 195 Å frame, which corresponds to the maximum of the flare (13:42 UT). We can see also two ejections,

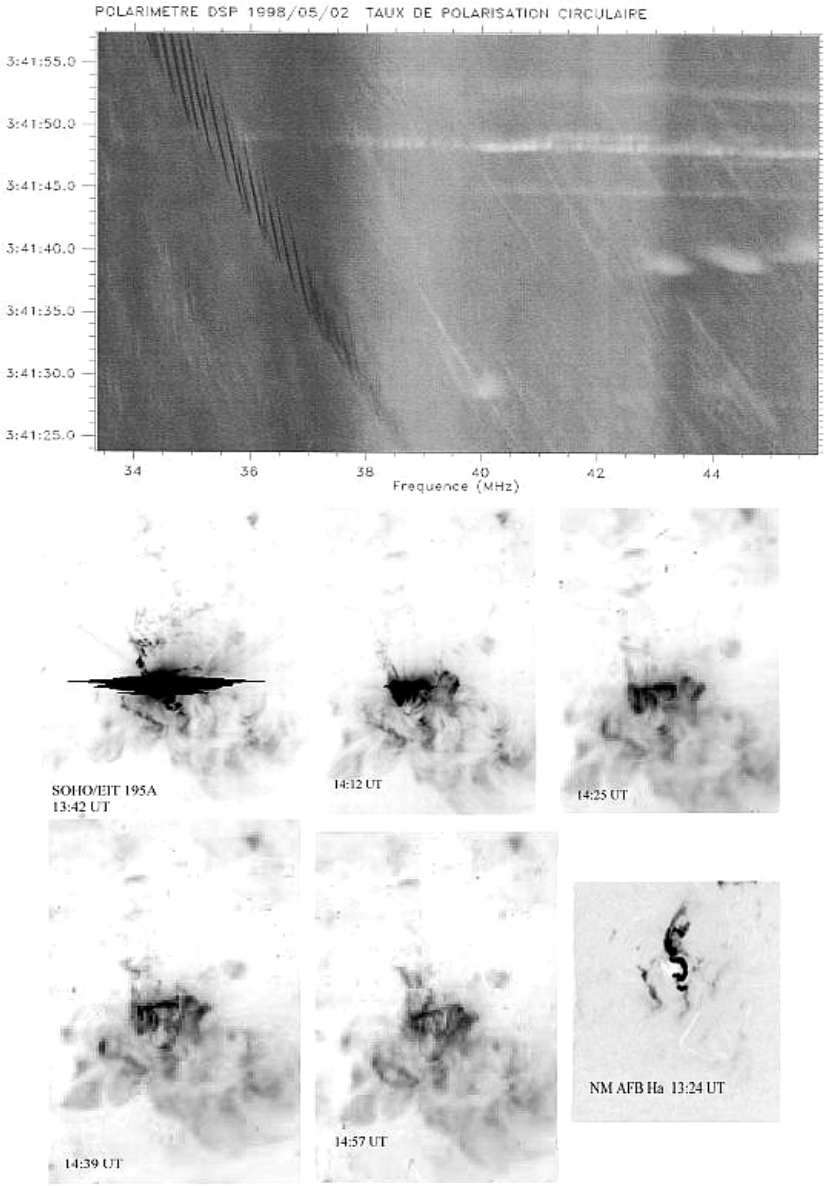

Fig. 4.30 The event of May 2, 1998. *The top panel* shows the degree of circular polarization in the dynamical spectrum obtained using the decameter spectropolarimeter (DSP) of the Nan¸cay Observatory (the time resolution is 0.05 s). *The lower panels* show the development of the outburst in the 195 Å EUV-line (SOHO/EIT) and the $H\alpha$ emission in the Active Region 8210) (from Chernov et al., 2006).

northwards and southeastern. Taking into account the presence of the two type II bursts, it is probable, that the upper ejection caused the first type II burst, and the lower - the second one. Each subsequent frame contains new fragments of ejected material in projection onto the disk.

According to Nançay spectra the first type II burst began at 70 MHz on 13:40 UT and the second one on 13:48 UT. The frequency drift of the first burst was ≈ -0.143 MHz s^{-1} which corresponded to the shock front velocity ≈ 960 km s^{-1} (using the density model of Leblanc et al.(1998), and the velocity of the second shock was much less, ≈ 380 km s^{-1} (Leblanc et al., 2000). This latter corresponds to the slower movement of the front in the southeast direction in the subsequent pictures in Figure 4.30. CME appeared at the height $1.0R\odot$ on 14:06 UT. Taking into account the CME velocity of 1040 km s^{-1} it is easy to show, that CME has arisen high in the corona, at any rate, near a plasma level of 80 MHz ($\approx 1R\odot$). Thus both shock fronts were blast, without any relation with CME.

The rope fiber structures were observed just at the flare maximum during the first type II burst. Behind this first shock front, the second slow shock front was located, and ahead of it was the CME with greater velocity, than the first shock front. Two type II bursts appeared at 14 MHz in *WIND* RAD2 spectrum approximately at 13:45 and 14:07 UT (the beginning of the first one hides behind the powerful type III bursts). The delay between them increased from 8 minutes on 70 MHz to 13 minutes at 14 MHz, which is related to the delay of the second slow shock front. It is obvious that, after the CME, the energy release proceeded in a vertical current sheet, which had structure with magnetic islands. Therefore the appearance of ZP in the decimeter range on 14:29 UT (shown in Jiricka et al. (2001) at the post-flare phase can be related with such magnetic islands. The appearance of a fiber structure in IP type II bursts it is probably connected with the passage of the shock front through a jet structure after CME. We exactly see such narrow streamers in the LASCO C2 image on 15:03 UT at the heights $\approx 3R\odot$, corresponding to plasma frequency of 4 MHz (according the model of Leblanc et al. (1998)). In the range 1 – 5 MHz the relative values of the parameters of fibers are greater approximately by an order of value, than in the metric range.

4.4.5 October 25, 1994 event: Observations

Some features of this burst were previously analyzed in Manoharan et al. (1996), Aurass et al. (1999), Zaitsev and Zlotnik (2002), Aurass et al. (2003),

Zlotnik et al. (2003); the main unusual properties of the ZP were not considered, however.

We used the data from simultaneous observations with several radiospectrographs (ARTEMIS, 100 – 500 MHz (Nançay), IZMIRAN, 25 – 270 MHz, Tremsdorf (Potsdam), 40 – 800 MHz), as well as the data from the radio-heliograph of Nançay (NRH) and the polarimeter in Trieste AO at frequencies 237, 327 and 408 MHz.

The radio event consisted of a type II burst drifting from frequencies below 90 MHz at 10:00 UT to 40 MHz at 10:06 UT, a short type IV burst (burst continuum) with a fine structure in the form of periodic type III bursts between 10:05:18 and 10:08:35 UT, and a ZP between 10:08:00 and 10:09:00 UT.

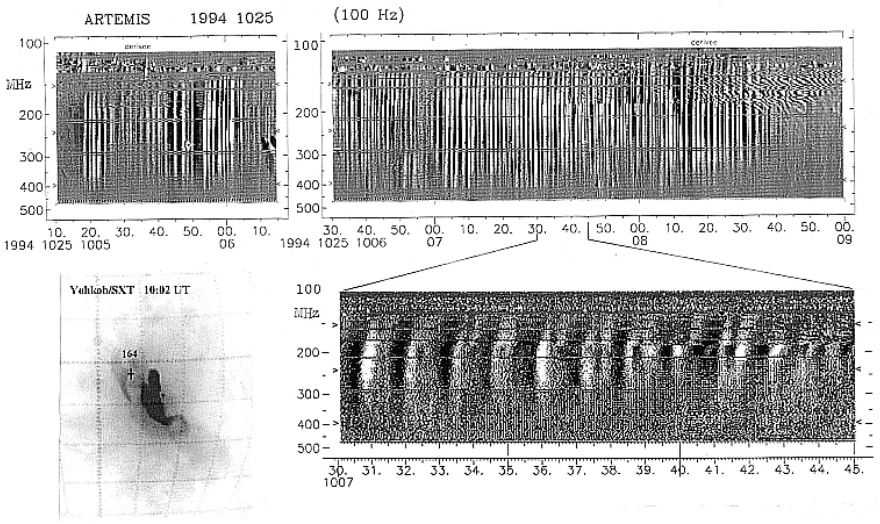

Fig.4.31 Dynamic spectrum of the periodic type III bursts (which are reminiscent of pulsations) in the event of October 25, 1994 over the entire range of the ARTEMIS spectrograph, 100 – 500 MHz (in the derivative of the signal). It can be seen *in the top panel* that a ZP appears in the frequency range of 135 – 210 MHz at the end of the event. *In the lower left panel*, a magnified fragment of the type III burst spectrum is shown, which demonstrates an abrupt stop of the frequency drift at a frequency of about 170 MHz just before the beginning of the ZP. It can be seen in *the lower left panel* that the center of the radio source at a frequency of 164 MHz (marked with *a cross* against a Yohkoh/SXT image with the thin A1.1 filter) is located beyond the bright flare region (from Chernov, 2005).

The dynamic spectrum observed with the ARTEMIS spectrograph is shown in Figure 4.31. The type III bursts drift very rapidly over frequency (perhaps, due to the elevated plasma density above the burst region). At lower frequencies, however, the drift is much slower. The energy release was mainly concentrated in the meter wavelength range. The maximal spectral intensity at a frequency of 204 MHz was 300- 400 s.f.u. between 10:08 and 10:09 UT. A minor (49 s.f.u.) GRF

type microwave burst was observed over about one hour. According to Solar Geophysical Data, No. 608 (II), 1994, a small *H*® flare of 1N importance was observed from 09:40 to 12:36 UT (with a maximum at 10:04 UT) in the 7792 (S09, W12) AR. An active dark filament and a filament system over this AR were also observed. Some details of this type IV radio burst with different locations of the radio source beyond the AR were discussed in Aurass et al. (1999).

In Figure 4.31 (the lower left panel) it can be seen that the center of the radio source of the fine structure at 164 MHz (NRH) superimposed on the soft X-ray (SXR) burst image (Yohkoh/SXT) recorded using a thin Al.1 filter is located beyond the AR. However, the source of the main continuum coincides with the maximum of the SXR burst. Each subsequent SXR image shows new bright sources both inside and beyond the main burst region; this points to the magnetic reconnection of the flare loop with neighboring loops. Probably, it is for this reason that repetitive bursts of radio emission at 327 and 408 MHz (Triest observatory) had different polarizations. The maxima of the SXR brightness occurred at the same place (in the center of the AR over the neutral line) at 09:59 UT (before the type II burst) and at 10:08 UT (during the type III burst). Sigmoid shape of the SXR burst followed the shape of the neutral line of the magnetic field. It was supposed in Manoharan et al. (1996) that the flare triggered a large-scale magnetic reconnection.

In this event, the ZP was observed in the frequency range 130 – 210 MHz against the background of type III bursts drifting from 400 to 150 – 125 MHz. Let us note the principal issues in Figure 4.31 that elucidate the event dynamics. The initial frequency of type III bursts varied between 300 and 450 MHz with a period gradually increasing from 10 -15 to 30 – 35 s during a series of type III bursts. This was possibly related to slow MHD oscillations of the region where the fast particles were accelerated. The lowest frequency of type III bursts varied asynchronously with their initial frequency and decreased to about 125 MHz between 10:08:12 and 10:08:30 UT.

An explicit indication of a new perturbation was that the frequency drift terminated abruptly between 10:07:38 and 10:07:57 UT at a frequency of 170 MHz (see the lower spectrum in Figure 31). About 3 s later, a ZP arose at frequencies of 140 - 170 MHz. By the end of the 8th min (10:08 UT), the ZP frequency range expanded to 130 - 210 MHz, whereas type III bursts gradually disappeared (their intensities and frequency bandwidths steadily decreased). In the time interval from 10:08:17 to 10:08:24 UT, within which the ZP was most pronounced, seventeen emission stripes with a frequency separation gradually increasing from 1.7 MHz at 140 MHz to about 2.2 MHz at 170 MHz were observed. The degree of polarization of radio emission in the ZP and type III bursts was rather moderate (25 - 30%) and reached its maximum in the ZS at the end of the 8th min. The right sign of polarization of radio waves emitted from the source above the southern-polarity tail spot corresponded to the predominance of ordinary waves.

A part of the ZP dynamic spectrum recorded with the Potsdam spectrograph is shown in Figure 4.32. It is almost identical to the spectrum recorded at IZMIRAN. The lower part of Figure 4.32 shows the contour lines of the south-north (SN) distribution of the radio emission intensity at a frequency of 164 MHz (NRH).

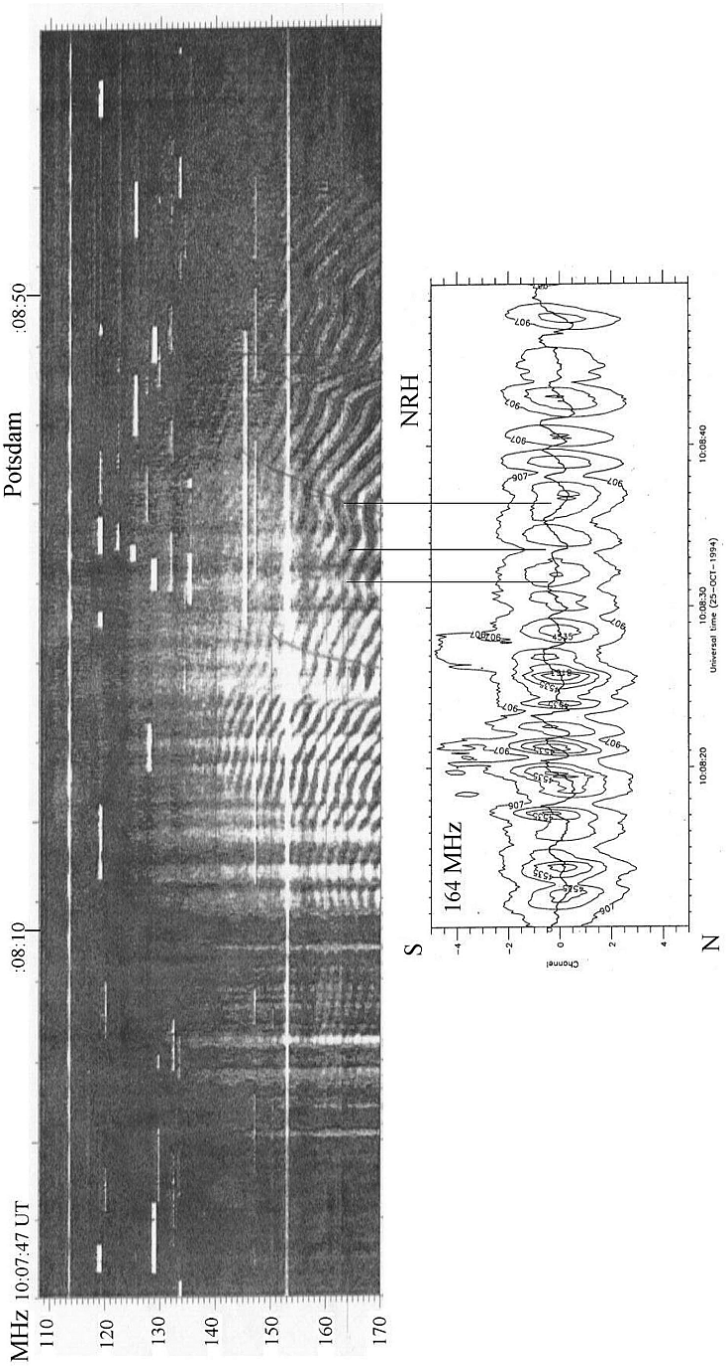
Potsdam
:08:10
:08:50
MHz
10:07:47 UT
110
120
130
140
150
160
170
NRH
164 MHz
S
N
Channel
10:08:20
10:08:30
10:08:40
Universal time (25-OCT-1994)

Fig. 4.32 *(Top)*: Dynamic spectrum of ZP against the background of periodic type III bursts in a part of the frequency range 110 – 170 MHz of the Potsdam spectrograph. *(Bottom)*: One-dimensional (S – N) contour plots of the relative brightness distribution at 164 MHz (Nan¸cay RH). The solid line passing through the maxima of the sources shows their spatial drift (from Chernov, 2005).

The maximal intensity corresponds to the center of the ZP source after 10:08:33 UT or to a type III burst before this instant. The solid line that passes through the source centers shows the spatial drift of the sources at a fixed frequency. We note that the centers of the sources of the ZP and type III bursts coincide not only in the NS direction but also in the east-west (EW) direction (i.e., on the Sun disk).

The III type sources (at the beginning of spectrum) drift from south to north, whereas the ZP sources (at the end of spectrum) drift from north to south. In all the ZP absorption stripes, the source drifts is the same way as in the type III bursts (one such instant corresponding to 10:08:33.4 UT is shown in Figure 4.32 by the heavy vertical line). The labels on the vertical axis correspond to the numbers of the spatial channels of the Nan¸cay radio interferometer. At a frequency of 164 MHz, one channel in the SN direction provides resolution of about 3.2'. Therefore, the average full width at half-maximum of the radio source (about 4.8') corresponds to one-and-a-half channel for both the ZP and type III bursts, whereas the maximal velocity of the spatial drift turns out to be > 90000 km s^{-1} (about 170 000 km s^{-1} for the last source). Taking into account the projection onto the disk, the actual velocities of the source are always > 10^{10} cm s^{-1} (i.e. close to the speed of light). Thus, the measured source size is actually the AR size and the observed drift velocities can only be attributed to fast (relativistic) particles. Approximately the same drift velocities of the ZP sources were observed earlier during the June 5, 1990 event (Chernov et al., 1994).

We also note the following important feature of the dynamic spectra: there are several humps in the ZP where the frequency drift changes its sign. The change in the sign of the frequency drift correlates with the change in the direction of the spatial drift of the ZP source. The negative frequency drift corresponds to the same source drift as for type III bursts. The change in the direction of the source drift is accompanied by the change in the sign of the frequency drift (see, e.g., the instants 10:08:32 and 10:08:36.5 UT in Figure 4.32, which are marked by thin vertical lines). These results allow one to choose model of the ZP generation and to explain the width of the frequency band occupied by the ZP in the dynamic spectrum (see Discussion). In the URAP experiment, the *Ulysses* satellite recorded one type III burst at 10:10 UT at frequencies below 1000 kHz. This burst was caused by an electron beam accelerated at the beginning of the flare.

4.5 ZP in microwave range: First zebra

In recent years because of the observations with the high resolution by the Chinese spectrometers, data about the detailed spectra of ZP in the microwave range (2.6-7.6 MHz) have appeared (Ning *et al.*, 2000).

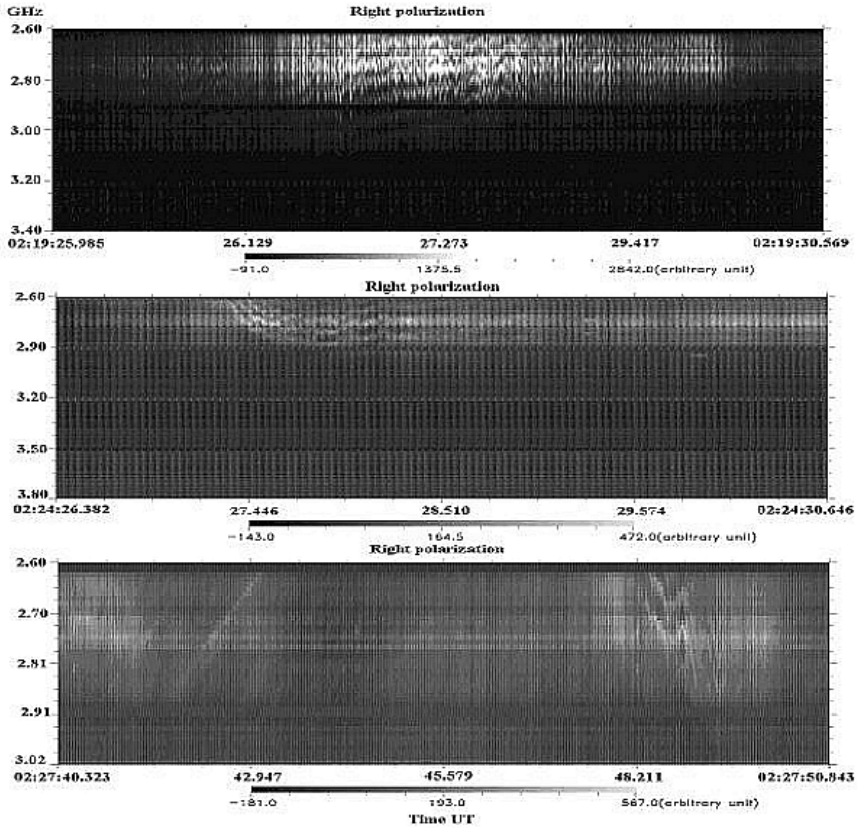

Fig. 4.33 Radio spectrograms of zebra patterns and fiber bursts during the evolution of the event of 29 October 2000 between 02:19 – 02:28 UT in right polarization recorded by the spectrometer of NAOC (2.6 – 3.8 GHz). The frequency difference between the 5 regular zebra stripes in the top panel depends weakly on the frequency (from Chernov et al., 2001b).

The event of October 29, 2000

The analysis of many cases of ZP near 3GHz in some events shows the full variety of fine structure similar to that seen in the meter range. In the event of October 29 2000, for about 20 minutes ZP and fiber bursts (FB) were followed by intermittent pulses of some seconds. An example of ZP evolution is shown in Figure 4.33.

This event was connected to the *Hα* 2B M4.4 flare in AR NOAA 9209, located at S25E35. The ZP shows different frequency drifts: slow negative, positive or switches between the two. The FB often overlap the zebra pattern, and the emission frequency band is about the same for both structures. After some fluctuations of ZP a strong series of FB with different periodicity and a constant frequency drift of -240 MHz s^{-1} was observed. The FB and ZP have about the same spectral parameters, e.g. the frequency bandwidth of emission stripes $\Delta f_e \approx 20 \div 30$ MHz and the frequency separation between emission lines is 50 – 80 MHz in the range 2.6 – 2.8 GHz.

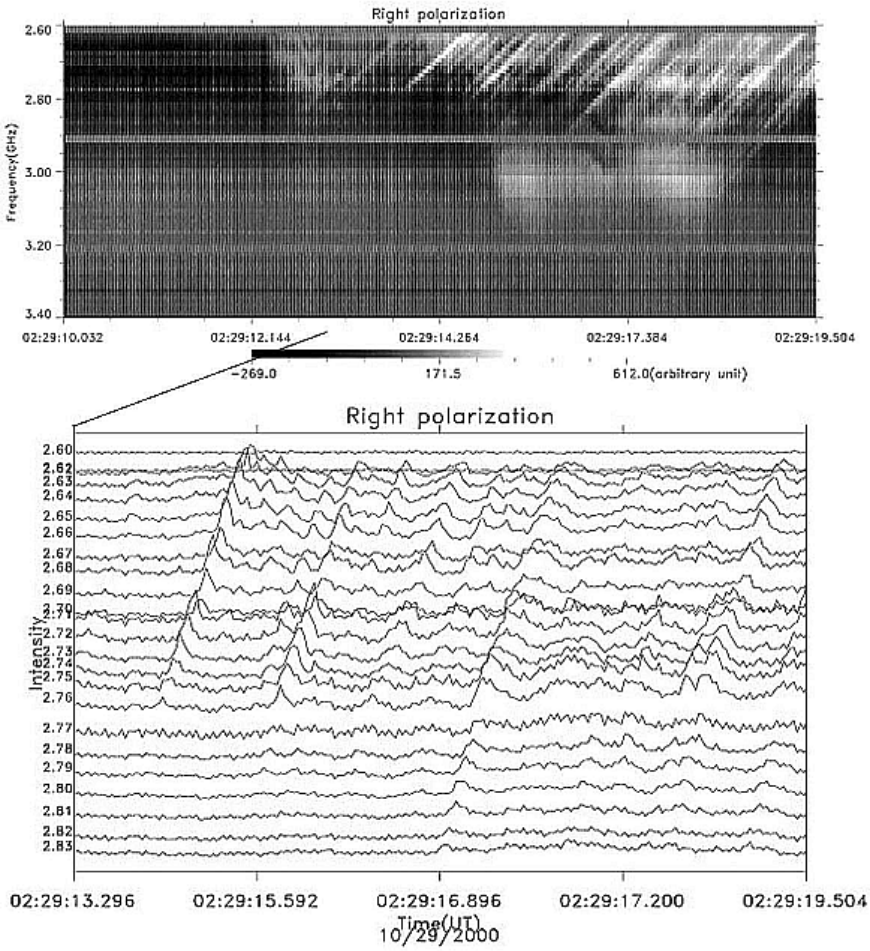

Fig. 4.34. Radio spectrograms of fiber bursts in the event of 29 October 2000. The multi-channel profiles (*bottom panel*) show irregular character of fibers in time and almost constant frequency drift. (from Chernov et al., 2001b).

In Figure 4.34 after some ZP wiggles we can see a series of strong fibers with different periodicities and almost constant frequency drift rate ~ -240 MHz s^{-1}. However, the multi-channel profiles in the bottom panel show the small retarding of the drift rate of some fibers, drifting from 2.83 to 2.60 GHz, which seems completely natural, in accordance with formula (1) (frequency drift is proportional to magnetic field strength). We see that the high frequency IDB are found to be identical in their relative characteristics with FB in the metric range.

A detailed analysis of the multi-channel time profiles (see Figure 3 in Chernov et al. (2001b) shows that the intensity level in the black stripes (between emission stripes) could be lower than the emission level of the main continuum (without ZP). Thus, the black zebra-stripes are visible not due to the absence of bright stripes, but due to an absorption of the main continuum emission (a modulation effect). In this connection the main parameter of ZP and FB is not frequency separation between emission stripes ($\Delta f_s \approx 60 - 70$ MHz on an average), but the frequency separation between the emission and the adjacent low frequency absorption with a mean value $\Delta f_{ea} \approx 30 - 40$ MHz. Therefore we can assume that both of the fine structures have the same origin.

The event of April 21, 2002

The eruptive long duration X1.5 class flare event of April 21 2002 occurred in AR 9906 close to the western solar limb (S14W84) between 00:43 and 02:38 UT. Images of TRACE data in the EUV 195 °A line show the formation of a bright post-flare arcade in the flare site (Gallagher et al., 2002). From 01:34 to at least 02:15, dark matter is seen falling onto the arcade from above. The dark matter apparently occults bright arcade loops.

The entire prolonged event was divided into two phases in the radio data and in hard X-rays: in the growing flow of soft X-rays (GOES) there was a first maximum in hard X-rays (about 01:15-01:18 UT, MTI/HXRS) and in the radio range (near 01:30 UT). In this phase the maximum energy release occurred in the decimeter wave band, which indicates magnetic reconnection at heights of the decimeter range. According to the data of radio-spectrographs (Hiraiso and IRS, Korea (Cho, personal communication)) high flux levels were recorded in the meter range (between 01:18 – 01:30), possibly with fine structure.

In the microwave range the maximum of the first phase was above that of the second phase. However, no fine structure in the first phase was registered around 3 GHz. The arcade of loops began to form only after approximately 01:30 UT.

The ZP are observed only during the second phase, between 01:44 and 02:05 UT, during the second phase of the HXR (MTI, HXRS) burst presented in Figure 4.35. In the loop arcade we see during this phase two new bright centers as X-points of magnetic reconnection (see top left panel in Figure 4.36). During the interval 01:51 – 01:53 UT the ZP was very weak. At this time in the TRACE 195 Å image some bright centers disappeared (see right top panel in Figure 36). The difference image between 01:50:57 and 01:48:16 shows many bright loops (middle left panel in Figure 4.36), where the radio sources of ZP could be located.

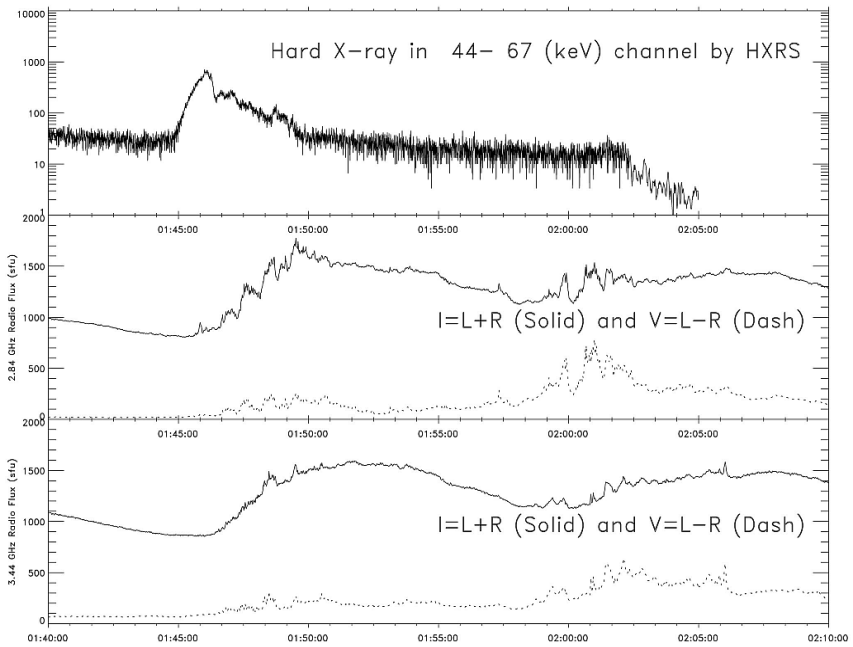

Fig. 4.35 The hard X-ray burst in the 44 – 67 keV channel of the HXRS during the period of ZP in 2.6 – 3.8 GHz. The Huairou radio profiles at 2.84 and 3.44 GHz showing the radio flux intensity (I = L + R) and the polarization component (V = L - R) are indicated by *solid and dashed lines* respectively (from Chernov et al., 2005).

At the same time three new sources of HXR (RHESSI, Gallagher *et al.*, 2002) appeared under the mentioned two X-points of the magnetic reconnection visible in the bottom left panel of Figure 4.36. Such a proposal is confirmed by radio source positions with SSRT data at 5.7 GHz for polarized emission (the parameter V, see two centers shown by isolines in the bottom right panel in Figure 4.36). White and black contours in the bottom left panel of Figure 4.36 show source positions of RHESSI/HXR energy channels respectively at 50 – 100 and 12 – 25 Kev (Gallagher et al., 2002). Radio sources of continuum emission in intensity with SSRT data (parameter I) have approximately the same positions. After 02:09 UT the arcade of bright loops in the line 195 Å rose to high altitudes (middle right panel in Figure 4.36), and the maximum of activity was displaced into the decimeter range.

All series of the ZP in this event represented zebra stripes with negative frequency drift, which is more inherent to fibers. In Figure 4.37 and 4.38 two intervals with the most pronounced ZP are shown, taken with the NAOC spectrometer at 2.6 – 3.8 GHz. In the first fragment of 20 second duration from 01:48:18 UT 34 zebra stripes are counted in the range 2.6 – 3.8 GHz with a barely noticeable increase in frequency separation between stripes from 27 MHz at 2.8 GHz to 43

MHz at 3.7 GHz. It is remarkable that the relative value of the frequency separation proves to be about the same as in the meter range $\Delta f/f \approx 0.012$.

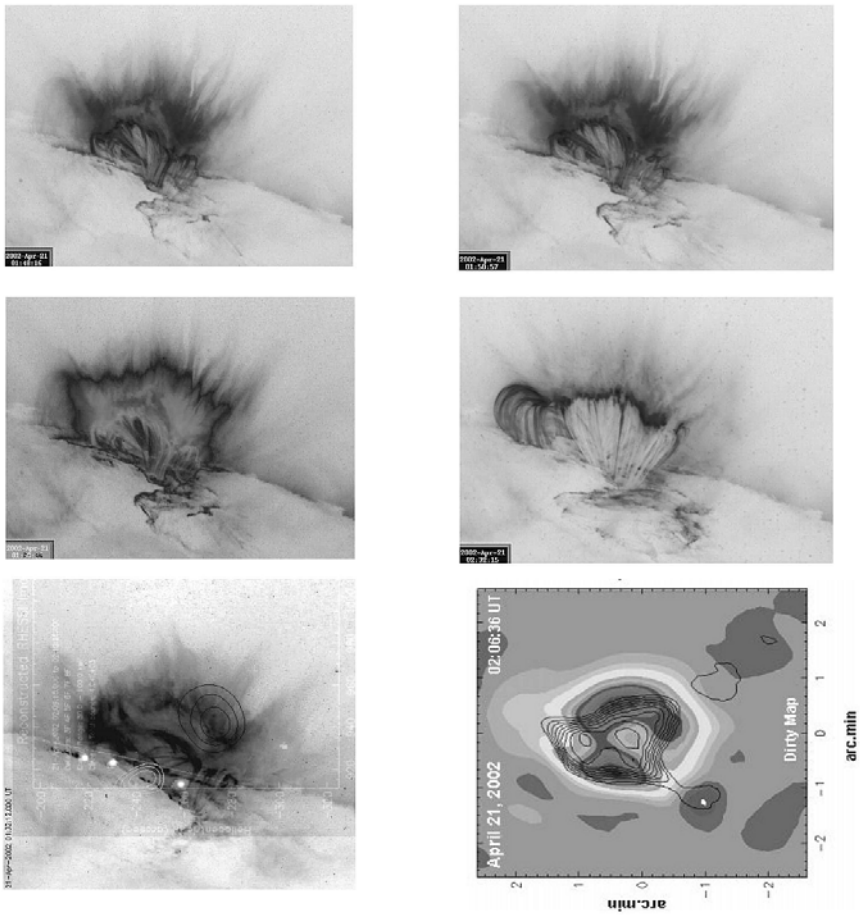

Fig. 4.36 The evolution of the flare of April 21, 2002 with TRACE data in EUV line 195 Å and RHESSI HXR data. The difference image between 01:50:57 and 01:48:16 UT is shown in (*middle left panel*). The *bottom left panel* shows three new sources (*white points*) of HXR (RHESSI, Gallagher, 2002). *The bottom right panel* shows radio source positions with SSRT data at 5.7 GHz (courtesy of R.Sych) in intensity (parameter I, shown by the *grey and black* background) and in polarization (parameter V shown by *contours*) (from Chernov et al., 2005).

The frequency drift of zebra stripes was negative and almost constant ≈ -120 MHz s^{-1} between 3.8 – 3.4 GHz, which is more characteristic of fibers. At the low frequency part of the spectrum a small deceleration of the frequency drift is observed. However, each 1 – 2 s, stripes undergo failures and jumps of frequency

drift, covering several adjacent stripes with a small time delay. Sometimes shifts in the frequency lead to merging or splitting of stripes. Such effects are well known in the meter wave band. In the bottom of Figure 4.37 a short fragment of intensity time profiles of about 3 s duration is shown at four frequencies.

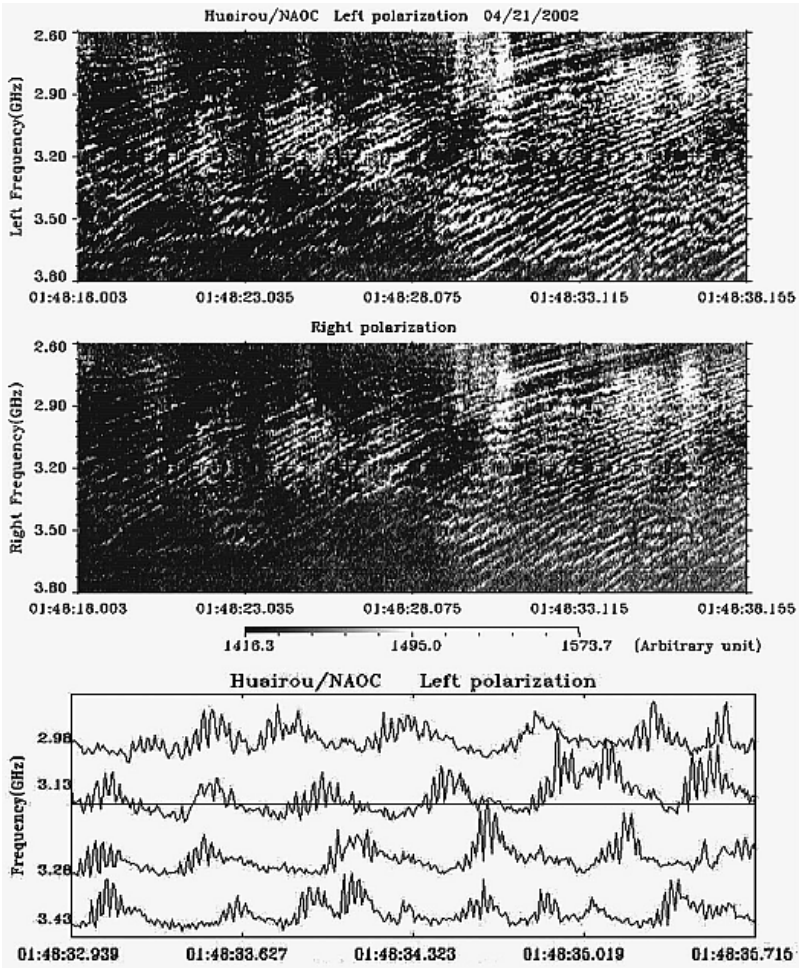

Fig. 4.37 Zebra structure in the event of April 21, 2002. *The two upper panels* show the Huairou radio spectrograms in the 2.6 – 3.8 GHz range in the left and right polarization components with a zebra pattern at 01:48:18 – 01:48:38 UT, in which 34 stripes can be distinguished and whose frequency separation grows smoothly with frequency. *The lower panel* shows profiles of the intensities at four fixed frequencies. The profiles confirm the spike-like structure of each zebra stripe in emission. The dark stripes do not contain a spike-like structure, and the radiation level proves to be lower than the average level of continuum, shown by the straight line at a frequency of 3.13 GHz (from Chernov et al., 2005).

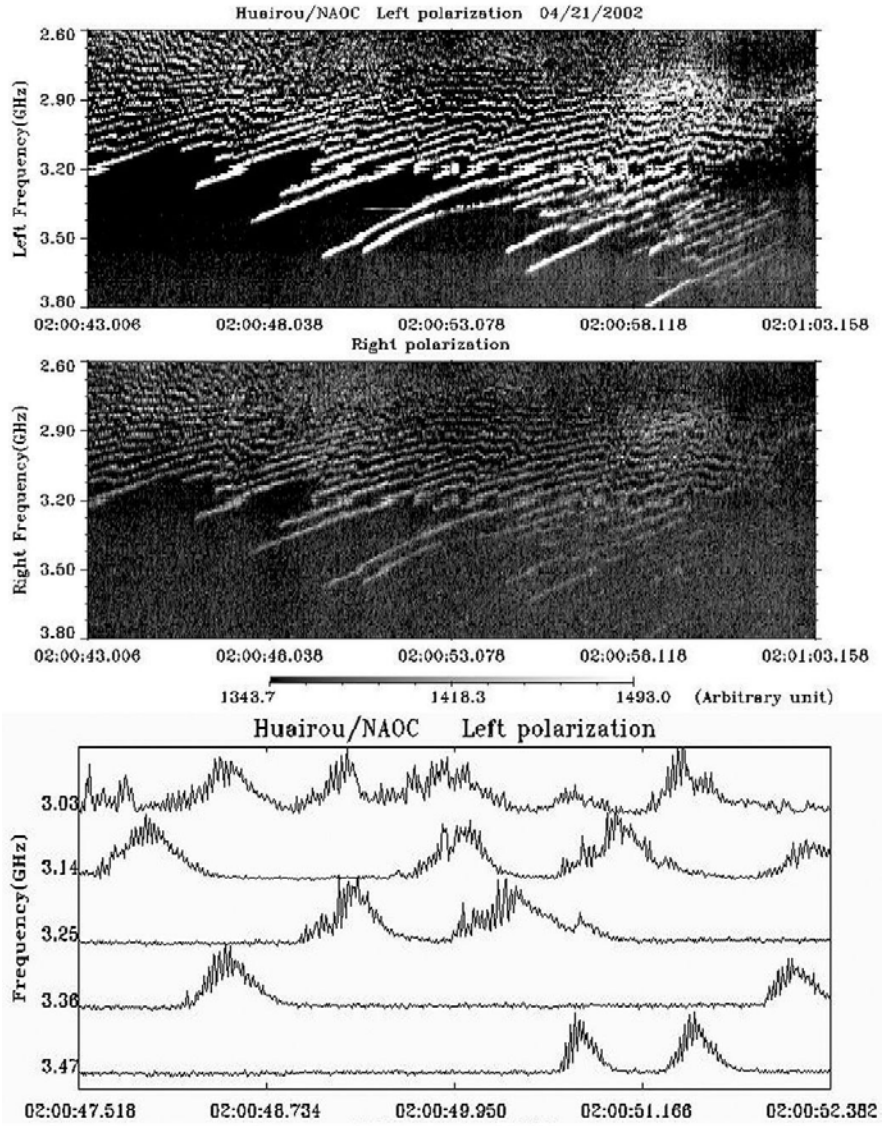

Fig. 4.38 Zebra structure in the event of April 21, 2002 at 02:00:43 – 02:01:03 UT. The zebra stripes on the high-frequency edge of the spectrum are more similar to isolated fibers without any strict periodicity. The multichannel time profiles (in *the bottom panel*) show stripes in emission consisting of spikes as before. However, in the dark stripes the residual emission remains at a fixed level (from Chernov et al., 2005).

A detailed analysis of multichannel time profiles shows that each zebra stripe in emission has a spike-like structure. In the dark stripes (between the bright zebra

stripes) the emission level can be lower than the level of burst background (lower than the average level of continuum, shown by a straight line at 3.13 GHz). Thus the presence of dark stripes is connected not with the absence of bright stripes (in emission), but with an absorption of background microwave emission. The polarization degree was weakly left-handed. We propose that two polarized radio sources at 5.7 GHz were located above the leading spot (the left polarized source) and above the tail spot (the right source in the bottom right panel of Figure 4.36). Therefore due to the limb position of the AR it is difficult to precisely define the magnetic polarity of the corresponding radio sources to define the type of radio wave.

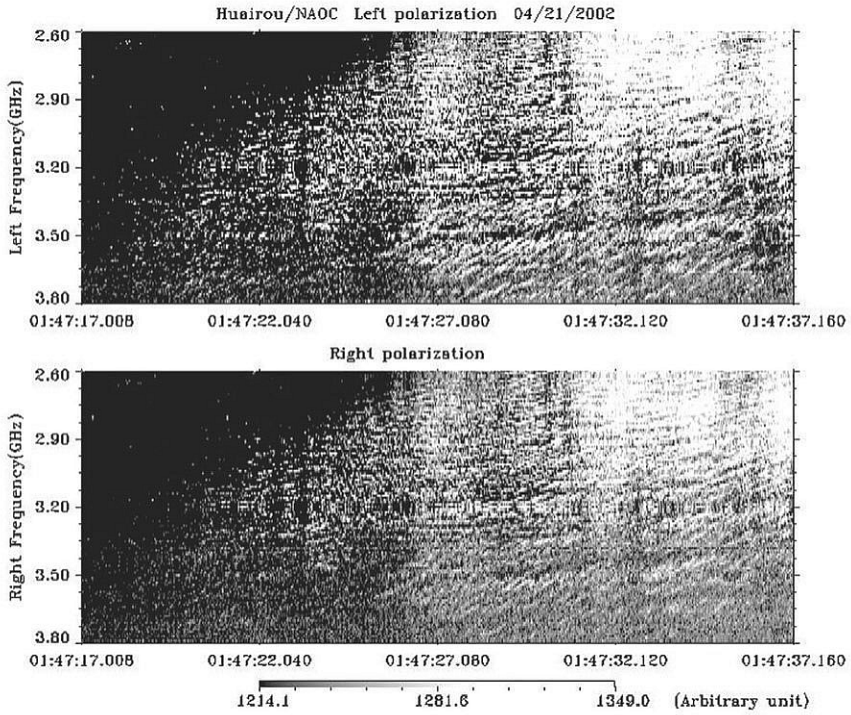

Fig. 4.39 Some series of ZP began from a cloud of millisecond spikes with gradual formation of zebra stripes (from Chernov et al., 2005).

The fragment in Figure 4.38 shows some changes of ZP properties: the polarization degree becomes stronger and it grows with time and frequency; the frequency drift almost stops in the low-frequency part of the spectrum (sometimes the stripes are almost parallel to the time axis); however, in the high-frequency part of the band they are more similar to isolated fibers with a negative frequency drift (there is no strict periodicity). The multichannel time profiles (in the bottom panel of Figure 4.38) show that stripes in emission consist as before of spikes,

however, in the dark stripes, deep dips in emission are not observed; the residual emission remains at a fixed level.

ZP was also observed in the pulsating regime, but almost all series of ZP were prolonged; in the examples in Figure 4.36 and 4.37 the duration exceeded 1 minute. The evolution of zebra stripes in several series began from a cloud of millisecond spikes with the gradual shaping of zebra stripes, as is shown in Figure 4.39.

4.5.1 A superfine spiky structure of ZP in microwave bursts

In this section we present observations of a new property of ZP. According to Chernov (2003), in 7 microwave bursts with ZP and FB a new effect was discovered by broadband radio spectrometer at Huairou station (Beijing, NAOC) (Fu et al., 1995) in the frequency range 2.6 – 3.8 GHz: zebra-stripes had own super fine structure, they were consisted of numerous fast spikes with duration at a limit of the time resolution of spectrometer ≈ 8 ms. The same superfine structure was present in Figures 4.36 – 4.38 in the event of April 21, 2002.

At two top panels of Figure 4.40 two spectra of the weak event January 21 2000 in left and right hand polarization are shown (the degree of polarization was moderate). A cloud of the emission (in the form of apple) consists of spikes, as well as zebra-stripes with negative and positive frequency drift. The emission bandwidth of zebra - stripes is equal about to the bandwidth of spikes (50-100 MHz), practically vertical white traits with duration at the limit of the time resolution 8 ms. In this connection we could conclude, that the source dimension of an isolated zebra stripe is about equal to the source dimension of spikes, and therefore their brightness temperatures are also about the same $T_b \geq 10^{13}$ K.

A fragment of similar structure in the strong radio burst November 25, 2000 is present at the bottom panel of Figure 4.40. The spectrum is shown in one left polarization channel, because the emission was full polarized at this moment. The emission on the whole includes numerous spikes, as well as zebra-stripes showing the oscillating frequency drift. The frequency separation between stripes and bandwidth of each stripe are smaller than at upper panels (~ 50 MHz).

The event November 24, 2000 was very dynamic, and 20 seconds after the first strong polarized ZP with the spiky structure a zebra stripes with moderate left polarization appeared (Figure 4.41), as well as two zebra stripes around 3 GHz at 05:00:56 UT that became more pronounced in right polarization, and at this time they consisted of spikes. The Nobeyama data show at this moment a double radio source above the neutral magnetic line, and the main, stronger radio emission (L-sign) corresponds to the ordinary mode. An enlarged fragment (3.54 s) of zebra stripes at the beginning of this interval is shown at the bottom of Figure 4.41. We can see that the majority of spikes have a duration of one pixel, i.e. ≤ 8 ms.

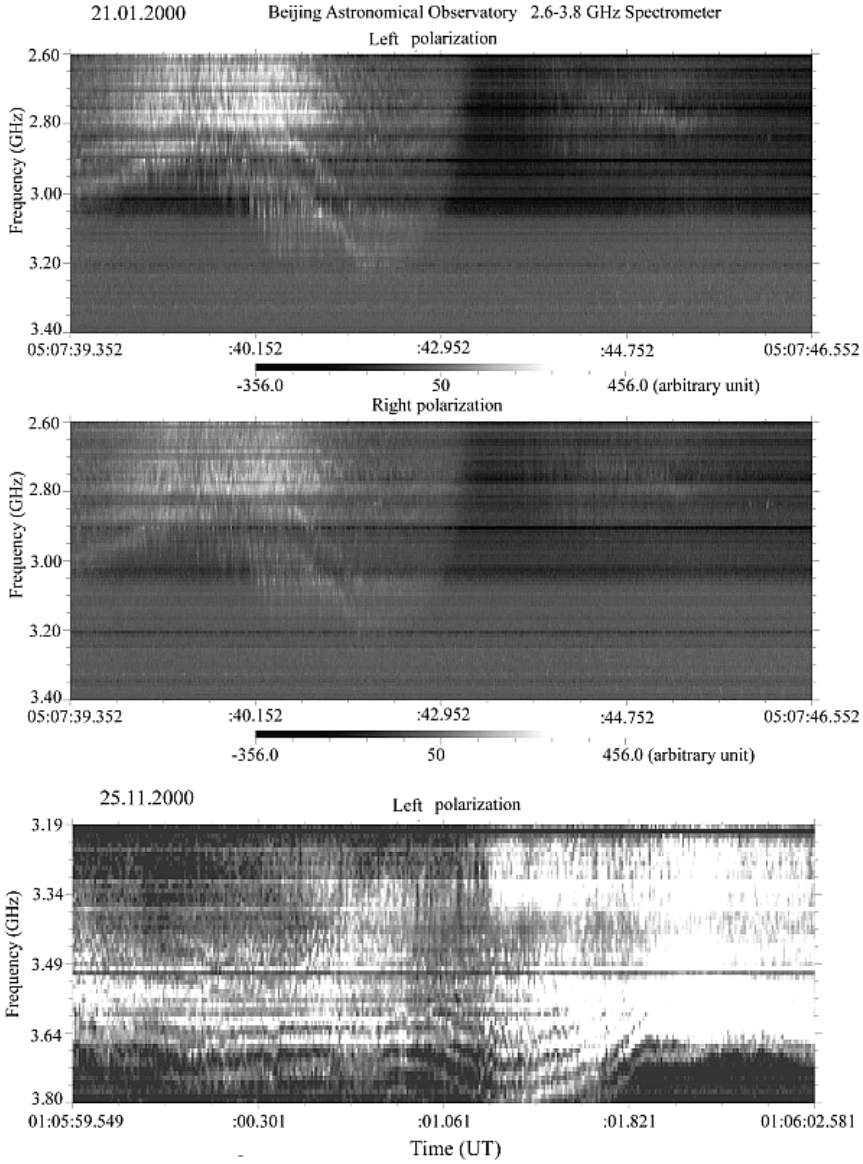

Fig. 4.40 Dynamical spectra of super fine structure of zebra-pattern in two events: 21 January 2001 (*two top panels* in left and right circular polarization in the frequency range 2.6 – 3.4 GHz) and 25 November 2000 (*bottom panel* of ~ 3 s duration in left polarization in the range 3.19 – 3.8 GHz) (from Chernov et al., 2003).

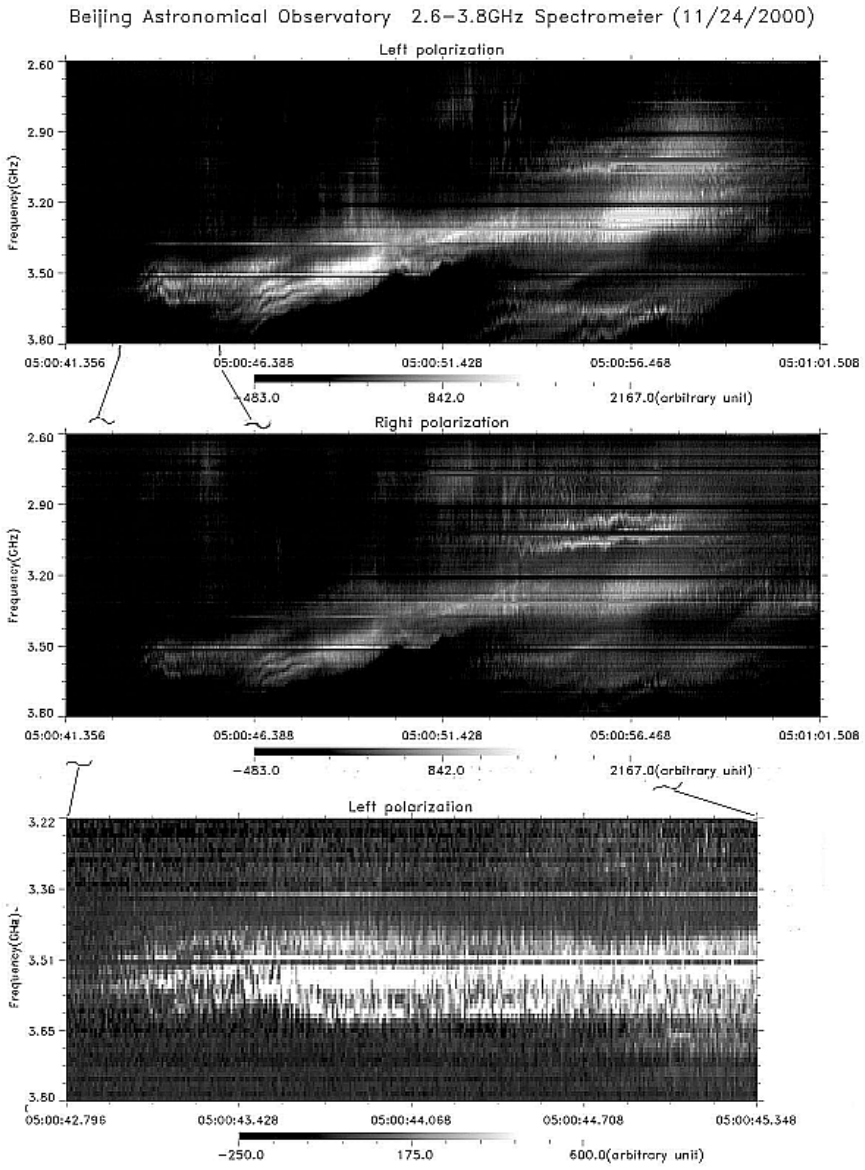

Fig. 4.41 The continuation of the event of 24 November 2000 showing a complex zebra- pattern with superfine structure. An enlarged fragment (3.54 s) of zebra-stripes in left polarization at the beginning of this interval is shown on *the bottom panel*. The radio emission on the whole has a moderate left polarization, but two zebra stripes around 3 GHz and 05:00:56 UT have a moderate right polarization (from Chernov et al., 2003).

The bandwidth of spikes is equal to about 35 - 45 MHz, and $\Delta f_e \approx 60$ MHz. Spikes in two neighboring zebra-stripes do not have any correlation, as shown in Figure 4.42 with a multichannel presentation of two short fragments of zebra patterns from the Figure 4.41: between 05:00:45.5 – 05:00:48.6 UT in left polarization and between 05:00:52.5 – 05:00:57.0 UT in right polarization. The frequencies of channels were chosen almost along zebra-stripes in emission. We see obvious chaotic behavior of spikes, as in practically all such events. Multichannel intensity profiles show also a very important result: the intensity between zebra stripes (in absorption stripes) remains lower than the intensity between spikes in emission stripes, but slightly higher than in parts of the spectrum without the background burst emission. Spikes almost disappear in absorption stripes, but the intensity level there testifies to a modulation effect. The flux density of spikes in the composition of zebra-stripes is usually about 20 – 50% (in different events) of the radiation of the background burst.

Another important observation was that the spiky structure is not pronounced in FB, when fibers appear simultaneously with ZP (October 29, 2000, see Figures 4.34). Zebra stripes as well as fibers can appear as isolated stripes, and all other parameters of both stripes in emission and in absorption are similar (Chernov et al., 2001b). We conclude that the spiky structure of ZP is seen almost in all events, when the time resolution of the spectrometer is high enough: some ms. In this connection the rapid frequency variations in the range 0.8 – 1.3 GHz observed by Karlicky et al. (2001) with 0.1 s resolution (called Lace- bursts) are possibly similar structures if observed with millisecond resolution.

The wealth of fine structure does not always correspond to the importance of the chromospheric flares and the intensity of the radio bursts. The relatively weak event of April 15, 1998 was very rich in spikes and ZP (see Chernov et al. (2001b)). Zebra patterns were usually observed after the burst maximum in all events.

Chernov et al. (2006) present the results of the first simultaneous observations of zebra patterns with superfine spiky structure in the microwave range made at two observatories 1000 km apart (Beijing and Nanjing, China). The fine structure was recorded by Huairou station with a spectra polarimeter in the 5.2 – 7.6 and 2.8 – 3.6 GHz ranges and by the Purple Mountain Observatory spectrometer in the 4.5 – 7.5 GHz range (Figure 4.43).

Identical spectra of zebra stripes with superfine structure (within the limits of instrument resolutions) obtained simultaneously at two observatories, confirm a solar origin of the ZP superfine structure.

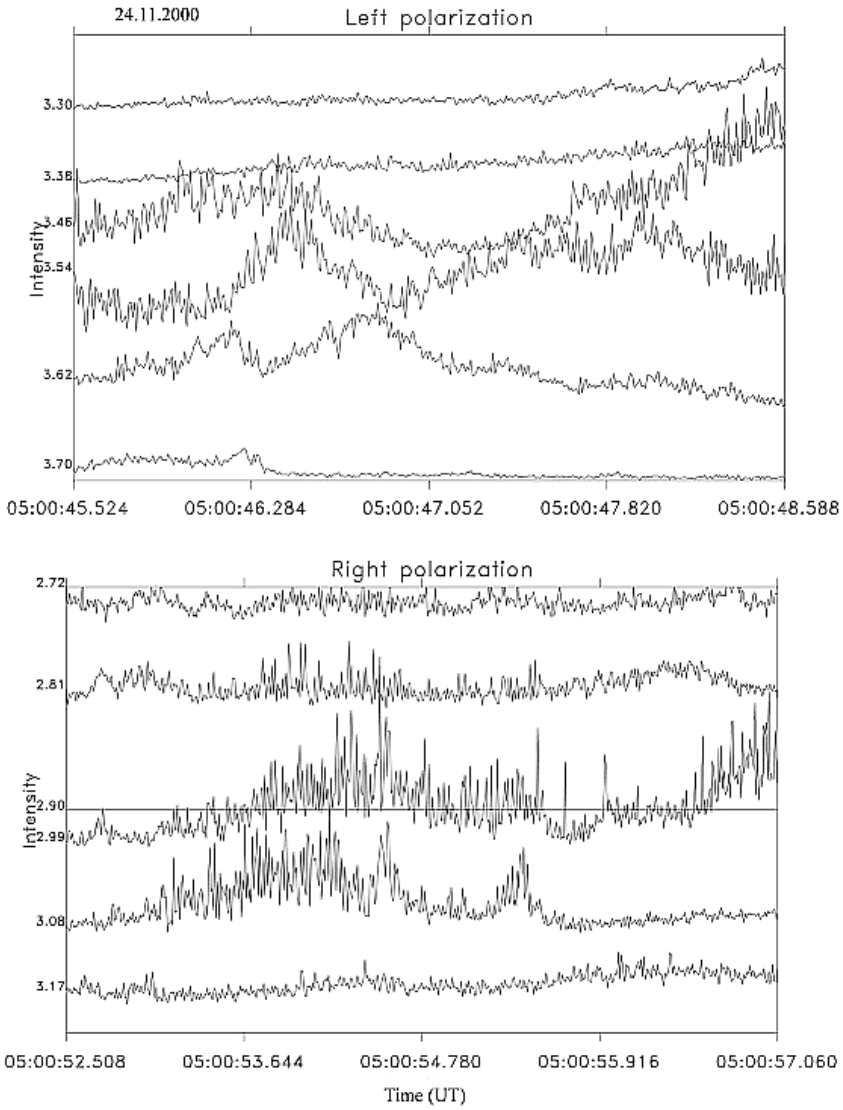

Fig. 4.42 A multichannel presentation of two fragments of ZP from Figure 4.41 with a duration of 3 s (in left polarization) and 4.5 s (in right polarization). The frequencies of channels were chosen almost along zebra-stripes in emission (from Chernov et al. 2003).

The circular polarization degree was very weak for the burst background radio emission and moderate to strong for the fine structure. The polarizaion sign in all

the cases probably corresponds to the extraordinary wave mode

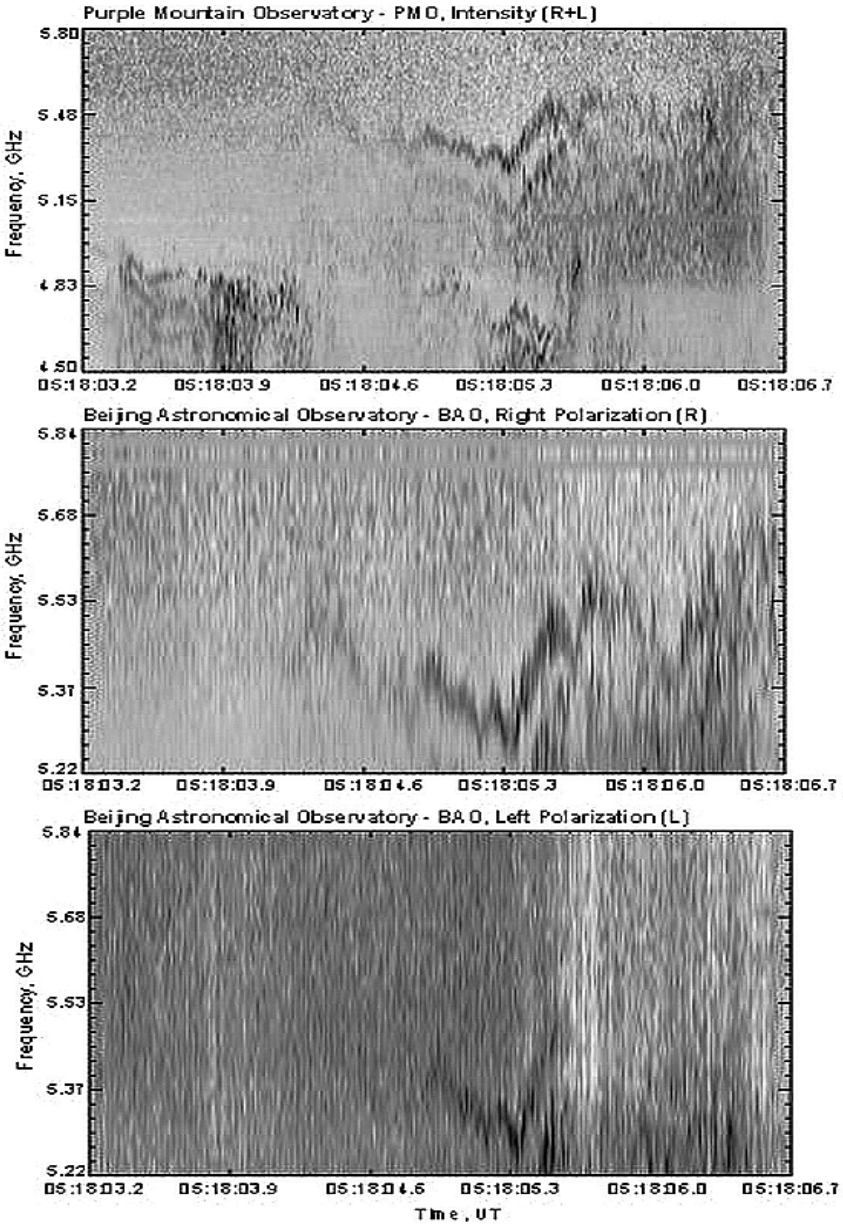

Fig. 4.43 Dynamic spectra of the zebra pattern in the April 10, 2001 event observed simultaneously by two observatories: Purple Mountain Observatory in intensity (*top*) and Huairou/Beijing Observatory in left (L) and right (R) polarization channels (*middle and bottom panels*) (from Chernov et al., 2006).

(see source positions with SSRT in Figure 4.44). But, these attempts show the difficulties involved in determining the wave mode for the fine structure. In all our cases the sources were located near the neutral magnetic line, and their positions at 15 – 20 thousand km do not necessarily correspond to the magnetic polarity sign at the photosphere level. Therefore it is not possible to regard our conclusions about the prevalence of the X- mode as absolute. The same note is also applicable to the conclusion made by Altyntsev et al. (2005) (see below Figure 4.47).

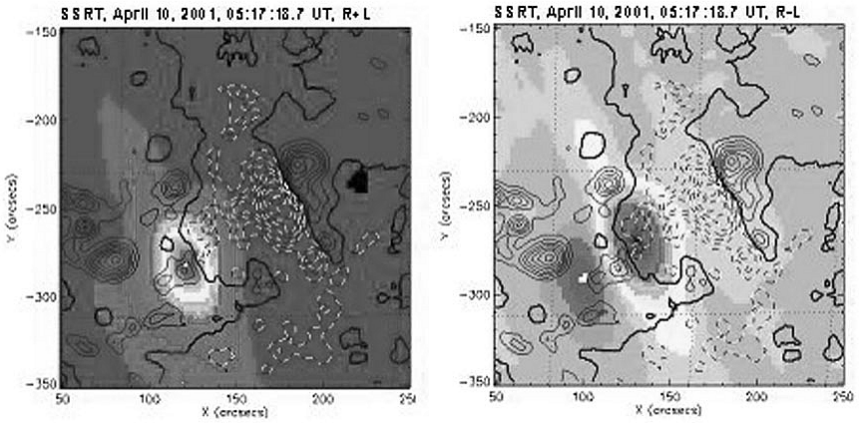

Fig. 4.44 SSRT 5.7 GHz source positions overlaid on the magnetic map from SOHO/MDI. *Solid thick line* is the neutral magnetic line. In the *left panel* the brightness distribution of intensity (parameter I=R+L) is presented. In the *right panel* the polarized sources (parameter V=R-L) are shown. To the left is the R radio source shown in halftone with a brightness center above the N magnetic polarity; to the right is the L radio source (*solid color contour*) above the S magnetic polarity. The radio emission corresponds to the extraordinary mode (L e S) (from Chernov et al., 2006).

The top panel of Figure 4.45 shows that all the spikes have peaks simultaneously in both R and L channels of the spectrometer, which proves the absence of any group delay between them within the limits of the spectrometer time resolution (5.0 ms). Thus, in this case, the degree of partial polarization is not related to the delay between ordinary and extraordinary wave modes discovered by Fleishman et al. (2002) (as for spikes of some events).

Two adjacent stripes of the zebra are shown in the lower panel of Figure 4.45. Although a strict correlation between spikes in the adjacent stripes is not observed, the largest elements of the superfine structure reveal the specific correspondence with small delays in the low-frequency stripe.

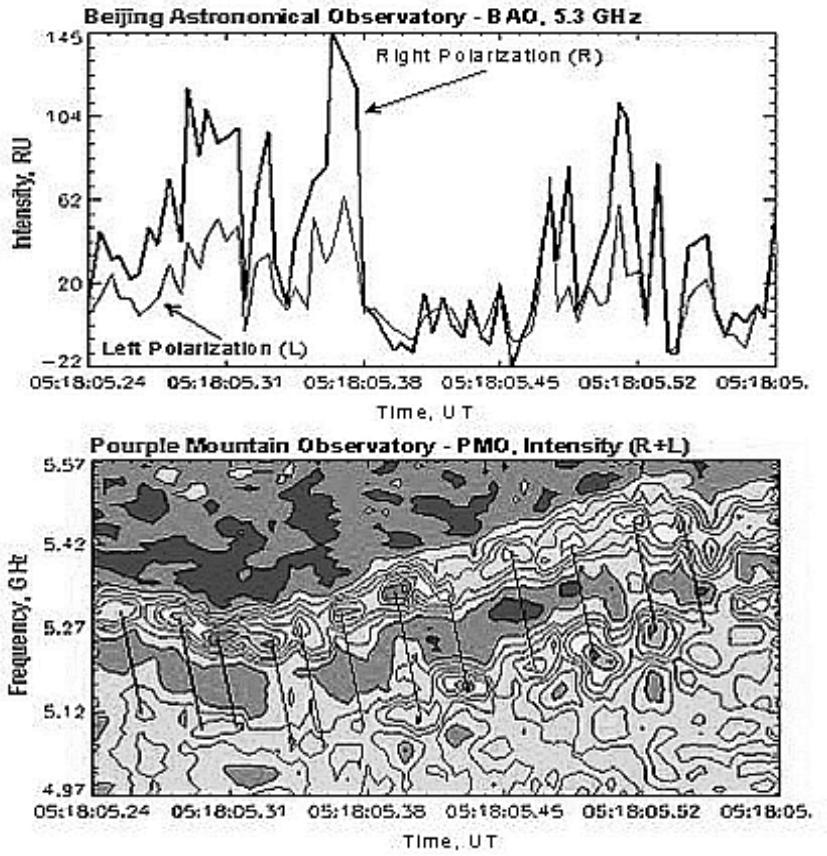

Fig. 4.45 Profiles at 5.3 GHz in the *top panel* show that all spikes (superfine structure of the zebra stripes) have peaks simultaneously in both R and L channels, proving the absence of any group delay between them within the time resolution of the spectrometer (5.0 ms). Two adjacent stripes of the zebra of the PMO spectrum are shown in the *lower panel*. Although no strict correlation between the spikes in the adjacent stripes is observed, the largest elements of superfine structure reveal specific correspondence with the low-frequency stripe, although with a small delay (from Chernov et al., 2006).

Straight, inclined lines connecting such details prove to be strictly parallel, suggesting the propagation of some agent. The speed of the frequency drift (df/dt) of the straight, inclined lines is approximately equal to 15 GHz s^{-1}, and in a realistic density model above the sunspot with a height scale: $Ln = 2n(dn/dh)^{-1} \sim 10^9$ cm, we obtain the speed of the agent $\approx 5.8 \cdot 10^9$ cm s^{-1}, which is suggestive of beams of fast particles.

In the whistler model the frequency separation between the stripe in emission and the adjacent absorption (Δf_{ea}) is approximately equal to the whistler frequency

$f_w \approx 0.1 f_B$, and we obtain, for Δf_{ea} = 70 MHz at 5.2 GHz (Figure 4.40), B = 250 G and consequently the plasma $\beta \approx 0.03$.

4.5.2. ZP at frequencies around 5.7 GHz

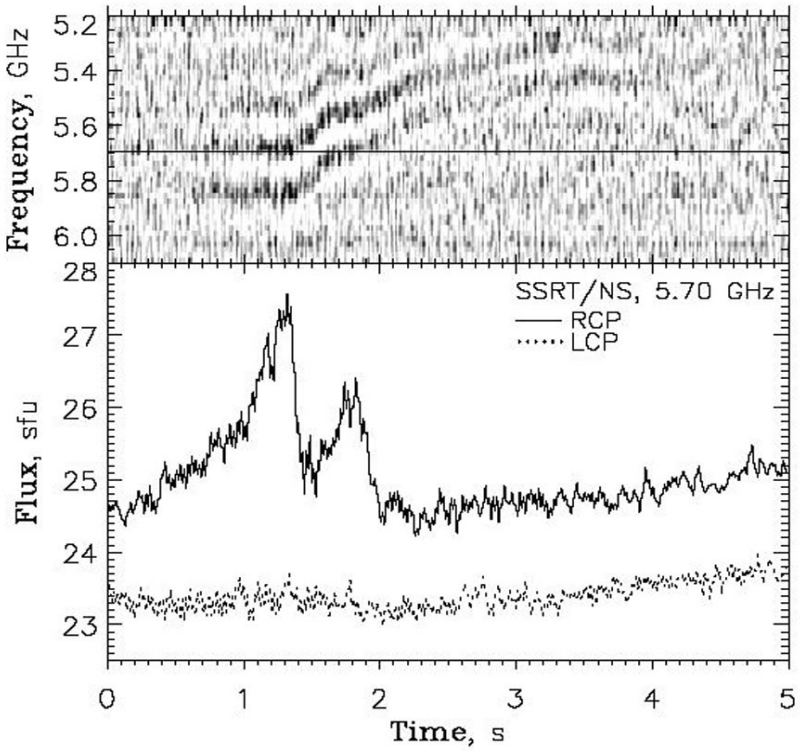

Fig. 4.46 *Top*: NAOC dynamic spectrum with zebra pattern, recorded on January 5, 2003 (06:06:10.3 UT). Darker areas correspond to the higher intensity of emission. The horizontal lines show the frequency 5.7 GHz. *Bottom*: the corresponding temporal profiles of emission with right (RCP) and left (LCP) circular polarization at 5.70 GHz, recorded by the SSRT linear interferometer. The circular polarization degree of the ZP reaches 100% (from Kuznetsov, 2005).

ZP was barely observed at frequencies higher than 5.5 – 6 GHz. Only one and very weak event was registered by China spectrometer (5.2 – 7.6 GHz) (Altyntsev *et al.* 2005; Kuznetsov, 2005). The radio flux of zebra stripes reaches only 2 – 3 s.f.u. above the burst background of 25 s.f.u. (Figure 4.46). The position of the radio source of ZP is shown by crossed straight lines at the background of SOHO/MDI magnetogram in Figure 4.47.

The main conclusions from these observations are:
- the frequency interval between adjacent stripes has almost constant value of 160 MHz;
- the instantaneous bandwidth of stripes is about 60 MHz;
- the apparent source size does not exceed 10 arcsec (7 thousand km), and the sources of the different stripes of the zebra structure coincide spatially (but at one frequency);
- the circular polarization degree reaches 100%, and the polarization sense corresponds to the extraordinary wave.

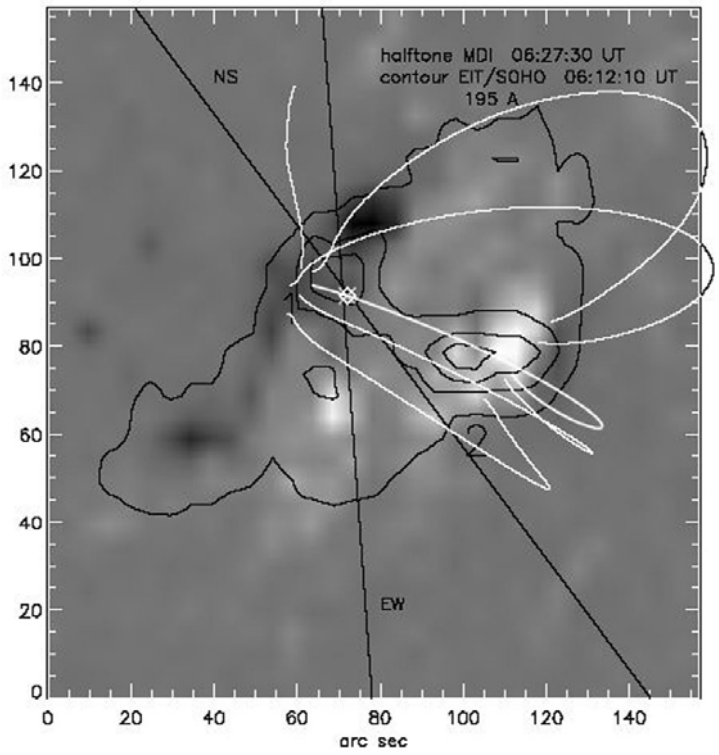

Fig. 4.47 The SOHO/MDI magnetogram (halftone) and the UV emission map (contour) of the AR 0243 flaring region. The crossed straight lines show the scanning directions of the EW and NS linear interferometers. The intersection point corresponds to the position of the zebra source. The contour levels are 45%, 60%, 75% and 90% of the maximum values. (From Altyntsev et al., 2005).

In connection with this rare event one should nevertheless note: first, during the precise study of the dynamic spectrum it is possible to note a smooth increase in the frequency separation between the five stripes with frequency; in the second, the identical position of the radio sources of different stripes was determined at

one frequency, therefore it is not amazing, that they coincide. In this case the sources of different stripes at different frequencies (at one time moment) can quite locate at the different heights, as in the distributed source (see below Figure 4.60b); in the third, the stripes reveal superfine structure (as millisecond spikes), and the authors in no way discuss it.

4.6. Models of fiber bursts (FB) and zebra pattern (ZP)

Concerning the interpretation of FB and ZP, the theory always lagged behind from obtaining of ever more diverse observational data.

4.6.1 Theory of the continuum emission

Our description of the theory would be incomplete, if we shall not illuminate briefly the mechanisms of the continuum radio emission against the background of which the fine structure develops. Type IV bursts are believed to originate from closed magnetic structures (magnetic traps) at heights up to $\approx 0.5R_{\odot}$. Winglee and Dulk (1986) indicate that the distribution of fast particles tends to be peaked at large pitch angles when the electrons are injected impulsively into a closed field loop, whereas loss-cone distributions tend to develop if continuous injection occurs.

Kuijpers in his review (Kuijpers, 1980) concluded that the most important high-frequency instability in stationary magnetic traps in the solar corona is the loss-cone kinetic instability of upper hybrid waves. This conclusion was specified by Winglee and Dulk (1986): after a broad consideration of different aspects of the continuum emission in the Introduction, and after the numerical simulation of the electron cyclotron maser instability, they conclude that the continuum emission results if the maser instability with the loss-cone distribution is saturated. Because zebra-stripes and continuum bursts are produced by the same mechanisms, his theory is able to account for the simultaneous continuum enhancement and ZP appearance (when the maser instability is not at saturation). But in any case the precise knowledge of the distribution function is of prime importance in determining the properties of the instability. In particular, (Kuijpers, 1980) gives an example of the loss-cone distribution when the generation of cyclotron waves become possible at frequencies above the hybrid band in contrast with conclusion of Zheleznyakov and Zlotnik (1975a).

The theory of Winglee and Dulk (1986) is well suited for the homogeneous plasma, and it is not known how it works under the conditions relevant a case when the dense background plasma is assumed to be locally in a highly turbulent state with a number of density irregularities. In plasmas of this kind it has been shown by Fleishmann (2001), referring to earlier suggestions of Ginsburg and Tsytovich (1984), that energetic particles moving across a turbulent plasma emit so-called transition radiation at frequencies above the average local plasma frequency. The first indications of the importance of the account of the transition emission were made by LaBelle et al. (2003) in connection with a new theory of ZP.

4.6.2 Theory of fiber bursts

The interaction of plasma electrostatic waves (*l*) with whistler waves (*w*) (generated by the same fast particles with loss-cone anisotropy) is a well-accepted emission mechanism for intermediate drift bursts (IDB) or fiber bursts: $l + w \rightarrow t$ with freely escaping electromagnetic waves (*t*) in the ordinary (*o*) mode. This model was proposed by Kuijpers (1975a,c). He calculated some principal whistler parameters in the case of longitudinal propagation for conditions in the solar corona: linear instability, cyclotron damping, coupling with Langmuir waves (admissibility) and a possibility of propagation in the form of discrete wave packets (with dimensions $\approx 10^8$ cm), called as solitons. This name, however, refers no to concept of the soliton within the framework of strong turbulence. He estimated that the whistlers must be generated in a periodic manner due to the quasilinear development of loss-cone instability with time interval exceeding ≈ 0.2 s.

The calculations of linear increments for loss-cone distribution (shown in the Figure 4.48) are one of the very crucial points of theory of Kuijpers (1975c). The calculation were made for typical conditions in the middle corona: the ratio of densities of hot particles to cold plasma ($n_h/n_c = 10^{-3}$), $T_e = 10^6$ K and velocity $V_h \approx 10^{10}$ cm s^{-1}.

4.6.2.1 Other models

The modulation of the emission into IDB was interpreted by a whistler wave packet propagating through a region of enhanced Langmuir waves. In the mean time this model has suffered criticism from several sides: (i) Melrose (1975) has pointed out that the parametric conditions of $l + w \rightarrow t$ are difficult to be met by beam-driven Langmuir waves, making this process very inefficient. (ii) Using nonlinear wave packets (solitons), Bernold and Treumann(1983), Treumann et al. (1990) have demonstrated that a nonlinear $l + w \rightarrow t$ process operates, but the emission of a single soliton is far too weak since whistler solitons have a small volume. Instead, they proposed the nonlinear process as the emission mechanism involving a large number of whistler solitons, but another process for the modulation producing IDB is required. As a possible candidate, they proposed Alfvén solitons changing the emission properties of the whistler solitons in a large volume and thus producing the observed drifting absorption and emission. Thus the drift rate would not be the whistler group velocity as assumed by Kuijpers (1975a), but the velocity of the Alfvén soliton.

Güdel et al. (1988) and Treumann et al. (1990) have investigated stationary solutions for Alfvén solitons propagating obliquely to the magnetic field in a two

component (hot and cold) corona. They apply a super-Alfvénic solution to modulate the emission and relate the observed range of drifts to velocities between 1 and 3 times the local Alfvén velocity.

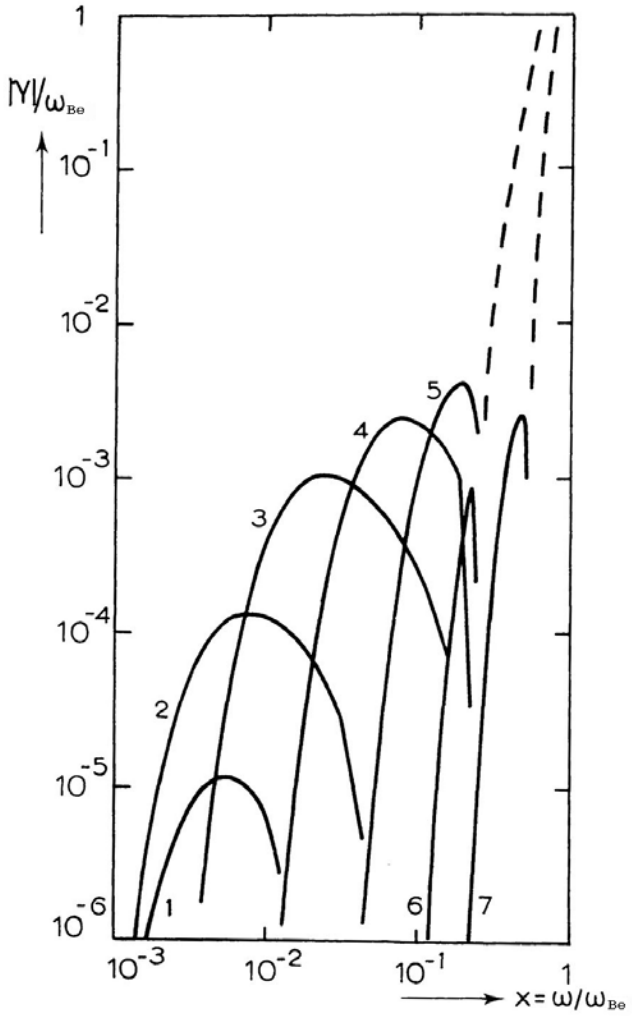

Fig. 4.48 Whistler growth rates in dependence of wave frequency with loss-cone distribution function. The numbered curves (1-6) correspond to increasing loss-cone angles α = 8o ÷ 86o and fixed ratio ω_{Pe}/ω_{Be} = 30; the curve 7 - to $\alpha = 90^{o}$ and ω_{Pe}/ω_{Be} = 10. The dashed curves present part of the cyclotron damping: at the left is common to cases 1-6, at the right - to case 7 (from Kuijpers, 1975c).

Another line has been followed by Mann et al.(1987), who proposed a different modification of the original model. They consider low-frequency, form-stable

whistler wave packets for both emission and modulation of IDB. The proposed wave packets do not satisfy the conditions for solitons, but are much larger. The ponderomotive force induces a density hump causing the observed absorption feature at the low-frequency side of IDB. The wave packets originate at the bottom of magnetic loops that trap energetic electrons and near the level where the whistler frequency equals the lower-hybrid frequency. The wave packets then propagate upward with the local whistler group velocity. Thus we are faced with two models of the IDB phenomenon interpreting the drift rate by a few times the Alfvén velocity and the whistler group velocity, respectively. The magnetic field derived from the observations differs by an order of magnitude for the two models. If the interpretation of IDB were settled in either way, the magnetic field in the source could be determined with accuracy.

Thus we have different understanding about the role of whistlers in the formation of FB. Moreover, a model is developed for explaining FB generally without participation of whistlers: Kuznetsov (2006) proposes modulation of upper-hybrid waves by the propagating MHD wave (sausage mode).

4.6.3 Whistler mode

In connection with different understanding of the participation of whistlers in the formation of FB one should first dwell on the general representation of the whistler mode, and mainly, on the conditions for their generation and propagation in the solar corona, since all attempts at the use of whistlers are introduced from the field of research of the magnetospheric whistlers.

It is known that whistlers are almost transverse waves which carry their energy predominantly along the magnetic field in both directions. The rotation of the electric vector of a whistler corresponds to the extraordinary wave (X- mode) (some renaming of the waves is allowed for oblique propagation (Gershman and Ugarov, 1960)). In contrast with other low-frequency waves, whistlers are purely electron oscillations at frequencies $\omega_w << \omega_{Be}$ and $>> \omega_{Bi}$ and can propagate in a dense plasma $\omega_w << \omega_{Pe}$ (ω_{Pe}- electron plasma frequency, ω_{Be}- electron cyclotron frequency, ω_{Bi} - ion cyclotron frequency). The expression for the index of refraction in the quasi-longitudinal approximation (valid for enough big angles) has a form (Edgar, 1972; Chernov, 1976):

$$\mu^2 = \frac{k_w^2 c^2}{\omega^2} = \frac{\omega_{Pe}^2}{M} \frac{\omega_{Be}^2}{\omega^2} \frac{1}{\cos\theta - (\delta\omega/\omega_{Be})\left(1 + \omega_{Be}^2/\omega_{Pe}^2\right)}, \tag{4.2}$$

where $\delta = 1 - \omega_{LHR}^2/\omega^2$, θ is the angle between the wave normal and the direction of the magnetic field, ω_{LHR} is the frequency of the lower hybrid resonance

$$\omega_{LHR}^2 = \frac{\omega_{Be}}{M}\frac{\omega_{Be}^2/M + \omega_{Pe}^2}{\omega_{Pe}^2 + \omega_{Be}^2} \quad . \tag{4.3}$$

M is the ratio of the proton (i) and electron (e) masses, k_w is the whistler wave number and c is the velocity of light. Under conditions of the middle corona $\omega_{Pe}^2 >> \omega_{Be}^2$, and (4.3) is simplified: $\omega_{LHR} \approx \omega_{Be}/M^{1/2} \approx \omega_{Be}/43$. The frequency ω_{LHR} is the resonance frequency in the case of $\delta \approx 0$, when θ approaches $\pi/2$, then $\omega \approx \omega_{LHR}$ and $\mu \to \infty$.

For quasi-longitudinal propagation at frequencies $\omega >> \omega_{LHR}$, $\delta \approx 1$ and the dispersion relation is simplified (Edgar, 1972):

$$\omega = \frac{\omega_{Be} k_w^2 c^2 \cos\theta}{\omega_{Pe}^2 + k_w^2 c^2} \quad . \tag{4.4}$$

The dispersive branch of the whistler wave is the high frequency extension of the fast magnetosonic wave (Kaplan and Tsytovich, 1973), but the analysis of just high-frequencies whistlers ($\omega_{Be} > \omega >> \omega_{Bi}$) excites the greatest interest, since at these frequencies the Cherenkov damping is exponentially small and whistlers can propagate in a dense plasma without appreciable absorption. The collisional damping is also small since the collisional decrement of whistlers (Kaplan and Tsytovich, 1972) $\gamma_\nu = \omega\omega_{Pe} \sin^2\theta / \left(\omega_{Be}\cos\theta\, n_e d_e^3\right)$ will be <<10 through the whole corona (d_e - Debye length). The whistler branch is not altered at the transition from cold plasma to a plasma with hot electrons.

It is known that in the quasi-longitudinal case the effect of the ions is not important, and a simplified equation is obtained for the group velocity of whistlers:

$$V_{gr} = 2c\frac{\omega_{Be}}{\omega_{Pe}}\sqrt{x(1-x)^3} \tag{4.5}$$

where $x = \omega/\omega_{Be}$ The values of V_{gr} calculated from Eq. (4.5) for the values of the ratio $f_{Pe}/f_{Be} \approx 1 \div 20$ are plotted in Figure 4.49. We can see that V_{gr} is always > 10^8 cm s^{-1} and in the middle corona ~ 10^9 cm s^{-1}. The qualitative decrease of V_{gr} for large angles θ is shown by a dashed line. The frequency $f_{LHR} \approx f_{Be}/43$ is marked by a vertical dashed line.

For low-frequency whistlers (more exactly for $x/\cos\theta \ll 1$) and in quasi-longitudinal approximation the whistler group velocity does not deviate from the direction of magnetic field more than on an angle 19°29' (the theorem of Storey (Storey, 1953)).

It is known from the magnetospheric whistler propagation that in the quasi-transverse case the effect of he ions comes down to the fact that the index of refraction does not go to infinity, thanks to which at a frequency $f \approx f_{LHR}$ in a very narrow height interval the group velocity reverses direction with insignificant damping of the wave (Edgar, 1972). This is a linear refraction effect described by

Snell's low. Furthermore, probably, nonlinear decay interactions are possible, causing low-frequency plasma turbulence. In Molchanov et al. (1974) such processes are examined for the explanation of the disturbances of linear refraction of the magnetospheric whistlers, when instead of the reflection, the wave packet can penetrate through the appropriate level of lower hybrid resonance. Probably, analogous behavior of whistlers should also be characteristic of magnetic traps in the solar corona.

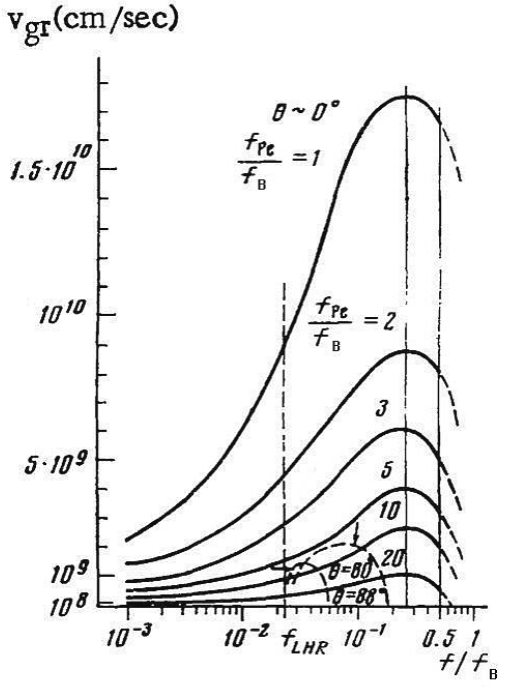

Fig. 4.49 Group velocity of whistlers in quasi-longitudinal propagation for values of ratio $f_{Pe}/f_{Be} = 1/20$ as a function of the relative frequency of whistlers f/f_{Be}. The qualitative decrease in V_{gr} for angles $\theta \approx \pi/2$ is shown by a dashed line (from Chernov, 1976b).

4.6.3.1 Cyclotron damping

Whistlers undergo strong cyclotron damping on the cold plasma. The first estimations of cyclotron damping for the solar corona were made by Kuijpers (1975a,c). Under coronal circumstances ($T_e = 10^6$ K, $\omega_{Pe}/2\pi = 300$ MHz, $\omega_{Pe}/\omega_{Be} = 30$, 10 and in the absence of a loss-cone distribution the role of the cyclotron damping is so important that the propagating whistlers will not occur above 0.5 ω_{Be}.

Such calculations were repeated by Mann et al. (1987) (Figure 4.50) with more various plasma parameters. But these authors overestimate the importance of the

cyclotron damping, so that they draw a conclusion about the impossibility of the whistler propagation in the corona and on this basis they developed the new model of FB (above mentioned) with the ponderomotive force as a main factor inducing a density hump causing the observed absorption feature. The interpretation was later revised (Benz and Mann, 1998; Aurass et al., 2005) where the initial version of model on whistlers of Kuijpers (1975) is accepted.

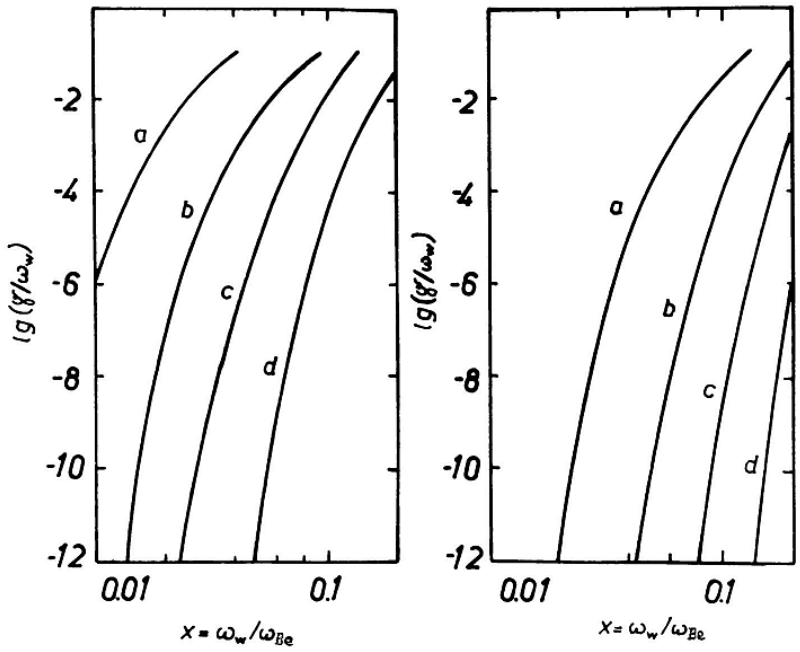

Fig. 4.50 Frequency dependence of the decrement of the electron cyclotron damping for whistler waves propagating along the external magnetic field in the case of $\omega_{Pe}/\omega_{Be} = 43$ (*left*) and $\omega_{Pe}/\omega_{Be} = 20$ (*right*) for various temperatures: a)10^7K, b) $4 \cdot 10^6$ K, c) $2 \cdot 10^6$ K, d) 10^6 K (from Mann et al., 1987).

Nevertheless, Figure 4.50 shows a strong dependence of the cyclotron damping on the ratio ω_{Pe}/ω_{Be} and especially on the plasma temperature. Therefore, if a chosen distribution function does not ensure maximum excitation at frequencies to the right of curves of the cyclotron damping, that indeed, the propagation of whistlers cannot be considered. At the same time one must take into account, that when this condition is satisfied, whistlers experience scattering on the background plasma with the transmitting to the low frequencies. Then, with the propagation to the side of the decrease of external magnetic field this transmitting detains the moment of switching on of the complete cyclotron damping. Moreover, according to the contemporary representations, the magnetic field changes very slowly with the height in the narrow magnetic loops (Aschwanden, 2004).

4.6.3.2 Whistler interaction with Langmuir waves

In the Kuijpers model the analysis of the interaction of Langmuir waves with whistlers was rather semi-qualitative, and there was no detailed analysis of such an interaction and its efficiency in the solar corona before the appearance of a theory of Fomichev and Fainshtein (1988). They showed that the observed fiber radio fluxes are explained in frameworks of weak plasma turbulence. Therefore, alternative models with solitons of Alfvén waves (Bernold and Treumann, 1983) and the strong whistler turbulence (Benz and Mann, 1998) are not required (in greater detail see Chernov (1990b)).

Following a formalism of Fomichev and Fainshtein (1988) first let us consider the kinematics of a three-wave interaction between a plasma wave (ω_l, kl), a whistler (ω_w, k_w) and an electromagnetic wave (ω_t, kt). As is well known, the condition of spatio-temporal synchronisation (conservation laws)

$$\omega_l + \omega_w = \omega_t, \quad k_l + k_w = k_t \tag{4.6}$$

must be satisfied in such an interaction. The frequencies and wave numbers must satisfy the dispersion relations for the corresponding branch of oscillations in a plasma for the case of longitudinal propagation:

$$\omega = \frac{\omega_{Be} k_w^2 c^2 \cos\theta_w}{\omega_{Pe}^2 + k_w^2 c^2}, \tag{4.7}$$

$$\omega_l^2 = \omega_{Pe}^2 + 3k_l^2 V_{Te}^2 + \omega_{Be}^2 \sin^2\theta_l \ , \tag{4.8}$$

$$\omega_t^2 = k^2 c^2 + \omega_{Pe}^2 \left[1 + \left(\omega_{Be}/\omega_t\right)\cos\theta_t\right]^{-1} \ . \tag{4.9}$$

Here $V_{Te} = (k_B T_e/m_e)^{1/2}$ is the thermal velocity, k_B is Boltzmann constant, θ_w, θ_l, θ_t- the angles between the direction of propagation of corresponding waves to the external magnetic field $\mathbf{B}$, $\omega_{Be} = eB/mec$ - the electron gyrofrequency, $\omega_{Pe} = (4\pi e^2 n_e/m_e)^{1/2}$ - the electron plasma frequency (c - the velocity of light, e and m_e - charge and mass of the electron), n_e- the electron density. Eq. (4.9) correspond to the ordinary wave (o- mode).

For a realistic case in the corona where $\omega_t > \omega_{Pe} >> \omega_{Be}$ and using the geometrical relations between wave vectors

$$k_t^2 = k_l^2 + k_w^2 \pm 2k_l k_w \cos\theta, \tag{4.10}$$

(where is the angle between the directions of wave vectors of whistlers and plasma waves) one can obtain from Eqs. (4.7)-(4.10) the expression for cos θ_t. In Eq. (4.10) the sign '-' before the third term to the right corresponds to the decay process $l \rightarrow t + w$ at the difference frequency $\omega_t = \omega_l - \omega_w$, $k_t = k_l - k_w$. As shown by Chernov and Fomichev (1989) and Chernov (1990b) such a process is quite possible, if the thermal additive (to the plasma frequency) in the dispersion relation in Eq. (4.8) will be more than the whistler frequency. Such a condition can be realized for the ratio $\omega_{Pe}/\omega_{Be} > 8$ for the whistler frequency $\omega_w \approx 0.1\omega_{Be}$.

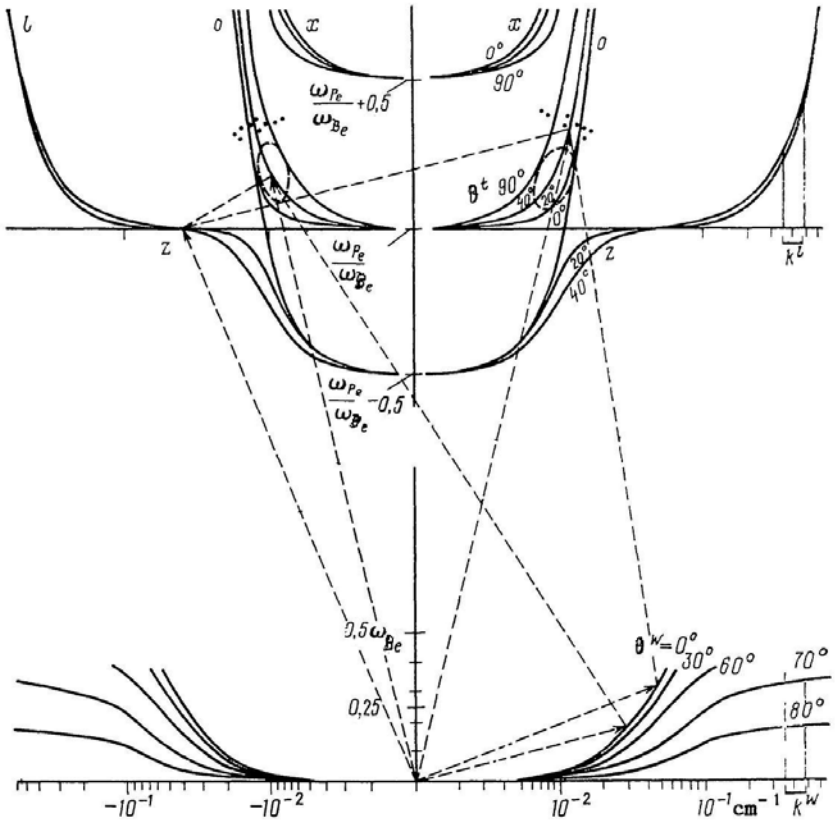

Fig. 4.51 Dispersion curves for electromagnetic (O- and X- modes), Langmuir waves (*l*) and whistlers (bottom) for different propagation angles (θi) with respect to the magnetic field. A graphic diagram of the $l + w \rightarrow t$ interaction at the sum frequency is shown by dashed lines for two whistler wave numbers and $\theta_w = 0^o$. The domains of values ω_t, k_t for the $l \rightarrow t + w$ decay process at the difference frequency are encircled by dashed curves on the branches for the ordinary wave. The corresponding values of k_l and k_w are marked by segments on the *k*- axes (from Chernov, 1990b).

From the natural requirement $|\cos\theta_t| < 1$, the range of possible values $k_l = k_w$ was obtained. It was shown that the interaction is possible for both relations $k_l / k_w > 1$ and $k_l / k_w < 1$ with $k_l \approx k_w$ and $\mathbf{k}_l = -\mathbf{k}_w$, i.e. Lengmuir wave and whistlers with approximately equal and oppositely directed wave vectors take part in the interaction. For the interaction at the difference frequency the vectors $\mathbf{k}_l$ and $\mathbf{k}_w$ must be in the same direction with a very small angle between them $\theta < 1.28^o$, but with a limitation of the angle θ_w, $\theta_l > 70 \div 80^o$. Chernov and Fomichev (1989) obtained the maximum plausible angles $\theta > 84^o$ at the difference frequency. In Figure 4.51 we show the dispersion curves and a graphic representation of the interaction of *l*, *w* and O- mode, $l + w \rightarrow t$ for the typical conditions in the middle corona: $\omega_{Pe}/\omega_{Be} = 30$ and $Te = 10^6$ K. The branches of whistlers for $\theta_w = 0^o$ and $\theta_w = 30^o$ are cut off at the frequency $\omega_w = 0.37\ \omega_{Be}$, since the strong cyclotron damping sets in at higher frequencies, and ω_w does not exceed $0.17\ \omega_{Be}$ for $\theta_w = 80^o$.

The interaction of waves at the sum frequency is shown schematically by dashed lines for two whistler wave numbers. The sum values ω_t and k_t for different frequencies ω_w are denoted by dots on the branches of O- mode (similar to Figure 5 in Kuijpers (1975c). The intervals of values of k_l and k_w for which the conservation laws are satisfied at the difference frequency are denoted by segments on the wave number axes. The domains of values of ω_t and k_t at the difference frequency are encircled by dashed curves on the branch of O- mode.

The synchronization conditions (conservation laws) are not satisfied for extraordinary (X) wave with any values k_l and k_w (Fomichev and Fainshtein, 1988). Therefore the polarization of the radio emission generated through the interaction plasma waves and whistlers will correspond to the ordinary wave, which agrees with observations.

For the interaction at difference frequency significant constraints are imposed on the range of wave numbers k_l and $k_w \approx 0.23 \div 0.45$ and consequently on the propagation angles θ_l, $\theta_w \geq 80^o$. Specifically these factors may explain the rare appearance of radio emission at the difference frequency (Figures 4.7 and 4.22). Oblique whistlers can be generated only at anomalous Doppler resonance, (see below the section 4.5.2.5) which can be realized rather during quasi-linear diffusion of whistlers on fast particles.

The conservation laws will be carried out analogously for interaction of plasma upper hybrid waves and whistlers with the escape of ordinary wave for the case, when both wave vectors $\mathbf{k}_{UH}$ and $\mathbf{k}_w$ are directed at large angles toward the magnetic field.

The estimation of effectiveness of the interaction of plasma waves and whistlers presents the main result of work of Fomichev and Fainshtein (1988), for the first time they solved the system shortened equations for complex amplitudes of interacting waves (in the steady-state case with $\partial/\partial t = 0$). In the case of fixed wave phases the amplitude of the electromagnetic wave increases linearly with distance. But the case with random wave phases is more realistic in the sources of type IV radio bursts. Performing the averaging over the wave phases the initial system of equations for the wave amplitude (a_i) is transformed into equations for the dimen-

sionless wave intensities $N_i = \left\langle a_i^2 \right\rangle \Delta\omega_i$. Here $\Delta\omega_i$ is the bandwidth of wave of type *i*.

In the general case, the solution of the system for the wave intensities was too unwieldy, and a numerical simulation were carried out. Taking into account the subsequent estimations of the interaction at the difference frequency (Chernov and Fomichev, 1989) we can state that coalescence and decay at the frequencies $\omega_t = \omega_l \pm \omega_w$ can be equally efficient in an optically thick source, and the maximum electromagnetic radiation intensity is given by the expression:

$$N_t \le \frac{N_l N_w}{(\omega_{Pe}/\omega_{Be})N_w \pm \sqrt{\omega_{Be}/\omega_{Pe}}(\omega_{Be}/\omega_{Pe})N_l} \ . \qquad (4.11)$$

Here '-' in the denominator - for the decay process at the difference frequency. Melrose (1983) has shown that four-plasmon coalescence and decay processes in an optically thick source at the combination frequencies $\omega_t = \omega_l \pm \omega_w \pm \omega_{w'}$ are also possible in the corona.

4.6.3.3 Weak or strong turbulence of whistlers

Fomichev and Fainshtein (1988) have estimated one important parameter, the turbulent level of whistlers in the source. The fiber fluxes ~10^{-19} W m^{-2} Hz^{-1} and brightness temperatures ~10^{14} K for the plasma wave power $W_l \approx 10^{-5} \div 10^{-6}$ erg cm^{-3} require a whistler power $W_w \approx 2 \cdot 10^{-10}$ erg cm^{-3}, which is only four to five orders of magnitude higher than the thermal noise of the whistlers and as many orders of magnitude lower than the energy of the plasma waves. Thus, a more detailed analysis of the interaction $l + w \rightarrow t$ confirms the result of Kuijpers (1975a,c), that usually observed radio fluxes in FBs are explained in the context of week turbulence.

However, observations of FB in very strong type IV bursts are stimulating many authors to employ strong turbulence of whistlers. On the basis of of an expression for the functional form of a onedimensional whistler soliton obtained by Karpman and Washimi (1977) it was proposed in Treumann and Bernold (1981), Bernold and Treumann (1983) and Treumann et al. (1990) that all the energy of the whistlers is concentrated in such solitons. This model subsequently encountered new difficulties.

i) It turns out that the emission of ~10^{14} solitons from a volume of ~ 10^8 km^3 is required to explain the observed fiber fluxes. The absorption cannot be explained in the usual way in this case, since the individual solitons in such a volume cause emission (and absorption) at frequencies which much differ, due to their very small size.

ii) For attaining strong turbulence at the reflection points of whistlers, the whistler frequency $\omega_w \approx \omega_{LHR} \approx \omega_{Be}/43$, that contradicts to the condition for the formation of whistler soliton, $\omega_w \geq \omega_{Be}/4$.

iii) A simple decrease in the group velocity cannot result in the formation of whistler solitons. Multiple reflections of whistlers are observed in the earth's magnetosphere, but solitons were not recorded. The reflection of whistlers occurs with a gradual reversal of $\mathbf{k}_w$ through the interaction with the electrostatic mode. A strong wave can therefore result in the formation of lower-hybrid solitons, which propagate perpendicular to the magnetic field and could interact with upper-hybrid waves.

It is thought that the level of strong turbulence of whistlers (and plasma waves, incidentally) may be reached in powerful events. But the analysis of the linear stage of modulational instability in Karpman and Washimi (1977) does not at all mean that all the energy of whistlers is concentrated in solitons. For FB it is necessary to consider the non-linear stage of modulation instability, and even more its saturation. Such a two-dimensional problem was solved numerically in Karpman and Shagalov (1988). They showed that the field of a powerful wave is concentrated in two types of narrow structure drawn out along field lines: fast magnetosonic waves with decreased density and magnetic field, propagating with whistler group velocity, and slow magnetosonic waves with increased density, moving with a very slow velocity ($< V_{Te}/43$). The first structures containing density cavities can be used to interpret the usual classic FB, and the slow magnetosonic structure can be used to interpret unusual slowly drifting fibers.

4.6.3.4 Formation of stripes in emission and absorption

Let us examine in more detail the yield of radio radiation in this process. First of all we enforce that the radiation at a fixed frequency can be generated in the corona in an extended region. This extent can be connected with the finite width of the spectrum of plasma waves due to the thermal spread of the background plasma and velocity dispersion of the fast particles. We designate the dimension of the emitting region at fixed frequency in the direction of ∇n_e as L, assuming that the intensity of the radiation of a given frequency declines exponentially in this region with height h : $W \sim \exp - (h/L)^2$. This means that from each level in the corona a spectrum of frequencies $\Delta\omega$ should be emitted. A realistic dimension of L can be of $\sim 10^8$ cm. And about the same value can be the dimension of whistler wave packet L_w, if to judge on the duration of fibers at a fixed frequency of ≈ 0.5 s (Figure 4.7), taking into account the group velocity of whistler $V_{gr} \approx 10^9$ cm s^{-1} for the ratio $\omega_{Pe}/\omega_{Be} \approx 20$ (Figure 4.49).

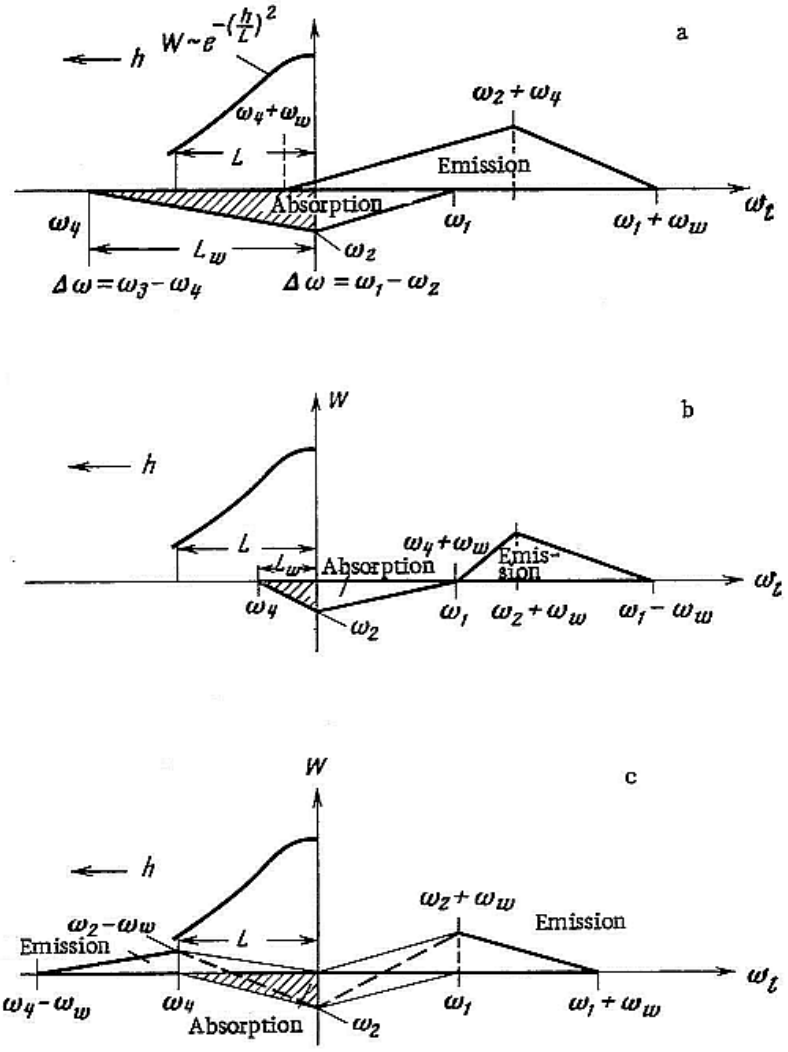

Fig. 4.52 Qualitative diagram of formation of stripes in emission with LF- absorption for different dimension of wave packets of whistlers (L_w); ω_l - Langmuir frequency and h-height in the corona. *a)* $L_w > L$, $\omega_w > \Delta\omega$, regions of emission and absorption are overlapped in frequency; *b)* $L_w < L$, $\omega_w \geq \Delta\omega$ these regions are separated; *c)* $L_w \approx L$, $\omega_w \leq \Delta\omega$, regions produce a form of a "tadpole" type owing to the yield of radiation at the difference frequency. In all cases the frequency separation between neighboring maxima in emission and absorption equals the whistler frequency ω_w (from Chernov, 1976b).

Figure 4.52 shows qualitative diagram of formation of stripes in emission and LF- absorption for different relation between L and L_w: *a*) $L_w > L$, $\omega_w > \Delta\omega$; *b*) L_w

< L, c) $L_w \sim L$, $\omega_w \leq \Delta\omega$. In all cases the frequency separation between neighboring maxima in emission and absorption equals the whistler frequency ω_w. The condition of frequency separation of stripes in emission (from neighboring whistler wave packet) means that the distance between packets must be greater than L. The stripes in emission will be separated by stripes in absorption if the condition for their formation is satisfied: $\omega_w > \Delta\omega = L \cdot \nabla\omega_l$.

The reality of the formation of stripes is confirmed in Chernov (1976) by the numerical calculations of intensity relative to continuum, based on the comparison of effectiveness in the processes of interaction $l+w \rightarrow t$ and induced scattering of l plasmons on ions. The modulation depth in the calculated profiles agrees with that observed in FB in the event May 3, 1973 (Figure 4.5) and in ZP in the event July 3, 1974 (Figure 4.19). The calculations show that the necessary whistler wave energy is much less than the energy of plasma waves.

The possibility of the escape of radio emission as on the sum, so at the difference frequency it is confirmed by the observations of FB and ZP. In the Figure 4.21 the absorption is located from the HF edge of fiber in the emission in the event on July 28, 1999. In the Figure 4.7 the exchange of the position of absorption from HF to LF is shown in the course of the drift of one fiber. In Figures 4.21 and 4.22 the position of absorption changed to the reverse one in one series the ZP during about 1 minute. Here, the different directivity of emission in these processes plays the dominant role.

4.6.3.5 Linear whistler instability

Linear cyclotron instability was investigated in some detail in application to magnetospheric whistlers by Kennel (1966) and Kennel and Thorne (1967). Jamin *et al.* (1974) analyzed firehose and mirror whistler instabilities for a large temperature anisotropy. They showed that the whistler wave field has the form of sporadic irregular oscillations with a transfer of energy inside the spectrum. The spectrum of whistlers in coordinates [γt; kx] resembles to a braided zebra patterns (see Figure 3 in Chernov (1976b). Yip (1970) calculated the first possible frequency and angular spectra of whistler at normal and anomalous Doppler resonance by electron streams in the solar corona. And in application directly to FB Kuijpers (1975a,c) calculated linear increments for loss-cone distribution with different plasma parameters (shown in the Figure 4.48). Berney and Benz (1978) used much more various loss-cone distribution function, and they confirmed in general calculations of Kuijpers. They compare also whistler and electrostatic instabilities, and conclude that the growth of electrostatic waves is at least an order of magnitude faster. However, according to Sharma and Vlahos (1984), the growth rates of Langmuir and upper hybrid waves for the loss-cone distribution are less than for whistlers.

In all papers above mentioned the instability was calculated only for the longitudinal whistlers at the normal Doppler resonance with monoenergetic electron

distribution. In order to examine the amplification of whistlers propagating in coronal plasma at arbitrary angles to the magnetic field, Mal'tseva and Chernov (1989) use an anisotropic Maxwellian distribution with a loss-cone in the perpendicular velocity $\upsilon_\perp$ and with the presence of a beam along the magnetic field **B**:

$$f_h(\upsilon) = \frac{n_h \upsilon_\perp^{2j}}{\pi^{3/2} \upsilon_{T||}^{2j+2}} exp\left[-\frac{(\upsilon_{||} - \upsilon_b)^2}{\upsilon_{T||}^2} - \frac{\upsilon_\perp^2}{\upsilon_{T\perp}^2} \right] \tag{4.12}$$

where n_h is the concentration of hot electrons, $\upsilon_\perp = \upsilon \sin \alpha$, $\upsilon_\parallel = \upsilon \cos \alpha$, α is the pitch angle, $\upsilon_{T\perp}$ and $\upsilon_{T\parallel}$ are the rms transverse and longitudinal velocities, υ_b is the velocity of the beam along **B** and j is the positive index of the loss-cone in $\upsilon_\perp$. In this case $f_h \sim \sin^{2j} \alpha_{lc}$, where α_{lc} is loss-cone angle. The temperature anisotropy is introduced by the parameter $a = 1 - \upsilon_{T||}^2 \big/ \upsilon_{T\perp}^2$. The cold background plasma is specified by the same Maxwellian distribution with $j = 0$; $a = 0$; $\upsilon_b = 0$ and the temperature $T_e \sim 10^6$ K.

A beam distribution with the loss-cone yields a beam with $\upsilon_\parallel > \upsilon_\perp$ (if $a < 0$, and $j \le 0.5$, which can be realized at the top of the magnetic trap), in which case Cherenkov and cyclotron resonances on the anomalous Doppler effect contribute to emission (Kennell, 1966; Gendrin, 1981). In such a case in the cyclotron resonance relation

$$\omega - k_{||} \upsilon_{||} - s\omega_{Be} = 0 \tag{4.13}$$

the harmonic number $s = -1$. With a strong transverse anisotropy ($a > 0$, and $j \approx 2$), we obtain $\upsilon_\perp > \upsilon_\parallel$ (rather at the base of the magnetic trap), and the resonance on the normal Doppler effect will basically responsible for whistler emission ($s = 1$ in Eq.(4.13)).

In the expressions for local growth rates of whistlers excitation by hot electrons (γ_h) and for damping decrements by cold plasma (γ_c) the three main resonances (Cerenkov and cyclotron on normal and anomalous Doppler effects) were summed. The calculations were carried out for large series of the parameters of anisotropic beam and cold plasma. For the energy of hot electrons $E \approx 30$ keV ($\upsilon \approx 10^{10}$ cm s^{-1}) and energy dispersion $\Delta E \approx 30$ keV the maximum growth rates locates near the relative whistler frequency $x = f_w/f_{Be} = 0.1 \div 0.15$ (for large loss-cone angles and velocity anisotropy $a = \pm 0.5$). Specifically, at this frequency the minimum of the absorption (γ_c) is located. This result confirms calculations of Kuijpers (1975c) for the longitudinal propagation. However, the account of three resonances made it possible to reveal the maximum of absorption (Landau damping) at the smaller frequencies, $x = 0.03 \div 0.05$. The main new inference to be drawn from calculations of Mal'tseva, Chernov (1989b) is complex behavior of instability as function of the angle of propagation (here the angle ψ) shown in Figure 4.53. The anisotropic high-energy beams produce emission at all angles ($0^o <$

$\psi < 90^{o}$) for $x \leq 0.1$ but only up to angles $\psi \approx 45^{o} \div 50^{o}$ for $x > 0.1$. The sign change of the velocity anisotropy from $a = 0.5$ to $a = -0.5$ at the high loss-cone anisotropy ($j = 1.5$) cause a pronounced shift of the curves towards larger ψ.

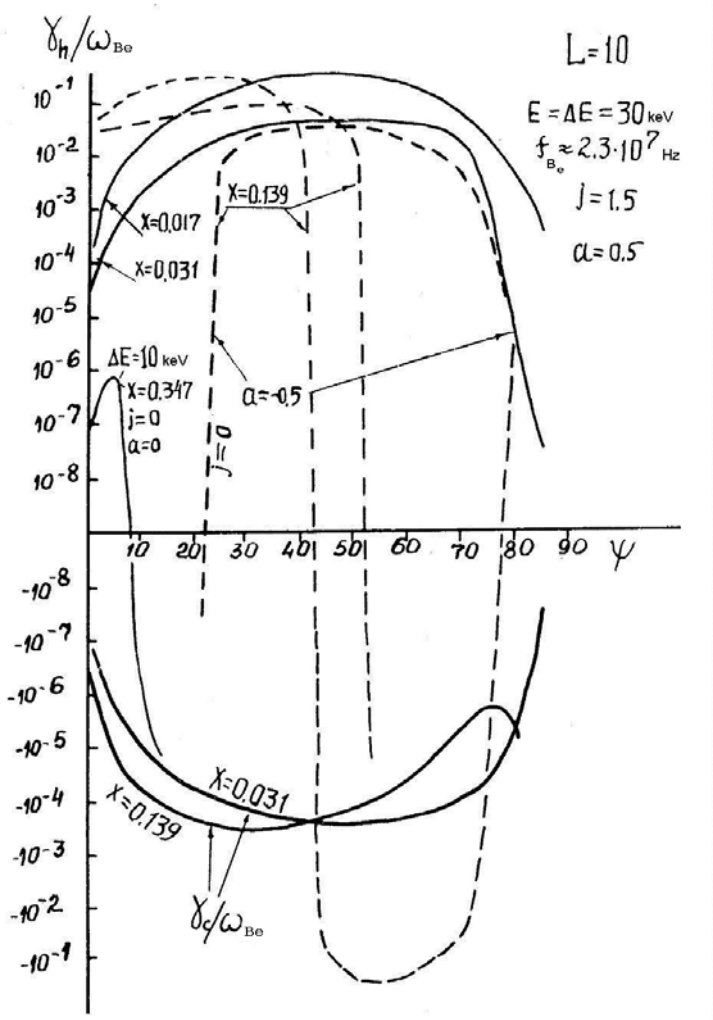

Fig. 4.53 Curves of γ_h and γ_c for several frequencies x. A negative velocity anisotropy shifts the γ_h curves towards larger ψ (the anomalous Doppler effect) (from Mal'tseva and Chernov, 1989b).

The complicate behavior of $\gamma_c(\psi)$ (γ_c curves are intersected twice) is explained by the increase in Landau damping as ψ increases at low frequencies. But for $x >$

0.1 and angles ψ near $\pi/2$, the cyclotron absorption begins to dominate and the curves are crossed again at $\psi \approx 80^o$.

It was found that the Landau damping peaks at intermediate angles $\psi \approx 30^o \div 50^o$ (although it remains small even there), and that the damping decreases with increase of ψ to $80^o \div 90^o$. Therefore whistlers can be reflected without appreciable damping in low-hybrid resonance regions. The Landau damping decrement begins to decrease as ψ approaches 90^o, since the components of the antihermitian part of the permittivity tensor ϵ_{yy}, ϵ_{yz} and ϵ_{zz} which are exponentials $exp\left(-X_0^2\right)$ with coefficients of different signs, contribute to it for $s = 0$ (see Appendix in Mal'tseva, Chernov (1989b)). There is a definite similarity between these calculations and the results of Hashimoto and Kimura (1977).

The actual variation of the wave amplitude (A_o) during propagation at group velocity is determined by the integral gain

$$\gamma_\Sigma = \int_0^l \left(\gamma / V_{gr}\right) dl'$$

in which the amplification (damping) contributions from hot particles and damping by the cold plasma along the path l are summed. Large negative values of γ_Σ (when $\gamma_\Sigma \gg 1$) characterize instantaneous damping of the wave, since its amplitude will decrease in accordance with the law $A = A_o \exp\gamma_\Sigma$.

Figure 4 in Mal'tseva and Chernov (1989b) shows small damping along whistler trajectory during 10 – 20 s even for extreme conditions for the instability with $E = 3$ keV, $\Delta E = 0.01$, $n_h/n_c \sim 10^{-7.}$ As a final result of calculations of Mal'tseva and Chernov (1989b) Figure 4.54 shows the frequency range of the positive total increments of whistlers, obtained on the totality values of γ_Σ. along 60 trajectories for different values of f_{Pe}/f_{Be}. The amplified whistler propagation is possible only, if $\gamma_h \gg |\gamma_c|$ (by two - three orders of magnitude with a maximum in the frequency interval $x = 0.022 \div 0.1$). This result is differed from those of Kuijpers (1975c) (see above Figure 4.47) and Berney and Benz (1978) in terms of cutting curves by low frequencies (due to Landau damping) and in terms of smoother decrease from the side of the high frequencies (due to contribution of three resonances).

Thus Mal'tseva and Chernov (1989b) showed that whistlers excited by anisotropic beams (as the most real distribution in the solar magnetic traps) can propagate in arbitrary angles to magnetic field in course of tens of seconds.

In connection with the new observations of FB in the microwave range, it is important to estimate the possibility of the excitation of whistlers in the dense hot flare plasma. The calculations of increments for such conditions were carried out by Yasnov et al. (2002). The position of the radio source near the acceleration region of particles justifies the use of the same distribution function (4.12) in the form of anisotropic beam.

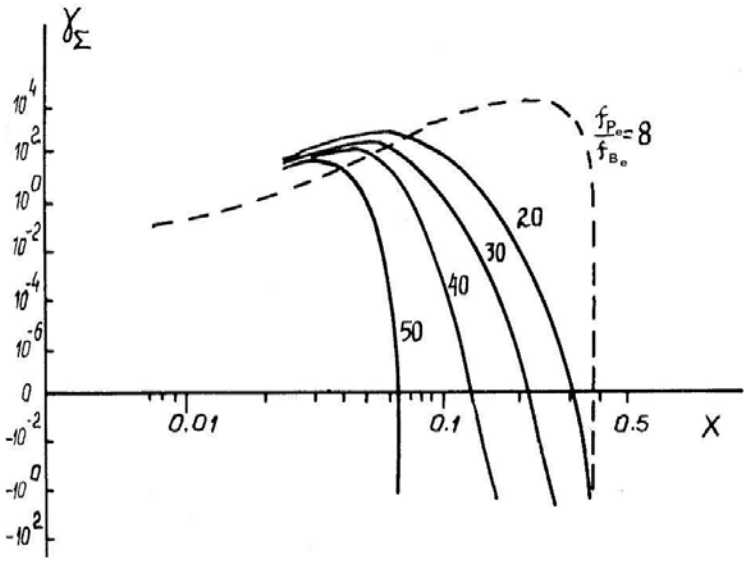

Fig. 4.54 Frequency range in which amplified whistler propagation is possible (with maximum positive gain to the first reflection) (from Mal'tseva and Chernov, 1989b).

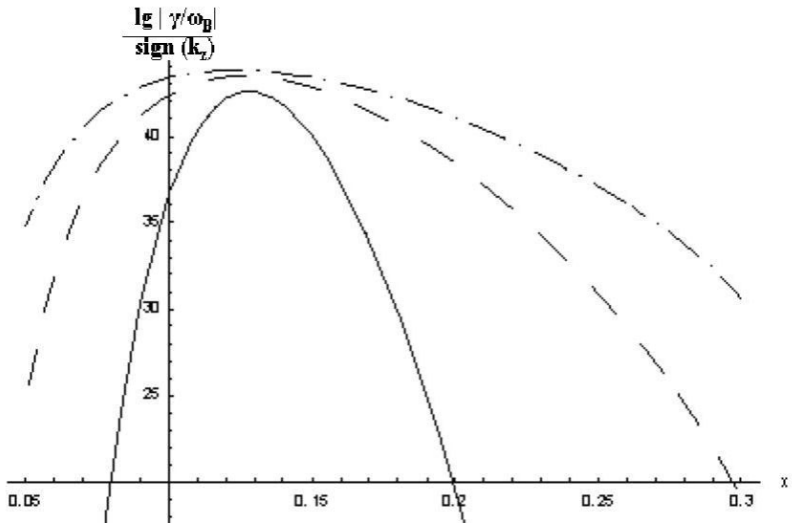

Fig. 4.55 Increment of whistler instability relative *!B* on the dependence of whistler frequency *x* for three values of the coronal temperature, from below to upward $T_e = 2 \cdot 10^6$ K, 10^7 K, $2 \cdot 10^7$ K (from Yasnov et al., 2002).

One example of calculations for $a = -0.5$ and $j = 0.2$ (the anomalous Doppler effect with a small loss-cone anisotropy) and different temperatures (to $2 \cdot 10^7$ K) is shown in the Figure 4.55.We can see, the whistler growth rates increase with T_e and the maximum is shifted with T_e to the lower frequencies, from $x = 0.13$ to $x \approx 0.1$ for $T_e = 2 \cdot 10^7$ K. The absolute values of increments prove to be even higher, than in the upper corona for the meter range.

4.6.3.6 Whistler ray tracing in the solar corona

Accordingly Kimura (1966) as a result of the account of ions in the dispersive relationship, refractive index at the mirror point acquires large, but end value. Only account of ions made it possible to calculate the trajectories of magnetospheric whistlers with the multiple reflections (Walter, 1969). The form of trajectory at the mirror point depends on the frequency of the whistlers: it is smooth oval, if $\omega \ll \omega_{LHR}$, sharp, if $\omega \approx \omega_{LHR}$, or even with the overlap, if $\omega > \omega_{LHR}$, (Edgar, 1972).

However, the simple transfer into the corona of all effects characteristic for the magnetospheric whistlers will be not completely correct, since coronal plasma is denser, hotter, and the relation of plasma frequencies changes in the larger interval of values (1 – 50). It was therefore very important to verify the possibility of reflections of whistlers in the solar corona.

The possible whistler trajectories in the solar corona were calculated by Mal'tseva and Chernov (1989a). The standard program of numerical integration of Haselgrove two-dimensional equations (usual for earth's magnetosphere) was used. This is system of four differential first order equations in the polar coordinates (r, Θ). The equations of ray are obtained from the differential form of Snell's law with the propagation of wave with the group velocity through the medium with the smoothly varying parameters (Haselgrove, 1955). The double Newkirk model of the electron density was chosen, as a convenient analytical form above the active region (Newkirk, 1961),

$$n_e = 16.52 \cdot 10^4 \cdot 10^{4.32/\rho} \text{ cm}^{-3} \tag{4.14}$$

where ρ is the height from the center of the Sun in solar radii ($R\odot$). And the dipole model of magnetic field above an active region was selected for the analogy with magnetospheric calculations, with a depth of the position of dipole under the photosphere L= 20000 km, which was utilized as the parameter of McIlwain with the calculation of the course of force line according to the formula: $r = L_0 \cos^2(90 - \Theta)$, where L_0 is the maximum height of the force line. The magnetic field strength at the photosphere level was chosen of 300 G for force lines in the height interval 0.015 – 0.1 $R\odot$ and of 1000 G for heights > 0.1$R\odot$.

The calculations of Mal'tseva and Chernov (1989) showed that the trajectories of whistlers in the solar corona can be such complex, with the multiple reflections, like magnetospheric ones.

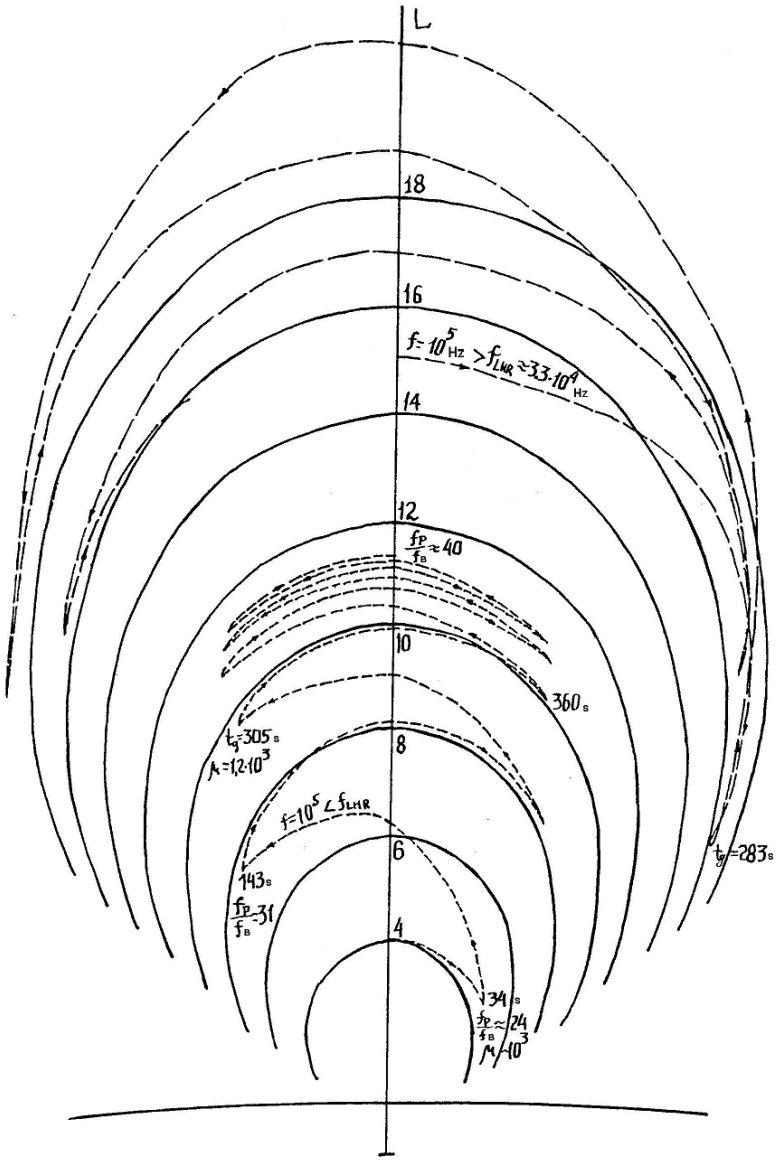

Fig. 4.56 Whistler trajectories (*broken line*) with repeated reflections against the background of dipole force lines (*solid line*). $L = 20000$ km is the depth of the position of dipole under the photosphere . The scale in the horizontale direction is the same (in L). The lower trajectory is seized at the level of $L \approx 11.5$. In some reflection points the parameters of trajectories are marked: time of group propagation t_g, ratio f_P/f_B and value of the refractive index μ (from Mal'tseva and Chernov, 1989a).

Mal'tseva and Chernov (1989) were limited to the most probable frequency range of whistlers, $0.02 \le x \le 0.25$ in which the propagation is possible without appreciable attenuation. With the inclined excitation and propagation of the whistlers (more precisely, when the angle between the wave vector **k** and the ray polar coordinate r, $\delta < 20^{o}$) they can experience reflections at the points of lower hybrid resonance and repeatedly intersect the source of radio emission. Figure 4.56 shows two of numerous trajectories beginning at the top of magnetic loops and interesting rather for the interpretation of ZP, when the oblique whistler wave is excited at anomalous Doppler effect. The lower trajectory is seized in the corona after numerous reflections, seven rays in the interval of 32 000 km. The periodic whistler wave packets are prove to be seized at a certain level in the corona in the time interval compared with one minute, then this can be used for the interpretation of the stationary stripes of zebra almost without the frequency drift.

If the longitudinal whistlers are excited in the base of magnetic trap (at the normal Doppler resonance), they propagates along the magnetic field and they can be responsible for FBs. The parameters of ducts capable of canalizing whistlers with the increased density and magnetic field strength (in 2 – 5 times) represent a special interest. The greatest cross size of duct should not exceed $2 \div 3 \cdot 10^{8}$ cm. A critical angle of capture of whistlers in the duct is found: $\psi \le 70^{o}$ (ψ is the angle between **k** and **B** in a point of whistler excitation).

4.6.3.7 Scattering of whistlers on thermal plasma and coupling with ion-sound waves

In the course of the propagations in the corona the whistlers undergo by the induced scattering on thermal ions and electrons. According to Livshits and Tsytovich (1972) the predominant scattering of whistlers by ions occurs only in strong magnetic field, more precisely for the coronal conditions, when $\omega_{Pe}/\omega_{Be} < 12$ (see in detail Chernov (1989)). During scattering by ions whistlers transfer to lower frequencies (to $\omega_w \approx 0.1\omega_{Be}$) and became aligned along the magnetic field. However this process is slow. The scattering by electrons is much faster, (approximately by a factor 43) and the continuous transfer to larger angle θ_w occurs.

Under conditions of a non-isothermal plasma $T_e \gg T_i$ the main process consists in the inter-conversion of ion-sound wave (s) (at frequency $\omega_s \approx \omega_{Pi}$- ion plasma frequency) into whistlers and back. Here, there is a strong constraint on the angle between $\mathbf{k}_w$ and the magnetic field $\theta_w \ge 70^{o}$. Angular scattering of whistlers by electrons satisfies this condition, although the main role plays the angles θ_w under which whistlers are excited.

The maximum increments for coupling and decay of whistlers and s waves occur only when their frequencies almost coincide, which means that $0.25\omega_{Be} \approx \omega_{Pi}$. Just such relation is satisfied in the solar corona. The approximate behavior of the main plasma frequencies in the corona is shown in Figure 4.57. The plasma frequency f_{Pe} is approximated by double Newkirk model. It is seen that the $0.25f_{Be}$

curve intersects the f_{Pi} curve in the vicinity of $f_{Pe} \approx 300$ MHz, so this level is the middle of the range where rapid conversion of whistlers into ion-sound waves and back in a pulsating regime can occur ($s + s' \leftrightarrow w$). This region is hatched in Figure 4.57.

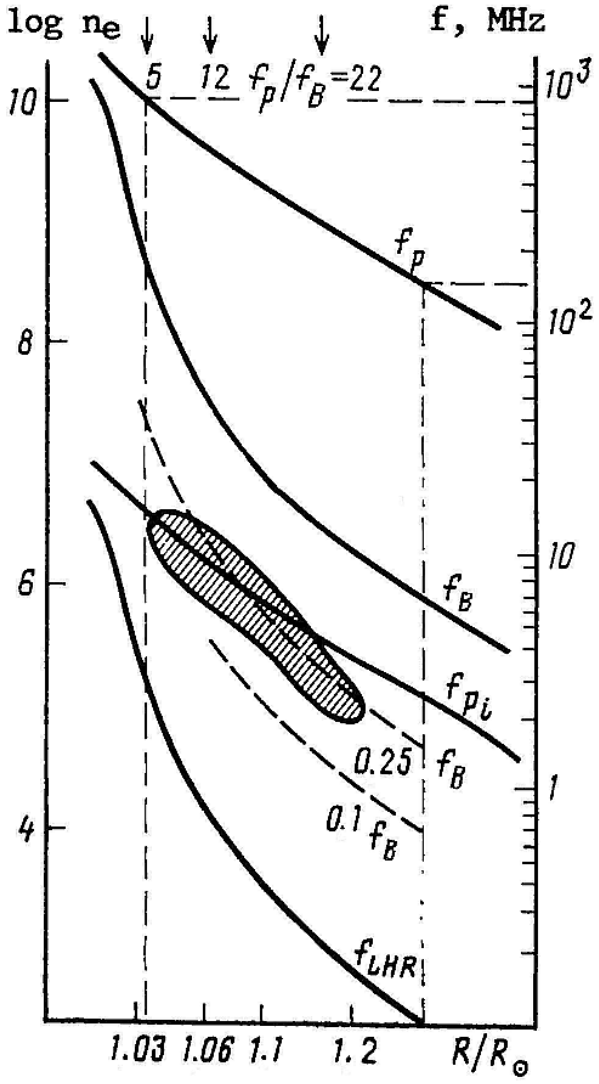

Fig. 4.57 Variation of characteristic frequencies with distance $R/R\odot$ in the corona. The interaction ($s+s' \leftrightarrow w$) is most efficient in the hatched region (from Chernov 1989).

This mechanism will useful to understand the nature of the superfine structure of zebra stripes consisting of millisecond spikes (Chernov et al. 2003). Couplings and decays of *s* waves and whistlers are observed in the laboratory experiments and are used for the interpretation of radio emission in the active rocket experiments with the injection of the electrons (Mishin et al. 1989).

4.6.3.8 Problem with magnetic field estimations using FB

Benz and Mann (1998) the first time presented IDB above 1 GHz (Figure 58) and they investigated the variation of the frequency drift rate with frequency as well as the magnetic field estimations in different models. In Figure 4.58 we see that *df/dt* is almost constant with frequency and high frequency IDB are found to be identical in their characteristics with FB below 1 GHz. The quantitative results on the first derivative (drift rate) and second derivative have been used to test the two existing models. At the newly accessible high frequencies, the Alfv´en soliton model by Treumann et al. (1990) predicts very high magnetic fields that are inconsistent with plasma emission.

The other model, suggesting whistler waves (e.g. Mann et al., 1987), predicts relations of $\dot{f}$ and $\ddot{f}$ with frequency dependances that are not consistent with the observations. However whistler wave model gives the reasonable magnetic field strengths using the whistler group velocity and *df/dt*: 212 G at 2000 MHz and 5.7 G at 200 MHz. But these estimations depend strongly on relative whistler frequency (x) and density model (Ln).

Dulk and Mclean (1978) did not include the estimations of the magnetic field strength using the frequency separation ($\Delta f_{ea} \approx f_w$) between emission stripe and LF absorption in FB due to a large arbitrariness in the choice of x. In Chernov (1990b) a special attention is given to the choice of x where the whistler growth rate is maximal.

At meter wavelengths ($f_{Pe}/f_{Be} \approx 30$) the distribution function should have a narrow loss-cone and the generation maximum falls at frequencies $x \approx 0.1$ (see Figure 4.48). In this case the fast differential scattering of whistlers on thermal electrons is predominant with transfer over the spectrum to low frequencies which may compensate the increase of x with upward whistler propagation toward lower magnetic field. Since the scattering on electrons has a low frequency limit $x \approx 0.1$ this value remains almost constant during life time of the fiber.

In the decimetric range fast electrons have larger loss-cone angle (near the magnetic mirror) and the maximum of the growth rate takes place at $x \approx 0.25$. For $f_{Pe}/f_{Be} < 12$ the differential scattering on ions is predominated and the value $x \approx$ 0.25 should be conserve along the fiber. By this reason the value Δf_{ea} usually hardly varies during life of one fiber (e.g. see Figures 6. 22).

Thus, in the metric range $x = 0.1$ must be used and in the decimetric range $x = 0.25$. The estimations of B with these values of x satisfy condition that plasma β would be ≤ 1 and they are close to model of Dulk and McLean (1978):

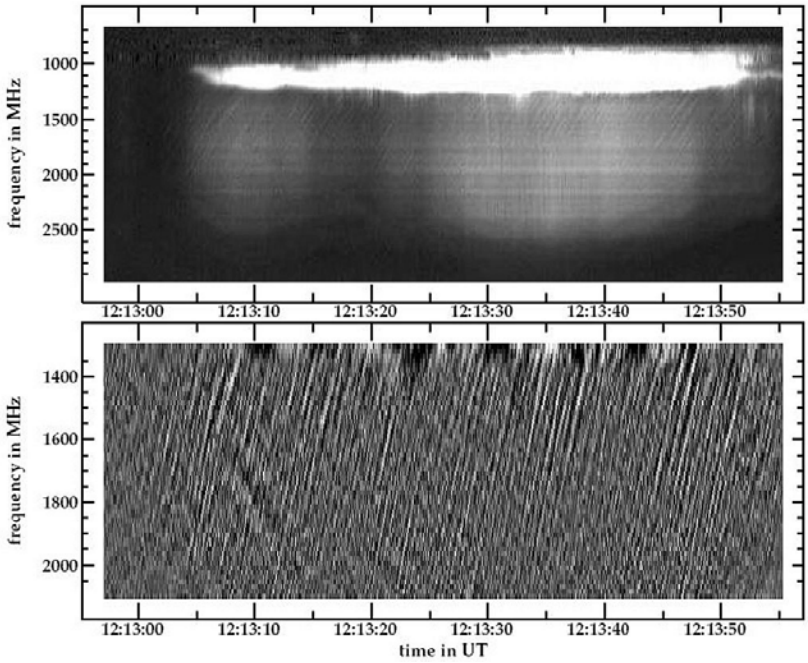

Fig. 4.58 *Top*: Spectrogram of a decimetric type IV burst observed with the Phoenix radio spectrometer of ETH Zurich on March 20, 1993. *Bottom*: The IDBs in the range 1200-2400 MHz; the intensity have been enhanced by subtracting a gliding average in frequency and time (from Benz and Mann, 1998).

$$B = 0.5(h - 1)^{-1.5}\,\mathrm{G}\,, \quad (1.02 \leq h \leq 10) \tag{4.15}$$

where h is the height in solar radii. The reliability of this procedure is checked by the simultaneous testing of the obtained estimations according to the frequency drift of fiber using the formula (4.1), obtained by Elgarøy (1982) via equating V_{gr} of whistlers (formula (4.5)) and speed of an agent, determined from the frequency drift

$$V \approx 2\frac{df/dt}{f}\frac{n_e}{dn_e/dh}\,. \tag{4.16}$$

For determining of the agent speed V the simple double Newkirk model (formula (4.14)) is traditionally used. Coefficients in the formula (4.1) must be different for different x.

4.6.4 Theory of Zebra patterns

Zebra-patterns are more complicated structures, and many mechanisms have been proposed to explain them (Kuijpers 1975a,b; Zheleznykov and Zlotnik 1975a,b; Chernov 1976a; Mollwo 1983; 1988; Winglee and Dulk 1986; Ledenev et al. 2001; Karlicky et al. 2001). The majority are based on electrostatic emission at double plasma resonance (DPR):

$$\omega_{UH} = \left(\omega_{Pe}^2 + \omega_{Be}^2\right)^{1/2} = s\omega_{Be} \tag{4.17}$$

with ω_{UH} - upper hybrid frequency and s- integer harmonic number. The most advanced model in this category, proposed by Winglee and Dulk (1986), is based on cyclotron non-saturated maser emission of electrostatic waves by a loss-cone electron distribution. However some difficulties remain with all these versions: the frequency separation between zebra stripes Δf_e must comprise certain portion of the electron cyclotron frequency (depending on the relationships of the scale heights of density and magnetic field in the corona), and this is hard to reconcile with its often irregular variation with frequency; the magnetic field deduced from Δf_e seems too low for the flare region and we are faced with the difficulty of having plasma $\beta \approx (\upsilon_s/\upsilon_A)^2 \leq 1$ (a well accepted value for magnetic traps in active regions). Practically all models explain only stripes in the emission, although the stripes are sometimes observed predominantly in the absorption. An important property of distribution with the loss-cone was missed in all models: it generates also whistlers, and interaction of whistlers with the fast particles changes radically the velocity distribution function, when the transverse anisotropy decreases, but a beam on the longitudinal velocities appears.

Probably, the noted difficulties always stimulated the new authors to the search for other mechanisms. For example, Fomichev and Fainshtein, (1981) proposed the generation of zebra pattern due to the excitation of nonlinear ion-sound waves and their scattering on fast particles.

4.6.4.1 Electrostatic waves perpendicular to the magnetic field

For the description of double plasma resonance (DPR)- model we will address to the primary sources of the theory of kinetic excitation of electrostatic plasma waves in the solar corona (Zheleznyakov and Zlotnik, 1975a) and on the motion of

description we will note the subsequent specifications and additions of the different authors. For the brevity of exposition we will not repeat long computations, requiring detailed descriptions and appendixes, which exist in the original papers.

If we assume that the density of non-equilibrium electrons is small compared to background plasma and if the wave length is much smaller than the gyroradius of thermal electrons (a parameter $\lambda = k_\perp^2 V_{Te}^2 / \omega_{Be}^2$,where $k_\perp$ is the transverse component of the wave vector **k**; V_{Te} is the thermal velocity), that the dispersion properties of the waves are determined by the equilibrium component and can be described by well-known equations (the equation (2.5) in Zheleznyakov and Zlotnik (1975a)):

$$\varepsilon_{||}^0 = 1 - \frac{\omega_{Pe}^2}{\omega^2 - \omega_{Be}^2} - \frac{3\omega_{Pe}^2 \omega_{Be}^2}{\left(\omega^2 - 4\omega_{Be}^2\right)\left(\omega^2 - \omega_{Be}^2\right)} - \frac{\omega_{Pe}^2}{\omega^2 - s^2\omega_{Be}^2} \frac{s}{(s-1)} \left(\frac{\lambda}{2}\right)^{s-1} = 0 \tag{4.18}$$

(s is the harmonic number).

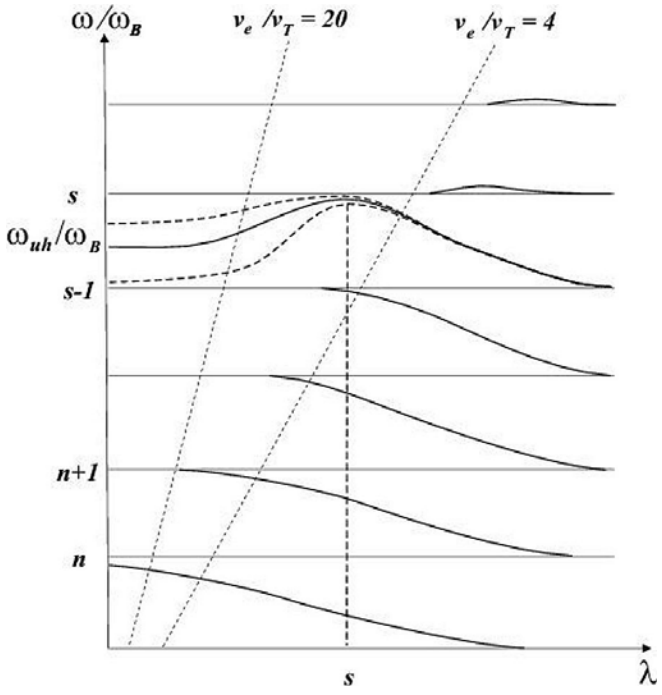

Fig. 4.59 Qualitative dispersion curves for Bernstein modes and plasma waves at the frequency of upper hybrid resonance. *Straight lines* mark the instability boundaries for two ratios of velocities v_e/V_{Te} (from Zlotnik et al., 2003).

Equation (4.18) has solutions at the frequencies close to the cyclotron harmonics $s\omega_{Be}$ (the so-called Bernstein modes):

$$\omega^2 - s^2\omega_{Be}^2 = \frac{\omega_{Pe}^2\,\omega_{Be}^2}{\left[\left(s^2-1\right)\omega_{Be}^2 - \omega_{Pe}^2\right]}\frac{s\left(s+1\right)}{\left(s-2\right)!}\left(\frac{\lambda}{2}\right)^{s-1} \tag{4.19}$$

and close to the upper hybrid resonance frequency ω_{UH}:

$$\omega^2 = \omega_{UH}^2 + 3\lambda\omega_{Be}^2 = \omega_{UH}^2 + 3k_\perp^2 V_{Te}^2 \tag{4.20}$$

The dispersion curves $\omega(\lambda)$ for the ratio $\omega_{UH}/\omega_{Be} = 15$ are shown in Figure 4.59. The Bernstein modes have anomalous dispersion passing from one harmonic to the other. A qualitative difference is present for the plasma waves in the vicinity of the hybrid frequency at $\lambda < s$: they have normal dispersion. Three curves inside the hybrid band correspond to different location of ω_{UH} within the given interval. The curves in Figure 4.59 at $\lambda << 1$ show that the dispersion relation (4.20) is valid only inside the hybrid band $(s-1)\omega_{Be} < \omega < s\omega_{Be}$ determined by $s \cong \omega_{UH}/\omega_{Be}$. It cannot be extended to the adjacent band to the hybrid band from above, as done by Winglee and Dulk (1986). Zlotnik et al. (2003) affirm that Winglee and Dulk (1986) neglected the resonance term in (4.18). This remark should shake (or reject) the subsequent statements of Winglee and Dulk (1986) about an opportunity of contributions from various harmonics to the emission at a fixed frequency as well as the numerical result of growth rates, represented in Figure 2 in Winglee and Dulk (1986): flat "piling" of 17 harmonics.

In Appendix B in Zlotnik et al.(2003) the calculation of growth rates for DPR instability is specified for non-relativistic case important for ZP. Zlotnik et al. (2003) consider the distribution function of fast electrons in the DGH form (Dory, Guest and Harris, 1965) without a loss-cone:

$$f\left(\upsilon_{||},\upsilon_\perp\right) = \frac{\upsilon_\perp^2 c^3}{4\pi\sqrt{2\pi}\upsilon_e^5} exp\left(-\frac{\upsilon_{||}^2+\upsilon_\perp^2}{2\upsilon_e^2}\right), \tag{4.21}$$

where $\upsilon_{||}$ and $\upsilon_\perp$ are the longitudinal and transverse components of electron velocity **v** relative to the magnetic field. The DGH distribution function (sometimes named as ring distribution) is too specific, in the sense that the maximal instability develops only for a strictly fixed velocity of fast electrons which sharply limits the possibilities of its use. ZP is usually observed in the post flare phase, when the energy particles manage repeatedly to be reflected from magnetic mirrors, as a result of which the loss-cone distribution is formed. Winglee and Dulk (1986) examine both these distributions in a comparative aspect, in order to show, what distribution and with what velocities can excite the isolated harmonics, not being merged

together into the continuum. Zlotnik *et al.* (2003) repeat all calculations of the growth rates from Zheleznyakov and Zlotnik (1975a), in order to precise the instability limits and to respond on some remarks of Winglee and Dulk (1986).

The growth rate of longitudinal waves (γ) is determined only by the nonequilibrium fast electrons (when a small addition of fast particles does not change the dispersive properties of plasma: $\gamma << \omega$) and is given by

$$\gamma = Im\,\omega \approx -\frac{Im\,\varepsilon_{||}^{(1)}}{\left[\partial\varepsilon_{||}^{(0)}/\partial\omega\right]_{\varepsilon_{||}^{(0)}=0}}\ , \tag{4.22}$$

where $\varepsilon_{||}^{(1)}$ is the antihermitian part of the dielectric tensor. For positive γ the value $Im\ \varepsilon_{||}^{(1)}$ should be negative which defines the instability boundaries: $\lambda > \lambda_{cr} \approx (sV_{Te}/\upsilon_e)^2$, shown in Figure 4.59 by dotted lines. A strong instability is realized at sufficiently great velocities υ_e, when the instability boundary is located in the region of normal dispersion ($\lambda_{cr} < s$). Zlotnik et al. (2003) emphasized that the Doppler shift (the value $k_{\|}\upsilon_{\|}$ in the resonance term in $\varepsilon_{||}^{(1)}$) was taken into account as necessary condition of such an instability in contrast of the statement of Winglee and Dulk (1986), that Doppler shift was neglected by Zheleznyakov and Zlotnik (1975a).

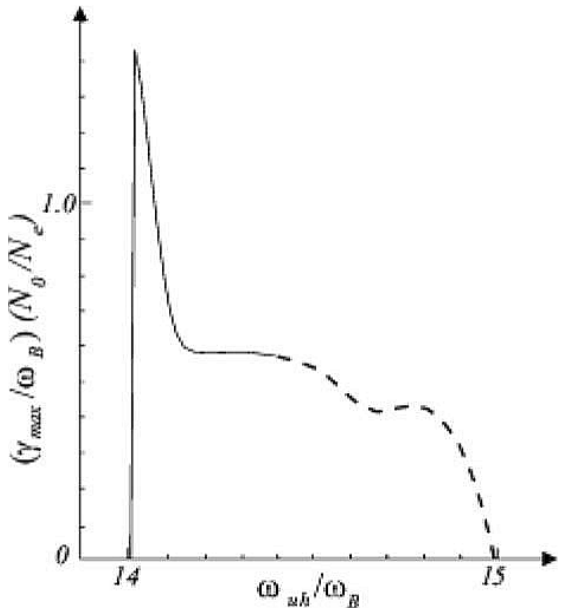

Fig. 4.60 The dependence of maximum growth rate on the position of ω inside the hybrid band (From Zlotnik et al., 2003).

In Appendix B of Zlotnik et al. (2003) it was confirmed the following peak growth rate of upper hybrid waves in the hybrid band for $\upsilon_e/V_{Te} = 20$ and $\omega_{Pe}/\omega_{Be} = 15$: $\gamma_{max} \sim \omega_{Be}(n_e/n_0)$. This value is one to two orders of magnitude greater than the growth rate of Bernstein modes. However the estimation of the relative frequency bandwidth of the excited waves

$$\delta\omega/\omega_{Be} \sim (3/2s)\left(V_{Te}^2/\upsilon_e^2\right) \tag{4.23}$$

for used values $s = 15$ and $\upsilon_e/V_{Te} = 20$ gives a too small unrealistic value $\delta\omega/\omega \approx 2.5\cdot10^{-4}$. And the reason is that at the estimation of $\Delta k_\perp/k_\perp$ (the expression B.15) the velocity dispersion $\Delta\upsilon_\perp/\upsilon_\perp$ was missed as the infinitesimal quantity.

In this connection the main qualitative conclusion that the frequency interval of enhanced generation is much less than ω_{Be} (represented in Figure 4.60) causes the doubt. Such a behavior of increment will be correct only for a distribution being peaked at large pitch angles and with the velocity dispersion $\Delta\upsilon_\perp/\upsilon_\perp$.

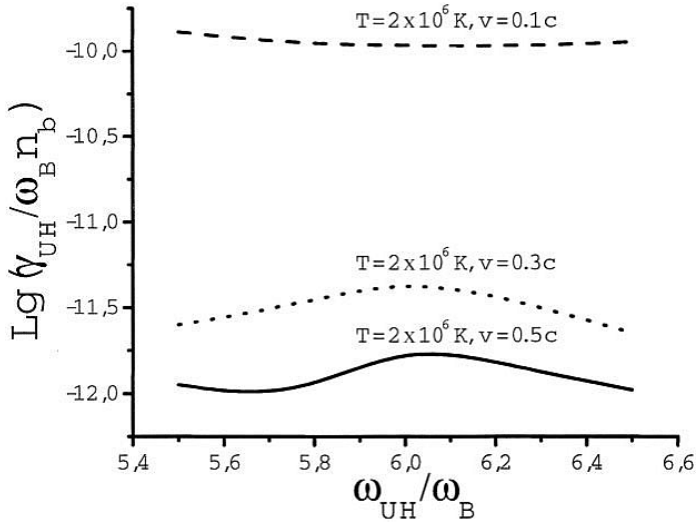

Fig. 4.61 The growth rate of the upper hybrid waves for the harmonic number s =6 and different temperature and velocities of fast particles (from Yasnov and Karlicky, 2004).

This remark is confirmed by new calculations carried out by Yasnov and Karlicky (2004) for the same distribution function of (4.21). The growth rate of the upper hybrid waves was computed for different velocities of fast electrons considering a finite temperature of the background plasma and relativistic corrections. One of examples of calculation is shown in Figure 4.61 for s=6. We see a noticeable maximum of γ only for greater velocities $\upsilon = 0.3 \div 0.5c$, but the bandwidth of the maximum occupies more than a half of ω_{Be} and its value decreases on more

than one order. The maximum of the growth rate appears only on harmonics s = 5÷10. According to results of Stepanov et al. (1999) the frequency interval of plasma wave excited in the DPR conditions occupies also about 0.3 – 0.5 part of the distance ω_{Be} between the adjacent harmonics.

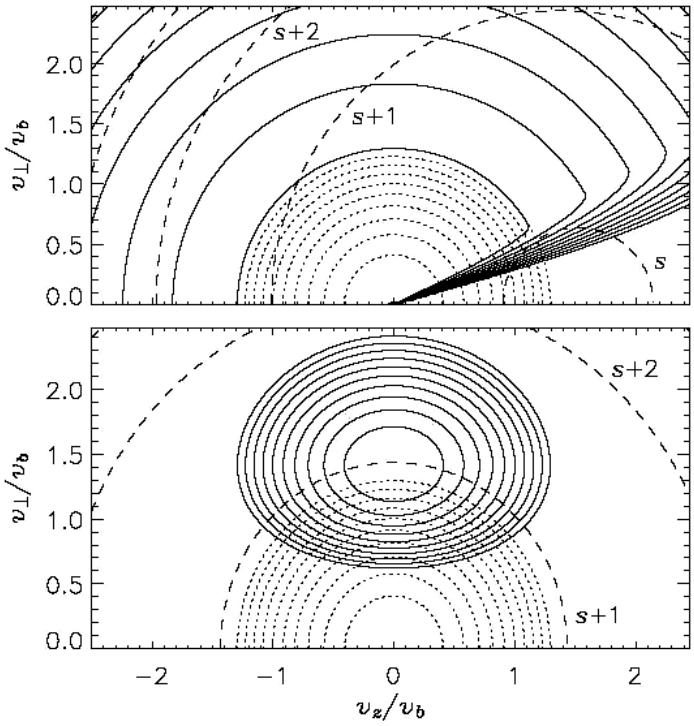

Fig. 4.62 Distribution functions of fast electrons with loss-cone (*(top)*) and DGH (ring) type (*bottom*). The dashed lines show the resonance curves corresponding to the maximal growth rate for Bernstein modes with frequency $s\omega_{Be} < \omega < (s+1)\ \omega_{Be}$. The dotted contours show the distribution of background plasma electrons (from Kuznetsov, 2005).

In such a case a problem arises with the overlapping of harmonics. The frequency bandwidth $\Delta f/f_{Be}$ of γ should be less than the frequency separation between harmonics which depends on the relative relationship of the height scales in the corona of the density $L_n = 2n(dn/dh)^{-1}$ and the magnetic field $L_B = B(dB/dh)^{-1}$ (Winglee and Dulk, 1986; Zlotnik et al., 2003):

$$\delta f/f_{Be} < L_B/\ (L_n\ - L_B) \tag{4.24}$$

For realization of DPR- levels it is required, that the height scales would noticeably differ, and usually $L_n >> L_B$ (the magnetic field changes with height faster

than the electron density). However if even $L_n/LB = 4$, we obtain the values $\Delta f/f_B$ and $\delta f/f_B$ of one order, thus harmonics will merge into a continuum emission.

Taking into account the given above valid remarks of Zlotnik et al. (2003) it should be nevertheless recognized to be accurate with the basic conclusion of Winglee and Dulk (1986): in most cases the emitted harmonics overlap in the continuum radiation and zebra stripes can appear only if the maser instability is not at saturation, if the fast electrons have a loss-cone distribution and their velocities are close to 0.1 c. This result seems natural, if we will compare resonance curves on both distribution functions, DGH and loss-cone distribution, represented in Figure 4.62: the resonance curve in the loss-cone distribution is located at the maximum of distribution near loss-cone with the lower perpendicular velocities, and on DGH - with the higher velocities without the maximum of distribution, that will require the higher concentrations of non-equilibrium particles.

Mollwo (1983; 1988) explained smooth changes of frequency drift by a movement of fronts of fast particles at various angles to the magnetic force lines. Thus, a certain restriction is imposed for the crosssection size of these fronts, so that the stripes are not merged into the continuum.

Up to now two versions of the radiation source of cyclotron waves are allowed for the explanation ZP: the first version is the excitation due to the kinetic cyclotron instability in a small-size source of Bernstein modes (Figure 4.63a). Such a scheme is apparently responsible for quasiequidistant on frequency ZP stripes. The second and more common version is the generation in a distributed source in the magnetic flux tube filled with hot electrons. Here, the emission stripes are formed at the levels of DPR in the different regions of the source (Figure 4.63b). In this case ZP stripes may be of essentially non-equidistant character.

Independently and almost simultaneously Kuijpers (1975a,b) suggested one of the possibility of ZP generation. His model coincides with Zhelnyakov and Zlotnik (1975c) model of the distributed source: excitation of cyclotron waves takes place in the region of DPR. However Kuijpers (1975) considers the hydrodynamic instability. His model permits to explain in a unified way the origin of the background continuum and zebra stripes. The background generates in regions between the levels $\omega_{UH} = s\omega_{Be}$ and the enhanced emission of zebra stripes emerges from these discrete levels. A version of the hydrodynamic instability was also developed by Berney and Benz (1978).

The hydrodynamic instability seems rather attractive to explain the ZP (due to the high increment). However, as Zlotnik (1979) shown, for the hydrodynamic approximation to be valid, it is necessary that in solving the dispersion equation in the integral which determines the imaginary part of the dielectric permittivity one could neglect the pole in the denominator of the integrand. Physically, this means that all non-equilibrium electrons interact similarly with a wave and in this sense the distribution function may be replaced by δ- function. Then, Zlotnik (1979)

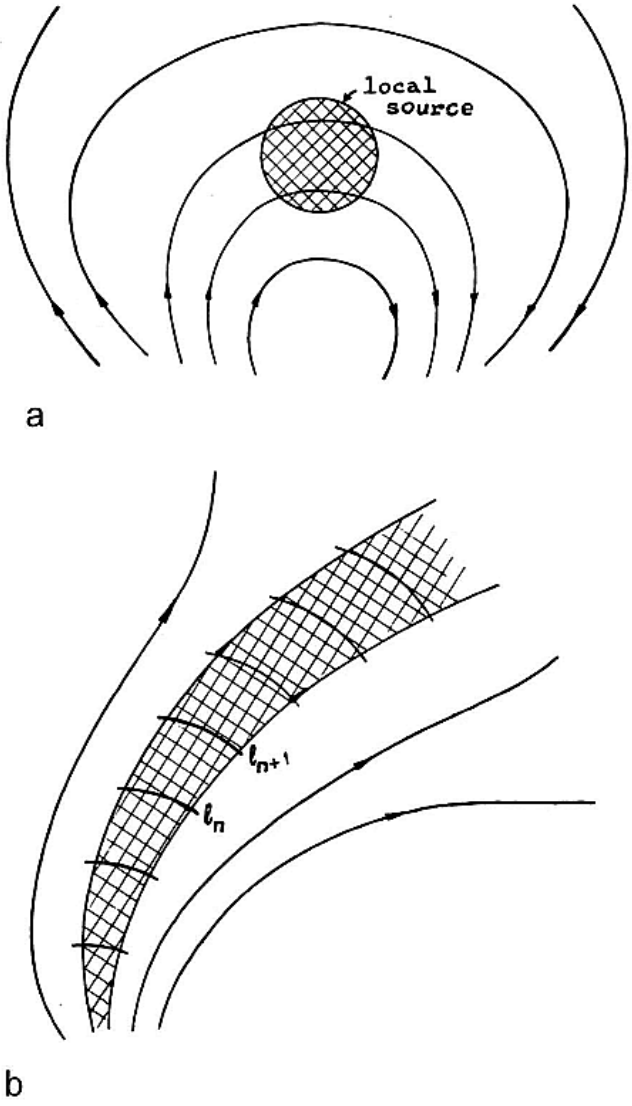

Fig. 4.63 (a)- Model of the local source localized at the apex of magnetic trap. (b)- Model of the distributed source extended along of flux tube (from Zheleznykov and Zlotnik, 1975b).

obtains the applicability limits of hydrodynamic approximation: $|\omega - s\omega_{Be}| >> \upsilon_e^2 s\omega_{Be} / 2c^2$. It is seen from this inequality that for weakly-

relativistic electrons the number of observable harmonics cannot be greater than ten, since for large s the mistuning $|\omega - s\omega_{Be}|$ exceeds the distance ω_{Be} between the harmonics. Moreover, even at low harmonics the hydrodynamic instability is unlikely excited under coronal conditions, because it is realized with impossibly large values of the hot electrons density $n_h >> 0.05 n_o$.

The kinetic instability has no density threshold to occur, and under conditions in the coronal magnetic trap it is realized at rather low densities: $n_h \geq 10^{-6} n_o$. And one more argument in favor of the kinetic instability in the double resonance region: it gives a possibility to explain absorption stripes near low frequencies of emission stripes. It is this frequency dependence which the kinetic increment has for cyclotron waves in the hybrid band in the normal dispersion region (Figure 4 in Zheleznyakov and Zlotnik (1975a)). In the hydrodynamic approximation the dispersion equation has purely real solution in that parameter region where the instability does not exist, and the absorption stripes cannot be explained.

The same argument is offered by Zlotnik (1979) not in favor of model suggested by Fedorenko (1975), according to which the ZP appears in a point source due to the kinetic instability of Bernstein modes at the harmonics above the hybrid band. In this frequency region Bernstein modes are closely adjacent the harmonics themselves (in a narrow part of the interval ω_{Be}, (Figure 4.59)) where one may obtain only the amplification band. Besides, additional calculations show that the increments of Bernstein modes at the harmonics above the hybrid band are rather small. They are less by an order of magnitude than the increments under the hybrid band and by several orders less than the increments of plasma waves in the double resonance region in the hybrid band.

4.6.4.2. The role of the relativistic effects

Zheleznyakov and Zlotnik (1975a) considered also the role of relativistic electrons (the velocity dependence of electron mass) in the kinetic instability of cyclotron waves in plasma and possible manifestation of this effect in the occurrence of the so-called "tadpoles" (Figure 4.18) in ZP (Zheleznyakov and Zlotnik, 1975b).

The relativistic effects are most important for the waves propagating perpendicularly to the magnetic field. This is easily seen from the Doppler resonance condition:

$$m\omega - s\, m_0 \omega_{Be} - k_{\|}\, m\, v_{\|} = 0 \tag{4.25}$$

which determines the interaction between particles and a wave. Really, for $k_{\|} = 0$ the bunching and re-distribution of particles affected by the wave field may be only due to the velocity dependence of mass. For Bernstein modes with anomalous dispersion the electrons with comparatively small velocities ($v_e/c \leq 0.1$) perpendicular to the magnetic field excite the waves in the narrow frequency interval

$\Delta\omega \approx s\omega_{Be}\upsilon_0^2 / c^2$, where for the inclined waves the absorption takes place. The maximal relativistic increment amounts to a value

$$\gamma_{max} = 10^{-3}\,\omega_{Be}\, n_h / n_0 \ , \tag{4.26}$$

which about one order less than for inclined waves, however in both cases the space amplification coefficients ($\mu = \gamma/V_{gr}$) can be comparable.

For Bernstein modes at the frequencies $\omega < \omega_{UH}$ (with anomalous dispersion) the absorption stripe is at the higher frequencies. It is this relative position of the frequency intervals of amplification and absorption takes place for "tadpoles", and it was the reason to use Bernstein modes with anomalous dispersion for interpreting its frequency spectrum with emitting tail, absorbtion body and bright eye. The relativistic amplification interval is situated in a place where the inclined waves are absorbed. In such a way a relativistic eye appears on the high frequency part of the absorption body (Zheleznyakov and Zlotnik, 1975b).

Thus, the relative position of absorption and amplification stripes in the ZP may serve as an indicator what model - point source with Bernstein modes or distributed source with plasma waves at DPR frequencies - is responsible for the origin of ZP. In this connection, we could however to mention, that in some events we observed simultaneously different positions of the absorption relatively the amplification (Figure 4.22), moreover this position could change during one interval of ZP.

And else a doubt arises with a such statement, when we see in Figure 4.18 some "tadpoles" almost simultaneously with eye and without it though the relativistic effect should be always present, then may be there are not Bernstein modes which are responsible for the appearance of the "tadpoles". In other events an isolated "tadpole" appear sometimes in the interval of the non-stationary ZP (Figure 4.19).

4.6.4.3 Polarization

The longitudinal cyclotron waves cannot escape outside the corona therefore one of the main processes is the conversion (coalescence) of plasma waves into the electromagnetic radiation. According to observations the polarization of ZP can be as very weak as well as very strong and in both polarization modes, but more often in ordinary mode than extraordinary.

The polarization is defined by escaping conditions and for cyclotron plasma wave was considered by Zlotnik (1977). The radio emission at the second harmonic due to the combinational scattering of plasma waves on each other may appear to be considerably stronger than the fundamental occurred as a result of spontaneous scattering by thermal ions. Then one can hardly expect the emission with a marked polarization since the condition of escaping at the frequency $\omega \approx 2\omega_{Pe}$ are practically the same for ordinary and extraordinary waves.

Another situation will be in the case when the level of excited plasma waves is sufficiently high and the efficiency of conversion into the radio emission of the fundamental is determined by induced process rather than spontaneous one. Then the emission at the fundamental may be stronger than at the second harmonic and we may expect the radio emission with a considerable polarization.

The problem of the induced scattering in plasma wave source in the corona was clarified by Zaitsev (1975). In particular he obtained the critical value W_l^{cr} of the energy density of plasma waves above which the processes of induced scattering are essential. A re-calculation of the criterium obtained under the conditions typical for ZP generation region leads to the estimation $W_l^{cr} \sim 10^{-8}$ erg cm^{-3}. For the comparison, one can estimate the plasma wave level from the observed radio emission intensity and from the known formula for the possibility of the combinational plasma wave scattering in the DPR conditions. For example, for the typical value of the emission flux density $f_\omega \sim 4 \cdot 10^{-17}$ erg s^{-1} cm^{-2} Hz^{-1} (observed in the March 2, 1970 event (Slottje, 1972)) the necessary energy density has to amount to $W_l \sim 2 \cdot 10^{-7}$ erg cm^{-3}. This value is close to W_l^{cr}, that means that depending on specific conditions in the ZP source the plasma wave scattering may be both spontaneous and induced process. Accordingly, we can observe mainly the unpolarized emission at the second harmonic or the fundamental emission with essential polarization with the sign of the ordinary mode.

As the point source model when the electromagnetic radiation occurs as a result of coalescence of Bernstein modes with plasma waves at the hybrid frequency $\omega = \omega_{UH} + s\omega_{Be}$, the situation there is nearly the same. A detailed analysis of this process of conversion (Zlotnik, 1976) shows that the intensity of the radio emission is proportional to $(1 \mp \cos\theta)^2$, where θ is the angle between the wave vector of electromagnetic wave and the magnetic field, the signs '−' and '+' correspond to extraordinary and ordinary modes. The circular polarization degree is determined by the relation

$$p_c = \frac{2\cos\theta}{1+\cos^2\theta}\ , \tag{4.27}$$

and depending on the angle θ changes from zero to unity (of the ordinary mode). In Chiuderi et al. (1973) an incorrect conclusion was made that the resultant electromagnetic radiation is unpolarized since they did not take into account a weak non-longitudinality of Bernstein modes. The dependence of polarization in accordance with the formula (4.27) should be reflected in the decrease of polarization degree with an increase in the source heliolongitude. However, in the observations the strong polarization was sometimes recorded in the limb events.

Thus, both models of ZP generation (of distributed and point source) may provide the appearance of both unpolarized and circularly polarized radio emission. However the increments of the upper-hybrid waves exceed significantly incre-

ments of Bernstein modes (by one-two orders of magnitude) therefore from all possible combinations of waves two main nonlinear coupling remain as the most probable to explain ZP: 1) the generation of plasma waves in a distributed nonuniform source, at levels of DPR with the escaping ordinary mode; 2) the generation of Bernstein modes in a point-like source and the coupling process ($\omega = s_1\omega_{Be} + s_2\omega_{Be}$) with the escaping extraordinary mode (Mollwo and Sauer, 1977; Willes, 1999).

In spite of fact, that the increments of Bernstein modes are considerably less, than for the plasma waves, Altyntsev et al. (2005); Kuznetsov (2005) utilized precisely Bernstein modes for interpretation of ZP, although the distribution function is selected with a large limitation on the particle energy. In any cases Kuznetsov (2005) calculated more detailed dependence of the growth rates of Bernstein modes on frequency (with a fast decrease after s =10), and he shown effectiveness of the nonlinear coupling of modes between themselves. There are a very weak flux (1.5 s.f.u.) against the background (20 s.f.u. at 5.7 GHz in discussed event of January 5, 2003), the defined extraordinary wave mode and the same space positions of radio sources of all zebra stripes which remain certain positive arguments in favor of this model.

In a number of last works the DPR mechanism continues to be improved. Ledenev *et al.* (2001) have chosen a scale of heights of a magnetic field much less than the scale of heights of plasma density. They have assumed that radiation originates in the second harmonic of f_{UH} and they have determined higher values of magnetic field strength B (comparable with values from Chernov et al. (2001b) in models with whistlers). However, ZP is usually strongly polarized and very seldom has moderate polarization, suggesting radiation in the fundamental frequency. Thus values B appear overestimated by more than twofold as the number of harmonics s is arbitrarily chosen. In Sawant et al. (2002) for the first time the fragment of ZP on harmonic frequencies (1700 and 3400 MHz) is discussed; such a trend was predicted in the model of Ledenev et al. (2001). However in the absence of information on polarization and also in the absence of any conformity of zebra stripes at harmonic frequencies, a certain doubt remains about the reality of harmonic structure.

For braided zebra (or lace bursts) Karlicky et al. (2001) proposed a version of DPR mechanism for flare plasma, when the radio source is considered to be in a turbulent state. Authors for the first time assume, that the different zebra lace lines can be generated in different magnetic flux tubes.

4.6.5 Detailed examination of the recent models of ZP at DPR

We are forced to examine in more detail interpretation of ZP in the event October 25, 1994, since below an alternative interpretation of this event will be presented.

In two papers, Aurass et al. (2003) (I.Observations) and Zlotnik et al. (2003) (II.Source model, theory), the DPR mechanism was used for the interpretation of the short type IV burst with ZP that occurred on October 25, 1994. In the first article, the results of the force-free extrapolated magnetic field of AR 7792 in the corona are presented. The extrapolated magnetic force line starting from the head spot and used in paper II is not connected to the radio source of ZP, since the positions of the fine structure radio sources are far to the NE of AR 7792.

The authors of paper II do not address the conclusion of paper I (at the end of section 3.2.2.) that particle acceleration took place most likely above the NE part of the loop LS1, instead of the SW part. The statement about the position of particle acceleration in the SW part of the loop LS1, made in II, contradicts Fig.5 in (I) where it is shown that the radio sources of type III bursts at 164 MHz are far to the NE of the bright area in which the main flare took place. The positions of radio sources of type III bursts and ZP coincided, therefore particles responsible for type III bursts should move upwards on the NE part of the loop LS1 and those responsible for ZP should move downwards in the same part of the loop.

In paper II, the opposite problem is solved: using multiple crossings of the calculated cyclotron harmonics with the fixed frequencies of ZP stripes (at a fixed time point) a dependence $f_p(h)$ is constructed (Fig.5). The authors have considered an arbitrary selected force line in the center of the coronal loop LS1. They assert that the electron density over height follows a barometric law.

From Fig.5 in paper II it is visible that for the extrapolated magnetic force line the cyclotron frequency drops approximately 4 times faster than the plasma frequency (for example, for the gyroharmonic number s =15). More precisely, the scale height for the magnetic field $L_B = B(dB/dh)^{-1}$ appears to be 4 times lower than the scale height for the electron density $L_n = 2n(dn/dh)^{-1}$. Thus, these relations satisfy a condition for realization of DPR with a large number of harmonics $L_n/L_B >> 1$. However, it does not satisfy a condition for the separation of zebra stripes on the continuum background, namely $\delta f/f_B < L_B/(L_n - L_B)$, at least for the nonrelativistic case.

In Appendix A, B of paper II the main formulae for the theory of growth rates for DPR instability are presented with some newer details than Zheleznyakov and Zlotnik (1975a) and Zheleznyakov (1995). In particular, these authors voice two objections, relating to Winglee and Dulk (1986). First, the dispersive curves of longitudinal electrostatic waves at the frequency of DPR (shown in Fig. A1 in II) $\omega^2 = \omega_{UH}^2 + 3k_\perp^2 V_{Te}^2$ are valid only inside the hybrid band. This cannot be extended to the band adjacent to the hybrid band from above, as done by Winglee and Dulk (1986).

Furthermore, in the footnote of Appendix A (in II) it is noted that Winglee and Dulk (1986) considered only the first order of the small parameters $k^2 V_{Te}^2 / \omega^2$ in the "thermal" dielectric tensor. That corresponds to neglecting the important resonance term. However, they do not discuss to what inaccuracies this leads in the final analysis. Thus, the main result, represented in Fig.2 in Winglee and Dulk

(1986) is inaccurate: a piling or comb of harmonics cannot be equal in intensity for s = 6 – 20.

However, in II, all formulae for similar estimations (after (B.7)) show only the qualitative behavior of the growth rate of upper hybrid waves in DPR conditions. If we choose (in more detail) the optimal value of the wave number k_{opt} (where the growth rates are maximal) for the velocity of fast particles $\upsilon_e \approx 5 \cdot 10^9$ cm s^{-1} and if we take into account the velocity dispersion $\Delta\upsilon_e/\upsilon_e \approx 1$ we obtain the relative bandwidth of the maximum growth rate inside the hybrid band $\Delta f/f_B$ approximately equal to the frequency separation between stripes $\Delta f/f_B \approx L_B/(L_n - L_B) \approx 0.3$. According to Stepanov et al. (1999), the frequency interval of a plasma wave excited in DPR conditions also occupies about 0.3 – 0.5 of the distance ω_B between the adjacent harmonics. The value of $\delta f/f_B \approx 1/10$ (see Figure 4.60) is obtained only for an unrealistically narrow velocity dispersion $\Delta\upsilon_e/\upsilon_e << 1$, since in the expression (B15) the term $\Delta\upsilon_e/\upsilon_e$ is omitted (i.e. as the infinitesimal).

Thus, for the calculated magnetic force line, the ZP stripes in Fig.5 (in II) should merge in a continuum, and the plotting of the dependence $f_p(h)$ becomes almost arbitrary. The authors of II discuss merging of zebra-stripes in a continuum (in section 4.2.), but do not check this condition further in the construction of Fig. 5.

Therefore the explanation of frequency drift of stripes due to a change of magnetic field and temperature cannot be accurate. The barometric formula: $f_p = f_{po} \exp(-h/10^4 T)$ (the formula (10) in II) is written by analogy to formula (3.9) in Priest (1982) for constant temperature, thus it is impossible to define from it a change of T. The real dependence on T is given by the much more complex expression (3.8) in Priest (1982). Heating and cooling of plasma are slow processes (in the coronal loop they last some minutes), therefore it is impossible to explain a change of frequency drift of stripes on time intervals of less than 1 second by these processes. The authors in II have obtained an underestimated electron concentration of almost two orders relative to any other model (f_{po} = 234 MHz for h = 0), and the footnote on this account (that in the base of a corona other temperatures could exist) only aggravates this question, since the local parameters will not be coordinated with the global parameters for the entire corona. The authors were forced to make this assumption because of the unrealistically calculated magnetic force line.

Thus, it was necessary to determine to what other density distributions the fitting corresponds better (for example, to the Newkirk model). If it is possible to choose any force line and to vary s, this method is not suitable for the solution of such a problem.

Smooth changes of frequency drift are explained by a movement of fronts of fast particles at various angles to the magnetic force lines (Mollwo, 1983; 1988). Thus, a certain restriction is imposed for the cross-section size of these fronts, so that the stripes are not merged into the continuum.

In the recent paper devoted to perfection of the DPR model of Yasnov and Karlicky (2004), the calculations of the growth rates of the upper hybrid waves are

carried out for various velocities of fast particles and various temperatures of the background plasma. From Figure 4.61, it is seen that the large width of the maximum of the growth rates does not satisfy the same condition $\delta f/f_B < L_B/(L_n - L_B)$, so that the zebra-stripes would not merge in the continuum.

In II the question of real absorption of the background continuum in dark ZP stripes is in no way discussed, although Zheleznyakov and Zlotnik (1975a,b) relate absorptions to the negative relativistic growth rates of cyclotron waves in the hybrid band at the low frequency edge of the positive growth rates. Winglee and Dulk (1986) do not discuss this at all due to the too large differences of the scale of negative and positive increments (of about two orders). Winglee and Dulk (1986) conclude that in most cases the emitted harmonics overlap in the continuum radiation and zebra stripes can appear only if the maser instability is not at saturation, if the fast electrons have a loss-cone distribution and their velocities are close to 0.1c.

4.6.6 New theories of zebra pattern

In search of an elimination of the difficulty with small values of magnetic field strength in the DPR model the new theory of ZP based on the radiation mechanism of auroral "choruses" - magnetospheric bursts observed at ground stations on frequencies of 2 – 4 MHz, with the fine structure similar to ZP is offered in LaBelle et al. (2003). It is supposed, that the Z-mode is radiated by the cyclotron maser mechanism (by the analogy with Winglee and Dulk (1986)). And though the Z-mode at the upper hybrid frequency does not escape from the source, it can be transformed in ordinary (O) mode at discrete frequencies (quasi-harmonics or eigenmodes) with the presence of density enhancements of the appropriate scales. The task is reduced to the solution of the equivalent Schrödinger equation for the Z- mode captured in a density inhomogeneity of an idealized cylindrical form. The Wentzel-Kramers-Brillouin approximation is used on the basis of the previous papers of co-authors. Harmonics will be derived due to the quantization in eikonal conditions with the leakage of the wave for appropriate quantum numbers in the eikonal conditions, azimuthal (m) and radial (n).

This complicated theory demands a some clarification of the physical sense of those numbers. With an analogy with quantum mechanics the azimuthal quantum number 'm' is a number of potential holes in a single inhomogeneity. The number 'm' defines the number of the angle modes along the coordinate 'r', and 'n' - the number of wave periods inside of the potential hole, i.e. the frequency of an eigenmode at a fixed level (the propagation is excluded in the consideration). Therefore 'm' defines the number of zebra stripes, and 'n' - the frequency separation between neighboring stripes. However, the numerical solution of dispersion equation (12), represented on figures 2 and 3 in LaBelle et al. (2003), reveals an increase of

the frequency separation with the decrease of the frequency, while the observations testify about the inverse dependence.

According to the estimation in LaBelle et al. (2003), the maximum number $m \approx \delta^{1/2}/\rho$, where the positive value $\delta < 1$ is a density increase inside the inhomogeneity, $\rho = \rho_e/L$ - the ratio of the electron gyroradius ρ_e to the size of the inhomogeneity L. Thus, bigger number of gyroradii gets in the scale of a single density enhancement bigger harmonic number m (the number of zebra stripes may approach to $m \approx 100$).

Thus, the generation of the Z- mode can occur in a point source at one level of the double plasma resonance (s - $const$ = 2 or 3 in (17)). Main difference and advantage of this model will be, that it provides generation of the big number of harmonics (up to 100) with the small frequency separation $\Delta f_s \approx 0.01 f_{Be}$. In LaBelle et al. (2003) the estimations of parameters of density inhomogeneities (~ 20%) and sizes $L = 1 \div 100$ m are obtained. The such density irregularities can form dispersing ion-sound waves. However authors do not discuss an important point: the time dependence of the own harmonics (dynamics of ZP), it is spoken only about a possible stability of irregularities during ~ 10 s. The generation conditions of ion-sound waves (a main condition - exceeding of the electronic temperature above ionic one $Te >> Ti$), are not discussed also, which in the solar coronae is realized only in turbulent plasma with an anomalous resistance (in current layers, in fronts of shock waves) (Kaplan and Tsytovich, 1973). Besides, the total picture from the set of discontinuities (they form by extending ion-sound waves) should lead to a merging of stripes into a continuous spectrum (continuum) taking into account, that approximately 10^8 of the such point sources are required to produce the observed power of the zebra emission. The simultaneous appearance of fibers bursts on background of ZP and also the stripes in absorption remain still away from the consideration.

There is also a doubt in applicability of model LaBelle et al. (2003) in the meter wave range, when the length of a wave becomes of one order of size with the size of irregularities ($\lambda \sim L$), as only the opposite relation ($\lambda \ll L$) is the basic condition of applicability of geometrical optics for the writing of the eikonal conditions (the equations (4) and (5) in LaBelle et al. (2003).

In this connection, we note that the zebra-structure model of LaBelle et al. (2003) is not able to explain the continuous transition between zebra structure and fiber bursts (shown in Figures 4.13 and 4.22), since only a stable point source is considered. It is not clear what variations of the positions of the absorption stripes should be expected in this model, or what their origin would be.

In recent paper of Ledenev et al. (2006) a new theory of ZP is offered: it is asserted that ZP can be formed as a result of interference between direct and reflected rays coming from a source of small size in a stratified atmosphere. The emission is generated by plasma mechanism. Full emission flux is contributed from a great number of narrow-band short-lived sources of small sizes, which are formed by plasma waves captured in density minima of background plasma fluctuations.

The formalism of geometric optics for solids (from the domain of crystal optics) adapts for obtaining of an interference pattern from the direct rays and reflected ones from the coronal heterogeneities. A doubt immediately appears about the reality of interference from the rays reflected from the heterogeneities with a smooth boundary (with a transition layer). O- and X-wave modes are reflected from the different levels in such heterogeneities (Hayes, 1985), and the necessary parallelism of rays will not be reached. The radio source should be of point-like size, of $< 10^6$ cm, and the sum emission from a great number of point sources should merge into the continuum.

Barta and Karlicky (2006) have proposed an interpretation of ZP close on the subject-matter to Ledenev et al. (2006). They show that ZP can be the result of the transillumination of the radio waves through the regular coronal density heterogeneities or the consequence of the reflection of radio waves from such heterogeneities. The same doubts appear, connected with the direct transfer of the optical properties of the propagation of the light through the crystal grid to the radio wave propagation through the coronal heterogeneities with a smooth change in the density. Moreover the dependence of the transmission coefficient on the frequency (shown in the Figure 3 in Barta and Karlicky (2006) does not reveal an increase in the frequency separation between the peaks with the frequency.

Previously, it was counted, that the propagation of the waves through the regular heterogeneities can cause diffraction pattern, (it is possible, in the form of stripes), passing over the Earth's surface from the East to the West (with the velocity $\approx$ 420 km s^{-1}), since the diffraction "grid" co-rotates with the corona. The first estimations of the corresponding delay (per-second scale) of peaks in the diverse observatories were made still by Pisareva (1958) and were checked by Chernov (1974). No delay of the fine structure between IZMIRAN (Moscow) and Nançay then there was discovered. The precise agreement of ZP stripes on the time and on the frequency in IZMIRAN and Potsdam is shown in the Figure 5 in Chernov et al. (1998). See also the precise agreement of ZP in IZMIRAN and Nançay in Figures 4.9 and 4.10. However, excluding the ray treatment (with the interference or the diffraction), it is possible to expect, that the radio waves can enter into a resonance inside the heterogeneities of the corresponding scale, locating directly above the radio source in the flare region. This approach was realized in Laptuhov and Chernov (2006).

In contrast to Ledenev et al. (2006) and Barta and Karlicky (2006), Laptuhov and Chernov (2006) are obtained dispersion equations for the spectrum of the eigen frequencies of the periodic medium, which can be created in the flare plasma due to the development of thermal instability in the form of nonlinear structures. The spectrum of the eigen frequencies of such periodic in the space resonators is calculated and it is shown, that they are completely capable generate tens of zebra stripes, number of which does not depend on the relationship of plasma and gyrofrequency in the source. This can remove all difficulties in the explanation of the large number of stripes ZP and low values of magnetic field. The periodic medium is a filter of frequencies with the numerous windows of transparency, divided

from each other by the zones of opacity. Number and frequency of the harmonics depends on the value of the spatial period of heterogeneities, which for the typical conditions of solar atmosphere is meters and decameters. The frequency separation between emission peaks grows with frequency, in accordance with observations.

4.6.7 The general scheme of formation of stripes in emission and absorption in the model with whistlers

An important point missing in previous theories is that the loss-cone distribution generates also whistlers, which in turn affect the electron velocity distribution (Chernov, 1996).

The most essential contradiction of numerous models of the ZP based on the emission of plasma waves on the DPR consists of that, that from one side, the explanation of the dynamics of the ZP stripes should assume fast changes of the magnetic field (or density of background plasma) in time (that is improbable), and on the other hand, the weak magnetic field are obtained (calculated according to the frequency separation between the stripes), insufficient for exceeding of magnetic pressure above the kinetic one (plasma β<1). The dark ZP stripes indicate not the simple absence of the increased emission, but a real absorption of the background continuum emission, which is modulated by ZP. New observations on TRACE mission showed, that the flare loops (in UV lines 171, 195 Å) consist of numerous narrow non-expanding upwards loops, in which density and magnetic field are barely changed with the height (Aschwanden, 2004). The existence of double plasma resonance levels in such loops is highly improbable.

The similarity of main properties of fibers and zebra stripes allows to apply the model with whistlers for zebra-stripes: both structures represent the parallel drifting stripes in emission and in absorption. This led Chernov (1976; 1989) to propose a common interpretation for these two kinds of fine structure based on the coupling of plasma wave and whistlers, but in different conditions of the whistler instability: for fiber bursts - at the cyclotron resonance with a normal Doppler effect when whistlers propagate along the magnetic loops; for zebra-stripes - with the anomalous Doppler effect, when whistlers propagate at the different angles to the magnetic force lines (Maltseva and Chernov, 1989; Chernov *et al.*, 1998). A system of quasi-standing whistler packets is driven by a loss-cone distribution of fast electrons in the entire magnetic trap at the cyclotron resonance:

$$\omega_w - k_{||}\upsilon_{||} - s\omega_{Be} = 0 \tag{4.28}$$

with s = +1 (the normal Doppler effect) or s = -1 (the anomalous Doppler effect) depending on the form of the distribution function (Maltseva and Chernov, 1989),

$k_{\|}$, $v_{\|}$ being the whistler wave number and fast electron velocity, both parallel to the magnetic field, ω_w - whistler wave frequency.

However, it paid little attention itself to a question of the whistler excitation in the solar corona. After Kuijpers (1975) only Berney and Benz (1978) showed the importance of examination under the solar conditions of the whistler instability in comparison with high frequency electrostatic waves. Then Sharma and Vlahos (1984) showed clearly in their calculations, that the whistler growth rates due to the loss-cone instability is higher than for upper hybrid waves.

It is important at once to note, that all previous calculations of the whistler instability are carried out by an analogy with the magnetospheric whistlers only for the longitudinal propagation at the normal Doppler effect (Kuijpers, 1975, Berney and Benz, 1978). The quasi-linear problem of the behavior of whistlers is not yet solved fully. Some special cases have been only examined also for the longitudinal whistlers. So, Stepanov and Tsap (2002) have obtained estimations of quantity and spectral indexes of the trapped electrons in relation to the precipitating ones in loss-cone for the comparison with the fast particle spectra obtained according to X-ray radiation. The oblique whistlers undergo a small Landau damping and the account of whistlers, propagating under large angles to the magnetic field and exciting on the anomalous Doppler effect, changes radically the estimations of the quasi-linear effects (Chernov, 1996).

The radiation source of type IV is usually represented as a magnetic trap, therefore it is natural to assume the distribution function of fast electrons, responsible for the continuum radiation, of a type anisotropic Maxwellian one with the loss cone and temperature anisotropy. As such cumulative distribution function is unstable also for the generation of the whistler waves it is necessary to take into account the dynamics of the cumulative distribution function due to the diffusion of fast electrons on the whistlers. We shall remark, that the generation and the propagation of the whistlers are quite possible in the narrow flare loops. The conservation laws of the processes of the coalescence $l+w \rightarrow t$ and the decay of whistlers $l \rightarrow t + w$ are examined in the monographs Tsytovich (1970; 1977), and for the conditions of coronal plasma they are examined in the papers Kuijpers (1975), Fomichev and Fainshtein (1988), Chernov and Fomichev (1989) and in the present brief description of basic aspects of the whistler model are considered executed.

The formation of stripes in emission and absorption is the basic property of the whistlers in the such sources of type IV radio bursts as a magnetic trap with the loss-cone distribution of the fast electrons (Chernov, 1990b). The calculations of the whistler kinetic instability have found out a very low power threshold of excitation (Maltseva and Chernov, 1989b). It has been shown there, that for the calculations of the integrated factors of the amplification of the whistlers, propagating under any angle to the magnetic field, it is necessary to take into account three basic resonances: the cyclotron resonance at normal and anomalous Doppler effects and the Cherenkov one.

The first consideration of quasi-linear systems of the equations (Jamin *et al.*, 1974) has shown, that the basic property of linear whistler instability is its perio-

dicity in time and space. But it is very fast (millisecond) periodicity. In the conditions of the coronal plasma in a magnetic trap the time of diffusion can be much more. Besides it should be modulated by the bounce period, (the time of the movement of fast particles between the magnetic mirrors) $l_B/2\upsilon \approx$ 0.5 s, where l_B - the length of a trap.

It follows from the calculations in Maltseva and Chernov (1989b), that the anisotropic electron beams depending on the degree of loss-cone and temperature anisotropy will excite whistlers, propagating towards the beam, on the normal Doppler effect, if $\upsilon_\perp > \upsilon_\parallel$ and $s = 1$ in the relationship (4.28). But if $\upsilon_\perp < \upsilon_\parallel$ and $s = -1$ in (4.28), then whistlers are excited on the anomalous resonance and propagate to the side of beam at large angles to the magnetic field.

Let us note an important role of the type of the electrons injection: if the injection is impulse, that quasi-linear effects on the normal resonance do not work (particle and wave disperse to the different sides), and on the anomalous one the role of injection grows with it's duration (or when new particles overtake wave).

During the prolonged particle injection the regime of whistlers generation should be periodic (in the time and the space), since the instability is sharply weakened with the precipitation of electrons into the loss-cone, and with the withdrawal of particles and whistlers (with the group velocity) from the region of excitation, the loss-cone instability is restored approximately through 0.2 – 0.3 s (Kuijpers, 1975, Bespalov and Trahtenherz, 1974). One should consider, that the particles can be scattered not only on the whistlers, but also on the electrostatic waves (Breizman, 1987; Omura and Matsumoto, 1987), the diffusion occurring first on the electrostatic waves to the side of an increase of $\upsilon_\parallel$. Then the diffusion on the whistlers along the diffusion curves begins to work. Accordingly Breizman (1987) the relaxation length of beam, excited whistlers:

$$l^w = \Lambda \frac{c}{\omega_{Pe}} \frac{\omega_{Be}}{\omega_{Pe}} \frac{n^c}{n^h} \ , \qquad (4.29)$$

(where $\Lambda = 25$ in the solar corona). For $\omega_{Pe} = 2\pi\ 1.5 \cdot 10^8$ Hz, $\omega_{Pe}/\omega_{Be} = 30$ and for a small fraction of the energetic particles relative to the background cold plasma $n^c/n^h \approx 3 \cdot 10^6$ we obtain relaxation length $l^w \approx 0.8 \cdot 10^8$ cm. The beam relaxation length on plasma waves with the same parameters and the velocity $\upsilon_\parallel \approx 1/3c$ occurs considerably bigger, $l^l \approx 2.3 \cdot 10^9$ cm (Chernov, 1989). Thus, the relaxation on the whistlers is considerably faster and a condition to the initial angular spread of the beam is easily satisfied: $\Delta\Theta_0 > (l^w/l^l)^{1/3}$, with which the relaxation on the Langmuir waves is insignificant (Breizman, 1987).

In the time of withdrawal out from the loss-cone of the precipitating electrons (Bespalov and Trahtenherz, 1986) $T_c \approx l_B/2\upsilon \approx 0.25$ s (for the trap length of $l_B = 5 \cdot 10^9$ cm) whistlers at frequency $\omega^w \approx 0.1\omega_{Be}$ pass with a group velocity of $V_{gr}^w \approx 5 \cdot 10^8$ cm s^{-1} an interval $\Delta l_B = T_c\ V_{gr}^w \approx 1.25 \cdot 10^8$ cm. Thus, as a result of the quasi-

linear relaxation of the beam on the whistlers the entire trap will consist of zones of the maximum whistler amplification with a thickness of l^w, divided by intervals of Δl_B. In this case the periodic packets of whistlers will create regular stripes of ZP with the frequency separation $\Delta f_s \approx (l^w + \Delta l_B)\nabla f_{Pe}$. It is known, that within the framework of the doubled Newkirk density model $|\nabla f_{Pe}| \approx 1$ MHz /10^8 cm, and for the frequency of 150 MHz we will obtain the frequency separation $\Delta f_s \approx 2$ MHz, coinciding with that observing in the event on 25 October, 1994.

Let us note, that the excited whistler spectra are sufficiently narrow (Kuijpers, 1975), and the group velocities along the edges of this spectrum change little with the maximum at frequency of $0.25 f_{Be}$ (especially for the oblique whistlers, see. Fig.5 in Chernov (1976) and in more detail Chernov (1990b)). This fact eliminates the group scattering of the whistler wave packet in the corona inherent for the magnetospheric whistlers. The calculations of the possible trajectories of the whistler propagation in the solar corona showed, that the whistlers in the frequency band $\approx 0.05 f_{Be}$ do not undergo any noticeable group dispersion in the propagation time ~ 10 s (Mal'tseva and Chernov, 1989a). The whistlers can experience reflections in the regions, where their frequency approaches the frequency of the lower hybrid resonance: $f_w \approx f_{LHR} \approx f_{Be}/43$. In the ducts with the increased density along the magnetic trap they go tightly along the duct for the entire frequency spectrum (a capture into the duct).

Thus, if the particle injection is prolonged, and a part of the trap is filled up with the periodic whistler packets (by thickness l^w along the trap), that each packet with the narrow whistler spectrum forms the stripe of zebra-structure in the emission as a result of the process of coalescence with the plasma waves at the summation frequency. The propagation of the system of such packets with the group velocity will cause a stripe system of the ZP, drifting in the frequency in dependence of the angle between the trajectory and the levels of the identical density. Since the ratio of frequencies f_{Pe}/f_{Be} changes little in the height interval of a radio source, giving the zebra, that the group velocities of different packets (even on the edges of the entire interval) are close in the value and in the direction, which excludes their rapid dispersion, and almost synchronous frequency drift of zebra stripes on the spectrum ensures (Mal'tseva and Chernov, 1989a).

The preferred appearance of the ZP stripes with the positive frequency drift can be connected with the excitation of the oblique whistlers on the anomalous Doppler effect in the loop apex (where $v_\perp < v_\parallel$) and with the non-ducted propagation downward to regions of the lower hybrid resonance, in which they experience reflections and then they can reach again the region at the apex with the maximum whistler instability. The propagation of the whistlers downward to the side of the growing magnetic field tension excludes the achievement of the level of the cyclotron damping (ω_w / ω_{Be} decreases). Therefore the separate stripes of ZP are usually prolonged than fiber bursts.

The system of fibers with the preferred negative frequency drift must be connected with the excitation of whistlers on the normal Doppler effect in the base of

a trap (more precise near the plug of the reflection of particles, where the distribution function has the maximum loss-cone angle). Such longitudinal whistlers are propagated along the trap to the level of the cyclotron damping (or up to reaching of absorption on the anomalous Doppler effect nearer to the loop apex). In this model the similarity of the basic properties of fibers and ZP stripes are naturally explained (frequency bandwidth, modulation depth, polarization of the ordinary type etc.) It makes possible to explain also a sometimes observed continuous transformation of fibers into the ZP stripes and vice versa. If a whistler trajectory goes at small angle to ∇f_{Pe} (almost along the trap), we could observe fibers. When the bent trajectory reaches the trap apex, it can be almost perpendicular to ∇f_{Pe}, and we could observe the decelerating frequency drift and a transformation of the fibers into the ZP stripes, which remain sometimes almost parallel to the time axis on the spectrum.

4.6.7.1 Manifestation of quasi-linear diffusion on whistlers in ZP and FB

The complete solution of the quasi-linear problem for the three resonances with particle sources and losses is very difficult, and has not yet been obtained either analytically or numerically. Usually, a simplified problem is posed, and quasi-linear equations are solved numerically for one resonance and one oscillation mode with a loss-cone distribution function (Ossakov et al., 1973; Ashour-Abdalla, 1972; Sazhin, 1987; Bespalov and Trakthenherz, 1986; Stepanov and Tsap, 2002).

Figure 4.64b schematically shows the shapes of the distribution function of type anisotrpic beam at small, moderate and large pitch angles for three improvised moments of time in the course of the diffusion: with large $\nu_{\|}$ at small pitch angles, and large $\nu_{\perp}$ at large angles; in an intermediate position the equal contribution of $\nu_{\|}$ and $\nu_{\perp}$ is possible. If fast particles interact with whistlers at the cyclotron resonance (4.28) they move on the ($\nu_{\perp}$, $\nu_{\|}$) plane along the diffusion curves (D)

$$\upsilon_{\perp}^2 + \left(\upsilon_{\|} - \omega/k_{\|}\right)^2 = const$$

in the direction of decrease of the distribution function $F(\upsilon_{\perp}, \upsilon_{\|})$ (Gendrin, 1981; Chernov, 1996).

Particles with the small pitch angles give their energy to the waves and they approach the loss-cone, and particles with large pitch angles increase their energy ($\upsilon_{\perp}$) due to the waves. However, only the part of the particles is poured out quickly into the loss-cone, directly it adjoining, and the loss-cone remains for a long time empty. Estimations of the time of life of the fast electrons with the scattering on the whistlers in the regimes of the moderate and strong diffusion give times 10 – 20 s (Bespalov and Trakhtenherz, 1986).

If the resulting flux of particles in velocity space is directed toward increasing particle energy, energy in the given range of velocities will be transferred from resonant waves to particles, and the wave will weaken. This physical process finds

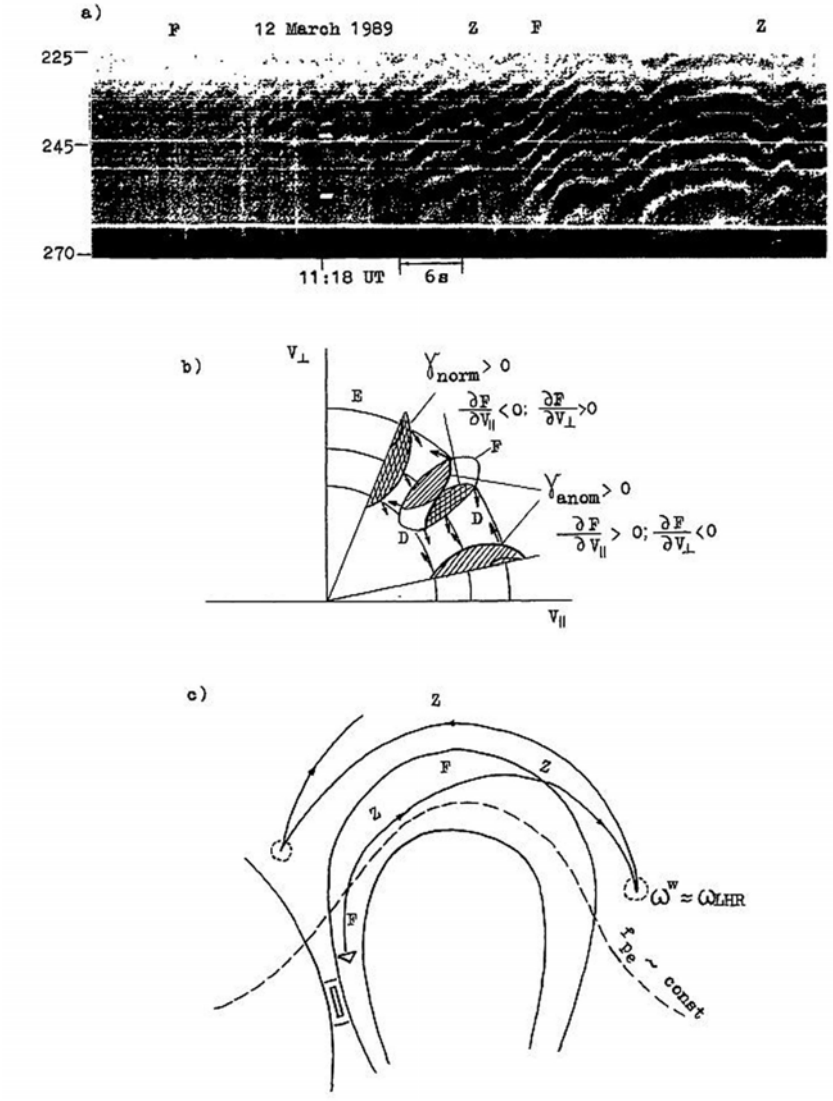

Fig. 4.64 *a)*: Dynamical spectrum of ZP with wave-like frequency drift in the type IV burst of March 12, 1989. The Z, F labels above the spectrum refer to the times when zebra stripes (Z) with a constant drift toward low frequencies become similar to fibers (F). *b)*: Schematic presentation of the fan instability switching of whistler instability from normal Doppler cyclotron resonance (cross-hatched F regions) to anomalous resonance (single-hatched regions) due to the shift of the maximum (bump) of the distribution function F during diffusion along the diffusion curves D (arrows) from large values of $\upsilon_\perp$ (where the operator $\hat{\Lambda} < 0$) to large $\upsilon_\parallel$ (where $\hat{\Lambda} > 0$). *c)*: qualitative scheme of a whistler trajectory explaining the possibility of ZP conversion into FB and inversely (from Chernov 1990a).

its theoretical reflection in the identity operator $\hat{\Lambda}$ (which has the meaning of a derivative along the curve D) in formulas for the whistler instability increment and the distribution function diffusion equation (Gendrin, 1981; Bespalov and Trakhtenherts, 1986):

$$\hat{\Lambda} = \frac{s\omega_{Be}}{\omega\upsilon_\perp}\frac{\partial}{\partial\upsilon_\perp} + \frac{k_\parallel}{\omega}\frac{\partial}{\partial\upsilon_\parallel} \ . \tag{4.30}$$

For positive values of the increment the operator $\hat{\Lambda}$ should be negative. In Figure 4.64b we show that at the normal Doppler effect the increment γ_{norm} will be positive with the derivatives $\partial F/\partial\upsilon_\parallel < 0; \partial F/\partial\upsilon_\perp > 0$, and at the anomalous Doppler effect γ_{anom} will be positive with $\partial F/\partial\upsilon_\parallel > 0; \partial F/\partial\upsilon_\perp < 0$. In the intermediate position the beam contributes in the instability at both resonances, and the parts with positive γ_{norm} are cross-hatched, and the parts with positive γ_{anom} are single-hatched.

The smooth switching of the predominant contribution from the anomalous to normal Doppler resonances (and inversely) occurs in accordance with the sign of an operator $\hat{\Lambda}$. Thus, if the entire trap is filled up with the fast particles (prolonged injection), that the continuous quasi-linear diffusion on the whistlers begins to work in a self-oscillatory regime, when it is possible a switching of the instability from the predominance of the normal Doppler resonance to the anomalous one and back (an analogy with the fan instability (Shapiro and Shevchenko, 1987) and with the spike regime in the TOKAMAK (Parail and Pogutse, 1981). Such switchings of the instability indicate smooth (or sharp) changes in the direction of the whistler group velocity, which explain the frequently observed smooth (undulating) changes in the frequency drift of the stripes or sharper jumps in the form of sawtooth stripes, if the distribution function is deformed by a new impulse particle injection (Chernov, 1996).

Thus, smooth changes in the frequency drift of zebra stripes and the gradual conversion of ZP into FB and vice versa, shown in Figure 4.64a, it is possible to explain by the precisely quasi-linear effects of scattering of fast particles on whis-

tlers. Changes in direction of V_{gr}^{w} to the opposite one during the switching of resonances it is confirmed by the observations of the positions of sources. In Figure 4.13 it is shown that the change of the sign of the frequency drift of stripes correlates with the change of the sign of the space drift of sources at the fixed frequency. Analogous correlation was shown in Figures 4.10 and 4.16 in two other events.

Figure 4.64c shows the qualitative scheme of the possible prolonged propagation of whistlers in the corona for the cases, when FB and ZP can appear alternatively during ~ 1 minute, and quasi-linear effects act in the shorter time intervals. Longitudinal whistlers excited in the base of the magnetic trap by particles accelerated in the region of magnetic reconnection at the normal resonance propagate upward along the trap and give fibers (F). The excitation on the anomalous Doppler resonance at large angle to the magnetic field can predominate at the apex of trap, and whistlers propagate downward (sometimes almost parallel to the level of constant f_{Pe}) to the possible mirror points (where $\omega \approx \omega_{LHR}$) (in ZP the positive frequency drift predominates).

4.6.8 Explanation of LF absorption

The dark stripes of the ZP indicate not the simple absence of the increased emission, but the real absorption of background continuous emission, which is modulated by the ZP. One of the very obvious cases of real absorption in the ZP is given in Figure 4.9 (Chernov et al., 1994), where the absorption of the continuum exceeded 90% according to the data of NRH at the frequency 237 MHz.

The most reliable explanation of the absorption at the low-frequency edge from the stripe in the emission is obtained, if we take into account, that in the quasi-linear diffusion time the intensity of the plasma waves (critical for the continuous emission) is reduced in the volume of the whistler wave packet due to the electron diffusion on the whistlers.

So, with the whistler excitation on the normal resonance ($\upsilon_{\perp} > \upsilon_{\parallel}$) the maximum of the distribution function is displaced almost instantly to the high longitudinal velocities (to smaller pitch angles) due to the diffusion of fast particles on the whistlers, and the instability of the plasma waves on the double plasma resonance sharply weakens, that also is exhibited in the form of the dark stripe of the zebra-structure. But if the initial diffusion on the whistlers occurs on the anomalous resonance ($\upsilon_{\perp} < \upsilon_{\parallel}$), and the plasma Langmuir waves along the field are emitted, that in this case their level will be reduced because of the turn of the beam to the high transverse velocities. Unusual fibers (without the noticeable absorption) in the type II bursts are sometimes observed. Such fibers structure can be naturally connected with the propagation of the whistlers through the clusters of the plasma waves before the shock wave front. But before the wave front there is no trap, particles and waves disperse in the space, and diffusion on the whistlers does not

work. Therefore the instability of plasma waves is not reduced in the volume of whistler wave packets and the absorption is absent. Thus, the natural and necessary consideration of the quasi-linear effects of the diffusion of fast electrons with the loss-cone anisotropy on the whistlers allows to explain a number of the important properties of fibers and ZP.

4.7 Discussion of the Selected Events

4.7.1 February 17, 1992 event

Besides, we can naturally explain other phenomena in Figure 4.15 (in the event February 17, 1992), taking into account the possibility of the whistler generation at both Doppler resonances simultaneously. When a new beam of particles is injected (new $v_{\|}$), ω_w changes suddenly according to Eq. (4.28), and the conservation laws break down locally, but are quickly restored at nearby plasma levels with a different value of ω_t. This will result in a sudden shift of the frequency ω_t, propagating from one zebra stripe to the next one at the speed of the beam. This corresponds precisely to the observed frequency shifts (Figure 4.16, top panel) at drift rates similar to type III bursts.

Another consequence of the injection of a new beam (at the moment marked by first arrow under the spectrum in Figure 4.16) is that the velocity distribution is suddenly filled up with high velocities parallel to the magnetic field, which tend to turn the instability on the anomalous Doppler resonance. This offers a natural explanation for the split zebra stripes as due to simultaneous whistler instability at normal and at anomalous Doppler resonances at slightly different frequencies, $\omega_{w,s=1}$ and $\omega_{w,s=-1}$ (at slightly different plasma levels). For the observed frequency splitting $(\omega_{w,s=1} - \omega_{w,s=-1})/2\pi = 2$ MHz we need $v_{\|,s=1} \approx 16 \cdot 10^8$ cm s^{-1} and $v_{\|,s=-1} \approx 26 \cdot 10^8$ cm s^{-1}, which are quite possible velocities in the source. Additional beams with a narrow velocity dispersion (high $v_{\|}$) do not change the conditions of instability for the normal Doppler effect (high $v_{\perp}$). Therefore, only the high frequency component of a split zebra stripe will be structured by these beams into a succession of emission dots, in synchronization with sudden reductions (see also Figure 4.17).

The $l+w \rightarrow t$ model thus nicely accounts for the characteristic features of zebra stripe frequency shifts and splittings, and for their occurrence at times of enhanced sudden reductions, that is in the midst of repeated injections of electron beams with high $v_{\|}$.

Interpreting zebra patterns with the (loss-cone driven) electron cyclotron maser emission theory, operating at upper-hybrid frequency at the double plasma reso-

nance, would give an average density of $n_e = 10^9$ cm^{-3} and a magnetic field of B = 2.5 G. Oscillations of a large magnetic loop in the sausage mode with an amplitude of 1 or 2% are sufficient to produce the temporal frequency oscillations and the band splitting of zebra patterns. But this model requires too low a magnetic field (plasma beta $\beta \approx 1$), and does not readily explain the characteristics of split stripes: at most two components and a dot-like structure for the upper-frequency component only.

4.7.2 Discussion of the October 25, 1994 event

In this short-term event, the ZP radio sources were located beyond the AR (see Figure 4.31). A detailed analysis of Yohkoh/SXT images in Manoharan et al. (1996) showed that an additional brightenings outside the main flare region was caused by the magnetic reconnection of the main flare loop with the upper loops that previously existed in the corona.

The frequency width of the ZP band is presumably determined by the distance between the X-point of magnetic reconnection above the flare loop and a point lying higher in the corona (in the shear region between the ascending flare loop and large transequatorial loops that are seen in Yohkoh/SXT images). An argument in favor of this assumption is that the low-frequency boundary of the ZP coincided with the frequency at which the drift of type III bursts terminated after 10:08:35 UT (see Figure 4.31). The ZP source at a frequency of 164 MHz drifted southward, i.e., in the direction opposite to the drift of the sources of type III bursts.

Taking into account the above assumption, this indicates that the fast electron beams accelerated in the lower lying current sheet (it is these beams that are responsible for periodic type III bursts) are reflected from the region with a magnetic shear. The loss-cone velocity distribution of the reflected particles leads to the generation of plasma waves and whistlers, whose interaction produces a ZP at corresponding frequencies. The fact that the direction of the spatial drift of the ZP source and the sign of the frequency drift change simultaneously indicates that the spatial drift at a fixed frequency is not an actual shift of the source, but rather a displacement of the energy maximum in the vertical direction within a finite-size plasma region that radiates at this frequency (due to the velocity spread of the fast particles) and also along a surface of equal density. Within the adopted whistler model, such a drift is quite realistic.

The excitation of whistlers by the reflected particles (which have a loss-cone velocity distribution) should occur at the anomalous Doppler resonance, at which the particles and waves propagate in the same direction. A positive frequency drift of the ZP stripes indicates that, in this case, whistlers propagate downward. Quasilinear scattering of whistlers by fast particles deforms the electron distribution function: the longitudinal velocities decrease, whereas the transverse anisotropy increases. As a result, the excitation of whistlers switches to the normal Doppler

resonance, at which the particles and waves propagate in different directions, and whistlers began to propagate upward. The switching occurs at the instants at which the ZP frequency drift changes its sign and the ZP source begins to drift in the opposite direction. Two such instants are marked in Figure 4.32 by thin vertical lines.

Even greater shifts of the source center occur at the instants corresponding to the boundaries of the ZP absorption stripes. In this case, an angular shift of ~ 4.8' over 1/3 s (e.g., within the time interval 10:08:41.3 – 10:08:41.7 UT), which formally corresponds to velocities exceeding the speed of light, cannot be associated with the actual motion of particles. Such a fast angular shift is actually related to the switching of the source image to the maximum of the emission continuum, which indeed corresponds to an angular shift of more than 4' in the south-west direction above the maximum of the SXR burst (see Figure 4.31).

Thus, although the centers of the sources of the ZP and type III bursts almost coincide, the emission is produced by different particles moving in different directions: for type III bursts, these are particle beams propagating from the acceleration region, which is the highest part of the burst current sheet (the height of this region corresponds to $f_{Pe} \approx 450$ MHz), whereas for the ZP, these are the particles reflected from the region with a magnetic shear (at the height that corresponds to the minimal frequency of type III bursts and where $f_{Pe} \approx 125$ MHz). A new abrupt perturbation, which partially stops the frequency drift of type III bursts at 10:07:37 - 10:07:58 UT, indicates the position of a new X-point of magnetic reconnection (at the height where $f_{Pe} \approx 170$ MHz). At such heights, the particles generating type III bursts are partially captured in a new magnetic cloud (an island above the X-point). The size of this new magnetic cloud (between the new X-point and the sheared magnetic field) determines the initial ZP frequency range. Over 1 min (from 10:08 to 10:09 UT), whistlers gradually propagate downward to the region where $f_{Pe} \approx 210$ MHz.

The large transverse size of the source indicates that whistlers are excited throughout the entire layer with a given plasma density above the AR. However, the maximum of the radio emission intensity can be greatly shifted along this layer from the center of continuum. In the whistler model, each ZP stripe is related to an individual whistler packet. The ZP periodicity is mainly related to the periodicity of the quasilinear interaction of whistlers with fast particles (the periodic deformation of the electron distribution function). The ZP periodicity can also be caused by the periodicity in injection of fast particles and by the bounce motion of particles in a magnetic trap.

In the event under study, there were no explicit evidence of a trap, but an amazing coincidence was observed between the number of type III bursts (24 bursts) within the time interval 10:08-10:09 UT and the number of the ZP stripes along the time axis in the dynamic spectrum. Quasilinear effects lead to an additional modulation along the ZP stripes. These effects come into play only when the particles propagate together with waves (whistlers). A gradual shift of the ZP hump accompanied by the change in the sign of the frequency drift (two such shifts are

marked by dark curves in Figure 4.32) is caused by the diffusion of whistlers on fast particles under conditions such that the switching between resonances (see above) at different frequencies (heights) occurs with a small time delay equal to the diffusion time at a given height.

The double plasma resonance model proposed for this event in Zlotnik et al. (2003) does not explain the effects observed. First of all, it fails to predict the number of the ZP stripes in the frequency range of interest. If we consider realistic (rather than hypothetical) height profiles of the plasma density and the magnetic field above the AR, e.g., the double Newkirk model (formula (4.14)) and a dipole magnetic field whose height scale is much smaller than the height scale of the plasma density, then, instead of the observed eighteen stripes in the 135 to 170 MHz frequency range, we will obtain only ten stripes with harmonic numbers s varying from 10 to 20, as was shown in Figure 3 in Chernov (2005). Moreover, this model predicts a sharp increase in the frequency separation between the stripes (from 2.5 to 7 MHz), rather than an actually observed gradual increase from 1.7 to 2.2 MHz.

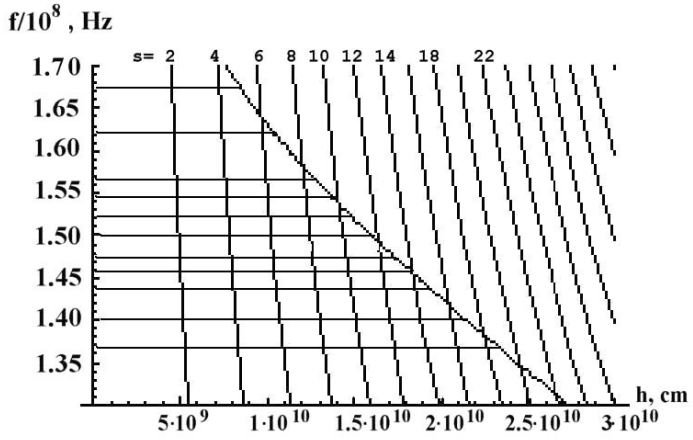

Fig. 4.65 The graph of frequency (Hz) against of the height in the corona h (cm). A grid of gyroharmonics (s= 2 – 26...) is plotted using the magnetic field model of Dulk and McLean, (1978). The point like curve is the barometric plasma frequency dependence over height: $fp = fpo\ exp(-h/10^4 T)$. The horizontal lines note the frequencies of zebra stripes at a fixed time moment (10:08:23 UT) (from Chernov et al., 2005).

Concerning the result of Zlotnik *et al.* (2003), namely the finding of the barometric model for the plasma frequency from the observations of the ZP, that for the comparison it is possible to construct an analogous graph, utilizing no calculated magnetic force line (Figure 4.65). It is possible to take the known model of magnetic field in the corona, obtained on numerous radio data (Dulk and McLean, 1978), $B = 0.5B_0(h/R_\odot)^{-1.5}$ G , and on the analogous graph to obtain even better agreement with the barometric dependence. Let us recall, that the horizontal lines

note the frequencies of zebra stripes at a fixed time moment. On the edges of the frequency range the zebra stripes fall even better on the levels of the DPR (harmonic from 5 through 19), than at Figure 5a in Zlotnik *et al.* (2003). However, this does not mean at all that the barometric formula actually assigns dependence $f_{Pe}(h)$. For this agreement we have selected completely unreal values of T_e = 0.9 10^7 K, although the initial frequency appears more adequate here, $fpo \approx 1.05 \cdot 10^9$ Hz, than in Zlotnik et al. (2003).

All the other models (e.g., those with the plasma density profile described by the barometric formula and the dipole magnetic field profile) even greater disagree with observations. We note that the magnetic field model proposed in Dulk and McLean (1978) is quite appropriate because it is confirmed by numerous radio observations. On the other hand, the barometric formula certainly does not apply to magnetic loops with plasma $\beta << 1$, because this formula describes the density distribution in a gravitational field at a constant temperature without allowance for the magnetic field.

The ZP contains not only the emission stripes but also absorption stripes, which are sometimes dominant. In this context and also taking into account the simultaneous generation of the ZP, fiber bursts, and fast pulsations, the main properties of the ZP in the event under study can hardly be explained in terms of the new model proposed in LaBelle et al. (2003). It is not so obvious whether there are necessary conditions (first of all, the condition $Te >> Ti$ (Kaplan, Tsytovich, 1973)) for the generation of small-scale inhomogeneities (ion-acoustic solitons); in LaBelle et al. (2003), their presence was merely postulated. It is quite reasonable to assume that electrostatic plasma waves and whistlers are excited in new burst loops by the trapped fast particles.

In contrast to the double plasma resonance model, the model involving quasilinear interaction of whistlers with fast particles allows one to explain all the fine effects of the ZP dynamics (frequency band, connection with III type bursts, changes of the spatial drift of radio sources synchronized with the frequency drift of the stripes).

4.7.3 Discussion of May 2, 1998 event

The rope of fibers shown in Figure 30 strongly resemble similar structures observed earlier at higher frequencies (200-250 MHz) and discussed in Mann et al. (1989), Chernov (1997) (Figure 4.26, 4.27). However, these latter structures were repeated multiple times over the entire decay phase of a flare (over more than an hour). They are associated with the whistler instability in a small magnetic trap that has formed between shock fronts moving away from a magnetic-reconnection X- point during the prolonged process of reestablishing the magnetic structure after a CME (Figure 4.27b).

In Figure 4.30 we can see ejections in various directions in five frames in the 195 Å line (SOHO/EIT), but two of these are most prominent: one toward the north from the main flare and the other toward the southeast (a slowly moving front). This is suggestive of a perturbation (shock front) moving toward the observer. According to the first EIT 195 Å image (13:42 UT), it is possible to assume, that the radio source of fine structure was located in a turbulent zone between two shock fronts. The different polarization signs of the main rope of fibers and surrounding its zebra structure (shown in Figure 4.30 at the top spectrum in circular polarization) testify to the presence within the source of different magnetic polarities, most likely in the form of the X- region of magnetic reconnection.

Thus, it is most probable that the source of the fiber rope is associated with the turbulent zone behind the fast shock fronts and is located in a narrow trap between the fast front and the slow front. The ropes are observed over only three minutes during the type II outburst, and the frequency drift of the main rope is determined by the motion of the shock front with a speed of 960 km s^{-1}, because the frequency drift of the main rope is almost equal to the drift of the fast front. Fast particles accelerated in the shock front were captured in this narrow trap. According to the dynamic spectra at the moment of the beginning of the second type II burst at 70 MHz the first burst through the crude estimate was located approximately at 20 MHz. Utilizing the density model of Leblanc et al. (1998), we estimate the distance between the shock fronts at this moment approximately of 300000 km. Trapped fast particles with the typical velocity for the type III bursts of order 10^{10} cm s^{-1} pass this distance for 3 s. Specifically, this is the average period between the separate fibers in composition of rope. As a result of the "bounce effect" - the motion of these particles between the two maxima of the magnetic field (between two shock fronts) - a loss-cone velocity distribution was formed, giving rise to a periodic whistler instability. The increasing distance between the two shock fronts can explain the smooth expansion of the main rope during the drift toward lower frequencies. In general, the shock front probably propagates at any angle to the magnetic field. In this case, the magnetic field and density of the shock front should have an oscillatory structure. This may be the origin of the presence of a number of other fragments of fiber ropes and zebra stripes at higher frequencies, whose sources are located further behind the fast shock front.

The whistlers propagate in the direction of propagation of the shock front. It is natural to assume, that whistlers are excited before the shock front (in parameters of the background plasma, with the ratio of cyclotron and plasma frequencies $f_{Be}/f_{Pe} = 1/30$ and the relative frequency $x = f_w/f_{Be} = 0.01$). The magnetic field varies a little (according to the constant parameters of narrow fibers), but whistlers scatter on the background plasma, that results in sharp reduction of x (Chernov, 1989). Besides, the presence of broadband main rope means a density heterogeneity with increased plasma density (2 – 3 times). Therefore the group velocity of the whistlers $V_{gr} = 2c\frac{\omega_{Be}}{\omega_{Pe}}\sqrt{x(1-x)^3}$ (Kuijpers, 1975) should be noticeably less than 10^8

cm s^{-1} (e.g. for f_{Be}/f_{Pe} =1/45 and x = 0.0033, V_{gr} =760 km s^{-1}), providing an explanation for the appreciably lower frequency drift of the fibers within the main rope in the comparison with the drift of the rope (whistlers lagged behind from the shock front). Thus, these unusual fiber ropes are most likely a manifestation of whistler wave packets propagation between two shock fronts in the corona. Short total duration of each fiber (gradually growing from approximately 2 s on 38 MHz to 7 s on 35 MHz), is determined by the not simply growing interval between the fronts, but most likely by cutting emission as a result of the cyclotron damping of whistlers with the decrease of the field strength and reaching x = 0.5. Evidently from Figure 4.30, that the shock fronts propagated at different angles, therefore it is possible to assume, that fibers and ZP were observed only in the time interval, thus far the fronts overlapped in space, that is below approximately 20 MHz (above $1.6R_{Sun}$). The type II bursts continued in IP space but only with the usual flocculent structure at frequencies of 14 – 8 MHz (Chernov et al. 2008).

4.7.4 Centimeter Wavelengths

4.7.4.1 October 29, 2000 event

Since ZP and FB display similar spectral characteristics, we will consider both structures to be manifestations of the whistlers in the radio source, due to their interactions with the electrostatic plasma waves: $l + w \rightarrow t$, with both waves being excited by the same fast particles in hot flare loops, which have an anisotropic loss-cone distribution. The computations of Yasnov et al. (2000) show a growth in the whistler increment with the temperature of the background plasma in the flare region, with the growth in the cyclotron decay being compensated by the decrease in the whistler frequency with the maximum increment to $0.1\omega_{Be}$. The mean duration of a series of zebra structures and fiber bursts was about two seconds, and the propagation of whistlers without damping over this time places a constraint on the whistler increment of < 0.5 s^{-1}. This constraint can be used to estimate the magnetic field strength in the region in which the flare is generated. Electron temperatures in the range 2 ÷ 20 MK yield magnetic fields of B = 125 ÷ 190 G for regions in which the electron density is $(8 \div 18) \cdot 10^{10}$ cm^{-3}.

These rough estimates coincide with estimates derived from the frequency-drift rate of the fiber bursts observed at the same time at these same frequencies, based on the formula $B = 15.43(lnf - 3)^{-2} df/dt$ (Elgarøy, 1982), which was obtained for a 60-fold Newkirk model and a whistler frequency of $\omega_w = 0.1\omega_{Be}$. In the model with the whistlers we can verify also the obtained values B using the frequency separation between the maximum in the emission and the adjacent minimum in the absorption (Δf_{ea}). This value must be equal to the frequency of whistlers, which is

selected equal to 0.1 of the cyclotron frequency (on which the increment of whistlers is maximum). Thus, $B = \Delta f_{ea} / (0.1 \cdot 2.8)$ G and for the observed value $\Delta f_{ea} \approx$ 40 MHz) we can estimate $B \approx 140$ G. This value is close to the values of field, obtained above by other two methods, which confirms the reliability of the determination of magnetic field in the model with whistlers.

If we estimate the magnitude of B in the new model of LaBelle et al. (2003), assuming that $\Delta f_s \approx 0.02 f_{Be}$, we obtain for $\Delta f_s = 80$ MHz implausibly high values $B \approx 1500$ G, close to photosphere values.

The alternative model based on the generation of plasma waves at the upper-hybrid frequency ω_{UH} under the conditions appropriate for the DPR was also considered. In the DPR model all estimations of field depend strongly (even in order of magnitude) on the unknown relationship between the scale heights in the corona for density and magnetic field, which was already noted above.

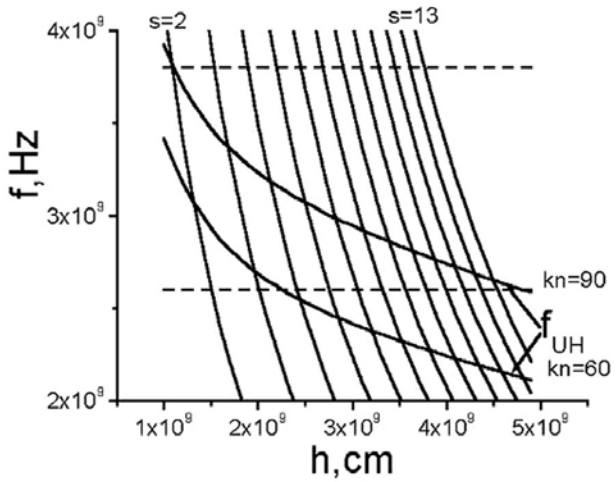

Fig. 4.66 Dependences of upper hybrid and cyclotron frequencies on the height in the corona in the magnetic field model of Dulk and McLean, (1978) and electron density model of Newkirk, multiplied by kn : ($n = kn \cdot 8.26 \cdot 10^4 \cdot 10^{4.32/h}$ cm^{-3}) (from Chernov et al. 2005).

We can see from Figure 4.66 that the main inadequacy of this model is associated with the increase in the frequency separation of the emission stripes Δf_s with increasing frequency: the model predicts an increase from 60 MHz at 2.7 GHz to ~ 450 MHz at 3.8 GHz, which is not generally observed. Usually, the frequency separation only slightly increases with frequency.

The conditions of the DPR realize probably rarely in the flare region with a set of thin magnetic loops. But if they nevertheless realize in the certain stable magnetic trap, that it follows to expect the stable emission of stripes, most likely, during entire event. Such stable stripes in emission were observed, for example, in the

decimeter range in the event February 17, 1992 (Chernov et al., 1998, (evolving emission lines, EEL)). The EEL with the slow wavy frequency drift of one or three harmonics during more than 2 hours satisfies actually to mechanism on DPR.

The frequency separation between harmonics in EEL (Figure 4.15) varies between ≈ 50 and 80 MHz, which corresponds to a maximum magnetic field strength in the source $B \approx 17 \div 28$ G, consistent with the 11 G deduced from the $l + w \square t$ model for ZP at a lower frequency (~250 MHz) where we do expect a weaker field. The electromagnetic maser would require too high a magnetic field.

4.7.4.2 April 21, 2002 event

The Figures 4.35 and 4.36 helps us to pay attention to the main flare moments to which appearance of a zebra can be connected. First, the interval of a zebra synchronizes precisely with HXR burst (44 – 67 keV, HXRS). Second, two most powerful series of ZP represented in Figures 4.37 and 4.38, coincide on time with appearance of two new HXR sources (RHESSI data in the lower left panel of Figure 4.36), which positions coincide with two maximum radio sources (Siberian Solar Radio Telescope (SSRT) data) in the polarized radiation. Thus, the formation of zebra was tightly connected with the presence of fast particles in the loop arcade, included two bright nodes in the form X- points of magnetic reconnection, visually seen on the difference picture in Figure 4.36. Certainly, the emission in line FeXII, 195 Å shows to us only bright loops with the temperature of $1.8 \cdot 10^6$ K, but radio sources at 5.7 GHz (SSRT) and 17 GHz (Nobeyama) in the polarized radiation were located exactly near two bright nodes, in which the bright being intersected loops had a configuration in the form of the singular X- points.

Dark material, falling out on top is probably overheated flare plasma (to 50 – 100 MK) ejected from the region of maximum energy release at the heights of decimeter range. Certainly, this prolonged flow of overheated plasma (from 01:34 through 02:15 UT) served as the source of heating of the entire arcade (but not only the mentioned nodes with the X- points), since the duration of its precipitation covered tightly the interval of the fine structure excitation.

It would be natural to connect radio sources exactly with these bright loops. Then the large number of loops with the bright apexes in the narrow height interval causes the specific doubt about the possibility of the realization of the condition of DPR in the wide interval of heights. In this connection, the example of the zebra structure shown in Figure 4.37, is noteworthy, since it shows that the DPR-model is not able to explain the presence of simultaneous emission in 34 zebra stripes with virtually identical intensities in the range 2.6 – 3.8 GHz.

At the same time, this situation is quite realistic in a whistler model, where strict periodicity of the stripes is specified by the whistler excitation mechanism itself (fluctuations in the instability under the action of quasi-linear effects, independent of the models for density and magnetic field in the corona). All the more,

that frequently the zebra stripes are more similar to isolated fibers, as, for example, we see on the high-frequency edge of the spectrum in the Figure 4.38. Therefore we could consider both fine structures in a common model, as the whistler manifestation. The isolated packages of whistlers are excited more effectively below, near magnetic mirrors and they propagate upward along the magnetic loops. Approaching the singular points (X- points), whistlers gradually fill the entire radio source with almost standing periodic wave packets, that also explains the presence of stripes barely drifting in the frequency at the low-frequency edge of the spectrum in Figure 4.38.

The new model of LaBelle et al. (2003) can theoretically explain any parameters of zebra structure and mainly - the large number of zebra-pattern stripes from a point radio source. But the stable appearance of series of zebra structures in a pulsating regime cannot be understood, since this model predicts a strong dependence for the frequency separation and the number of zebra stripes on the parameters of the inhomogeneities, while we observe only a very small growth in the frequency separation with increasing frequency. The parameters of inhomogeneities such as propagating ion-sound waves cannot remain so similar over a wide range of frequencies (interval of heights) over extended periods of time. Furthermore, large problem remains to explain the large intensity of all zebra stripes from numerous point radio sources, exciting the total (incoherent) emission i.e., the spectrum of the stripes would be expected to blend into the continuum.

The frequency profiles in Figure 4.37 and 4.38 demonstrate rapid pulsations in the bright ZP stripes with a well defined period of 30 ms. Thus, these new observations support the conclusions of Chernov et al. (2003), that the ZP at centimeter wavelengths has always fine spike-like structure, which can be explained in a natural way in whistler models for zebra structure.

Figure 4.39 shows, that in the cloud of spikes zebra stripes are gradually formed. Therefore it is possible to assume, that the emission of spikes is a primary process. In dm- range the analogous conversion was observed by Kuijpers et al. (1981). They assumed even, that spikes and zebra can be excited by the same mechanism. On the basis of our previous results (Chernov et al., 2003), we can assume, that near the flare region spikes can be excited by the nonlinear mechanism of interaction of plasma Langmuir waves with ion-sound waves. The ionic sound can be always present in shock wave fronts, departing from regions of magnetic reconnection (Chernov et al., 2001a). But zebra appears with the excitation of whistlers by fast particles with the loss-cone distribution, forming only after the reflection of particles from the magnetic mirrors. So that a certain delay is always permissible.

If we determine the magnetic field strength on the frequency separation between the maximums in emission and absorption in one stripe (Δf_{ea}), that for the moment 01:48:34 UT we will obtain the small value $B \approx 90$ G.

After 02:00 UT we do not have a possibility to estimate B thus, since the zebra stripes did not detect noticeable absorptions even in the single stripes at HF edge. A decrease in the intensity of plasma waves due to scattering of fast particles on

the whistlers in the periodic wave packets is the basic reason for absorptions. Therefore we are right to assume, that in this case the particles and waves diverged in the space, which completely is allowed with a fast particle injection and the emission of whistlers on the normal Doppler effect (in a regime of weak diffusion). It is not excluded also, that the large number of stripes with the narrow frequency separation is the result of the imposition of emission from the different loops with the observation in the projection of radio sources at the solar limb. In this case the polarization will be most likely determined by propagation conditions of radio emission perpendicularly to the magnetic field.

Thus, new data on zebra structure and fiber bursts at centimeter wavelengths testifies that they have similar structures to those observed at meter wavelengths. ZP was not observed at frequencies higher than ~ 6 GHz. The radiation of electrostatic plasma waves at higher frequencies is probably suppressed in the dense flare plasma. A unified model for zebra structure and fiber bursts involving whistlers can yield realistic values for the magnetic field strength B ~ 140 ÷160 G at a plasma level of about 3 GHz. Using realistic dependences for the electron density and magnetic field, the DPR- model for zebra structure predicts a frequency dependence for the frequency separation between stripes that is much stronger than is observed. Altyntsev et al. (2005) and then Kuznetsov (2005) (in more detail) assume, that properties of ZP in the January 5, 2003 event are more inherent to the point-like radio source, and the authors conclude that the most probable generation mechanism of this zebra pattern is nonlinear coupling of Bernstein waves. In this case the value of the magnetic field in the burst source, determined by the frequency separation between the adjacent stripes, is 60 – 80 G, too low values at the level of plasma frequency about 5.7 GHz. Altyntsev et al. (2005) and then Kuznetsov (2005) do not discuss in their model the superfine structure of ZP (as millisecond spikes), observed in this event.

4.7.5 Discussion of the superfine structure of ZP

The superfine structure of ZP allows the possibility to compare different models. Let us be turned to parameters of ZP with the superfine structure. In the bottom panel of Figure 4.40, in left polarization with a well pronounced ZP one sees about 6 zebra stripes between 3.5 and 3.8 GHz, so the separation is Δf_e = 60 MHz. If one interprets the zebra bands as harmonics of the gyrofrequency, $f_{UH} = sf_{Be}$ one would get a gyrofrequency of f_{Be} = 60 MHz, which corresponds to $B \approx 20$ G, and a harmonic of s = 3600/60 = 60. If we believe the model at the double plasma resonance of Zheleznyakov and Zlotnik (1975) or Winglee and Dulk (1986), $s > 20$ are unlikely at the fundamental frequency f_{UH}. We cannot believe the emission at the second harmonic of f_{UH}, because in most cases the zebra pattern is strongly polarized. But at the frequency near 3.5 GHz a density of $ne = 1.5 \cdot 10^{11}$ cm^{-3} and a magnetic field of B = 20 G is unreasonable near a reconnection site in a flare loop.

At the same time an interpretation in terms of the sum of the local upper hybrid frequency and low harmonics of the electron cyclotron frequency $f = f_{UH} + sf_{Be}$ is less likely, because it requires multi-step processes of wave coupling from a compact radio source.

In two recent papers (Karlicky et al., 2001 and Barta and Karlicky, 2001) it is supposed that the radio emission at double plasma resonance is generated in plasma with rapidly changing plasma parameters in turbulent magnetic loops. A possible source of the turbulence can be the plasma outflows from the magnetic field reconnection. It is supposed that scales of heights of density and the magnetic field in a loop vary chaotically along the loop, and the condition of double plasma resonance can be realized only at certain points along a loop. It is supposed that the area around each such point can be a source of spike emission accompanying ZP. However, the authors do not discuss processes that could result in such a loop structure with strongly turbulent plasma. Thus spikes can form chaotic chains, however the occasional realization of a double plasma resonance (both in one loop and in neighboring ones) excludes formation of parallel drifting zebra stripes.

Recent SOHO and TRACE data suggest narrow pre-flare loops, along which the density and magnetic field change very slowly (Aschwanden et al., 1999; 2002), when density and magnetic field scale heights are about the same, ~ 55±10 Mm, comparable with the length of the loop. This proves that double plasma resonance surfaces cannot exist in such loops.

In Karlicky et al. (2001) and Barta and Karlicky (2001) the nonlinear process that causes saturation of the instability is not studied in detail, nor are the wave transformation processes. Notice that in our case spikes as superfine structure of zebra stripes have much smaller duration (8 ms). For an explanation of the discussed structure we will consider alternative models of whistlers and ion-sound waves, in which the radio emission is formed as a result of the more effective interactions: $l + s \to t$ and $l + w \to t$.

Microwave spikes as a part of ZP have millisecond durations, and for such spikes a new model was proposed in Chernov et al. (2001a), namely the coupling of plasma and ion-sound waves: $l+s \to t$ in a radio source, related to fast shock fronts in the flare region. The behavior of ion-sound waves and whistlers in coronal magnetic traps was considered in Chernov (1989), where it was shown that a dynamic energy transfer between s- waves and whistlers can operate in a pulsating regime with the processes $s + s' \to w$. The efficiency of these processes becomes maximal when the whistler frequency is about equal to the ion plasma frequency: $\omega_w \approx \omega_{Pi}$.

In the meter and decimeter ranges such a coincidence takes place when $\omega_w \approx (0.1 \div 0.25)\omega_{Be}$ (see Figure 4.57). In our case the generation of whistlers occurs in the flare region, where the plasma temperature is higher than in the corona. According Yohkoh/SXT data it may be $\geq 10^7$ K (Yasnov et al., 2002), and the maximum of whistler instability displaces to $\omega_w \leq \cdot\, 0.1\omega_{Be}$ (Figure 4.52). In such a case the condition $\omega_w \approx \omega_{Pi}$ should be realized in the microwave range around 3 GHz.

Thus, the radio emission of zebra stripes in the process of the coupling $l + w \rightarrow t$ could be modulated due to the oscillating whistler spectrum caused by the interaction $s + s' \rightarrow w$.

Ion-sound waves can be excited in the whole radio source connected with magnetic reconnection in the flare region, but whistlers only near magnetic plugs or in the upstream of fast shock fronts. This explains, why sometimes spikes cover entire burst continuum and not only zebra stripes (see Figures 4.39, 4.40). The process $s + s' \rightarrow w$ has a limitation with regard to the angles of whistler wave vectors to the magnetic force line (Chernov, 1989) (they must be $> 70^{o}$), that explains why the spiky structure is almost not present in FB: because in this case whistlers propagate along magnetic loops. This process works effectively for inclined whistlers generated at anomalous Doppler resonance and responsible for ZP.

However, in the metric range we did not practically observed similar superfine structure in ZP (see time profiles in Figures 4.5, 4.7, 4.8, 4.26, obtained with 0.01 s time resolution. Therefore it is possible to expect, that this structure will be discovered by observations with the higher millisecond resolution.

The dot-like structure with the period ≈ 0.25 s in event February 17, 1992 in the splitted stripes of ZP synchronously with the same structure in EEL (Figures 4.16 and 4.17) has other nature. They appeared only during fast broadband pulsations of type sudden reductions with the same period, and the dot-like structure was connected with new injections of fast particles with the period of 0.25 s. The emission/absorption character of dot-like structure in the EEL is simply explained in frames of the sudden reduction mechanism proposed by Zaitsev and Stepanov (1976) and Benz and Kuijpers (1976). The EEL is emitted at double plasma resonance and the dots in absorption correspond to a quenching of the upper hybrid wave instability at moments of new fast particle injections. In the ZP we do not see dots in absorption (Figure 4.16), the usual absorption stripes in ZP do not distorted, since the absorption is defined there by whistlers. So, on this example we are once again convinced of different generation mechanisms of ZP and EEL in this event.

4.7.6 Interpretation of rope-like fibers

Comparing the rope-like fibers in Figures 4.26 – 4.29, it is possible unambiguously to conclude, that these are the kindred phenomena and they require special consideration.

One published theory (Mann et al. 1989) was based on a threshold switch-on process of whistler loss-cone instability in a localized wave packet of the fast magneto-acoustic mode. The critical loss-cone angle is exceeded due to additional perturbation of the magnetic trap by the fast magneto-acoustic mode. However, this model is applicable only in the case of injection of a large relative number of energetic particles $n_h/n_c \sim 10^{-2}$ into a magnetic trap with a large plug ratio. A whis-

tler excitation threshold in terms of the loss-cone angle that is realized only when we take into account the contribution of thermal ions in the dispersion relation is of general importance for sources of type II/IV radio emission.

An analogy with the X-ray spikes in TOKAMAK plasmas excited by tearing instability was initially used to explain the rope of fibers on November 3, 1997 (Klassen et al. 2001). In general, however, this process is more suitable for explaining the simultaneous impulsive X-ray bursts and type III bursts.

Subsequently, the same authors suggested a different mechanism, a model with kink instability at anomalous plasma resistance (Karlicky et al. 2002), based on the fact the simplest process can be the density and magnetic field modulation in a loop. It is assumed that the emission should originate from the levels of double plasma resonance, where the upper hybrid frequency ω_{UH} is equal to a whole number (s) of electron cyclotron harmonics ω_{Be} (the mechanism by Zheleznyakov and Zlotnik (1975) and Winglee and Dulk (1986)). The authors describe the electric field of a wave under the action of two oscillators with frequencies ω_{UH} and $s\omega_{Be}$ with a positive feedback. If the local density and magnetic field strength underwent oscillations in time or space, then both these frequencies would undergo the corresponding oscillations. The radio flux, which is proportional to the square of the wave amplitude at the upper hybrid frequency, would then undergo oscillations. Various possible models of these oscillations are considered. In comparison with the wave model (MHD wave) and balloon instability, kink instability at anomalous plasma conductivity was chosen as the most suitable model. The anomalous conductivity is needed to suppress the instability. The effect of rapid heating in a source of small sizes (~10 km) in the shape of a loop with a temperature $T_e \sim 10^7$ K is used.

It is hard to expect the parameters used at the heights of the meter wave band. However, they also allow one to obtain the suppression and recovery of emission (without any overlap in time) with great reserve only for periods of 5–15 s. The short periods of ~1 s cannot be explained, nor can the fiber frequency drift, the formation of absorptions, and frequency splitting be explained. Therefore, let us consider in more detail another possible interpretation.

4.7.6.1 Model of periodic fibers in the reconnection region with fast shock fronts

We must stretch the theory to explain the more rapid repetition of the fibers in ropes, the deep modulation of the continuum and certain other properties accompanying the ropes - the slowly drifting absorption fibers and the millisecond pulsations (see Figure 4.27a). We will, therefore, consider another probable source of rope-like fibers, which directly related to the reconnection model of Anzer and Pneuman (1982) (for CME during two ribbon flare) and which is located in a ver-

tical current sheet with magnetic X- points (Chernov, 1990a; 1997). Similar scheme of the radio source was used by Aurass et al. (1987), which first have presented the chains of these fibers. The multiple formation of magnetic islands along a vertical current sheet with X-points high in the corona was calculated by Forbes and Priest (1983).

A reconnection between the magnetic island and lower closed loop begins from a stationary phase (Figure 4.27b). With the onset of nonstationary reconnection two pairs of slow shock waves (S^-) and two fast shock fronts (S^+) move outward from the reconnection region (Sidneva and Semenov, 1985; Xu and Forbes, 1992). The fast shock fronts form here, because streams of plasma flowing upward and downward from the rarified region (surrounded by the slow fronts) with the Alfvén velocity are encountered with the transverse magnetic field. The fast shock front appearance was predicted and confirmed in the calculations by Podgornii and Syrovatskii (1981). The numerical calculations of Sakai and Ohsava (1987) indicate that during the explosive reconnection the magnetic field triples in the fast fronts and ions and electrons undergo quasi-periodic acceleration by the induced electric field.

The accelerated fast particles could be reflected off the fast fronts and became captured in a small trap between the upper and lower fast fronts (S^+). The reflected particles form the loss-cone distribution and a sharp increase of whistler loss-cone instability develops near the fast fronts. The whistlers propagate toward the slow fronts (S^-) until the instantaneous cyclotron damping in the minimum of the magnetic field strength in the slow front. The whistler trajectories are shown by dashed line in Figure 4.27b.

The most obvious and necessary effect from this picture is a decrease of the continuum emission from the rarified regions due to the screening by the shock fronts. Because of this screening, the slowly moving rarified region between shock fronts should give rise to slowly drifting absorption fibers, which are in fact the most characteristic features accompanying ropes. Their bandwidth of ≈2 MHz corresponds to the size of the rarified region along ∇f_{Pe} in the corona $\approx 2 \cdot 10^8$ cm. Using this estimation we can roughly estimate the time for whistler propagation between the fast and the inclined slow fronts with the group velocity $\approx 5 \cdot 10^8$ cm s^{-1} (for $\omega_{Pe} / \omega_{Be} \sim 15$ and $x = 0.03$, determined for this event by Mann et al. (1989)). The result is ≈ 0.4 s, which corresponds to the observed duration of separate fibers in a rope.

The whistlers propagate toward decreasing density, which explains the observed negative frequency drift of individual fibers in a rope. The periodicity of the fibers is associated with the bounce motions of particles in the small trap between the fast fronts. This leads to the higher periodicity of the fibers in a rope ~ 5 – 6 s^{-1} in comparison with the periodicity of usual fibers bursts ~ 1–2 s^{-1}.

In this model, the plasma in the reconnection region should not be isothermal ($Te >> Ti$), primarily due to the predominant heating of electrons in the shock fronts. Therefore, a mechanism in which the millisecond pulsations are the result of a pulsating regime of the coupling whistlers and ion-sound waves should work

(Chernov 1989). The ion-sound waves should encompass a large height interval in the reconnection region, so that the millisecond pulsations appear at a wide range of frequencies.

Thus, this model should work in the direct association with reconnection region during big flares (with CME), it does not require any additional disturbances, and it can explain not only all main properties of the rope-like fibers but also a number of accompanying features of the radio fine structure.

4.7.6.2 Discussion of the November 3, 1997 Event

The observational data on four events in Chernov (2008) suggest that the ropes of fibers are usually observed in the time interval when the shock front (even in the absence of the corresponding type II burst) catches up with the leading edge of CME. In large events at the post-maximum flare phase, the ropes can reappear periodically together with new ejections from the flare region accompanied by shock waves near the special X- points of magnetic reconnection high in the corona.

According to the IZMIRAN spectra on February 17, 1992 (Figure 4.29), even the main rope of fibers at 09:09 UT does not completely satisfy the condition when the succeeding fiber begins only after the switch-off of the emission from the preceding one, although precisely this condition should have justified both the new name and the new mechanism suggested by Klassen et al. (2001) and Karlicky et al. (2002). In addition, the appearance of additional short fibers resembling a frequency splitting at the end of each fiber was disregarded in these papers.

A close relationship is traceable between the appearance of ropes and type III bursts in all four events considered, suggesting a common particle acceleration mechanism. The beams of particles escaping along open field lines produce type III bursts, but some of the particles are trapped. Karlicky et al. (2002) even compare the number of type III bursts with the number of fibers in a rope. In the November 3, 1997 event in the interval 09:08:50–09:09:30 UT, all type III bursts did not drift below approximately 150–160 MHz (Fig. 3 in Chernov (2008)), while the presence of many U- bursts points to the existence of closed magnetic loops at these heights in the corona. The formation of ropes exactly near 150 MHz is clearly related to this fact. At this level in the corona, some of the particles were reflected back from the lower CME edge (or the special X- point of magnetic reconnection) and conditions for periodic excitation of plasma waves and whistlers were realized in a narrow region of reflection. Thus, our model (Chernov 1997) may also be applicable here if the peculiarities of the conditions in the radio source are taken into account. The narrow band of the fibers (Δf) is related not to the sizes of the trap for particles, but to the narrow range of heights at which the whistlers can propagate until their total cyclotron damping. An even faster termination of emission can be caused by the suppression of plasma wave instability

through the interaction of fast particles with whistlers, which deforms the distribution function of the fast particles.

The minimum period of ~1 s in the rope at 210 MHz is precisely determined by the bounce period of the fast particles in the range between 215 MHz (~ $0.24R_{Sun}$) and 150 MHz (~ $0.37R_{Sun}$). This range of heights (≈ 90 000 km) are traversed by the fast particles with a velocity of ≈1/3 c (typical of type III beams) approximately in 0.9 s. The initial period of ≈ 4.5 s in the main fiber (Figure 4.29) is probably related to the capture of particles into a large trap between the shock front located at the height of the plasma level, ≈ 200 MHz (≈ $0.25R_{Sun}$), at 09:09 and the leading CME edge located at a height of ≈ $0.9R_{Sun}$ at this time (according to the diagram in Fig. 6 in Chernov (2008)). This distance, ≈ 450 000 km, is traversed by the fast particles precisely in 4.5 s. The further increase in period may be related to a new rate of particle acceleration with a gradually increasing period. It should be recognized that each fiber can be associated with a new particle injection, not with the bounce motions of one beam, which is not surprising for such large trap scales, ≈ $0.65R_{Sun}$.

In this scheme, the identified ropes of fibers can appear as the whistler wave packets pass through narrow loops with an enhanced density in which the excitation of a small level of plasma waves (flare continuum) is achieved. The periodic whistler packets are most likely generated immediately upstream of the shock front, but they manifest themselves only indirectly, encountering the identified regions with an enhanced level of plasma waves in their path as a result of the coalescence $l + w \rightarrow t$. The reduced frequency drift rate of the fibers in ropes compared to that of usual fibers can be explained by the propagation of whistlers inside inhomogeneities (whistler trapping), where their group velocity decreases sharply (Chernov et al. 2007a, b).

It may well be that the enhanced level of plasma waves can be caused by transition radiation; the latter can be responsible for the entire flare continuum emission. The assumption about an important role of transition radiation in the ZP sources was first made by LaBelle et al. (2003).

The appearance of a frequency splitting at the end of fibers is quite admissible in this model. As a result of quasi-linear effects and deformation of the distribution function for fast particles as the maximum in the distribution function shifts to the high velocities, whistlers can be excited along the magnetic field precisely at the end of fibers not only at normal Doppler resonance, but also simultaneously at anomalous one (this effect was considered in detail previously (Chernov 1996)). The emission frequency shifts in accordance with the expression for the cyclotron resonance (Eq. (4.28). The frequency splitting of the ZP stripes estimated above (Subsection 4.6.1) in terms of this model showed that a splitting of ≈ 2 MHz at 250 MHz required a small shift in the longitudinal particle velocity, from 1.6×10^9 to 2.6×10^9 cm s^{-1}.

4.7.6.3 Some concluding remarks

Under the condition of a unified approach to interpreting the ropes of fibers in all events, their basic properties can be explained in terms of the standard model of IDBs or fiber bursts by taking into account the plasma parameters in the radio source. The following subtle effects in ropes can be understood by taking into account the behavior of whistlers in the corona and quasi-linear effects when the whistlers are scattered by fast particles: the different periods, durations, and frequency bandwidths of the fibers, the formation of LF absorption of different level, and the frequency splitting. The connection of fibers with the developed ZP also becomes clear within the framework of a unified approach to the formation of stripes in emission and absorption in the model with whistlers.

4.8 Summary

We have considered several of the most recent events with the radio fine structure of type ZP and FB using a multi-faceted approach to study the flare processes based on all new data available from the Yohkoh, SOHO, TRACE and RHESSI satellites. A complex study of flare processes has allowed us in some cases to find a connection of the occurrence of the fine structure with shock waves and CME. The fine structure was observed simultaneously with the ascent into the corona of new, hot magnetic loops, and the frequency range occupied by the fine structure in the dynamical spectrum is determined by the extent of these new loops in the corona. In the April 21, 2002 event, the zebra structure was developed in the area of the magnetic reconnection at the apexes of loops, at the base of which the new hard X-ray sources appeared, and the entire interval of structure was accompanied by precipitation from above the overheated plasma. In each new event the new special features of the fine structure are revealed, however, they are usually connected with the varied conditions in the source. Therefore, one ought not to find a special mechanism of emission for each event, which was repeatedly done before. In recent years a new page is opened of similar experiments in connection with detection ZP and FB in the microwave range due to the observations on the Chinese spectrometers with a high resolution (10 – 20 MHz and 5 – 8 ms). New data on the zebra structure and fiber bursts at centimeter wavelengths show that they are similar to the corresponding structures at meter wavelengths. The discovery of the superfine structure, in the form of millisecond spikes is the most significant new effect in cm range. Zebra structure and fiber bursts are observed at the frequencies from 20 to ~ 6000 MHz. The radiation of electrostatic plasma waves at higher frequencies is, probably, suppressed in the dense flare plasma. The main relative spectral parameters and the degree of circular polarization of the zebra structure and fiber bursts are nearly identical. The continuous transition from fiber bursts to

zebra structure and vice versa testifies to a single nature of these two structures. Important new results are obtained by simultaneous studies of the positions of radio sources, using Nançay Radio Heliograph at 164 and 236 MHz, and SSRT at 5.7 GHz. In particular, correlation between the direction (sign) of the frequency drift of stripes on the spectrum and the direction of the drift of source in space is discovered. In most events the polarization corresponds to the O- radio mode. In some events with X-emission mode a polarization conversion in the course of propagation across the magnetic field is supposed. All new properties are considered in the light of both earlier and new theoretical models. All the main properties of the emission and absorption stripes can be explained in a model involving interactions between electrostatic plasma waves and whistlers, taking into account the quasi-linear diffusion of fast particles with the loss-cone distribution on whistlers. Within the framework of this mechanism alone not simply the stripes in the emission and the absorption are explained, but also the entire dynamics of the stripes on the spectrum and of their radio sources (splitting of stripes, movements of the sources, superfine spiky structure). In this model it is possible to obtain realistic values for the magnetic field strength of $B \approx 5$ G at the plasma level in the corona about 250 MHz, $B \approx 160$ G at the plasma level of about 3 GHz and $B = 250$ G at the level of 5.7 GHz and consequently the plasma $\beta << 1$. The double-plasma-resonance model for the zebra pattern based on the well-known realistic dependences for the electron density and magnetic field yields a frequency dependence for the frequency separation between stripes that does not agree with the observations. The mechanism at double plasma resonance can be invoked to account for the large-scale stripes in the emission whose duration is comparable to that of the entire event, as was shown, for example, for the fibers (EEL), oscillating during two hours in the event of February 17, 1992. The relative significance of several possible mechanisms remains uncertain. The future observations should provide better definition of the some ZP and FB features, for example, through simultaneous observations of spectra and source positions at microwaves and millisecond resolution in the metric range (such as Frequency Agile Solar Radiotelescope (Owens Valley Radio Observatory). Such experiments could confirm or disprove many theoretical models.

Chapter 5

Recent results of zebra patterns in solar radio bursts

5.1 New observations

5.1.1 2004 July 24 Event

Chernov et al. (2008) analyzed strange fiber structures in four events in decimeter range when small-scale fibers are organized into large-scale ZPs. They used spectral observations from the new Chinese spectrometer (Huairou station of NAOC, Beijing) in the range of 1.1 – 2.0 GHz with extremely high resolution of 5 MHz and 1.25 ms (Fu et al., 2004).

Figures 5.1 demonstrates a new variety of stripes in emission in the event on 2004 July 24. At the beginning of the event, separate narrow-band stripes (small fibers) were located along the frequencies, forming almost instantaneous pulsations (around 06:04:20 UT); then they were decomposed and aligned along the inclined straight lines that are parallel to the individual small fibers. At the end of this time interval the small fibers formed an almost braided ZP (around 06:04:26 UT). The circular polarization of the fibers was dominantly of right-hand sign.

One second later (Figure 5.1a), they were located once more along the inclined straight lines (06:04:27.0 – 06:04:28.5 UT), and a new special feature was seen two seconds later (06:04:30 UT): they were localized along the straight lines, but with the reverse (positive) drift. In one more second (06:04:31 – 06:04:33 UT), this special feature was already clearly the basic prevailing structure (Figure 5.1b) which is basically regarded as large-scale ZP stripes drifting to higher frequencies with the speed of about 270 MHz s^{-1}. These structures were terminated at a certain high-frequency boundary which drifted to lower frequencies with the speed of approximately – 67 MHz s^{-1}.

In Figure 5.1 only right polarization channels are presented because the polarization degree was 100%. The fiber structure appeared as a forerunner of the rise of continuum which continued for more than three minutes, but no more fine structure was observed.

The flare of M1.0 1F class occurred at 06:01 – 06:04 – 06:10 UT in the active region (AR) 10652 (N07W20). The analyzed fiber structure was observed after

several strong pulsations at the very beginning of the smooth rise of a flare continuum in the unpolarized emission whose duration was about 5 minutes.

According to the spectral data of IZMIRAN in the frequency range of 270 – 25 MHz, the pulsations had a continuation in the meter-wave range in the form of type III bursts, where they stopped at frequencies near 200 MHz in the form of J-bursts. Later the flare continuum lost any fine structure, and the event ended, without type II bursts or any coronal mass ejection (CME).

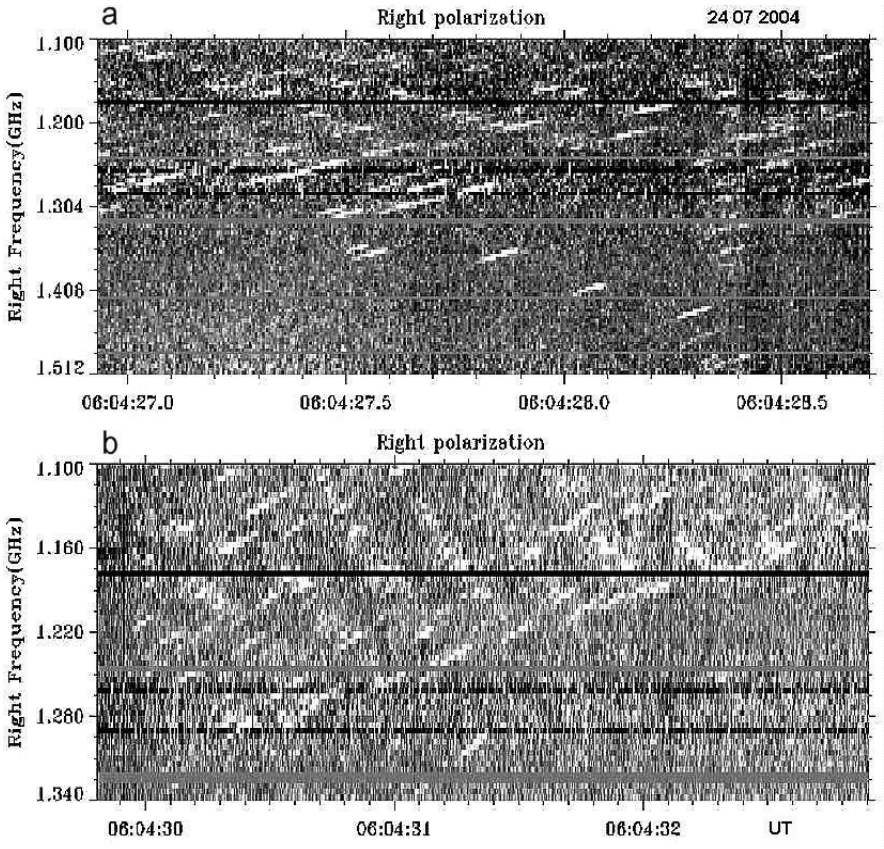

Fig. 5.1 (a) Dynamic spectrum in the range 1.100 – 1.512 GHz in left and right circular polarizations recorded by the spectrometer of NAOC on 24 July 2004. (b) The continuation of the 24 July 2004 event in the range 1.100 – 1.340 GHz in the right- circular polarization (the radio emission is fully polarized) (from Chernov et al., 2008).

In the absence of spatially-resolved radio observations, the position of the radio source can be inferred from the image of the flare in the chromosphere of

TRACE 1700 Å data (Strong *et al*. 1994). At the moment 04:07 it was superimposed on the magnetogram (Solar Flare Telescope, NAOJ/Mitaka). Three bright flare kernels were located to the west of the preceding sunspot of this AR, above the quadrupole-like structure of the magnetic field with a peculiar X- point at the center of the flare region.

The two flare kernels were located above the S- magnetic polarity; therefore the radio emission of right circular polarization should correspond to the ordinary wave mode. The flare kernels in the 195Å images were also located exactly above the bright regions seen in the 1700 Å images, and the radio source in right circular polarization at 17 GHz (Nobeyama Radio Heliograph) was also located in this place. The largest radio flux was recorded in decimeter and meter ranges, indicating the magnetic reconnection occurred high in the corona. As a matter of fact, in the 1700 Å images we see bright tops of the flare loops. The decimeter radio source is expected to be found below the flare current sheet (where the acceleration of fast particles would take place). The positive frequency drift of the large scale ZP stripes may be caused by the downward motion of a plasma ejection from the reconnection region with the Alfvén velocity. On its way this ejection would meet a flare loop arcade that was expected to be rising. The high-frequency boundary of the termination of emission can be the consequence of this collision.

5.1.2 2004 November 3 Event

This event was most powerful and most prolonged, with diverse fine structures and duration of about 2 hours, over the course of repetitive brightenings of the flare. For the analysis we selected only its first part (with a duration of about 25 minutes), at the beginning of which small-scale fibers were observed (Figure 5.2), and, as in the previous events, it was also a forerunner of the entire event.

The first glance at Figure 5.2 reveals certain similarity to the event of 2004 July 24: at first, the small-scale fibers occurred chaotically scattered along the frequencies, then they were localized at some frequencies and formed large-scale ZP stripes, and at the end they broke up again to separate into chaotic fibers, which gradually (during ≈ 1.5 min) broke up into a cloud of chaotic spikes. The essential difference lies only in different polarization. Here, it was of moderate right-hand sign.

Figure 5.3 helps to better estimate the parameters of the small fibers that composed the large-scale ZP. The time profiles at the fixed frequency of 1.216 GHz show that all profiles are symmetrical, and have an almost Gaussian shape. The frequency drift of fibers was stable and constant, ≈ -270 MHz s^{-1}, and for the large-scale ZP, it was ≈ 630 MHz s^{-1}.

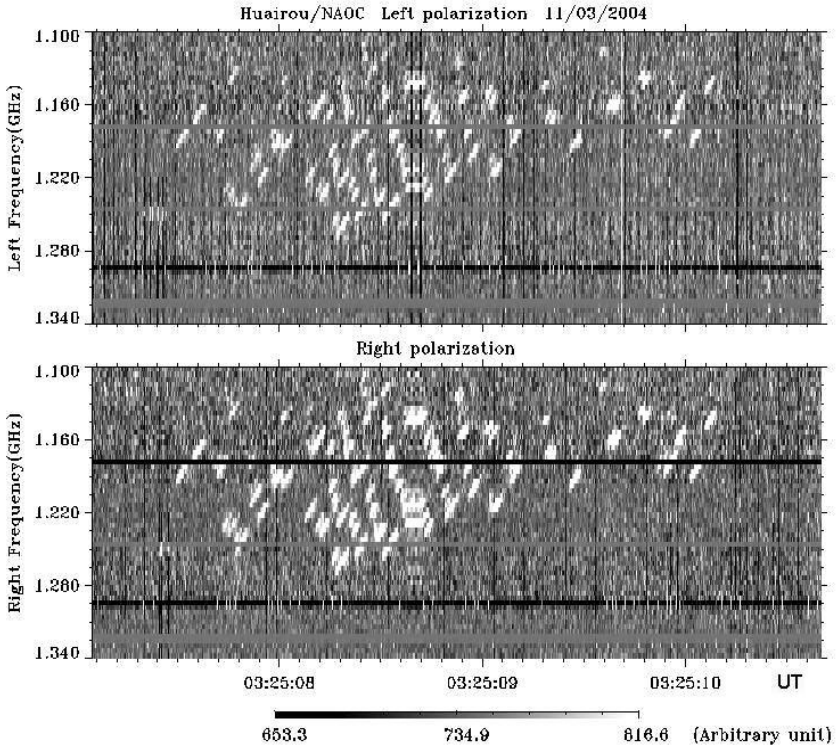

Fig. 5.2 The beginning of the 2004 November 3 event in the frequency range 1.100 – 1.340 GHz, showing moderate right-hand polarization: the small-scale fibers are re-grouped into large-scale ZP stripes (from Chernov et al., 2008).

The flare of M1.6 1N class has occurred at 03:23 – 03:35 – 03:57 UT in AR 10696 (N09E45). The analyzed fiber structure was observed at 03:25:07 UT at the very beginning of the smooth rise of a flare continuum in the non-polarized emission whose duration was about 25 minutes. According to Culgoora spectral data, strong type II bursts began at 03:33 UT at frequencies near 120 MHz (estimated shock speed 750 km s^{-1}), accompanied by a powerful CME (SOHO/LASCO C2) after 03:54 UT (whose estimated speed was 918 km s^{-1}).

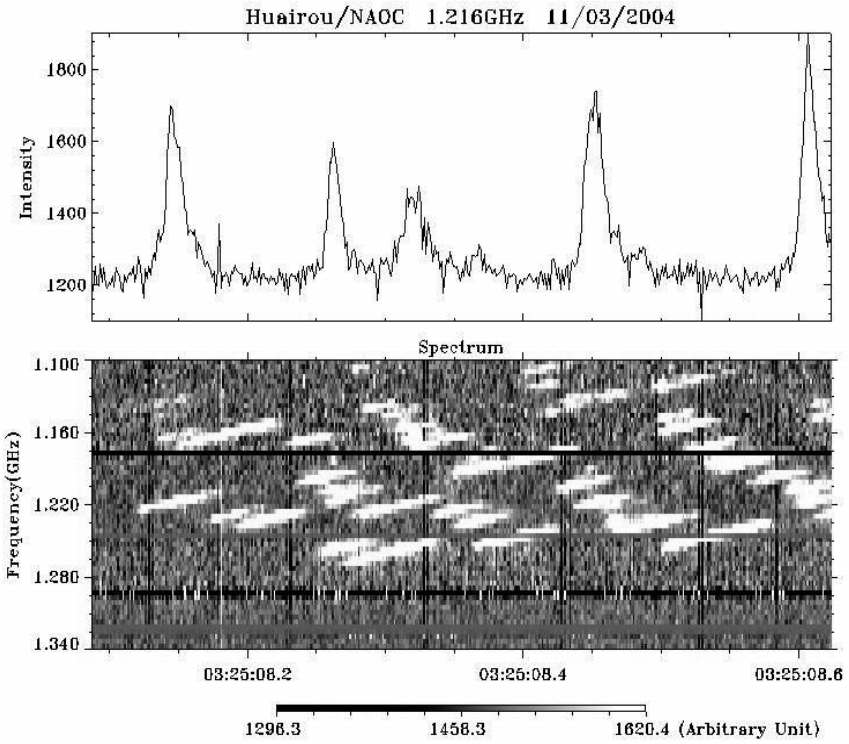

Fig. 5.3 The magnified dynamic spectrum (*bottom*) and the time profile at 1.216 GHz (*top*) of the fiber structure on 2004 November 3 (from Chernov et al., 2008).

After about 03:30 UT the polarization of the fine structure changed sign, and the left-handed polarization became predominant. The dynamics of flare processes can be tracked according to RHESSI hard X-ray data in the 6.0 – 7.0 keV energy band, the Nobeyama radio map at 17 GHz (Chernov et al. 2008). At 03:26 UT the radio source had a triple structure (in accordance with the distribution of sunspots in the AR) with a big source of predominantly right-hand circular polarization above the following spot of the S-polarity. A single HXR- source was located above this radio source. At 03:30 UT a new HXR source appeared in the south-western portion of the AR. Thus, the strengthening of the radio source at this moment was connected with the development of the flare above the small leading spot of N-polarity. In the higher energy band 14.0 – 16.0 keV, even two new sources have appeared in the same location. So, it is possible to conclude that the radio emission corresponded to the ordinary wave mode both at the beginning and in the maximum of the event.

We can derive the following conclusions from the observations of two events with small-scale fiber bursts as a substructure of large-scale ZPs:

Narrowband fibers almost always drift to lower frequencies with the speed that is typical in usual fiber bursts, and sometimes they are similar to the ropes of fibers in the meter range.

In two events the fibers evolved from chaotic features in the dynamic spectrum to a regular structure (in the form of large-scale ZP stripes) and again to disorder, being gradually converted into the spike-bursts.

Large-scale ZPs were limited at high frequencies by a boundary drifting to lower frequencies with the speed of – 70 to – 90 MHz s^{-1}.

The radio emission was moderately or strongly polarized and corresponded to the ordinary wave mode.

The fiber structure appeared as a forerunner of the entire event.

The fibers, as well as large-scale ZP, do not reveal absorptions at the low frequency edge.

A superfine structure in small-scale fibers was not detected with a time resolution of 1.25 ms.

In two other events (2004 December 22 and 2004 October 31) small-scale fibers can be regarded as the fine structure in type III bursts and broadband pulsations (Chernov et al. 2008).

5.1.3 2006 December 13 Event

5.1.3.1 Introduction

The most recent large flare of the 23rd cycle was observed on 2006 December 13 (02:10 – 05:10 UT) in the active region NOAA 10930 (S05W24–27). This was an unusual event by its importance (X3.4/4B) and fast coronal mass ejection (CME). The flare also provided the richest material for the analysis of fine structures of radio emission in the microwave range. Numerous spikes in absorption of millisecond duration are the main feature of radio emission observed during the decay phase of the flare. The Solar Broadband Radiospectrometer (SBRS) in the range of 2.6–3.8 and 5.2–7.6 GHz (Huairou Station, NAOC) carried out the radio observations (Fu et al. 2004). The frequency resolution of the SBRS is 10 MHz, and the cadence is 8.0 ms.

During this long-lasting event, different types of common fine structures were observed (e.g. spikes in emission, usual zebra-patterns and fast pulsations). However, during the decay phase together with the spikes in emission, spikes in absorption began to appear. The latter were first randomly distributed in the frequency range 2.6–3.8 GHz, then they exhibited fast pulsations and trajectories of

type III-like bursts in the dynamic spectrum. Furthermore, numerous type III bursts in absorption were observed for about one hour.

The impulsive phase of this event with some fragments of zebra patterns has already been described by Yan et al. (2007). Fast radio pulsations were examined in Tan et al. (2007). They assumed that a resistive tearing-mode oscillation in the current-carrying flare loops modulated the microwave emissions and formed the pulsating structures. The positions of X-points is between two magnetic islands. There are many X-points in each flare loop.

The spikes in emission and fiber bursts were studied by Wang *et al.* (2008). Chen and Yan (2008) already reported the absorptive spikes in this event. The type III-like burst in absorption had been explained by Chen and Yan (2008) as a fragmentary injection of new particles in a loss-cone leading to quenching of the loss-cone instability of plasma waves at the upper-hybrid frequency. Parameters of the bursts in absorption (instantaneous frequency bandwidth and duration, frequency drift *etc*.) depend on parameters of new beams of particles.

A general description of absorptive spikes in this event was carried out by Chernov et al. (2010). The reason for the appearance of spikes in absorption at the decay phase of the event should be understood. It was necessary to estimate how the physical parameters vary in the event, and how the type III-like bursts are formed from the absorptive spikes (with elements of ZP stripes).

The first spikes in absorption appeared at 02:53:08 UT. Further, over more than one hour, different combinations of the spikes in absorption and the type III-like bursts in absorption and in emission were observed. The latter appeared simultaneously and both with positive and negative frequency drift. For the analysis, it is important to know what kind of specific features of the flare were associated with the appearance of bursts in absorption.

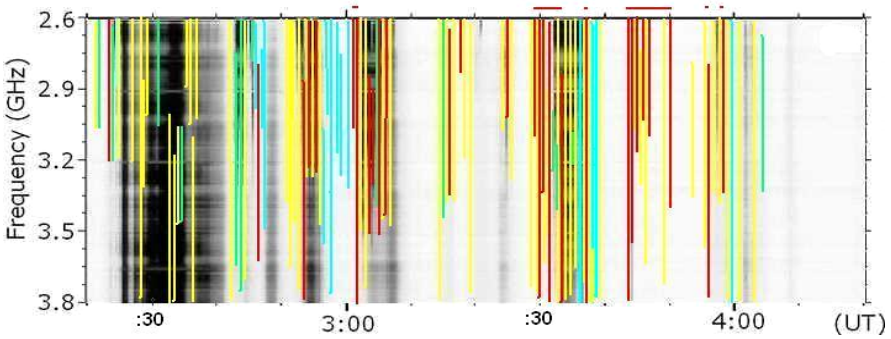

Fig. 5.4 The dynamic spectrum of the whole event 13 December 2006 in the frequency range of 2.6 – 3.8 GHz. The emission is displayed in a negative picture (darker means stronger emission). The color bars indicate timing and frequency range of fine structures: yellow – spikes in emission, red – spikes in absorption, blue – fiber bursts, green – zebra pattern. The red horizontal bars at the top show the time intervals when spikes in absorption formed type III-like bursts (from Chernov et al., 2010).

Figure 5.4 shows the timing and frequency range of fine structures in the dynamic spectrum of the whole event. It is evident that spikes in emission (yellow bars) were observed over the whole event while the spikes in absorption (red) were only observed in the decay phase. Typical fragments of bursts in absorption are shown in Figures 5.6 and 5.7. It should be noted that the usual fine structures in emission, zebra pattern (green bars in Figure 5.4) and fiber bursts (blue bars) were observed over the whole event as well (see also Figures 5.8 and 5.9).

5.1.3.2 New flare brightening in TRACE- images

The further dynamics of the flare was outlined in more detail with the TRACE-images in the 195 Å passband. They show flare loops with temperature of $1.8 \cdot 10^6$ K. Six images taken from TRACE catalog data (http://trace.lmsal.com/trace _cat.html) are shown in Figure 5.5.

According to the TRACE images of the 195 Å passband at the impulsive phase, the flare consisted of many bright kernels distributed over the entire active region and bright large-scale loops, which extended predominantly from the north-west to the south-east, connecting to distant spots. During the impulsive phase in the eastern part of the active region, five consecutive flare brightenings were observed. After approximately 02:40 UT the TRACE images show thin loops (arcades) along the large-scale X-ray loop which began to be formed westwards. After approximately 02:47 UT, the new loops started to appear successively towards the west.

On the first TRACE 195 Å image in Figure 5.5 (02:48 UT) new bent loops appeared in the western part of the region and began to ascend. The three images (03:02, 03:20, and 03:23 UT) illustrate the subsequent rising of these bent loops and some changes above them which suggest rapid flows. At 03:20 UT the bent loop did look like a cusp for the first time.

After approximately 03:36 UT, the restoration of the magnetic structure began, and the bent loops (with a possible apex) began to descend. At 04:23 UT, the bent loops finally descended, and the burst activity completely ceased after that. During this time, about ten peaks of radio emission occurred at 2.84 MHz (Figure 1 in Yan, et al. (2007)). Diverse bursts in absorption were observed during practically each peak.

According to the Nobeyama Radio Heliograph (NRH) data at 17 GHz (see Figure 2 in Chen and Yan (2008) the peak of the radio continuum burst was located above the northern flare ribbon in the negative magnetic polarity. During the new flare brightening at 03:28 UT, the radio source revealed asymmetry with a second maximum above the western part of the northern flare ribbon. This location coincides with the new helmet-shaped loop in the western part of the loop arcade after 03:23 UT (Figure 5.5).

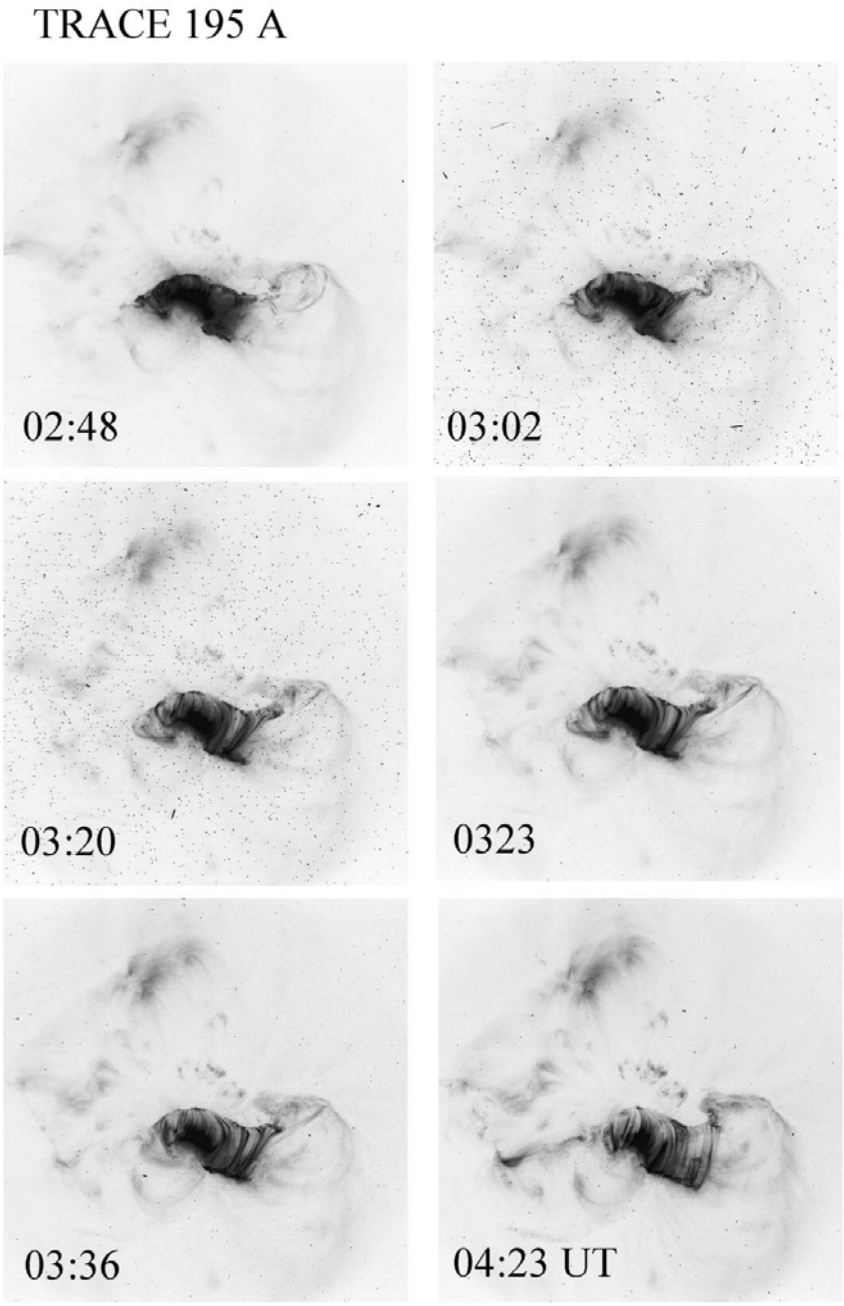

Fig. 5.5 The development of the flare in the western part of the post-flare arcade in the TRACE EUV passband 195 Å (from Chernov et al., 2010).

5.1.3.3 Features of bursts in absorption

Figures 5.6 and 5.7 show the appearance and the detailed development in time of spikes in absorption according to the data of SBRS (in the frequency range 2.8–3.6 GHz). Only the right-handed circular polarization (RHCP) components of SBRS are shown because, during the decay phase of the event, the emission was fully right-handed polarized.

The first spikes in absorption appeared at 02:53:08 UT (Figure 5.6a). All spikes had different frequency bandwidths, from point-like (in one pixel with the size of 10 MHz, 8 ms) to 400 MHz, but no bursts showed frequency drift. Therefore, each spike represents an instantaneous frequency bandwidth. Most of them were scattered randomly in the frequency and time domains. During the time interval shown in Figure 5.6a, we did not notice specific patterns in appearance of spikes in absorption and in emission. The spikes in absorption and emission appear simultaneously at different frequencies and they are distributed randomly with respect to each other.

After 03:01:28 UT, the non-drifting spikes began to be built along the inclined trajectories and to form the absorptive bursts, similar to type III bursts, shown in Figure 5.6b. The analysis of such bursts in the interval 03:01:28 – 03:01:37 UT is very important. The first group of isolated spikes at 03:01:29.5 UT were built along two type III-like trajectories, with different frequency separations between spikes. Then, the large dark type III-like burst in absorption with a longer duration of 0.12 s appeared. The subsequent two trajectories consisted of isolated spikes again. In addition, several following type III trajectories were accompanied by spikes with diversified frequency bandwidths and frequency drift rates (see the continuation of possibly similar activity in Figure 5.6e).

It is important to note that the isolated spikes along the type III trajectories were shifted in frequency with separations approximately equal to the bandwidth of the spikes (≈ 80 MHz). However, in the following type III-like large bursts, they overlapped in frequency (they became more broad-banded, ≈ 160 MHz). The strongest spikes appeared one after another, *i.e.*, with the period equal to their duration (8 ms). Thus, it is not completely excluded that spikes actually have smaller bandwidths and shorter duration, due to the limited frequency and time resolution of the instrument (10 MHz and 8 ms). After 03:01:31 UT, clouds of spikes in emission began to appear, with approximately the same parameters, but they did not form type III bursts in emission.

In the interval 03:03:00 – 03:03:10 UT, fragments of the large-scale ZP in emission appeared in the HF edge of the powerful emission (the top panel in Figure 5.8). A large-scale ZP means that the frequency separation between stripes is around 170 MHz, the largest value found in this event (see Table 1 in Yan et al. 2007). Numerous spikes in emission and absorption were seen superimposed on ZP stripes. The spikes in absorption constituted the absorption stripes of the ZP.

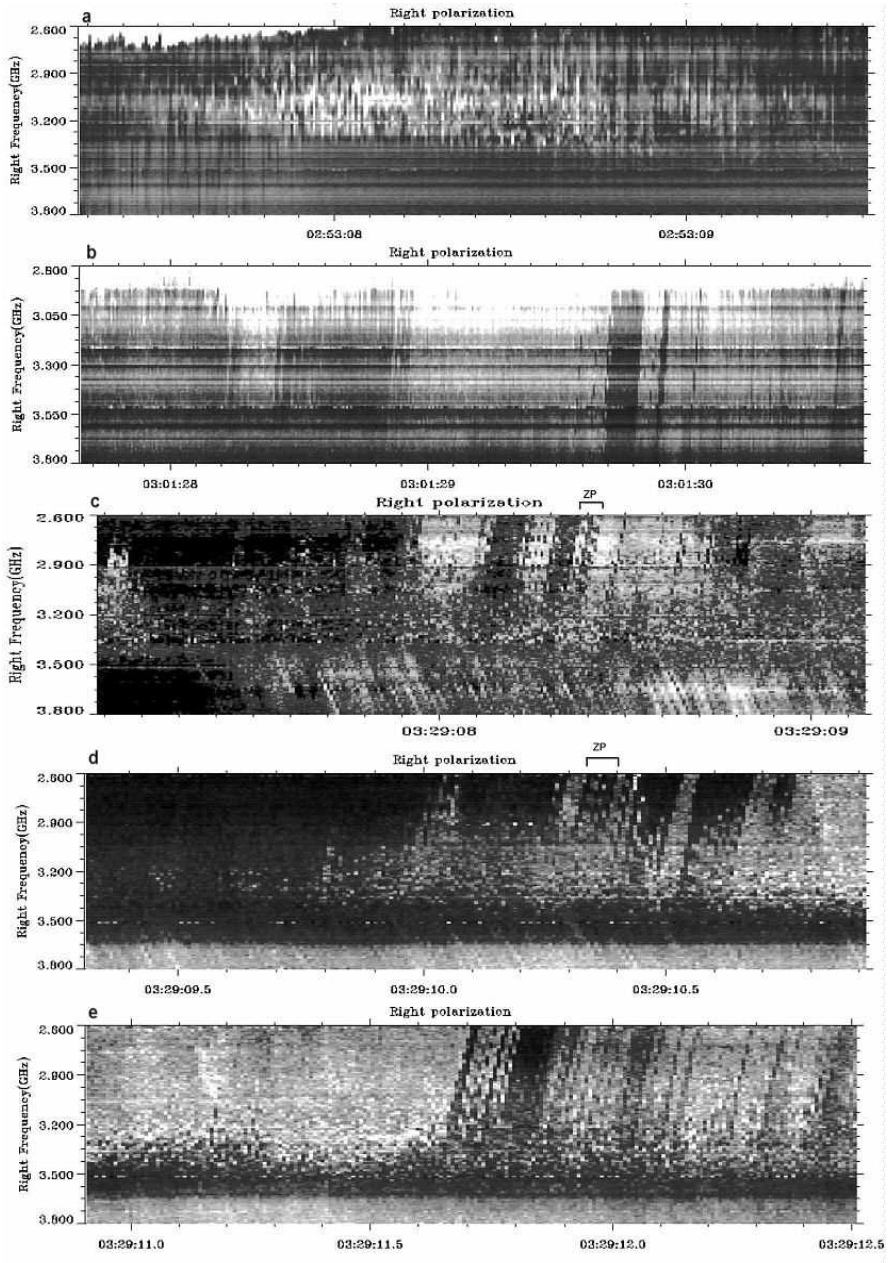

Fig. 6 Dynamic spectra of the component of the right-handed circular polarization in 2.6 – 3.8 GHz showing the consecutive development of the absorptive spikes at 02:53 UT (a) and of type III-like busts consisting of spikes in absorption at 03:01 (b) and 03:29 UT (c). The frequency and time scales are different in different panels (from Chernov et al. 2010).

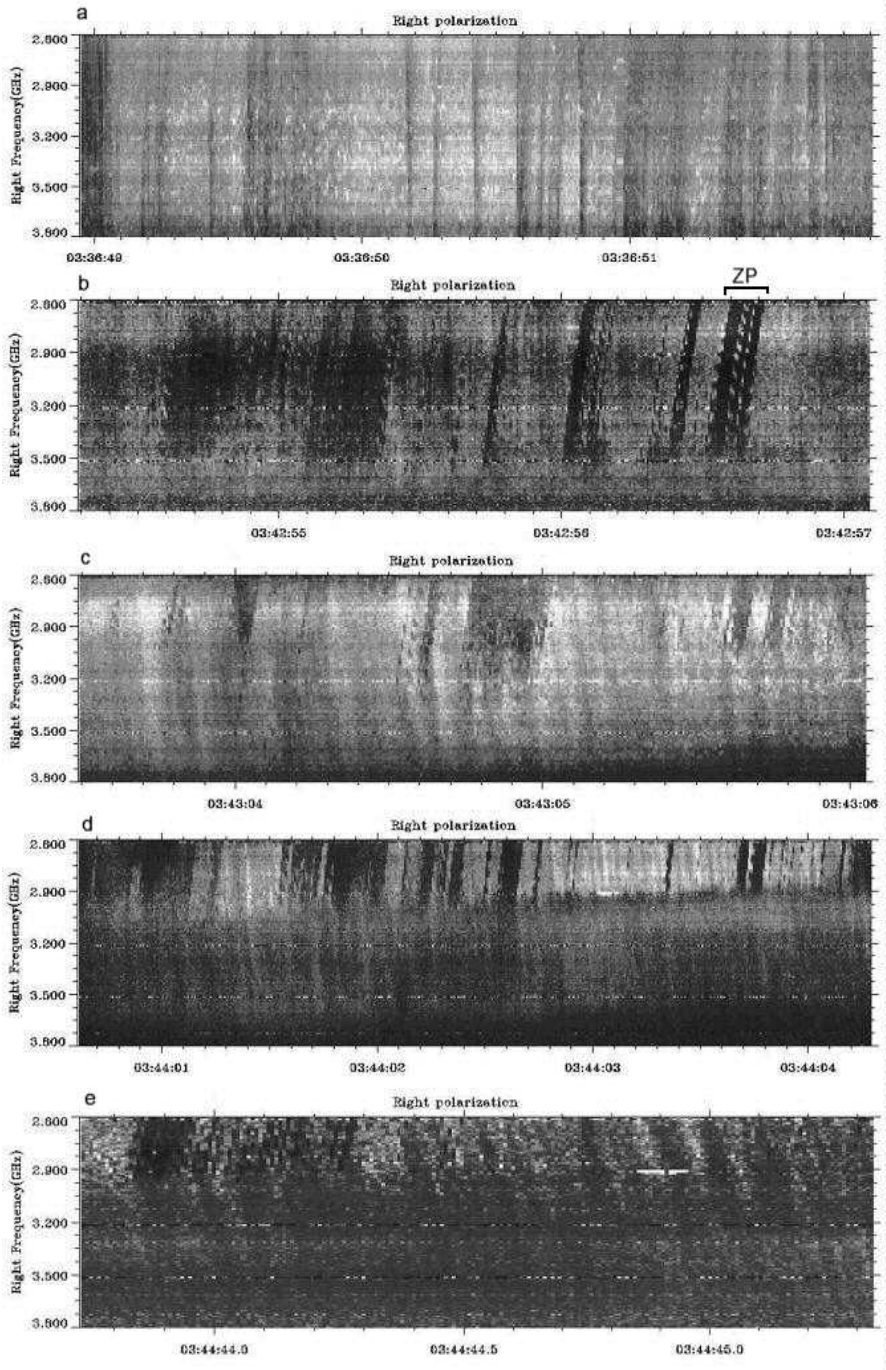
a
Right polarization
Right Frequency(GHz)
2.600
2.900
3.200
3.500
3.800
03:36:49
03:36:50
03:36:51
b
Right polarization
ZP
Right Frequency(GHz)
2.600
2.900
3.200
3.500
3.800
03:42:55
03:42:56
03:42:57
c
Right polarization
Right Frequency(GHz)
2.600
2.900
3.200
3.500
3.800
03:43:04
03:43:05
03:43:06
d
Right polarization
Right Frequency(GHz)
2.600
2.900
3.200
3.500
3.800
03:44:01
03:44:02
03:44:03
03:44:04
e
Right polarization
Right Frequency(GHz)
2.600
2.900
3.200
3.500
3.800
03:44:44.0
03:44:44.5
03:44:45.0

Fig. 5.7 The continuation of the development of the right-hand circularly polarized component in 2.6 – 3.8 GHz in the time interval 03:36 – 03:44 UT showing the absorptive type III-like bursts (b, c, d) accompanied by the reverse-drifting bursts in emission and absorption (c, d, e) (from Chernov et al. 2010).

Previously, only spikes in emission were reported as substructures of ZP emission stripes (Chernov et al., 2003; Chernov et al., 2005).

Such a complex combination of different structures continued up to 03:24:30 UT, when the reverse drifting bursts in absorption appeared as the prevailing structure. However, in contrast to type III-like bursts in absorption, they did not show clear spike substructures. To be more precise, maybe the spikes were not resolved by the instrument, or perhaps substructures do not exist at all. Over the next few seconds the reverse-drifting bursts in emission appeared, and alternated with the bursts in absorption almost over the entire frequency range of the spectrometer. Until 03:25:22 UT, the range of the intermittent reverse-drifting bursts was from 2600 to 3000 MHz.

After 03:29 UT a new powerful flare brightening began, and in the mean time bursts in absorption with new properties appeared (Figures 5.7c and 5.7d). The frequency of ≈3400 MHz became the "boundary" between the bursts of the opposite drifts. The bursts in absorption with the fast direct (negative) drift appeared at the higher frequencies, and the reverse-drifting bursts in emission and absorption appeared at the lower frequencies. We did not notice any correlation between bursts of different drift. Moreover, the drift to higher frequencies of the latter bursts was approximately three times slower, around 3.6 GHz s^{-1}, and they actually looked like classical fiber bursts with typical absorption from their LF edge (Chernov, 2006) but with reverse drift.

The low-frequency bursts in absorption were composed of spikes with almost no frequency separation (03:29:08.15 – 03:29:08.25 UT). The spikes that formed the type III-like bursts had a wide range of parameters and showed no regularity in appearance. The spikes, as the substructures of type III-like bursts, are clearly visible in Figures 5.10 and 5.11 with enlarged spectra and time profiles at two fixed frequencies.

However, at 03:29:08.4 – 03:29:08.5 UT in Figure 5.6c in the type III-like bursts (in the frequency range 2.60 – 3.05 GHz) it is possible to distinguish absorptive ZP-like stripes (noted on top by symbols ZP), which drifted to higher frequencies and consisted of spikes. A similar but short fragment of ZP-like stripes repeated at 03:29:10.3 in the frequency range of 2.60 – 2.90 GHz (Figure 5.6d).

In the subsequent two minutes (03:30 – 03:32 UT) the powerful pulsations in emission (partially interrupted with broadband pulsations in absorption) and clouds of narrow-band spikes in emission were observed. At 03:32:16 UT, several stripes with a usual ZP appeared (the second panel in Figure 5.8) with the narrow

frequency separation (of ≈40 MHz). Numerous spikes in emission and absorption accompanied these several ZP stripes.

In Figure 5.7, further development of bursts in absorption is represented, when the helmet-shaped flare loop on the western edge of the arcade began to descend (the image at 03:36 UT in Figure 5.5). In Figure 5.7a, pulsations in absorption (or type III-like bursts), are seen against the background of a large cloud of spikes in emission. The pulsations did not reveal a strict periodicity, but the spikes in absorption are visible as the substructures of pulsations.

Against the background of such pulsations during 03:36:57 – 03:36:58 and 03:37:04 – 03:37:05.5 UT, the type III-like trajectories containing isolated almost point-like spikes in emission appeared. Again, the classical fiber bursts at 03:37:12 – 03:37:25 UT against the background of pulsations in emission and absorption were observed (a part of these fibers is shown in the middle panel of Figure 5.9), when the flare brightening was decaying. These fiber bursts were gradually transformed into broadband stripes predominantly in absorption with the decreasing frequency drift. Then the reverse-drifting (almost through the entire range) fiber bursts appeared again during 03:37:34 – 03:37:38 UT. Further, the fibers against the background of powerful pulsations and the clouds of spikes in emission (03:37:49 – 03:38:10 UT) appeared again.

This entire dynamics is very important for understanding the appearance and development of the uncommon bursts in absorption. During three more minutes, the clouds of strong spikes in emission were observed. At the end of this interval, broadband pulsations in emission and absorption with the reverse drift accompanied these clouds. The pulsations were followed by the type III-like bursts in absorption which consisted of non-drifting spikes in absorption. During the time interval 03:42:56.5 – 03:42:56.7 UT (Figure 5.7b), spikes in absorption formed the absorptive ZP-like stripes. In this time interval, all features of the type III-like bursts in absorption noted above (during the different moments) were seen.

The initial HF boundary of the absorptive bursts was slightly displaced downwards, up to ≈3500 MHz. In the middle part of this spectrum, weak non-drifting pulsations with the same HF boundary remained noticeable. The main structure here – the non-drifting spikes in absorption – is the building blocks of all other forms of bursts (see also Figure 5.7c). Let us note the basic properties of type III-like bursts in absorption we observed.

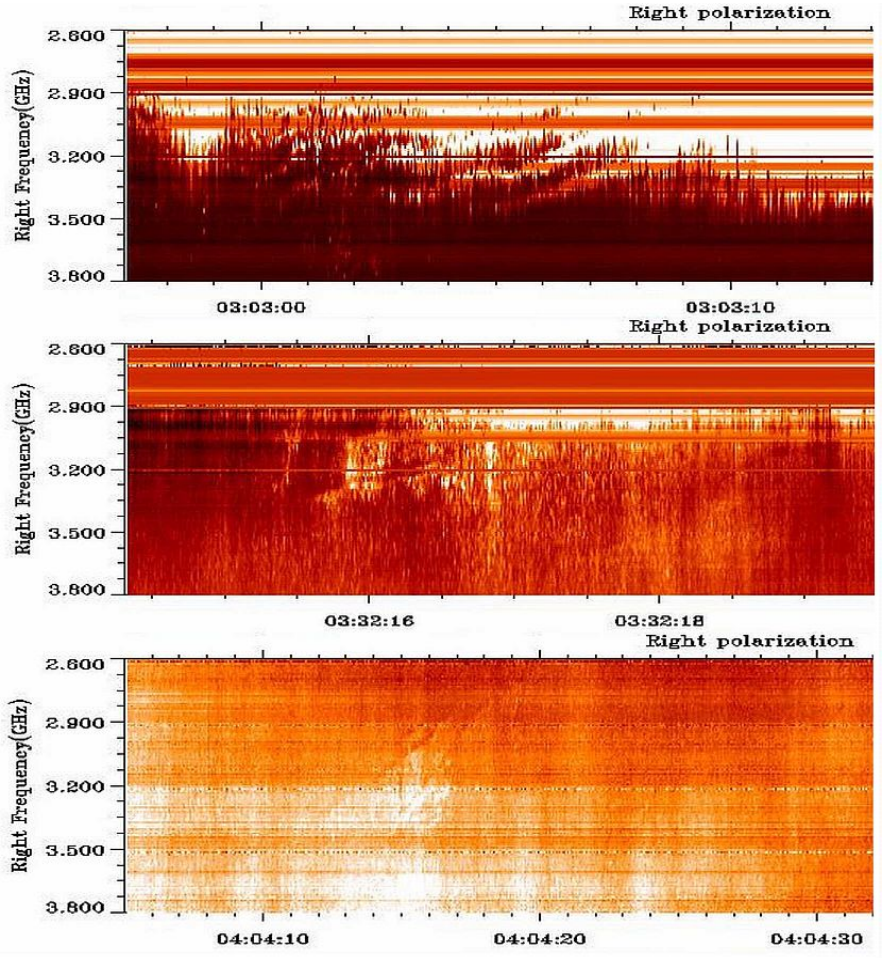

Fig. 5.8 Enlarged spectra showing the ZP at the post-maximum phase of the event. The top panel shows spikes in emission and absorption superimposed on ZP stripes. The spikes in absorption constituted the absorption stripes of the ZP. Numerous spikes in emission and absorption were accompanied several ZP stripes in the middle panel. Note the unusual (braided) ZP in emission and absorption - in the bottom panel (from Chernov et al. 2010).

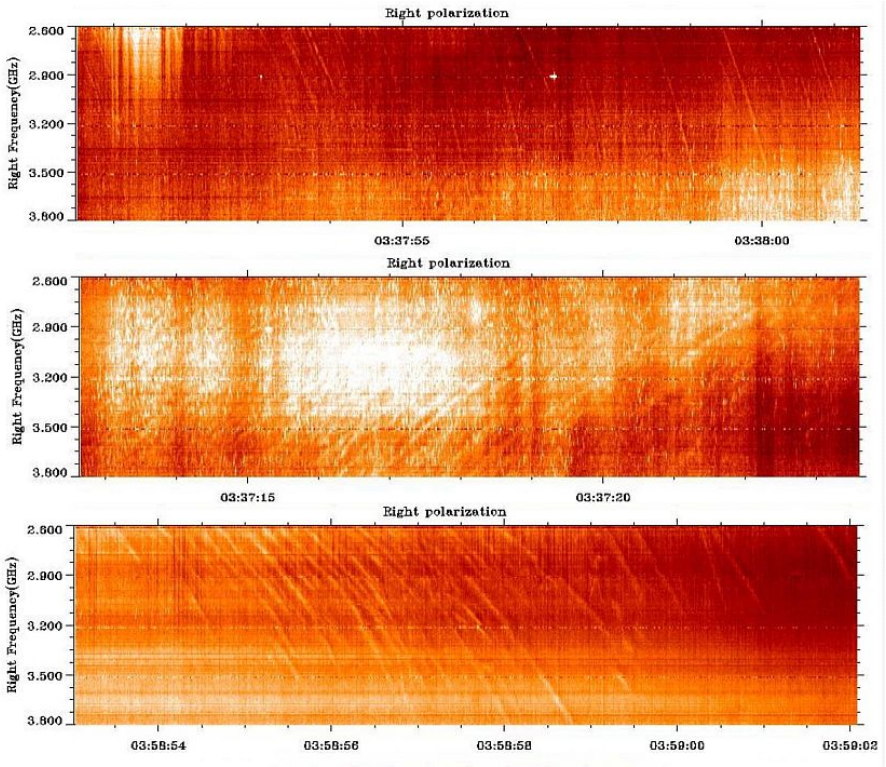

Fig. 5.9 Fiber bursts at the decay phase of the event. In the three panels spikes in emission and absorption are superimposed on fibers or are simultaneously visible. The time scales are different in different panels (from Chernov et al. 2010).

- The type III-like trajectories consisted of isolated spikes which overlap both in frequency (from the HF part) and frequency separation (from the LF part of the spectrum). These single (broken) trajectories appeared prior to the larger dark type III-like bursts, as well as after them.
- In the large absorptive bursts we were able to count 4-5 sequential trajectories of spikes, which did not show a noticeable frequency-time correlation between them. The drift velocity of type III-like bursts was ≈ -12 GHz s^{-1}.
- In several moments, the spikes in absorption in sequential trajectories displaced smoothly to HF, and formed the ZP-like stripes; the maximum duration of stripes was about of 0.12 s in the last burst in Figure 5.7b. The frequency drift of the

stripes was ≈1700 MHz s^{-1}, almost the same as that in the first absorptive ZP-like stripes during 03:29:08 – 03:29:14 UT.

All these details are more easily visible in enlarged spectra in Figures 5.10 and 5.11. Similar short ZP elements drifting like type III bursts (or almost vertical columns) are known in the meter range. For example, Slottje (1972, in his fig. 6C) showed numerous almost vertical columns of the ZP. In this case, repeating columns of the ZP can be explained by fast pulsations in absorptions (sudden reductions). Several examples of fast, almost vertical, columns of the ZP in emission (without sudden reductions) were presented in Chernov (1976a) (see also Figure 4.19). Here, we will examine similar fast elements of the ZP, but in absorption and with a much higher time resolution in the microwave range.

Parameters characterizing the observed spikes in emission and absorption are summarized in Table 5.1. Let us note that the spikes of type 3 have more strictly fixed duration of 8 ms and smaller spread of the frequency bandwidth, and they are repeated strictly through 8 ms.

Table 5.1: Parameters of Spikes in Emission and Absorption

Type	Range (GHz) [1])	Duration (ms)	Bandwidth (BW) (MHz)	Relative BW (%)	Period (ms)	Frequency drift
1	0.3 - 1.2	8–16	10–220	0.3 – 7.4	8 ▯ 50	| [2])
2	0.3 - 1.2	8–16	20–400	0.67 – 13.3	8 ▯ 50	|
3	0.3 - 1.0	8	30–160	1.0 – 2.4	8	|
Average absolute error						
		8	10	0.3	8	

[1]) Frequency range inside 2.6 – 3.8 GHz.

[2]) | - means vertical spikes, the frequency drift approaches infinity.

Type 1 – spikes in emission; Type 2 – groups of spikes in absorption; Type 3 – spikes in absorption as substructures of type III-like bursts.

Five seconds after the absorptive type III bursts (at 03:43:03 UT), a new special feature appeared. The HF boundary of bursts in absorption shifted to lower frequencies, down to 3000 MHz (*i.e.* the radio source must have been displaced upward). Simultaneously, the bursts in emission drifting to HF (or the reverse-drifting type III bursts) with a fixed period ≈ 0.1 s appeared (Figure 5.7c). Their drift velocity was approximately the same as that in the dark bursts, namely of 12 GHz s^{-1}. Then, during almost one minute after 03:43:03 UT the clouds of spikes in emission began to be superimposed on such structures. From Figure 5.7d, it is evident that at 03:44:01 UT a new property appeared: the HF boundary of type III-like absorptive bursts smoothly displaced to lower frequencies; simultaneously the

reverse-drifting bursts in emission stopped at the same frequency boundary; in this case they became less prolonged and more frequent (the period became ≈ 0.03 s).

We note that at frequencies higher than the HF boundary, the reverse-drifting bursts continued in absorption and with the period that characterized the reverse-drifting bursts in the emission one minute ago (≈0.1 s). The general appearance of this fragment began to resemble a "herringbone structure" (well known in type II bursts in the meter wave band). The only difference is that it was related to the bursts in absorption. The type III-like burst in absorption and reverse-drifting bursts started at the same frequency, and the starting frequency slowly drifted to the low-frequency region with a drift rate of about –60 MHz s^{-1}. As indicated by Klassen (1996), this could be a signature of propagating bidirectional electron beams originating near the reconnection area. In our event, the reverse-drifting bursts in emission with their starting frequency below 2.6 GHz may indicate the existence of the second site of acceleration above in the corona. At this time (after 03:36 UT), the cusp-shaped flare loop continued to descend (Figure 5.5), and the activity rapidly changed.

After 03:44:05 UT, the bursts in absorption disappeared together with the HF boundary. The reverse-drifting bursts in emission which covered almost the whole frequency range became dominant bursts. During 03:44:41 – 03:44:44.5 UT the bursts in absorption reappeared, partially with the fragments of the "herringbone structure". This is shown in Figure 5.7e, where it is also possible to note that at the end of this interval, the reverse-drifting bursts (almost over the entire range) in absorption followed. In the course of the subsequent several minutes after 03:44:45 UT, the bursts in emission and absorption in different combinations with the spikes in emission and absorption still existed. In the course of the last flare brightening (03:55 – 04:05 UT), the bursts in emission (pulsations and spikes) predominated, although the complex forms of bursts in absorption (without type III-like bursts) irregularly appeared.

During 03:58:54 – 03:58:59.2 UT the classical fiber bursts with the reverse drift appeared once more (see the bottom panel in Figure 5.9). It is remarkable that several stripes of the ZP (with the spiky structure) were observed at the higher frequencies (5.2 – 5.7 GHz) at this moment. Thus, in the course of the whole period discussed here, the conditions for the excitation of a usual ZP and fiber bursts irregularly appeared. During 04:04:12 – 04:04:20 UT the final series of peculiar slow-drifting stripes, exhibiting different absorption and emission characteristics (as elements of the ZP), were observed (the bottom panel in Figure 5.8).

After 04:05 UT, several small events appeared in the radio emission at 2.84 GHz (Figure 1 in Yan et al. (2007)), but the continuum level gradually decreased to the pre-flare level.

5.1.3.4 Time profiles of bursts in absorption

Figure 5.10 shows the enlarged spectrum of the sharpest type III-like bursts in absorption at 03:42:56 UT whose duration was ≈ 0.7 s. The intensity profiles at two frequencies (2.85 and 3.06 GHz) clearly show the modulations due to the bursts in emission and absorption. In terms of the absolute scale in solar flux units (s.f.u.) the maximum flux in emission reached 330 s.f.u. and the minimum flux (in absorption) ≈ 240 s.f.u. with the average level of the continuum of ≈ 280 s.f.u. The maximum of modulation depth at frequency 3.060 GHz was observed between the spike in absorption at ~ 03:42:56.60 UT and the spike in emission 03:42:56.68 (about 80 s.f.u.).

Between the three type III-like bursts in absorption, the ZP looks like the classical one (Chernov, 2006): the increased emission in the bright stripes (two high picks on the profiles) and the moderate absorption in the dark ones (here the absorption is even with respect to the average level of flux in the type III-like bursts in absorption). In the spectrum of Figure 5.10 another property of the usual ZP is clearly seen: the smooth increase with frequency of the frequency separation between the stripes. It increased from ≈ 80 MHz at the frequency of 2700 MHz to ≈ 150 MHz at 3400 MHz.

In the type III-like bursts consisting of isolated spikes in absorption (for example, a trajectory at 03:42:56.3 UT), the instantaneous frequency bandwidth of the spikes also increased with frequency from of 30 to 100 MHz. The decreasing frequency separation between them, disappeared at the frequency of ≈ 3400 MHz. The latter was not coordinated with the frequency separation of the absorptive stripes of the ZP. However, at other onsets noted above for similar bursts this property was not observed.

The ZP-like stripes appear to be parallel. We can distinguish six stripes against the background of type III-like bursts in absorption (they are marked by thin black lines in the spectrum) and three stripes from the LF edge remained diffuse. However, this conclusion depends on many factors: on the conditions in the radio source and on the rate of particle acceleration in different parts of the radio source.

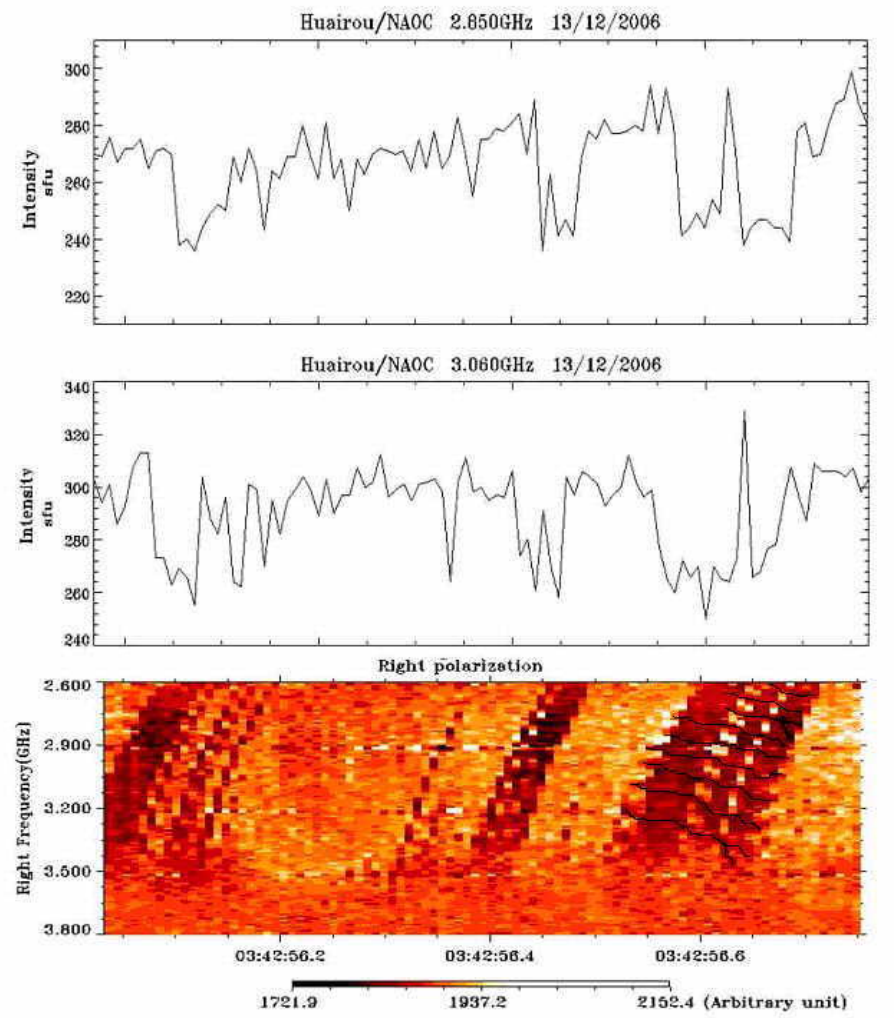

Fig. 5.10 Enlarged spectrum and time profiles at two fixed frequencies (2.85 and 3.06 GHz) of ≈ 0.7 s duration showing the modulations during the type III-like bursts in absorption with a ZP. The absorptive ZP-like stripes are marked by thin black lines (from Chernov et al., 2010).

The precise measurements of the frequency drift showed that its speed also increased with the frequency: from 1000 MHz s^{-1} to 1700 MHz s^{-1}. Thus, it is possible to say that this was a usual ZP, but it was observed against the background of type III-like bursts in absorption. The ZP-like absorptive stripes remained noticeable even against the background of the type III-like absorptive bursts.

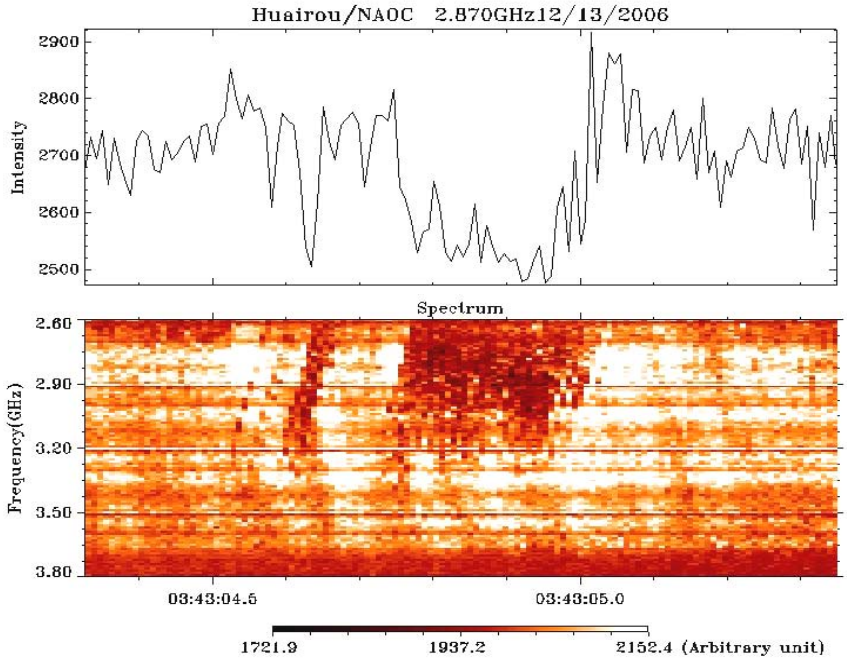

Fig. 5.11 Enlarged spectrum and time profile of ~ 1 s duration at a fixed frequency of 2.87 GHz, showing the modulations during the type III-like bursts in absorption. The intensity scale is in arbitrary units. The spikes, as the substructures of type III-like bursts, are clearly visible (from Chernov et al., 2010).

Figure 5.11 shows the distribution of the spikes in absorption in the background of another type III-like burst in absorption. The spikes were distributed randomly, but they tended to form several short stripes. Such structures of the spikes were called 'braided ZP' by Slottje (1981) (see the event 1970-07-27) and 'lace bursts' by Karlicky et al. (2001) because of the variety of the ZP.

Brief Conclusion from Observations

In spite of the complexity of the analyzed phenomenon, let us isolate the basic properties of the bursts in absorption.

The basic structural element (a building block) of all bursts in absorption was the spikes whose duration was close to the limit of the instrument resolution (8 ms) and the instantaneous frequency bandwidth was on average $\approx$ 70- 80 MHz.

The dynamics of appearance and development of spikes is very rapid. It changed every several seconds.

The type III-like bursts in absorption were basic structures of the absorptive spikes. In three brief moments, the absorptive spikes created ZP-like stripes which lasted for $\lesssim 0.1$ s.

The complex combinations of the drifting bursts in emission and absorption sometimes exhibited the form of a `herringbone structure.'

The activity of absorptive bursts alternated (or were simultaneously observed) with the usual fine structure in emission: spikes, broadband pulsations, ZPs and fiber bursts.

This entire interval of the peculiar fine structure was observed during several flare brightenings in the western part of the flare arcade above the south magnetic polarity. We believe that during this time the magnetic reconnection probably took place. The right sign of polarization corresponded to the ordinary wave mode.

The bursts in absorption were sometimes observed in the meter-wave range (Chernov et al., 1998), but the event discussed here for the first time revealed a wide variety of absorptive bursts in the microwave range.

5.1.4 Other events

Small fibers similar to ones shown in Figure 5.1 were observed by Dabrowski et al. (2005) (Figure 5.12). However, the authors discuss them as drifting spikes. Dynamical radiospectrograms of the spikes were recorded in the 1352–1490 MHz frequency band which was split into 46 channels each 3 MHz wide. The time resolution of the collected data is equal to 80 μs, the highest ever obtained. The observations of the radio spikes have been collected with the 15 m radio telescope of Torun Centre for Astronomy, Nicolaus Copernicus University in Torun, Poland. The observed radio spikes have internal structure and form chains (rope-like fibers and braided ZPs). They occurred during the bulk motion of the plasma along the long loops, observed with the TRACE telescope in the 171 Å band.

Another kind of spike (called dot emissions) was observed with the Brazilian Solar Spectroscope (Meszarosova et al., 2008) in the dm range of 950–2640 MHz with variable time and frequency resolution between 10–1000 ms and 1–10 MHz, respectively. An example of a group of dot emissions arranged as zebra-like chains observed on 1999 March 19 is shown in Figure 5.13 (as a part of fig. 1 from Meszarosova et al. (2008)). Figure 5.13b presents a global view of the dot emissions. The time and frequency resolution is 100 ms and 5 MHz, respectively. Figure 5.13c reveals a detailed view showing the dot emissions with undulating chains resembling the zebra pattern. Figure 5.13d shows the radio flux in time at 1400 MHz where peaks with an intensity of ~ 130 SFU correspond to individual dot emissions (horizontal line in panel *c*).

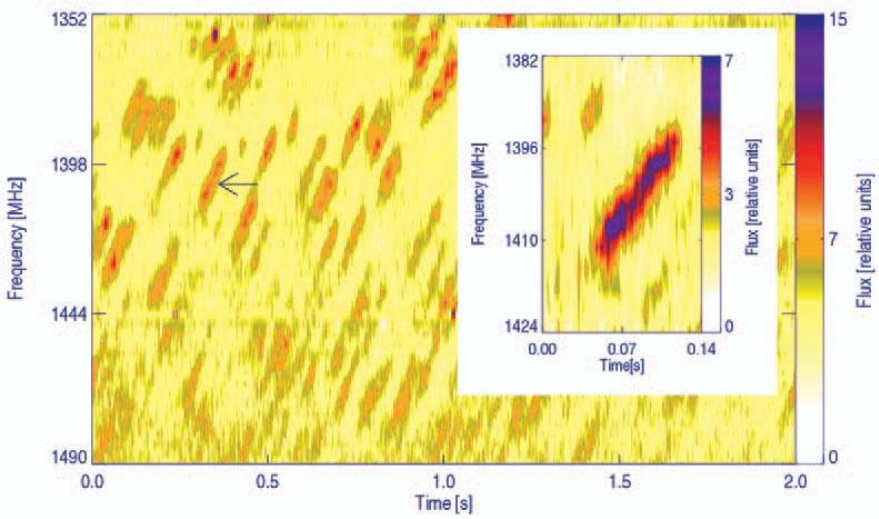

Fig. 5.12 Dynamic radio spectrogram of the dm radio spikes recorded on 2001 October30, beginning at 12:20:27 UT (from Dabrowski et al., 2005).

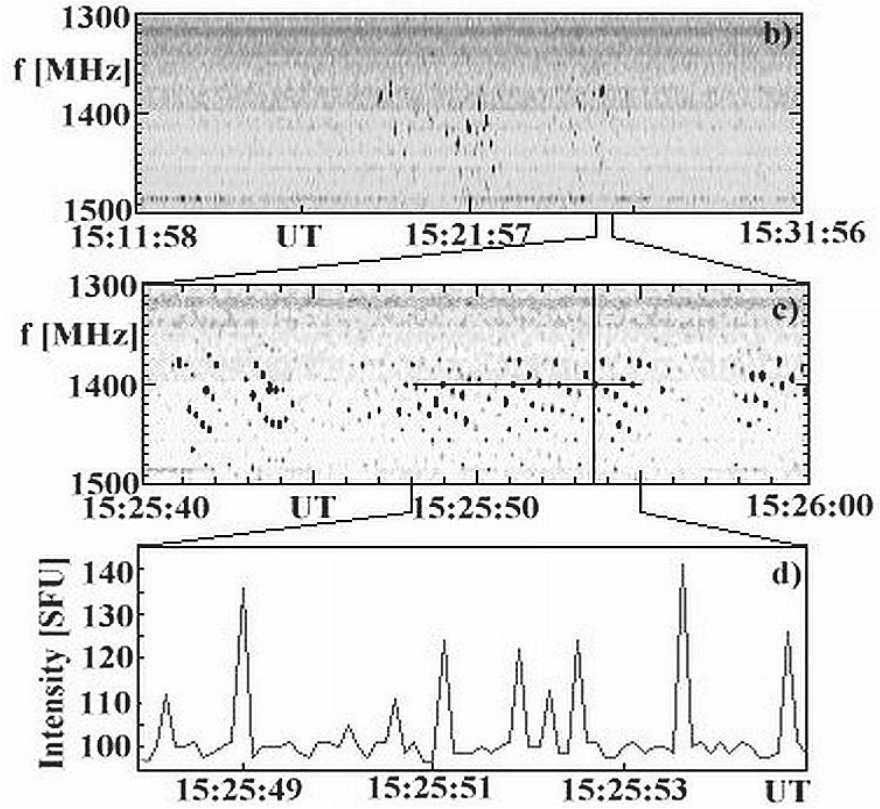

Fig. 5.13 Dot-emissions (in black) arranged as zebra-like chains observed on 1999 March 19: *b*) global view of dot emissions, *c*) zebra-like chains, *d*) radio flux in time at 1400 MHz (horizontal line in *c*) (from Meszarosova et al., 2008).

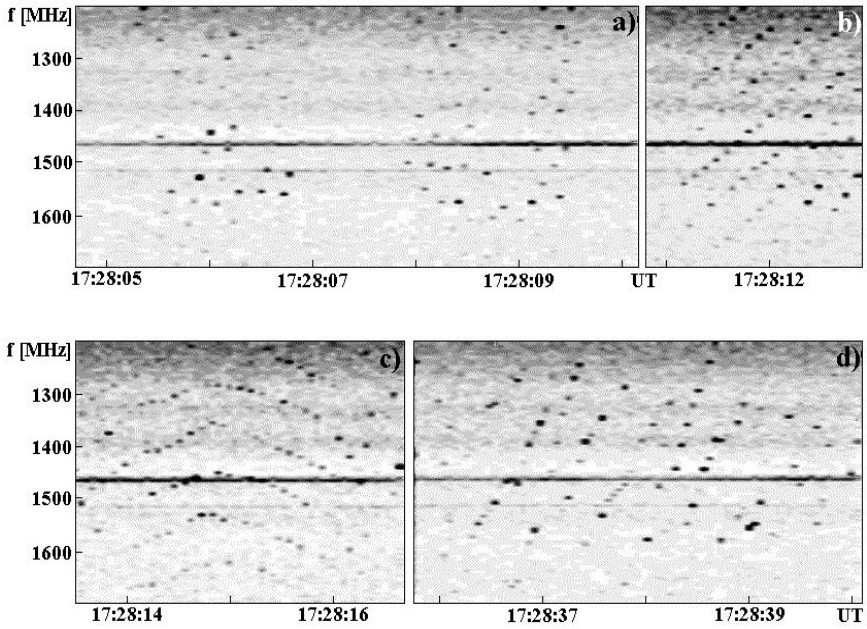

Fig. 5.14 Example of the arrangement of the series of the dot emissions (in black) observed on, 1999 October 19: irregular dot emissions (panel *a*)), fiber-like chains (panel *b*)), zebra-like chains (panel *c*)), and irregular dot emissions (panel *d*)) (from Meszarosova et al., 2008).

Figure 5.14 shows an example of the structural evolution of the group of dot emissions observed on 1999 October 19. This group starts with some irregular dot emissions (panel a) but later they evolve into almost regular fiber-like (panel b) and zebra-like (panel c) chains. At the end, the group of dot emissions again becomes irregular (panel d). During times of dot emission, no background burst emission was detected.

Sych et al. (2006) and Zlobec and Karlicky (2007) studied the characteristics of the zebra-associated spike-like bursts during 2003 August 5 event that were recorded by the Ondrˇejov radio spectrograph in the range 1 – 2 GHz with time resolution 100 ms (upper panel in Figure 5.15). Simultaneously, the spiky structure was examined using the 1420-MHz polarization profiles of the Trieste Astronomical Observatory with a very high time resolution of 1 ms (bottom panel in Figure 5.15). The selected spike-like bursts show a duration (with a mean value of about 7.4 ms at half power) and it is not influenced by the polarization. For the selected bursts there was just a “tendency” that the weaker component (L- polarization channel) should be delayed. Zlobec and Karlicky (2007) realized that the L continuum was generally low with respect to the R continuum; however, the polarization of the spikes does not always match the contemporaneous polarization of the continuum.

The observed superfine structure (spikes) of zebras can be interpreted as proposed by Chernov, Yan, and Fu (2003). Nevertheless, Zlobec and Karlicky (2007) think that the model based on the double plasma resonance (DPR) as proposed by Bárta and Karlický (2001) and Karlický et al. (2001) is also possible. Namely, this model explains both the zebras and the spikes by the same double plasma resonance process; the spikes are generated by the interruption of the DPR process by assumed turbulence (density or magnetic field variations).

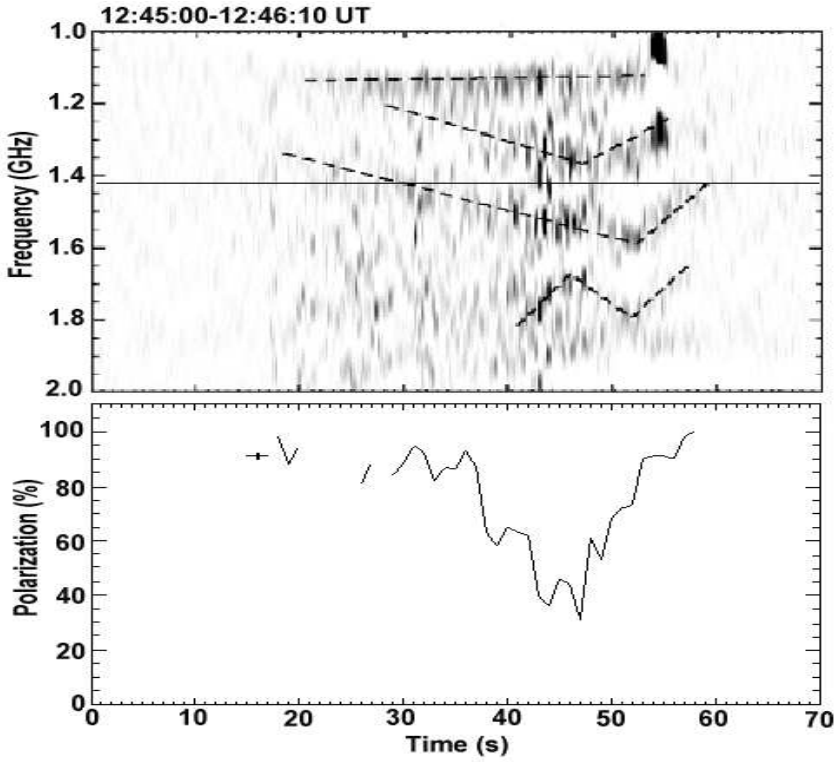

Fig. 515 *Upper panel*: Part of Figure 5 from the paper by Sych et al. (2006) showing the time evolution of the spike-like bursts clustered into zebras forming "V" like structure (in the event August 5, 2003). *Bottom panel*: contemporaneous time evolution of the mean polarization (in R-sense) of the selected spike-like bursts at 1420 MHz (from Zlobec and Karlicky, 2007).

Magdalenic' et al. 2006 reported supershort structures SSSs (spikes), in particular as substructures of the ZP and as tadpoles in the range 265 – 350 MHz using the solar radiospectrograph Artemis IV (Greece) with a time resolution of 10 ms (Figure 5.16). The spikes in the ZP exhibit a duration of 11 – 13 ms, shorter than what was reported earlier in the meter range. Tadpoles are comprised of an emission "eye" with a duration of $\approx$50 ms at the high-frequency side of the burst

and a stretched absorption "body" with a bandwidth of ≈ 40 MHz. In spite of distinctive differences (the emission tails of the tadpoles are not visible), the Slottje (1972) tadpoles and these tadpole-like SSSs belong to a class of physically equivalent bursts.

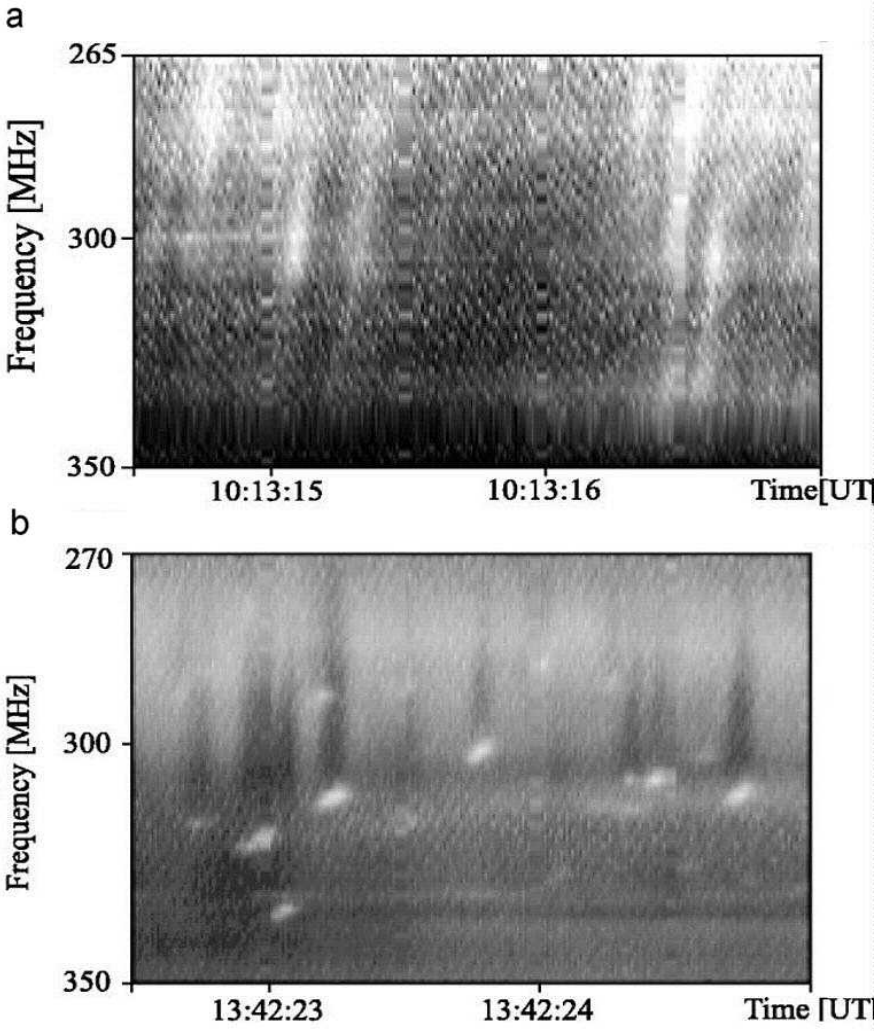

Fig. 5.16 Artemis IV dynamic spectra of negatively drifting supershort structures (SSS) in the background of the ZP with a superfine structure (*a*) and tadpole-like bursts (*b*) in the event 2000 April 15, (from Magdalenic' et al. 2006).

5.2 General Discussion of the events

5.2.1 2004 July 24 and November 3 Events

Small-scale fibers differ from usual fiber bursts only by narrow total frequency bandwidth and they are similar to ropes of fibers, therefore the usual (that is, most accepted) mechanism for fiber bursts should work, namely the coalescence of a plasma wave (*l*) with whistlers (*w*): $l + w \rightarrow t$ (Kuijpers, 1975b; Chernov, 1976a; 1990). However, the propagation of whistlers is limited by a small magnetic trap in the form of fast shock fronts escaping from a region where magnetic reconnection occurs (Chernov, 1997). In our case the periodicity of fibers was not so evident, and fibers were organized as large-scale stripes of a ZP. So, these ZP stripes become visible only when whistlers propagate through the ZP source.

In our events the radio sources cannot be point-like ones, since in such a case one whistler wave packet should produce all zebra stripes simultaneously, but we did not see such a feature. Since the small fibers were not connected by a unique straight line in the dynamic spectra, we cannot assume that one whistler wave packet passes through several DPR levels consecutively in an extensive source. So, the unique possibility remains that whistlers are excited at the same DPR level simultaneously with the plasma waves. Without whistlers, ZP stripes cannot be visible, at least in the DPR model with loss-cone distribution function, in accordance with numerical results of electrostatic instability in Kuznetsov and Tsap (2007). Whistlers without a plasma wave cannot be detected either, but a plasma wave of low energy will be sufficient (at places of DPR) to emit radio waves of sufficient intensity. Thus, whistlers "highlight" DPR levels.

In order to confirm this hypothesis, let us estimate the magnetic field strength *B* in two ways. One is from the observations of separate fibers using the model of the whistlers, and the other is from large-scale ZP in the DPR model. If the hypothesis is correct, these values of the field strengths should be equal.

From the whistler model for small fibers we have $\Delta f_e \approx f_w \approx 0.1\, f_{Be}$ (f_w is the whistler frequency), and a mean value $\Delta f_e = 12.5$ MHz (for the events of July 24 and November 3), and we obtain $B \approx 45$ G.

In the DPR model the frequency separation depends on the scale heights of density (N_e) and magnetic field ($L_{Ne} = 2N_e\, (dN_e/dr)^{-1}$ and $L_B = B\, (dB/dr)^{-1}$ (Zlotnik et al., 2003):

$$\Delta f_s / f_B \approx LB / |L_{Ne} - L_B| \qquad (5.1)$$

For Δf_s = 72 MHz (for the November 3 event) we could obtain about the same value B = 46 G for $L_{Ne} = 1.4 \cdot 10^9$ cm and $L_B = 5 \cdot 10^8$ cm. In the flare region the plasma is very inhomogeneous and such scale heights are realistic. In our events only 3 – 4 large-scale stripes of ZP (or DPR- levels) are simultaneously formed in the spectrum which demonstrates the small sizes of local L_{Ne} and L_B in flare inhomogeneities. Four DPR levels are simply produced at harmonic number s = 10 – 14 with such a ratio of scale heights.

The stable frequency drift of fibers implies that the magnetic field changes little during the lifetime of the structure (Chernov, 1990). The frequency drift of fibers is mainly determined by the group velocity (υ_{gr}) of whistlers, and we have $\upsilon_{gr} = 2c \times f_{Be}/f_{Pe} \times [x(1-x)^3]^{1/2}$, where $x = f_w/f_{Be}$ is the ratio of whistler frequency to cyclotron frequency (Kuijpers, 1975a). If we assume the parameter x varies little during the lifetime of the structure, and f_{Be}/f_{Pe} has a consistent value due to the DPR condition, then υ_{gr} would vary little and consequently the whistlers would cause a stable frequency drift of fibers, at least within a certain DPR level. Therefore the positive frequency drift of large-scale ZP can be connected with the downward motion of the source. In the absence of a good analytical model of electron concentration in the upper chromosphere, we will use a graphical representation given, for example, in the model of Allen (in Figure IV.1 of Krüger (1979)). Utilizing the dependence of plasma frequency (f_{Pe}) on height (r), it is possible to roughly estimate the value of the gradient of f_{Pe} between 1000 and 2500 MHz to be on the order of 240 MHz/10^8 cm. Then, we can use the simplest expression for the definition of the velocity of propagation:

$$V \approx 2 \frac{df/dt}{f} \frac{N_e}{dN_e/dr} = \frac{df/dt}{df_{Pe}/dr} \tag{5.3}$$

The frequency drift df/dt = 630 MHz s^{-1} will correspond to the velocity of about 2590 km s^{-1}. Such a value might be more than a typical Alfvén velocity. Therefore it is possible to assume that the plasma ejection that moves downward from the magnetic reconnection region has caused a shock wave.

In the July 24 event the drift of 220 MHz s^{-1} implies the velocity $\approx$ 900 km s^{-1}, which is somewhat more than the Alfvén velocity ($V_A \approx$ 700 km s^{-1} for the estimated value of B = 45 G).

The drifting boundary of the emission termination at the high frequency edge of a large-scale ZP may mean that a moving shock front meets a rising closed magnetic loop. So, the conditions for DPR are satisfied only in a narrow height interval, below the magnetic reconnection region, and only at the very beginning of events. After such a collision they will be destroyed, and large-scale zebra stripes will be transformed into a braided ZP (Figure 5.1b). Thus, the radio source showing such a fiber structure differs from the radio source of the rope of fibers only by the absence of a magnetic trap (only one shock front) where fast particles could make periodic bouncing motions, and by short lived conditions for the DPR. The absence of any absorption is simply explained by the absence of continuum emis-

sion at the very beginning of events. Only the pulsations in the October 31 event were observed against a weak continuum, and we could detect some fragments of absorption between fibers (fig. 6 in Chernov et al. (2008)).

Thus, we assume that the usual mechanisms can be applied for the interpretation of such a fiber structure: the coalescence of whistler waves with plasma waves producing fiber bursts and the DPR- model for large-scale ZPs. However, the following special features of the plasma wave excitation in the radio source must be present. Both whistler and plasma wave instabilities are too weak at the very beginning of the events (the continuum is almost absent), and the fine structure is almost invisible. Moreover, according to the recent simulations of Kuznetsov and Tsap (2007), the fast electrons with a loss-cone distribution cannot excite a high enough level of electrostatic waves in the DPR levels, so that the separate stripes would be visible. Then, whistlers generated directly at the DPR levels by the same fast electrons will "highlight" the radio emission only from these levels due to the interaction with plasma waves and we observe small-scale fibers as a substructure of a ZP. More precisely, the whistler packets may bring about sufficient plasma wave energy as well as a new composition of the particle distribution, therefore the DPR levels could be more pronounced and "highlighted".

Wu et al. (2007) interpreted the small-scale fibers in the November 3 event as drifting spikes emitted from "solitary kinetic Alfvén waves" (SKAWs) by fast electrons accelerated by the electric field and trapped in SKAWs. However, they did not discuss the reasons for the formation of fibers along the stripes of large-scale ZPs. Furthermore, the source of the strong Alfvén waves, which accelerates a large fraction (≈ 0.1) of the background electrons at the beginning of the event also was not examined.

We have not adopted the model of LaBelle et al. (2003), since it is supposed to be applied to the explanation of a large number of stripes with a narrow frequency separation. In the large-scale ZP in question, on the contrary, the frequency separation is considerably wider than in the usual ZP. Recent evaluation by Chen and Yan (2008) on the validity of the mechanism of LaBelle et al. (2003) indicated that, with the realistic values of the density contrast (with ≤ 0.2) the model cannot account for the large number of ZP stripes.

However, we cannot completely exclude the possibilities of application of the new models, based on the existence of the bands of transparency and opacity when the radio waves propagate through spatially periodic medium (for example, Laptuhov and Chernov, 2006). It is possible that the large-scale ZP is the result of this selectivity with the specific scale of thermal heterogeneities, which move downward from the flare region, and small-scale fibers are caused by additional quasi-periodic modulation of these heterogeneities, for example, by a fast magneto-sonic wave propagating from below. Or alternatively and more simply, the radio waves meet on their way the small- and large-scale heterogeneities which move in different directions, *i.e.* a radio wave is filtered by transparency bands twice. These possibilities require more detailed study.

5.2.2 Other events

Considering all aspects of the observed dot emissions, Meszarosova et al. (2008) think that the dot emissions are generated in a similar way as zebras (Ledenev et al. 2001) or lace bursts (Karlický et al. 2001). Thus, they propose that the dot emissions are produced in the solar atmosphere at the locations where the so-called double plasma resonance condition is fulfilled. The upper-hybrid waves at these locations can be generated e.g. by the anisotropic beam ($T_\perp > T_\parallel$, where $T_\perp$ and $T_\parallel$ are the temperatures of energetic electrons across and along the magnetic field, respectively) accelerated during the flare's primary energy processes. The beam anisotropy can be naturally formed along magnetic field lines by an escape of fast electrons from slower ones. Then these upper-hybrid waves are transformed to electromagnetic waves (with the frequency $\omega_{el} \approx \omega_{\mathrm{uh}}$ or $\omega_{el} \approx 2\omega_{\mathrm{uh}}$), which are observed by radiospectrographs on the Earth. This process is a resonant one which means that its intensity can be several orders of magnitude higher than those associated with non-resonant processes. This can explain the fact that, at times of dot emission, no background burst emission was detected.

Using this model, we can explain not only individual dot emissions, but also their chains. The beam along its trajectory generates dot emissions in several resonance locations (*s*-harmonics). The higher *s* means a higher height of the dot emission source in the solar atmosphere. Thus fiber-like chains of the dot emissions can be formed. On the other hand, zebra-like chains of the dot emissions can be explained by a sequence of anisotropic beams producing dot emissions nearly at the same position on the same *s*-harmonic. Even the whistler waves, which are considered in the model of fibers, can enhance emission at the locations with double resonance conditions. Therefore both forms of zebra-like and fiber-like chains are possible.

Due to similarities in morphology and characteristic properties between the dot emissions and dots in the fine structures of zebras and fibers, Meszarosova et al. (2008) think that both have a similar physical origin. They found that fiber-like chains of the dot emissions evolve into zebra-like chains and vice versa. These changes are in agreement with the idea of Chernov *et al*. (1998) who proposed that both the zebras and fibers are generated by whistler packets. The propagating whistler packets may also generate dot emissions at the positions in the solar atmosphere where the double resonant conditions are fulfilled (see also, Sawant et al. 2002; Krishan et al. 2003). Furthermore, they propose that the chaotic character of some groups of dot emissions is due to rapidly varying plasma parameters (in the MHD turbulence) in the region of dot-emission sources.

5.2.3 2006 December 13 event

From the observations discussed above in detail, we are able to understand the reason for the appearance of the spikes in absorption, as well as the variable nature of their parameters. The main task is to explain formation of the absorptive type III-like bursts and absorptive ZP-like stripes of the absorptive spikes, in combination with different bursts in emission.

Let us recall that the loss-cone instability is the most probable mechanism of the continuous radio emission of the type IV bursts (including microwave bursts). Plasma waves are excited at the upper hybrid frequency by the fast electrons, captured in a magnetic trap, where the particle-velocity distribution with the loss-cone is formed (Stepanov, 1974; Kuijpers, 1975a; Zhelezhyakov, 1995; Kuznetsov and Tsap, 2007). The maximum amplification of waves occurs under the conditions of double plasma resonance (DPR, when the upper hybrid frequency is close to integer harmonics of the electron cyclotron frequency). The appearance of a usual ZP and fiber bursts during the entire event attests to the fact that the loss-cone velocity distribution actually existed.

The dips in emission (corresponding to bursts in absorption) mean the quenching of the loss-cone instability. According to Zaitsev and Stepanov (1975), Benz and Kuijpers (1976), and Fleishman et al. (1994), this quenching can occur because of additional injection of fast particles, which fill the loss-cone. The process of the quenching of instability is examined in detail in a recent paper by Chen and Yan (2008). The authors showed (Figure 5.17) that the beam with a linear dimensions of ≈ 220 km and a Maxwellian particle-velocity distribution inside the loss-cone causes absorption with a frequency bandwidth of ≈ 60 MHz (due to the cyclotron self-absorption of upper-hybrid waves). The calculated absorptive depth corresponds to the observed value: the modulation in the growth rate in Figure 5.17 corresponds exactly to the observed absorption depth of ≈17% in our Figure 5.10. Let us note that according to the calculations by Kuznetsov and Tsap (2007), the beams with the power-law spectrum with a large spectral index should give bursts in emission (the spiky superfine structure of the ZP stripes).

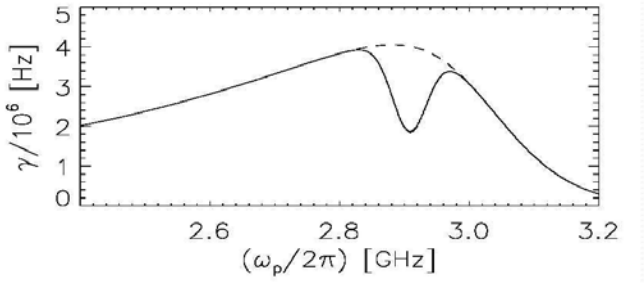

Fig. 5.17 Dependence of the total growth rate of the upper hybrid waves on the plasma frequency. The initial growth rate result corresponds to a value of s = 15. Signs of an absorption feature with a frequency bandwidth of about 60 MHz can be clearly seen (from Chen and Yan, 2008).

Taking into account the fact that absorptive spikes do not always follow type III trajectories, and that they are often a random collection of instantaneous bursts, it is natural to assume a random acceleration of small-scale beams occurs. The dimensions of the beam would then determine the instantaneous frequency band. The quenching of instability occurs only when the instability develops in the location of the beam. Then the beam rapidly leaves the region, and the emission will be restored there. Most likely, the maximum effect is achieved in the DPR conditions. Therefore, when the moving beam reaches a neighboring DPR- level, a certain space between the spikes in absorption will be formed. By this method, it is possible to explain the discrete nature of absorptive spikes. Various parameters of the absorptive spikes can be associated with different local gradients of density and magnetic field. At the beginning of the interval of bursts in absorption, the spikes in absorption were still accompanied by spikes in emission with the similar parameters (Figure 5.6a). It means that at this moment not all beams were confined in the trap. This untrapped part of the beams would have given off bursts of emission, although the beams did not move ahead further, possibly, they were reflected.

In the mildly inhomogeneous corona, the DPR- levels are the surfaces whose size perpendicular to the line of sight is more than 10,000 km. Compared to this size, the magnetic loops are very narrow and inhomogeneous in density, so that the DPR- levels in the adjacent loops cannot coincide with each other. If the beams of particles were periodically injected along one loop, then we should always see ZPs. Therefore, most likely they are injected consecutively in time and simultaneously in several loops. In cases like this, we would often observe almost random distributions of spikes in the type III-like bursts (Figure 5.11). However, if the DPR- levels almost coincide among the adjacent loops, then a smooth displacement of dark spikes would be produced, and at these moments the ZP will appear. The frequency drift of the ZP- stripes ($\approx$ 1700 MHz s^{-1}) can be explained by an appropriate displacement of the DPR- levels in the corona. Even a slow downward motion of a loop making a sharp angle with respect to the gradient of plasma frequency (which exactly occurred, according to the TRACE images in Figure 5.5) could lead to rapid lowering of DPR- levels in the corona, which will also explain the frequency drift of ZP stripes. During the resistive tearing-mode instability (see below), the condition of frozen magnetic flux is disrupted, and magnetic field line can move independently of the plasma (Aschwanden, 2004, p. 414).

The beam traveling between the DPR- levels can give impulsive contributions to the emission on the Cerenkov resonance, so that the appearance of bright ZP stripes (spikes in emission) is entirely expected (the plasma mechanism of type III bursts). The frequency drift of type III-like absorptive bursts ($\approx$ 12 GHz s^{-1}) would correspond to the speed of the electron beam not exceeding of 10^{10} cm s^{-1} in accordance with Allen's density model of the corona (see Fig. IV.1 in Krüger (1979)).

Wang et al. (2008) considered that the spikes in emission are generated by the electron cyclotron maser (ECM) mechanism. However, the majority of spikes with

right circular polarization were observed during flare brightening in the northern flare ribbon in the south magnetic polarity. Thus, the radiation mode was ordinary. Two episodes with left circular polarization were connected with the brightening in the southern flare ribbon (see the black rectangle in fig. 3b of Wang et al. (2008)) where the north magnetic polarity could be dominant. This also means the ordinary wave mode dominates, while in the ECM radiation the extraordinary mode should dominate (Fleishman and Melnikov, 1998). For this very reason the estimations of the magnetic field strength obtained by Wang et al. (2008) in the ECM model almost exceed by an order of magnitude the ones obtained by Yan et al. (2007) using the frequency separation of ZP stripes.

The simultaneous presence of bursts in emission and absorption with different drift rates (Figure 5.7c and 5.7d) testifies that at least two places of particle acceleration exist at the different heights. In accordance with Figure 5.5 (the pictures at 03:23 and 03:36 UT) we can assume that above the cusp-loop, in the course of the post-flare restoration of the magnetic structure, a magnetic island was probably formed, and particle acceleration occurred in the two current layers located above the flare cusp-loop (upward) and above the magnetic island (downward). Such an assumed scheme coincides with the sketch of the magnetic configuration proposed for this flare in fig. 8 in Guo et al. (2008).

As Schwenn et al. (2006) diligently noted, despite many decades of indirect observations suggesting the presence of a current sheet, such as soft X-ray cusp structures (Tsuneta, 1996) and horizontal inflow, direct observations of the formation and evolution of a current sheet in the solar atmosphere have been missing. Strong observational evidence for reconnection comes from the post-eruption emission and dynamics. Our radio observations also testify to the probable case for reconnection in the erupting solar corona.

The rise of helmet-shaped loops in three TRACE images at 03:02, 03:20 and 03:23 UT in Figure 5.5 allows us to propose the existence of a single X- point above the helmet-shaped loop, and the initiation of flows due to the magnetic reconnection. The consecutive flows may be associated with the formation of magnetic islands above the helmet loop. The sketch of the magnetic configuration can be similar to Figure 8 of Pick et al. (2005) as a two-dimensional cut of the three-dimensional configuration across the twisted flux rope. Similar two-dimensional magnetic configurations were often discussed in many numerical simulations (Tsuneta, 1996, Lin and Forbes, 2000, Aschwanden, 2004, and references herein). The three-dimensional flux rope is in fact anchored (line-tied) to the photosphere. The theory of three-dimensional reconnection is presented in greater detail in the book of Priest and Forbes (2000). The two-dimensional representation is mostly done for convenience, but the magnetic structure is three-dimensional (see fig. 4 in Roussev et al. (2003) for a view of the very complicated magnetic field configuration). All special features of two-dimensional reconnection enumerated in Pick et al. (2005), are also valid in our case. In the framework of an erupting flux rope, magnetic reconnection occurs behind the twisted rope. The accelerated particles form beams along the newly reconnected field lines and propagate both upward and downward.

Two places of acceleration, separated in height suggest the tearing-mode instability, in that two (or more) magnetic islands were formed and the entire activity at the post-eruptive phase is associated with the restoration of the magnetic structure.

The analysis of microwave pulsations by Tan et al. (2007) confirms such an evolution of the flare. They concluded that the flaring region consisted of many current-carrying compact loops. In each current-carrying flare loop, the resistive tearing-mode instability will trigger the formation of a series of multi-scale magnetic islands. The X-point is located between the two magnetic islands. The opposite frequency drifts of pulsations also suggest the particle acceleration occurs in the opposite directions.

The radio bursts drifting in the opposite directions in the frequency coverage of the spectrograph (Figure 5.7c and 5.7d) indicate the simultaneous existence of two places of particle acceleration in the current sheets between the magnetic islands. The fast particles moving from the higher to the lower corona are responsible for the type III burst in emission with the reverse drift. The fast particles moving from the lower to the higher corona are seized in the magnetic trap and give off the type III-like bursts in absorption with negative drift.

Karlicky and Barta (2007) found that electrons are accelerated most efficiently in the region near the X-point of the magnetic reconnection at the end of the tearing process and the beginning of the restoration of the magnetic configuration.

In this connection, all intervals of new peaks in the burst profile at the decay phase (Figure 1 in Yan et al. (2007)) were very rich in spikes of absorption, type III–like bursts consisting of spikes in absorption and usual ZPs and fiber bursts with different frequency drifts (see Figures 5.6–5.9). The appearance of ZP and fiber bursts means the loss-cone velocity distribution of fast particles inside the radio source (magnetic islands) exists.

The beams, accelerated above the flare loop would have propagated upward and fallen into the magnetic trap, where the loss-cone distribution of fast particles was already present, and would have caused bursts in absorption. The particles accelerated above the magnetic island would have probably propagated along the overlying magnetic loops downward (where the loss-cone distribution was absent). They might have simultaneously produced the reverse-drifting bursts in emission. The comparison of spectra in Figure 5.7b – 5.7d suggests a slow lift of the lower site of particle acceleration, which may have created a kind of `herringbone structure'. After ≈ 03:44:01 UT, the reverse-drifting bursts in emission were stopped by the drifting boundary (a hump of the `herringbone structure'). At higher frequencies, their continuation transformed to bursts in absorption (though their relationship is not very clear). The loss-cone distribution was probably formed there up to this moment and the quenching of instability by additional beams already became the main effect.

The difference in the parameters of these bursts in absorption (they were prolonged, broad-banded and diffuse) indicates that these beams were larger in scale and their velocity dispersion was wide (≈1). The velocity dispersion in the beams, critical for the spikes in absorption, was much less than 1. New beams with great longitudinal velocities stimulate the whistler generation at the anomalous Doppler resonance and as a consequence, the formation of ZP stripes in emission (in Fig-

ure 5.10 at 03:42:56 UT) could be explained in the whistler model (Chernov, 1996).

When the slowly drifting boundary became almost indistinguishable at 03:44:44 UT, the diffuse reverse-drifting bursts in absorption covered the whole frequency range (2.6 – 3.8 GHz), and the spikes in absorption almost disappeared. At this moment, the existence of the magnetic island must have ended.

5.3 New theories of ZPS

5.3.1 WHAT IS NEW IN IMPROVED DPR-BASED ZP THEORIES?

The mechanism proposed in LaBelle et al. (2003) can be regarded as an important step in attempts to improve the DPR-based model. The escape of the Z mode is considered at one DPR level (a point radio source), whereas the harmonics are assumed to be eigenmodes that propagate through regular inhomogeneities, such as an ion-acoustic wave. The number of harmonics is large only if density variations in the ion-acoustic wave reach ~20%. However, as was shown in Chen and Yan, (2008), it is hardly possible that such a strong ion-acoustic wave can be generated in the solar corona; in fact, the amplitude of density variations is no more than ~2%. In this case, only several ZP stripes can be generated by this mechanism, whereas up to a few tens of stripes are usually observed. In our opinion, a disadvantage of this theory is that it fails to explain the high intensity of radiation emitted by separate incoherent sources.

In the basic papers on the DPR theory (Zheleznyakov and Zlotnik, 1975; Winglee and Dulk, 1986) the velocity distribution function of fast particles was assumed to be narrow, with an infinitely small spread in velocities; therefore, calculations of the growth rates of upper hybrid waves could hardly provide a realistic picture (Chernov, 2006). Besides, Winglee, and Dulk (1986) restricted themselves by consideration of the Maxwellian distribution of particles over momentum that could significantly affect the results obtained. This was clearly demonstrated in Kuznetsov and Tsap (2007), where the following electron distribution function of the loss-cone type was chosen (see Figure 5.18):

$$f_p(p,\theta)=\varphi(p)\begin{cases}0, & \theta \le \theta_c-\Delta\theta_c \\ \dfrac{\theta-\theta_c+\Delta\theta_c}{\Delta\theta_c}, & \theta_c-\Delta\theta_c<\theta<\theta_c, \\ 1, & \theta>\theta_c\end{cases} \tag{5.3}$$

where the function $\varphi(p)$ describes the electron distribution over momentum and θ_c is the loss-cone boundary with a width $\Delta\theta_c << 1$.

In old papers, the term associated with the velocity spread, to be more exact, the spread over particle momenta ($\Delta p/p$), was left in the expression for the anti-Hermitian part of the plasma permittivity. In the course of the new analysis Kuznetsov and Tsap (2007) conclude that the non-relativistic approximation cannot be used for investigation of the generation of upper-hybrid waves at the double plasma resonance when $s >> 1$. The authors used the condition of the cyclotron resonance of waves and accelerated electrons in the form:

$$\dot{\psi}_s = \omega - \frac{s\omega_B}{\Gamma} - k_z \upsilon_z = 0 \quad , \tag{5.4}$$

where $\dot{\psi}_s$ is the time derivative of the phase difference between the waves and the gyrorotating particles, υ_z is the longitudinal component of electron velocity (υ), and $\Gamma = (1 - \upsilon^2/c^2)^{-1/2}$ is the relativistic factor.

Here, it is necessary to recall that Zlotnik *et al.* (2003) assume that the dispersion relation (A.6) is correct only inside the hybrid band. They obtained a very narrow maximum of the growth rate due to at the estimation of $\Delta k_\perp/k_\perp$, the velocity dispersion $\Delta\upsilon_\perp/\upsilon_\perp$ was missed as the infinitesimal quantity.. Zlotnik *et al.* (2003) assume also that many authors (Winglee and Dulk, 1986; Kuznetsov and Tsap, 2007) erroneously conclude that the kinetic instability of plasma waves described by the dispersion relation (A.6): $\omega^2 \cong \omega_p^2 + \omega_B^2 + 3k_\perp^2\upsilon_T^2$ - may contain several harmonics, while it is valid only inside the interval $\Delta\omega \le \omega_B$. This assertion is correct, mainly, without taking into account relativistic correction and for the strictly perpendicular propagation. Zlotnik and Sher (2009) showed that in this case the harmonics, which adjoin the hybrid band on the top, give the overstated contribution to the value of increment, and this leads to the expansion of its maximum. To answer this question, new calculations with the precise dispersion relation will only help. At least, Kuznetsov and Tsap, 2007 assert that comparison with the exact solution of the dispersion relation shows that the equation of upper-hybrid waves (A.6) describes well the behavior of the oscillation branch with normal dispersion even at $\lambda \geq 1$, including the frequencies above the hybrid band. Moreover, Robinson (1988) has shown that weakly relativistic effects (especially in the case of *slightly non-transversal propagation*) cause the branches with normal dispersion corresponding to different harmonics to reconnect to one another at $\omega \approx s\omega_B$. As a result, a single continuous branch is formed. In addition, the condition of touching of the loss-cone boundary and the resonance curve can be satisfied only for one certain value of *s*. Since the contribution of the term associated with this harmonic will considerably exceed the contribution of other terms in the sum for the loss cone with a sharp boundary (when $\theta_c \to 0$; see the follow-

ing), we can neglect the summation over harmonics and assume that the growth rate $\gamma \approx \gamma_s$, where γ_s is the growth rate at the *s*-th harmonic.

In the course of the analysis Kuznetsov and Tsap (2007) derived the final form of the imaginary part of the dielectric permeability (in the relation for γ):

$$Im\,\varepsilon_{||}^{(s)} \approx -2\pi^2 m^4 c^2 \frac{\omega_p^2}{k^2}\frac{n_b}{n_0}\Gamma^3 J_s^2\left(\frac{k_\perp p_\perp}{m\omega_B}\right)\times \left[\frac{\partial\varphi(p)}{\partial p}+\frac{\varphi(p)tan\,\theta_c}{p\Delta\theta_c}\left(\frac{s\omega_B}{\Gamma\omega sin^2\theta_c}-1\right)\right]\frac{\Delta p_z}{p} \qquad (5.5)$$

where the momentum $\mathbf{p} = (p_z; p_\perp)$ and the parameter Γ correspond to the point of tangency $p_{\perp 0} = p_{z0}\ tan\,\theta_c$ (see Figure 5.18); $J_s(\xi)$ is the first-order Bessel function.

The derivation of Formula (5.5) somewhat differs from the corresponding procedure in the work of Zheleznyakov and Zlotnik (1975) because of another normalization condition for the function $f\mathbf{p}(\mathbf{p})$ and a misprint in the tensor of the dielectric permeability by the coefficient in front of the matrix (which contains the relativistic electron mass ($\tilde{m}$) rather than the rest one (see Appendix in Kuznetsov and Tsap (2007).

As a result of calculations, for the Maxwellian distribution of particles over momentum ($\varphi_1(p) = A_1 exp(-p^2/2p_h^2)$) of the loss-cone type (5.3) and real values of the velocity spread (~0.1), the modulation depth between the peaks of the growth rates turns out to be too small. However, calculations performed with a power-law velocity distribution function with an index of power of 8–10 yielded a modulation depth that was quite sufficient for the ZP formation at many harmonics (Figure 5.19).

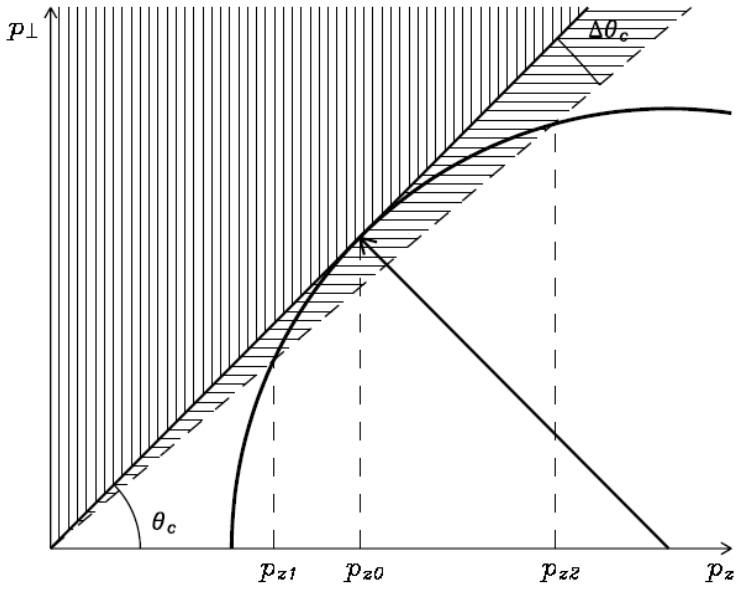

Fig. 5.18 Schematic of the loss-cone distribution and the resonance curve in the space of electron momenta (from Kuznetsov and Tsap, 2007).

A steep power-law spectrum of particles can be considered as an analog of a small velocity dispersion, although such spectra are sometime observed, especially in repeated bursts of hard X-ray emission (data from RHESSI).

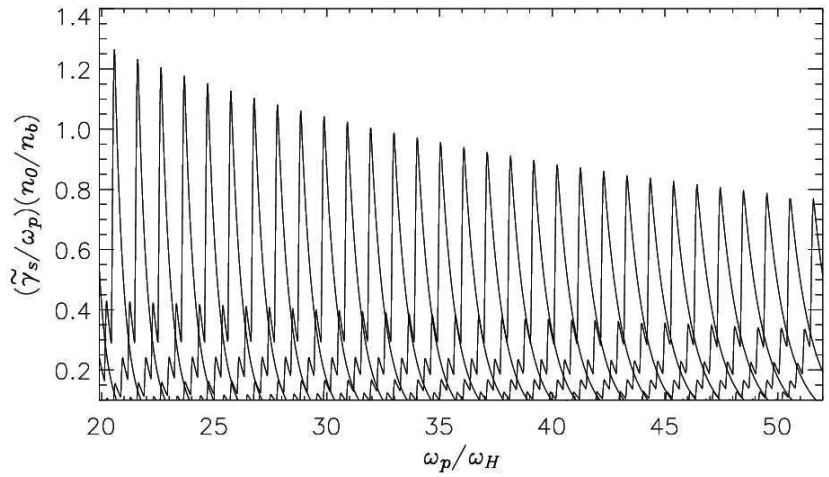

Fig. 5.19 The dependence of the maximal growth rate of upper-hybrid waves on the plasma parameters for the power-law distribution of electrons over momentum (from Kuznetsov and Tsap, 2007).

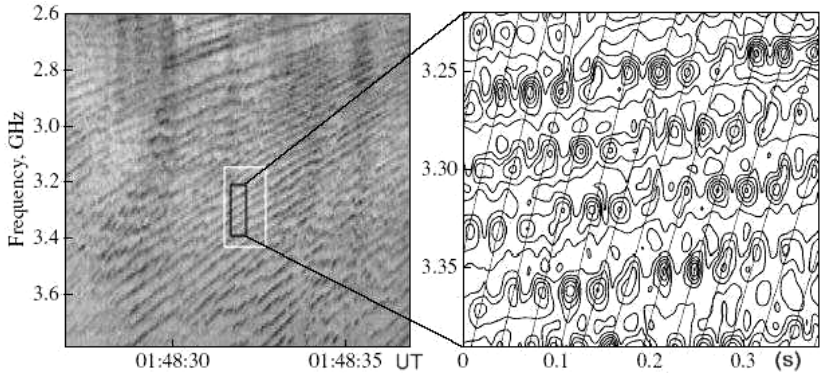

Fig. 5.20 ZP in the frequency range 2.6–3.8 GHz in the event 2002 April 21. The magnified fragment of the spectrum (on the right) demonstrates the superfine structure of stripes in the form of periodic millisecond spikes, which, for better visualization, are shown by contour levels of the intensity (adapted from Kuznetsov, 2007).

Kuznetsov and Tsap (2007) and Kuznetsov (2007) applied their results to interpret 34 ZP stripes with a superfine structure in the form of millisecond spikes in the 2.6–3.8 GHz frequency range (Figure 5.20) under the assumption that the elec-

tron beams were generated strictly periodically. It is important to note that the straight lines, which connect spikes in the adjacent ZP stripes (in the right panel in Figure 5.20) can be drawn at any inclination. Thus, the velocity of beams can be any value, and it is selected arbitrarily.

However, if we consider the possibility of simultaneous excitation of waves at 34 DPR levels in the corona, assuming that the plasma density depends on the altitude by the conventional barometric formula $f_P = f_{P0} \exp[-(h - h_{B0})/10^4 T]$ and the magnetic field, by the formula derived in Dulk and McLean (1978) from the radio data, $B = 0.5\ (h / R_s)^{-1.5}$ where R_s = is the Sun's radius, then we obtain that 34 DPR levels extend in the corona up to altitudes of ~65000 km, which, according to current knowledge, correspond to the plasma frequency ~250 MHz.

We calculated the DPR levels shown in Figure 5.21 by using a barometric formula with the commonly accepted coronal plasma parameters: the electron temperature $T_e = 1.2 \cdot 10^6$ K and the initial plasma frequency $f_{P0} = 3800$ MHz at the altitude $h_{B0} = 20000$ km. If we use a dipole dependence of the magnetic field for cyclotron harmonics, then the DPR resonances at harmonics with $s \geq 50$ will occur at altitudes higher than 100000 km. Thus, the simultaneous excitation of waves at 34 levels in the corona is impossible for any realistic profile of the plasma density and magnetic field (if we do not assume it to be smaller, on the order of magnitude of the local density and magnetic field scale heights). For example, if we assume that the magnetic field decreases with altitude more slowly (see, e.g. fig. 55 in Zheleznyakov (1995)), then there will only be a few DPR levels at low harmonics. It should be noted that, as a rule, only the first several cyclotron harmonics are easy to excite, whereas the excitation of harmonics with $s > 50$ is hardly possible.

In this connection, let us note that in the following paper (Kuznetsov, 2008) the author proposed an alternative mechanism: a model in which the superfine temporal structure is formed due to modulation of the radiation by downward propagating MHD- oscillations. The wavelet analysis shown a decrease of the period of spikes (from 40 ms at 2.6 GHz to 25 ms at 3.8 GHz). Variation of the observed period of oscillations is caused by a variation of the speed of the DPR levels (due to the Doppler effect). It was found that in the considered event on 2002 April 21 the MHD oscillations should have a period of about 160 ms and a speed of about 1500 km s^{-1}. This model allows us to explain the observed variation of the pulse period with the emission frequency.

At the same time, the frequency drift rate of the zebra stripes (increasing with an increase of the frequency from 60 to 160 MHz s^{-1}) was explained by the upward moving DPR levels. The observed polarization degree was connected with a partial depolarization when the emission propagates through a region with a transverse magnetic field. Both of these last effects were often used in many other papers (other events). However, there cannot be an universal interpretation because the frequency drift is often oscillating (like a saw-tooth) and the degree of polarization may be very different (sometimes with a change of sign during the event).

However, the superfine stripe structure in the form of millisecond spikes is apparently produced during the generation of the primary continuum radio emission,

rather than arising in the course of ZP formation. This is confirmed by the detailed analysis of the time evolution of the spectral amplitudes of continuous radiation several seconds before the appearance of the ZP. It is seen from Figure 5.22 that, when there is no yet regular ZP stripes, the time dependence of the radiation intensity at the frequency 3.19 GHz clearly exhibits regular spikes with a period of ~30 ms. This period is then present in the ZP (see Figure 5.20). Thus, the superfine structure is not a consequence of wave excitation at DPR levels.

The superfine structure was also observed in the meter wavelength range. It was shown in Chernov et al. (1998) that such a spiky structure can arise due to periodic acceleration of fast particles provided that the simultaneous splitting of the ZP stripes is caused by the excitation of whistlers under the conditions of normal and anomalous Doppler effects (new beams).

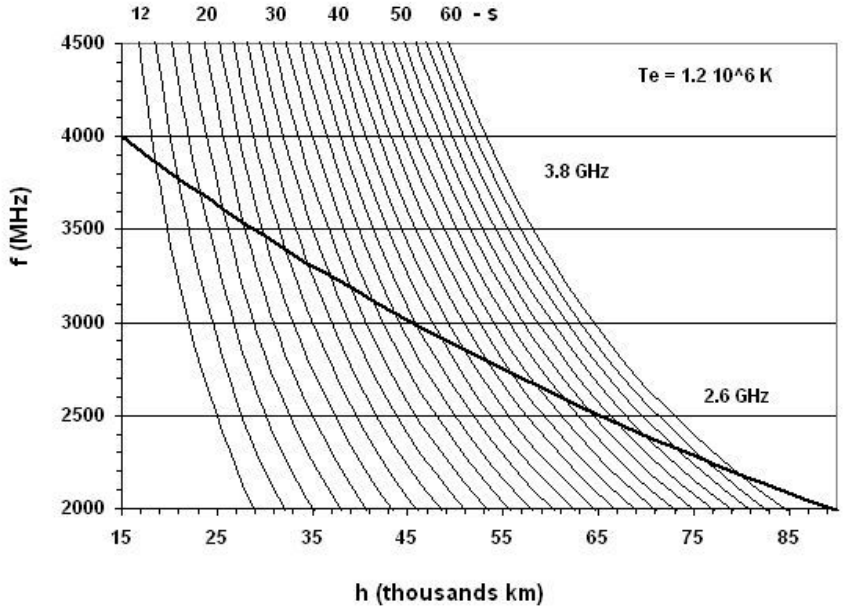

Fig. 5.21 Altitude dependence of the plasma frequency in accordance with the barometric law (heavy line) and altitude profiles of the electron cyclotron harmonics *s* (light lines) in the solar corona. For the electron temperature $T_e = 1.2 \cdot 10^6$ K and initial frequency $f_{P0} = 3800$ MHz at an altitude of $h_{B0} = 20\,000$ km, 34 DPR levels form between 2600 to 3800 MHz plasma layers (from Laptuhov and Chernov 2009).

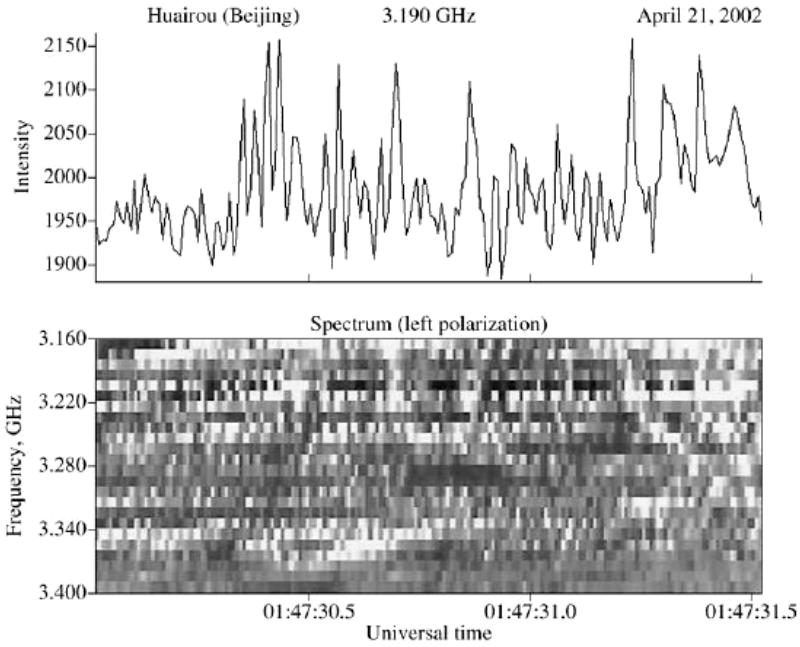

Fig. 5.22 Superfine structure of the continuum in the form of spikes with a period of ~30 ms (from Laptuhov and Chernov 2009).

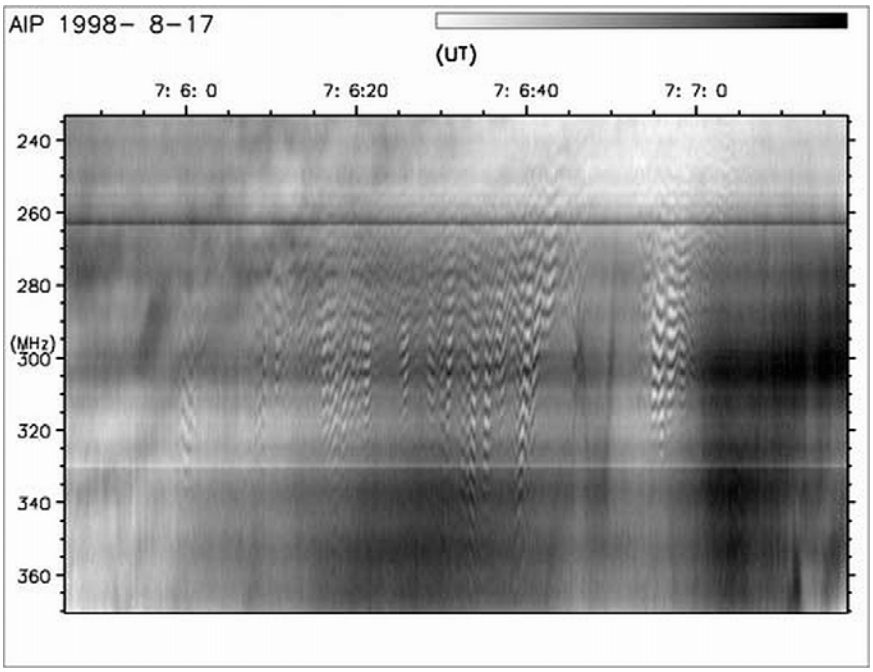

Fig. 5.23 Dynamic radio spectrum with zebra patterns in fast drifting envelopes recorded on 17 August 1998 by the spectrograph of the Astrophysical Institute Potsdam (from Zlotnik et al. 2009).

Zlotnik et al. (2009) give an analysis the occurrence of zebra patterns in a fast drifting envelopes of continuum absorption, based on radio spectra of the Astrophysical Institute Potsdam shown in Figure 5.23. For the explanation of ZP in fast drifting (type III burst-like) envelopes it is proposed to consider complementary multinonequlibrium components of the coronal plasma in the DPR model. ZPs should be related with the emergence of fast particle beams. But prior to the electron beam emergence, the nonequilibrium plasma consists of two components: one having a loss-cone distribution f_1 with velocity υ_1 and causing the background continuum and another one f_2 of DGH type (Dory, Guest, and Harris, 1965) with velocity υ_2 being able to provide the DPR effect and thus causing the ZP.

The loss-cone component is denser and cooler than the DGH component. Thus, for many reasons the stronger continuum can dominate the zebra pattern, making it invisible on the dynamic spectrum. If the electron beam emerges, it fills the loss cone, quenches the loss-cone instability (according to Zaitsev and Stepanov (1975)), and causes a type III-like burst in absorption. The switch-off of the continuum during electron beam passage makes the zebra pattern visible against the absorption burst background. Some specific parameter conditions should be fulfilled:

- for the zebra structure excitation by the DGH component f_2 ($\upsilon_2/\upsilon_T \sim 15 - 30$) there exist reasonable intervals of velocity $\upsilon_1 \sim (1/6 - 1/2)\ \upsilon_2$ and electron number density $N_2 < N_1 < (10^2 - 10^7)N_2$ for the component f_1 where the proposed generation scheme is valid;

- $N_b >> N_1$ is a necessary condition for the absorption burst;

- the proposed scenario is only valid if the beam velocity ($\upsilon_b \approx c/3$) is much greater than the bulk velocity of electrons at the loss cone ($\upsilon_2/\upsilon_1 \approx 3 - 6$) but the beam does not excite plasma waves.

- the beam electrons with great longitudinal and small transverse velocities fill the loss cone, while the electrons with great transverse and small longitudinal velocities enrich the DGH function f_2 with additional electrons, then an enhanced brightness of zebra stripes is observed.

If even one of these conditions is broken, the ZP can hardly appear. The authors conclude that the described scheme quite naturally explains the (at first glance enigmatic) appearance of a zebra pattern during electron beam passage without a type III burst in emission. However, two distributions (DGH and loss-cone) can exist simultaneously but rather in different places of the radio source.

Besides, it should be assigned several properties of ZP stripes in the spectrum, not noted in Zlotnik et al. (2009). Not all the type III-like envelopes have negative frequency drift, it is possible to note almost instantaneous in the broadband (07:06:31 UT) or even with the positive drift (07:06:25 UT). ZP is visible between the envelopes. It is possible to trace continuous ZP stripes lasting through five envelopes with the spasmodically changing drift. ZP is only strengthened during the envelopes and it is experienced the sharp jumps of drift (by zigzags).

Such almost vertical pulsating envelopes of ZP are not so rare phenomena. For instance, let us see an excellent sample in Figures 6C in Slottje (1972). And in the event 3 July 1974 similar ZP envelopes were continuing during several hours (Slottje ,1981; Chernov, 1976b). Smooth or abrupt changes in the frequency drift of ZP stripes in the event 25 October 1994 were discussed in Chernov (2005) on the basis of the natural mechanism of the formation of stripes in absorption due to the diffusion of fast particles on whistlers. The whistler waves are always generated simultaneously with the plasma waves at upper hybrid frequency by fast particles with the loss-cone velocity distribution. This diffusion process is examined in Chernov (1990b) and in more detail in Chernov (1996; 2005). The important feature was there noted: the changes in the sign of the frequency drift correlate with the change in the direction of the spatial drift of the ZP radio source (see Figure 4.32 and 4.64). The loss-cone distribution function changes due to the diffusion and the whistler generation switches from normal Doppler resonance to anomalous one. In such a case whistler group velocity changes the direction to the opposite, which results the change of the sign of the frequency drift of ZP stripes. Additional particle injection can only accelerate this process and strengthen the instability of whistlers, with which can be related the strengthening of ZP in drifting envelopes in the event examined in Zlotnik et al. (2009).

Thus, in the model with the whistlers the absorptive ZP stripes are formed also due to the quenching of the loss-cone instability, but due to only the scattering of fast particles on whistlers and only in the whistler wave packet volume. This

mechanism explains the spasmodically changing frequency drift, and it does not require any complementary strict specific parameters.

The appearance of absorptive bursts depends strongly of parameters of new beams. Chen and Yan (2008) shown that the large scale beams with longtime injection (~ 1 s) are responsible for broadband type III- like absorptive bursts, and only the small scale beams with very short injection time (~ 0.2 ms) could be responsible of absorptive spikes (see Figure 5.17). New beams with great longitudinal velocities enrich the whistler generation at anomalous Doppler resonance (Chernov, 1996) and as a consequence, the formation of ZP stripes. This explains strengthening of ZP- stripes during drifting envelopes (Figure 5.23). We could propose the same effect includes in bright ZP stripes in absorptive type III- like bursts in the event 13 December 2006 (Figure 5.12). However, in such a case the whistler generation and as a consequence, the formation of ZP stripes depends strongly also of the velocity distribution in the new beams.

In the recent small critical review of Zlotnik (2009) the advantages of DPR model and the main failures of the model with whistlers are refined. The author asserts that the theory based on the DPR effect is the best-developed theory for ZP origin at the meter-decimeter wavelengths at the present time. It explains in a natural way the fundamental ZP feature, namely, the harmonic structure (frequency spacing, numerous stripes, frequency drift, etc.) and gives a good fit for the observed radio spectrum peculiarities with quite reasonable parameters of the radiating electrons and coronal plasma. The statement that the theory based on whistlers is able to explain only a single stripe (e.g., a fiber burst) was made in Zlotnik (2009) without the correct ideas of whistler excitation and propagation in the solar corona.

First of all, Zlotnik uses a wrong term “oscillation period” of whistlers. Actually, the loss-cone particle distribution is formed as a result of several passages of the particles in the magnetic trap. But the whistler amplification length is always small (of $\leqslant 10^8$ cm in comparison with the length of the magnetic trap of $>10^9$ cm) for any energy of fast particles (Breizman, 1987, Stepanov and Tsap, 1999). According Gladd (1983) the growth rate of whistlers for relativistic energies of fast particles decreases slightly if the full relativistic dispersion is used. In this case, the whistlers are excited by anisotropic electron distributions due to anomalous Doppler cyclotron resonance. Thus, our conclusion, that the entire magnetic trap can be divided into the intermittent layers of whistler amplification and absorption remains valid for a broad energy range of fast particles.

In Zlotnik (2009) the main matter is ignored that the model involving quasilinear interaction of whistlers with fast particles allows one to explain all the fine effects of the ZP dynamics, mainly the superfine structure of ZP stripes and oscillating frequency drift of the stripes synchronously with the spatial drift of radio sources.

5.3.2 MODELS OF ZP FORMATION DURING RADIO WAVE PROPAGATION IN THE CORONA

Let us consider the capabilities of alternative models. One of the first such models was proposed in Laptuhov et al. (2005) and further developed in Laptuhov and Chernov (2006), where a one-dimensional inhomogeneity was considered in which the plasma and field parameters varied periodically in space along one coordinate x with a period $L_x = L$ (e.g., in the presence of nonlinear thermal structures) and the magnetic field $\mathbf{B} = (0, 0, B)$ was perpendicular to the inhomogeneity gradient and directed along the z axis.

The wave equation obtained from Maxwell's equations and hydrodynamic equations for the perturbed velocity of electrons and ions in a cold nonuniform magnetoactive plasma yields a generalized vector equation for the perturbed electric field, which has separate solutions for ordinary and extraordinary waves. The problem is reduced to deriving the corresponding dispersion relations in a spatially inhomogeneous medium in which the profiles of both the plasma density and magnetic field are approximated by stepwise functions. An analysis of the solutions to this problem revealed the existence of transparent regions separated by opaque regions of different width depending on the inhomogeneity scale L.

Thus, the dark ZP stripes observed in the radio emission spectrum can form due to the existence of opaque regions in a spatially periodic medium. The frequency separation between transparent regions increases with frequency (in agreement with observations). The number of harmonics grows with increasing amplitude of the inhomogeneity, but is independent of the ratio of the plasma frequency to the gyrofrequency in the source. This may help to overcome all the difficulties in explaining the large number of ZP stripes and small values of the magnetic field determined from the frequency separation of stripes (e.g., in the DPR-based model).

Practically at the same time, Barta and Karlicky (2006) analyzed a similar problem in which the formation of harmonics during the propagation of a wave through regular inhomogeneities (such as oscillations behind a shock front) was considered in a simplified approach. The wave equation was written for an unmagnetized plasma, the dispersion relations for harmonics were not derived, and solutions for the amplitudes of reflected and transmitted waves were searched. From the conservation laws and boundary conditions admitting the existence of nontrivial solutions, the frequency dependence of the transmission coefficient was found. As a result, multiple narrow harmonics (transmission regions, called interference stripes) separated by opacity (reflection) regions were obtained. In view of analogy with the results of Laptuhov and Chernnov (2006), it is worth comparing the parameters of transmission regions obtained in these two papers.

In Ledenev *et al.* (2006), a similar problem was considered in an even simpler approach in which the interference pattern produced by the incident rays and those reflected from regular inhomogeneities was analyzed. The problem was solved in the geometrical optics approximation by using the eikonal equation (by analogy with the problem of light propagation through a crystal lattice). The size of the radio emission source was assumed to be infinitely small, and the emission spectrum was considered to be sufficiently broad. Evidently, in case of radio wave reflection from smooth inhomogeneities, the interference pattern cannot be as contrast as that produced by light reflected from a solid body. Moreover, the ordinary and extraordinary waves are reflected from layers with different plasma densities. Therefore, the modulation depth of the total interference pattern produced by many small-size sources is relatively small.

In Laptuhov and Chernov (2006), the propagation of electromagnetic waves through a spatially periodic plasma was investigated to explain the ZPs observed in solar radio bursts. The possibility of existence of one-dimensional spatially periodic structures in the solar atmosphere was demonstrated in Kovalev (1990); Laptuhov (1991). Laptuhov and Chernov (2006) assumed that the waves propagate in a unbounded collisionless plasma along the x axis perpendicular to the magnetic field $\mathbf{B} = (0, 0, B(x))$.

In Laptuhov and Chernov (2009), a more realistic model in which a spatially periodic plasma occupies a region of thickness NL containing N identical plasma layers of thickness L was consider. For simplicity, each layer is assumed to consist of two piecewise-homogeneous layers with the thicknesses $a < L$ and $b = L - a$. In the regions $x < 0$ and $x > NL$, the plasma is uniform.

Let us consider the propagation of broadband radio emission in such a plasma. As a matter of fact, the region occupied by the spatially periodic plasma is a frequency filter with multiple transparency windows separated by opaque regions (see Figure 1 in Laptuhov and Chernov (2006)). If a broadband radiation is incident at the filter input ($x = 0$), then, at the output ($x = NL$), the radiation spectrum will contain only the frequencies that correspond to the transparency windows of the filter, while the amplitudes of waves with frequencies corresponding to opaque regions will be practically zero. As a result, after passing through such a filter, a structure similar to the ZP observed in the solar radio spectrum will form. This is the essence of the physical mechanism that was proposed in Laptuhov and Chernov (2006) to explain the ZP formation in solar radio emission. In this case, the mechanism for the generation of primary broadband radio emission can be arbitrary (e.g., beam – plasma or cyclotron loss-cone instability (Zheleznyakov, 1995).

Let us first analyze the propagation of an ordinary wave, the field of which is described by the following simple formula (see Eq. (8) in Laptuhov and Chernov (2006)):

$$\frac{d^2E}{dx^2} + k^2E = 0, \quad k^2 = \frac{\omega^2 - \omega_p^2}{c^2}, \quad \omega_p^2 \equiv \omega_e^2 + \omega_i^2 \tag{5.6}$$

The plasma frequency $\omega_p(x)$ and the corresponding constants k_m in different plasma regions are defined by the formulas

$$\begin{aligned}
&\omega_p(-\infty < x < 0) = \omega_0, \quad \omega_p(NL < x < \infty) = \omega_3, \\
&\omega_p((n-1)L < x < a + (n-1)L) = \omega_1, \quad n = 1,2...N, \\
&\omega_p(a + (n-1)L < x < nL) = \omega_2, \quad \omega_0 \geq \omega_3 \geq \omega_1, \\
&k_m \equiv \sqrt{(\omega^2 - \omega_m^2)}/c, \quad m = 0,1,2,3.
\end{aligned} \tag{5.7}$$

where all of the four frequencies ω_j, ($j = 0,1,2,3$) are constant. In this case it is assumed that in the regions $x < 0$ and $x > NL$ the plasma is uniform, and between them $(0 < x < NL)$ it is located N of the identical layers, each of which is piecewise-uniform and has a thickness L. Let an electromagnetic wave with the frequency $\omega > \omega_0$ propagates along the x axis in the region $x < 0$. Then, taking into account wave reflection from the region $0 < x < NL$, a general solution to Eq. (5.6) in the region $x < 0$ can be written as

$$E(x < 0) = E_0 \exp(ik_0 x) + E_r \exp(-ik_0 x), \tag{5.8}$$

where E_0 is the amplitude of the incident wave, which is assumed to be given, and E_r is the amplitude of the reflected wave.

In the region $x > NL$, there is only the transmitted wave. Therefore, in this region, we have

$$E(x \geq NL) = E_t \exp(ik_3(x - NL)), \tag{5.9}$$

After simple manipulations, we obtain the transmission and reflection coefficients

$$K_t \equiv mod\left(\frac{k_3 E_t^2}{k_0 E_0^2}\right), \quad K_r = mod\left(\frac{E_r^2}{E_0^2}\right) = 1 - K_t, \tag{5.10}$$

By definition, the coefficient K_t is equal to the ratio of the intensity $\mathbf{Q} = c[\mathbf{E},\mathbf{B}]/4\pi$ of the transmitted wave to that of the incident wave. It can easily be shown that the coefficient of reflection from N inhomogeneous plasma layers is $K_r = 1 - K_t$.

Note that the results obtained can also be generalized to the case of extraordinary waves described by Eq. (17) in Laptuhov and Chernov (2006) (cf. Eq. (5.6)). Below, we will consider some examples of calculating the reflection and transmission coefficients for different parameters of plasma inhomogeneities.

The number of stripes and their shape depend on the parameters (such as the size and number) of inhomogeneities. The profile of the harmonics of the reflection coefficient in the form of narrow peaks separated by a relatively wide frequency intervals (see Figure 5.24) can be interpreted as radiation stripes similar to those present in the lower spectrum in Figure 4.16. Thus, in this case, the ZP is probably observed in reflected radiation. Note that the harmonics of the reflection coefficient in Figure 5.24 agree better with observations than the results of similar calculations in Barta and Karlicky (2006) presented in Figure 5.25. In our case, this is an even comb of harmonics in which the frequency separation between neighboring harmonics increases gradually with frequency, whereas in Barta and Karlicky (2006), intense harmonics alternate with weak ones. Presumably, inhomogeneities in the form of density dips, which were considered in Barta and Karlicky (2006), cannot provide the observed widths of the ZP stripes. Moreover, we take into account the magnetic field and harmonics of an ordinary wave agree better with observations.

For a smaller number of larger inhomogeneities with a = 45 m, the frequency profile of the transmission coefficient (see Figure 5.26) yields nearly symmetric harmonics, which are most frequently observed (see the upper spectrum in Figure 4.16).

Figure 5.27 shows the results of calculations of the transmission coefficient in the microwave range. It is seen that, after passing through inhomogeneities with a thickness of L = 3 m, the spectrum of ordinary waves consists of symmetric harmonics, the frequency separation between which increases gradually with frequency, which agrees with observations. The sufficiently large number of harmonics are produced when the number of inhomogeneities is >10.

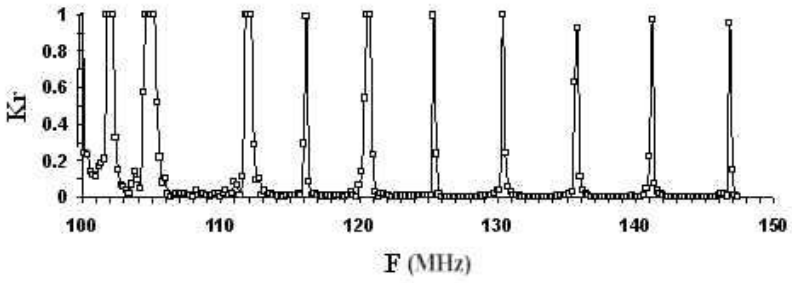

Fig. 5.24 The reflection coefficient K_r of ordinary waves as a function of the frequency F for $n_1 = n_2 \cdot 0.84 = n_3$, $n_0 = n_2$, $a = b$ = 10 m, $n_2 = 1.2d + 8$, and N = 50 (from Laptuhov and Chernov, 2009).

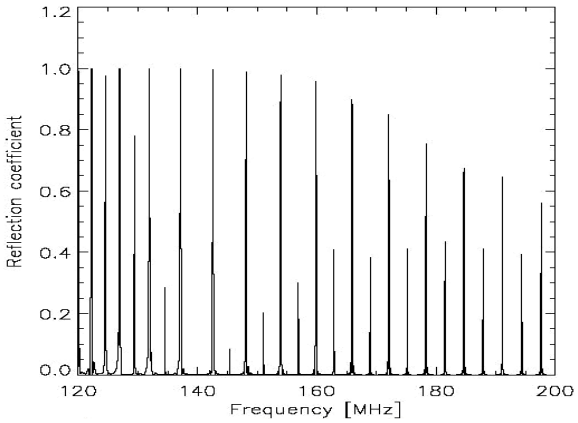

Fig. 5.25 The reflection coefficient $R = 1 - T$ for the series of 50 density wells finished by the density drop as a function of the frequency of an incident wave (from Barta and Karlicky, 2006).

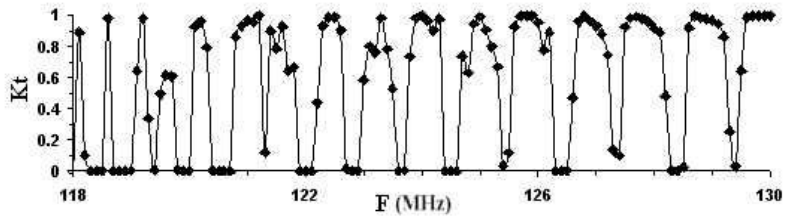

Fig. 5.26 The transmission coefficient K_t of ordinary waves as a function of the frequency F for $n_0 = n_3 = 1d + 8$, $n_2 = 1.5n_0$, $n_1 = n_2/2$, $a = 45$ m, $b = a$, $N = 10$, and $B = 5$ G (from Laptuhov and Chernov, 2009).

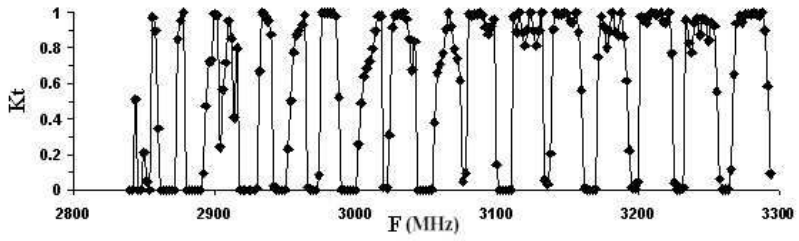

Fig. 5.27 The transmission coefficient K_t of ordinary waves as a function of the frequency F for $n_1 = n_2/\alpha$, $n_0 = 2n_2/(1 + \alpha) = n_3$, $b = L/(1 + \alpha)$, $a = \alpha b$, $L = 3$ m, $\alpha = 2$, $n_2 = 1.0d + 11$, and $B = 100$ G (from Laptuhov and Chernov, 2009).

Some concluding remarks

An analysis of the difficulties arising in different models shows that the improvement of these models necessitates imposing new stringent conditions on the parameters of plasma and waves in the source. The simplest model is related to the propagation of radio waves through regular inhomogeneities, because inhomogeneities are always present in the solar corona. However, for cm range the effectiveness of this model requires inhomogeneities with the sizes of several meters. Such scales can be produced by ion-acoustic waves or the oscillator structure of the density and the magnetic fields behind the shock wave front. Existence of such waves in the flare region with the magnetic reconnection is completely probable. The alternative mechanism of the formation of small-scale heterogeneities could be the tearing-mode instability of the current-carrying loops in the process of the magnetic reconnection (Tan, 2010). In this case, the dynamics of ZP stripes (variations in the frequency drift, stripe breaks, etc.) may be associated with the propagation of inhomogeneities, their evolution, and their disappearance.

The observed frequency difference between neighboring ZP stripes increases with frequency. This corresponds to the propagation of ordinary waves, the electric field of which is parallel to the unperturbed magnetic field, through a spatially periodic plasma. The number of discrete harmonics does not depend on the ratio of the plasma frequency to the gyrofrequency in the source. The latter circumstance can eliminate all the difficulties that arise in explaining the large number of ZP stripes and the small magnetic field value determined from the frequency separation of stripes (e.g., in the DPR based model).

The superfine structure observed in the microwave range, when all the continuous emission consists of spikes (Figure 5.20), indicates the presence of plasma wave – whistler interaction in the pulsed regime of whistler interaction with ion acoustic waves in the radio emission source generating ordinary waves (this mechanism was considered in Chernov et al. (2003)). An alternative source of pulsed radio emission may be associated with plasma density pulsations caused by the propagation of a finite amplitude wave. The generation of electron cyclotron maser radiation, which is considered a possible cause of the observed spikes Fleishmann and Mel'nikov (1998), is dominated by extraordinary waves.

5.3.3 OTHER RECENT MODELS

Nonlinear periodic space – charge waves in plasma

Kovalev (2009) have investigated periodic nonlinear waves that can arise in plasma due to the excitation of potential oscillations by accelerated electrons with unstable distributions. As was noted in Kovalev and Petviashvili (1994), one- dimensional single-peak distributions of accelerated electrons are most likely to exist in the solar flare plasma. Such electron distributions excite resonance Langmuir oscillations with frequencies $\omega_2 < \min\{\omega_B, \omega_P\}$, due to the anomalous Doppler resonance. Low- and high- frequency modes of Langmuir oscillations can form large-amplitude periodic nonlinear waves. The corresponding spectrum of electromagnetic waves excited resonantly by the current of a potential wave is calculated. It is shown that an equidistant spectrum of electromagnetic radiation in plasma can form in the presence of a periodic potential wave.

Thus, the radio emission harmonics can be generated directly in the source in the form of a nonlinear periodic space charge wave in plasma. In Kovalev (2009), a solution in the form of such a wave propagating in a magnetic field was obtained in the hydrodynamic approach (without taking into account wave dispersion). The spectrum near the breaking point, in the vicinity of which the number of harmonics increases substantially, was calculated. Due to electron bunching, the periodic wave with the spatial period $l = 2\pi u/\omega_2$ has the form of spatially alternating negatively and positively charged layers with an increased and a decreased electron density. In the presence of a wave electric field, the accelerated particles are subject to additional periodic acceleration and deceleration, due to which an electromagnetic wave is generated.

For a sufficiently large amplitude of density oscillations (a), a large number of harmonics with the frequency separation close the electron-cyclotron frequency can be excited. The number of these harmonics is determined by the parameter $N = \dfrac{3}{2^{3/2}(1-a)^{3/2}}$, characterizing the degree of nonlinearity. Thus, for $a \sim 0.9$, we have $N \approx 34$. Since the radio emission can be generated in a relatively small-size source, the key difficulty of the DPR-based model, namely, the excitation of a large number of harmonics in a distributed source, is overcome (Figure 5.20). The number of harmonics can be fairly large when one of the plasma oscillation modes is dominating. In this case, the amplitudes of harmonics decrease fairly slowly ($\propto s^{-1/3}$) with increasing harmonic number s.

Due to inverse processes, the energy of background electromagnetic waves can transform into the energy of potential oscillations at the resonance frequencies $s\,\omega_2$. This can lead to the formation of an absorption zebra pattern consisting of stripes with a depressed radiation intensity.

The efficiency of the quite natural mechanism associated with nonlinear space charge waves depends on whether strong nonlinearity is reached; however, conditions for achieving the nonlinear regime were not considered in Kovalev (2009). The nonlinearity should rapidly increase and disappear in the course of wave-breaking (at $a = 1$).

The new alternative mechanism of the ZP due to development of explosive instability in the system beam – plasma

Observations of ZP during the powerful flares make possible to assume that the particle acceleration to the relativistic velocities and excitation of different wave modes occurs in the radio source. Therefore, probably, it should be take into account other possible interactions of waves and particles. For example, into Fomichev and Fainshtein (1981) was proposed the decay instability of whistlers to the harmonics of the ion sound, which have weak spatial dispersion and small damping at frequencies much less than the ion Langmuir frequency ω_{0i}. In Fomichev *et al.* (2009) an alternative mechanism of ZP is discussed, due to the development of explosive instability in the system weakly–relativistic beam – nonisothermic plasma. The explosive instability appears in the nonequilibrium system, where there are waves of negative energy (Kadomtsev, *et al.* 1964), moreover in the resonance triplet negative energy must possess the wave of the highest frequency of ω_3, and two lowest waves ($\omega_{1,2}$) have positive energy. Fomichev *et al.* (2009) have shown, that the mechanism of the generation of the ion-acoustic "saw" as a result of the development of explosive instability in the system the weakly-relativistic flow of protons – strongly nonisothermic plasma is more effective in the energy sense.

The number of harmonics of ionic sound *n* is determined by two factors: 1) the dispersion of ion sound must be sufficiently small [1]); 2) $\nu_{ef} << \omega$ (ω – the angular frequency of sound), i.e., the *n*- harmonic of sound must weakly attenuate.

The quasi-hydrodynamic approximation was utilized for describing interaction of the particles of the beam and plasma (Fainshtein and Chernova, 1996; Ginzburg, 1967). Linearizing the hydrodynamic equations for the processes of ~ *exp(i ω t–ikx)*, a dispersion equation for the system the flow–plasma was obtained:

$$1-\frac{\omega_{0\mathrm{i}}^2}{\omega}-\frac{\omega_{0\mathrm{i}}^2}{c_{\mathrm{s}}^2k^2}-\frac{\omega_{0\mathrm{s}}^2}{(\omega-kV_0)^2\left(1-\frac{\omega-ck}{3ck}\right)}=0, \qquad (5.11)$$

where $\omega_{0\mathrm{s}}^2=4\pi e^2 N_{0s} M_0^{-1}$, $\omega_{0i}^2=4\pi e^2 N_0 M^{-1}$; ω is the cyclic frequency, *k* is the wave number; *e, M₀, M* – electron charge, the rest mass of ion beam, the mass of the ion of the plasma; $\overline{\rho}_s = N_{0s} + \rho_s$; $\overline{V}_s = V_0 + V_s$; ρ_s, V_s, ρ_i, V_i –

[1]) $n^2 q^2 c_s^2 \ll \omega_{0i}^2$; q – wave number of the base ion-sound mode; c_s – ion-sound speed ($c_s^2 = æT_e M^{-1}$), M – ion mass , $æ$ – Boltzmann constant.

the deviation respectively of ion concentrations of beam, speed of the ions of beam, concentration of the ions of plasma, velocity of the ions of plasma from their equilibrium values N_{0s}, V_0 , N_0 , 0. With $V_0/c_s >> 1$, $N_{0s}/N_0 << 1$ from (5.11) the approximate dispersion equations were obtained:

$$\omega_1 \equiv \Omega \approx c_s k_1 \equiv c_s m q; \tag{5.12}$$

$$\omega_{3,2} - k_{3,2} V_0 \approx \mp \omega_{0s} + \delta; \frac{\delta}{\omega_{0s}} << 1. \tag{5.13}$$

Equation (5.12) describes the ion-acoustic wave (energy positive), and (5.13) - slow (ω_3 , negative energy) and rapid (ω_2 , positive energy) beam waves. The number $m > 0$- is selected from the escape condition of radio emission from the corona. It is easy to determine, that for the slow beam wave (ω_3 , k_3), the fast beam wave (ω_2 , k_2) and the sound (Ω , q) the conditions of synchronism are satisfied (Tsytovich, 1970). From the conditions of synchronism taking into account (5.12), (5.13) we will obtain:

$$mq \approx 2\omega_{0s} V_0^{-1} \tag{5.14}$$

Since the sound has weak dispersion, the cascade process is possible:

$$mq + mq \to 2mq + mq \to 3mq + mq \ldots mnq \cdot$$

Then, after decomposing nonlinear terms up to the quadratic terms and after using standard procedure in the weak turbulence (Weiland and Wilhelmsson, 1977; Tsytovich, 1970), the shortened equations for the complex amplitudes of coupling modes are obtained: beam modes $a_j \ (j = 1,2)$ and ion sound $b_k \left(k = 1,2,\ldots mn\right)$.

The analysis of interaction coefficients showed that the systems of such equations describe the stabilized “explosion” (Fainshtein, 1976).

It is shown also, that the increment of the growth of ion sound in this case exceeds considerably the values, obtained in Fomichev and Fainshtein (1981). Therefore the mechanism in question occurs much more effective.

The generable sound is scattered on the fast protons, which move with a speed of $V \sim V_0 \sim 10^{10}$ cm s^{-1} and according to the mechanism, described in Fomichev and Faishtein (1981), the radiated from the source frequency of $\omega^t \approx mqnV$, and frequency separation between the stripes $\delta\omega^t = mqV$. Taking into account the equation (21) and selected parameters ($N_0 \sim 5 \cdot 10^9$ cm^{-3}, $N_s \cdot N_0^{-1} \sim 10^{-3}$, the constant magnetic field ~ 30 G) we obtain for the emission frequency of $\geq$ 634 MHz the value of coefficient $m = 15$, ($7 \cdot 10^2 \leq mn << 15 \cdot 10^3$) and the frequency separation

between the adjacent stripes $\delta\omega^t \approx$ 15 MHz. The obtained value of $\delta\omega^t$ corresponds to the observed frequency separation in the decimeter wave band. In the given above estimations the wavelength of the ion sound ~ 100 m, the initial frequency ~1.0 kHz and the cyclic frequency of the slow beam wave $\omega_3 \sim 7 \cdot 10^2\, \omega_{0i}$ (that correspond to ~ 10 GHz).

Discrete emission bands are possible when the width of each emission band will be less than the value of frequency separation. This condition imposes restriction on the dispersion of the beam velocities. As show such estimations, executed in Fomichev and Fainshtein (1981), the beam of protons must be sufficiently quasi-monoenergetic, in the case in question $\Delta V_0 / V_0 < 10^{-3}$.

5.4 Fine Structure of Decametric Type II Radio Bursts

Chernov et al. (2007) have performed a comparative analysis of the fine structure of two decametric type II bursts observed on July 17 and August 16, 2002, with the 1024-channel spectrograph of the UTR-2 radio telescope in the frequency range 18.5–29.5 MHz and with the IZMIRAN spectrograph in the frequency range 25–270 MHz.

The August 16 burst (Figure 5.28) was weak, ~2–5 s.f.u., but exhibited an unusual fine structure in the form of broadband fibers (Δf_e > 250–500 kHz) that drifted at a rate characteristic of type II bursts and consisted of regular narrowband fibers (Δf_e > 50–90 kHz at 24 MHz) resembling a rope of fibers (Figure 5.29).

The July 17 burst was three orders of magnitude more intense (up to 4500 s.f.u. at 20 MHz) and included a similar fiber structure (Figure 5.30). The narrow fibers were irregular and shorter in duration (Figure 5.31). They differed from an ordinary rope of fibers by the absence of absorption from the low-frequency edge and by slow frequency drift (slower than that of a type II burst).

Both type II bursts were also observed in interplanetary space in the WIND/WAVESRAD2 spectra, but without any direct continuation. Analysis of the corresponding coronal mass ejections (CMEs) based on SOHO/LASCO C2 data has shown that the radio source of the type II burst detected on August 16 with UTR-2 was located between the narrow CME and the shock front trailing behind that was catching up with the CME.

The July 17 type II fiber burst also occurred at the time when the shock front was catching up with the CME. Under such conditions, it would be natural to assume that the emission from large fibers is related to the passage of the shock front through narrow inhomogeneities in the CME tail.

To clearly understand the relationship between the shock waves (type II bursts, after 07:20 UT) and the CMEs, we will use the lucky coincidence of the C2 coronagraph heights (2–5R_{Sun}) with the range of heights (1.8–6R_{Sun}) from which the radio emission in the WIND RAD2 frequency range (1–14 MHz) originates. Such height estimates can be easily obtained using a model electron density (plasma frequency) distribution in interplanetary space calculated by Leblanc et al. (1998), which agrees well with the Newkirk model above an active region in the corona.

The Radio Burst Fine Structure in the 18.5–29.5 MHz Frequency Band

The radio bursts in Figure 5.28b are the various elements of the weak type II burst and the numerous type III bursts drifting almost through the entire range. The fibers exhibit the most unusual fine structure: irregular broadband (with different instantaneous widths Δf_e > 250–500 kHz) fibers with a superfine structure in the form of narrow-band fibers (with bandwidths Δf_e > 50–90 kHz).

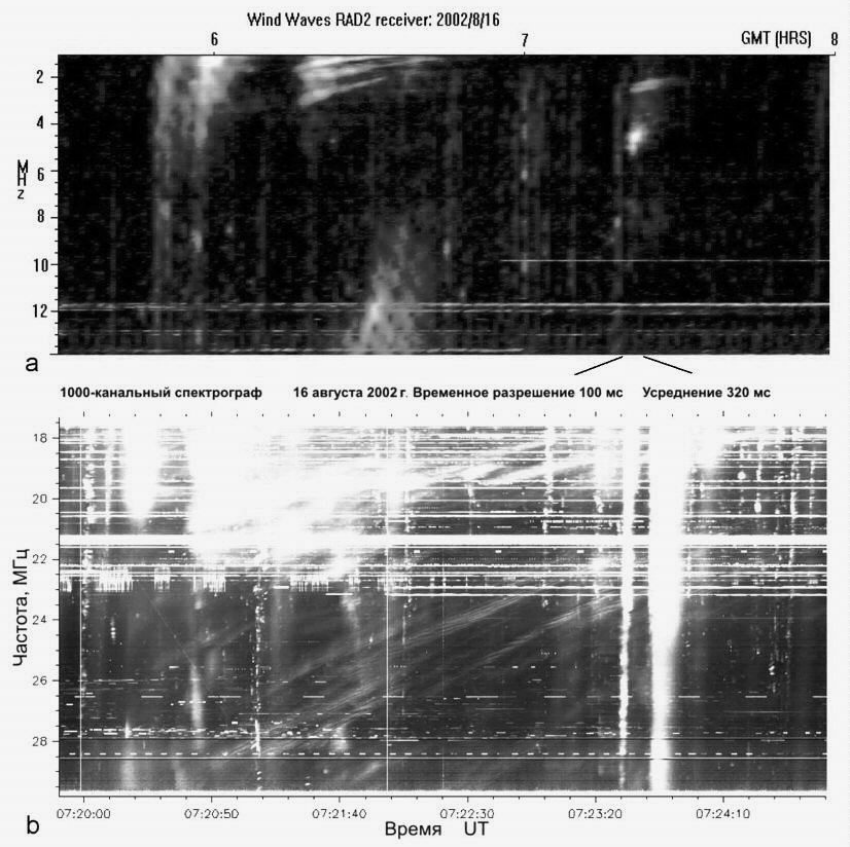

Fig. 5.28 (a) WIND/WAVE RAD2 spectrum in the frequency range 1–14 MHz (http://lep694.gsfc.nasa.gov/waves/waves.html) containing three different type II bursts against the background of numerous type III bursts. (b) UTR-2 spectrum in the frequency range 18.5–29.5 MHz showing an unusual fine structure of broadband fibers with a superfine structure in the form of narrow-band fibers.

The frequency separation between the latter rarely exceeds 50 kHz. Large fibers have a frequency drift rate $df/dt > -0.0365$ MHz s^{-1} characteristic of type II bursts at these frequencies, while small fibers (in large ones) have a frequency drift rate from a value almost equal to the drift rate of large fibers (parallel fibers at 07:22:30-50 UT in the largest fiber) to a minimum (on average) value, > -0.019 MHz s^{-1}. All large fibers have similar frequency drift rates, but they are spread randomly over the spectrum, with some of them exhibiting virtually no superfine structure. Narrow-band fibers are observed only in large fibers. Five narrow parallel fibers forming a so-called rope of fibers well known in the metric wavelength range (Chernov 1997) can be simultaneously distinguished in the largest fiber. In the event under consideration, the narrow fibers differ from a rope of fibers only by a slower frequency drift.

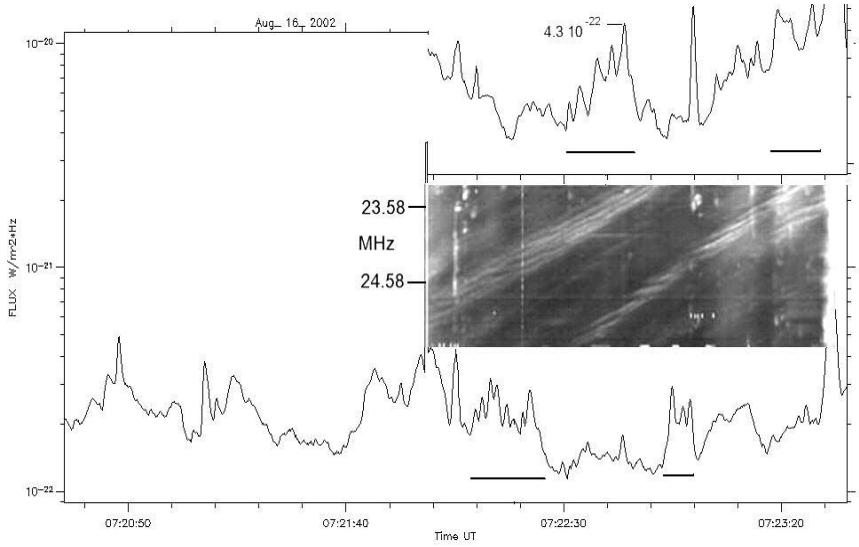

Fig. 5.29 Profiles of the 1024-channel spectrograph at two frequencies combined with the dynamic UTR-2 spectrum. The times of the fiber profiles are marked by the straight line segments under the profiles. The profile for a frequency of 23.58 MHz is shown at the top.

Note the following important property of this event: it was a limb one and very weak in intensity: the flux density in weak fibers was, on average, 2– 3 s.f.u. (1 s.f.u. = 10^{-22} Wm^{-2} Hz^{-1}), while for the two successive type III bursts after 07:23:20 UT (the brightest ones in the spectrum in Figure 5.28b) at 20 MHz the flux density was 24 s.f.u. The flux densities are presented in Figure 5.29 at two

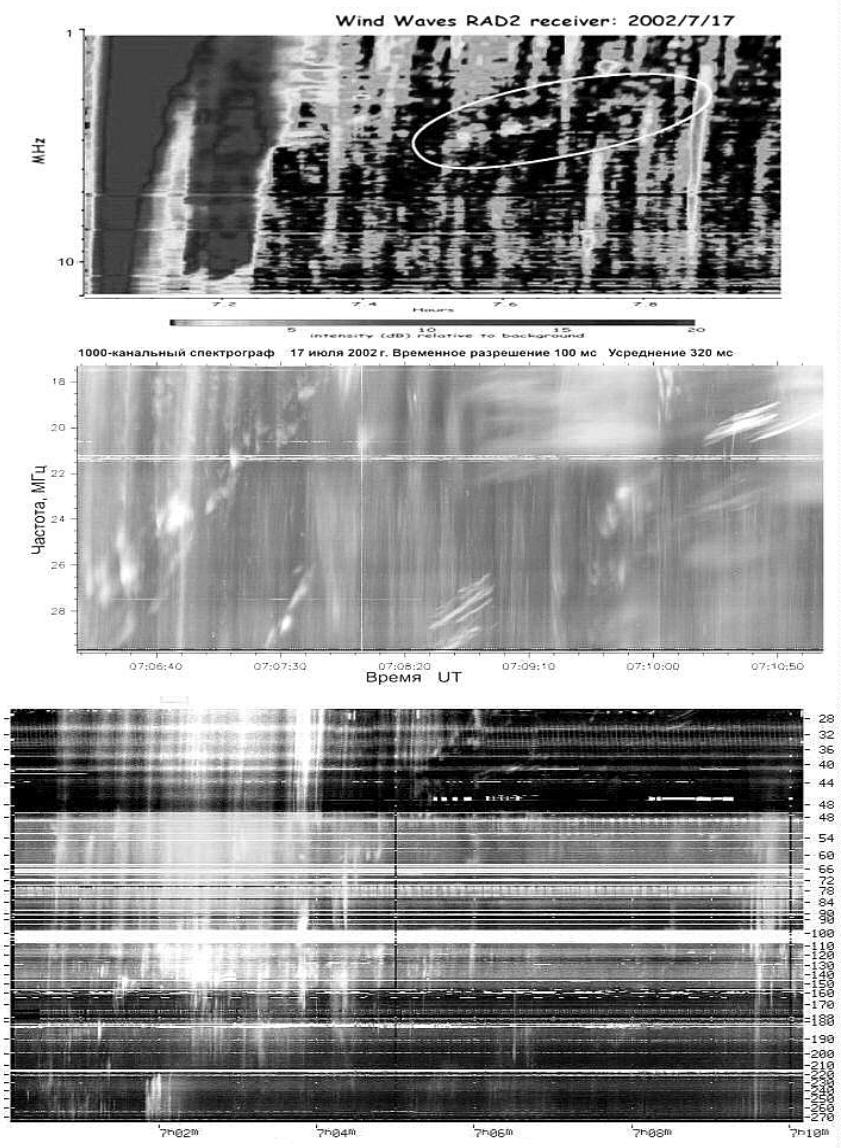

Fig. 5.30 Combined spectrum of the July 17, 2002 event. The IZMIRAN spectrum in the metric range (26− 270 MHz) is shown in the lower panel. The UTR-2 spectrum in the frequency range 18.5− 29.5 MHz exhibiting patches of the type II burst and three groups of unusual fibers is shown in the middle panel; their frequency drift rate is lower than the mean drift rate of the type II burst and decreases with time and frequency. The 1− 14 MHz (WIND/WAVE RAD2) spectrum containing a weak. type II burst (in the oval) against the background of numerous type III bursts is shown in the upper panel.

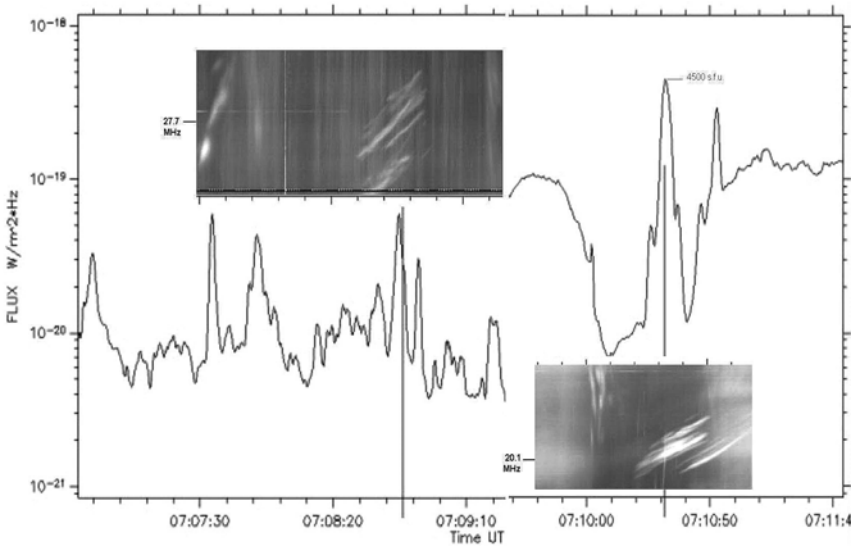

Fig. 5.31 Fiber profiles at two frequencies, 27.7 and 20.1MHz, combined with the spectra on the same scale in the July 17, 2002 event. The peak flux at 20.1MHz reached 4500 s.f.u. The width of the spectra is ~3.7 MHz.

frequencies together with a magnified fragment of the fiber spectrum. The fiber profile times are marked by the straight line segments under the profiles. The profiles reveal no clear absorption of the background burst between the fibers, i.e., there is no low-frequency absorption characteristic of intermediate drift fibers (IDB fibers or a rope of fibers).

Some of the type III bursts also exhibit a fine structure in the form of stripes or patches; the stripes occasionally drift with the same rate as the narrow fibers, when they are near the fibers, for example, at 07:21:08 UT. The spectrum is further complicated by the presence of reverse-drifting type III bursts, which also contain stripes with a drift similar to that of the fibers (e.g., at 07:21:40 and 07:23:20 UT).

We see a clear analogy of the fiber structure in this event with that at close frequencies in the May 2, 1998 event described in section 4.4.4, although the latter was much more intense and had a larger scale. The parameters of both large and small fibers are approximately identical and the small fibers in a large fiber (rope) then also drifted with a lower rate. The main difference of the May 2, 1998 event was that the large fiber was then a single and longer-lived one, while the small fibers appeared throughout the spectrum, grouping only occasionally into large ropes.

Thus, narrow fibers are the fine structure of large fibers and, although they are similar in overall spectral shape to a rope of fibers, no intermediate drift rate is reached in these two events. However, as was shown for the May 2, 1998 event, a

slow drift is determined by a reduced whistler group velocity at the shock front (Chernov et al. 2006). The absence of low-frequency absorption is often also characteristic of ordinary fibers in the metric range.

The Fine Structure of the July 17, 2002 Radio Burst in the 18.5–29.5 MHz Frequency Band

Note that the fine structure in the form of fibers differs from the August 16, 2002 event by a shorter duration, ≈20–30 s. Instead of large fibers, they form two groups. The diffuse group between 22–24 MHz under the intense second group can also be noted. Apart from the type III bursts, the spectrum simultaneously exhibits a number of other bursts: shortlived forward and reverse drift bursts, longlived diffuse bursts. Moreover, the groups of fibers are observed against the background of diffuse emission. Note the following important fact: the fibers in the 27–29.5MHz band (as well as other features) closely coincide in time in theUTR-2 and IZMIRAN spectra (Figure 5.26), suggesting that the fine structure is solar in origin. The fibers in groups follow irregularly both in time and in frequency. All of the fibers also differ in bandwidth; they appear as individual bursts. The band width Δf_e changes from its minimum value, >0.028 MHz, to its maximum value, >0.1 MHz. The frequency drift rate of the fibers in the first group is −0.08 MHz s^{-1}, i.e., it is lower than that of the patchy type II stripe, where $df/dt > -0.11$ MHz s^{-1}. In the second group, the frequency drift rate is the same as that for the large fibers on August 16, 2002, $df/dt > -0.036$ MHz s^{-1}.

The fibers do not exhibit a clear low-frequency absorption either. The large dips between the fibers of the second group (Figure 5.31) are most likely related to the absence of diffuse emission at these times in a broad frequency band and not directly to the fibers.

Thus, the main difference between the fibers in the weak and strong events-manifested itself mainly in the breakdown of a strict fiber periodicity in the strong event. The low intensity of the August 16, 2002 burst is most likely related to the directivity of the radio emission from the limb source, since the flares differ little in X-ray importance.

Discussion

The August 16, 2002 Burst Recall that we determined the position of the type II radio burst source between the narrow CME and the shock front trailing behind that was catching up with the CME. In terms of the plasma mechanism and the model of density *Ne* in interplanetary space calculated by Leblanc et al. (1998), the plasma frequency gradient is $df/dr > -4.79 \times 10^{-5}$ MHz km^{-1} (in the frequency range 10– 40 MHz). The shock front velocity

$$V \approx 2\frac{df/dt}{f}\frac{N_e}{dN_e/dr} = \frac{df/dt}{df/dr} \tag{5.15}$$

determined from the frequency drift $df/dt = -0.04$ MHz s^{-1} is 830 km s^{-1}. The minimum drift of the narrow fibers was ~ -0.02 MHz s^{-1}. The smooth increase in drift rate points to a change in the agent velocity from 400 to 830 km s^{-1}. In the May 2, 1998 event, the source was located between two diverging shock fronts also in the CME tail. The large fibers can be explained most naturally by the emission excited when the shock front passes along the elongated narrow streamers, the inhomogeneities remaining behind the leading CME edge. The instantaneous bandwidth of the large fibers, $\Delta f_e > 250$–500 kHz, allows the inhomogeneity thickness in the propagation direction of the shock front, $\Delta f_e/(df/dr)$, to be estimated. The maximum thickness can be $\approx 10\,000$ km.

The density inside the streamers can be twice the ambient plasma density and we see the maximum emission only from the streamers (Vrsnak et al. 2004). The presence of fast particles accelerated at the shock front may be considered obvious, given the appearance of oppositely drifting type III bursts in our spectrum and the numerous ordinary type III bursts at lower frequencies (Figure 5.24a), many of which are the herringbone structure of a type II burst. Therefore, it would be natural to assume that the enhanced radio emission from large fibers is the transition radiation, the radiation from fast particles at the boundary between two media with different refractive indices (Fleishman 2001). The transition radiation has already been suggested to explain the continuum in the zebra-pattern sources in the metric range by La Belle et al. (2003). In interplanetary space, it can be much more efficient, since the transition radiation flux is proportional to the square of the density contrast in percent ($\rho\,\%$)^2 (Eq. (15) in LaBelle et al. (2003)). Whereas in the metric range ρ can reach only a few percent, the density contrast in the streamers in the CME tail can be ~100%. In addition, the resonant radiation increases sharply if the wavelength becomes equal to the density inhomogeneity sizes (the so-called resonant transition radiation (Nita et al. 2005). The satisfaction of this condition is much more likely in the CME tail at large heights.

In the August 16, 2002 event, we estimated the shock velocity, ~830 km s^{-1}, at a frequency of 24 MHz (in the model by Leblanc et al. (1998)). Our estimates of the magnetic field strength, $B \sim 0.9$ G (see below), allow the Alfvén velocity, $V_A \sim$ 730 km s^{-1}, and the Mach number, ~1.14, to be estimated at the boundary of the critical value for the emission of plasma waves at the fronts of collisionless type II shock waves in the upper corona (Fomichev, 1986). The shock wave in specific segments of its path can be both quasi-longitudinal and quasi-transverse with respect to the background magnetic field. However, particles are known to be accelerated at the shock front in both cases (Zaitsev and Ledenev 1976; Holman and Pesses 1983).

Fast particles accelerated at the shock front can be captured into a small trap between the leading CME edge and the shock front. The electrons reflected from the

shock front form a loss-cone velocity distribution unstable for the generation of whistlers. Therefore, even one particle beam will lead to periodic whistler excitation through bounce motions in such a trap. According to Fig. 2 in Chernov et al. (2008), the separation between the leading CME edge and the presumed shock front (the position of the plasma level corresponding to the onset of emission at 30 MHz) is ~1R_{Sun} and fast particles with velocities ~1010 cm s^{-1} characteristic of type III bursts provide a whistler excitation period of ~7 s. In the spectrum of Figure 5.24b, this proves to be the maximum period between narrow fibers at the same frequency. Shorter periods (2–3 s at 07:22:30 UT) result from the reflection of two beams from both mirrors.

Thus, we can explain the presence of narrow fibers only in large fibers and it is related to a modulation of the continuum emission from large fibers by whistlers as a result of their merging with plasma waves (this is the widely known formation mechanism of fiber bursts (Kuijpers 1975). In this model, we can estimate the magnetic field inside an inhomogeneity from the frequency separation between the light and dark stripes in narrow fibers Δf_e: it is approximately equal to the whistler frequency. The accuracy of our observations allows us to equate Δf_e and half the frequency separation between the fibers Δf_s (e.g., at frequencies near 24 MHz). For the relative whistler frequency $x = f_w/f_{Be} = 0.01$ (at which the whistlers have the maximum growth rate at moderate loss cone angles ~70° (Kuijpers, 1975), we obtain the maximum field strength inside the inhomogeneity, $B \approx 0.9$ G. The plasma β for such a field at a 24-MHz level will be negligible, $\beta << 1$, which is expected for the inhomogeneities inside a CME (magnetic cloud).

The whistlers propagate in the propagation direction of the shock front, i.e., in the direction of a decrease in magnetic field and an increase in density (inside the inhomogeneity). However, the whistler excitation location remains uncertain. It would be natural to assume that the whistlers are excited upstream of the shock front (in background plasma parameters). When the whistlers enter an inhomogeneity with a density enhanced by a factor of 2 or 3, they are trapped into the inhomogeneity region. In this case, the magnetic field changes little (in accordance with the constant parameters of narrow fibers), but the whistlers are scattered by the background plasma, which causes a sharp decrease in x (Chernov 1989). Therefore, the whistler group velocity (Kuijpers 1975) $Vgr = 2c(f_{Be}/f_{Pe})[x(1 - x)^3]^{1/2}$ should be $\leq$760 km s^{-1}, for example, for the ratio of the gyrofrequency to the plasma frequency $f_{Be}/f_{Pe} \leq 1/45$ and the relative whistler frequency $x = f_w/f_{Be} \approx 0.0033$ (inside the inhomogeneity). Thus, the whistlers should lag behind the shock front, which is why the narrow fibers have a slower frequency drift. After about 07:22:40 UT, the narrow fibers became parallel large ones and, hence, the whistlers proved to be standing downstream of the shock front at this time.

The magnetic field can also be determined from the frequency drift of narrow fibers. According to the formula from Elgaroy (1982) for the model of a doubled Newkirk density at $x = 0.01$, equating the whistler group velocity and the velocity determined from the frequency drift , we obtain

$$B = 41.8(\ln f - 1.29)^{-2}|df/dt|. \quad (5.16)$$

For the frequency $f = 24$ MHz and the drift rate $df/dt = -0.04$ MHz s^{-1}, we obtain $B = 0.47$ G. Thus, it is clear that the density inside inhomogeneities should be approximately doubled in order that Eq. (5.16) give $B = 0.9$ G determined from the frequency separation. During their drift, the narrow fibers remain parallel ones (the whistlers are not damped for almost 1.5 min). This is indicative of an almost constant magnetic field strength along the inhomogeneities on scales of ≈75 000 km. A no less complex behavior of the fine structure is observed in type III bursts. Thus, for example, in the type IIIb burst at 07:21:07–10 UT, the entire emission consists of stripes and patches, with the stripes appearing in the spectral segments adjacent to large fibers. Their bandwidth and drift velocity are approximately the same as those for the narrow fibers, which provides evidence for the same whistler– plasma wave interaction mechanism. The point like patches are most likely of the same nature, but are short in duration, i.e., the fine structure of the burst results from the passage of a type III beam through a turbulent zone downstream of the shock front.

We cannot see fast bursts in the WIND/WAVE spectra, since the time resolution is limited by 16 s, the time of one scan through the entire frequency range 1–14 MHz (Bougeret et al. 1995). The type II burst consisting of four stripes that form pairwise harmonic structures in the frequency range 0.7– 3.5 MHz coincides in time with the overtaking and absorption of the slow CME by the fast one. These four stripes can be explained by the generation of two shock fronts during the collision of two CMEs.

An additional splitting of broad stripes into narrower ones is observed at frequencies near 2 MHz. Their regular frequency drift breaks down, suggesting a possible contribution from the transition radiation that depends on inhomogeneity parameters inside the CME.

The July 17, 2002 Burst

The general interpretation of the fibers in this event can be the same as that for the August 16, 2002 event. At this time, the shock front was catching up with the CME and the entire fine structure can be associated with the emission from inhomogeneities in the CME tail, including the patchy structure and diffusive bursts. The fibers most likely appear also inside the inhomogeneities. Incidentally, traces of fibers are also seen in the diffuse burst under the second group. The absence of fibers in other diffuse bursts most likely points to different locations of the sources (e.g., along the shock front). The excitation of whistlers is suppressed in these places or, more precisely, the trap for the locked particles does not enclose the entire shock front. The absence of a strict fiber periodicity may be related to a high (plasma wave) emission level: if the emission frequency depends on intensity, then an additional positive nonlinear addition is added to the emission frequency. The shorter fiber duration is also difficult to explain by a high intensity. It is de-

termined by the inhomogeneity sizes, which can be very different and can have very unusual configurations. The absence of absorption from the low-frequency edge of the fibers is an ordinary property of the fibers in type II bursts. It can be explained by the divergence of fast particles and waves (whistlers) in the space upstream of the shock front (Chernov 1997).

Concluding remarks

We analyzed two type II radio bursts in the decametric wavelength range with a fine structure in the form of unusual slowly drifting fibers. For our general analysis of the events we used all the available data in other ranges, in particular, WIND, SOHO, and TRACE data. This provided an insight into the development of flare processes and allowed the possible positions of radio sources to be determined. Both type II bursts were observed simultaneously at various frequencies of the decametric range with the 1024-channel spectrograph of the UTR-2 radio telescope and the IZMIRAN spectrograph as well as in the WIND/WAVES RAD2 spectra. In contrast to the well-known herringbone structure and patches in the spectrum, this fine structure is distinguished by the formation of narrow-band fibers (Δf_e > 50–90 kHz at 24 MHz) and is characterized by the possible generation of whistlers between the leading CME edge and the shock front. SOHO/LASCO C2 data were used to analyze the CME. The fiber drift velocity is assumed to be determined by the whistler group velocity inside the inhomogeneities in the CME tail. Like the continuum modulation in the form of fibers in type IV bursts, the whistlers excited at shock fronts manifest themselves only against the background of enhanced emission from large fibers, which can be the transition radiation from fast particles at inhomogeneities in the CME tail. The unusually low drift velocity of narrow fibers may be determined by the reduction in whistler group velocity inside the inhomogeneities to 760 km s^{-1}. The magnetic field inside the inhomogeneities at the frequency of 24 MHz was $\approx$ 0.9 G.

5.5 FINE STRUCTURE OF SOLAR RADIO BURSTS OBSERVED IN INTERPLANETARY SPACE

The observations with *WIND/WAVES* receiver (1 ÷ 14 MHz) also show fine structure in interplanetary (IP) radio bursts (Bougeret et al., 1995). Flocculent (wisp or patch) structure in II type bursts and rapid pulsations in IV type continuum are frequently present (see http://lep694.gsfc.nasa.gov/waves/waves.html). There also exist shock-associated (SA) events in the decametric (DCM) range as the extension into IP bursts of “herringbone structure”, which are generally considered as evidence of shock acceleration (Bougeret et al., 1998). In addition, different fiber-like structures are sometimes observed in conjunction with type II or type IV

IP bursts. The object of this section is to study similar fiber structures in relation to ZP and IDB in the metric ranges.

All of the main properties of the selected 14 events are summarized in Table 5.2. In the latter four columns the spectral parameters of the fiber structure are collected: Δf – total frequency band, encompassed by structure; Δf_e – frequency bandwidth of isolated fiber in emission; Δf_s – frequency separation between adjacent fibers; df/dt – frequency drift of the fibers. In the fourth column, in addition to the speed, the abbreviation of the observatory where the dynamic spectrum of type II meter burst was observed is also noted.

The fiber fine structure is rather rare event among numerous IP bursts, but not less rare than analogous structure in the meter wave band. Statistics will be inaccurate, if we will attempt to determine it.

Of the 14 selected events, seven exhibit the fiber structure in type II bursts, five in type IV continuum bursts, and two – as striae – in type III bursts. The clear, reliable continuation of meter type II burst into IP type II burst was observed only in the events of May 2 1998 and November 3 2003 (10:00 UT, together with the type IV continuum) in agreement with the results of Cane and Erickson (2005) about the rarity of such events. In four events (September 17 2001, October 27 2002, November 13 2003, and July 13 2005) we see only the continuation of the continuum emission with fiber structure mainly at frequencies 14 – 5 MHz.

December 12 1997 event

The event was rare according to all of its properties. First of all, the continuum is located separately from DCM spectrum (Figure 5.32), but in the same continuum it is possible to distinguish type III bursts, consisting of striae. According to Hiraiso data, the metric radio burst was very weak: there are continuum with type III bursts and fairly present type II burst. The corresponding CME was very slow

Table 5.2: Selected fiber patterns in IP radio bursts with *WIND/WAVE* RAD2 spectra

Date UT	Dur min	Flare, coord.	Type II V km s^{-1}	CME V km s^{-1}	Δf MHz	Δf_e kHz	Δf_s kHz	df/dt kHz s^{-1} Type
12Dec97	30	B9.4	1000	LE loop	1 – 5	200	400	-1.8
22:30		N25W52	Hir	207				IV fibers
02May98	130	X1.1	960 N	Halo	1 – 6	200 -	>500	<-2.78
14:10		S15W15	400 N	1040		300		II fibers
18Apr 00	68	No data	?	No	1.5 –	100	>200	-0.69

22:10		N17E90	Wind		4			II fibers
		EIT195	IP630					
19Apr 00	210	C1.2	?	No	1 – 2	105	>300	-0.40
01:30		N19E73						II fibers
17Sep 01	32	M1.5	685	P. Halo	5 –	500 -	>1200	-8.33
08:30		S14E04	5540	1000	14	700		II + IV
			Izmi	1400				fibers
20Jul02	30	X3.3	600	OAHalo	7 –	1000	>1500	-8,93
21:30		SE limb	Culg	1941	14			IV fibers
27Oct 02	20	C4.3	900	OA halo	6 –	1000	>3000	-22.2
23:10		?N24W42	Culg	2115	14			IV fibers
03Nov03	15	X2.7	705	W65	1.3 –	150	>300	-0.926
01:12		N10W83	Hir	827	3.2			III striae
03Nov03	30	X3.9	1700	W103	6 –	800	>1000	-12,35
10:10		N08W77	Izmi	1420	14		IV	fibers
							200	Type II
13Nov03	18	M1.4	714	P. Halo	6 –	150 -	> 300	-4.29
09:30		E limb	Izmi	1141	14	200	rope	II fibers
			Ip1500					
18Nov03	>84	M4.5	4000	P. Halo	2 –	200	300	-1.85
10:10		S04E16	800	1824	4.5			II fibers
			Ip656					
13Jul05	57	M5.0	457	Halo	1.6 –	300 -	Isol.	-16.7
14:08		N11W90	Nan Ip ?	1423	14	1000	fibers	-2.08
23Aug05	36	M2.7	SAG	P. Halo	8 –	1000	>1500	-11.1
14:42		S14W90	IP 738	2090	14			II + IV
								fibers
31Aug05	20	C2.0	?680N	Halo	1 –	100	200	-0.79
11:40		N13W13	IP III	860	14			III striae

(207 km s^{-1} and shown streamer structure. The IP burst is not an extension of metric activity. But if we assume these striae to be ZP, then the relative values of the parameters ($\Delta f_e/f \approx 0.067$ and $\Delta f_s/f \approx 0.14$) exceed by more than an order of magnitude the analogous values for ZP in the meter range.

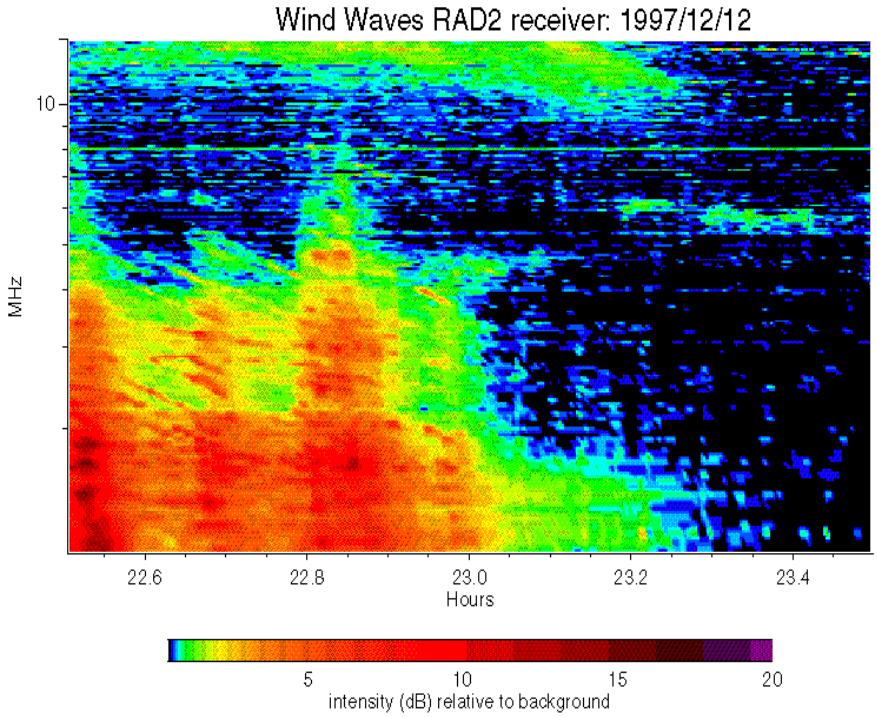

Fig. 5.32 Multiple fibers and striae similar to zebra pattern in a type IV continuum burst (Chernov et al. 2007).

May 2 1998 event (Observations)

This is one of the most interesting event, because both in meter and decameter ranges two type II bursts were observed, and in both ranges fiber structure was also recorded. In this connection, this event can be a key for understanding of the generation mechanism of this structure.

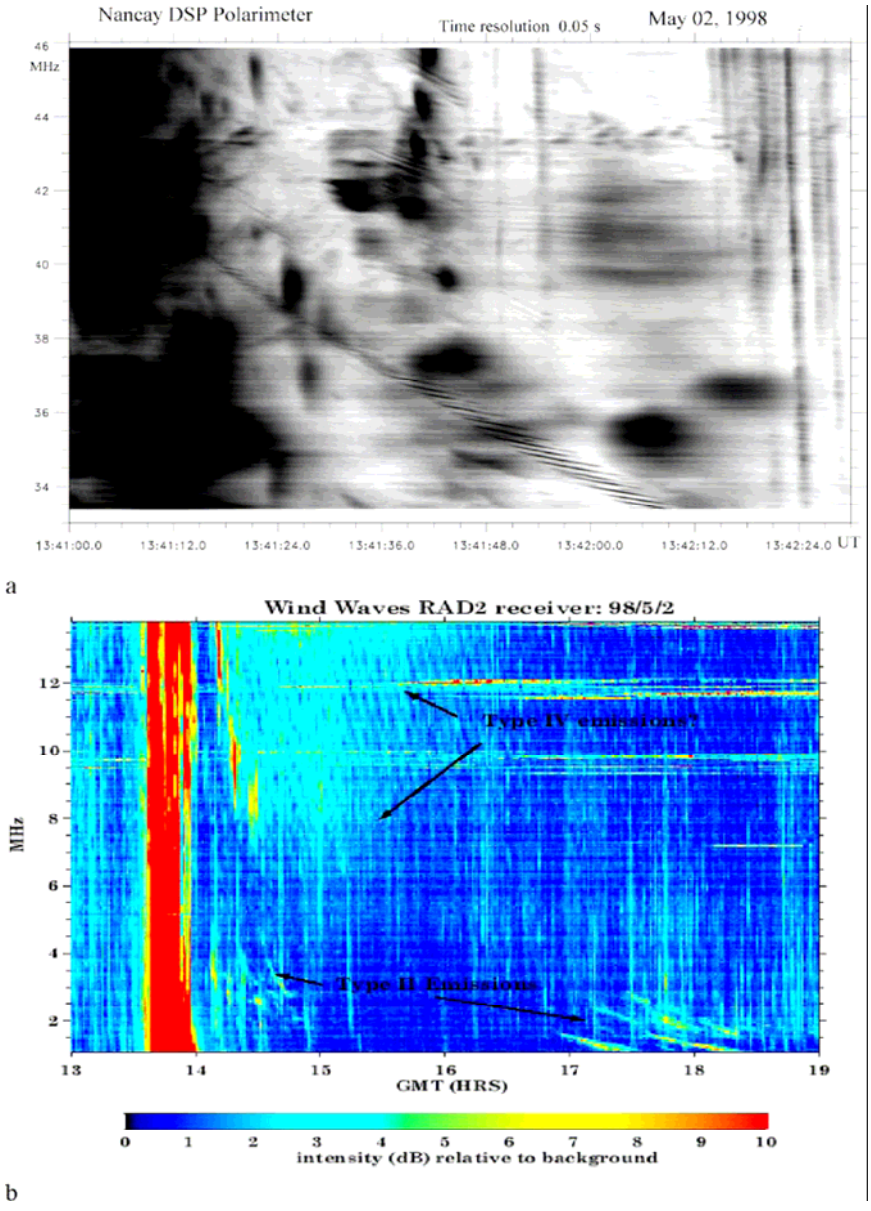

Fig. 5.33 (a)- dynamical spectrum obtained by the decameter spectropolarimeter (DSP) of the Nançay Observatory. (b)- Two IP type II bursts consisting of narrowband fibers. Strictly straight stripes in the continuum are caused by an artifact, of the spin modulation of the spacecraft (Chernov et al. 2007).

The meter burst was described and discussed in the section 4.4.4 and 4.7.3. Two type II bursts with fiber structure observed also by *WIND* RAD2 receiver in the frequency range Δf ~1 ÷ 6 MHz (Figure 5.33). However, it is difficult to distinguish fiber structure at frequencies 14 ÷ 6 MHz. Strictly parallel stripes in the type IV continuum (similar to the zebra) are caused by spin modulation of the spacecraft (the spin rate is about 20 per minute).

The absence of spin modulation in type II and III bursts could be explained by their weak polarization, since this modulation arises only with two perpendicular *X,Y*- antenna (Reiner et al., 2006). In such a case, the type IV continuum was strongly polarized. In this event we see the fiber structure of the type II bursts with large diversity in the frequency separation between the fibers. Thus, here no similarity with the ZP is observed. The frequency drift of separate fibers is approximately equal to the drift of the type II burst as a whole.

September 17 2001 event (Observations)

The IP burst, shown in Figure 5.34c, presents fiber structure as it expands from the metric range (may be of type II burst and group of strong type III bursts), containing strange fragments of reverse drift bursts (similar to U bursts). In the metric range, the radio event consisting of strong type III bursts and two type II bursts (Fig. 5 in Chernov et al.(2007) began simultaneously with the M1.5/2N flare on 08:20 UT in Active Region 9616 with coordinates S14E04. Both type II bursts began almost simultaneously at 08:24:50 UT and consisted of fundamental and harmonic bands, but they drifted with sharply different drift velocities: the first slow burst (but prolonged), with $df/dt \approx$ -0.135 MHz s^{-1} reached the frequency of 25 MHz at 08:33 UT, the second (rapid) burst ended on 25 MHz approximately at 08:27 UT and had a drift velocity almost five times greater than the slow one.

The analysis of SOHO/EIT images in the 195 Å line shows two ejecta at 08:24 UT which propagated at different angles and were visible until 08:36 UT. At the same time interval, the two-dimensional maps of the Nançay radioheliograph at 164 MHz show two radio sources approximately in these directions. So, two type II bursts could not be radiated by one shock front, *e.g.* by different parts of this front with different density gradients. Unusually high frequency drift, – 0.6 MHz s^{-1} is certainly connected to this effect.

The SOHO/LASCO data show the partial halo CME, and on the its height-time diagram at the moment of type II burst beginning (08:25 UT) the CME was located at the height of 1.5 $R_\odot$ (or at the level of 25 MHz), *i.e.* much higher in the corona.

In Figures 5.34a,b the increased fragments of the metric spectrum are shown. The first spectrum presents numerous narrow frequency fibers between 190 ÷ 175 MHz with some elements of rope like similar to ropes discussed in Chernov (1997). The second spectrum shows the "herringbone" structure at the low - frequency part of the fundamental band of the slow type II burst, and this structure

(between 08:33-08:49.5 UT) passes continuously into fibers in the range 14 – 5 MHz in the *WIND*/RAD2 spectrum. Some type III bursts are also observed in IZMIRAN.

Thus, some analogy is found with the event on May 2 1998. Here fiber ropes and two type II bursts in the meter range as well as the expansion of one of them into the WIND spectrum as drifting fibers were also observed.

The clear difficulty for interpretation represents the transition of the "herring-bone" structure with separate very-quickly drifting bursts (and with different sign) into slowly- drifting fibers with the drift speed close to the usual drift of type II bursts.

November 3, 2003 event (Observations)

The similar transition of fiber structure in the metric range into fibers in the WIND spectrum is shown in Figures 5.35a and b. The event was related to a large X3.9/2F flare in AR 0488 on the west part of the disc at N08W77. Taking into account all of the harmonic relations between the bands of complex type II bursts, shown in Figure 7 in Chernov et al (2007), we are compelled to recognize the presence of two type II bursts. The low-frequency burst (140 ÷ 40 MHz) with a frequency drift df/dt = -0.3 MHz s^{-1} was obviously caused by another shock front judged by its complete stop (attenuation) at frequencies ~ 40 MHz. The first type II burst with harmonic structure drift to 25 MHz (at 10:05 UT), though with a somewhat lower frequency drift. The velocities of the shocks estimated within the framework of the double Newkirk model are equal about 1770 km s^{-1} for the fast burst and about 1000 km s^{-1} for the slow one. Both shocks were of the blast type and were related with the eruptive phase of the flare. The CME began some minutes later and its velocity was 1420 km s^{-1}, thus both shock fronts were propagating far ahead of CME. Although the fast type II burst stopped at 40 MHz, on *WIND* spectrum we notice its continuation after 10:10 UT but with two strange harmonically related type U bursts (with turnover frequencies near 3 MHz and 6 MHz for the fundamental and harmonic respectively) and subsequent narrow stripes (or fibers also with harmonics) which appear as a continuation of falling branches of U bursts between 5 ÷1.5 MHz in the interval 10:20 - 10:40 UT (Figure 5.35b). The velocity of IP front determined by the frequency drift of narrow fibers in the Leblanc, Dulk, and Bougeret (1998) model, is about 700 km s^{-1}, *i.e.* the CME was overtaking it. Thus this strange IP burst could not be initiated by the forward edge of CME, as in this case the speeds of the CME and the shock front should be approximately equal.

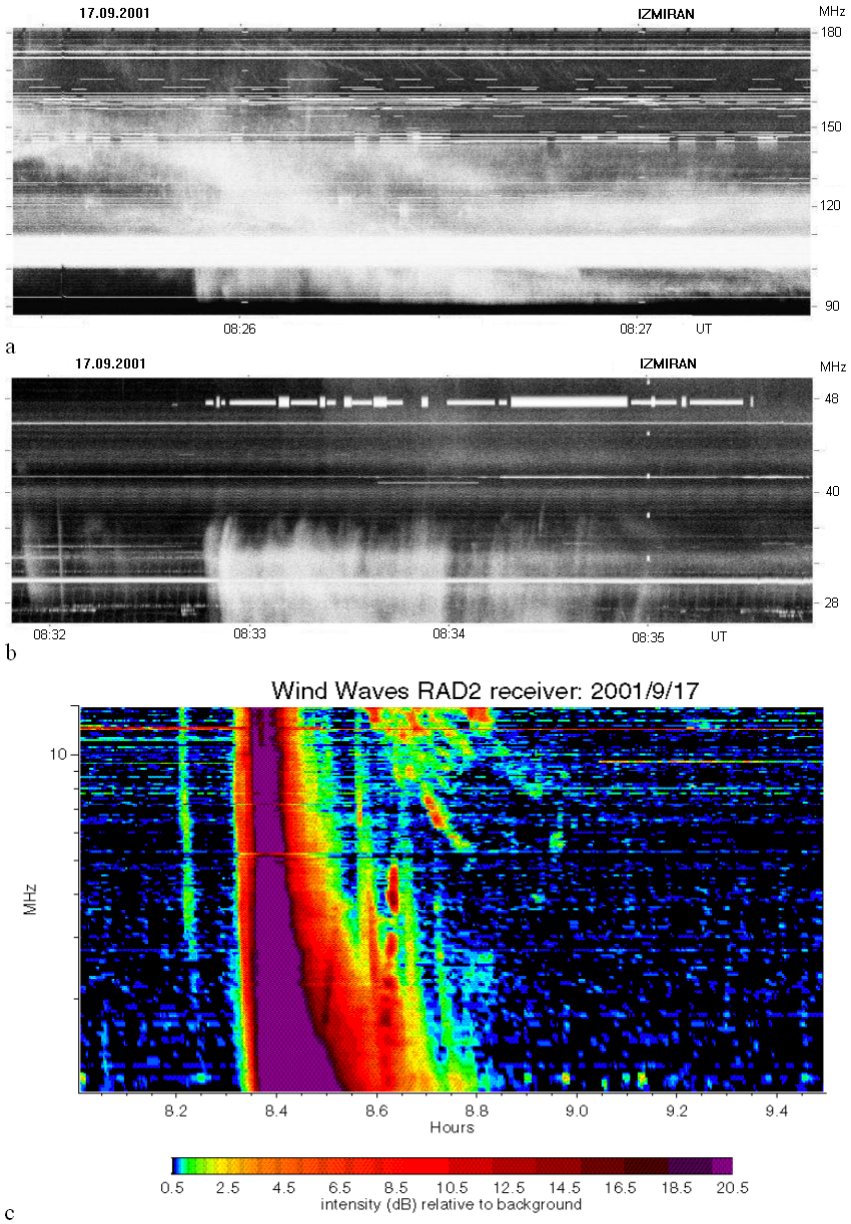

Fig. 5.34 Increased fragments of the metric spectrum (IZMIRAN) show numerous narrow frequency fibers between 190 ▯ 175 MHz (a) and the "herringbone" structure at the low frequency part of the fundamental band of the slow type II burst (b). (c)- Multiple fibers as extension of the metric type II bursts into the RAD2 spectrum. After strong type III bursts two fragments with reverse frequency drift, like type U– bursts, are also visible between 1.6 ÷ 4.6 MHz (Chernov et al. 2007) .

The fibers in the range 90 - 30 MHz against the background of wisp structure of the second type II burst (Figure 5.35a) are similar to fiber bursts (IDB), however the speed of the frequency drift is about equal to the drift speed of the type II bursts and even less, and they cannot be classified as fiber bursts (IDB). They also cannot be identified with ropes (Chernov, 1997) because they are more large-scale. As always, in each event fibers in type II bursts are varied and depend on the shock front structure. It is possible to say quite definitely, that their source was located between two shock fronts.

Comparing this event with the two previous ones, we nevertheless notice the clear analogy in the origin of the fine structure in *WIND* spectra. But first of all we should note that the continuum emission in the *WIND* spectrum (14 ÷ 5 MHz) is a direct expansion of flare continuum from the meter range, as well as the fibers are direct continuation of those of the meter range. The fibers are formed as a result of the interaction of plasma waves with whistlers, generating and propagating inside a magnetic trap, in this case between two shock fronts.

We assume that the CME overtook the slow front, and this happened about 10:02 UT, at the beginning of the ascending branches of the U bursts. This assumption, on the whole, is supported in the paper Vrsnak et al. (2006), where the diagram of this overtaking is shown.

Unusual U bursts in the *WIND* spectrum testify to the clear closed magnetic configuration at heights $2 - 4\ R_{\odot}$ (a magnetic cloud) that specifies a capture of fast particles in this interval of heights between shock front of the IP burst and the forward edge of the CME. Recall that this IP shock front lagged behind the CME. Therefore the generation of narrow-band fibers in the IP takes place in elongated density heterogeneities in the wake after CME passage, well visible on the SOHO/LASCO image (Fig. 5.36). Moreover, in the left bottom image at 10:32 UT a diffuse emission strip behind the forward edge of CME (marked by the arrow in Fig. 5.36) is probably the manifestation of the shock front against the background of the CME wake.

November 13, 2003 event (Observations)

The main peculiarity of this event is an occurrence of structure such as the rope in IP burst (Figure 5.38b). In contrast to all other events, this one was connected with the flare on the east limb in AR 0501 of importance M1.4. The CME began almost simultaneously with the type II burst in the metric range about 09:26 UT. Most likely the CME and shock front were independent as the velocity of the CME was much higher (1140 km s^{-1}) than that of the shock front (~700 km s^{-1}). Therefore all of the fine structure was connected with a source between the forward edge of the CME and the shock front going behind it.

We see in Figure 5.37a only the part of the “herringbone” structure drifting to high frequencies. The low frequency part of this “herringbone” structure with opposite frequency drift is also seen in the *WIND* spectrum at the same time.

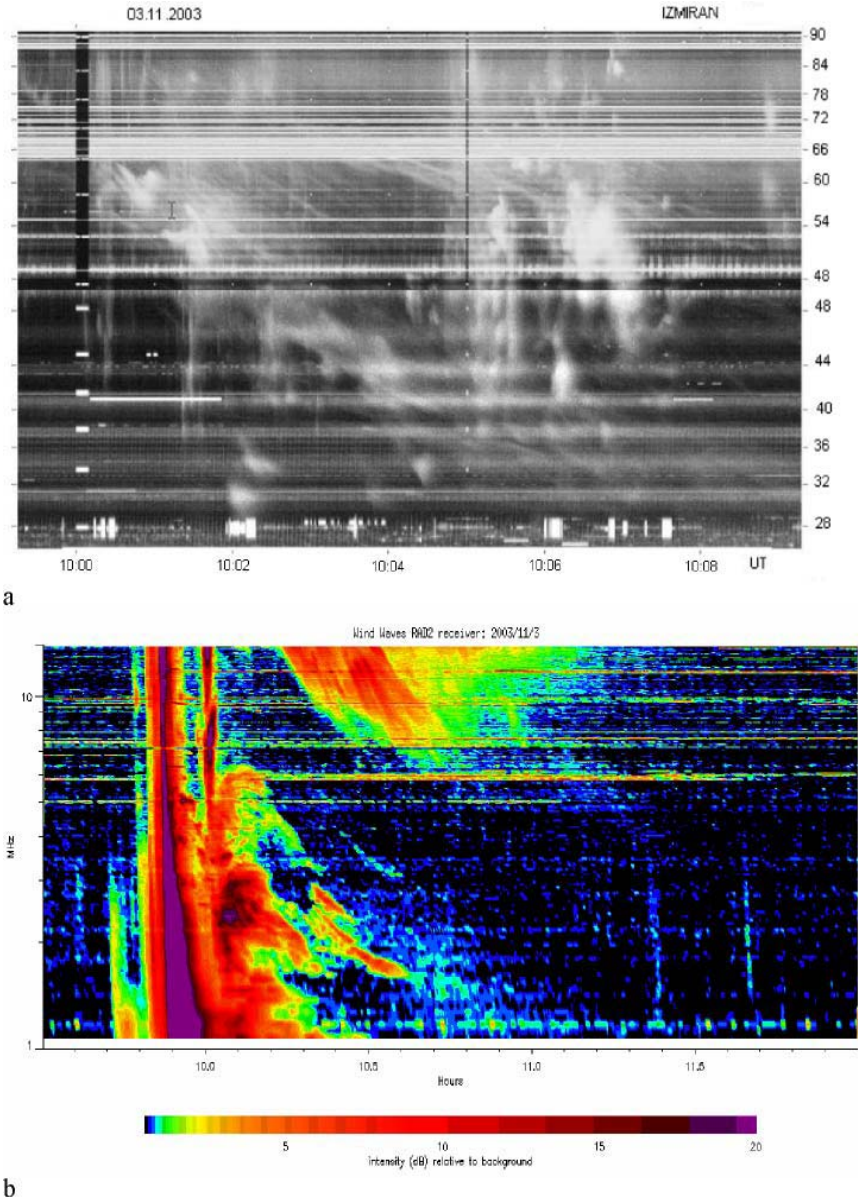

Fig. 5.35 The continuation of fiber structure from the DCM range in the continuum emission and fragments of type U burst and fibers in type II burst at low frequency part of the RAD2 spectrum (Chernov et al. 2007).

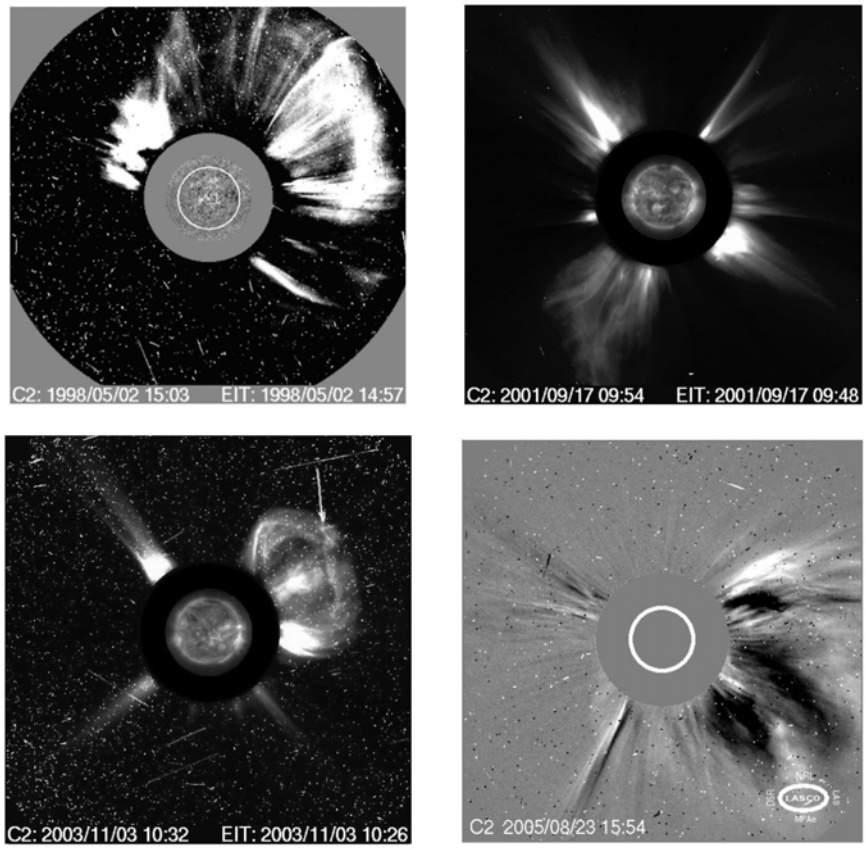

Fig. 5.36 SOHO/LASCO C2 difference (May 2 1998 and August 23 2005) and original (September 17 2001 and March 3 2003) images with the streamer structure behind the CME leading edge. The CME on 3 November 2003 overtook the shock front, and the perspective position of the front is shown by *an arrow* (Chernov et al. 2007).

The fast particles responsible for the "herringbone" structure could be then trapped between the forward edge of CME and the shock front, and we see only some manifestations of their possible bounce motions with the generation of plasma waves and whistlers. So, the mechanism should be the same as for the fiber rope structure in the metric range.

The termination of radiation is not necessarily connected with a scattering or merging of fronts, it is more natural to assume an angular divergence CME and shock front.

Some stria structure in continuum emission after type III bursts below six MHz is similar to the stria structure in the December 12 1997 event (Figure 5.32), although here any frequency drift of striae is absent.

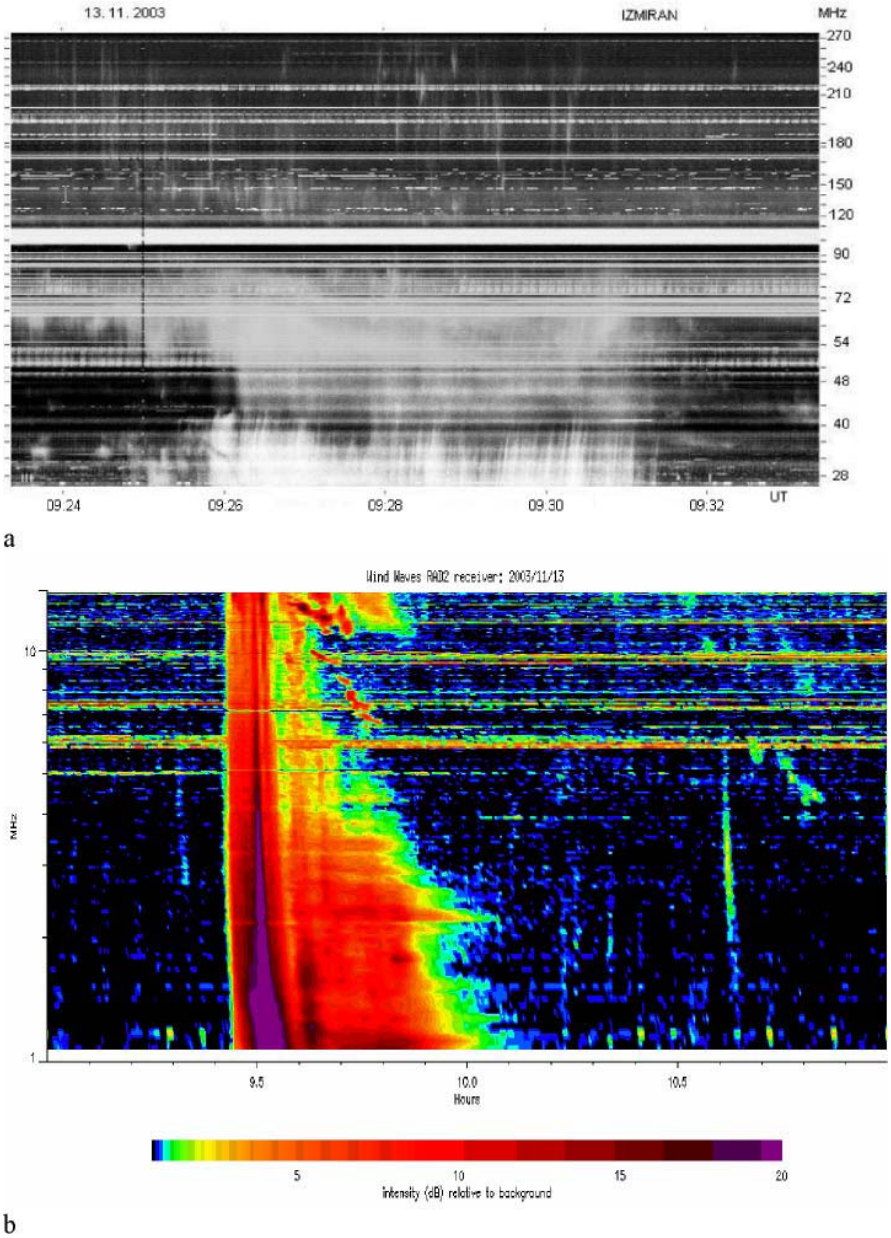

Fig. 5.37 Herringbone structure in the metric type II burst *(a),* its expansion into RAD2 spectrum *(b)* but in another quality as some short slow drifting (-4.3 kHz s^{-1}) fibers forming a rope (Chernov et al. 2007) .

Other events

For the April 18 2000 event we have no information about flares and metric type II bursts, however it is very interesting and consists of two bursts with fine structure (Figure 38 and 39). Despite of numerous IP type III bursts, there are no bursts in the meter range in the spectrum from the Hiraiso observatory, and only weak continuum presents in the band 25 ÷ 35 MHz in the interval 21:30 - 24:00 UT. Thus, it is obvious that the type III beams were accelerated at heights ~2 $R_{\odot}$. At the same time, the first event (Figure 5.38) was accompanied by a powerful CME, and we have an opportunity to look for the CME site which is responsible for this radioburst. In the events discussed above, we followed only that heterogeneities the shock front propagated through after CME.

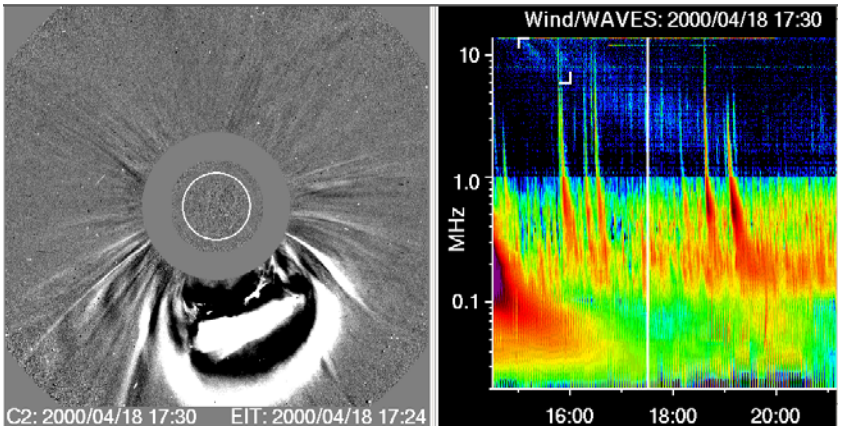

Fig. 5.38 The combined LASCO C2 image and WAVE (RAD2+RAD1) spectrum allowing the connection of the moment of radiation (marked by *the straight vertical line* on spectra,) with a locating in the CME, as a source of radiation (Chernov et al. 2007).

In the RAD2 spectrum a broadband drifting continuum is present, and against this continuum two drifting stripes are located in the high frequency part of the spectrum. The common frequency drift of the continuum is some less than the drift of fibers; it drifts through the whole range 14 ÷ 1 MHz in approximately 80 minutes. In the model of Leblanc, Dulk, and Bougeret (1998) this drift corresponds to the speed 660 km s^{-1}, which practically coincides with the speed of the CME (668 km s^{-1}). In the absence of a type II burst (shock front), it specifies that the continuum is direct radiation in front of the CME.

The structure of the CME (Figure 5.38) does contain two fronts, therefore it is quite obvious that the first wide front is responsible for the radiation of the first broadband fiber, and the second one (narrow internal) for radiation of the second narrowband fiber. There is a break in the continuum emission between these fi-

bers, which, probably, is connected with an area of rarefaction between the two fronts. A somewhat larger speed of the frequency drift of the fibers is determined by the large density gradients in the CME fronts. However the disappearance of fibers at 16:00 UT remains to be explained because the structure of the CME with two fronts remained long lasting after 16:00 UT. The speed of the CME allows us to assume the occurrence of the shock front driven by the CME, then the rarefaction area is actually a reverse shock wave of rarefaction. It is known that the speed of the reverse shock wave is less than that of the forward wave. The somewhat smaller drift velocity of the rarefaction area in comparison with the drift of fibers could be connected with that.

The second April 18 2000 event at 22:30 UT is a typical IP type II burst in the range $4 \div 1.5$ MHz (Figure 10 in Chernov et al (2007)), and it is similar to the May 2 1998 event. LASCO C2 images show a faint additional CME, a little to the north of the previous one (not included in the Catalog). It is possible that the shock front is too connected with this ejection. The IP space at the heights $2 \div 5\ R_{\odot}$ remained perturbed after the previous CME passage, and the shock front radiated maximum emission from density enhancements similar to other events.

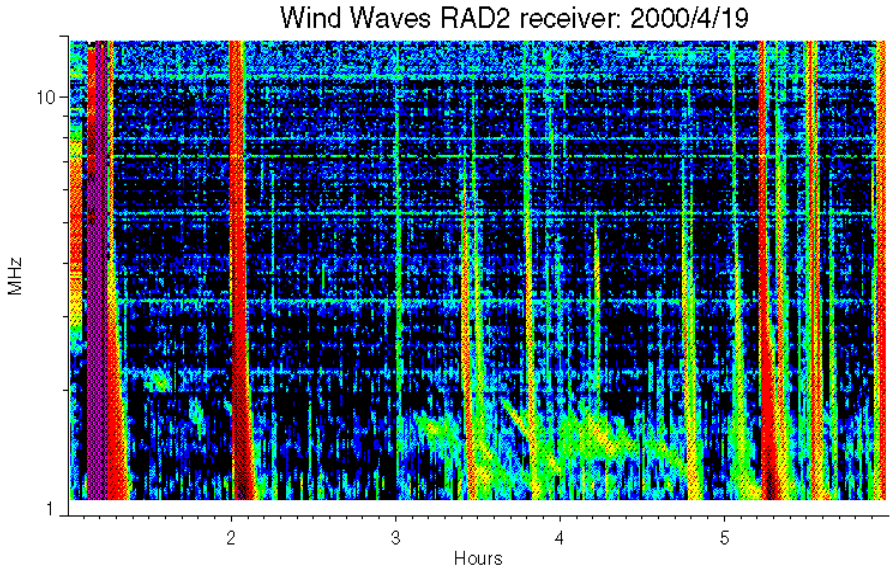

Fig. 5.39 Multiple drifting fibers in type II burst with a noise of type III bursts (Chernov et al. 2007) .

The April 19 2000 event (Figure 5.39) is similar to the previous one. It presents a series of fibers repeating in time without a simultaneous CME. But during the day, a type III noise bursts were observed and all strong bursts were accompanied by narrow ejecta in LASCO C2 images, and the IP space was very structured.

Taking into account some patch structure before fibers we can only propose the IP shock front propagating through these inhomogeneities. The fibers do not show strict periodicity and occupy different ranges of frequencies. In April 18 and 19 events the general view of fibers are really similar to fiber bursts (IDB) in the meter range.

Striae in type III bursts

In Figure 5.40, two groups (may be unique) of type III bursts with striae are shown. Parameters of the events are shown in Table 5.2. It is evident that the striae occur only in the narrow zone of frequencies (heights). In contrast to striae in the meter range, here they drift to low frequencies, thus they almost do not differ from fibers shown on Figure 5.39. Therefore their origins can be identical, with the only difference being that here type III beams of fast particles meet a turbulent zone on the way, and in April 19 2000 event the shock front crosses a similar zone, though it is clear that fast particles accelerated in the shock front are also responsible for formation of fibers.

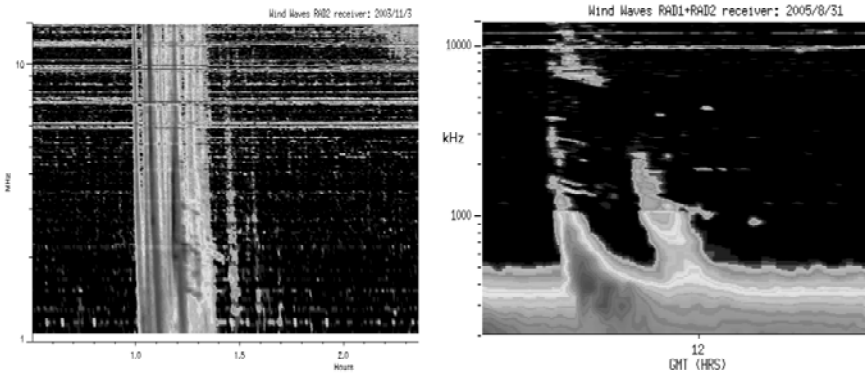

Fig. 5.40 Two events with striae in the type III bursts (Chernov et al. 2007).

The type III bursts are the most numerous phenomena in IP spectra, but such

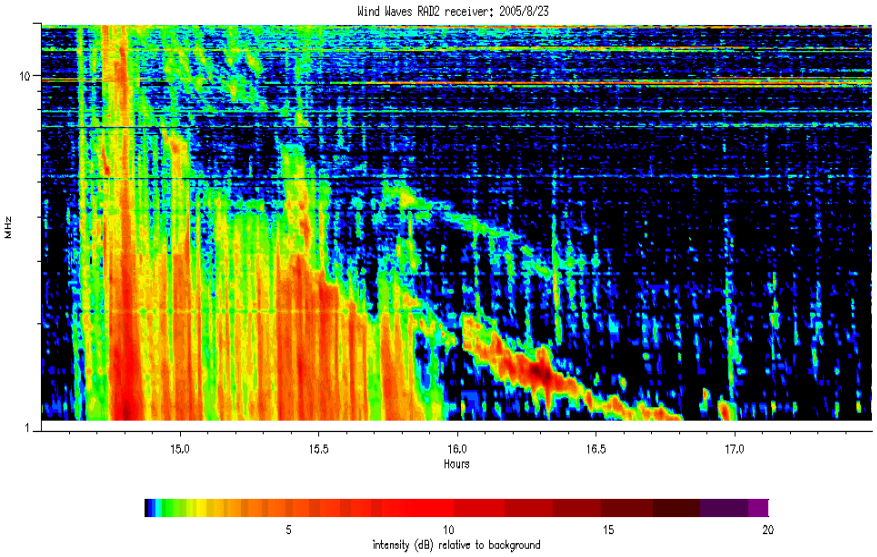

Fig. 5.41 The August 23 2005 event, showing the entire collection of fine structures: fiber structure in 14 - 7 MHz, two harmonic bands of type II burst, and strong SA bursts (Chernov et al. 2007).

rare occurrences of stria structure could be explained by the fact that their large part usually is not connected with CME as well as with shock fronts, as happened in these two events.

The August 23 2005 event (Figure 5.41) shows the entire collection of fine structure: fiber structure in 14 ÷ 7 MHz, two harmonic bands of type II burst with a patch structure and strong SA bursts. But we have no spectra in the metric range. LASCO C2 images show streamer structure after the strong CME. This event was preceded by a radio source at 164 MHz moving to the West, it was probably the source of the metric type II burst.

The July 20 and October 27 2002 events are similar to the September 17 2001 event. A direct expansion of the metric type II bursts (both observed by the Culgoora spectrograph) was manifested only as fibers at high-frequency edge of the *WIND*/*RAD*2 spectrum. LASCO C2 images show the bright jet structure (narrow streamers) behind the CME front simultaneously with fibers and at the same heights (as well as in others events).

The November 18 2003 event show some peculiarity: after the strong metric type II burst only some striae were observed at 08:30 UT, but after the second faint type II burst we see very marked fibers in IP type II bursts after 10:20 UT. A

very marked jet structure after the partial halo CME remained at a distance $2 \div 5\ R_{\odot}$.

The event of July 13 2005 shows many isolated fibers in the whole RAD2 range after a strong, drifting continuum in the metric range (Nançay DCM spectrum, 20 □ 70 MHz). Some small scale jets remained at the distance 2 □ 4 $R_{\odot}$ in the wake behind the halo type CME.

General Discussion

First of all it should be noted that the time resolution of *WIND*/RAD2 spectra is limited by the time of one scan through 14 – 1 MHz, once each 16 seconds and by averaging time of one minute, and thus we can not distinguish all the fine structure elements as in the metric range with the IZMIRAN and Nançay spectrographs with the time resolution 0.04 - 0.05 seconds. So, *WIND/WAVES* receiver can record only large features or sets of fibers. It is still necessary to specify in each event that the fibers have the peculiarities in all parameters (drift, frequency range, duration of separate fibers). Only the instant frequency bandwidth is stable, 200 - 300 kHz for slow-drifting fibers in the type II burst, and 700 – 1000 kHz for fast-drifting fibers in the type II+IV (continuum). In addition, we have not found in IP bursts periodic and parallel-drifting fibers typical for meter and decimeter wave ranges, as well as classical zebra pattern with variable frequency drift of stripes. Only in the first event (Figure 5.32) the stripes are hardly similar to the zebra pattern. The relative fiber parameters ($\Delta f_e/f$, $\Delta f_s/f$) exceed as a rule by an order of magnitude those in the meter range.

It is important to note that in practically all the events with the expressed fine structure (as fibers), shock fronts of IP type II bursts went behind the leading edge of CME. In all the events, a certain connection between the occurrence of fibers and the presence of streamers (narrow jets remaining after the passage of CME) is looked through, when the shock front passes through them. However it is impossible now to establish unequivocal dependence between jets parameters (all their variety) and parameters of separate fibers (their duration, radiation bandwidth). It is clear only that a certain agent must exist which propagates with a speed exceeding or less than the speed of the shock front in order that the drift speed of the fibers would also be more or less than the drift speed of the type II burst. To answer the question on the origin of fibers in the IP bursts we will briefly summarize the known models and generation mechanisms of fiber bursts and zebra pattern.

Interpretation of the fine structure in IP bursts

Let us note, that in almost all the enumerated mechanisms, the electron cyclotron frequency (or its a portion) is used as the harmonic frequency. Therefore it is possible to draw a conclusion that neither the frequency of whistler nor electronic cyclotron frequency determines the frequency bandwidth of the fibers, as well as the frequency separation between them, since in the events discussed the observed values are greater by an order of magnitude. It is known, that in fronts of IP shocks whistlers are observed, and the CMEs represent a magnetic clouds with the braided magnetic loops (flux-rope). Besides, it is possible to consider the presence of fast particles in front of the front as the obvious fact providing to be true by occurrence of the SA bursts. The propagation of fronts through the elongated density heterogeneities (in the wake behind the CME) allow to assume about an opportunity of generation of transition radiation which was already supposed above (in section 5.4) in sources of the decametric fine structures. In interplanetary space it should radiate much more effectively. By varying other parameters the radio flux can not be lower, (*e.g.* in dependence on temperature and energy of electrons). The intensity of the transition radiation can be greatly enhanced by plasma resonance at frequencies just above the local plasma frequency (the resonance transition radiation (RTR). RTR arises as fast particles move through a plasma with small scale variations (as short as the wavelength of the emitted wave) of the refractive index. Such variations may be provided by microturbulence-induced inhomogeneities of the plasma density or magnetic field (Nita, Gary, and Fleishman, 2005). The RTR component is associated with a region of high density, and the RTR emission is *o*-mode polarized. Such conditions are indeed present in IP shock fronts propagating through the wake of CME, especially regarding the occurrence of a resonance between the emitted wavelength and density irregularities.

Different frequency drift of fibers can arise from different propagation angle of the shock front relative to jets with a high density gradient. But the main parameter, the complete duration of each fiber, is determined by the time of the presence of fast particles on the boundary of two media with different density gradients. In the case of shock front, this will be the transit time of the front through the heterogeneity, since the fast particles are present only directly in the front. This time depends on the difference between the speeds of heterogeneity and front. The shock front is absent in type III bursts, and the duration of striae is determined also by the time of the intersection of fast particles with heterogeneity. Fast particles of type III beam fly away in the space providing the emission of type III mainly from its forward edge, but the transition emission is excited throughout the entire beam length of the boundary of heterogeneity, therefore striae have a somewhat larger duration in the comparison with the basic type III burst, that we see on Figure 5.40. Thus, the frequency drift of fibers and striae is defined by the speed of the heterogeneity, which can be somewhat more or less than the speed of the shock front.

The transition of the herringbone structure for meter waves (to 25 MHz) into the large-scale and rather slowly-drifting fibers becomes clear (September 17

2001, Figure 5.34). Small-scale (fast) details are no longer visible in the WIND spectrum, but at the same time the shock front entered into the region of heterogeneities behind the forward edge of the CME, then the transition radiation from the heterogeneities becomes more intense. The drift velocity of the fibers between 12 and 5 MHz in Figure 5.34 corresponds to the velocity of heterogeneities ~ 1400 km s^{-1} in the model of Leblanc, Dulk, and Bougeret (1998), close to speed of CME, which argues in favor of this model. The U bursts in Figure 5.34c have probably the same nature as in the November 3 2003 event. The beginning of the ascending branch at 08.6 UT is joined with the type III burst, therefore it is obvious that the type III beam was trapped into the magnetic cloud of the CME, and a part of fast particles was reflected back into the corona. According to the height-time diagram of the CME it was just located at the distance about 5 $R_{\odot}$ corresponding to the reflection frequency of 1.5 MHz.

On November 13, 2003 (Figure 5.37) we see another scenario of the fine structure. The fibers between 14 ÷ 5 MHz are the continuation of metric fiber structure against the continuum emission, resulting the propagating whistler wave packets. Only in IP space we see some fibers (with harmonics) due to the transition radiation during the shock propagation through the CME wake (after CME overtook the shock front).

Fiber structure of the May 2 1998 IP burst is not the direct continuation of fine structure from the meter range. The general view of the spectrum differs considerably; therefore the mechanism of their formation is different also, apparently. In that case, the fibers are the result of the propagation of the fronts along narrow density heterogeneities (seen in Figure 5.36), and we observe the maximum emission only from these structures (streamers after the passage of the CME). In such a case, the main contribution could give the transition radiation.

The discussed fibers are observed only at the selected frequency range 14 □ 1 MHz. The absence of these fine structures in RAD1 and TNR spectra can be naturally explained by the considerable expansion of CME in space and by the vanishing of the wakes, when heterogeneities are no longer encountered on the path of the shock fronts.

Some Conclusions

We have analyzed *WIND/WAVES* RAD2 spectra with fine structure in the form of different fibers in 14 events covering 1997 □ 2005. A splitting of broad bands of IP type II bursts into narrow band fibers of different duration is observed. The instant frequency bandwidth of fibers is stable enough, 200 □ 300 kHz for slow-drifting fibers in the type II burst, and 700 □ 1000 kHz for fast-drifting fibers in the type II+IV (continuum). In addition, we have not found the IP bursts with periodic and parallel-drifting fibers typical of meter and decimeter wave ranges as well as classical zebra pattern with variable frequency drift of stripes. Only on the April 19 2000 fibers in the range 2 ÷ 1 MHz are somewhat similar to metric IDB, and on November 13 2003 a set of fibers is somewhat similar to rope of fibers in the met-

ric range, but in both case the scales of fiber parameters, and consequently of the source sizes in the IP space, are much larger.

In some events an expansion of metric fiber structure or "herringbone" structure into *WAVES* RAD2 spectra (14 ÷ 5 MHz) was observed. In such cases the radio emission mechanism can be the same as in the metric range, mainly the modulation of radio continuum emission by whistler wave packets before the shock front (or between two shock fronts).

But in most of the events, with the splitting of the usual patch structure in IP type II (or II+IV) bursts into the narrow band fibers, the comparison of spectra with LASCO C2 images testifies to the passage of shock fronts at these moments through narrow jets in the wake of the CME. The propagation of fronts through the elongated density inhomogeneities, (in the wake behind CME), allows one to assume an opportunity of generation of transition radiation (rather resonance transition radiation), when the scales of the density variations in the jets are as short as the wavelength of the emitted wave. The 300 m scales of inhomogeneities are very realistic over the distance $2 \div 4\ R_{\odot}$.

More precise estimations for checking the proposed scheme of the fiber formation in IP type II bursts could be made if we would have more reliable values of density and magnetic field inside CME, positions and sizes of the radio sources, which can be obtained by STEREO mission.

5.6 Summary

We have considered several of the most recent events with new peculiar elements of the zebra patterns. All new properties are considered in the light of both earlier and new theoretical models.

In two events (24 July 2004 and 3 November 2004) the large-scale ZP consisted of small-scale fiber bursts. The appearance of such an uncommon fine structure is connected with the following special features of the plasma wave excitation in the radio source: both whistler and plasma wave instabilities are too weak at the very beginning of the events (the continuum was absent), and the fine structure is almost invisible. Then, whistlers generated directly at DPR levels "highlight" the radio emission only from these levels due to their interaction with plasma waves.

A unique fine structure was observed in the event of 13 December 2006: spikes in absorption formed dark ZP stripes against the absorptive type III-like bursts. The spikes in absorption can appear in accordance with the well- known mechanism of absorptive bursts. The fast particles filled the loss-cone (breaking the loss-cone distribution), and the generation of continuum was quenched at these moments, which was evinced by the formation of bursts in absorption. The maximum absorptive effect realizes at the DPR levels. The parameters of millisecond spikes are determined by small dimensions of the particle beams and local scale heights in the radio source.

Thus, in each new event, new special features of the fine structure are revealed. However, they are usually related with the varied conditions in the source. In such a case, one ought not to find the special emission mechanism for each event, which was repeatedly done before.

The DPR model helped us to understand several aspects of unusual elements of ZP. In this connection, the calculations of growth rates of the upper hybrid waves with different distribution function of fast electrons inside the loss-cone is very important (Kuznetsov and Tsap, 2007). However, discussions concerning the validity of taking into account one or several harmonics in the hybrid band continue. At the same time, Laptuhov and Chernov (2009) showed that the simultaneous existence of several tens of the DPR levels in the corona is impossible for any realistic profile of the plasma density and magnetic field (if we do not assume smaller, by an order of magnitude, local density and magnetic field scale heights).

Since any known model does not avoid deficiencies, the attempts to create new theories continue. We examined three new theories.

The formation of transparency and opacity bands during the propagation of radio waves through regular coronal inhomogeneities is the most natural and promising mechanism. It explains all main parameters of regular ZP. The dynamics of ZP stripes (variations in the frequency drift, stripe breaks, etc.) can be associated with the propagation of inhomogeneities, their evolution, and disappearance. Inhomogeneities are always present in the solar corona, however straight evidence of the existence of inhomogeneities with the scales of several meters in the corona is absent. Although ion-sound waves could serve as the same.

The model of nonlinear periodic space – charge waves in plasma (Kovalev, 2009) is also a very natural mechanism in the solar flare plasma. However, in the case of the intrinsic plasma emission it gives constant frequency separation between stripes of $\approx \omega_B$, while the observations testify to an increase of the frequency separation with frequency. Besides, the condition for achieving strong nonlinearity remains uncertain.

The mechanism of scattering of fast protons on ion-sound harmonics in explosive instability seems very uncommon, which requires a number of strict conditions. However, the fast protons always exist in large flares, and the presence of nonisothermic plasma is completely feasible in the shock wave fronts.

Two last models could be rather realized in large radio bursts. And all three models are related with a compact radio source. The number of discrete harmonics does not depend on the ratio of the plasma frequency to the gyrofrequency in the source in all three models. The latter circumstance can eliminate all the difficulties that arise in the DPR model.

We analyzed two type II radio bursts in the decametric wavelength range with a fine structure in the form of unusual slowly drifting fibers. For our general analysis of the events we used all data available in the other ranges, in particular, WIND, SOHO, and TRACE data. This provided an insight into the development of flare processes and allowed the possible positions of radio sources to be determined. Both type II bursts were observed simultaneously at various frequencies of the decametric range with the 1024-channel spectrograph of the UTR-2 radio

telescope and the IZMIRAN spectrograph as well as in the WIND/WAVES RAD2 spectra. In contrast to the well-known herringbone structure and patches in the spectrum, this fine structure is distinguished by the formation of narrow-band fibers (Δf_e > 50–90 kHz at 24 MHz) and is characterized by the possible generation of whistlers between the leading CME edge and the shock front. SOHO/LASCO C2 data were used to analyze the CME. The fiber drift velocity is assumed to be determined by the whistler group velocity inside the inhomogeneities in the CME tail. Like the continuum modulation in the form of fibers in type IV bursts, the whistlers excited at shock fronts manifest themselves only against the background of enhanced emission from large fibers, which can be the transition radiation from fast particles at inhomogeneities in the CME tail. The unusually low drift velocity of narrow fibers may be determined by the reduction in whistler group velocity inside the inhomogeneities to 760 km s^{-1}. The magnetic field inside the inhomogeneities at a frequency of 24 MHz was $\approx$ 0.9 G.

We have analyzed *WIND/WAVES* RAD2 spectra with fine structure in the form of different fibers in 14 events covering 1997 -- 2005. A splitting of broad bands of IP type II bursts into narrow band fibers of different duration is observed. The instant frequency bandwidth of fibers is stable enough, 200-300 kHz for slow-drifting fibers in the type II burst, and 700 - 1000 kHz for fast-drifting fibers in the type II+IV (continuum). In addition, we have not found the IP bursts with periodic and parallel-drifting fibers typical of meter and decimeter wave ranges as well as classical zebra pattern with variable frequency drift of stripes. Only the April 19, 2000 fibers in the range 2 ÷ 1 MHz are somewhat similar to metric IDB, and on November 13, 2003 a set of fibers is somewhat similar to rope of fibers in the metric range, but in both cases the scales of fiber parameters, and consequently of the source sizes in the IP space, are much larger.

In some events an expansion of metric fiber structure or “herringbone” structure into *WAVES* RAD2 spectra (14 ÷ 5 MHz) was observed. In such cases the radio emission mechanism can be the same as in the metric range, mainly the modulation of radio continuum emission by whistler wave packets before the shock front (or between two shock fronts).

But in most of the events, with the splitting of the usual patch structure in IP type II (or II+IV) bursts into the narrow band fibers, the comparison of spectra with LASCO C2 images testifies to the passage of shock fronts at these moments through narrow jets in the wake of the CME. The propagation of fronts through the elongated density inhomogeneities, (in the wake behind CME), allows one to assume an opportunity of generation of transition radiation (rather resonance transition radiation), when the scales of the density variations in the jets are as short as the wavelength of the emitted wave. The 300 m scales of inhomogeneities are very realistic over the distance 2 ÷ 4 $R_\odot$.

More precise estimations for checking the proposed scheme of the fiber formation in IP type II bursts could be made if we would have more reliable values of density and magnetic field inside CME, positions and sizes of the radio sources, which can be obtained by STEREO mission.

References

Abada-Simon, M., Lecacheux, A., Louran, P., Dulk, G.A., Belkora, L., Bookbinder, J.A., Roso len, C.: In: Grenier, J., et al. (eds.) Proceeding of IAU colloquium 151, flares and flashes, Monograph, vol. 454, pp. 32–35. Springer, Berlin (1995)

Akhiezer, A.I. (ed.): Plasma Electrodynamics. Nauka, Moscow (1974) (in Russian)

Alekseev, V.A., Dugin, N.A., Lipatov, B.N., Melnikov, V.F., Cnegirev, S.D., Tihomirov, J.V.: Izv. VUZov Radiofizika **40**, 1063 (1997) (Rus), Radiophys. Quantum Electron. **40**, 713

Altyntsev, A.T., Grechnev, V.V., Hanaoka, Y.: Solar Phys. **178**, 575 (1998)

Altyntsev, A. T., Grechnev, V. V., Konovalov, S. K.: Astrophys. J. **469**, 976 (1996)

Altyntsev, A.T., Kuznetsov, A.A., Meshalkina, N.S., Rudenko, G.V., Yihua, Y.: Astron. Astrophys. **431**, 1037 (2005)

Altyntsev, A.T., Lesovoi, S.V., Meshalkina, N.S., Sych R.A., Yan Yihua: Astron. Astrophys. **400**, 337 (2003)

Anzer, U., Pneuman, G.W.: Solar Phys. **79**, 129 (1982)

Aschwanden, M.J.: Solar Phys. **111**, 113 (1987)

Aschwanden, M.J.: Particle Acceleration and Kinematics in Solar Flares. Kluwer Academic Publ, Dordrecht (2002)

Aschwanden, M.J.: Astrophys. J. **515**, 842 (2004a)

Aschwanden, M.J.: Physics of the Solar Corona: An Introduction. Springer/Praxis, Berlin/ Chichester (2004b)

Aschwanden, M.J, Güdel, M., Ap.J. **401**, 736 (1992)

Aschwanden, M.J., Newmark, J.L., Delabouniere, J.-P., Neupert, W.M., Klimchuk, J.A., Gary, G. A., Portier-Fornazzi, F., Zucker, A.: Astrophys. J. **515**, 842 (1999)

Ashour-Abdalla, M.: Planet. Space Sci. **20**, 639 (1972)

Aubier, M., Boischot, A.: Astron. Astrophys. **19**, 343 (1972)

Aurass, H., Chernov, G.P.: Solar Phys. **84**, 339 (1983)

Aurass, H., Chernov, G.P., Karlicky, M., Kurths, J., Mann, G.: Solar Phys. **112**, 347 (1987)

Aurass, H., Vrˇsnak, B., Hofmann, A., Ruˇzdjak, V.: Solar Phys. **190**, 267 (1999)

Aurass, H., Klein, K.-L., Zlotnik, EYa, Zaitsev, V.V.: Astron. Astrophys. **410**, 1001 (2003)

Aurass, H., Rausche, G., Mann, G., Hofmann, A.: Astron. Astrophys. **435**, 1137 (2005)

Bakunin, L.M., Chernov, G.P.: Sov. Astron. **29**, 564 (1985)

Bakunin, L.M., Ledenev, V.G., Nefedyev, V.P., et al.: Solar Phys. **135**, 107 (1991)

Barrow, C.H., Sounders, H.: Astrophys. Lett. **12**, 211 (1972)

Barta, M., Karlicky, M.: Astron. Astrophys. **379**, 1045 (2001)

Barta, M., Karlicky, M.: Astron. Astrophys. **450**, 359 (2006)

Bastian, T.S., Benz, A.O., Gary, D.E.: Annu. Rev. Astron. Astrophys. **36**, 131 (1998)

Benz, A.O.: Solar Phys. **96**, 357 (1985)

Benz, A.O.: Solar Phys. **104**, 99 (1986)

G.P. Chernov, *Fine Structure of Solar Radio Bursts*, Astrophysics and Space Science Library 375, DOI 10.1007/978-3-642-20015-1,

Benz, A.O.: Plasma Astrophysics. Kluwer Academic Publisher, Dordrecht (1993)
Benz, A.O., Güdel, M.: Solar Phys. **111**, 175 (1987)
Benz, A.O., Kuijpers, J.: Solar Phys. **46**, 275 (1976)
Benz, A.O., Mann, G.: Astron. Astrophys. **333**, 1034 (1998)
Benz, A.O., Wentzel, D.: Astron. Astrophys. **94**, 100 (1981)
Benz, A.O., Saint-Hilaire, P., Vilmer, N.: Astron. Astrophys. **383**, 678 (2002)
Berney, M., Benz, A.O.: Astron. Astrophys. **65**, 369 (1978)
Bernold, T.: Astron. Astrophys. Suppl. Ser. **42**, 43 (1980)
Bernold, T.E.X.: Fibre fine structure in solar flare radio emission observations and theoretical interpretation. Dissertation ETH No 7409, Swiss Federal Institute of Technology, Zurich (1983)
Bernold, T.E.X., Treumann, R.A.: Astrophys. J. **264**, 677 (1983)
Bespalov, P.A., Trakhtenherz, VIu: Geom. Aeron. **14**, 321 (1974)
Bespalov, P.A., Traxtenherz, V.Iu.: Alvenic Mazers, IPFAN, Gorkii (in Russian). Rev. Plasma Phys. **10**, 155 (1986)
Boischot, A.: Ann. Astrophys. **21**, 273 (1957)
Boischot, A., Haddock, F.T., Maxwell, A.: Ann. Astrophys **23**, 478 (1960)
Bougeret, J.-L., Kaiser, M.L., Kellogg, P.J., et al.: Space Sci. Rev. **71**, 5 (1995)
Bougeret, J.-L., Zarka, P., Caroubalos, C., et al.: Geophys. Res. Lett. **25**, 2513 (1998)
Breizman, B.N.: In: Kadomtsev, B.B. (ed.) Problems in Plasma Theory, vol. 15, p. 55. Energoatomizdat, Moscow (1987)
Cane, H.V., Erickson, W.C.: Astrophys. J. **623**, 1180 (2005)
Caroubalos, C., Maroulis, D., Patavalis, N., et al.: Exp. Astron. **11**, 23 (2001)
Chernov, G.P.: Sov. Astron. **17**, 788 (1974a)
Chernov, G.P.: Solnechnye Dannye **N12**, 75 (1974b) (in Russian)
Chernov, G.P.: Sov. Astron. **20**, 449 (1976a)
Chernov, G.P.: Sov. Astron. **20**, 582 (1976b)
Chernov, G.P.: Sov. Astron. **21**, 612 (1977)
Chernov, G.P.: Sov. Astron. **22**, 330 (1978)
Chernov, G.P.: Sov. Astron. Lett. **8**, 54 (1982)
Chernov, G.P.: Sov. Astron. **33**, 649 (1989)
Chernov, G.P.: Solar Phys. **130**, 75 (1990a)
Chernov, G.P.: Sov. Astron. **34**, 66 (1990b)
Chernov, G.P.: Kinemat. Fiz. Neb. Tel **6**, 27 (1990c)
Chernov, G.P.: Astron. Rep. **40**, 561 (1996)
Chernov, G.P.: Astron. Lett. **23**, 827 (1997)
Chernov, G.P.: Astron. Rep. **48**, 853 (2004)
Chernov, G.P.: Plasma Phys. Rep. **31**, 314 (2005)
Chernov, G.P.: Space Sci. Rev. **127**, 195 (2006)
Chernov, G.P., Fomichev, V.V.: Sov. Astron. Lett. **15**(5), 410 (1989)
Chernov, G.P., Kurths, J.: Sov. Astron **34**, 516 (1990)
Chernov, G.P., Zlobec, P.: Solar Phys. **160**, 79 (1995)
Chernov, G.P., Chertok, I.M., Fomichev, V.V., Markeev, A.K.: Solar Phys. **24**, 215 (1972)
Chernov, G.P., Korolev, O.S., Markeev, A.K.: Solar Phys. **44**, 435 (1975)
Chernov, G. P.. Stanislavskii, A. A. Konovalenko, A. A, et al., Astron. Lett. **33**, 192 (2007b)
Chernov, G.P., Chertok, I.M., Fomichev, V.V., Gnezdilov, A.A., Gorgutsa, R.V., Markeev, A.K.: Report UAG-96, p. 88. World Data Center, Boulder (1984)
Chernov, G.P., Klein, K.-L., Zlobec, P., Aurass, H.: Solar Phys. **155**, 373 (1994)
Chernov, G.P., Markeev, A.K., Poquerusse, M., Bougeret, J.-L., Klein, K.-L., Mann, G., Aurass, H., Aschwanden, M.: Astron. Astrophys. **334**, 314 (1998)
Chernov, G.P., Poquerusse, M., Bougeret, J.-L., Zlobec, P.: Proceedings of the 9th European Meeting on Solar Physics, Magnetic Fields and Solar Processes', Florence, Italy, 12–18 September 1999 (ESA SP-448), p. 765 (1999)
Chernov, G.P., Fu, Q., Lao, D.B., Hanaoka, J.: Solar Phys. **201**, 153 (2001a)

Chernov, G.P., Yasnov, L.V., Yan, Y., Fu, Q.: Chin. J. Astron. Astrophys. **1**, 525 (2001b)
Chernov, G.P., Poquerusse, M., Bougeret, J.-L., Zlobec, P.: Radio Sci. **36**, 1745 (2001c)
Chernov, G.P., Yan, Y., Fu, Q.: Astron. Astrophys. **406**, 1071 (2003)
Chernov, G.P., Yan, Y.H., Fu, Q.J., Tan, ChM: Astron. Astrophys. **437**, 1047 (2005)
Chernov, G.P., Sych, R.A., Yan, Y.H., Fu, Q.J., Tan, ChM, Huang, G.L., Wang, D.Y., Wu, H.G.: Solar Phys. **237**, 397 (2006)
Chernov, G.P., Kaiser, M.L., Bougeret, J.-L., Fomichev, V.V., Gorgutsa, R.V.: Solar Phys. **241**, 145 (2007a)
Chernov, G.P., Yan, Y.H., Fu, Q.J., Tan, ChM, Wang, ShJ: Solar Phys. **250**, 115 (2008)
Chernov, G.P., Yan, Y.H., Tan, ChM, Chen, B., Fu, Q.J.: Solar Phys. **262**, 149 (2010)
Chernov, G.P., Cych, R.A., Meshalkina, N.S. Yan, Y., and Tan, Ch.M.: Astron. Astrophys. (accepted) (2011)
Chen, B., Yan, Y.: Astrophys. J, **689**, 1412 (2008)
Chertok, I.M.: Sov. Astron. **16**, 1023 (1973)
Chiuderi, C. Giashetti, R., and Rosenberg, H.: Solar Phys. **33**, 255 (1973)
Dabrowski, B.P., Rudawy, P., Falewicz, R., Siarkowski, M., Kus, A.J.: Astron. Astrophys. **434**, 1139 (2005)
De Groot, T.: Int. Bull. Sol. Radio Obs. Eur. **9**, 3 (1962)
Dory, R.A., Guest, G.E., Harris, E.G.: Phys. Rev. Lett. **14**, 131 (1965)
Droge, F.: Astron. Astrophys. **57**, 285 (1977)
Droge, F., Riemann, P.: Int. Bull. Sol. Radio Obs. Eur. **8**, 6 (1961)
Dulk, G.A., McLean, D.J.: Solar Phys. **57**, 279 (1978)
Edgar, B.C.: The Structure of the Magnetosphere as Deduced from Magnetospherically Reflected Whistlers. Stanford University, Stanford (1972)
Elgarøy, Ø.: Nature **184**, 887 (1959)
Elgarøy, Ø.: Astrophys. Norv. **7**, 123 (1961)
Elgarøy, Ø.: Astrophys. Norv. **10**, 127 (1963)
Elgarøy, Ø.: Astrophys. Lett. **3**, 39 (1969)
Elgarøy, Ø.: Report of the first Meeting of C.E.S.R.A., Utrecht, p. 48 (1971)
Elgarøy, Ø.: Astron. Astrophys. **82**, 308 (1980)
Elgarøy, Ø., Rosenkild, P.H.: IAU Symposium, Australia (1973)
Elgarøy, Ø., Sveen, O.P.: Solar Phys. **32**, 231 (1973)
Elgarøy, Ø.: Intermediate Drift Bursts, Report N 53. ITA, University of Oslo, Oslo (1982)
Fainstein, S.M.: Zh. Eksp. Teor. Fiz **71**, 1021 (1976) [Sov. Phys. JETP **44**, 534]
Fainstein, S.M., Chernova, E.A.: Zh. Eksp. Teor. Fiz **109**, 821 (1996) [JETP **82**, 442]
Fedorenko, V.N.: Sov. Astron. **52**, 978 (1975)
Fleishman, G.D.: Astron. Lett. **27**, 254 (2001)
Fleishman, G.D., Melnikov, V.F.: Usp. Fiz. Nauk **168**, 1265 (1998) [Soviet Phys. Usp. **41**, 1157]
Fleishman, G.D., Stepanov, A.V., Yurovsky, Y.F.: Solar Phys. **153**, 403 (1994)
Fleishman, G.D., Fu, Q.J., Huang, G.L., Melnikov, V.F., Wang, M.: Astron. Astrophys. **385**, 671 (2002)
Fomichev, V.V., Chertock, I.M.: Sov. Astron. **12**, 21 (1968)
Fomichev, V.V., Chertock, I.M.: Sov. Astron. **13**, 1032 (1970)
Fomichev, V.V., Chertock, I.M.: Izvest. Vuzov Radiofizika **20**, 1255 (1977)
Fomichev, V.V., Fainshtein, S.M.: Solar Phys. **71**, 385 (1981)
Fomichev, V.V., Fainshtein, S.M.: Sov. Astron. **32**, 552 (1988)
Fomichev, V.V.: Sporadic Solar Radio Radiation on meter waves and diagnostics of the Solar Corona, Ph.D. Dissertation in mathematical physics, IZMIRAN, Moscow (1986)
Fomichev, V.V., Fainshtein, S.M., Chernov, G.P.: Plasma Phys. Rep. **35**, 1032 (2009)
Forbes, T.G., Priest, E.R.: Solar Phys. **84**, 169 (1983)
Fu, Q.J., Gong, Y.F., Jin, S.Z., Zhao, R.Y.: Solar Phys. **130**, 161 (1990)
Fu, Q.J., Qin, Z.H., Ji, H.R., Pen, L.B.: Solar Phys. **160**, 97 (1995)
Fu, Q.J., Ji, H.R., Qin, Z.H., Xu, Z.C., Xia, Z.G., Wu, H.A., et al.: Solar Phys. **222**, 167 (2004)
Gallagher, P.T., Dennis, B.R., Krucker, S., Schwartz, R.A., Tolbert, A.K.: Solar Phys. **210**, 341 (2002)

Gary, D.E., Hurford, G.J., Flees, D.J.: Astrophys. J. **369**, 255 (1991)
Gendrin, R.: Geophys. Space Phys. **19**, 171 (1981)
Gershman, B.N., Ugarov, V.A.: Usp. Fiz. Nauk Sovjet Usp. **72**, 235 (1960)
Ginzburg, V.L.: Propagation of Electromagnetic Waves in Plasma. Nauka, Moscow (1967)
Ginzburg, V.L., Rukhadze, A.A.: Waves in Magnetoactive Plasma. Nauka, Moscow (1975) (in Russian)
Ginzburg, V.L., Tsytovich, V.N.: Transition Radiation and Transition Scattering. Nauka, Moscow (1984);1990, Bristol: Adam Hilger
Gladd, N.T.: Phys. Fluids **26**, 974 (1983)
Gotwols, B.L.: Solar Phys. **25**, 232 (1972)
Güdel, M.: Astron. Astrophys. **239**, L1 (1990)
Güdel, M., Benz, A.O.: Astron. Astrophys. **231**, 212 (1990)
Güdel, M., Zlobec, P.: Astron. Astrophys. **245**, 299 (1991)
Güdel, M., Aschwanden, M.J., Benz, A.O.: Astron. Astrophys. **251**, 285 (1991)
Güdel, M., Benz, A.O., Treumann, R.A.: Proceedings of Workshop on Plasma Astrophysics, Varenna, Italy, ESA SP-285, V.1, 95 (1988)
Guo, Y., Ding, M.D., Wiegelmann, T., Li, H.: Astrophys. J. **679**, 1629 (2008)
Gurnett, D.A., et al.: J. Geophys. Res. **84**, 2029 (1979)
Haselgrove, J.: Ray Theory and a New Method for Ray Tracing, in Physics of the Ionosphere, p. 355. The Physical Society, Cambridge (1955)
Hashimoto, K., Kimura, J.: J. Plasma Phys. **18**, 1 (1977)
Hayes, L.M.: Aust. J. Phys. **38**, 705 (1985)
Hillaris, A., Chernov, G.P., Zlobec, P., Caroubalos, C.: Proceedings 10th European SPM, Solar Variability: From Core to Outer Frontiers, Prague (ESA SP-506), Vol. 2, p. 637 (2002)
Holman, G.D., Pesses, M.E.: Astrophys. J. **267**, 837 (1983)
Huang, G.-L.: New Astron. **8**, 313 (2003)
Huang, G.-L.: In: Dere, K., Wang, J., Yan Y. (eds.) Proceedings of the IAU Symposium 226, Beijing, p. 95, Cambridge University Press, Cambridge (2004)
Huang, G.L., Nakajima, H.: Astrophys. Space Sci. **295**, 423 (2004)
Huang, J., Yan, Y., Liu, Y.: Adv. Space Res. **39**, 1439 (2007)
Isliker, H., Benz, A.O.: Astron. Astrophys. **104**, 145 (1994)
Jamin, E., Parkinson, D., Rogister, A., Bernatici, M.: Phys. Fluids **17**, 419 (1974)
Jiřička, K., Karlicky, M., Meszarosova, H., Snizek, V.: Astron. Astrophys. **375**, 243 (2001)
Kaastra, J.S.: Solar flares, an electrodynamic model. Ph. D. thesis, Utrecht University, Utrecht, p. 161 (1985)
Kadomtsev, B.B., Mihailovsky, A.B., Timifeev, A.V.: Zh. Eksp. Teor. Fiz. **47**, 2266 (1964)
Kaplan, S.A., Tsytovich, V.N.: Plasma Astrophysics. Pergamon Press, New York (1973)
Karlicky, M., Barta, M.: Adv. Space Res. **39**, 1415 (2007)
Karlický, M., Bárta, M., Jiřička, K., Meszárosová, H., Sawant, H.S., Fernandes, F.C.R., Cecatto, J.R.: Astron. Astrophys. **375**, 638 (2001)
Karlický, M., Bárta, M., Klassen, A., Aurass, H., Mann, G.: Proceedings 10th European SPM, 'Solar Variability: From Core to Outer Frontiers', Prague (ESA SP-506), p. 303 (2002)
Karpman, V.I., Shagalov, A.: J. Plasma Phys. **38**, 155 (1987); 1988, **39**, 1
Karpman, V.I., Washimi, H.: J. Plasma Phys. **18**(1), 173 (1977)
Kennel, C.F.: Phys. Fluids **9**, 2190 (1966)
Kennel, C.F., Thorne, R.M.: J. Geophys. Res. **72**, 871 (1967)
Kimura, I.: Radio Sci. **1**, 269 (1966)
Klassen, A.: Solar Phys. **167**, 449 (1996)
Klassen, A., Aurass, H., Mann, G.: Astron. Astrophys. **370**, L41 (2001)
Kliem, B., Karlicky, M., Benz, A.Q.: Astron. Astrophys. **360**, 715 (2000)
Kovalev, V.A.: Kinemat. Fiz. Nebesn. Tel **6**, 38 (1990)
Kovalev, V.A.: Plasma Phys. Rep. **35**, 394 (2009)

Kovalev, V.A., Petviashvili, V.I.: Russ. Phys. J. **37**, 699 (1994) [Russ. Izv. Vyssh. Uchebn. Zaved., Fiz., No. 7, 118]
Krishan, V., Fernandes, F.C.R., Cecatto, J.R., Sawant, H.S.: Solar Phys. **215**, 147 (2003)
Krucker, S., Benz, A.O.: Astron. Astrophys. **285**, 1038 (1994)
Krucker, S., et al.: Astron. Astrophys. **302**, 551 (1995)
Krüger, A.: Introduction to Solar Radio Astronomy and Radio Physics, p. 128. D. Reidel Publ. Comp, Dordrecht (1979)
Kuijpers, J.: *Collective wave-particle interactions in solar type IV radio sources*. Ph.D. Thesis, Utrecht University, Utrecht (1975a)
Kuijpers, J.: Astron. Astrophys. **40**, 405 (1975b)
Kuijpers, J.: Solar Phys. **44**, 173 (1975c)
Kuijpers, J.: Theory of type IV dm bursts. In: Kundu, M.R., Gergely, T.E. (eds.) Radio Physics of the Sun, p. 341. D. Reidel Publishing Company, Dordrecht (1980)
Kuijpers, J., Van der Post, P., Slottje, C.: Astron. Astrophys. **102**, 331 (1981)
Kundu, M.: Solar Radio Astronomy. Interscience, New York (1965)
Kuznetsov, A.A.: Astron. Astrophys. **438**, 341 (2005)
Kuznetsov, A.A.: Solar Phys. **237**, 153 (2006)
Kuznetsov, A.A.: Astron. Lett. **33**, 319 (2007)
Kuznetsov, A.A.: Solar Phys. **253**, 103 (2008)
Kuznetsov, A.A., Tsap, YuT: Solar Phys. **241**, 127 (2007)
Kuznetsov, A.A., Vlasov, V.G.: Astron Rep **47**, 129 (2003)
LaBelle, J., Treumann, R.A., Yoon, P.H., Karlicky, M.: Astrophys. J. **593**, 1195 (2003)
Laptuhov, A.I., Chernov, G.P.: Plasma Phys. Rep. **32**, 866 (2006)
Laptuhov, A.I., Chernov, G.P.: Plasma Phys. Rep. **35**, 160 (2009)
Laptuhov, A.I., Chernov, G.P., Kovalev, V.A.: In: International symposium "Astronomy-2005: Current state and prospects," Moscow, 2005, Book of abstracts, Paper P2.31; Tr. GAISh **78**, 31 (2005)
Laptukhov, A.I.: Interplanetary Medium and Magnetospheric Processes. Nauka, Moscow (1991) [in Russian]
Leblanc, Y., Dulk, G.A., Bougeret, J.-L.: Solar Phys. **183**, 165 (1998)
Leblanc, Y., Dulk, G.A., Cairns, I.H., Bougeret, J.-L.: J. Geophys. Res. **105**(A8), 18215 (2000)
Ledenev, V.G., Karlicky, M., Yan, Y., Fu, Q.: Solar Phys. **202**, 71 (2001)
Ledenev, V.G., Yan, Y., Fu, Q.: Solar Phys. **233**, 129 (2006)
Lin, J., Forbes, T.G.: J. Geophys. Res. **105**, 2375 (2000)
Livshits, V.A., Tsytovich, V.N.: Sov. Phys. JETP **35**, 321 (1972)
Magdalenić, J., Vršnak, B., Zlobec, P., Hillaris, A., Messerotti, M.: Astrophys. J. **642**, L77 (2006)
Maltseva, O.A., Chernov, G.P.: Kinemat. Fiz. Neb. Tel **5**, 32 (1989a)
Maltseva, O.A., Chernov, G.P.: Kinemat. Fiz. Neb. Tel **5**, 44 (1989b)
Mann, G., Karlick´y, M., Motschmann, U.: Solar Phys. **110**, 381 (1987)
Mann, G., Baumgaertel, K., Chernov, G.P., Karlický, M.: Solar Phys. **120**, 383 (1989)
Manoharan, P.K., van Driel-Gesztelyi, L., Pick, M., Demoulin, P.: Astrophys. J. **468**, L73 (1996)
Markeev, A.K., Chernov, G.P.: Astron. Zhurnal **47**, 1044 (1970) (Sov. Astron. **14**, 835)
McLean, D.J., Sheridan, K.V.: Solar Phys. **32**, 485 (1973)
Melnik, V.N., Konovalenko, A.A., Stanislavsky, A.A., et al.: Radiofix. Radioastron. **9**, 237 (2004)
Melnik, V.N., Konovalenko, A.A., Dorovsky, V.V., et al.: Solar Phys. **231**, 143 (2005)
Melrose, D.B.: Solar Phys. **87**, 359 (1975)
Melrose, D.B.: Plasma Astrophysics. Gordon and Breach Publishers, New York (1980)
Melrose, D.B.: Solar Phys. **87**, 359 (1983)
Melrose, D.B.: Solar Phys. **119**, 143 (1989)
Melrose, D.B.: Astrophys. J. **380**, 256 (1991)
Meshalkina, N.S., Altyntsev, A.T., Sych, R.A., Chernov, G.P., Yan, Y.H.: Solar Phys. **221**, 85 (2004)
Messmer, P., Benz, A.O., Monstein, C.: Solar Phys. **187**, 335 (1999)
Messmer, P., Chernov, G.P., Zlobec, P., Gorgutsa, R.V.: Proceedings 10th European SPM, 'Solar Variability: From Core to Outer Frontiers', Prague (ESA SP-506), Vol. 2, p. 701 (2002)

Mészárosová, H., Veronig, A., Zlobec, P., Karlicky, M. In: Solar Variability: From Core to Outer Frontiers, Prague (ESA SP-506, December), Vol. 1, p. 347 (2002)
Mészárosová, H., Veronig, A., Zlobec, P., Karlicky, M.: Astron. Astrophys. **407**, 1115 (2003)
Mészárosová, H., Karlický, M., Sawant, H.S., Fernandes, F.C.R., Cecatto, J.R., de Andrade, M.C.: Astron. Astrophys. **491**, 555 (2008)
Mishin, E.V., Rouzhin, YuYa, Telegin, V.A.: Interaction of Electron Fluxes with the Ionospheric Plasma, p. 264. Gidrometeoizdat, Leningrad (1989)
Molchanov, O.A., Trahtendertz, VJu, Chmyrev, V.M.: Izv. VUZov Radiofizika **17**, 325 (1974)
Mollwo, L.: Solar Phys. **83**, 305 (1983)
Mollwo, L.: Solar Phys. **116**, 323 (1988)
Mollwo, L., Sauer, K.: Solar Phys. **51**, 435 (1977)
Nakariakov, V.M.: Adv. Space Res. **39**, 1804 (2007)
Newkirk, G.: Astrophys. J. **133**, 983 (1961)
Ning, Z., Fu, Q., Lu, Q.: Astron. Astrophys. **364**, 853 (2000)
Nita, G.M., Gary, D.E., Fleishman, G.D.: Astrophys. J. **629**, L65 (2005)
Nita, G.M., Fleishman, G.D., Gary, D.E.: Astrophys. J. **689**, 545 (2008)
Omura, Y., Matsumoto, M.: J. Geophys. Res. **92**(A8), 8649 (1987)
Ossakov, S.L., Ott, E., Haber, I.: J. Geophys. Res. **15**, 2314 (1972)
Ossakov, S.L., Ott, E., Haber, I.: J. Geophys. Res., **16**, 2945 (1973)
Osten, R.A., Bastian, T.S.: Astrophys. J. **637**, 1016 (2006)
Parail, V.V., Pogutse, O.P.: In: Kadomtsev, B.B. (ed.) Problems in Plasma Theory, vol. 11, p. 5. Atomizdat, Moscow (1981)
Pick, M., Démoulin, P., Krucker, S., Malandraki, O., Maia, D.: Astrophys. J. **625**, 1019 (2005)
Pick, M., Vilmer, N.: Astron. Astrophys. Rev. **16**, 1 (2008)
Pisareva, V.V.: Sov. Astron. **35**, 112 (1958)
Podgornii, A.I., Syrovatskii, S.I.: Phyz. Plaz. **7**, 1055 (1981)
Priest, E.R.: Solar Magnehydrodynamics. D. Reidel Publishing Company, Dordrecht (1982)
Priest, E., Forbes, T.: Magnetic Reconnection. Cambridge University Press, New York (2000)
Qin, Z.H., Huang, G.L.: Astrophys. Space Sci. **218**, 213 (1994)
Reiner, M.J., Kaiser, M.L., Fainberg, J., Bougeret, J.-L.: Solar Phys. **234**, 301 (2006)
Riddle, A.C.: Solar Phys. **34**, 181 (1974)
Roberts, B., Edwin, P.M., Benz, A.O.: Astrophys. J. **279**, 857 (1984)
Robinson, P.A.: Phys. Fluids **31**, 525 (1988)
Rosenberg, H.: Astron. Astrophys. **9**, 159 (1970)
Rosenrauh, J.M., Stepanov, A.V.: Contrib. Astron. Obs. Skalnate Pleso **15**, 409 (1986)
Roussev, I.I., Forbes, T.G., Gombosi, T.I., et al.: Astrophys. J. **588**, L45 (2003)
Rozhansky, I.V., Fleishman, G.D., Huang, G.-L.: Astrophys. J. **681**, 1688 (2008)
Sakai, J.-L., Ohsava, Y.: Space Sci. Rev. **46**, 113 (1987)
Sawant, H.S., Fernandes, F.C.R., Cecatto, J.R., et al.: Adv. Space Res. **29**(3), 349 (2002a)
Sawant, H.S., Karlický, M., Fernandes, F.C.R., Checatto, J.R.: Astron. Astrophys. **396**, 1015 (2002b)
Sazhin, S.S.: Planet. Space Sci. **35**, 753 (1987)
Schwenn, R., Raymond, J.C., Alexander, D., et al.: Space Sci. Rev. **123**, 127 (2006)
Shapiro, V.D., Shevchenko, V.I.: Plasma Turbulence in Space. Itogi Nauki i TekhSer. Astronomiya, p. 235. VINITI, Moscow (1987)
Sharma, R.R., Vlahos, L.: Astrophys. J. **280**, 405 (1984)
Sidneva, M.V., Semenov, V.S.: Geomagn. Aeronomy, **25**, 806 (1985)
Sirenko, E.A., Fleishman, G.D.: Astron. Rep. **53**, 369 (2009)
Slottje, C.: Solar Phys. **25**, 210 (1972)
Slottje, C.: Nature, **275**, 520 (1978)
Slottje, C.: Atlas of fine structures of dynamic spectra of Solar type IV-dm and some type II bursts, Utrecht Observatory, Utrecht (1981)
Smolkov, G.Y., Pistolkors, A.A., Treskov, T.A., et al.: Astrophys. Space Sci. **119**, 1 (1986)

Stahli, M., Magun, A.: Solar Phys. **104**, 117 (1986)
Stepanov, A. V.: Soviet Astronomy, **17**, 781 (1974)
Stepanov, A.V., Tsap, Y.T.: Astron. Rep. **43**, 838 (1999)
Stepanov, A.V., Tsap, Y.T.: Solar Phys. **211**, 135 (2002)
Stepanov, A.V., Kliem, B., Krúger, A., Hilderbrandt, J., Garaimov, V.I.: Astrophys. J. **524**, 961 (1999)
Storey, L.R.: Philos. Trans. **A246**, 113 (1953)
Strong, K.T., Bruner, M., Tarbell, T., Title, A., Wolfson, C.J.: Space Sci. Rev. **70**, 119 (1994)
Sych, R.A., Sawant, H.S., Karlický, M., Mészárosová, H.: Adv. Space Res. **38**, 979 (2006)
Tan, B.: Solar Phys. **253**, 117 (2008)
Tan, B.L.: Astrophys. Space Sci. **325**, 251 (2010)
Tan, B.L., Yan, Y.H., Tan, C.M., Liu, Y.Y.: Astrophys. J. **671**, 964 (2007)
Tapping, K.F.: Solar Phys. **87**, 177 (1983)
Tarnstrom, G.L., Philip, K.W.: Solar Radio Spike Bursts, UAG-217, University of Alaska, College, Alaska, p. 186 (1971)
Thompson, A.R., Maxwell, A.: Astrophys. J. **136**, 546 (1962)
Treuman, R.A., Bernold, T.E.X.: Phys. Rev. Lett. **47**, 1455 (1981)
Treuman, R.A., Güdel, M., Benz, A.O.: Astron. Astrophys. **236**, 242 (1990)
Trottet, G., Kerdraon, A., Benz, A.O., et al.: Astron. Astrophys. **93**, 129 (1981)
Tsang, K.T.: Phys. Fluids, **27**, 1659 (1984)
Tsuneta, S.: Astrophys. J. **456**, 840 (1996)
Tsytovich, V.N.: Nonlinear Effects in Plasma. Plenum Press, New York (1970)
Tsytovich, V.N.: Theory of Turbulent Plasma. Plenum Press, New York (1977)
Vrsnak, B., Magdalenc, J., Zlobec, P.: Astron. Astrophys. **413**, 753 (2004)
Vrsnak, B., Warmuth, A., Temmer, M., Veronig, A., Magdalenich, J., Hillaris, A., Karlicky, M.: Astron. Astrophys. **448**, 739 (2006)
Walter, F.: Nonducted VLF propagation in the magnetosphere: Technical Report N 3418–1, p. 145. Stanford University, Stanford (1969)
Wang, D.Y., Li, D.Y.: Solar Phys. **135**, 393 (1991)
Wang, D.Y., Chernov, G.P., Oraevsky, V.N.: Astrophys. Space Sci. **288**, 293 (2003)
Wang, S.J., Yan, Y.H., Liu, Y.Y., Fu, Q.J., Tan, B.L., Zhang, Y.: Sol. Phys. **253**, 133 (2008)
Weiland, J., Wilhelmsson, H.: Coherent Non-linear Interaction of Waves in Plasma. Pergamon Press, Oxford (1977)
Wentzel, D., Aschwanden, M.J.: Astrophys. J. **372**, 688 (1991)
Wild, J.P., Smerd, S.F.: Ann. Rev. Astron. Astrophys. **10**, 159 (1972)
Wild, J.P., Smerd, S.F., Weiss, A.A.: Ann. Rev. Astron. Astrophys. **1**, 291 (1963)
Willes, A.J.: Solar Phys. **186**, 319 (1999)
Winglee, R.M., Dulk, G.A.: Astrophys. J. **307**, 808 (1986)
Wu, D.J., Huang, J., Tang, J.F., Yan, Y.H.: Astrophys. J. **665**, L171 (2007)
Xu, P., Forbes, T.G.: Solar Phys. **139**, 315 (1992)
Yan, Y., Huang, J., Chen, B., Sakurai, T.: PASJ **59**, S815 (2007)
Yasnov, L.V., Karlický, M.: Solar Phys. **219**, 289 (2004)
Yasnov, L.V., Chernov, G.P., Yan, Y., Fu, Q.: Proceedings 10th European SPM, 'Solar Variability: From Core to Outer Frontiers', Prague (ESA SP-506), vol. 2, p. 791 (2002)
Yip, W.K.: Austral. J. Phys. **23**, 161 (1970)
Young, C.V., Spenser, C.L., Moreton, C.E., and Roberts, J.A..: Astrophys. J. **133**, 243 (1961)
Zaitsev, V.V.: Sov. Astron. Lett. **1**, 28 (1975)
Zaitsev, V.V., Ledenev, V.G.: Sov. Astron. Lett. **2**, 172 (1976)
Zaitsev, V.V., Stepanov, A.V.: Astron. Astrophys. **45**, 135 (1975)
Zaitsev, V.V., Stepanov, A.V.: Astron. Astrophys. **40**, 135 (1976)
Zaitsev, V.V., Zlotnik, EYa: Astron. Lett. **12**, 311 (1986)
Zaitsev, V.V., Mityakov, N.A., Rapoport, B.O.: Solar Phys. **24**, 444 (1972)
Zaitsev, V.V., Kunilov, M.V., Mityakov, N.A., Rapoport, B.O.: Sov. Astron. **18**, 147 (1974)

Zaitsev, V.V., Stepanov, A.V., Chernov, G.P.: Solar Phys. **93**, 363 (1984)
Zaitsev, V.V., Stepanov, A.V., Sterlin, A.M.: Sov. Astron. Lett. **11**, 192 (1985)
Zaitsev, V.V., Stepanov, A.V., Urpo, S., Pohjolainen, S.: Astron. Astrophys. **337**, 887 (1998)
Zheleznyakov, V.V.: Radiation in Astrophysical Plasmas, engl. transl. (in Russ., Izdat. Nauka, Moscow, 1977). Kluwer Academic Publisher, Dordrecht (1995) .
Zheleznyakov, V.V., Zaitsev, V.V.: Sov. Astron. **14**, 47 (1970)
Zheleznyakov, V.V., Zlotnik, EYa: Solar Phys. **43**, 431 (1975a)
Zheleznyakov, V.V., Zlotnik, EYa: Solar Phys. **44**, 447 (1975b)
Zheleznyakov, V.V., Zlotnik, EYa: Solar Phys. **44**, 461 (1975c)
Zheleznyakov, V.V.: Radio Emission of the Sun and Planets (in Russ), Izdat. Nauka, Moscow (engl. transl. Pergamon Press, Oxford, 1970) (1964)
Zimmerman, Z.: Astron. Astrophys. **15**, 433 (1971)
Zlobec, P., Karlický, M.: Solar Phys. **182**, 477 (1998)
Zlobec, P., Karlický, M.: Solar Phys. **246**, 419 (2007)
Zlobec, P., Li, H.W., Messerotti, M., Comari, M., Barry, M.B.: Solar Phys. **114**, 375 (1987)
Zlotnik, EYa: Izv. VUZov Radiofizika **19**, 481 (1976)
Zlotnik, EYa: Cent. Eur. Astrophys. Bull. **33**, 281 (2009)
Zlotnik, E.Ya., Zaitsev, V.V.: Proceedings of the conference: Active processes on the Sun and Stars, NIIRF, Spb. University, St Petersburg, p. 257 (in Russian) (2002)
Zlotnik, E.Ya.: Issled. po geomagnetismu, aeronomii i physike Solntsa , SibIZMIR, Irkutsk **48**, 132 (in Russian) (1979)
Zlotnik, EYa, Sher, E.M.: Izv. VUZov Radiofizika **52**, 95 (2009) (Rus), Radiophys. Quantum Electron. **52**, 88
Zlotnik, E.Ya., Zaitsev, V.V., Aurass, H., Mann, G., Hofmann, A.: Astron. Astrophys. **410**, 1011 (2003)
Zlotnik, EYa, Zaitsev, V.V., Aurass, H., Mann, G.: Solar Phys. **255**, 273 (2009)

Index